INELASTIC STABILITY OF PLATE STRUCTURES USING THE FINITE STRIP METHOD

by

NABIL S. MAHMOUD

A thesis submitted to the
University of Sheffield
for the Degree of Doctor
of Philosophy.

Department of Civil and
Structural Engineering,
University of Sheffield,
January, 1981

To my mother

CONTENTS

CONTENTS (continued)

CONTENTS (continued)

CONTENTS (continued)

CONTENTS (continued)

CONTENTS (continued)

CONTENTS (continued)

CONTENTS (continued)

CONTENTS (continued)

SUMMARY

In this thesis, some nonlinear effects associated with the buckling behaviour of plated steel structures are examined using a modified finite strip method. To include the effects of plasticity over parts of the cross-section, a more general stress-strain relationship than previously included has been used. The method is also extended to account for the large deflection behaviour of perfect and imperfect plates in the elastic range. The only restriction on the method presented here is that the buckling mode varies sinusoidally in the longitudinal direction, which implies either that the ends of the structure are simply supported or that the wave-length of the buckled mode is small in comparison with the overall length of the structure.

The present study may be divided into three parts. In the first part the small deflection theory is used to determine the stiffness and stability matrices of an individual strip and these are assembled to form an overall stiffness matrix, representing a structure which may be under concentric load, eccentric load or pure bending. In some cases a structure with an overall initial imperfection is considered. The Wittrick-Williams Algorithm is used to obtain the smallest critical buckling load. The method is applicable to the analysis of various structures such as isolated plates, stiffened panels, rolled sections and stiffened box-girder bridges. To check the accuracy of the method a comparison with some published theoretical and experimental results is undertaken.

Secondly, a parametric study for stiffened panels, columns, and beams is presented. For the stiffened panels, the effect of seven parameters (slenderness ratio, residual stress, dimensions and shape of the stiffener, mode of buckling, the longitudinal boundary conditions, and the yield stress) has been investigated. Approximate design curves for the optimum dimensions of panels stiffened by flat stiffeners are given. The capability of the method for the analysis of a stiffened box-girder in bending is also shown. The effect of seven parameters (dimensions and shape of the cross-section, the slenderness ratio, the material yield stress, the residual stress, the initial overall imperfection and the eccentricity of the applied load) on the inelastic buckling of columns and beams has been studied. All the results are given in non-dimensional graphs or tables.

Finally large deflection plate theory is applied to study the post-buckling behaviour of both perfect plates and those with initial imperfections. The work in this section is restricted to the elastic state. The longitudinal axial compression is assumed to act on the plate through two rigid bars at the ends, and various in-plane boundary conditions for the longitudinal unloaded edges have been considered. The Newton-Raphson method is used for the solution of the non-linear equations.

ACKNOWLEDGEMENTS

This research was carried out in the Department of Civil and Structural Engineering at the University of Sheffield. The author gratefully acknowledges the concern and interest of Professors D. Bond and T. H. Hanna. Financial support was provided by the University of Mansoura, Egypt, to whom the author is indebted.

Special thanks are given to Drs. R. J. Plank and D. A. Nethercot, supervisors of this work, for their helpfulness and criticism, and for the many hours they spent in useful discussions with the author.

The assistance of the Computing Services staff in allowing the author to run his many jobs is greatly acknowledged.

Finally, the author wishes to thank his mother for her unfailing and unconditional support throughout the course of this research.

LIST OF FIGURES

LIST OF FIGURES (continued)

LIST OF FIGURES (continued)

LIST OF FIGURES (continued

LIST OF FIGURES (continued)

LIST OF FIGURES (continued)

LIST OF FIGURES (continued)

LIST OF TABLES

LIST OF TABLES (continued)

NOTATION

The following is a list of symbols which occur most commonly in the various chapters of the thesis - other symbols are defined in individual chapters. All symbols are defined in the text when they first appear.

a	Length of a plate
b, b_f, b_w	Widths of rectangular strip, flange and web
b_e	Effective width of a plate
e	Average longitudinal strain or eccentricity of the applied load
h_s	Stiffener depth
k_x, k_y, k_{xy}	Curvatures
ℓ	Length of a structural member
m, n	Numbers of harmonics chosen for a particular solution
r	Radius of gyration
t, t_s, t_w	Thickness of plate, stiffener and web
u, v, w	Longitudinal, transverse and out-of-plane displacements
w^o	Initial out-of-plane deflection
x, y, z	Axes of co-ordinates
A_s	Cross-sectional area of a stiffener
B	Width of a plate
D	Flexural rigidity of a plate
E, E_{sec}, E_t	Young's, secant and tangent moduluses

NOTATION (continued)

$[F]$	Elastic or elasto-plastic matrix
K	Buckling coefficient
$[K]$	Stiffness matrix
$[KO]$	Stiffness matrix due to initial imperfections
$[KT]$	Incremental stiffness matrix
M_s	Number of strips in which a plate is discretized
N_x, N_y, N_{xy}	Components of internal stresses
$\{P\}$	Load vector
$[S]$	Stability matrix
W	Strain energy of a plate
α_n	Amplitude of initial imperfection
β	Slenderness ratio of a plate

$$\beta = \frac{B}{t}\sqrt{\frac{\sigma_Y}{E}\,\frac{(1-\nu^2)}{\pi^2}\,\frac{12}{K}}$$

δ	Ratio of stiffener area to plate area
$\{\delta\}$	Amplitude of nodal lines displacements
ε_x, ε_y, γ_{xy}	Strain components at a point
ε_b	Bending strain
η	Dimensionless co-ordinate defined by $\eta = y/b$
λ	Half wavelength of buckling
$\bar{\lambda}$	Slenderness ratio of a structural member

$$\bar{\lambda} = \frac{\pi^2 E}{(\frac{\ell}{r})^2}$$

NOTATION (continued)

ν	Poisson's ratio
ν_e, ν_p	Elastic and plastic Poisson's ratio
μ	Applied stress to yield stress ratio σ/σ_Y
ζ	Dimensionless co-ordinate defined by $\zeta = x/a$
θ	Rotation of the nodal line
σ_{av}	Average longitudinal stress
σ_{cr}	Critical stress
σ_r	Residual compressive stress
σ_x, σ_y, σ_{xy}	Components of the stress
σ_Y	Yield stress

CHAPTER 1

INTRODUCTION

The failure of four box-girder bridges - at the beginning of the present decade - has focused attention on many apsects of steel bridges and lead to extensive research in steel structures. In order to understand the behaviour of a complete structure, the behaviour of each of its components should be capable of being predicted up to and beyond collapse. A study of the interaction of all such components should then lead to a complete understanding of the behaviour of the system. In the case of a box-girder bridge, a typical component might be the stiffened compression flange which has itself been fabricated by welding together a number of flat plates. When subjected to compressive loading such components tend to fail by instability.

The buckling of a structure is associated with a reduction in its stiffness and a rapid increase in out-of-plane deformation. The determination of the initial buckling load is of great importance, especially when the distortion of the cross-section is not allowed, i.e. no account can be taken of the post-buckling strength. The analysis of this buckling is more difficult in the presence of residual welding stresses. These stresses are of such a magnitude that localised yielding occurs under relatively light loads, and hence part of the section behaves plastically under subsequent loading. In addition the pattern of residual

stresses is frequently highly nonuniform, leading to a net distribution of stresses which varies over the cross-section even for a uniform applied loading.

Rigorous analysis of the buckling behaviour of such structures is, of course, possible using standard finite element techniques, but because of the very large number of degrees of freedom associated with, for instance, a box-girder modelled in this way, such an analysis becomes very lengthy and expensive in terms of computational effort. The finite strip method on the other hand is very efficient for this class of structure and is now well established as an economical way of analysing the elastic buckling behaviour. In the present work the finite strip method is modified to include the effects of plasticity over parts of the cross-section.

Analysis of the behaviour of component plates after local buckling taking into account the material nonlinearity, geometric initial imperfection and the residual stress is very complicated. Nonetheless, such an analysis is of great importance to the steelwork designer because it can provide information about the collapse load and the determination of this ultimate load for other than simple structural components has in recent years become possible as a result of the increasing power of the digital computer.

The initial buckling of structures with relatively thick stiffened plates (e.g. component plates of suspension bridge towers) or structures controlled by serviceability

limit state (supersonic aircraft construction) is often more important than the post-buckling behaviour. In the first type of structure residual stresses influence the ultimate strength rather more than initial imperfections or post-buckling behaviour. In the second, to maintain the aerodynamic shape of the aircraft, large deflections and the post-buckling deformations must be prevented. In either case such structures may buckle in the elastic or in inelastic range and clearly the initial buckling load is of great interest.

The purpose of the present project is to investigate the initial buckling of these structures and in particular to study the inelastic buckling of various plate assemblies. An analytical technique based on the finite strip approach has been developed to include the effects of plasticity over parts of the cross-section. The project involves the preparation of a computer program which is sufficiently flexible in scope to enable the analysis of a wide variety of plate assemblies.

For more slender plates, the effect of initial geometrical imperfection and post-buckling strength are the major factors influencing ultimate load. The analytical techniques developed for initial buckling have therefore been extended to include large deflection behaviour. This is,however, restricted to the elastic stage.

The work can be divided into three main parts. In the first part (Chapters 3 and 4) the theory is developed and results obtained using this are compared with previously published results from various sources. Parametric studies for a range of panels are presented in the second part (Chapters 5 and 6) and in the third part (Chapters 7 and 8) large deflection theory is discussed.

Finally, the major findings from this work are discussed, and some suggestions for future work in this area are given.

CHAPTER 2

BUCKLING AND COMPRESSIVE STRENGTH - LITERATURE SURVEY

More than two centuries ago, Euler first studied the problem of plate analysis. About sixty years later, Saint Venant (1,2) developed the plate deflection equation for in-plane load and it was a further sixty years before the equation was solved by Bryan (1,2) to obtain the elastic buckling load. The early developments of the plate problem have been well documented (1,2) and are summarised in Tables 2.1(a), (b) and (c). Table 2.1(a) deals with the historical development of the partial differential equation for small deflections, whilst Table 2.1(c) relates to the large deflection equation. Table 2.1(b) summarises the major developments in studying the initial buckling load for plates, based upon small deflection theory.

The buckling behaviour of thin rectangular plates under uniaxial in-plane compression has attracted considerable attention during the ninety years since Bryan first analysed the stability of a simply supported plate in 1891. About the turn of the century, timber had largely been replaced by structural steel in ship construction. This change in structural material was extremely fruitful in furthering the development of plate theory. It was in Russia that the first contributions to naval architecture using the theory of solid mechanics took place. However,

Name (1,2)	Year	Work
Euler	1766	Formulated the first mathematical approach to the membrane theory of plates. Using the analogy of two systems of stretched strings perpendicular to each other he studied the problem of free vibration of rectangular and circular elastic membranes.
J. Bernouli	1789	Extended Euler's analogy to plates by introducing the grid-work analogy and developed the partial differential equation governing small deflections. He did not consider the torsional resistance of the plate.
Lagrange Navier	1811 1820	Derived the correct partial differential equation for the small deflections of an isotropic plate under surface load.
Saint Venant	1833	Extended the work of Navier and Lagrange to include in-plane forces applied at the edges.

Table 2.1(a). Analysis of Plates-Early Developments

Name (1,2)	Year	Work
Bryan	1891	Presented the buckling analysis for a rectangular plate simply supported on all its edges subjected on two opposite sides to a uniformly distributed compressive load in the plane of the plate. He was the first to apply the energy criterion of stability to the solution of the plate buckling problem.
Timoshenko	1907	In a series of papers he used Bryan's approach to determine the critical stress of plates with different boundary conditions.
Reissner	1909	Independent of Timoshenko, he presented the solution for an edge compressed rectangular plate with two clamped edges and for plates having one edge clamped and the other free.
Bleich	1924	Made an attempt to extend the theory of flat plate stability into the inelastic range by considering the plate as nonisotropic and by tentatively introducing a variable modulus of elasticity into the basic differential equation upon which the solution for elastic buckling is based.
Kollbrunner	1935 and 1946	Reported the results of his tests on large scale plates under edge compression. He investigated the buckling behaviour of the plates in both the elastic and the inelastic range.

Table 2.1(b). Initial Buckling of Plates - Early

Name (1,2)	Year	Work
Kirchhoff	1877	Developed the theory of large deflections of plates.
Föppl	1907	Introduced the use of the stress function to simplify the form of the equation.
Von Karman	1910	Was the first to derive the partial differential equation of large deflections in its current form.
Marguerre	1938	Extended the Von Karman equations to include initial deflections.

Table 2.1(c). Large Deflection of Plates- Early Developments

the Western world was slow to recognize this Russian research because of the language barriers and it was Timoshenko who directed the attention of the Western scientists towards the new Russian work in the theory of elasticity. These early developments have all been well documented (1-3) and are included here for completeness.

The increased activity in aircraft design between the two world wars provided a strong impetus towards more rigorous analytical investigations of plate problems. Buckling of plates under combined loading, inelastic buckling, post-buckling behaviour and buckling of stiffened panels, were investigated by many researchers during this period. Again this work has been well documented, and in particular Bleich (1) and Timoshenko (3) have reviewed the development of the stability of columns, beams, plates and stiffened panels up to the middle of this century.

In 1950 the arrival of the high speed electronic computer exerted a considerable influence on the analysis of plates. As a result of this new tool special numerical techniques, e.g. finite difference, finite element and finite strip methods, have been developed to solve the complex plate problems in an economical way.

Bulson (4) gives a comprehensive review of available solutions and references (up to 1970) relating to the critical buckling of flat plates subjected to a wide variety of in-plane loading conditions.

Because of the availability of several general reviews of the subject the remainder of this chapter will consider only those contributions which relate directly to the present study. These fall into three areas: the isolated plate, the stiffened panel and the structural sections (e.g. I-beams). For isolated plates and stiffened panels developments in inelastic buckling, large deflection and ultimate strength analysis will be considered, while only those studies on the interactive buckling (combined local and overall buckling) will be reviewed for structural members.

2.1 Buckling and Compressive Strength of Isolated Rectangular Plates

The isolated rectangular plate is the basic element in many structures. The buckling of plates in the inelastic range has been studied by many investigators starting over 40 years ago. Two theories of plasticity, deformation theory and incremental theory (5) have been used.

In 1947 Bijlaard (6) used the energy theory to study plastic buckling. He was the first to apply deformation stress-strain relations to the stability problem. Ilyushin (7) attempted to formulate a rational theory for the inelastic buckling of plates, but Bijlaard comparing his theory with the test results by Kallbrunner, showed that his theory was more accurate. Modifying and

improving Ilyushin's general relations Stowell (8) succeeded in developing a theory of inelastic buckling which apparently leads to theoretical results in good agreement with the observations made in the laboratory.

The more general theory of plasticity - incremental theory - was used by Haaijer (9) to investigate the buckling of steel plates including the effect of strain hardening.

When studying the collapse of plates however, it is not only material nonlinearity which is important. While the critical buckling load for a column is an upper bound to the collapse load, plates can sustain loads greater than this critical load (Figure 2.1). The behaviour of perfect and imperfect elastic plates after buckling has been studied by many researchers (10-15). The mathematical treatment of the interaction between the initial imperfections and the in-plane loading leads to a set of non-linear algebraic equations, commonly referred to as large deflection equations (von Karman's equation) for which no general solution is known.

Coan (10) used Levy's approach to solve this equation for two specific forms of boundary condition. Yamaki (11) extended this work to investigate a rectangular plate under eight different boundary conditions. Four terms for the double Fouries series representing the deflected shape were considered and so his solution is generally regarded as accurate up to quite high loads. The same problem has

been examined by Walker (12), again solving von Karman's equations, this time using Galerkin's method with a technique based on perturbation about the bifurcation load. Many researchers (12-14) have presented explicit expressions for the strength of a square plate, assuming that collapse corresponds to the condition when the maximum in-plane stress (at the unloaded edge) equals the material yield stress.

All these solutions have been restricted to isotropic plates of constant thickness and a limited range of boundary conditions. The ever-increasing computational capacity of computers has facilitated the derivation of specific solutions using numerical techniques and these are finding increasing practical application. Plates with variable thickness, orthotropic plates and a variety of boundary conditions can be included by these numerical methods.

One of these techniques is based on representing the governing differential equations in terms of finite differences which are solved iteratively using a computer program. There is sometimes a tendency for the direct iterative method to converge on the wrong deformed shape (16) and to avoid this, two dynamic terms one involving acceleration and the other viscous damping are added to the static equations. If the damping coefficients are arranged to give critical damping, the oscillations die

out quickly and a solution to the static form of the finite-difference equations is obtained. Rushton (17) has shown that dynamic relaxation can be a reliable solution procedure for elastic nonlinear plate problems. The same method has been used by Frieze et al (18) to examine the interactive buckling of box sections.

The finite element method has been applied to obtain elastic and inelastic solutions for similar problems (19-22). It is a general method and has no restriction on the mode of buckling but is approximate in that it is based upon an assumed displacement function.

Real plates exhibit certain characteristics, some of which have been ignored in the above development. To be valuable to the designer, the ultimate strength of the plate, rather than the elastic post-buckling behaviour must be considered. The investigations of the maximum strength must include:

1. The large deflection behaviour.
2. The spread of yielding through the volume of the plate.
3. The possibility of unloading from the yield surface.
4. The effect of the initial imperfection.
5. The effect of the residual stress.

Since 1960 a comprehensive study of the ultimate strength of plates has been conducted at Cambridge

University (23-30) and more recently at Imperial College (35, 36) and other research centres in the UK (21).

The experimental investigations of the maximum strength of plates have been carried out using individual plate specimens (23, 24) or square box columns (25-30). For the unloaded edges of the individual plates two boundary conditions - simply supported and clamped - have been considered. As an alternative to the conventional V-notches system, Ractliffe et al (23) developed cantilever racks (Figure 2.2) to supply the required boundary conditions. The thickness of the plates used by Ractliffe et al were 6.3 mm. Some specimens were tested as delivered while others contained severe residual stresses due to welding. Similar experiments were carried out by Moxham et al (24) using Ractliffe cantilever racks. One hundred and forty plates were tested with b/t between 36 and 80. The thickness of all specimens was 3 mm and the aspect ratio was 4.0. The conclusions of these two investigations (23, 24) were that:

1. The maxima on the average stress-average strain curves were more rounded for the plates with longitudinal imperfection.
2. The welded plates had an earlier departure from linearity and a lower maximum strength, but were more ductile.

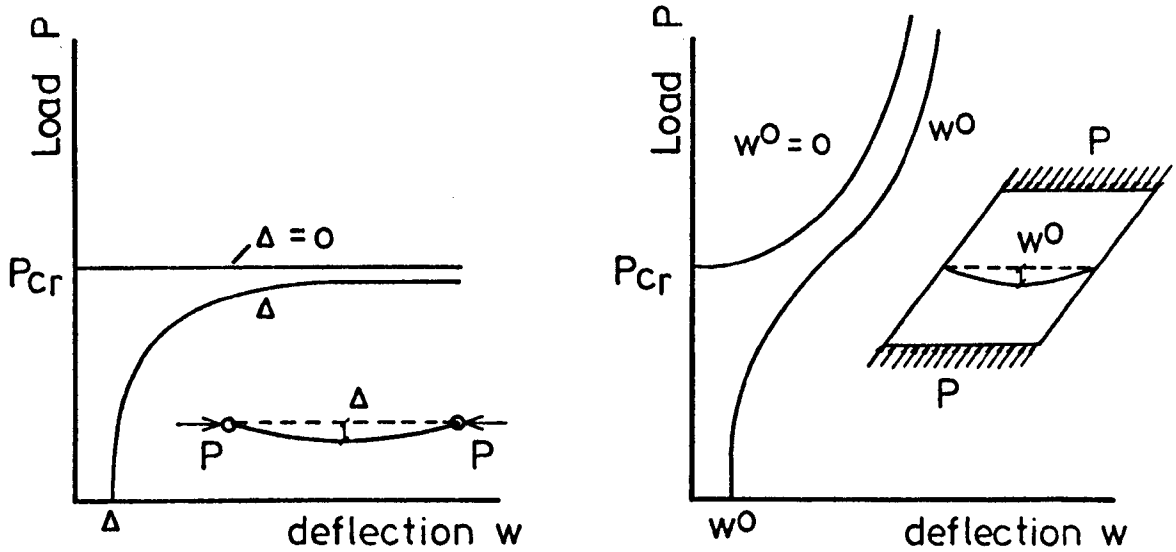

FIG. 2·1. DIFFERENCE IN BEHAVIOUR OF COLUMN AND PLATE.

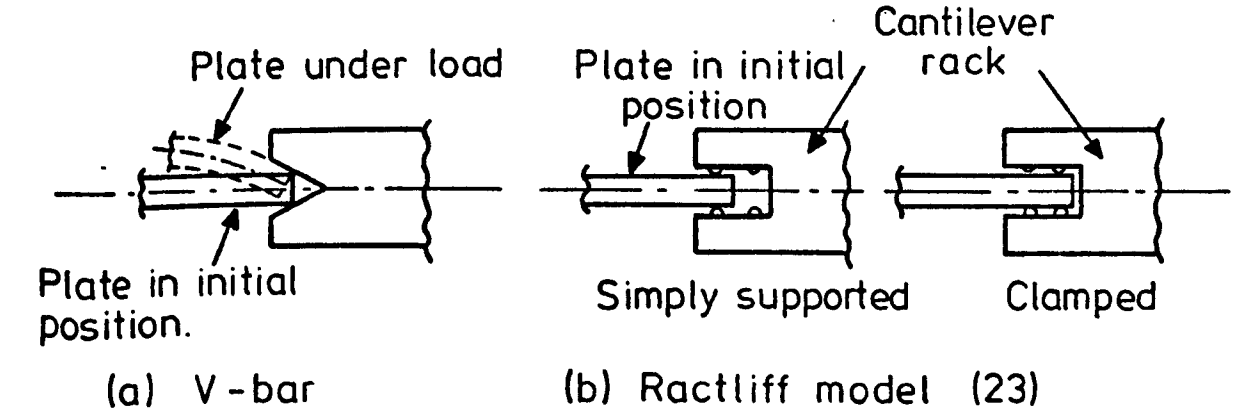

FIG. 2·2. THE SUPPORT OF THE UNLOADED EDGE OF TESTED PLATE.

3. Little difference in behaviour was observed between the simply supported and clamped specimens, except at high b/t.

In his theoretical analysis, Moxham used the energy method (Rayleigh-Ritz type) to determine the compressive strength of the plate. The plate was assumed to be simply supported with the unloaded edge free to pull-in. Moxham considered the overall equilibrium of one quadrant of the plate dividing this into 9 x 9 x 5 volumes. The strain energy density was calculated at the centre of each volume and then summed over the whole quadrant. By repeating the process for increments of applied compressive load, a complete loading curve was obtained. Moxham and Ractliffe have considered both residual stresses and initial imperfections in their analysis.

To overcome the difficulty of accurately representing the boundary conditions of the unloaded edges, box columns have been tested to find the compressive strength of plates with simply supported edges. In 1973 Little (25) has reported the results of more than 60 tests on box columns conducted by several investigators (26-30) at Cambridge. A method of analysis for the plate strength based on a Perry equation was presented and the theoretical results were shown to be in good agreement with the test results. Three design curves were provided depending on the magnitude of residual stress.

In a more recent paper Little (31) presented an accurate analysis for the collapse behaviour of a simply supported rectangular plate loaded by uniaxial or biaxial in-plane compression. Again the analysis was based on the Rayleigh-Ritz method. He used the plastic flow theory and took into account, as before, the effect of initial imperfections and residual stress. For numerical integration, Little divided one quadrant of the plate into grid points. Six systems of grids were examined. The smallest system had 80 points (4 x 4 x 5) and the largest one 252 points (6 x 6 x 7).

Later Little reported the results of applying this approach to the analysis of 960 different simply supported rectangular plates under longitudinal compression (32). By controlling the transverse displacement function, the longitudinal in-plane boundary conditions and the aspect ratio the actual plate panels of a box-girder bridge have been modelled. The minimum total number of variables which have been used to represent the displacements was 9. It was observed that the critical aspect ratio for the simply supported plate in the inelastic stage was not unity and this is in contrast with classical elastic buckling analysis. In most cases, the minimum plate strength was shown to occur at $a/b = 0.6$ while Moxham (24) suggested a critical ratio $a/b = 0.875$. Little suggested that this was due to the very small initial imperfection and the limited boundary

conditions used by Moxham (the unloaded edges were free to pull-in). Little in fact observed that the maximum effect of the longitudinal boundary conditions on the plate strength was less than 7% (32) and these new results gave support to his empirical design curves (25).

At other research centres, different numerical methods - finite element, finite difference and dynamic relaxation - have been developed to examine the elasto-plastic behaviour of unstiffened and stiffened plate panels up to ultimate load. At TRRL Crisfield (21) has used the finite element method to study large deflection elastic-plastic plate behaviour. Two approaches have been considered - the volume approach and the area approach. The first depends on the incremental theory of plasticity and integration is carried out over the volume of the plate. The area approach depends on the deformation theory of plasticity and sudden plastification of the plate section is assumed. The area approach is more economical but less accurate than the volume approach. In later work (33) Crisfield has modified the area approach to allow for spread of yield through the fibres before full section yield, but the accuracy is still less than for a full volume approach.

It has been observed by many researchers that the incremental theory of plasticity usually gives results further from experimental results than does the deformation

theory of plasticity. Neal (34) has referred this to the high sensitivity of the flow theory to initial imperfection. Moreover, the slenderness ratio and the material constants affect the difference between deformation theory and flow theory results.

At Imperial College, Frieze et al (35) and Harding et al (36) have used the dynamic relaxation method for the analysis of isolated plates in the elasto-plastic range, using the flow theory of plasticity. The main differences between these two investigations are:

Frieze et al (35)	Harding et al (36)
1. The plate is loaded by uniaxial or biaxial compressive stress.	The plate is loaded by complex load (shear, compression and in-plane bending).
2. Ilyashin single-layer has been used, with a sudden plastification at any section occurring over the full depth.	The plate thickness has been divided into layers and the yield of each layer has been determined from the von Mises criterion.
3. Uniaxial residual stress.	Biaxial residual stress.

Frieze et al found that the influence of aspect ratio was dependent upon both the magnitude of the initial deformation and the slenderness ratio. They considered only one

value of slenderness ratio and two values of the initial imperfection to calculate the preferred aspect ratio. They observed that increasing the initial imperfection, increasing the residual stress or allowing the unloaded edge to move freely, reduced the ultimate strength of the plate. Design curves were presented for unstiffened compression plates and data useful for the design of stiffened panels using a strut approach were also given.

Harding (36) was the first to investigate the ultimate strength of plates under complex loading conditions. He also used dynamic relaxation, and to save computer time he used an 8 x 8 mash for square plates, although this mash was known to lead to an error of up to 5% in some cases. As most of the computer time has been used in the main dynamic relaxation loops, Harding's method (the calculation of elasto-plastic rigidities by the multi-layer approach rather than by the Ilyushin single layer approach) does not have a significant computer time penalty. From this investigation, it has been found that:

1. The very slender panels ($b/t \geq 180$) cannot sustain any significant level of compressive loading with the assumed residual stress and initial imperfection present.
2. The panels loaded under combined shear - up to 0.4 times the shear yield stress - and compression were not affected by shear if the edges were unrestrained.

3. The strength of restrained panels under shear loading only was almost independent of slenderness ratio and initial imperfection.

Interaction curves were presented by Harding for square panels to show the relationship between the peak shear stress and the corresponding direct stress.

2.2 Stiffened Panels

An economical means of increasing the critical stress of a plate is to provide reinforcement in the form of longitudinal and/or transverse stiffeners. Two types of stiffener, open section and closed section (as shown in Figure 2.3) may be used. Ships, suspension bridge towers, box girder bridges, dock gates, etc. are essentially a collection of stiffened plates under various loading conditions.

The elastic analysis of stiffened plates has been based, in the past, on certain idealizations or restrictions. As an approximation it was normally assumed that the stiffener did not resist twisting during buckling of the plate (1). Timoshenko (3) was the first to determine the critical load of rectangular stiffened plates under various loading conditions. Wah (37) included the effect of torsional rigidity in his analysis of the same problem, showing it to be significant, particularly for closed section stiffeners.

To obtain the overall buckling load of panels stiffened by a large number of identical equally spaced stiffeners, the panel may be treated as an orthotropic plate and a number of authors have used this approach to study this particular problem (38-42).

Stiffened plates may be able to support ultimate loads considerably above the load for local buckling of the component plates. Three main approaches have been adopted by researchers for the inelastic analysis of stiffened plates in compression. These are:

1. The strut approach (25, 43-47).
2. The orthotropic plate approach (48, 49).
3. The discretely stiffened plate approach (50-53).

2.2.1 The Strut Approach

In this approach it is assumed that the panel is wide enough that orthotropic plate action can be neglected and hence the stiffened panel is treated as a pin-ended column. Every stiffener together with its associated width of plate is considered as a strut and no consideration is given to the effect of any possible restraint arising at the longitudinal edges of the "strut" due to transverse continuity with neighbouring "struts" (Figure 2.4). The effect of the initial imperfection, the residual stress and the loss of effectiveness due to buckling of the plating must be considered in the analysis. This may be achieved by using either:

1. Theoretical average stress-strain curve (approach I).
2. Experimental results (approach II).
3. Effective width approach (approach III).

Three modes of failure have been assumed,

1. Failure of the plating in compression due to squashing or buckling (mode I).
2. Failure of the stiffener by yielding (mode II).
3. Torsional buckling of the stiffener with subsequent lateral collapse towards the plating due to loss of lateral stiffness (mode III).

Different theoretical analyses can be used to calculate the ultimate strength of the strut. These are

1. The moment-curvature-thrust relationship (method I).
2. Perry formula (method II).
3. Approximate analysis (method III).
4. Finite element analysis (method IV).

A comparison of some studies (25, 43-47), based on the strut approach, is shown in Table 2.2. Little (25) used Moxham's theoretical stress-strain curves, which were calculated for simply supported plates with unloaded edges free to pull-in, and this is not reasonable for a very wide panel. A similar investigation was made by Moolani et al (43) assuming that the edges of the plate were simply

Data Considered	Little (25)	Moolani (43)	Horne (44,45)	Smith (46)	Carlson (47)
1. Mode of buckling	I & II	I & II	I	I & II	I, II & III
2. Plate buckling approach	I	I	III	-	III
3. Theoretical method	I	I	III	III	II & III
4. Number of spans	1	≥ 1	1	≥ 1	≥ 1

Table 2.2. Comparison Between Different Strut Solutions

supported or fixed against the out-of-plane deflections. The unloaded edges were constrained in-plane to remain straight but were free to pull-in. Single panel and multi-panel stiffened compression flanges were considered. They observed that the effects of continuity on the multispan panels did not necessarily lead to increased strength as compared with similar single panels.

Horne et al (44, 45) proposed an approximate method dependent on the effective width associated with the theoretical deflected form. Expressions for the effective width of perfect and imperfect plates have been obtained by assuming that the buckling shape in the post-buckled stage was sinusoidal. The analysis was restricted to the case where all edges of the simply supported plates are held straight both in-plane and out-of-plane, but free from restraining or applied moment. They also assumed that the stress at any stiffener section remains in the elastic range.

An alternative approximate investigation was conducted by Smith et al (46). They approached the problem by studying the inelastic buckling behaviour of a plane frame of general geometry. For stiffened panels, every stiffener with the attached strip of plating was treated as a beam-column, i.e. as a special case of a plane frame. The local buckling of the plating was neglected in the range studied ($b/t \leq 40$). They accounted for the change in the position

of the elastic neutral axes, caused by progressive yielding or local buckling of the cross-section, along the beam. The analysis was based on a small deflection approach. After every increment of load every fibre was checked to see whether it had yielded or not; the stiffness of the yielded fibres being then neglected.

More general loading conditions were considered by Carlsen (47). Emphasis was placed on the uniaxial compression case, while the effect of transverse compression, shear and lateral hydrostatic load were also considered to some extent. Carlsen used two simplified methods for collapse analysis, the ideal elastic-plastic strut analysis and the initial yield method (Perry-Roberston formula). In the first method the collapse load was given by the intersection point of the load-deflection curves calculated for an ideal elastic column and an ideal plastic column (Figure 2.5). The initial yield method defined collapse as the state of initial yielding of the outer fibres due to compression and bending. The residual stress in the stiffener was neglected; and this led to discrepancies between theoretical and experimental results.

2.2.2 Orthotropic Plate Action

In the case of a plate stiffened by a large number of equal and equidistant stiffeners either in one direction parallel to one of the sides or in both directions, the plate can be treated as an orthotropic plate. The local

(a) Open stiffeners.

(b) Closed stiffeners.

FIG. 2·3. STIFFENER SECTIONS.

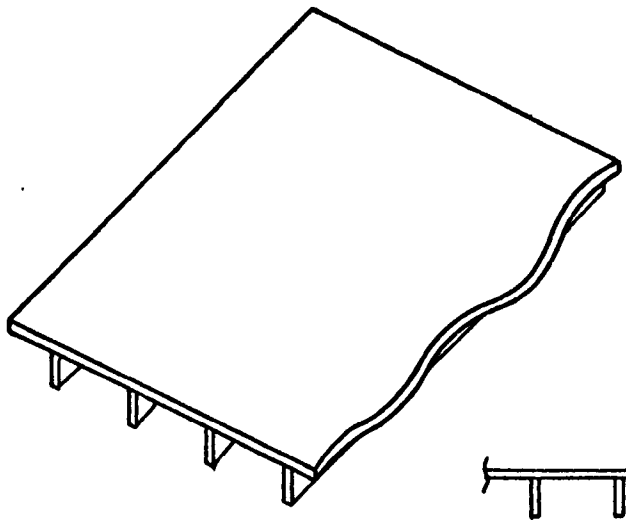

FIG. 2·4. IDEALIZED OF THE STIFFENED PANEL BY STRUTS.

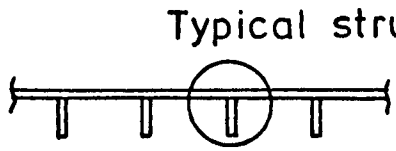

(a) Isometric view. (b) Cross section.

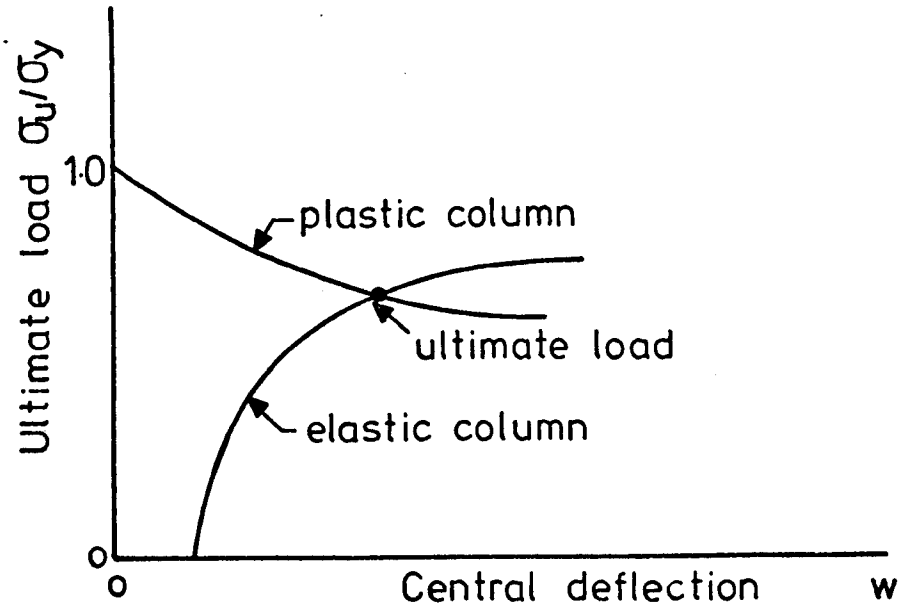

FIG. 2·5. ULTIMATE LOAD FOR A STRUT (Ref. 40)

buckling of the plate between stiffeners may be allowed for by using the effective width approach this implies that the local buckling of the stiffener is assumed to be prevented. Assuming that the failure of the orthotropic plate corresponds to yielding of the unloaded edge, the ultimate strength of the stiffened panel can be obtained (48, 49). Although this is an approximate approach, it can give a general picture of the behaviour of stiffened panels in the post-buckling range.

2.2.3 Discretely Stiffened Plate Approach

To overcome the approximations inherent in the two previous approaches, especially the orthotropic plate approach, discrete stiffened panel methods have been devised. In this approach the effect of the longitudinal boundary conditions of the panel can be considered. The finite difference method and the finite element method (50, 51) have been used in the theoretical analysis. One method, using a combination of finite element (local) and Rayleigh-Ritz (global) has been developed by Tvergaad and Crisfield (52, 53) to reduce the number of degrees of freedom. In this approach the Rayleigh-Ritz method was used for the out-of-plane displacements and the finite element method for the in-plane displacements. This approach was adopted because it is much more difficult to guess good in-plane trial functions than to guess good out-of-plane trial functions.

The triangular plate element and the beam element have been the main elements used to model the plate and the stiffener respectively (50, 51). The flow theory of plasticity with von Mises yield criterion has been used in the analysis. Soreide et al (50) used two approaches - the fixed co-ordinate system and the updated co-ordinate system in their finite element analysis. A similar investigation was made by Fujita et al (51). In order to check their theoretical results they carried out collapse tests on three girder specimens. The effect of the distribution of the stiffeners on the collapse load and mode was included in their study.

Tvergaad et al (52) used both theories of plasticity - deformation theory and flow theory - to study the inelastic buckling of stiffened panels. Two modes - local buckling mode and wide column buckling mode were considered. In the wide column buckling mode, it was found that the results from the two theories were indistinguishable from one another. In the post-buckling phase, an incremental method based on finite element/Rayleigh-Ritz was used. A similar investigation was made by Crisfield (53), who used the von Mises yield criterion in conjunction with an integration through the depth of the plate. He also allowed for elastic unloading from the yield surface and modified the area approach (21) to allow for yield in the fibres before full section yield. A reduction in computer time of

about 50% was achieved by using global variables only but the accuracy was observed to decrease by up to 13%.

In all the above approaches the torsional instability of the stiffener was neglected.

2.2.4 Stiffened Panels - Experimental Work

Panels stiffened by flats, bulb flats, angles, tees or closed stiffeners have been tested by many investigators in different countries (47, 51, 54-58). The effect of cross sectional shape, residual stresses, initial imperfections and the eccentricity of the applied load, have been studied. Three modes of buckling have been observed in the laboratory. These are

1. The local torsional buckling of the stiffener (mode I).
2. The buckling of the stiffened plate towards the free edges of the stiffeners (mode II).
3. The buckling of the stiffened panel away from the stiffeners (mode III).

Murray (54) and Faulkner (55) tested panels stiffened by bulb flats and tee stiffeners respectively. Murray's panels were loaded axially or in bending and only two modes of buckling, mode I and mode II, were observed. About 65 specimens were tested by Faulkner (55) under axial load.

Over a four year period Horne et al (56-58) tested 86 panels with different slenderness ratios stiffened with flats, bulb flats and angle stiffeners loaded in longitudinal compression. For all the specimens the unloaded edges were free whilst the loaded edges were fixed for the short test specimens and hinged for the longer specimens. They used intermittent and continuous plate/stiffener welds to study the effect of the residual stresses and found that the Merrison Rules (59) underestimate the residual stresses by a factor of order 2. The change in the value of the residual stress due to the different methods of welding was found not to be a significant factor for panels with low slenderness ratios. This was put down to separation occurring between plate and stiffeners as the failure load is approached for the intermittent case. For the panels with torsionally weak flat stiffeners, intermittent welding reduced the strength of the panel as compared with the continuously welded case. The influence of the local plate imperfection, torsional imperfections in the stiffeners and overall imperfection of the stiffened panel were also studied. It was shown that very large plate panel imperfections had, on the average, no deterimental effect on continuously welded panels and a slight deterimental effect on intermittently welded panels. The overall imperfection reduced the strength of the most slender panels but had almost no effect on the strength of the other panels.

In order to account for the effect of the boundary conditions of the unloaded edges, Fukumoto et al (60) tested 27 stiffened panelssimply supported along the four edges. The panels were stiffened by three to five flat stiffeners of the same grade of steel as the plate panels. In order to simulate the welding conditions in actual box section members, welding bead was provided along each unloaded edge. By measuring the residual stresses it was found that the compressive residual stresses increased as the width-to-thickness ratio of the plate became smaller. For panels with b/t = 22, the compressive residual stress was 0.70 σ_y. It was observed that the stresses in the stiffeners had little correlation with the width-to-thickness ratio of the panels or the stiffeners. All three modes of buckling were observed.

Stiffeners of closed section, e.g. trapezoidal, triangular, rectangular and semi-circular, have structural and economic advantages. Due to their high torsional stiffness, they elastically restrain the plate sub-panels and hence enhance the corresponding ultimate stress. Moreover, the geometrical configuration alone allows a greater spacing between the stiffeners due to their own width. Also the connection with the plate requires only two fillet welds which is no more than required for a single open-section stiffener. Girders stiffened by triangular section stiffeners have been tested (61) and showed the improved behaviour of this kind of stiffeners as compared to open sections.

2.3 Interaction Buckling in Beams and Columns

Structural sections, e.g. I beams, may buckle in one of three buckling modes - local, overall or combined local and overall (Figure 2.6). The critical mode depends on the geometry and properties of the cross section, the slenderness ratio, the initial imperfections, and the residual stresses. In analysing local buckling it is typically assumed that the lines of junction between the plate assemblies remain straight. This mode is critical when the component plates are wide in comparison with their thickness. Overall buckling may be flexural, torsional or flexural-torsional. It is usually assumed that the cross-section of a structural member buckling in an overall mode remains undistorted - that is, each cross-section of a member deforms as if it were a rigid body with only three degrees of freedom in the plane of the cross-section. If the cross-section is made unduly compact, the flexural properties are poor and the tendency for this mode of buckling increases. To achieve an economic (optimum) design a section should be designed such that failure in local and overall buckling modes ocurr at the same load. In such cases the actual failure mode involves distortion of both a local and overall nature. This type of buckling is called distortional buckling (or interaction buckling) because the cross-section of the member is free to distort and displace. This interaction buckling is critical for intermediate length structural members (Figure 2.7) with relatively large width-to-thickness ratios of the component plates of the cross section.

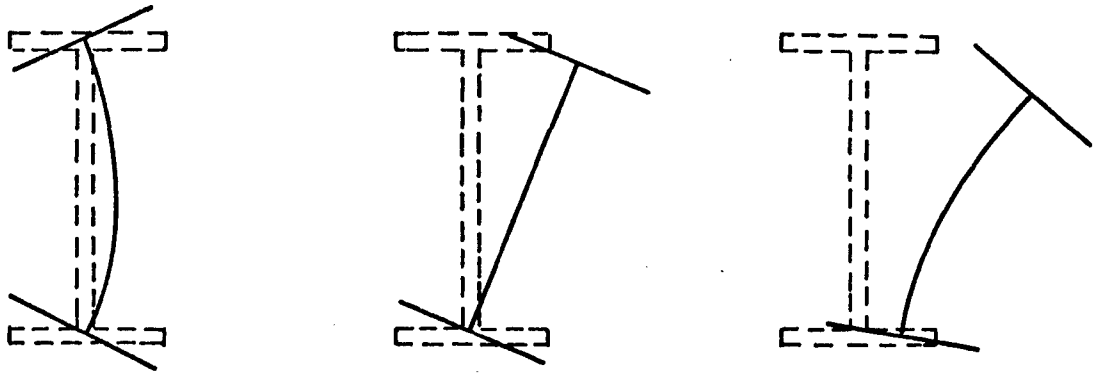

FIG. 2·6 THE BUCKLING MODE OF A STRUCTURAL MEMBER.

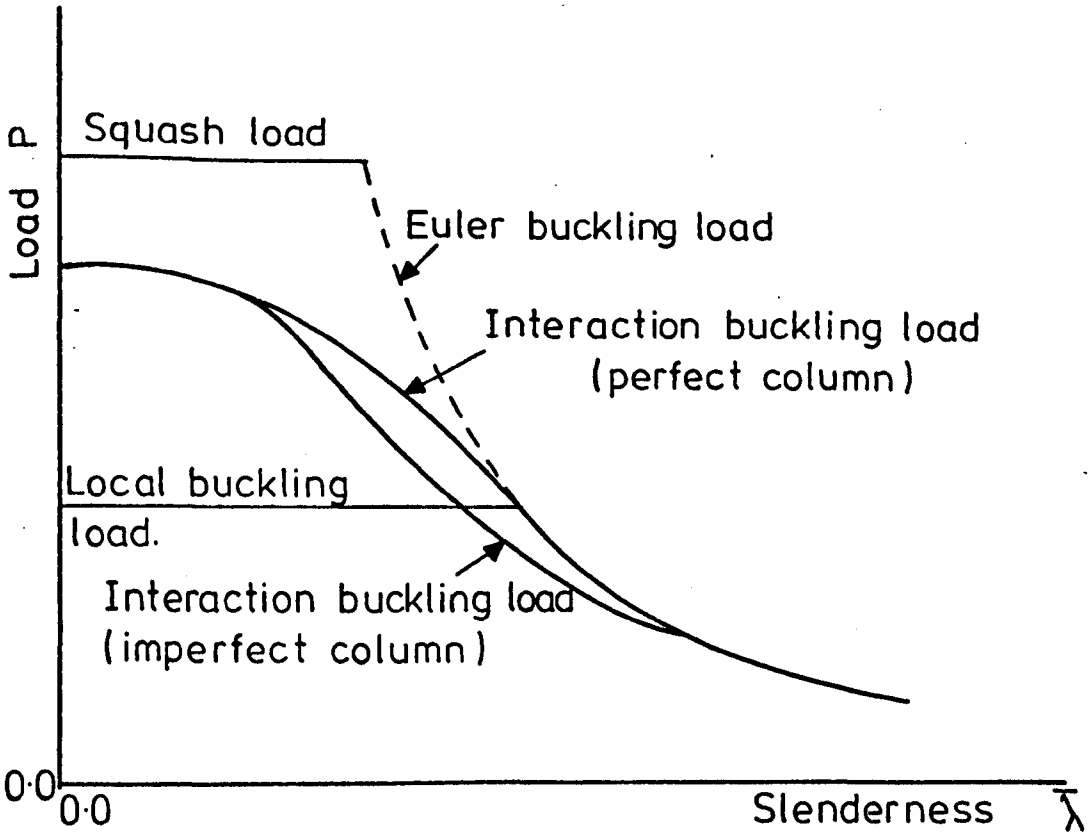

FIG. 2·7. LOAD SLENDERNESS CURVE FOR INTERACTION BUCKLING.

Over the last 30 years the problem of interaction buckling has received a great deal of attention from various researchers. Theoretical and experimental investigations have been carried out on members with different cross sectional shapes.

However, up to the present date there is no general study which has accounted for residual stress, initial imperfection and interaction between local and overall buckling (lateral, torsional and lateral-torsional). Many researchers (62-64, 66-68, 70-77, 79-82) have made assumptions limiting their work to (Table 2.3):

1. Elastic plate behaviour (62-64, 66, 70-77, 79).
2. Plates with small deflection (66, 70-73, 76, 77).
3. Members deflecting without twisting (62, 63, 67, 68, 79-82).

Various theoretical approaches (methods) have been used in the analysis of interaction buckling of a structural member. These are:

1. Rayleigh-Ritz energy method (80-81).
2. Moment-curvature-thrust relation (82).
3. Finite element method (70-75).
4. Finite strip method (76, 77, 79).
5. Approximate method.

Bijlaard and Fisher (62, 63) were first to study H-section columns in the post-local buckling range. They tested columns which had minimal geometric imperfections.

Reference	Inelastic behaviour	Imperfection (local and overall)	Large deflection of plate component	Overall torsional buckling	Residual stress
Bijlaard and Fisher (62,63)	x	x	✓	x	x
Cherry (64) and Wang et al (74,75)	x	x	✓	✓	x
*(66,70-73,76,77)	x	x	x	✓	x
De Wolf et al (67) and Kalyanaraman et al (68)	✓	x	✓	x	x
Hancock (79)	x	(local) ✓ / x (overall)	✓	x	x
Graves Smith (80,81)	✓	(local) ✓ / x (overall)	✓	x	x
Little (82)	✓	✓	✓	x	✓

Notes:
1. "*" indication for the following references
   Goldberg et al (66), Rajasekaran et al (70), Johnson and Will (71), Akay, Johnson and Will (72), Bardford et al (73), Plank et al (76), and Hancock (77).
2. "✓" and "x" indication for taking into consideration and neglecting respectively.
3. Column 5 to show that not only lateral buckling but also torsional and lateral-torsional buckling have been considered.

Table 2.3. Limitation on the Previous Interaction Buckling Researches

In 1960 Cherry (64) proposed an approximate method for estimating elastic instability of beams. The method is applicable only for those sections in which the compression flanges alone have buckled, the webs are assumed to be undistorted. To account for the post-buckling effect of the flanges, he used the effective width concept. For the converted section the corresponding beam properties (flexural, torsional and warping rigidities) have been computed and taken as the effective properties of the section. To compare this theoretical approach with experiments., Cherry tested a series of H-section and T-section beams loaded by pure end couples. The theoretical approach overestimated the test results by 30% maximum, in the range of the local buckling. He suggested that this may have been due to neglecting the effect of initial imperfections. Ten years later Skaloud and Zornerova (65) tested a series of columns which had both local and overall imperfections. The columns demonstrated a significant reduction in load carrying capacity compared with straight columns with perfect plate elements.

In 1964 a more sophisticated buckling analysis (although still within the limitations of elastic small deflection theory) for members of arbitrary cross section was presented by Goldberg, Bogdanoff and Glanz (66). By coupling membrane and plate bending equations, eight first order partial differential equations were obtained. The critical load - corresponding to vanishing of the determinant of these equations - was obtained by iteration.

Recently, the results of the tests which have been performed at Cornell University on 34 H-section and rectangular tubular columns have been published by De Wolf, Pokoz and Winter (67). These columns were manufactured by connecting cold formed channels back to back (H-section) or the flanges of two channels together (rectangular section). The columns, which had a minimal initial imperfection, were loaded by concentric load (67). These tests are useful for estimating the effect of local buckling phenomena on the overall buckling of columns. De Wolf et al have developed an analytical iterative approach for the interaction buckling of rectangular box column. The method is based on the tangent modulus and the effective width concept. The same cold formed channel was used by Kalyanaraman, Pekoz and Winter (68) to manufacture and test inverted hat section and H-section columns. Based on these test results they determined the local buckling coefficient and an expression for the effective width of a stiffened plate. They applied the method to develop an empirical model, based on the effective section of the column and either the CRC formula (69) in the region of inelastic column behaviour or the Euler formula in the region of elastic behaviour.

The finite element method has been used by many researchers (70-75) to study the interaction behaviour of structural members. None of them have accounted for the post-buckling of the components plate and all have used the

small deflection theory. Rajasekaran and Murry (70) have restricted their analysis to a beam-column with open section only. The analysis superimposed the displacement due to out-of-plane flexure of the flanges on the displacements which occurred in one dimensional undistorted thin-walled beam element. The web was not allowed to distort. Eleven degrees of freedom were used at each node of the cross-sectional element. In order to account for the distortion of the web as well as the flanges, it is necessary to adopt a more general finite element such as that of Johnson and Will (71). They sub-divided the beam into a large number of rectangular elements. It was necessary to sub-divide a simple beam into 96 elements to achieve an accurate solution. Another model has been used by Akay et al (72) based on idealising the flange and the web by beam and plate elements. By this model only the distortion of the web was considered. It was assumed that straight lines across the flanges and normal to the web remain straight during buckling. They isolated the out-of-plane buckling from the in-plane stress analysis. This separation led to a reduction in the number of equations required for buckling analysis. Again the number of degrees of freedom is relatively large. Recently Bradford et al (73) used one dimensional beam elements with six nodal displacements of the cross-section following Akay et al (72) they assumed that the flanges remained undistorted. It was found that two elements (18 degrees of freedom) gave an error about 0.5% and 2% in the buckling load of a column under concentric compression and beams under pure bending respectively.

To account for the post-buckling effect in the finite element analysis, Wang et al (74, 75) used the effective width approach. Under a general loading condition, the beam section became monosymmetrically nonprismatic. The buckled compression flange was narrowed because of local buckling, but no reduction was necessary at locations with stress less than the critical stress. The effective flexural rigidity and the effective warping coefficient of the section was based on the effective width while the torsional rigidity was obtained from either the original full cross section or the effective cross section. It was found that the two values of the torsional rigidity were close to each other. Since the buckled section properties, applied loads and the laterail buckling loads for buckled section were independent, an iterative analysis procedure has become necessary. Wang et al have used the finite element formulation with small deflection theory to obtain the critical load of the structural member.

More recently, the finite strip method which is reviewed in the next section, has been used to study the interaction between the local and overall buckling of simply supported beams (76, 77) in the linear buckling range. Hancock has extended the finite strip approach to the post-buckling range (78), and proposed a method for calculating the effective flexural rigidity of imperfect box and H-sections. For the box-section the flexural rigidity compared well with

the flexural rigidity based on the effective width concept. Using the proposed flexural rigidity, the interactive buckling of the H-section column was obtained (79). Again an iterative analysis procedure was necessary. The theoretical results were compared with Cornell test results (67, 68) and with results which he calculated from the effective section approach described by Kalyanaraman et al (68).

The most sophisticated work on the problem of interaction buckling to date has been done by Graves Smith (80, 81) and Little (82). Graves Smith has presented a numerical method to predict the ultimate strength of locally buckled rectangular members under concentric compression (80) or pure bending (81). Strain reversal was not allowed, so the column proportions must be chosen such that it has buckled locally in the elastic range. He used the Rayleigh-Ritz energy method in conjunction with the flow theory of plasticity. The stress-strain relation was assumed to be elastic-perfectly plastic and the onset of plasticity was governed by the von Mises criterion. The deflection was assumed to be basically the same as the deflection of the completely elastic column. Graves Smith obtained complete theoretical curves of ultimate stress against slenderness " $\bar{\lambda}$" for various values of β greater than unity. In addition, he performed a carefully conducted series of model tests on square columns of aluminium and steel. The test specimens were approximately free from initial imperfection

and residual stress. He obtained very good comparison with the theory.

Little (82) used the moment-curvature-thrust relation to study the ultimate strength of the square box column. The method had been used previously for stiffened panels (83). The local buckling of the flange was allowed for by applying an appropriate average stress-strain curve to M-ϕ-P relation. Two cases for the web behaviour were assumed - unbuckled web (which was treated simply as elastic-perfectly plastic material) and buckled web (which was treated by using appropriate average stress-strain curve). No attempt was made to allow for strain reversals. Little proposed a design approach for the box column based on the modified Perry equation and ECCS column curves (69). The effective yield stress (the value at which the column curve cuts the stress axis) with the full cross section properties were used. The method has the advantage that it does not require iteration.

A similar design method has been recently proposed by Hancock (79) for H-columns. The method was based on the SSRC multiple column curves (69) and on the effective section (stocky columns) or on the local buckling of component plates (slender columns).

2.4 The Finite Strip Method

Wittrick and his colleagues (84-86) have developed a generalised matrix approach for calculating the buckling stresses of plate assemblies using what might be called an exact finite strip method (i.e. exact within the limitations of linear theory in the elastic range). Each component flat was treated as a single strip and it was assumed that all three components of displacement vary sinusoidally along any longitudinal line when buckling occurs. To satisfy this, either the half wavelength is small compared with the length of the plate assembly, or all the component plates are simply supported at their ends. This assumption enables the partial differential equations governing the in-plane and out-of-plane deformations of the component flats to be reduced to ordinary differential equations which can then be solved. Thence stiffness matrices are derived, relating the amplitudes of the sinusoidally varying forces and displacement on the longitudinal edges of the plate. These matrices have components which are complicated transcendental functions of a loading factor and the half wavelength. Therefore, the critical loading factor cannot be obtained by standard eigenvalue methods. To overcome this difficulty an algorithm was developed (87). The local, overall and interaction buckling can be investigated by this exact approach.

Parallel to the development of the exact method by Wittrick, an approximate finite strip method has been presented by Cheung (88), initially for plate bending problems, to solve the plate buckling problem. In this method, polynomial functions are used to describe the variation of the displacements in the transverse direction. The advantage of this approach over the exact finite strip method described above is that the coefficientsof the overall stiffness matrix are linear functions of the load factor, and standard eigenvalue routines can therefore be used to extract the buckling loads. Another advantage is that the approximate finite strip approach is more general than the exact approach. Any cross section under complicated variations of loads can be considered. Furthermore, boundary conditions for the loaded edges other than simply supported can be considered with the appropriate longitudinal variation for the distortion.

The disadvantage of it is that, in order to achieve sufficient accuracy, it is almost always necessary to subdivide the components flats into two or more finite strips, so that the order of the overall stiffness matrix is usually at least twice that arising from the exact finite strip approach. The approximate finite strip method is now well established as an economical and efficient way for the analysis of elastic buckling (76, 77, 88-95).

Recently the finite strip method has been extended to study the inelastic buckling behaviour of plate assemblies (60, 96, 97). Fukumoto et al (60) and Yoshida et al (95) have used the method to investigate axially compressed panels stiffened by longitudinal stiffeners and longitudinal and transverse stiffeners respectively. Yoshida et al (97) has studied H-columns. The effect of the residual stress was considered in all these studies. They assumed that the material stress-strain relationship was elastic-perfectly plastic. The strain reversal at the instant of buckling and the strain hardening were not considered in the analysis. They applied the deformation theory of plasticity in the inelastic range, and the inelastic moment curvature and the inelastic stress-strain relationship were used.

On the other hand, Graves Smith et al (98) have extended the elastic finite strip to the elastic post-buckling range. They have assumed that the strips were perfect. The two well known in-plane boundary conditions of the unloaded edges of the plate were considered. The in-plane displacement functions used by them differ from those conventionally used in linear finite strip analysis, in the longitudinal harmonic series assumed. This is because this function must satisfy the in-plane equilibrium equations. The compatibility between the out-of-plane displacement and the transverse in-plane displacement at the corners of structures where plates meet at an angle cannot be maintained by using these functions (Figure 2.8). To

achieve this compatibility, Sridharan (99) has assumed another function for the transverse in-plane displacement. The required number of harmonics is higher, in this case, than that required in the first assumption. Graves Smith et al (98) have assumed that the distribution of Possion's ratio in the post-buckling range is equal to that before buckling and have neglected the effect of the nonuniform stress in this range.

More recently the finite strip method has been developed to include the effect of the initial imperfection by Hancock (78). He assumed displacement functions which were different from those used by Graves Smith and Sridharan (98, 99), the main differences being

1. Graves Smith assumed that Possion's ratio is uniform in the post-buckling range while Hancock modified it by a factor dependent on the stress distribution.
2. The longitudinal harmonics which were used by Graves Smith for the in-plane displacement were sine and cosine functions, for longitudinal and transverse respectively, where Hancock used squared functions.

Hancock assumed that the in-plane displacement functions were divided into two components, one corresponding to the Hookean deformation (due to compressive stress) and the

other due to flexural displacement of the strip. Only one term of the Fourier series was used to describe the displacement fields along the length of the stip. This approach produced an accurate solution up to approximately 1.5 times the critical load. The assumed longitudinal in-plane harmonic series eliminated shear straining at the ends of the strip. Moreover, it allowed for compatibility between the out-of-plane and the in-plane displacements at plate junction (Figure 2.8). It was assumed that the load is acting through a very rigid loading bar. The initial out-of-plane imperfection of the plate was taken to be of the same form as the out-of-plane displacement.

To study the post-buckling behaviour of simply supported square plate, Graves Smith et al (98) divided it into 24 strips to achieve acceptable accuracy but Hancock (78) found that 8 strips were enough.

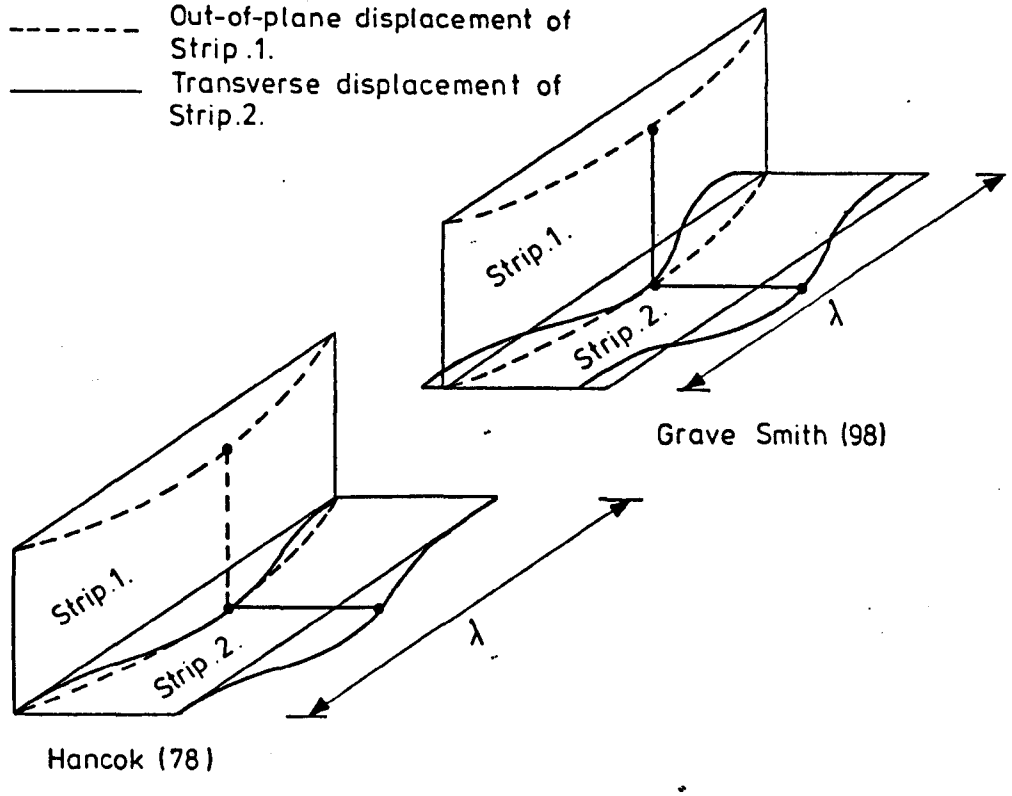

FIG. 2·8. GRAVE SMITH AND HANCOK'S DISPLACEMENT FUNCTIONS.

CHAPTER 3

THE FINITE STRIP METHOD IN INELASTIC STABILITY

3.1 Introduction

The finite strip method is now well established as a powerful method of solution in structural analysis and as such has been well documented. In the present work the emphasis is on the inelastic application of the method. In this chapter attention will therefore be concentrated on the details of the finite strip approach specifically related to inelastic buckling behaviour of plated structures and only a brief description of the established theory will be given for completeness. The basis of the current approach can be summarised as follows.

1. The structure is divided into a number of longitudinal strips. For a typical strip a displacement function describing the buckled deformation in terms of the nodal displacements is assumed.
2. A nonlinear stress-strain relationship for the material is used.
3. Applying the principal of virtual work stiffness and stability matrices can be derived for every strip.
4. The generated matrices are modified to include the effect of the boundary conditions of the longitudinal edges of the strip. The overall matrix is then assembled from these matrices.

5. An iterative procedure is used to obtain the inelastic critical load.
6. The residual stresses due to welding or rolling can be considered as additional nonuniform loads.

The present chapter concludes with a description of some of the routines used in the computer program developed on the basis of this theory for the determination of the smallest inelastic critical load of any plated structure.

3.2 The Finite Strip Method

In the finite strip method the structure is divided into a number of longitudinal rectangular strips (Figure 3.1) connected along their longitudinal edges (nodal lines). A typical strip (Figure 3.2) is assumed to be perfect and plane with constant geometry along its length. It may be connected along one or both of its nodal lines to the adjacent strips. The behaviour of each strip can initially be studied independently of the behaviour of other strips by assuming a set of functions approximating the displacement in that region. Due to the use of continuous function in the longitudinal direction the number of degrees of freedom at a strip nodal line is usually less than that at an element node (the conventional in finite element approach). The buckled mode is assumed to be sinusoidal and this implies that there are four degrees

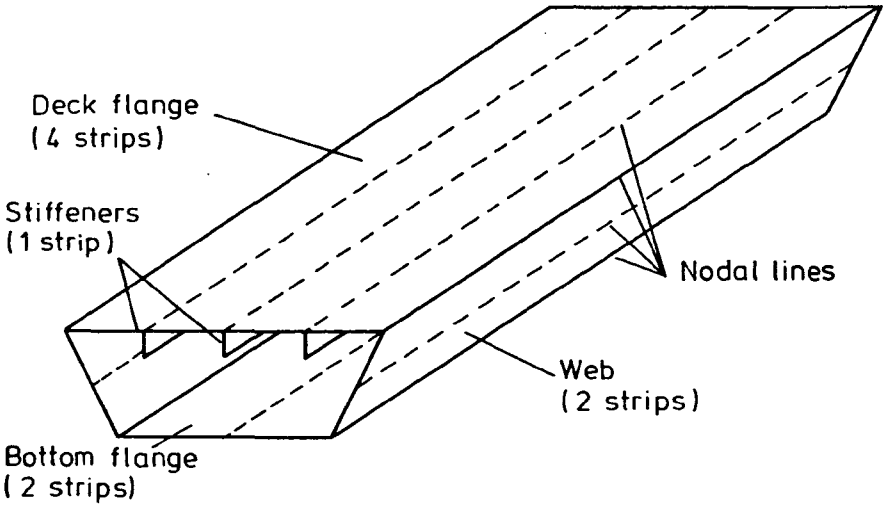

(a) Box girder.

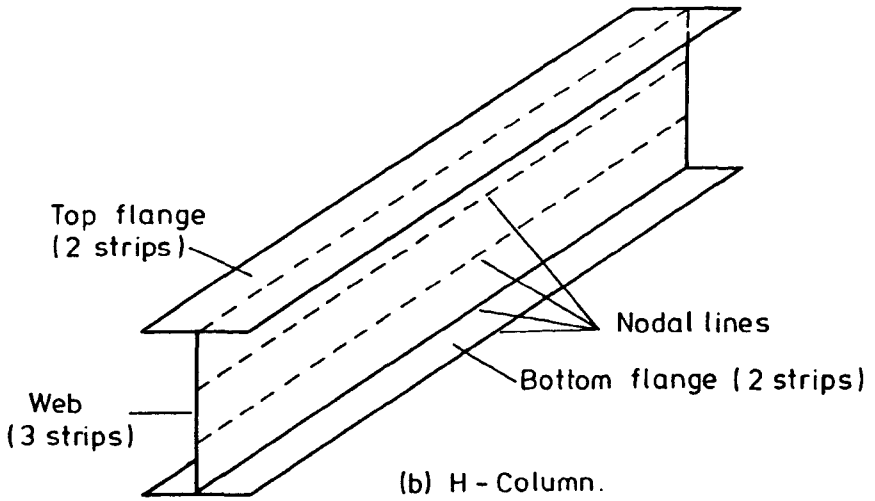

(b) H - Column.

FIG. 3·1. DIVISION OF STRUCTURES INTO STRIPS.

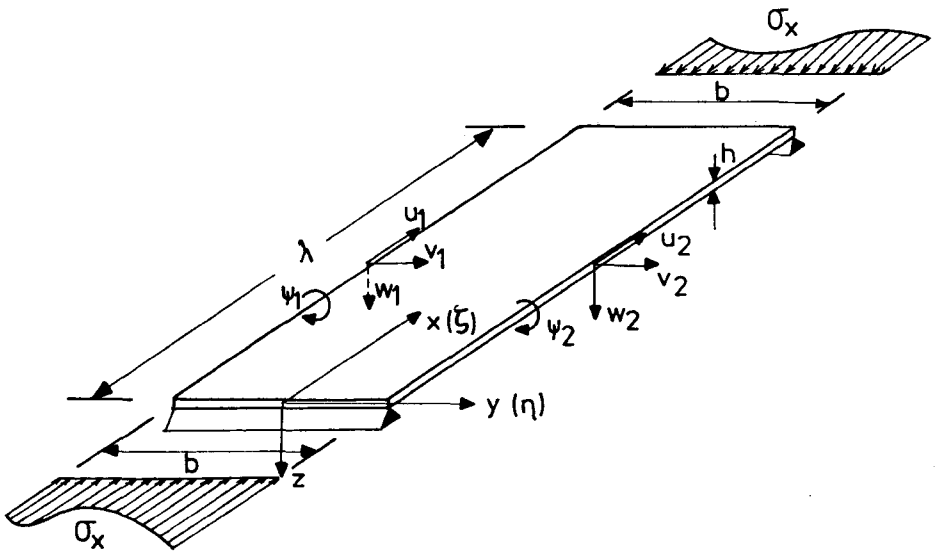

FIG. 3·2. A TYPICAL STRIP SHOWING THE EDGE DISPLACEMENT AND THE APPLIED STRESS.

of freedom - longitudinal, transverse and out-of-plane displacement and rotation - at each nodal line as shown in Figure 3.2.

The fundamental assumptions on which the current work is based are:

1. The cross-sectional dimensions of the structure and its components are the same throughout the length of the structure.
2. All components of the structure are initially perfectly flat.
3. In any buckling mode the displacement, under the action of axial stress, varies sinusoidally in the longitudinal direction.
4. The second order terms in the strain-displacement relations can be neglected.
5. The applied loads act in the middle plane of the strip.

3.3 Displacement and Shape Functions

A typical strip with the geometry and conditions shown in Figure 3.2 will be considered. Displacement functions which are simple polynomials in the transverse direction and continuously differentiable smooth series in the longitudinal direction, as shown in Figure 3.3 have been assumed. The displacements of any point in a strip are (u, v, w) in (x, y, z) directions and the displacement vector {f} can therefore be written

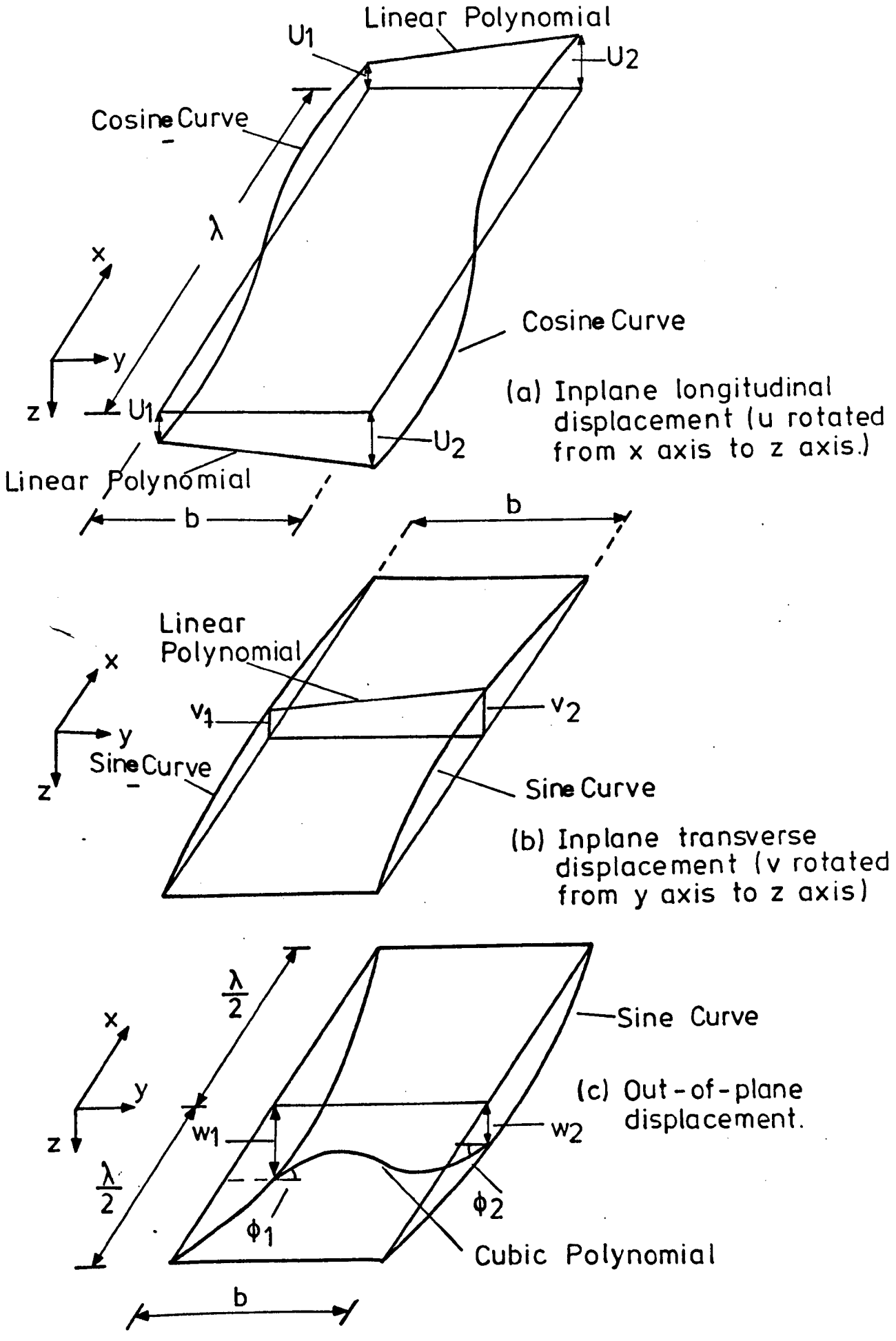

FIG. 3·3. DISPLACEMENT FIELDS OF STRIP.

$$\{f\} = \{u\ v\ w\}^T \tag{3.1}$$

The displacement functions are chosen to represent these displacements $\{f\}$ at any point in terms of the nodal displacements $\{\delta\}$ which are given by

$$\{\delta\} = \{\theta_1\ w_1\ v_1\ u_1\ \theta_2\ w_2\ v_2\ u_2\}^T \tag{3.2}$$

where θ_i and w_i, v_i and u_i are the rotation and displacements amplitude at edge (i). The chosen displacement functions consist of two parts. The first is the shape function which represents the change in the displacement in the transverse direction, while the second is the series which represents the change of the displacement in the longitudinal direction. The displacement function must be assumed so as to satisfy the following conditions (88).

(i) The series part of the displacement function should satisfy the end conditions. For the case of simply supported ends the conditions are that the out-of-plane displacements and the normal curvature at the two ends are equal to zero. Thus

$$w = w_{,xx} = 0.0 \qquad \text{at } x = 0 \ \& \ \lambda \tag{3.3}$$

Or in nondimensional form

$$w = w_{,\zeta\zeta} = 0.0 \qquad \text{at } \zeta = 0 \ \& \ 1 \tag{3.4}$$

where $\zeta = x/\lambda$ and λ is the half wavelength.

Because the strip is under longitudinal stress it is assumed that the longitudinal displacement at the ends is constant, i.e.

$$u = \text{constant} \qquad \text{at } \zeta = 0,1 \tag{3.5}$$

The two ends are assumed to be undistorted which means that the transverse displacement at the ends must equal zero.

i.e.

$$v = 0.0 \qquad \text{at } \zeta = 0,1 \tag{3,6}$$

The following displacement functions clearly satisfy the above conditions

$$u = \sum_{n=1}^{r} f_n(y) \cos \frac{n\pi x}{\lambda} \tag{3.7a}$$

$$v = \sum_{n=1}^{r} f_n(y) \sin \frac{n\pi x}{\lambda} \tag{3.7b}$$

$$w = \sum_{m=1}^{r} f_m(y) \sin \frac{m\pi x}{\lambda} \tag{3.7c}$$

where n and m are the number of harmonics chosen for a particular solution. In the present work only the first term in the assumed basic series function will be used, i.e. m = n = 1 (100).

(ii) The polynomial part in the displacement equation must be capable of representing a state of constant strain in the transverse direction. This can be achieved by satisfying the following conditions.

(a) The polynomial is complete up to or above the order of the necessary differentiation required to obtain the strain. For example to obtain the transverse in-plane strain and the bending curvature (ε_y and k_y) a first and second order differentiation ($v_{,y}$ and $w_{,yy}$) are required respectively. Thus the polynomial must be complete, at least up to the first term for v and up to the quadratic term for w.

(b) A constant term must be obtained after this differenation.

(ii) The displacement function must be continuous within the element. Furthermore it must be such that conditions of compatibility along the common edges of adjacent strips are satisfied in respect of the displacement u, v, w and θ. The continuity will be achieved if the partial derivatives of the displacement function w.r.t. y (to one order less than the highest order appearing in the strain displacement relationship) are continuous.

If these three conditions are satisfied convergence on the correct results will be ensured and the summation of the sum total of the virtual work of all strips will

be equal to the total virtual work of the structure. The displacement functions which satisfy these conditions are given by:

$$\{f\} = \begin{Bmatrix} u \\ v \\ w \end{Bmatrix} \tag{3.8}$$

$$= \begin{Bmatrix} \{x\}^T \{\delta\} \cos \frac{\pi x}{\lambda} \\ \{Y\}^T \{\delta\} \sin \frac{\pi x}{\lambda} \\ \{Z\}^T \{\delta\} \sin \frac{\pi x}{\lambda} \end{Bmatrix} \tag{3.9}$$

$$= \begin{Bmatrix} \{x\}^T \{\delta\} \cos\pi \\ \{Y\}^T \{\delta\} \sin\pi \\ \{Z\}^T \{\delta\} \sin\pi \end{Bmatrix} \tag{3.10}$$

$$= [N] \{\delta\} \tag{3.11}$$

where the shape functions $\{x\}$, $\{Y\}$ and $\{Z\}$ which describe the variation of the nodal line displacements $\{\delta\}$ across the strip width are given by

$$\{x\}^T = \{0, 0, 0, C_1, 0, 0, 0, C_2\} \tag{3.12}$$

$$\{Y\}^T = \{0, 0, C_1, 0, 0, 0, C_2, 0\} \tag{3.13}$$

$$\{Z\}^T = \{C_3, C_4, 0, 0, C_5, C_6, 0, 0\} \tag{3.14}$$

C_i is a polynomial function (i = 1,6) defined by

$$C_1 = \frac{1}{2}(1 - 2\eta), \tag{3.15a}$$

$$C_2 = \frac{1}{2}(1 + 2\eta), \tag{3.15b}$$

$$C_3 = b/8\ (1 - 2\eta - 4\eta^2 + 8\eta^3), \tag{3.15c}$$

$$C_4 = \frac{1}{2}(1 - 3\eta + 4\eta^3), \tag{3.15d}$$

$$C_5 = b/8\ (-1 - 2\eta + 4\eta^2 + \delta\eta^3), \tag{3.15e}$$

and $$C_6 = \frac{1}{2}(1 + 3\eta - 4\eta^3) \tag{3.15f}$$

where

$$\eta = y/b$$

These shape functions are compelete up to the first term for in-plane displacement, and up to the cubic term for out-of-plane displacement and hence satisfy condition (ii) above. From equation (3.10) the matrix [N] is given by

$$[N] = [\{x\}^T \cos\pi\zeta \quad \{Y\}^T \sin\pi\zeta \quad \{Z\}^T \sin\pi\zeta]^T \tag{3.16}$$

This matrix is a 3 x 8 rectangular matrix, where 3 corresponds to the component of displacement of any point and 8 corresponds to the total number of degrees of freedom per strip.

3.4 Material Nonlinearity

Much of the research work on stability of plates assumes a linear elastic relationship between stress and strain. Although for certain materials this might be quite acceptable up to the proportional limit, it is clearly inappropriate for stresses above this limit

With regard to the plastic behaviour beyond the yield stress, there are two major theories - the deformation theory and the incremental or flow theory (5). In the deformation theory the total strain depends on the current state of stress and is independent of the history of loading. In flow theory additional factors, such as the increments of stress and strain, affect the state of plastic strain. The basic assumption in the deformation theory is that no strain reversal occurs and therefore the relationship between increment in stress and increment in strain may be obtained from the tangent modulus.

Both theories of plasticity have been used in the stability problem (21, 52, 60). The elasto-plastic buckling stress of a perfect plate based on deformation theory of plasticity often agrees with experimental results more closely than the flow theory. Neal (34) referred this to the high sensitivity of the flow theory to initial imperfections. He found that the difference between deformation theory and flow theory results were due to the value of the initial imperfection, the slenderness ratio and the material constants.

Based on the flow theory Zienkiewicz et al (101) and Yamada et al (107) presented separately elasto-plastic matrices which can be used in incremental analysis. These matrices depend on the state of total stress. The method is valid for ideal plasticity as well as work hardened materials.

In the present work the more sophisticated stress-strain relationship (103) shown in Figure 3.4 is used. The fundamental assumptions can be summarized as follows:

1. Deformation theory can be applied.
2. Strain reversal, as shown in Figure 3.5, due to unloading can be neglected.
3. Although the strain hardening can be considered by modifying the stress-strain relationship (Figure 3.6), this strain hardening will be neglected in this work.
4. The whole section depth of the plate can be yielded suddenly.

The stress-strain curve (Figure 3.4) can be represented mathematically (103) by

$$\varepsilon = \frac{\sigma_x}{E} \left(\frac{1 - c\mu}{1 - \mu}\right) \tag{3.17}$$

where

$$\mu = |\sigma_x|\sigma_y| \tag{3.18}$$

$$\leq 1.0$$

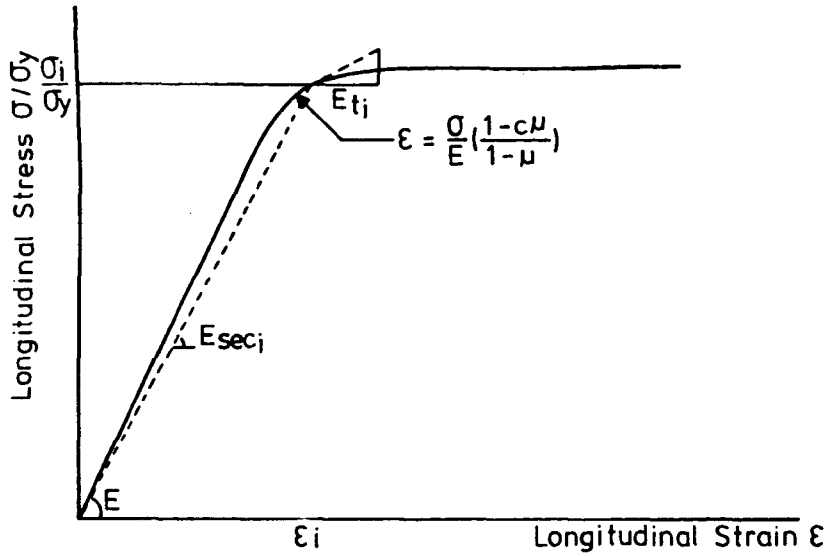

FIG. 3·4. THE IDEALISED STRESS - STRAIN CURVE.

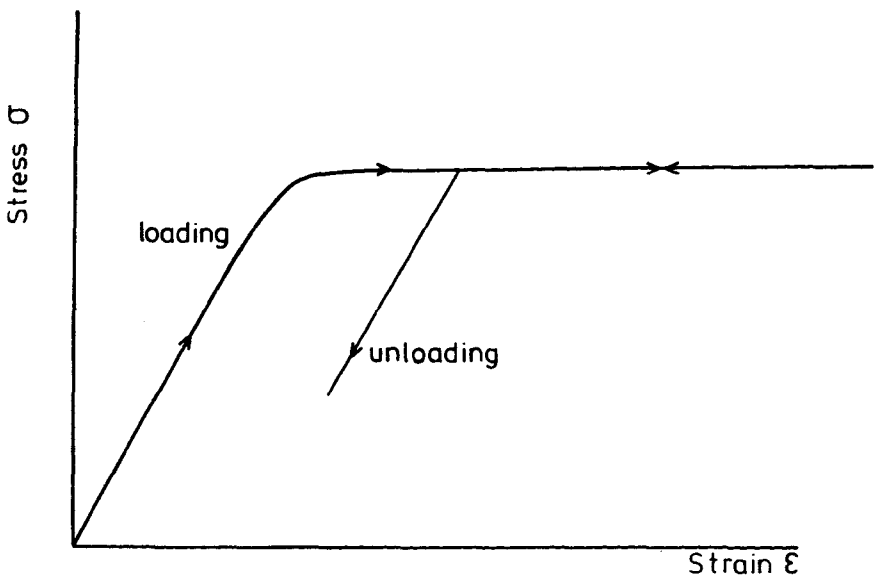

FIG. 3·5. STRAIN REVERSAL BEHAVIOUR DURING UNLOADING.

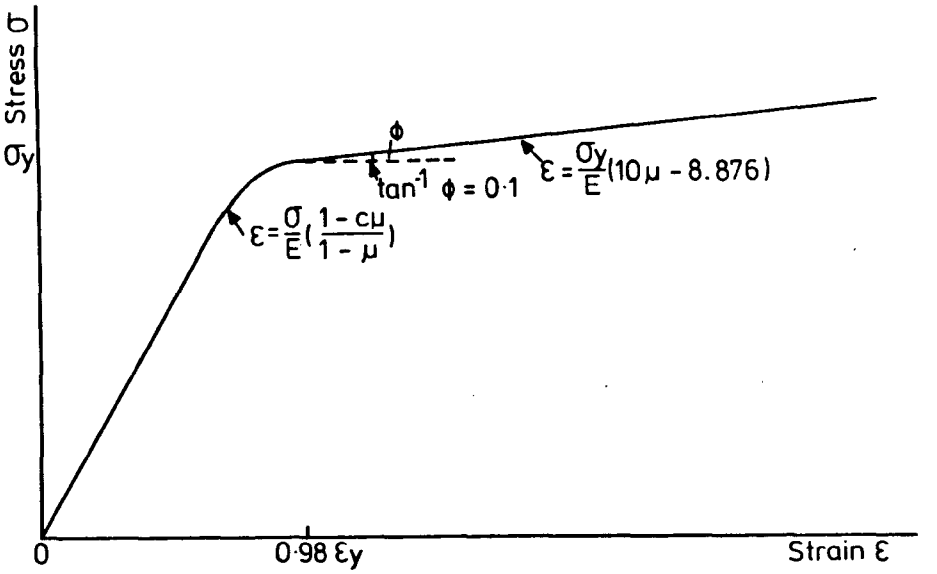

FIG. 3·6. STRESS-STRAIN RELATIONSHIP FOR STRAIN HARDENING MATERIAL.

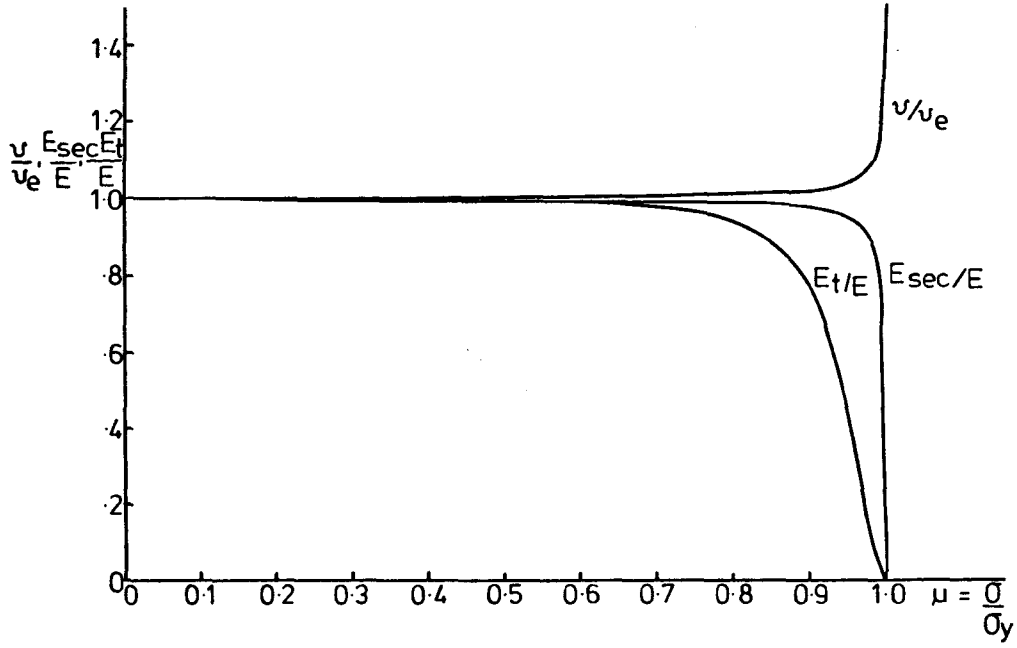

FIG. 3·7. μ VERSUS Et/E, Esec/E AND ν/νe.

σ_Y the yield stress

C = 0.997 for steel

The tangent modulus E_t which can be defined as the slope of the stress vs strain curve at a point (104) is given by

$$E_t = \frac{d\,\sigma_x}{d\varepsilon} \tag{3.19}$$

differentiating equation (3.17) with respect to σ_x gives

$$\frac{d\varepsilon}{d\,\sigma_x} = \frac{1}{E}\,\frac{(1-2C\mu+C\mu^2)}{(1-\mu)^2} \tag{3.20}$$

$$= \frac{1}{E_t} \tag{3.21}$$

The tangent modulus may be written as

$$E_t = E\,\frac{(1-\mu)^2}{(1-2C\mu+C\mu^2)} \tag{3.22}$$

The secant modulus E_{sec} can also be defined in terms of the total stress and strain at a given stage as

$$E_{sec} = \frac{\sigma_x}{\varepsilon} \tag{3.23}$$

From equation (3.17)

$$E_{sec} = E\,\frac{(1-\mu)}{(1-C\mu)} \tag{3.24}$$

The effective Poisson's ratio ν is given by (103)

$$\nu = \nu_p - (\nu_p - \nu_e) \frac{E_{sec}}{E} \tag{3.25}$$

where ν_p and ν_e are the plastic and elastic Poisson's ratios. In this work, it is assumed that $\nu_p = 0.5$. Below the proportional limit, the ratio of the secant modulus to elastic modulus, $E_{sec}/E = 1$ and the effective Poisson's ratio ν will be equal to the elastic value (ν_e). Above this limit, E_{sec}/E will be greater than unity and so the effective Poisson's ratio ν will be less than the elastic one.

The relation between the applied stress and elastic properties of the material is shown in Figure 3.7 and Table 3.1. If the applied stress is less than or equal to 80% of the yield stress, the tangent modulus may be considered equal to the elastic modulus. This means that the material is linear elastic for all values of $\mu < 0.80$. The reduction in the secant modulus and the increase in effective Poisson's ratio due to plasticity of the material can be neglected for $\mu < 0.90$.

3.5 Inelastic Stiffness Matrix

The strain $\{\varepsilon\}$ at any point on the strip consists of two parts - the axial strain of the middle plane and the bending strain. At a depth z from the middle plane the strain will be given by

$\mu = \sigma/\sigma_y$	E_t/E	E_{sec}/E	ν/ν_e
0.1	1.00	1.00	1.00
0.5	0.99	1.00	1.00
0.70	0.97	0.99	1.01
0.75	0.96	0.99	1.01
0.80	0.93	0.99	1.01
0.90	0.77	0.97	1.02
0.99	0.03	0.77	1.15
0.999	0.00	0.25	1.50

Table 3.1. Relation Between Applied Stress and Material Properties

$$\{\varepsilon\} = \{\varepsilon_o\} - z\,\{k\} \tag{3.26}$$

where

$$\{\varepsilon\} = \{\varepsilon_x \;\; \varepsilon_y \;\; \gamma_{xy}\}^T \tag{3.27}$$

$$\{\varepsilon_o\} = \{\varepsilon_{xo} \;\; \varepsilon_{yo} \;\; \gamma_{xyo}\}^T \tag{3.28}$$

$$= \{u_{,x} \;\; v_{,y} \;\; u_{,y} + v_{,x}\}^T \tag{3.29}$$

$$= \{\frac{1}{\lambda} u_{,\zeta} \;\; \frac{1}{b} v_{,\eta} \;\; \frac{1}{b} u_{,\eta} + \frac{1}{\lambda} v_{,\zeta}\}^T \tag{3.30}$$

$$\{k\} = \{k_x \;\; k_y \;\; 2k_{x,y}\}^T \tag{3.31}$$

$$= \{w_{,xx} \;\; w_{,yy} \;\; 2w_{,xy}\}^T \tag{3.32}$$

$$= \{\frac{1}{\lambda^2} w_{,\zeta\zeta} \;\; \frac{1}{b^2} w_{,\eta\eta} \;\; \frac{2}{b\lambda} w_{,\eta\zeta}\}^T \tag{3.33}$$

ε_x, ε_y and γ_{xy} are the axial strains in x, y directions and the shear strain in xy plane at any point. ε_{xo}, ε_{yo} and γ_{xyo} are the axial and shear strains at any point in the middle plane. k_x, k_y and k_{xy} are the curvatures.

The strains are related to the displacements by

$$\begin{Bmatrix} \varepsilon_x \\ \varepsilon_y \\ \gamma_{xy} \end{Bmatrix} = \begin{Bmatrix} u_{,x} \\ v_{,y} \\ u_{,y} + v_{,x} \end{Bmatrix} - z \begin{Bmatrix} w_{,xx} \\ w_{,yy} \\ 2w_{,xy} \end{Bmatrix} \tag{3.34}$$

$$= \begin{Bmatrix} \frac{1}{\lambda} u_{,\zeta} \\ \frac{1}{b} v_{,\eta} \\ \frac{1}{b} u_{,\eta} + \frac{1}{\lambda} v_{,\zeta} \end{Bmatrix} - z \begin{Bmatrix} \frac{1}{\lambda 2} w_{,\zeta\zeta} \\ \frac{1}{b^2} w_{,\eta\eta} \\ \frac{2}{b\lambda} w_{,\eta\zeta} \end{Bmatrix} \qquad (3.35)$$

From the differentiation of equation (3.10)

$$u_{,\zeta} = -\pi \{x\}^T \{\delta\} \sin\pi\zeta \qquad (3.36a)$$

$$u_{,\eta} = \{x_{,\eta}\}^T \{\delta\} \cos\pi\zeta \qquad (3.36b)$$

$$v_{,\zeta} = \pi \{Y\}^T \{\delta\} \cos\pi\zeta \qquad (3.36c)$$

$$v_{,\eta} = \{Y_{,\eta}\}^T \{\delta\} \sin\pi\zeta \qquad (3.36d)$$

$$w_{,\zeta\zeta} = -\pi^2 \{Z\}^T \{\delta\} \sin\pi\zeta \qquad (3.36e)$$

$$w_{,\zeta\eta} = \pi \{Z_{,\eta}\}^T \{\delta\} \cos\pi\zeta \qquad (3.36f)$$

$$w_{,\eta\eta} = \{Z_{,\eta\eta}\}^T \{\delta\} \cos\pi\zeta \qquad (3.36g)$$

Substitute equations (3.36) into equation (3.35)

$$\begin{Bmatrix} \varepsilon_x \\ \varepsilon_y \\ \gamma_{xy} \end{Bmatrix} = \begin{Bmatrix} -\frac{\pi}{\lambda} \{x\}^T \{\delta\} \sin\pi\zeta \\ \frac{1}{b} \{Y_{,\eta}\}^T \{\delta\} \sin\pi\zeta \\ \{\frac{1}{b} \{X_{,\eta}\} + \frac{\pi}{\lambda} \{Y\}\}^T \{\delta\} \cos\pi\zeta \end{Bmatrix} - z \begin{Bmatrix} -\frac{\pi^2}{\lambda^2} \{Z\}^T \{\delta\} \sin\pi\zeta \\ \frac{1}{b^2} \{Z_{,\eta\eta}\}^T \{\delta\} \sin\pi\zeta \\ \frac{2\pi}{b\lambda} \{Z_{,\eta}\}^T \{\delta\} \cos\pi\zeta \end{Bmatrix}$$

(3.37)

From equation (3.37) the strain $\{\varepsilon\}$ related to the nodal displacement $\{\delta\}$

$$\{\varepsilon\} = [B]\{\delta\} \text{ by} \tag{3.38}$$

where [B] is the strain matrix and given by

$$[B]_{3x8} = \begin{bmatrix} \frac{\pi}{\lambda}\{-\{x\} + z\frac{\pi}{\lambda}\{Z\}\}^T \sin\pi\zeta \\ \frac{1}{b}\{\{Y,_\eta - z\frac{1}{b}\{Z,_{\eta\eta}\}\}^T \sin\pi\zeta \\ \{\frac{1}{b}\{X,_\eta\} + \frac{\pi}{\lambda}\{Y\} - z\frac{2\pi}{\lambda b}\{Z,_\eta\}\}^T \cos\pi\zeta \end{bmatrix} \tag{3.39}$$

The change in the internal virtual work is equal to dW_i

where

$$dW_i = \int_{vol} \{d\varepsilon\}^T [F]\{\varepsilon\}\, dvol \tag{3.40}$$

Now from equation (3.38)

$$\{d\varepsilon\} = [B]\{d\delta\} \tag{3.41}$$

Substituting for $\{\varepsilon\}$ and $\{d\varepsilon\}$ into equation (3.40) gives

$$dW_i = \int_{vol} \{d\varepsilon\}^T [B]^T [F][B]\{\delta\}\, dvol \tag{3.42}$$

Now $\{\delta\}$ is the amplitude of the nodal displacement and constant within the strip. Hence

$$dW_i = \{d\delta\}^T \int_{vol} [B]^T [F] [B] \, dvol \, \{\delta\} \tag{3.43}$$

$$= \{d\delta\}^T [K] \{\delta\} \tag{3.44}$$

where [K] is the stiffness matrix of the strip

$$[K] = \int_{vol} [B]^T [F] [B] \, dvol \tag{3.45}$$

The matrix [F], the elastic-plastic matrix, depends on on the properties of the material.

$$[F] = \begin{bmatrix} F_{11} & F_{12} & 0 \\ F_{21} & F_{22} & 0 \\ 0 & 0 & F_{33} \end{bmatrix}$$

For elastic material with linear stress-strain relationship, the elements of the matrix [F] are constant and given by

$$F_{11} = F_{22} = \frac{E}{1-\nu^2} \tag{3.47a}$$

$$F_{21} = F_{12} = \nu F_{11} \tag{3.47b}$$

$$F_{33} = \frac{E}{2(1+\nu)} \tag{3.47c}$$

where E is the elastic modulus,

and ν is the Poisson's ratio.

For the inelastic material, nonlinear stress-strain relationship, the value of F_{ij} (i & j = 1, 3) is given by

$$F_{11} = \frac{E_t}{(1-\nu^2)} \tag{3.48a}$$

$$F_{12} = \nu F_{11} \tag{3.48b}$$

$$F_{33} = \frac{E_{sec}}{2(1+\nu)} \tag{3.48c}$$

The tangent modulus E_t, the secant modulus E_{sec} and the effective Poisson's ratio ν are given by equations (3.22), (3.24) and (3.25) respectively.

An expression for the matrix [K] obtained by substituting equation (3.39) into equation (3.45) and carrying out the integration through the depth and along the length of the strip is given in Appendix A. The integration through the width of the strip, i.e. in the transverse direction, cannot be carried out simply in the inelastic analysis of a strip under nonuniform compression. This is because the properties of the material will not be constant through the width and hence the matrix [F] will change from point to point. A numerical integration routine in which the strip is divided into a number of substrips will therefore be used, the matrix [F] being assumed constant for each substrip. The number of substrips into which each strip is divided will of course depend on the rate of variation of stress across

the width, and the accuracy required. For every substrip the stress level and hence the properties of the material can be determined at its two nodes. Using any numerical integration method, the stiffness matrix can thus be obtained. In the case of elastic analysis the stiffness matrix [K] is independent of the stress level which makes the solution of the problem much easier and direct.

3.6 The Stability Matrix

The virtual work, dW_m, done by the basic membrane stress system during a virtual displacement is

$$dW_m = \int_{vol} \{d\ \epsilon_b\}^T \{\sigma\}\ dvol \tag{3.49}$$

where the stress vector $\{\sigma\}$ is defined by

$$\{\sigma\} = \{\sigma_x\ \sigma_y\ \tau_{xy}\} \tag{3.50}$$

and σ_x is the longitudinal stress,

σ_y is the transverse stress,

τ_{xy} is the in-plane shear stress.

Note that because residual stresses are to be included, and hence some strips (or parts of strips) may be subjected to tensile stresses, it is important to introduce a sign convention. In this work compressive stress will be taken as positive and tensile stress as negative.

The bending strain $\{\varepsilon_b\}$ is given by

$$\{\varepsilon_b\} = \frac{1}{2} \begin{Bmatrix} u,_x^2 + v,_x^2 + w,_x^2 \\ u,_y^2 + v,_y^2 + w,_y^2 \\ 2u,_x\, u,_y + 2v,_x\, v,_y + 2w,_x\, w,_y \end{Bmatrix} \tag{3.51}$$

$$= \frac{1}{2} \begin{bmatrix} u,_x & v,_x & w,_x & 0 & 0 & 0 \\ 0 & 0 & 0 & u,_y & v,_y & w,_y \\ u,_y & v,_y & w,_y & u,_x & v,_x & w,_x \end{bmatrix} \begin{Bmatrix} u,_x \\ v,_x \\ w,_x \\ u,_y \\ v,_y \\ w,_y \end{Bmatrix} \tag{3.52}$$

Differentiation of equation (3.1) gives

$$\{f,_x\}^T = \{u,_x\ v,_x\ w,_x\}, \tag{3.53a}$$

$$\{f,_y\} = \{u,_y\ v,_y\ w,_y\}, \tag{3.53b}$$

Substituting equations (3.53) into equation (3.52), the bending strain becomes

$$\{\varepsilon_b\} = \frac{1}{2} \begin{bmatrix} \{f,_x\}^T & 0 \\ 0 & \{f,_y\}^T \\ \{f,_y\}^T & \{f,_x\}^T \end{bmatrix} \begin{Bmatrix} \{f,_x\} \\ \{f,_y\} \end{Bmatrix} \tag{3.54}$$

Using $\zeta = \frac{x}{\lambda}$ and $\eta = y/b$ to obtain in nondimensional form

$$f_x = \frac{1}{\lambda} f_{,\zeta}, \tag{3.55}$$

$$f_y = \frac{1}{b} f_{,\eta}, \tag{3.56}$$

and

$$\{\varepsilon_b\} = \begin{bmatrix} \frac{1}{\lambda}\{f_{,\zeta}\}^T & 0 \\ 0 & \frac{1}{b}\{f_{,\eta}\}^T \\ \frac{1}{b}\{f_{,\eta}\}^T & \frac{1}{\lambda}\{f_{,\zeta}\}^T \end{bmatrix} \begin{matrix} \frac{1}{\lambda}\{f_{,\zeta}\} \\ \\ \frac{1}{b}\{f_{,\eta}\} \end{matrix} \tag{3.57}$$

From equation (3.11)

$$\{f_{,\zeta}\} = [N_{,\zeta}]\{\delta\} \tag{3.53a}$$

$$\{f_{,\eta}\} = [N_{,\eta}]\{\delta\} \tag{3.58b}$$

Substituting equations (3.58) into equation (3.57)

$$\{\varepsilon_b\} = \frac{1}{2}\{\delta\}^T \begin{bmatrix} \frac{1}{\lambda}[N_{,\zeta}]^T & 0 \\ 0 & \frac{1}{b}[N_{,\eta}]^T \\ \frac{1}{b}[N_{,\eta}]^T & \frac{1}{\lambda}[N_{,\zeta}]^T \end{bmatrix} \begin{bmatrix} \frac{1}{\lambda}[N_{,\zeta}] \\ \\ \frac{1}{b}[N_{,\eta}] \end{bmatrix} \{\delta\} \tag{3.59}$$

$$\{d\varepsilon_b\} = \{d\delta\}^T \begin{bmatrix} \frac{1}{\lambda}[N_{,\zeta}]^T & 0 \\ 0 & \frac{1}{b}[N_{,\eta}]^T \\ \frac{1}{b}[N_{,\eta}]^T & \frac{1}{\lambda}[N_{,\zeta}]^T \end{bmatrix} \begin{bmatrix} \frac{1}{\lambda}[N_{,\zeta}] \\ \\ \frac{1}{b}[N_{,\eta}] \end{bmatrix} \{\delta\} \tag{3.60}$$

Substituting equations (3.50) and (3.60) into equation (3.49) we obtain

$$dW_m = \frac{1}{\lambda^2} \int_{vol} \sigma_x \{d\delta\}^T [N,_\zeta]^T [N,_\zeta] \{\delta\} \, dvol$$

$$+ \frac{1}{b^2} \int_{vol} \sigma_y \{d\delta\}^T [N,_\eta]^T [N,_\eta] \{\delta\} \, dvol$$

$$+ \frac{1}{by} \int_{vol} \tau_{xy} \{d\delta\}^T [[N,_\eta]^T [N,_\zeta] + [N,_\zeta]^T [N,_\eta] \{\delta\} \, dvol \quad (3.61)$$

If it is assumed that the structure is under pure longitudinal axial compressive stress σ_x and neglect the transverse stress σ_y and the shear stress τ_{xy} equation (3.61) becomes

$$dW_m = \frac{1}{\lambda^2} \int_{vol} \sigma_x \{d\delta\}^T [N,_\zeta]^T [N,_\zeta] \{\delta\} \, dvol \quad (3.62)$$

$$= \{d\delta\}^T \int_{vol} \frac{\sigma_x}{\lambda^2} [N,_\zeta]^T [N,_\zeta] \, dvol \{\delta\} \quad (3.63)$$

$$= \{d\delta\}^T [S] \{\delta\} \quad (3.64)$$

where [S] is the stability matrix and given by

$$[S] = \frac{1}{\lambda^2} \int_{vol} \sigma_x [N,_\zeta]^T [N,_\zeta] \, dvol \quad (3.65)$$

An expression for the matrix [S] obtained by differentiating the matrix [N] (equation (3.16)), substituting it into equation (3.65) and carrying out the integration through the depth and along the length of the strip is given in Appendix B. If the longitudinal stress σ_x is uniform a direct integration can be carried out across the width of the strip in both elastic and inelastic analysis. But for the case of nonuniform stress as in the case of a strip under axial and residual stresses, the integration can be carried out numerically as mentioned above (Section 3.5). It is clear that this matrix is independent of the material properties and is a linear function of the stress.

3.7 Equilibrium Condition

For equilibrium the virtual work done by the basic membrane stress system dW_m must equal the virtual work done by the internal strains dW_i.

$$dW_i = dW_m \tag{3.66}$$

Substituting expressions for dW_i and dW_m from equations (3.44) and (3.64) we obtain

$$\{d\delta\}^T [K] \{\delta\} = \{d\delta\}^T [S] \{\delta\} \tag{3.67}$$

$$\{d\delta\}^T [[K] - [S]] \{\delta\} = 0 \tag{3.68}$$

$$\{d\delta\}^T \neq 0 \tag{3.69}$$

i.e. $$[[K] - [S]]\{\delta\} = 0 \tag{3.70}$$

For the case of uniform stress, equation (3.70) may be written as

$$[[K] - \sigma_x [S]_o]\{\delta\} = 0 \tag{3.71}$$

where

$$[\bar{S}] = \frac{1}{\lambda^2} \int_{vol} [N,_\zeta]^T [N,_\zeta] \, dvol \tag{3.72}$$

The matrix $[\bar{S}]$ is independent of the load and will be constant for every strip. It depends on the geometric properties of the strip, and for this reason it is called the geometric stiffness matrix. If the material is elastic then the matrix [K] will also be constant and independent of the stress level.

3.8 The Boundary Conditions

After the stiffness and stability matrices of the strip have been obtained as described in the preceding sections, the boundary conditions at the longitudinal edges of the strip must be considered. These longitudinal edges may be one the following:

i - Connected to other strip

ii - Free to move and rotate

iii - Simply supported

iv - Built in

One restriction of the finite strip method is the impossibility of mixing more than one condition along one edge which is an easy task in the finite element method. In the finite element method there will usually be more than one node along any longitudinal edge and these nodes may have different degrees (types) of restraint. In the finite strip method however the longitudinal edge is considered as one nodal line and must therefore have only one type of restraint. For example if an edge is simply supported, then that condition must apply over the whole length of the edge.

The first and the second conditions will not affect the stiffness or the stability matrices. The third condition prevents the edge from moving normal to the middle plane but allows any other in-plane displacements as well as a rotation (i.e. $w_i = 0$). The fixed edge cannot move in the out-of-plane direction or rotate about the longitudinal axis ($w_i = \theta_i = 0$).

To introduce a certain displacement (boundary condition) into the overall matrix, consider first the general case of a set of algebraic equations

$$\begin{bmatrix} e_{11} & e_{12} & -- & e_{1n} \\ e_{21} & e_{22} & -- & e_{2n} \\ -- & -- & -- & -- \\ e_{n1} & e_{n2} & -- & e_{nn} \end{bmatrix} \begin{Bmatrix} \delta_1 \\ \delta_2 \\ -- \\ \delta_n \end{Bmatrix} = \begin{Bmatrix} P_1 \\ P_2 \\ -- \\ P_n \end{Bmatrix} \tag{3.73}$$

or in brief

$$[E]\ \{\delta\} = \{P\} \tag{3.74}$$

in which any variable, δ_2 for example, should be zero (or have a constant value β). There are two approaches by which this may be achieved.

1. The first approach is to modify the row and the column of the matrix [E] which corresponds to the constrained (or the known) displacement. All elements in this row and column are in fact reduced to zero, with the exception of the diagonal element which becomes unity. The corresponding element in the force vector must also be set to zero if the displacement is fully restrained (or the known value β). For instance if δ_2 is the constrained (or the known) displacement then the second row and the second column in the matrix [E] become zero and the diagonal e_{22} becomes unity. The value of p_2 must also be set to zero (or β). The modified form of equation (3.73) will then be

$$\begin{bmatrix} e_{11} & 0 & e_{13} & -- & e_{1n} \\ 0 & 1 & 0 & 0 & 0 \\ e_{31} & 0 & e_{32} & -- & e_{3n} \\ -- & 0 & -- & -- & -- \\ e_{n1} & 0 & e_{n2} & -- & e_{nn} \end{bmatrix} \begin{Bmatrix} \delta_1 \\ \delta_2 \\ \delta_3 \\ -- \\ \delta_n \end{Bmatrix} = \begin{Bmatrix} P_1 \\ 0 \\ P_3 \\ -- \\ P_n \end{Bmatrix} \tag{3.75}$$

2. The second approach involves modifying the diagonal element of [E] corresponding to the constrained displacement by adding a very high value. This is equivalent to applying a very large stiffness at the particular boundary, with the effect of reducing the corresponding displacement to a negligible small value. The modified form of equation (3.73) will be

$$\begin{bmatrix} e_{11} & e_{12} & -- & e_{1n} \\ e_{21} & e_{22}+10^{30} & -- & e_{2n} \\ -- & -- & -- & -- \\ e_{n1} & e_{n2} & -- & e_{nn} \end{bmatrix} \begin{Bmatrix} \delta_1 \\ \delta_2 \\ -- \\ \delta_n \end{Bmatrix} = \begin{Bmatrix} P_1 \\ P_2 \\ -- \\ P_n \end{Bmatrix} \tag{3.76}$$

In either case all degrees of freedom which are restrained can be treated in this way. In the present work the second method has been used and the stiffness matrix for each strip modified before the overall matrix of the structure is assembled.

3.9 The Overall Matrix

After the stiffness and stability matrix for each strip has been obtained and modified to account for the edge conditions, the overall matrix can be assembled. If all strips are coplaner, i.e. the local axes of each strip coincide with the global axes of the structure the assembly of the overall matrix can be done directly. However, if the local axes of the strip do not coincide with the global axes of the structure the stiffness and stability matrices for each strip must be transformed to a consistent set of axes. The transformed stiffness matrix [K] of the strip is given by

$$[K] = [R]^T [K]_1 [R] \tag{3.77}$$

where $[K]_1$ is the stiffness matrix referred to local axes and [R] is 8 x 8 transformation matrix.

$$[R] = \begin{bmatrix} [r] & [O] \\ [O] & [r] \end{bmatrix} \tag{3.78}$$

[O] is 4 x 4 null matrix and

$$[r] = \begin{bmatrix} 1 & 0 & 0 & 0 \\ 0 & \cos\beta & \sin\beta & 0 \\ 0 & -\sin\beta & \cos\beta & 0 \\ 0 & 0 & 0 & 1 \end{bmatrix} \tag{3.79}$$

β is the angle of rotation of the local axes measured in clockwise direction as shown in Figure 3.8.

In elastic buckling problems where two basic types of strip matrices (stiffness and stability matrix) are involved, it is required to assemble the two corresponding overall matrices, since the parameter σ_x must vary untill a certain condition is satisfied. The matrices [K] and $[\bar{S}]$ for all strips are independent of the load and thus the overall equilibrium equation becomes

$$[K - \sigma_x \bar{S}] \{\delta\} = 0.0 \tag{3.80}$$

where K is the assembled stiffness matrix,
and $\bar{S}$ is the assembled stability matrix.

In the inelastic buckling problems with nonuniform applied stress, both matrices [K] and [S] are functions of the stress σ_x. The separation of the two matrices (stiffness and stability) is no longer an advantage. They must both be updated with every iteration and the overall equilibrium equation becomes:

$$[K - S] \{\delta\} = 0 \tag{3.81}$$

$$[E] \{\delta\} = 0 \tag{3.82}$$

where

$$[E] = [K - S] \tag{3.83}$$

The matrices K, S and E are square matrices of order n x n, and $\{\delta\}$ is a nodal displacement vector of order n where n is the total number of degrees of freedom.

With regard to updating the stability matrix, there are two approaches. In the first the updated matrix [S] for any strip is given by

$$[S] = [S]_o - \Delta\sigma_x [\bar{S}] \tag{3.84}$$

where $[S]_o$ is the stability matrix obtained at initial axial stress σ_{xo} (equation (3.65)). $\Delta\sigma_x$ is the change in the initial axial stress σ_{xo}. This change in the axial stress, $\Delta\sigma_x$, is uniform and the stability matrix $[\bar{S}]$ can be obtained by direct integration (equation (3.72)). So, the numerical integration will be done in the first cycle only to obtain $[S]_o$. Thus, the two matrices $[S]_o$ and [S] will be calculated only once. The stability matrix at any stress level, σ_x, can then be obtained from equation (3.84). The second approach involves regeneration of the stability matrix using the updated axial stress, σ_x. In this case the numerical integration will be used in every cycle. The second approach, which has been used in the present work, needs less core store but is more time consuming in terms of computational effort.

3.10 Determination of the Critical Load and Mode of Buckling

3.10.1 Linear Eigenvalue Problem

In the elastic buckling problem the coefficients of the equation

$$[K - \sigma_x \bar{S}] \{\delta\} = 0 \tag{3.80}$$

are linear functions of the load and the simultaneous equations are homogeneous. The nontrivial solution of these equations is given by

$$|K - \sigma_x \bar{S}| = 0 \tag{3.85}$$

This means that the criterion for buckling is in general the vanishing of the determinant of the overall matrix $[K - \sigma_x \bar{S}]$. Standard eigenvalue routines (105) can be used to determine the critical load. In order to use direct methods for solution of the standard eigenvalue problem, equation (3.80) can be reduced to

$$[A] \{\delta^*\} - \sigma_x^* [I] \{\delta^*\} = 0 \tag{3.86}$$

where

$$[A] = [L]^{-1} [\bar{S}] [L]^{-T} \tag{3.87}$$

$$[K] = [L] [L]^{T} \tag{3.88}$$

$$\{\delta^*\} = [L]^T \{\delta\} \tag{3.89}$$

$$\sigma_x^* = 1/\sigma_x \tag{3.90}$$

The reduction of equation (3.80) to equation (3.86) consists of symmetric triangulation of the stiffness matrix [K] to [L] $[L]^T$. The matrix [A] is calculated by pre- and post-multiplication of the stability matrix $[\bar{S}]$ by $[L]^{-1}$ and $[L]^{-T}$ respectively.

A comparison between three of the most successful direct methods, Lanzos, Givens and Householder's for finding the eigenvalues of a general symmetric matrix can be found elsewhere (106). In all these methods the matrix reduces to triple-diagonal form. Householder's method is generally held to be the fastest and most accurate of known methods (106).

Because only the smallest eignevalue is desired, an iterative method rather than a direct one may be convenient to apply. In this method (107) a trial displacement vector $\{\delta\}_i$ is assumed and an approximate eigenvalue and a second trial eigenvector $\{\delta\}_{i+1}$ can be determined from

$$[\bar{S}]^{-1} [K] \{\delta\}_i = \sigma_x \{\delta\}_{i+1} \tag{3.91}$$

or from

$$\{\delta\}_{i+1} = \sigma_x [K]^{-1} [\bar{S}] \{\delta\}_i \tag{3.92}$$

The iteration may be based on a trial eigenvalue σ_x. The value of the stability determinant at $0 \leq \sigma_x < \sigma_{cr}$ is always positive as shown in Figure 3.9. With the trial σ_x, the determinant $[K - \sigma_x \bar{S}]$ is evaluated. If the determinant is equal to zero, the trial value of the stress, σ_x, will correspond to one of the critical loads (eigenvalues). If the determinant has a value other than zero, a new stress, σ_x, will be selected and the determinant is again calculated. A comparison is made with the results of the previous trial and, based on this comparison, a new stress, σ_x, is selected for trial. This should be repeated until the value obtained for determinant is equal to zero. For practical applications in fact it is extremely unlikely that a trial value for the stress will be identically equal to the critical stress, and an absolute value for the determinant of zero will not be realised. However, it is clearly a simple matter to check the upper and lower bounds to the critical load at any iteration. Once the difference between these is sufficiently small, the value of the critical load can be given to the appropriate degree of accuracy. Using this method of iteration however, there is no guarantee that the obtained critical load is the smallest one.

These standard methods of solutions for the eigenvalue problem are however only applicable to linear eigenvalue problems. As mentioned in the previous section,

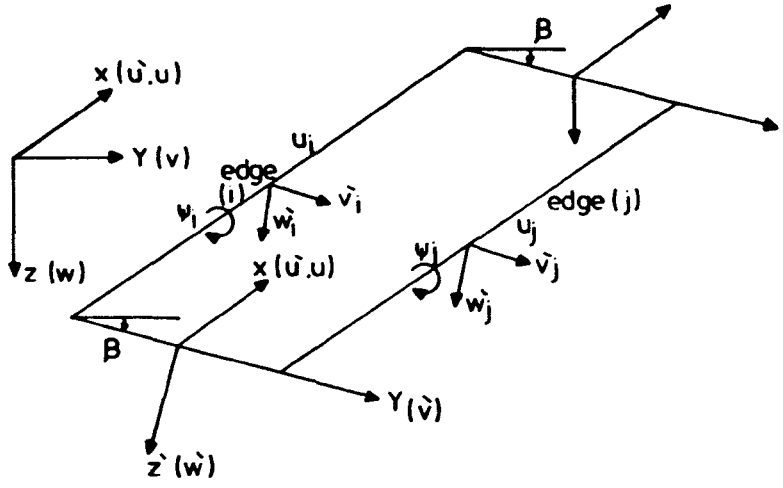

FIG. 3·8. LOCAL AND GLOBAL COORDINATE SYSTEMS.

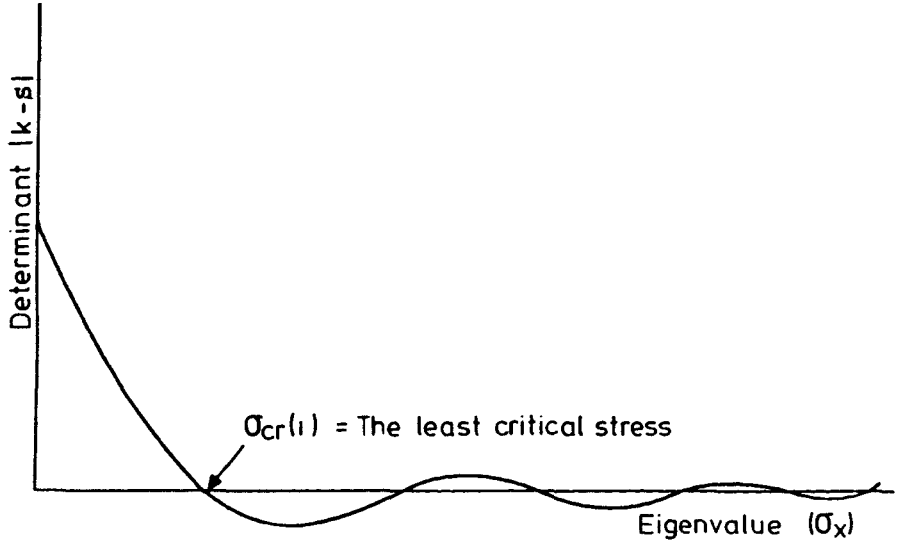

FIG. 3·9. EIGENVALUE OF THE DETERMINANT |k - s|

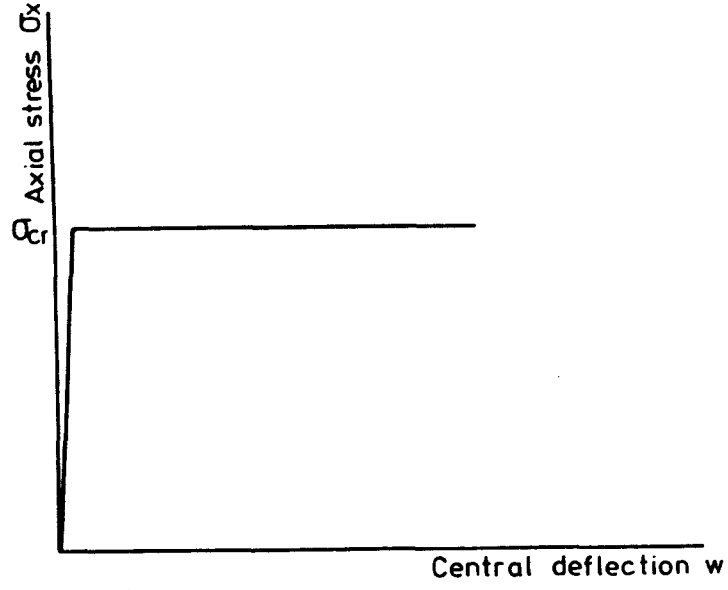

FIG. 3·10. LOAD DEFLECTION CURVE FOR PERFECT PLATE UNDER INPLANE LOAD.

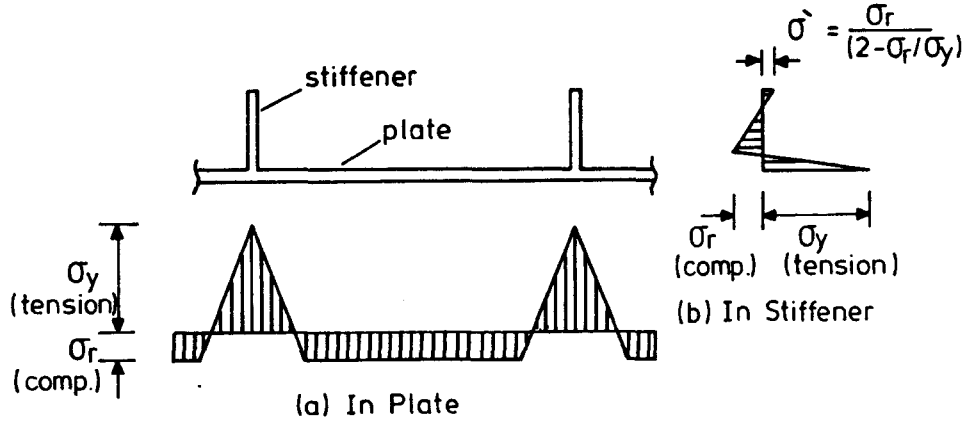

FIG. 3·12. THE IDEALISED RESIDUAL STRESS PATTERNS.

but the stiffness and stability matrices vary with the applied stress in a nonlinear manner, and hence these forms of solutions are not applicable. In the methods for the determination of the eigenvalues described above an ideal, perfect panel is considered and displacements prior to instability are ignored. An approximate method based on the load deflection relationship (Figure 3.10), for perfect and imperfect panel, can also be used. For any increment of load, the deflection behaviour can be obtained from a direct solution of the equilibrium equations and the critical load corresponds to that load at which the deflection becomes very large. Usually this approach underestimates the critical load and is also difficult and time consuming (69) to use. However it does have the advantage that the mode of buckling will be provided and the critical load will always correspond to the lowest eigenvalue. More importantly, it can be applied to the nonlinear relationships represented by the stiffness and stability matrices in the current work.

A general algorithm presented by Wittrick and Williams (87) eliminates the drawbacks of all these methods. Using this algorithm the number of critical buckling loads exceeded by any specified load can be obtained for the case in which the overall stiffness matrix is nonlinear. It can also be applied to the computation of the natural frequencies of elastic structures.

Because it enables convergence on the lowest eigenvalue with absolute certainty, this method has been used in the current work to obtain the critical loads. The method will be briefly described in the following section for completeness.

3.10.2 Wittrick-Williams Algorithm

In the inelastic problem, the stress at any point in the panel prior to buckling is a pure membrane axial stress combining the sum of the longitudinal residual stresses and the applied longitudinal compression. This stress may be tensile at some points and compressive elsewhere but the critical load can still be determined in the same manner as for the elastic case. However, as the coefficients of the matrix [E] (equation (3.82)) will no longer be linearly dependent on the load factor, standard eigenvalue routines are not applicable, and instead the Wittrick-Williams algorithm (87) is used to ensure automatic convergence on the lowest buckling stress, σ_{cr}. The only difference between the elastic and inelastic analysis using this algorithm is the updating of the stiffness and stability matrices with every iteration in the inelastic case.

The determination of the inelastic critical load using this algorithm is described below.

1. The panel is divided into a number of strips and every strip into a number of substrips. An applied stress σ_x is assumed and the elastic properties of the material for

every substrip is determined. The stiffness and stability matrices are generated and the overall matrix [E] assembled.

2. Using Gauss elimination the matrix [E] is transformed to an upper triangular matrix [E*].

3. The number of the negative elements on the leading diagonal of the matrix [E*] is calculated. This number (m) is equal to the number of critical loads exceeded. To obtain the first critical load this number must be zero or one, i.e. the first critical load is the load which changes the number of the negative elements in the leading diagonal from 0 to 1 when this load increases by a small amount.

4. If the number of negative elements m is greater than one, the assumed applied stress must be reduced and if m is less than one the assumed stress must be increased. The stiffness and stability matrices are then regenerated and steps 1 to 4 repeated. In every cycle the assumed stress is compared with the previous one. If the change in the critical load is within the accuracy specified, the current value of stress will be taken as equal to the smallest critical load.

A flow chart for calculating the inelastic critical load for plate structuresis shown in Figure 3.11.

3.10.3 The Determination of Buckling Mode

The previous section has been concerned with the calculation of the smallest critical stress of a plate

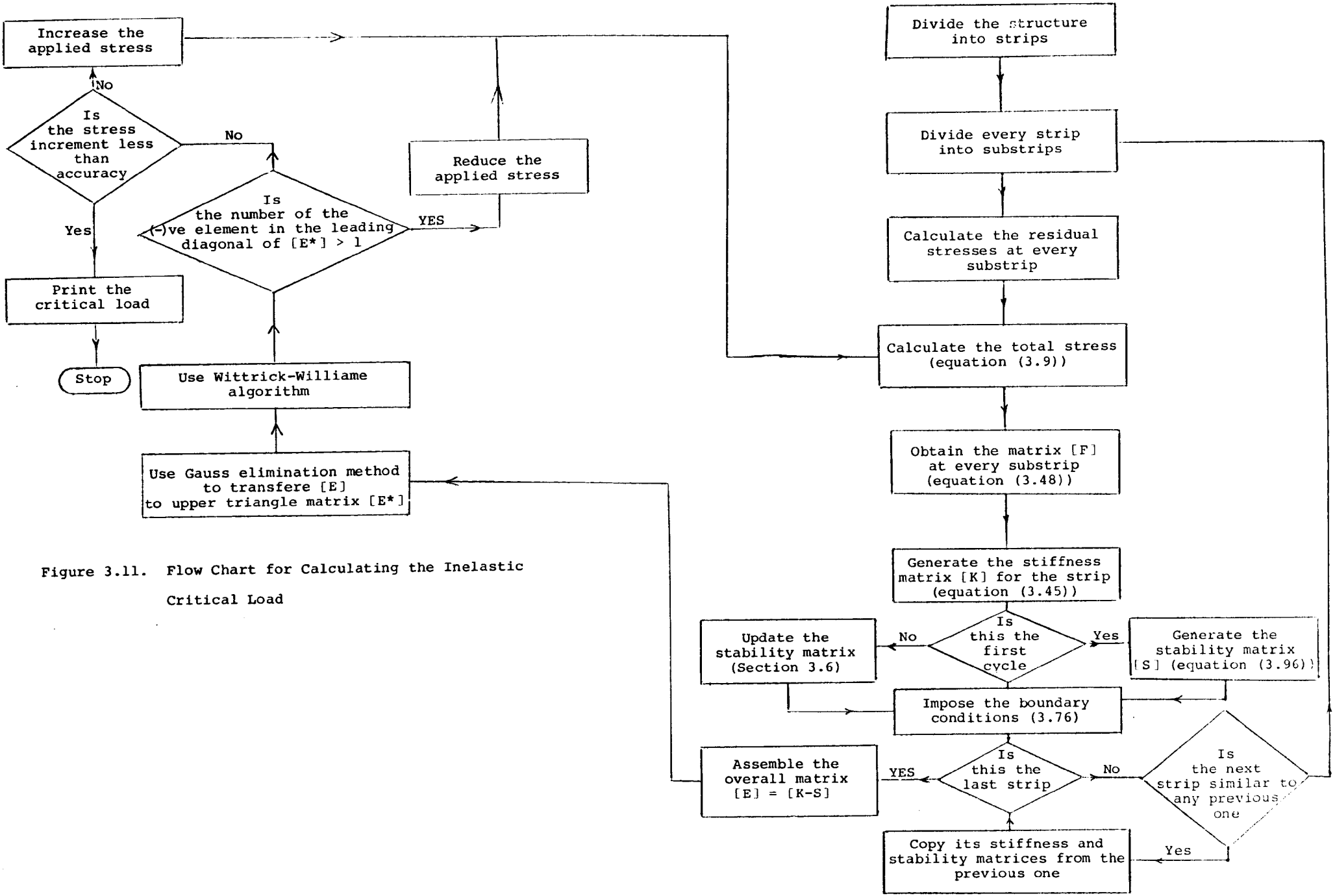

Figure 3.11. Flow Chart for Calculating the Inelastic Critical Load

assembly. However, it is often useful to know the corresponding mode of buckling (eigenvector) and a means of obtaining this will be described in the present section.

After the determination of the critical stress σ_{cr} equations (3.81) and (3.82) become

$$[K - S] \{\delta\} = 0$$

$$[E] \{\delta\} = 0$$

where the stiffness matrix [K] and the stability matrix [S] are both functions of the critical stress. These equations represent a system of simultaneous equations, the solution of which yields the required eigenvector $\{\delta\}$. However, because these equations are all homogeneous, an absolute solution is not possible, and it is therefore necessary to specify arbitrarily one of the elements of $\{\delta\}$. Thus, the eigenvector represents simply the magnitudes of the nodal displacement relative to this specified displacement.

Care must be taken in selecting a suitable displacement to form the base which the values of the eigenvector are determined from since many of the degrees of freedom could be implicitly zero in a given buckled shape. It has been found that problems can be avoided if the element of $\{\delta\}$ to be specified is the one corresponding to the negative element of the leading diagonal of the upper triangulated overall matrix [E*] at the final upper bound to the critical load (22). Note that since the critical stress is

calculated using a trial and error procedure, it will in general be an upper or a lower bound to the absolute value of the critical stress. It is assumed that the convergence procedure has been pursued to such an accuracy that the critical stress exceeds at most one eigenvalue. This implies that only one negative element appears on the leading diagonal of $[E^*(\sigma_{cr})]$ and the corresponding element of $\{\delta\}$ is set to unity.

Because this element may appear any where on the diagonal the following computational procedure can be adopted:

1. Obtain the upper bound to the critical load σ_{cr}.
2. Detect the negative element (ne) of the leading diagonal of the upper triangularized overall matrix $[E^*]$.
3. Generate the overall matrix

$$[E] = [K - S]$$

or

$$\begin{bmatrix} e_{11} & e_{12} & -- & e_{1,ne} & -- & e_{1,n} \\ e_{21} & e_{22} & -- & e_{2,ne} & -- & e_{2,n} \\ -- & -- & -- & -- & -- & -- \\ e_{ne,1} & e_{ne,2} & -- & e_{ne,ne} & -- & e_{ne,n} \\ -- & -- & -- & -- & -- & -- \\ e_{n,1} & e_{n,2} & -- & e_{n,ne} & -- & e_{n,n} \end{bmatrix} \begin{Bmatrix} \delta_1 \\ \delta_2 \\ -- \\ \delta_{ne} \\ -- \\ \delta_n \end{Bmatrix} = \begin{Bmatrix} 0 \\ 0 \\ 0 \\ 0 \\ 0 \\ 0 \end{Bmatrix} \qquad (3.93)$$

4. Prescribe a unit value to δ_{ne} by means of the transformation

$$\begin{bmatrix} e_{11} & e_{12} & -- & 0 & -- & e_{1,n} \\ e_{21} & e_{22} & -- & 0 & -- & e_{2,n} \\ -- & -- & -- & 0 & -- & -- \\ 0 & 0 & 0 & -e_{ne,ne} & 0 & 0 \\ -- & -- & -- & 0 & -- & -- \\ e_{n,1} & e_{n,2} & -- & 0 & -- & e_{n,n} \end{bmatrix} \begin{Bmatrix} \delta_1 \\ \delta_2 \\ -- \\ \delta_{ne} \\ -- \\ \delta_n \end{Bmatrix} = - \begin{Bmatrix} e_{1,ne} \\ e_{2,ne} \\ -- \\ e_{ne,ne} \\ -- \\ e_{n,ne} \end{Bmatrix}$$

5. Solve this linear system of equations (3.94) to obtain the required eigenvector.

3.11 The Residual Stresses

Many structural members, such as plate girders and box girders, are fabricated by welding plates along their longitudinal edges. The metal around the welds in these structures is stressed up to yield in tension. The rest of the section must be in a state of compression (residual compressive stress σ_r) in order to preserve longitudinal equilibrium (108, 109). This residual stress is due to the longitudinal shrinkage of the welds on cooling. The residual stresses can be introduced as an imperfection or as additional stresses on the panel (59). In this work it is assumed that the residual stresses act as additional stresses in the direction of loading (longitudinal direction only).

The slenderness ratio of the panel, the size, method and type of welding (continuous or intermittent) and the treatment process all have an effect on the residual stresses (56-58). The shape and the amplitude of the post-welding distortions of plates are dependent upon the welding process and the dimension of the plate. The distortion increases with increasing weld size, which is a function of the plate thickness. The post welding distortions are a function of the transverse shrinkage of the edge welds (108). The compressive residual stresses due to longitudinal shrinkage will increase this distortion. There are three procedures for straightening the panel to overcome these distortions. The effect of the three methods-localized heating, clamping of some parts of the panel and mechanical loading - on the residual stress have been examined by Horne et al (56-58).

There are many assumed patterns for the distribution of the residual stresses in plate structures (21, 60, 96, 109) but in this work the idealized pattern shown in Figure 3.12 will be used.

3.12 The Computer Program

A program was written to calculate the inelastic critical load for stiffened panels, rolled sections or box columns. The routines of the program perform the following functions.

1. Read and print the input data.
2. Generate the substrips and determine the residual stresses.
3. Obtain the elastic properties of the material.
4. Generate the stiffness matrix for each strip.
5. Generate the stability matrix for each strip.
6. Introduce the geometric boundary conditions.
7. Transform the stiffness and stability matrices if required.
8. Assemble the overall matrix.
9. Determine the first critical load.
10. Print the results.

3.12.1 Generate the Substrips and Obtain the Residual Stress

The strip is divided into a number of substrips - up to 30 - dependent on the accuracy required from the numerical integration. The program generates the position of the strip - and hence each substrip - relative to the panel. From the assessed pattern of residual stress, the value of the residual stresses at each substrip node can be calculated and stored. The total stress will then be

$$\sigma_x(i) = \sigma(i) + \sigma_r(i) \tag{3.95}$$

where $\sigma_x(i)$ is the total stress at substrip node (i),

$\sigma(i)$ is the applied longitudinal stress at substrip node (i),

$\sigma_r(i)$ is the residual stress at substrip node (i).

3.12.2 Obtain the Inelastic Properties of the Material

Knowing the value of the total stress at every substrip node, the material properties such as tangent modulus E_t, secant modulus E_{sec} and effective Poisson's ratio can be obtained from equation (3.22), (3.24) and (3.25) respectively. The elasto-plastic matrix [F] (equation (3.48)) is then generated at every substrip node.

3.12.3 Generate Strip Stiffness Matrices

To generate the stiffness matrix of a strip equation (3.45) will be used. Because the width of individual strips is not constant in most cases, a routine to form the shape function for any strip width is used. It is clear from the stiffness matrix equation that the first and the second order differentiation of the shape functions are required. A routine for differentiation of the equation presented in the element "ii" of any vector such as {X} has been written. A flow chart for the generation of the stiffness or stability matrices of a strip is shown in Figure 3.13.

The generated stiffness matrix will be stored. The next strip will be compared with the previous strip. If both strips have similar conditions, such as geometry, residual stresses and applied stresses, the same stiffness matrix will be used for the new strip. If any condition is different, a new stiffness matrix will be generated as

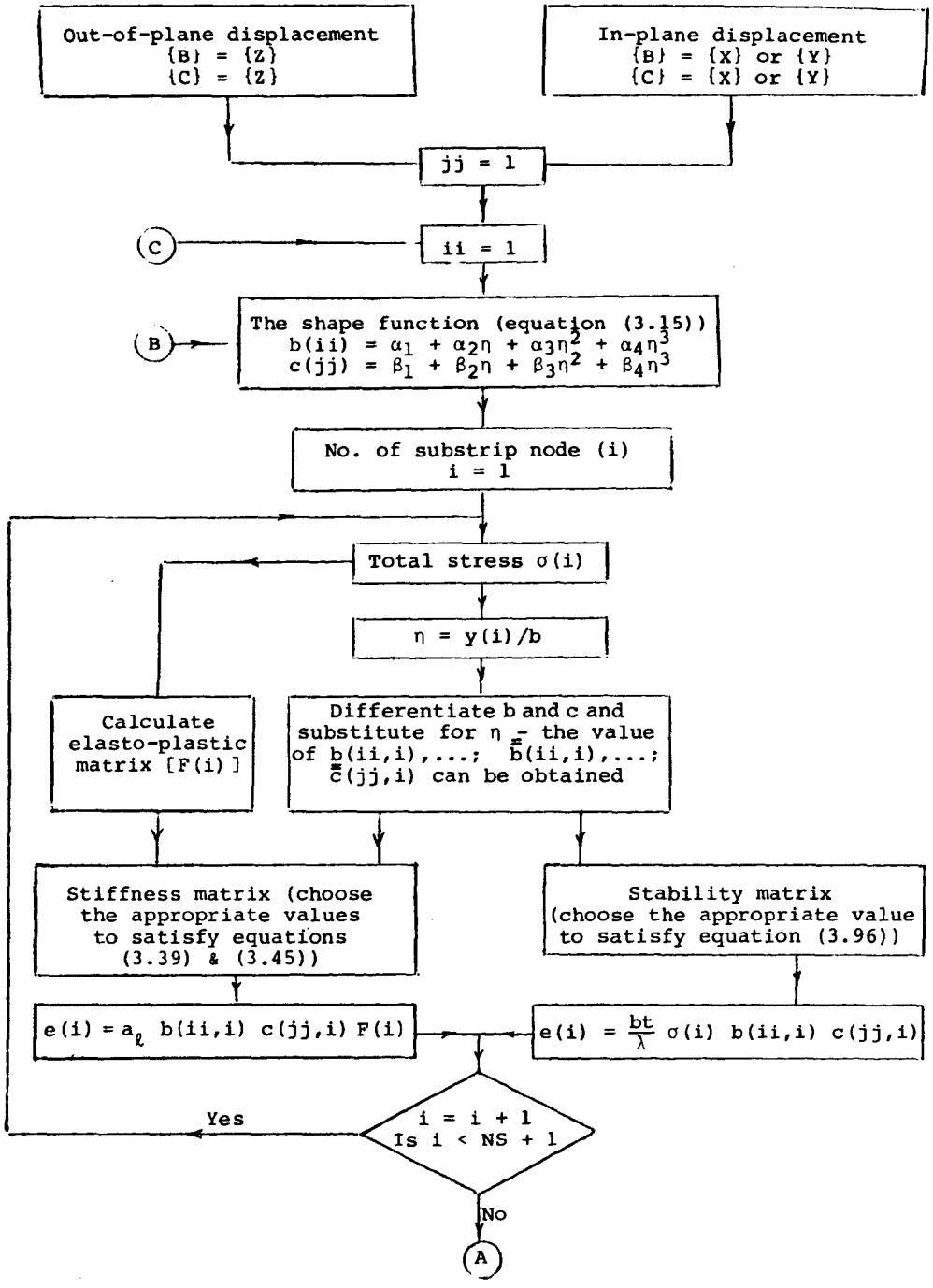

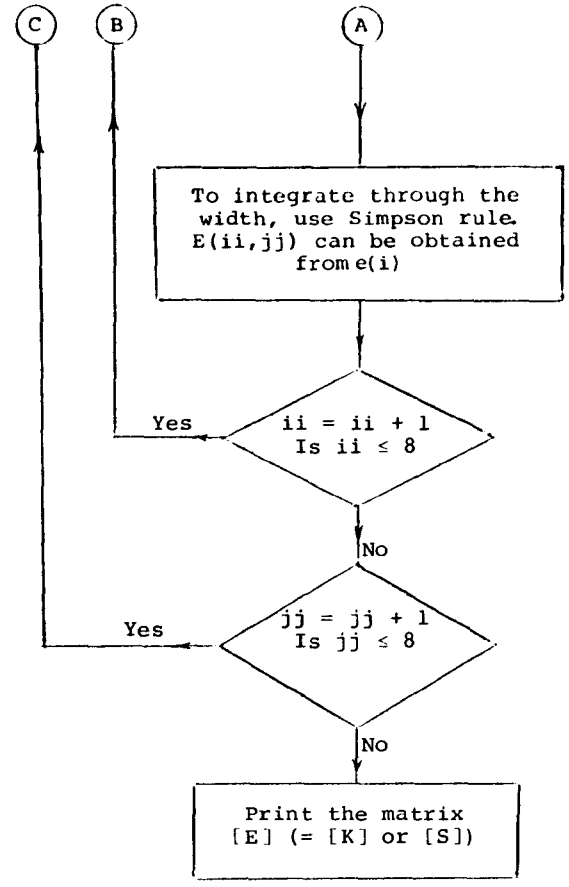

Figure 3.13. Flow Chart for the Generation of the Stiffness and the Stability Matrices

described above. So every new strip will be checked with all the previous strips before deciding whether stiffness matrix is to be copied from any of the existing stiffness matrices or generated as a new one.

3.12.4 Generate Strip Stability Matrices

The total stress at every substrip is calculated from the equation

$$\sigma_x(i) = \sigma(i) + \sigma_r(i)$$

The stability matrix is given by

$$[S] = \frac{bt}{\lambda} \int_{-.5}^{.5} \sigma_x (i) \, [\{x\} \{X\}^T + \{Y\} \{Y\}^T + \{Z\} \{Z\}^T] d\eta \tag{3.96}$$

A flow chart for the generation of the stiffness and stability matrices is shown in Figure 3.13. The stability matrix will be stored. If the next strip is similar to the previous one the stability matrix will be copied otherwise it will be generated as described.

3.12.5 Impose the Geometric Boundary Conditions, Assemble the Overall Matrix and Determine the Smallest Critical Load

The boundary condition will be considered for every strip by checking the two edges. If the first edge is

free or continuous the routine will check the second edge and if that too is free or continuous the routine will do nothing and the strip stiffness and stability matrices will not change. If one edge is hinged, the diagonal element of the stiffness matrix corresponding to the out-of-plane deflection will be replaced by a very high value such as 10^{30}. The corresponding element in the stability matrix will be replaced by zero. If the edge is fixed not only the out-of-plane deflection but also the diagonal elements corresponding to the combined rotation will be modified as before.

If the angle between the panel global axes and the strip local axes is β the stiffness and stability matrices must be transformed. A routine has been written to transform these matrices using the equation

$$[K] = [R]^T [\bar{K}] [R]$$

The transformed stiffness and stability matrices are used to assemble the overall matrix. This overall matrix is transformed to an upper triangular matrix using Gauss elimination. The Wittrick-Williams algorithm is then used to determine the critical load. If the change in the assumed stress is within 0.1% the program will terminate and print this value as the critical load.

CHAPTER 4

COMPARISON BETWEEN THE THEORY AND PREVIOUS WORK

4.1 Introduction

In order to establish to what level of accuracy the finite strip method can be used to predict the failure load of plate structures, a number of comparisons have been made with previously published results. Before presenting these, however, it is necessary to evaluate the number of strips into which the structures should be divided in order to achieve a reasonable level of accuracy. Furthermore, where the stress varies across the plate width - and the elastic properties are therefore not constant - the number of substrips to be used in the numerical integration for the internal virtual work must be assessed.

This checking procedure has been carried out in stages, each of which are described in detail in the following sections. The first stage was the comparison with established results for the elastic buckling of a rectangular plate, followed by a similar study for plate assemblies - in particular stiffened panels.

The next stage was to check the nonlinear parts of the current method, and this again was done first for isolated plates, and then for plate structures, including those with residual stresses.

Unfortunately some of the published work on buckling of plate structures is not directly suitable for comparison, but these points are discussed more fully where applicable.

4.2 Elastic Buckling Behaviour of Plate Structures

4.2.1 Elastic Buckling of Isolated Plates

The stability of rectangular plates has been thoroughly studied by many authors and represents an ideal starting point for assessing the accuracy of the current method. This problem has been solved for various boundary conditions and for loading conditions including uniform compression, pure bending and combinations of the two (1, 3, 4). Although the present program can be used for all such cases, it was checked first for the simple case of a rectangular plate under uniform compressive stress. Two restraint conditions were considered along the two longitudinal edges - simply supported and clamped. The wavelengths used for obtaining the critical stresses were those used in the exact solution. A number of solutions were obtained with the plate divided into different numbers of strips between 1 and 8. Although direct integration could be used for this simple case, the more general method of numerical integration was used, with every strip divided into four substrips. For this simple case the number of substrips should have negligible effect on the buckling load. This in itself provided a useful check on

the program, and indeed it was found that with each strip divided into two substrips identical results were obtained.

To use the routines described in Chapter 3, a very high value of yield stress was assumed, so the ratio of the applied stress to yield stress (μ) was negligeably small. Therefore the tangent modulus and secant modulus could be considered as equal to the elastic modulus.

Thus, $\mu = \sigma/\sigma_Y$

and for very high values of σ_Y

$$\mu \simeq 0$$

$$E_t = \frac{E\ (1 - \mu^2)}{(1-2\ C\mu + \mu^2)} \simeq E,$$

$$E_{sec} = \frac{E\ (1 - \mu)}{(1 - C\mu)} \simeq E, \text{ and}$$

$$\nu = \nu_p - (\nu_p - \nu_e)\ \frac{E_{sec}}{E} = \nu_e$$

The buckling coefficients K for simply supported and clamped rectangular plates are given in Table 4.1, where

$$K = \frac{12\ (1 - \nu^2)}{E\ \pi^2}\ \left(\frac{b}{t}\right)^2\ \sigma$$

The results compared very well with Plank's results (76), the small difference between the two being possibly due to a higher accuracy used by Plank.

It appears from Table 4.1 that an error of about 0.2% compared with the exact critical stress will arise if the rectangular plate is divided into two strips. Considering the two important approximations which are made in the remainder of this work, this level of accuracy can be considered quite acceptable. The first of these approximations is that the structure behaves in an inelastic way according to the assumed stress-strain relationship described in Section 3.4. The second approximation concerns the residual stress pattern which is idealized as described in Chapter 3, and this will generally differ from the actual pattern of the measured residual stresses (56-58, 60). For these reasons, in the present work every component of the structure will be represented by two strips unless otherwise stated.

4.2.2 Elastic Buckling of Stiffened Panels

Skaloud and Kristek (113) have examined the relationship between elastic critical load and stiffener size using folded plate theory. They considered simply supported panels with eight or two longitudinal flat, angle, tee or closed stiffeners under uniform axial compression and analysed both local and overall buckling modes. Their results for the case of eight flat stiffeners are shown in Figure 4.1 together with those predicted by the finite strip method (as curves of critical stress versus the stiffener size h_s/t_s).

Boundary Conditions	No. of strips	Buckling Coefficient (K)	
		Ref. (76)	Present work
Simply Supported Edges $\lambda/b = 1.0$	1	4.2583	-
	2	4.0086	4.0097
	3	4.0017	4.0019
	4	4.0005	4.0006
	6	4.0001	4.0001
	8	4.0000	4.0000
	Exact result (2)	4.000	
Built in edges $\lambda/b = 0.661$	2	7.2261	7.2597
	3	7.0280	7.0348
	4	6.9908	6.9930
	6	6.9753	6.9757
	8	6.9724	6.9725
	Exact result (2)	6.9709	

Table 4.1. Elastic buckling of flate plate

For overall buckling ($\lambda/b = 4.5$), agreement between the two methods is good, but the finite strip results for local buckling ($\lambda/b = 1$) of panels with stiffeners with a depth to thickness ratio $h_s/t_s < 8$ are considerably lower than those of reference (113). This is because of interaction between local and overall buckling modes. For

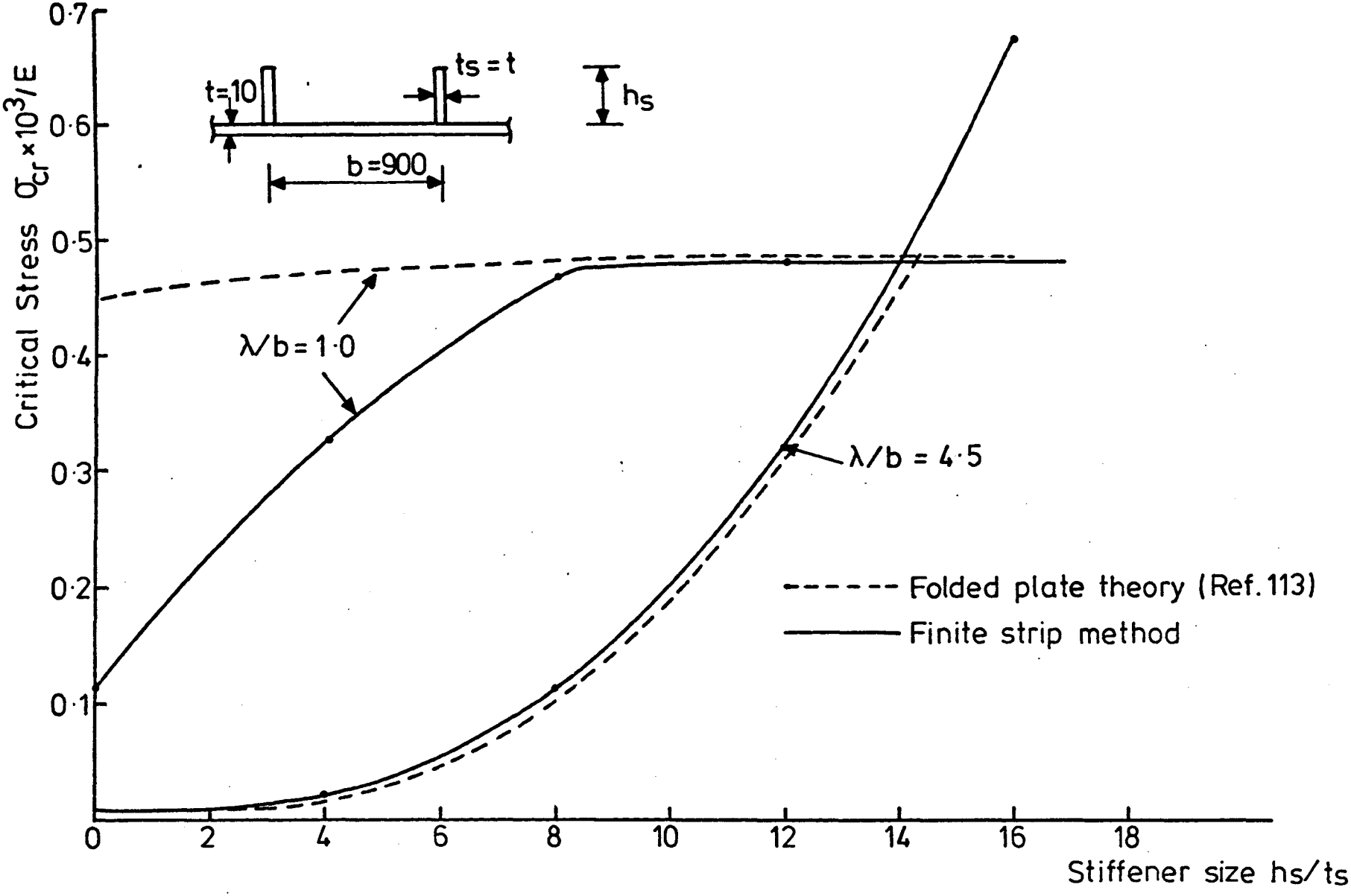

FIG. 4·1 COMPARISON BETWEEN THE FINITE STRIP AND FOLDED PLATE RESULTS.

small stiffener sizes the assumption that for local buckling the longitudinal lines at the stiffener-plate connections remain straight is unrealistic. Whilst the method used by Skaloud and Kristek imposed such a restriction, the finite strip method described here is more general, and because in-plane destabilising effects are included, full interaction between buckling modes is accounted for.

The intersection of the overall and local buckling curves may be considered as defining the optimum size of the stiffeners (113), the increase in the local buckling stress being very small above this "optimum" size.

Skaloud and Kristek found that the behaviour of a plate fitted with two stiffeners was similar to the one fitted with eight flat stiffeners.

A point to note is that the folded plate theory of reference (113) is entirely elastic. If typical values for steel of elastic modulus E = 210000 N/mm^2 and yield stress σ_Y = 240 N/mm^2 are assumed, it is clear that the critical stress does not exceed 0.5 σ_Y, well below the limit of proportionality, and hence the assumption of elastic behaviour is justified.

It would appear from this comparison that the computer program based on the finite strip approach (Chapter 3) is capable of analysing accurately the buckling behaviour of plate assemblies within the elastic region.

4.3 Inelastic Buckling Behaviour of Rectangular Plates

4.3.1 Plate Buckling Curve-German Design Rules

After the program had been checked for obtaining the elastic critical load of a rectangular plate and plate assembly, it was used to investigate the inelastic behaviour of isolated plates to check the present non-linear approach. An initially perfectly flat, simply supported square plate under a uniform longitudinal compressive stress was considered. No residual stresses were included and the stress-strain relationship given in Chapter 3 was assumed.

The plate was divided into four strips and instead of direct integration which is possible for this simple case of uniform stress, the more general method of numerical integration was used to obtain the stiffness and stability matrices, every strip being divided into four substrips for this purpose.

To revise the German Standard for Stability Problems DIN 4114 and to prepare a new edition, Scheer et al (111) proposed a quadratic parabola as a transition curve between the elastic buckling curve and the squash line corresponding to $\sigma_{cr}/\sigma_Y = 1.0$ (Figure 4.2). This transition curve was established by comparing the following formulae (111):

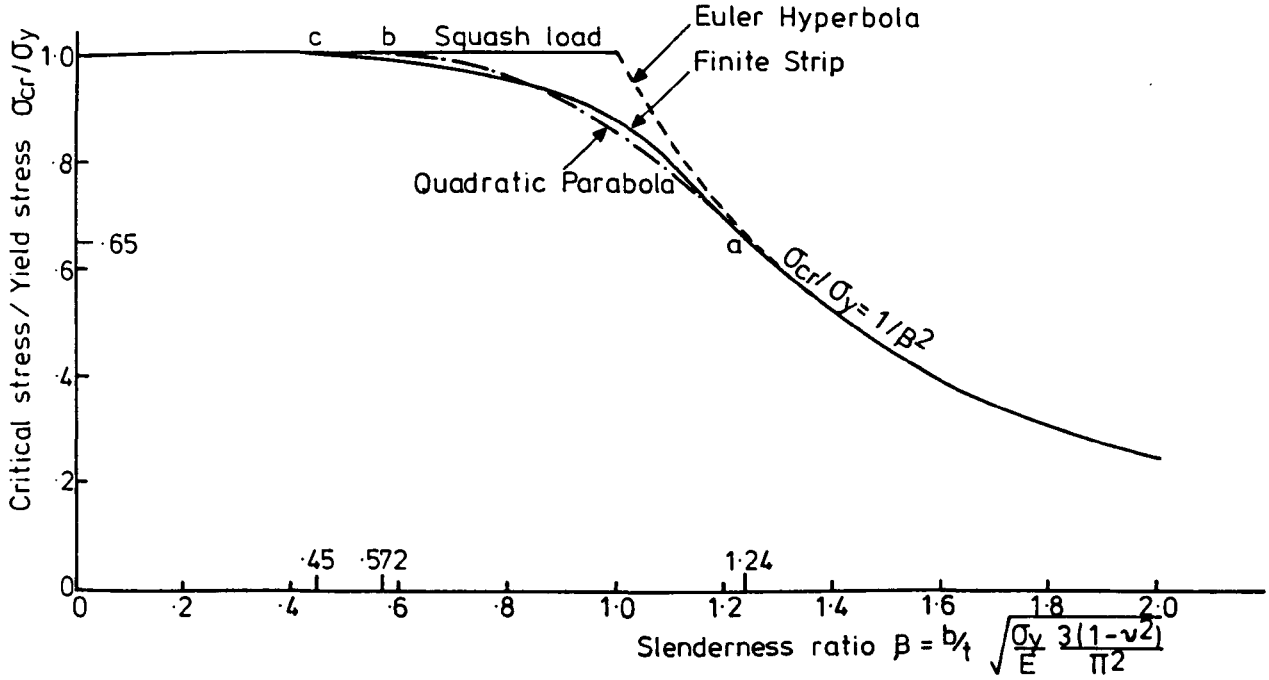

FIG. 4·2. PLATE BUCKLING CURVE (COMPARISON BETWEEN FSM AND QUADRATIC PARABOLA)

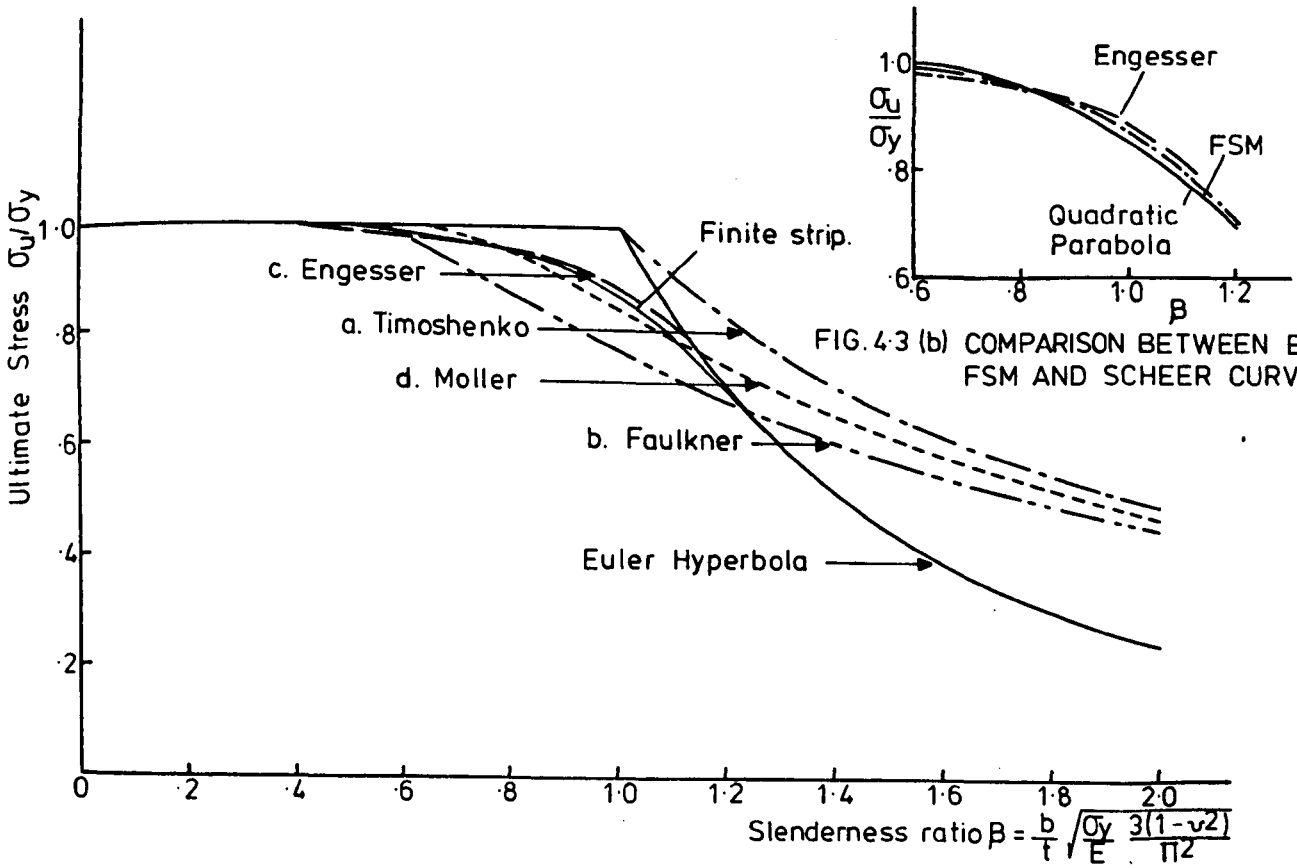

FIG. 4·3 (b) COMPARISON BETWEEN ENGESSER, FSM AND SCHEER CURVES.

FIG. 4·3 (a) BUCKLING CURVES FOR SIMPLY SUPPORTED LONG PLATE.

a. Timoshenko

$$\frac{\sigma_u}{\sigma_Y} = \frac{\pi}{\sqrt{3\ (1 - \nu^2)}} \frac{t}{b} \sqrt{\frac{E}{\sigma_Y}}$$

$$= \frac{1}{\beta}$$

b. Faulkner

$$\frac{\sigma_u}{\sigma_Y} = \frac{2t}{b} \sqrt{\frac{E}{Y}} - \left(\frac{t}{b}\right)^2 \frac{E}{\sigma_Y}$$

c. Engesser

$$\frac{1}{\beta} = \sqrt{\frac{\sigma_u}{\sigma_Y}} \left[0.5 + \frac{0.1}{\sqrt{0.04 - (\sigma_u/\sigma_Y - 0.8)^2}}\right], \sigma_u/\sigma_Y \geq 0.8$$

d. Möler and Donat

$$\frac{\sigma_u}{\sigma_Y} = \left[1 - \frac{0.148}{\beta^2}\right] \frac{1}{\beta}$$

Each of these curves is plotted in Figure 4.3(a) together with the results obtained using the inelastic finite strip approach. It is clear that for a slender plate the curves a, b and d are higher than the finite strip and this may be due to neglecting the post-buckling effect in the present approach.

The finite strip method, in the elastic range ($\beta > 1.25$), gave a curve of critical stress versus slenderness which coincides exactly with the Euler curve as shown in Figure 4.2. The finite strip results for the inelastic range are shown by the solid curve ac. These compare very favourably with the quadratic parabola proposed by Scheer et al (111). The tangent of this transition curve is equal to the tangent of the Euler hyperbola at the point $\sigma_{cr}/\sigma_Y = 0.65$; the vertex of the curve corresponds to the ordinate $\sigma_{cr}/\sigma_Y = 1$. The difference between the two curves is more marked at the lower end where Scheer et al assume a starting point of $\beta = 0.572$ compared with a value of about 0.45 given by the finite strip results. It should be noted that as the effects of strain hardening are not considered in either finite strip or Scheer's work the curves start as horizontal line $\sigma_{cr}/\sigma_Y = 1.0$ at small values of β. Furthermore for slender plates, the post-buckling reserve, which may be many times larger than σ_{cr}, has been neglected in both approaches.

Comparing the Engesser curve for plate buckling with the quadratic parabola, Scheer et al found that the latter is lower for values of slenderness ratio β about 1.0 (Table 4.2). On the basis of some unspecified test results they decided that this reduction was more correct. It is of interest to note that the finite strip results fall between these two curves - Scheer and Engesser - in the range of β between 0.8 and 1.2 (Figure 4.3b). At $\beta = 1.0$ the ratio of

the critical stress to the yield stress - σ_{cr}/σ_Y - is 0.85, 0.873 and 0.890 where the calculations were based on the quadratic parabola, finite strip and Engesser curve respectively.

The above comparison for an isolated plate in the inelastic range would suggest that the current method of allowing for nonlinear material behaviour is sound.

Formula or approach		σ_{cr}/σ_Y
FSM	2 strips	0.874
	3 strips	0.873
	4 strips	0.873
Ref. (111)	Faulkner	0.769
	Moller	0.852
	Scheer	0.856
	Engesser	0.890
	Timoshenko	1.000

Table 4.2. Inelastic buckling of simply supported plate with $\beta = 1.0$

4.3.2 Inelastic Buckling of Rectangular Plates With Residual Stress (25)

To check the finite strip approach when residual stress is included a comparison has been made with some test

results obtained at Cambridge University (25). In the previous section it was assumed that the plate was initially stress free and direct integration might be used to obtain the stiffness and the stability matrices. For a residual stress other than zero, the strip has to be divided into a number of substrips. The effect of this number on the buckling strength of plates has also been studied.

For a square box section the local buckling can be modelled as a simply supported plate (25) with (4n + 4) degrees of freedom, where n is the number of strips. Generally, in the analysis of local buckling of box columns four models can be investigated (Figure 4.4). The first is a complete box section with 16n degrees of freedom where n is the number of strips on one side only. This model is necessary where there is no symmetry in geometry or in loading conditions. For symmetrical cross-sections, only one half of the cross-section - as shown in Figure 4.4(b) - need be used. The number of degrees of freedom will be reduced to (8n + 4). If the section is under pure axial compression mode C which is based on the very wide panel approach (112) can be used. The displacement of the nodes a and c (Figure 4.4(c)) are identical so the total degrees of freedom is only (8n).

In comparing the current results with the published test results (25) models A, C and D have been used and in each case the critical stress was the same , confirming

that the box column test results can be used for comparison with a simply supported rectangular plate.

4.2.3.1 Division of Strips into Substrips - Convergence Tests

The failure stress of a square box column loaded in axial compression has been analysed using different numbers of strips and substrips. The residual stress pattern shown in Figure 4.5 has been assumed, and two levels of residual stress - $\sigma_r = 0.1\ \sigma_Y$ and $0.3\ \sigma_Y$ where σ_Y is the yield stress - have been considered. The results are shown in Table 4.3 with the results of both the theoretical and experimental work carried out at Cambridge University for identical box columns with measured residual stresses between $0.08\ \sigma_Y$ and $0.13\ \sigma_Y$.

It is clear from Table 4.3 that convergence is quite rapid and that with each component divided into two strips, and six substrips used for the numerical integration, the results appear to be satisfactory. However it has been found that in some circumstances a finer subdivision is necessary, and as this involves little additional computational effort, ten substrips have been used throughout this work wherever the stress is varying across the strip width.

Comparison of the finite strip results and the work undertaken at Cambridge University will be discussed more fully in the following section.

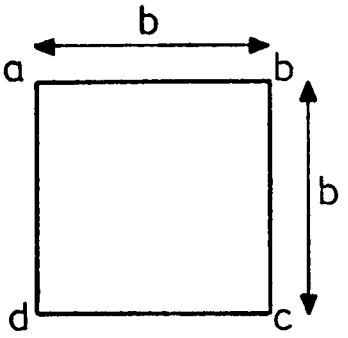

(a) Model A.

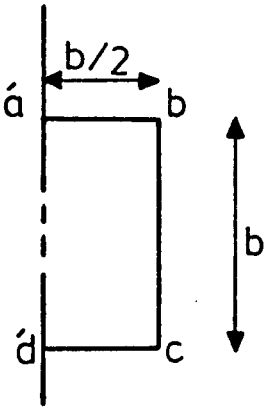

(b) Model B.

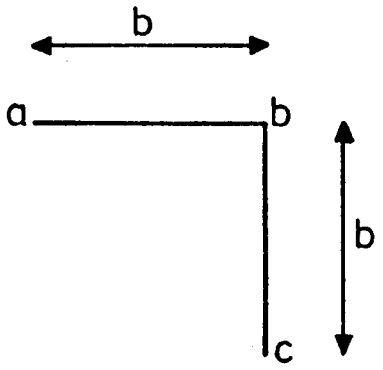

(c) Model C.

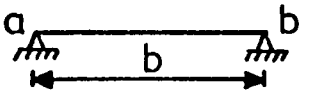

(d) Model D.

FIG. 4·4. MODELS FOR BOX COLUMN.

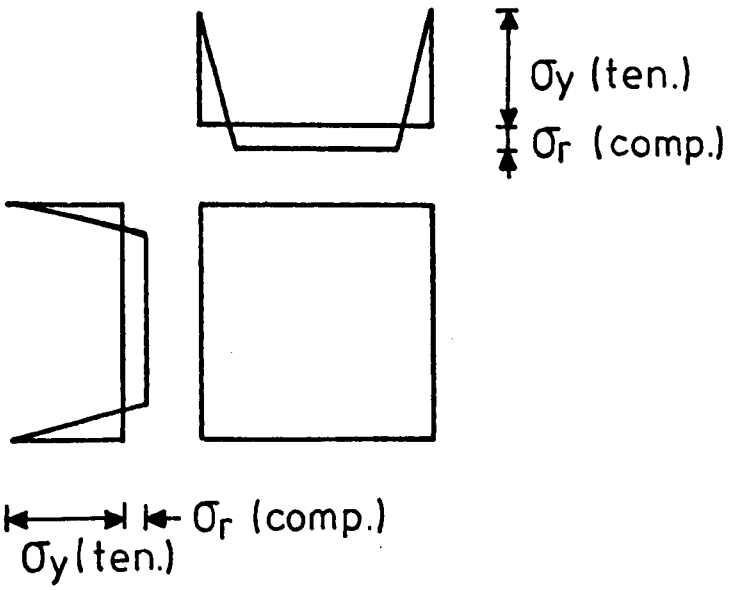

FIG. 4·5. ASSUMED RESIDUAL STRESS PATTERN.

No. of strips	No. of substrips	Critical stress/Yield stress σ_{cr}/σ_Y					
		β = 1.26		β = 0.92		β = 0.79	
		$\frac{\sigma_r}{\sigma_Y}$ = 0.1	0.3	0.1	0.3	0.1	0.3
1	4	0.5523	0.3515	0.8330	0.6329	0.8622	0.6621
	6	0.5579	0.4483	0.8328	0.6691	0.8611	0.7675
	10	0.5590	0.4234	0.8318	0.6581	0.8598	0.6899
	20	0.5642	0.4179	0.8356	0.6555	0.8637	0.6854
	30	0.5631	0.4164	0.8351	0.6547	0.8632	0.6841
2	4	0.5226	0.3774	0.8225	0.6365	0.8553	0.6642
	6	0.5252	0.3650	0.8245	0.6341	0.8570	0.6628
	10	0.5257	0.3690	0.8238	0.6360	0.8543	0.6645
	20	0.5254	0.3689	0.8239	0.6365	0.8547	0.6652
	30	0.5253	0.3692	0.8196	0.6365	0.8547	0.6650
3	4	0.5242	0.3642	0.8241	0.6339	0.8568	0.6627
	6	0.5253	0.3695	0.8237	0.6368	0.8562	0.6652
	10	0.5240	0.3671	0.8232	0.6354	0.8543	0.6640
	20	0.5243	0.3685	0.8191	0.6364	0.8543	0.6633
	30	0.5242	0.3683	0.8191	0.6362	0.8543	0.6628
4	4	0.5257	0.3708	0.8240	0.6366	0.8564	0.6644
	6	0.5243	0.3693	0.8235	0.6365	0.8543	0.6645
	10	0.5242	0.3656	0.8234	0.6347	0.8543	0.6624
	20	0.5240	0.3658	0.8234	0.6341	0.8543	0.6624
	30	0.5240	0.3658	0.8233	0.6341	0.8543	0.6624
Average test result		0.5600	-	0.7720	-	0.8590	-
Theo. results (25)		0.5800	-	0.7330	-	0.8400	-
No. of specimens		2	-	5	-	3	-
Measured σ_r/σ_Y		0.0800	-	0.1200	-	0.1300	-

Table 4.3. Convergence with box column test results

4.2.3.2 Comparison With the Available Results

A considerable amount of experimental work has been performed at Cambridge University (25-30) to study the maximum strength of short, square, welded steel box columns. Some tests were done on "as-welded" and others on stress-relieved specimens. The results for all tests, which included specimens with measured compressive residual stresses between 0.0 and 0.25 σ_Y, are compared in Figure 4.6 with the finite strip solution for σ_r/σ_Y = 0.0, 0.1 and 0.2. In this analysis every side of the box column was divided into two strips and every strip was divided into ten substrips. For columns with a slenderness ratio $\beta < 1.4$ the theoretical predictions are generally in good agreement with the test results. For columns with more slender plating the test results tend to be a little higher than the theoretical predictions and this may be due to post-buckling effects which are not included in this analysis. Similarly at low values of β, some of the test results are underestimated by the current theory, possibly due to the influence of strain hardening. This last effect could in fact be included in the current analytical treatment by suitable modification of the stress strain curve.

It is of interest to observe that the buckling curve for $\sigma_r = 0.1\ \sigma_Y$ is horizontal for columns with stocky plating - $\beta < 0.35$. The difference between this constant strength curve and the crushing strength is equal to the level of the residual stress. In this range the curve is

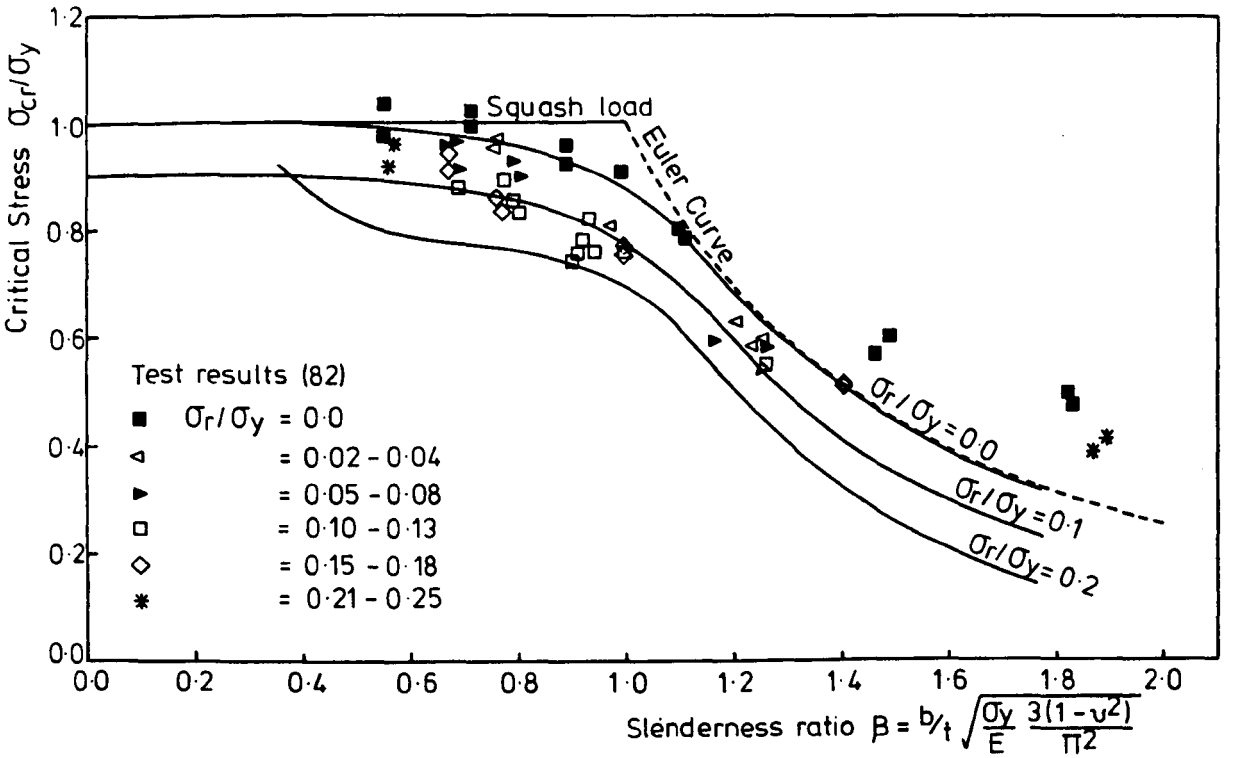

FIG. 4·6 FINITE STRIP RESULTS COMPARED WITH CAMBRIDGE BOX COLUMN TEST RESULTS.

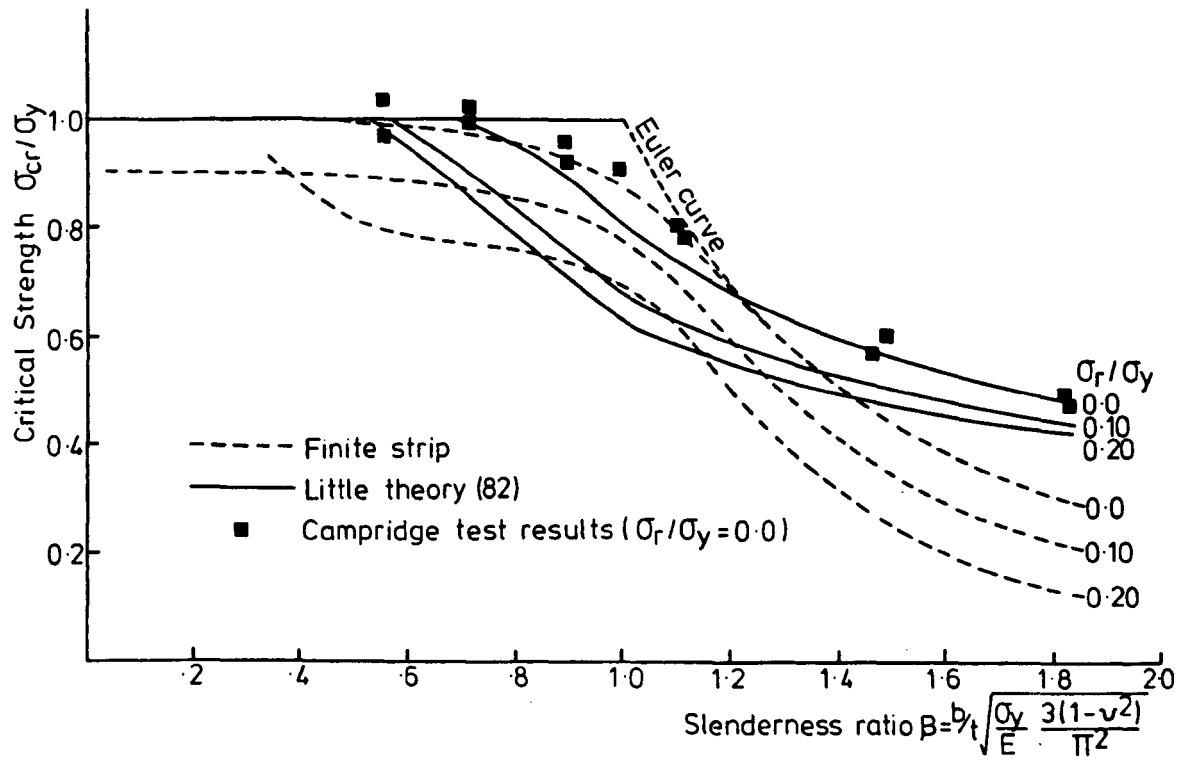

FIG. 4·7 COMPARISON WITH LITTLE THEORETICAL CURVES FOR LOCAL BUCKLING OF SQUARE BOX COLUMN.

lower than the corresponding curve for $\sigma_r = 0.2\ \sigma_Y$ - the strength of stocky columns increases as the residual stress increases. This may be due to the fact that the central area of the plate subjected to compressive stresses is larger in the case of lower residual stress. A similar increase in strength was observed by Little in his tests on eccentrically loaded columns (82).

In addition to his experimental work, Little developed curves for local buckling of square box columns based on the Perry formula using the available experimental and theoretical data. For a slender column with $\beta > 1$, he used an empirical expression to obtain the post-buckling strength. His theoretical curves, the finite strip results for different residual stress levels and the test results for initially stress free columnsare shown in Figure 4.7.

For columns with $\beta > 1.2$ the finite strip results are lower than those predicted by Little's theory and the difference increases as the slenderness ratio β increases. This is because in the current work the post-buckling reserve is ignored.

In the range of slenderness ratios $1.2 > \beta > 0.8$ the finite strip results are greater than those of Little and as the residual stress increases, this difference increases. In this range - for zero residual stress - the test results are in fact closer to the finite strip curve than to Little's theoretical curve.

Again, for columns with relatively stocky plating $\beta < 0.8$, Little's theory predicts higher critical stresses than the finite strip method. This may be due to the early yielding assumed in the present stress-strain relationship (Chapter 3) compared with elastic-perfectly plastic stress-strain material used by Little.

It can be concluded from this comparison that the present approach gives results for inelastic buckling of rectangular plates with residual stress which are generally in good agreement with the test results, confirming the validity of the current work.

4.4 Buckling of Panels Stiffened with Longitudinal Stiffeners

A panel stiffened with longitudinal stiffeners can collapse in two different modes. The first is a plate collapse (local mode) and the second is a stiffener collapse (overall mode). The slenderness ratio of the plate, the rigidity of the stiffener and the eccentricity of the load are three factors which affect the mode of collapse.

Many tests have been carried out to study this effect. Some investigators have measured and recorded the initial imperfections and the residual stresses and these provide a basis for comparison with the present theory. In the following sections the finite strip results will be compared with both test and theoretical results from various sources.

These comparisons are provided to show the capability of the current work for studying the inelastic - local and overall - buckling of plate assemblies with different levels of residual stress.

4.4.1 Inelastic Buckling of Wide Panels (52)

In the following section the finite strip approach is compared with theoretical results based on various plasticity theories. Not only the local buckling - as in the previous section - but also the overall buckling has been considered.

The panel stiffened with flat stiffeners used by Tvergaard et al (52) to study the elastic-plastic buckling of a wide panel (Figure 4.8(a)) has been examined using the current approach. Tvergaard et al (52) considered two cases for the end boundary conditions. The first was a panel simply supported on the two edges on which the loading acts and the second was a panel continuous in the direction of applied compressive load and supported on several transverse supports. The panels were perfectly flat prior to buckling and the residual stresses were assumed to be zero. The local buckling of the plate between two adjacent stiffeners and the overall buckling of the panel as a wide column have been studied for different values of σ_Y/E. In their work, Tvergaard et al included the effect of the material strain hardening.

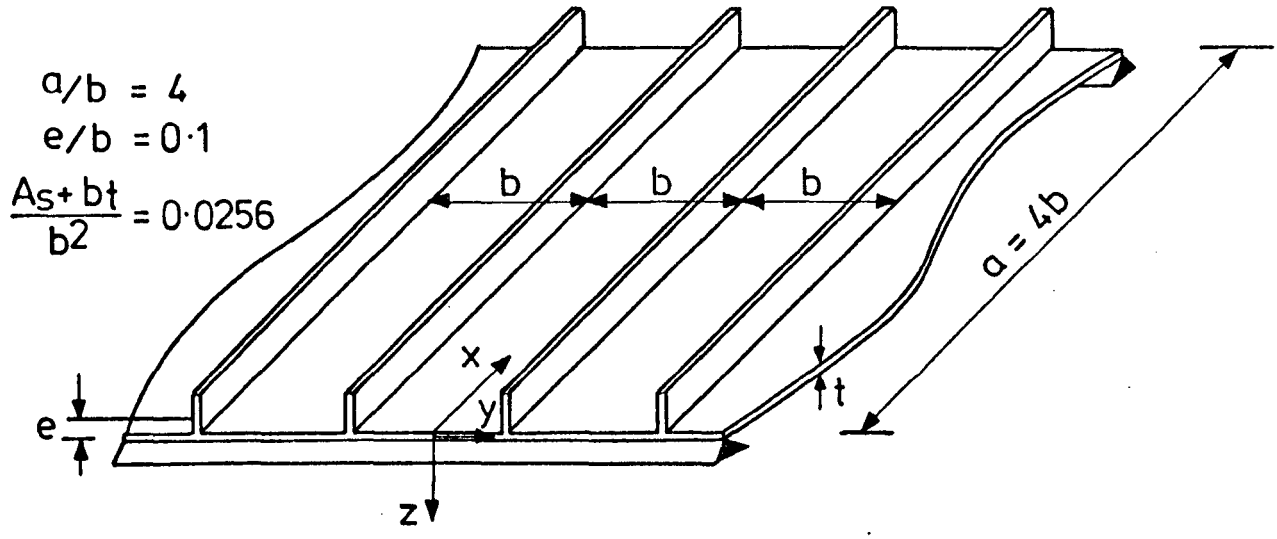

(a) Part of Tvergaard panel (52)

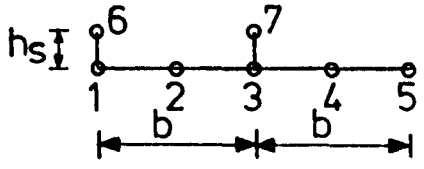

(b) Finite strip local buckling model.

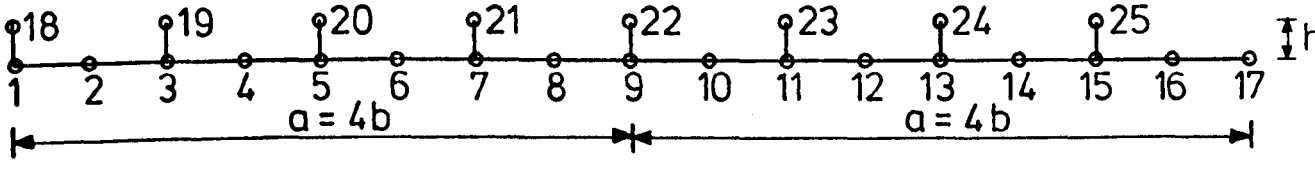

(c) Finite strip overall buckling model.

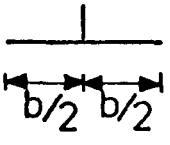

(d) Tvergaard model.

FIG. 4·8. ACTUAL AND MODELED PANEL.

For comparison only the simply supported panels will be considered and the inelastic critical load corresponding to local and overall buckling modes will be calculated. Tvergaard et al found that for wide column buckling (Figure 4.9) the flow theory and the deformation theory gave identical results. The finite strip results for the same mode with $\sigma_Y/E = 0.001$, are about 10% less than Tvergaard's results for a large range of panel geometries α. This underestimation increases to 12.5% and 15% when the yield stress, σ_Y, is increased to 0.0015 E and 0.002 E respectively.

For the local buckling mode (Figure 4.10) the finite strip method - as expected - gives a result somewhat closer to the deformation theory than the flow theory. This is because the present approach is based on the deformation theory. As the ratio of the plate area to the total area (α) decreases the three local buckling curves (Tvergaard's flow and deformation theories and the finite strip results) become closer. The difference between Tvergaard's results and the finite strip results may be due to the following points:

a. The effect of strain hardening which is neglected in the present work (in fact this effect can be included in the current analysis by suitable modification of the assumed stress-strain curve). As α increases - i.e. the panel becomes more stocky - the effect of the strain hardening becomes more significant.

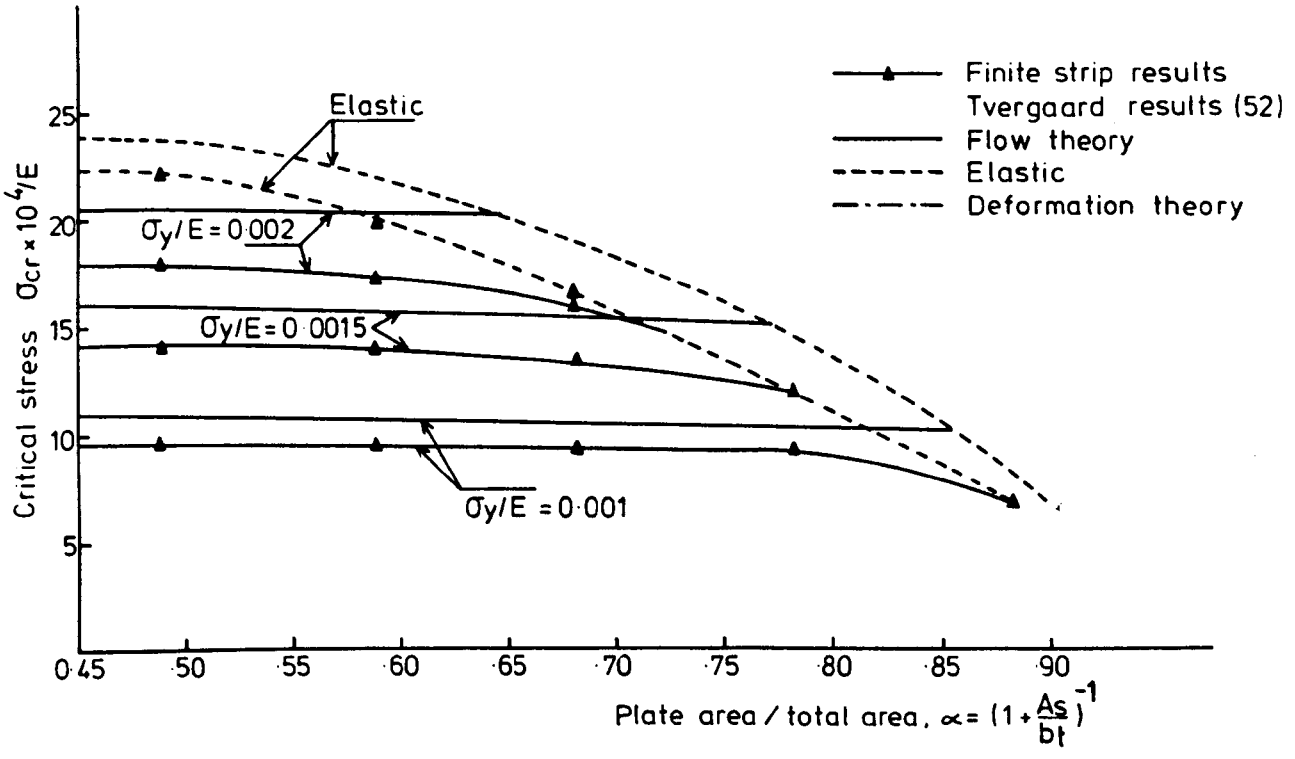

FIG. 4·9. OVERALL BUCKLING OF TVERGAARD PANEL.

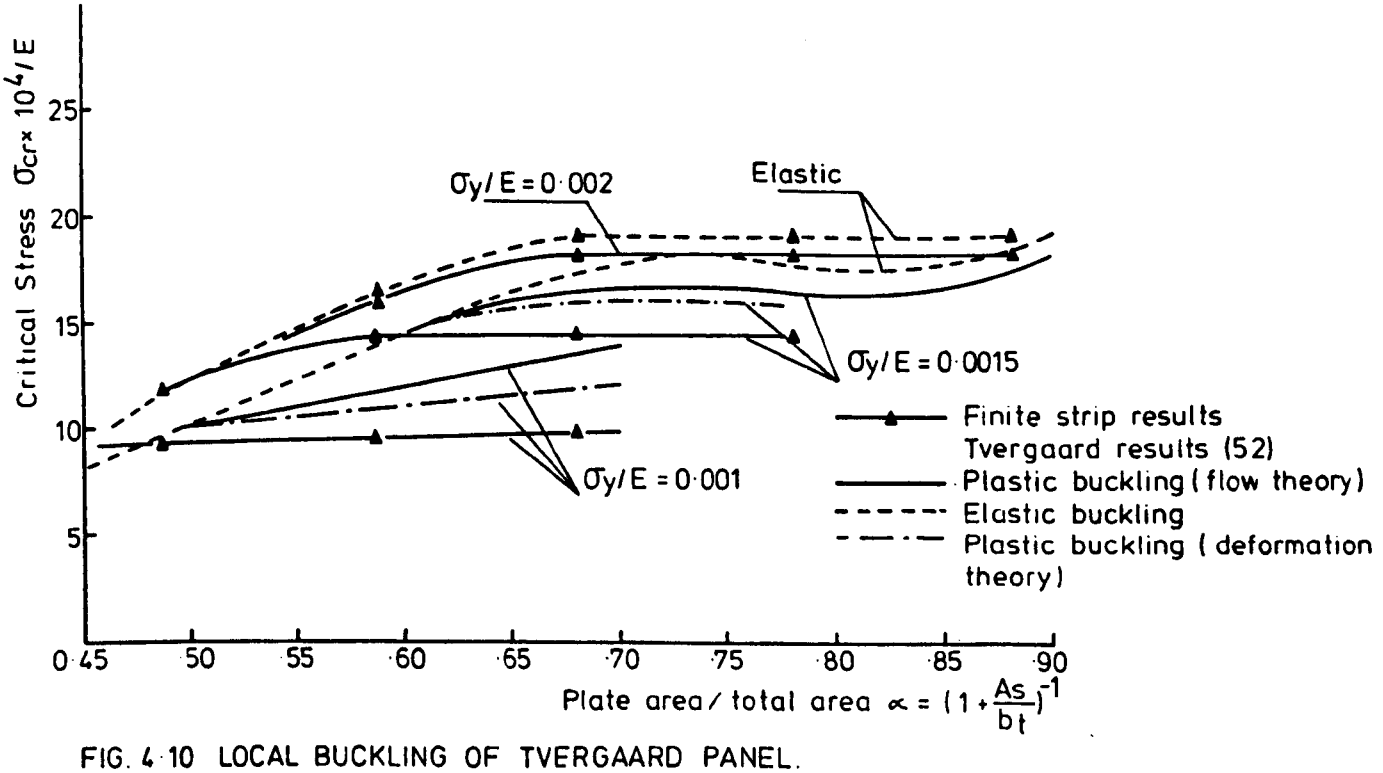

FIG. 4·10 LOCAL BUCKLING OF TVERGAARD PANEL.

b. Tvergaard et al treated the stiffener as a beam with elastic torsional rigidity. In a wide column buckling mode where the stiffeners remain untwisted this is valid, but if the stiffeners twist this approximation leads to an overestimate of the torsional stiffness and hence the critical load. In the finite strip analysis, in any buckling mode, the stiffeners are allowed to distort and to become inelastic and this will contribute to giving a lower critical load than the results obtained by Tvergaard et al.

c. For overall buckling, Tvergaard et al modelled the panel as a pin-ended column thus implying that the out-of-plane buckling displacement at any cross-section is constant. In the current analysis however the panel is treated as a very wide panel (Figure 4.8(b-d)). This means that the out-of-plane buckling displacement is not constrained to be constant and this will also contribute to a lower value of critical stress.

d. The depth to thickness ratio of the stiffeners in the panel is less than 5 for a wide range of α. This ratio is relatively low and a thick finite strip approach (88) may be necessary. The relation between α and h_s/t_s for the panels considered by Tvergaard is shown in Figure 4.11.

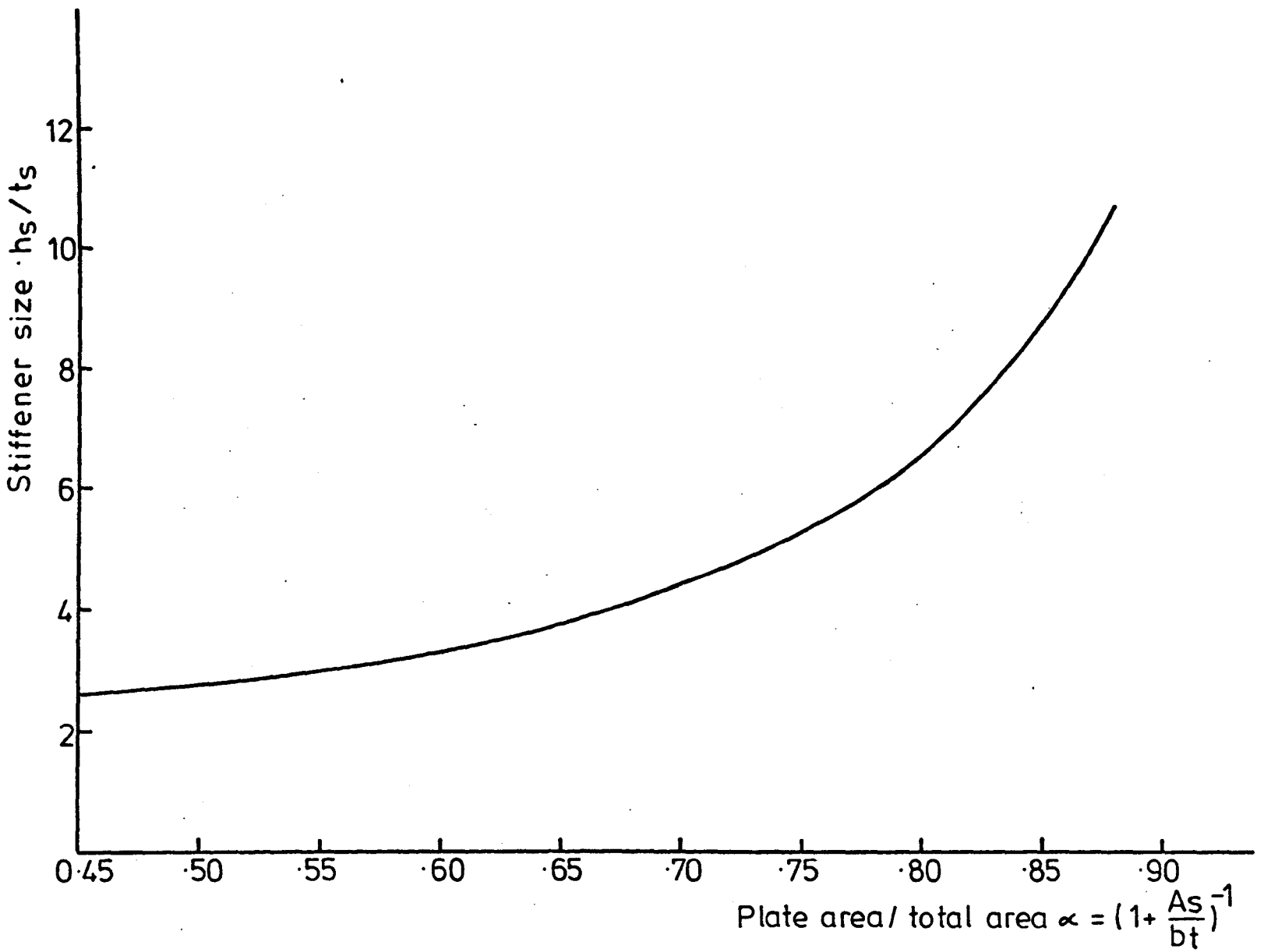

FIG. 4·11. RELATION BETWEEN STIFFENER DEPTH TO THICKNESS RATIO AND AREA OF TVERGAARD PANEL.

4.4.2 Comparison With Experimental Work on Longitudinally Stiffened Panels (54)

In Monash University, panels stiffened with five longitudinal flat stiffeners have been tested (54). The longitudinal edges were allowed to move longitudinally in-plane but the out-of-plane displacements were constrained. The panels were loaded axially and in bending. To compare these test results with the FSM results it has been assumed - as did Horne et al (44) in their theoretical comparison - that the panel can be treated as a very wide panel and the bulb flat stiffeners may be substituted with flat stiffeners having the same area. Murray (54) did not report the values of initial imperfection of the plates or overall imperfection, so it has been assumed that the panels are nominally straight. Only those results for the three panels which were tested under concentric axial load will be discussed.

A further convergence study to examine the effect of the number of strips and substrips on the accuracy was undertaken for one panel and the results are shown in Table 4.4. From this table it is clear that by dividing each plate into two strips each of which is divided into ten substrips, sufficient accuracy is achieved and this will be used for all other panels.

Murray's test results (54), Horne's theoretical results (44) and the finite strip results are shown in Table 4.5. Since the actual residual stresses present in

No. of strips bet. adj. stiff.	No. of sub-strips per strip	Critical stress/yield stress σ_{cr}/σ_Y		
		$\sigma_r/\sigma_Y = 0.1$	$\sigma_r/\sigma_Y = 0.3$	$\sigma_r/\sigma_Y = 0.5$
1	4	0.793	0.609	0.612
	6	0.793	0.659	0.497
	10	0.792	0.648	0.546
	20	0.799	0.644	0.502
2	4	0.622	0.482	0.357
	6	0.624	0.473	0.362
	10	0.624	0.476	0.362
	20	0.624	0.476	0.363
3	4	0.622	0.471	0.361
	6	0.623	0.476	0.363
	10	0.622	0.474	0.363
	20	0.622	0.475	0.363
4	4	0.623	0.477	0.363
	6	0.622	0.476	0.363
	10	0.622	0.475	0.363
	20	0.622	0.475	0.363

Table 4.4. Convergence of the critical load of a wide panel (panel H)

Dimension of the panel		Panel H	Panel M	Panel U
b/t		54	54	63
Stiffener spacing		533.4	266.7	609.4
Plate thickness		9.86	4.93	9.66
Stiffener used		6" x 7.42 lb	-	4" x 4.51 lb
Equivalent stiff. thick		9.6	4.8	8.8
Length of the panel		3450	1725	1700
ℓ/r		75.3		66.6
Yield stress σ_Y		377 N/mm^2	317 N/mm^2	377 N/mm^2
Observed σ_{max}/σ_Y (54)		0.70	0.73	0.59
Manchester theor. $\frac{\sigma_u}{\sigma_Y}$ (44)		0.62	-	0.64
Finite strip σ_{cr}/σ_Y	σ_r/σ_Y			
	0.0	0.71	0.82	0.53
	0.1	0.62	0.73	0.44
	0.2	0.55	0.65	0.35
	0.3	0.48	0.57	0.28
	0.4	0.42	0.50	0.23
	0.5	0.36	0.42	0.18

1. All dimensions are in mm
2. Panel M is half scale of panel H
3. Panel U from Ref. (44)

Table 4.5. Comparison with Monash University Test

each individual specimen were not recorded in reference (54) the pattern of Figure 4.12 has been assumed with calculations being performed for values of σ_r/σ_Y between 0.0 and 0.5. Horne et al (44), ignored the effect of the residual stress although the finite strip results indicate that the strength can be reduced by up to 17% by increasing σ_r/σ_Y from 0.0 to 0.1 (panel U). The finite strip results for panels with residual stress σ_r/σ_Y between 0.0 and 0.1 were in close agreement with the observed results. In all cases, it is clear that the effect of the panel slenderness ratio (ℓ/r) on the strength can be neglected because the failure was due to local buckling of plate between two adjacent stiffeners.

Comparing panels U and H, it is clear that while the plate slenderness ratio β of the first panel (U) is the higher, the panel slenderness ratio (ℓ/r) is less than that for panel H. These two panels failed by local buckling of the plating and hence the slenderness ratio of the plating β rather than ℓ/r is the governing factor. From this, it would be expected that the strength of panel U would be less than that of panel H and indeed the experimental results confirm this. Whilst the results obtained using this finite strip method also demonstrate this, the theoretical results of Horne et al indicate the opposite.

Again, from these convergence and comparison studies it is clear that - with each component of the plate assembly divided into two strips each of which is divided into ten substrips - the results based on the present approach are in good agreement with Murray's test results.

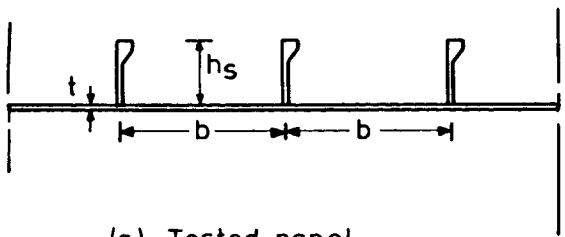

(a) Tested panel.

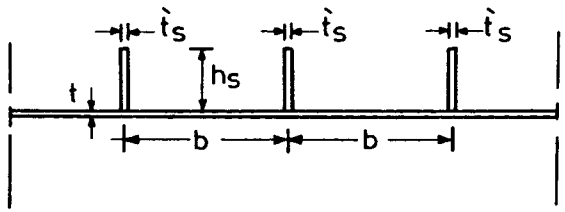

(b) Idealized panel.

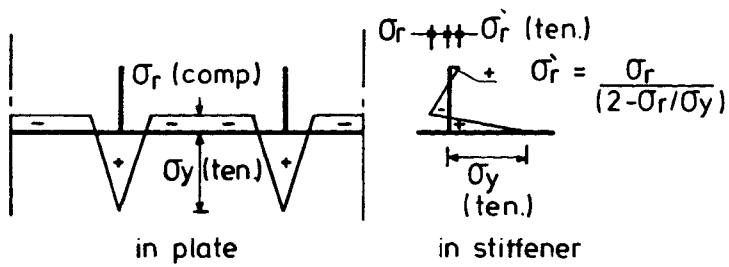

(c) Assumed residual stress.

FIG. 4·12. MONASH PANEL. (54)

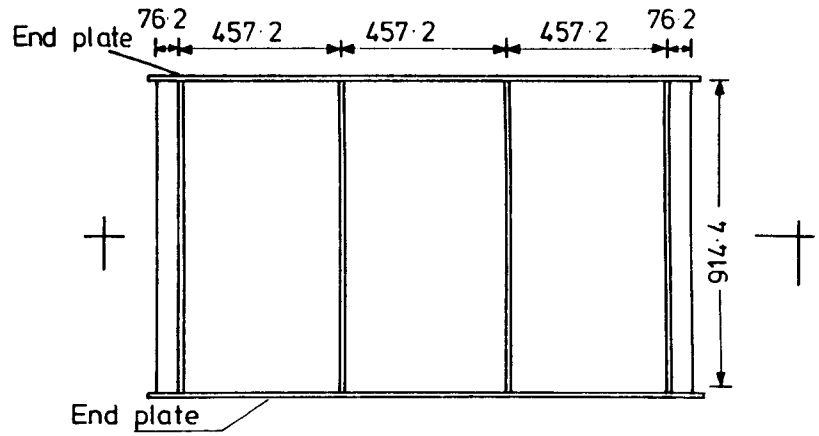

(a) Tested panel.

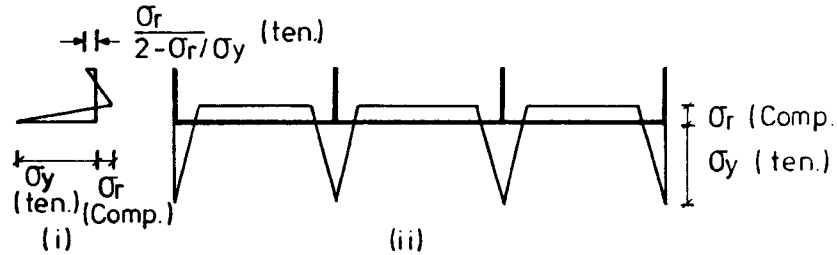

(b) Assumed patterns for residual stresses.
(i) for stiffeners
(ii) for plate

FIG. 4·13. MANCHESTER PANEL (56-58)

4.4.3 Comparison With Experimental and Theoretical Work on Longitudinally Stiffened Panel (56-58)

A series of tests have been carried out by Horne and Narayanan (56-58) on longitudinally stiffened plates (Figure 4.13) under axial load. In these tests not only residual stresses, but also initial imperfections and eccentricity of the applied loading were considered. Some of the results are therefore not suitable as a direct comparison with the current finite strip predictions of critical stress, and only those panels with small imperfections and no eccentricity of loading have been included here.

As a means of comparison the experimental results obtained by Horne and Narayanan have been reproduced in Table 4.6 together with the critical stresses calcuated using the current approach. In determining the finite strip results the actual values of residual stress have been used, and the pattern indicated in Figure 4.13 assumed. Unfortunately the information provided in reference (56-58) gives only the average residual stresses in both the stiffener and the plate and this may lead to some inaccuracy, particularly when detailing the distribution of residual stress within the stiffener.

In studying Table 4.6 some general comparisons can be made. For the four panels 7, A_{23}, E_{23} and C_2 where the measured residual stresses on the plates is high ($\sigma_r/\sigma_Y \geq$

Specimen	7	8	9	D_{12}	D_{22}	A_{12}	A_{23}	E_{12}	E_{23}	C_2
Stiffner size	16 x 152.5	16 x 152.5	9.5 x 152.5	12 x 80	12 x 80	9.5 x 152.5	9.5 x 152.5	12.5 x 76	12.5 x 76	9.5 x 152.5
Measured (plate)	0.410	0.125	0.122	0.132	0.315	0.066	0.424	0.088	0.330	0.386
σ_r/σ_{YP} (stiff)	0.082	0.100	0.100	0.077	0.228	0.025	0.111	0.039	0.046	0.073
b/t	48.0	48.0	48.0	45.7	45.7	70.3	70.3	70.3	70.3	45.7
ℓ/r	37.6	37.6	42.0	92.7	92.7	40.6	40.6	88.1	88.1	44.7
Observed $\frac{\text{ultimate load}}{\text{squash load}}$ (56-58)	0.79	0.85	0.78	0.65	0.60	0.56	0.62	0.48	0.45	0.87
Calculated $\frac{\text{critical load}}{\text{squash load}}$ (FSM)	0.60	0.85	0.83	0.78*	0.66*	0.52	0.31	0.55	0.35	0.60

* Panel buckled in overall mode

Table 4.6. Comparison between Manchester test results and finite strip results

0.32) relative to the other panels, the finite strip method underestimates the test results by about 32% on average. This may be due to the way in which the residual stress pattern has been modelled, and it is worth noting that although the measured value of σ_r in the plate is high, the corresponding value in the stiffener is very low. It is of interest to observe that the difference between the squash load and the calculated critical load for panels 7 and C_2 is approximately equal to the measured residual stresses on the plate. Although Horne and Narayanan expected failure of panel C_2 by stiffener buckling, it was the plate which collapsed in their test and buckled in the present work. Furthermore the observed failure stress for this panel was unusually high, and in fact exceeded the corresponding value for a similar panel with fixed ends by some 10%. Horne and Narayanan did not explain this apparent inconsistency.

Panels D_{12} and E_{12} have different values of measured residual stress on the plate. The finite strip results overestimate the test results of these two panels and this may be due to the fact that the present analysis ignores the initial imperfection which was approximately equal to 0.40 times the plate thickness.

For the three panels 8, 9 and A_{12} with measured residual stress on plate between 0.07 σ_Y and 0.13 σ_Y, the finite strip method results are in good agreement with the

test results. Panel 8 is similar to panel 7 and differs from it only in the magnitude of residual stress. For this panel the theoretical result is identical with the experimental result. Horne and Narayanan found that for panel 9 stiffener buckling was the dominant failure mode which means that the pattern of the residual stress in the stiffener is an important factor. In the finite strip analysis the maximum value of residual stress in the stiffeners was assumed to be equal to the recorded value. In the present work the maximum σ_r occurred only in one point on the stiffener while the measured values are the average of the compressive residual stress on the stiffener. This led to 6.4% overestimation compared with observed failure load. The local buckling stress for this panel, based on the finite strip method, is less than the overall buckling stress by 4.6%.

Panel D_{22} was nominally straight, the plate imperfections being in fact equal to about two-thirds of the Merrison tolerance (59). It was not possible for Horne and Narayanan to obtain the exact value for the ultimate collapse load taken by the panel and the value given in reference (56-58) represents the maximum load that could be recorded. Subsequent load increases, resulted in a sudden collapse of the specimen after a short time and Horne et al referred this to the fact that the stiffness of the test rig was lower than that of the unloading

specimen. The finite strip method overestimates the maximum recorded load by 10%.

According to the present theory all panels, except panels D_{12} and D_{22} buckled in local mode. Horne and Narayanan observed that these two panels collapsed by a plate failure at σ_{max}/σ_Y = 0.65 and 0.60 respectively. The finite strip method gives a result of σ_{cr}/σ_Y = 0.82 and 0.67 for local buckling and σ_{cr}/σ_Y = 0.78 and 0.66 for overall buckling respectively. Horne and Narayanan found that as the failure load was approached a seperation between plate and stiffeners for panels of low ℓ/r and welded intermittently occurred. The finite strip method is unable to consider this seperation which caused a significant decrease in carrying capacity for these panels.

Considering only the five continuously welded panels 7, D_{22}, A_{23}, E_{23}, and C_2 - the finite strip method underestimates the test results by an average of 27% while for the other five intermittently welded panels it overestimates the test results by an average of 7%.

Horne and Narayanan demonstrated that for the relatively thin plate which they used, the influence of residual stresses on the failure stress is much less than that of initial imperfections. These are of course not included in the current approach, and hence good agreement could not be expected where such effects are important.

It should be noted that for the panels included within Table 4.6, initial imperfections were within the recommended limits given by Merrison (59). Clearly even if a panel is nominally flat, it does not necessarily imply that the finite strip method will give an accurate prediction of the failure load. Nonetheless the results do indicate that for panels in which initial imperfections are small the current approach compares well with the observed failure stresses.

In addition to their experimental work, Horne and Narayanan proposed a theoretical treatment of the failure of stiffened panels, (44,45) based upon the "effective width" concept. They found in their tests that the Merrison Interim Design Rules (59) underestimated the actual welding residual stress by a factor of about 2. Their theoretical comparison however were not based on the measured level of residual stress, but on the values calculated in accordance with the Merrison Rules. They also computed the maximum strengths for $\sigma_r = 0$. Their analysis was based on the assumption that the panel was wide and hence a single plate-stiffener combination could be considered even though the test panels each comprised of four flat stiffeners. The finite strip method can also be used efficiently to study very wide panels (112) and this approach has been adopted here for consistency.

The theoretical results (44,45), based on Merrison Rules (56,57) and the finite strip method results are shown in Table 4.7. The residual stresses used in the finite

Spec. No.	Observed σ_{max}/σ_Y	Predicted values of σ/σ_Y						
		Finite strip method			Manchester theory		Merrison Rules	
		σ_r (measured)	σ_r (average)	$\sigma_r = 0.0$	σ_r (Merr. R.)	$\sigma_r = 0.0$	σ_r (as impr.)	σ_r (add. str.)
7	0.79	0.60	0.75	0.95	-	-	0.64	0.48
8	0.85	0.85	0.86	0.96	-	-	0.61	0.66
9	0.78	0.83	0.84	0.94	-	-	0.59	0.66
D_{12}	0.65	0.78*	0.78*	0.79*	0.65	0.69	0.54	0.58
D_{22}	0.60	0.66*	0.67*	0.72*	0.64	0.78	0.52	0.47
A_{12}	0.56	0.50	0.51	0.55	-	-	0.58	0.48
A_{23}	0.62	0.29	0.38	0.59	-	-	0.60	0.39
E_{12}	0.48	0.53	0.55	0.61	0.46	0.48	0.48	0.42
E_{23}	0.45	0.33	0.44	0.62	0.46	0.47	0.50	0.37
C_2	0.87	0.60	0.74	0.90*	-	-	-	-

* Panel buckled in overall mode

Table 4.7. Comparison between Manchester theoretical work and the finite strip method

strip calculation were as measured, zero and an average value between the measured values on the plate and on the stiffener (Table 4.8). In the latter case it has been assumed that the residual stresses on the plate and on the stiffener are equal which is consistent with both Horne et al (44) and the Merrison Rules (59).

It is clear from the comparison of Table 4.6 and Table 4.7 that the finite strip results for a very wide panel are approximately the same as those obtained from a complete panel analysis. The results for panels 7, 8, 9, D_{12}, D_{22} and C_2 are in fact identical for both approaches. For all the other panels the results obtained by considering the panel as very wide slightly underestimate the results obtained for the complete model.

For the four panels - 7, A_{23}, E_{23} and C_2 - if the average residual stress has been used in the calculation of the critical load, the finite strip method underestimates the observed results by 15% compared with 32% if the measured residual stresses are used. Because the measured residual stresses on the stiffeners are close to those measured on the plate for panels 8, 9, D_{12}, A_{12} and E_{12} the change in the critical stress due to using the average residual stress is very small.

For panels D_{22} and E_{23} with b/t equal to 48.0 and 70.3 respectively, the residual stress according to Merrison Rules is about 0.20 σ_Y. Using this value of residual stress the strength of the two panels is reduced

by 18% and 2% respectively according to Horne. This may be reasonable if the second panel collapsed in an overall mode but in fact the two panels were shown to collapse by plate failure. When an average residual stress of 0.23 σ_Y is used for the same two panels the reductions in the strength based on the finite strip method are 6.9% and 29% respectively. This difference in reduction is due to the fact that the first panel buckled in an overall mode while the second panel buckled in a local mode.

Horne and Narayanan found from their theoretical work that for normal panels with a moderate amount of welding the effect of residual stresses on the failure load is very small. For panels with a higher level of residual stress they suggested a reduction factor of 5% to 8% on the calculated ultimate stress to allow for any adverse effect of welding. The current finite strip results confirm this for a panel buckling in an overall mode (D_{12} and D_{22}) but for the case of local bucklingabigger stress reduction would be suggested.

Although separation between the plate and the stiffeners - leading to a reduction in the collapse load - occurred in some panels Horne's results were very close to the observed strength.

These comparisons show that, generally, there is good agreement between the current approach and the test results.

Spec.	σ_r/σ_Y (measured)		Average σ_r/σ_Y	σ_r/σ_Y (Merr. R.) (59)
	Plate	Stiff.		
7	0.410	0.082	0.25	0.16
8	0.125	0.100	0.11	0.05
9	0.122	0.100	0.11	0.06
D_{12}	0.132	0.077	0.11	0.07
D_{22}	0.315	0.228	0.27	0.20
A_{12}	0.066	0.025	0.05	0.06
A_{23}	0.424	0.111	0.27	0.16
E_{12}	0.088	0.039	0.06	0.07
E_{23}	0.330	0.046	0.19	0.21
C_2	0.386	0.073	0.23	0.17

Table 4.8. The residual stresses used in comparison

4.4.4 Nagoya University Test Results (60)

The results of a series of tests on steel panels stiffened with three, four or five flat stiffeners have been presented by Fukumoto et al (60). For each test specimen the critical stress has been calculated using the present finite strip approach and these theoretical predictions are compared with the test results in Table 4.9. Since measurements of the actual residual stresses present in each individual specimen were not provided in reference (60) the pattern shown in Figure 4.12(c) has been assumed

and results obtained for values of σ_r/σ_Y of 0.3 and 0.5. Comparison with the information on residual stresses given in reference (60) suggests that these levels bracket the likely values. Unfortunately values of the initial imperfections in the panels have not been reported.

Table 4.9 includes the mean and standard deviation for the ratio σ_{cr}/σ_{max} for both sets of calculations. It is noticeable that whilst certain individual results are affected by up to about 23% the two means for the series of 24 tests are almost identical. Moreover, the values of 0.86 and 0.89 suggest that on average the analysis is capable of providing good, if slightly conservative, predictions of panel strength. Whilst lack of input data (exact residual stress, level of imperfections, etc.) for individual panels make it impossible to discuss the comparisons on an individual basis, some rather more general observations may be drawn from the complete set of data.

Referring to Table 4.9 it can be seen that for the panel with the stockiest plating (β = 0.457) a change in the level of residual stress has negligible effect on buckling strength. As the plating slenderness in the panels increased so the trend changes from a tendancy of over-prediction to one of the underprediction. Taking β = 0.55 as a reference value, for the 4 specimens with lower β the mean values of σ_{cr}/σ_{max} are 1.01 and 1.04 for σ_r/σ_Y = 0.3 and 0.5 respectively, figures that are reduced to 0.82 and 0.85 for the 20 tests with $\beta > 0.55$. It seems likely that

Spec.	d_s/t_s (1)	$m = \frac{\gamma}{\gamma_{req.}}$ (2)	Slenderness ratio β	Test results[3] σ_{max}/σ_Y	Finite strip results σ_{cr}/σ_{max}	
					$\sigma_r/\sigma_Y = 0.3$	$\sigma_r/\sigma_Y = 0.50$
B-1-1	10.3	0.97	0.682	0.785	<u>0.88</u>	0.79
B-1-1_r	10.0	1.15	0.733	0.789	<u>0.87</u>	0.72
B-1-2	12.1	1.67	0.698	0.853	<u>0.81</u>	0.71
B-2-1	9.1	1.03	0.623	0.794	0.88	<u>0.90</u>
B-2-4	10.5	4.25	0.608	1.003	0.70	<u>0.81</u>
B-3-1	6.9	1.07	0.472	0.941	0.93	<u>1.01</u>
C-1-2	18.5	2.62	0.784	0.746	<u>0.91</u>	0.67
C-1-4	15.3	5.10	0.766	0.889	<u>0.77</u>	0.66
C-2-1	12.8	1.14	0.695	0.803	<u>0.86</u>	0.77
C-2-2	16.2	2.04	0.964	0.853	<u>0.81</u>	0.73
C-2-4	13.8	4.36	0.697	0.927	<u>0.75</u>	0.71
C-3-2	14.5	2.11	0.606	0.820	0.85	<u>0.94</u>
C-3-4	12.8	4.19	0.607	0.885	0.81	<u>0.93</u>
C-4-1	9.5	1.09	0.543	0.806	<u>0.99</u>	1.07
C-4-2	12.8	2.29	0.554	1.004	0.77	<u>0.85</u>
C-5-1	8.7	1.15	0.481	0.862	<u>1.01</u>	1.09
C-6-1	13.7	1.24	0.756	0.945	<u>0.81</u>	0.70
C-7-1	11.7	1.07	0.671	0.890	0.78	<u>0.80</u>
D-1-1	9.9	1.08	0.657	0.814	0.86	<u>0.88</u>
D-1-2	15.2	2.04	0.683	0.947	<u>0.74</u>	0.70
D-1-3	15.0	3.16	0.652	0.955	0.73	<u>0.77</u>
D-2-1	8.6	1.03	0.578	0.856	0.89	<u>0.99</u>
D-2-3	13.4	3.20	0.597	1.013	0.72	<u>0.82</u>
D-3-1	7.0	1.10	0.457	0.946	<u>1.06</u>	<u>1.06</u>
Mean average					0.84	0.83
Standard deviation					0.09	0.13
Mean average of the chosen values[3]					0.86	0.89
Standard deviation of the chosen values					0.10	0.09

1. d_s/t_s is the stiffeners width to thickness ratio
2. $m = \gamma/\gamma_{req.}$ is the relative flexure rigidity to the required relative flexure rigidity
3. The selected values are the predicted critical stresses closer to the observed maximum stress. They are indicated by underline in the table

Table 4.9. Comparison between Fukumoto test results and FSM

part of the reason for the overprediction at very low β is the presence of unflat plating in the test specimens, a feature that is not allowed for in the analysis. Moreover, at high values of β the plating would be expected to possess some postbuckling strength leading to experimental maximum loads being somewhat higher than the predictions of a theory which did not include this effect. It is of interest to note how for every panel with plating in the range $0.46 < \beta \leq 0.67$ a higher value of σ_{cr} has been obtained when the larger residual stress has been assumed. Further study of this point shows that it occurs consistently for panels having these proportions; it may be due to the reduction of the plate area - between stiffeners - in which the residual stresses are compressive. This effect has also been observed by Little (82) in his work on box columns.

For the 11 panels with relatively weak stiffeners ($m < 1.2$) the finite strip results underestimate the collapse loads slightly, the mean σ_{cr}/σ_{max} being 0.94 for both levels of σ_r. However, this underestimate increases for the panels with $m > 1.2$ for which the mean values of σ_{cr}/σ_{max} are 0.80 and 0.85 for $\sigma_r/\sigma_Y = 0.3$ and 0.5 respectively. It is possible that for this second series the buckling deformations are more concentrated within the plating and that the effects of plate post-buckling are significant. On the other hand when weak stiffeners are used buckling may be expected to occur in a more predominantly overall mode in which case the post-buckling of the plating would be expected to be rather less important.

For those panels in which the stiffeners had a width-to-thickness ratio in excess of 10 the theory generally underestimated the buckling load. This was in line with the analysis made by Fukomoto et al for panels having stiffeners with a width to thickness ratio less than 14. For the other panels this is in contrast to Fukumoto's analysis which tended to overpredict the strength of such panels. Although Fukumoto et al could not properly explain this they suggested that residual stresses higher than the assumed values might be a factor. Since in general the present calculations suggested that a change from σ_r/σ_Y of 0.3 to σ_r/σ_Y of 0.5 only produces a reduction in strength of about 8% at high values of β compared with an increase in strength at low values of β, this does not appear to be an adequate explanation.

Fukumoto et al's assumption of elastic-plastic material behaviour implies that nonlinear behaviour starts at rather higher loads than does the present analysis which is based on the stress-strain curve given in Chapter 3. While they consider that the material is linear elastic up to applied stresses equal to the yield stress, in the present approach the material is no longer linear elastic in the range of $\sigma_r/\sigma_Y \geq 0.8$. Consequently it is to be expected that the present analysis, since it leads to an earlier and more gradual drop in stiffness due to the effects of plasticity, would produce results generally lower than those of Fukumoto (60).

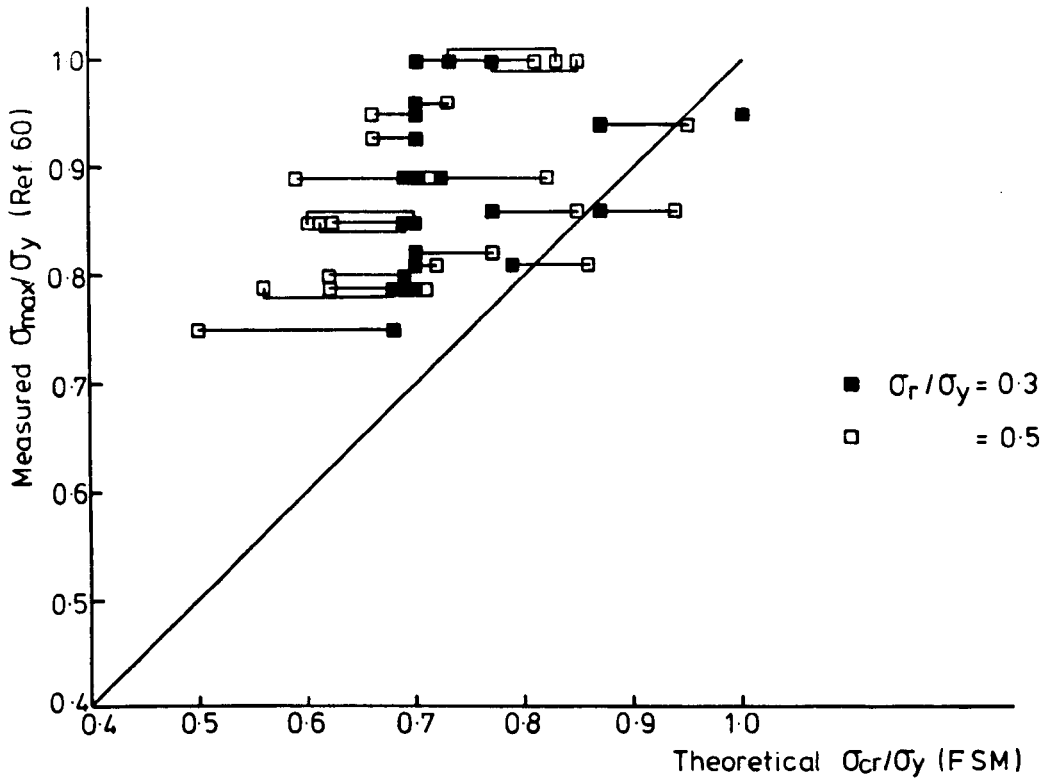

FIG. 4·14. COMPARISON BETWEEN FUKUMOTO TEST RESULT (60) AND FINITE STRIP FOR THE TWO LEVELS OF $\sigma_r/\sigma_y = 0·3$ AND 0·5.

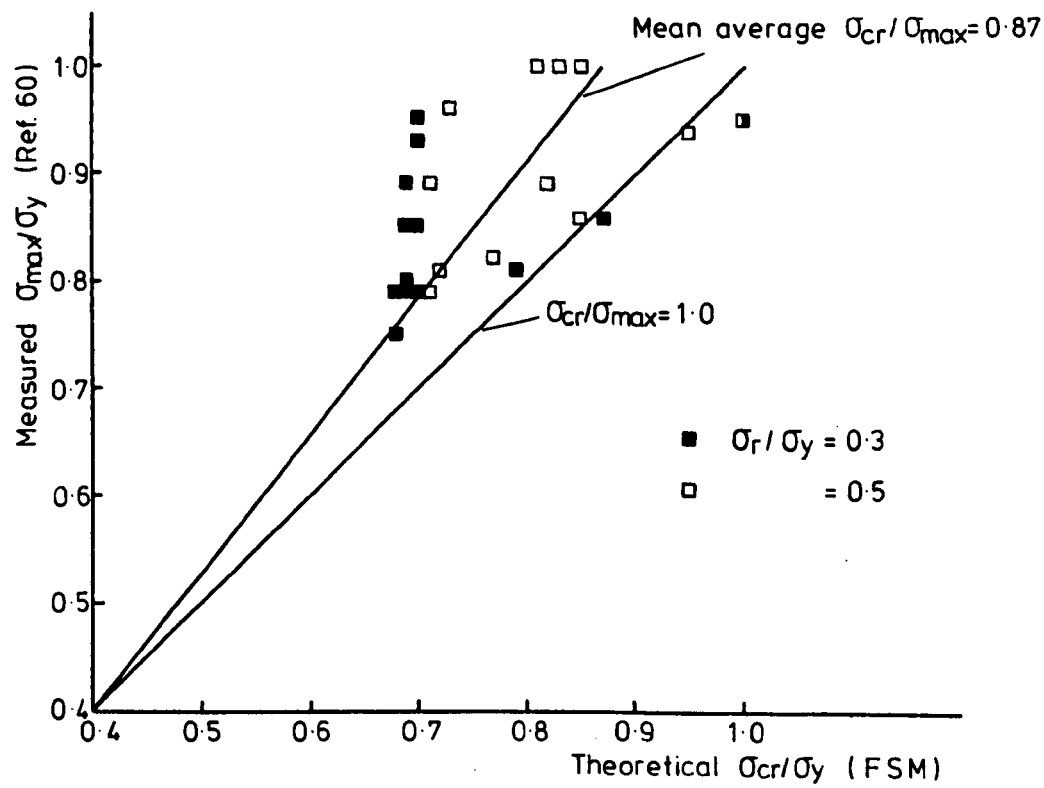

FIG. 4·15. COMPARISON BETWEEN FUKUMATO TEST RESULTS (60) AND FINITE STRIP FOR A CHOSEN LEVEL OF σ_r/σ_y.

The finite strip results are shown in Figure 4.14 for the two levels of σ_r/σ_Y - 0.3 and 0.5 - as curves of σ_{cr}/σ_Y against the observed collapse stress σ_{max}/σ_Y. The 45^o line corresponding to σ_{cr}/σ_{max} is also shown and it is evident that in some levels the results for $\sigma_r = 0.3\,\sigma_Y$ are closer to the test results, in others closer agreement occurs for residual stresses, $\sigma_r = 0.5\,\sigma_Y$. In the subsequent comparison the finite strip results closest to the experimental values have been used and this has been necessary because of the lack of data in reference (60). These selected results are shown in Figure 4.15 with the mean average line.

It is of interest to note that changing the shape of the stress-strain curve (Figure 3.4) by increasing the value of C in equation (3.17) to 0.999 increases the value of σ_{cr}/σ_Y for each panel by up to 5% (Table 4.10).

Spec.	Fukumoto test results σ_{max}/σ_Y	Predicted critical stress σ_{cr}/σ_Y					
		σ_r/σ_Y = 0.3			σ_r/σ_Y = 0.5		
		C = 0.997	C = 0.998	C = 0.999	C = 0.997	C = 0.998	C = 0.999
B-1-1	0.785	0.688	0.692	0.694	0.618	0.624	0.630
B-1-1_r	0.789	0.683	0.689	0.690	0.564	0.569	0.577
B-1-2	0.853	0.689	0.690	0.694	0.608	0.614	0.622
B-2-1	0.794	0.698	0.698	0.700	0.714	0.720	0.728
B-2-4	1.003	0.702	0.706	0.710	0.808	0.817	0.829
B-3-1	0.941	0.874	0.874	0.876	0.950	0.954	0.960
C-1-2	0.746	0.675	0.679	0.685	0.499	0.499	0.499
C-1-4	0.889	0.687	0.690	0.694	0.589	0.595	0.605
C-2-1	0.803	0.690	0.692	0.694	0.618	0.622	0.630
C-2-2	0.853	0.690	0.692	0.694	0.618	0.624	0.630
C-2-4	0.927	0.696	0.698	0.698	0.661	0.665	0.667
C-3-2	0.820	0.698	0.700	0.700	0.767	0.772	0.780
C-3-4	0.885	0.720	0.724	0.728	0.821	0.829	0.841
C-4-1	0.806	0.794	0.800	0.810	0.860	0.864	0.868
C-4-2	1.004	0.772	0.776	0.782	0.849	0.853	0.860
C-5-1	0.862	0.874	0.874	0.874	0.940	0.944	0.952
C-6-1	0.845	0.688	0.690	0.694	0.595	0.601	0.610
C-7-1	0.890	0.698	0.698	0.700	0.712	0.718	0.726
D-1-1	0.814	0.698	0.698	0.700	0.718	0.724	0.731
D-1-2	0.947	0.696	0.698	0.698	0.663	0.665	0.669
D-1-3	0.955	0.698	0.698	0.700	0.733	0.739	0.749
D-2-1	0.856	0.765	0.771	0.776	0.847	0.851	0.858
D-2-3	1.013	0.733	0.737	0.743	0.829	0.837	0.847
D-3-1	0.946	0.999	0.999	0.999	0.999	0.999	0.999

Table 4.10. Effect of the shape of stress-strain curve on the results

4.5 Buckling of Beams and Columns

Having checked the present approach (Chapter 3) for plate structures - rectangular plates and stiffened panels - it can now be compared with results for beams and columns which may also be considered as plate assemblies. The main difference between the buckling of a slender plate and the buckling of a slender column is the appreciable positive post-buckling stiffness of the plate compared with zero post-buckling stiffness of the column. Note that this post-buckling effect, has not been considered in the present approach.

In the following section theoretical predictions are compared with the experimental results for beams under pure bending moment and columns under axial compression. This comparison also demonstrates the wide variety of plate assemblies which can be analysed using the present approach.

4.5.1 Beams Under Pure Bending

A series of tests on beams of I-section under a uniform bending moment has been carried out by Dibley (114). Four sections - two universal columns and two universal beams - were chosen to cover a wide range of section geometry and slenderness ratio. The residual stress distribution and the initial imperfection, in the test section, were reported by Dibley and in only two specimens was there found to be any measurable initial bow. Four-point loading was used so that the centre unsupported span carried a uniform bending moment, the load being applied vertically

downwards at the ends of the beam which were constrained in guides to move vertically only. Dibley found that the ratio of the effective length to the actual length increased as the residual stress increased while the effectiveness of the lateral and warping restraint stiffnesses was reduced.

The observed values of the maximum bending moment were reduced to account for the effect of the dead load bending moment of the beam itself and friction in the loading and support structure. However the effect of the dead load was very small and it has been neglected in the current finite strip analysis. Dibley's estimation of error due to friction was relatively high and the maximum correction was about 16% for some test results. The actual slenderness ratios were modified to account for end restraint and nonuniform bending moment.

The relationship between the critical moment and both actual and effective slenderness ratio is shown in Figures 4.16 and 4.17. The finite strip results which of course were based upon the assumtpion of ideal end support and uniform bending moment loading conditions, are also shown in Figures 4.16 and 4.17. Two levels of residual stresses - 0.1 σ_Y and 0.3 σ_Y for the UB sections and zero and 0.1 σ_Y for the UC sections - have been used in the present calculations.

It is apparent that for slender beams - $\ell/ry > 120$ - the effect of the residual stresses on the finite strip results is negligible. For beams UB17 and UB19 the measured residual stress was approximately 0.12 σ_Y and 0.24 σ_Y

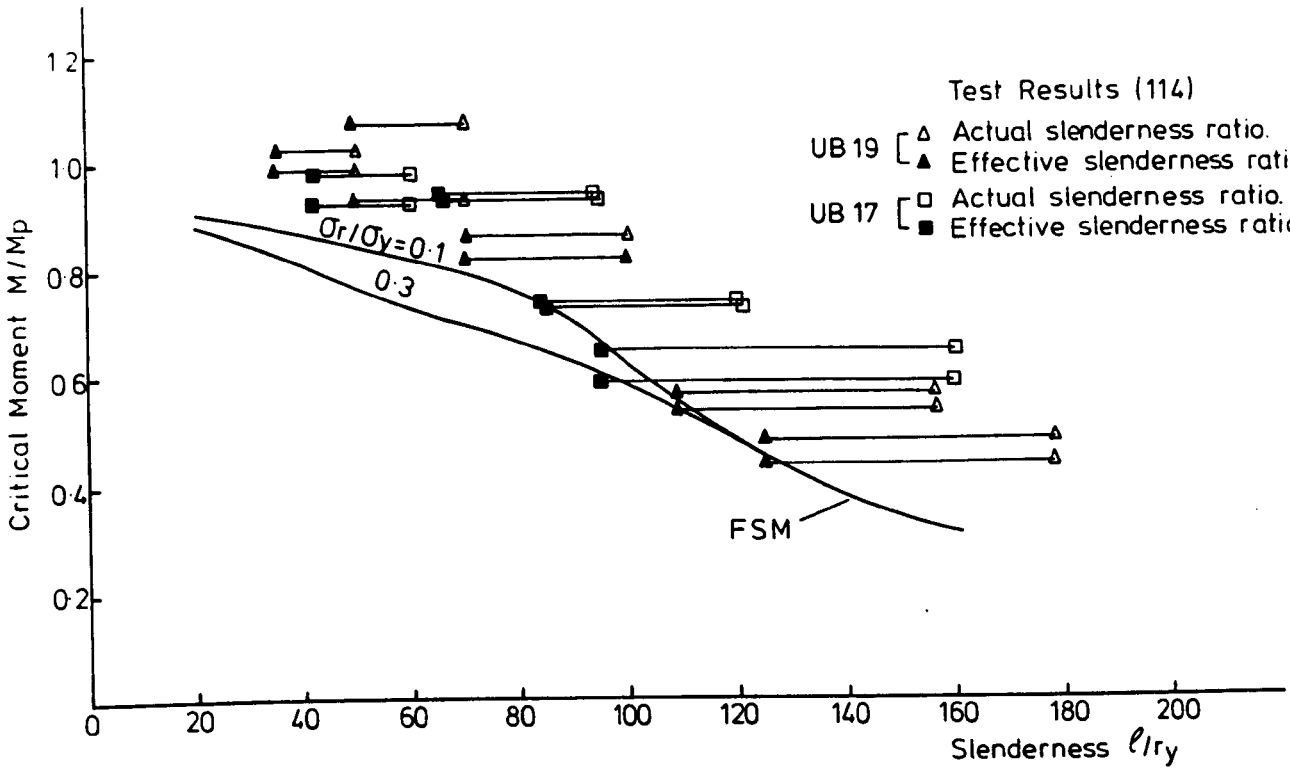

FIG. 4·16. COMPARISON BETWEEN DIBLEY RESULTS (114) AND FSM.

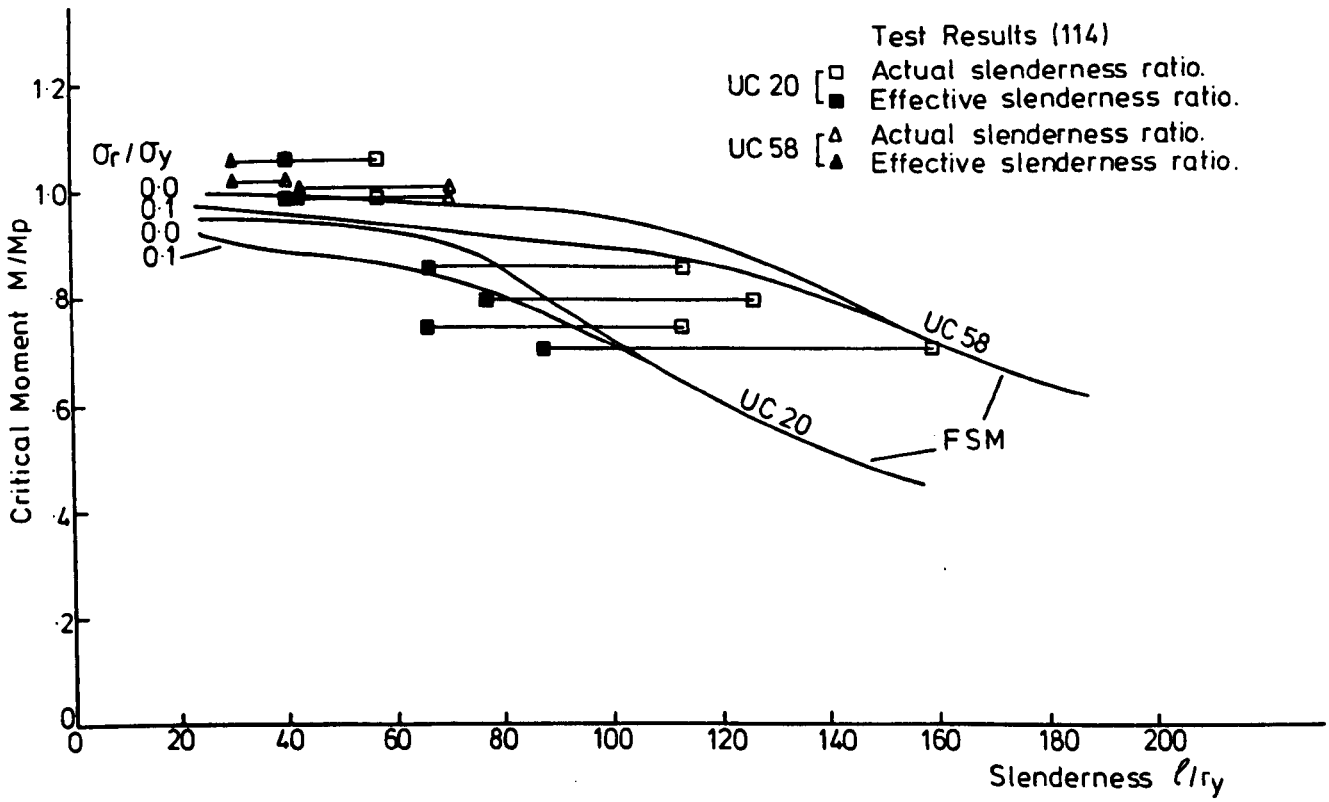

FIG. 4·17. COMPARISON BETWEEN DIBLEY RESULTS (114) AND FSM.

respectively but the actual pattern of the residual stress is in fact quite different from the assumed pattern used in the finite strip analysis (Figure 4.18). In the observed patterns both flanges were in tension and the web was in compression, while the assumed pattern was based on self equilibrium of each flange. This pre-tension in the flanges would increase the experimental collapse moment of a short column.

For beams with effective slenderness ratios $\ell/r_y \geq 60$, the finite strip results are in good agreement with the test results. The use of the actual slenderness ratio instead of the effective one leads to an underestimate of the collapse load by about 0.3 M_p based on the finite strip method. For beams with $\ell/r_y < 60$ the finite strip method underestimates the test results by about 18%. This underestimate may be due to the residual stress which gives rise to pre-tension in the flanges of the test specimens.

In Dibley's work five of the beams were observed to collapse at a maximum bending moment higher than the plastic moment (Figures 4.16 and 4.17). The reason for this would appear to be the strain hardening which has been neglected in the present analysis.

4.5.2 Columns Under Axial Compression

One hundred and thirty strut tests have been carried out by Strymowicz and Horsley (115) on high-strength steel

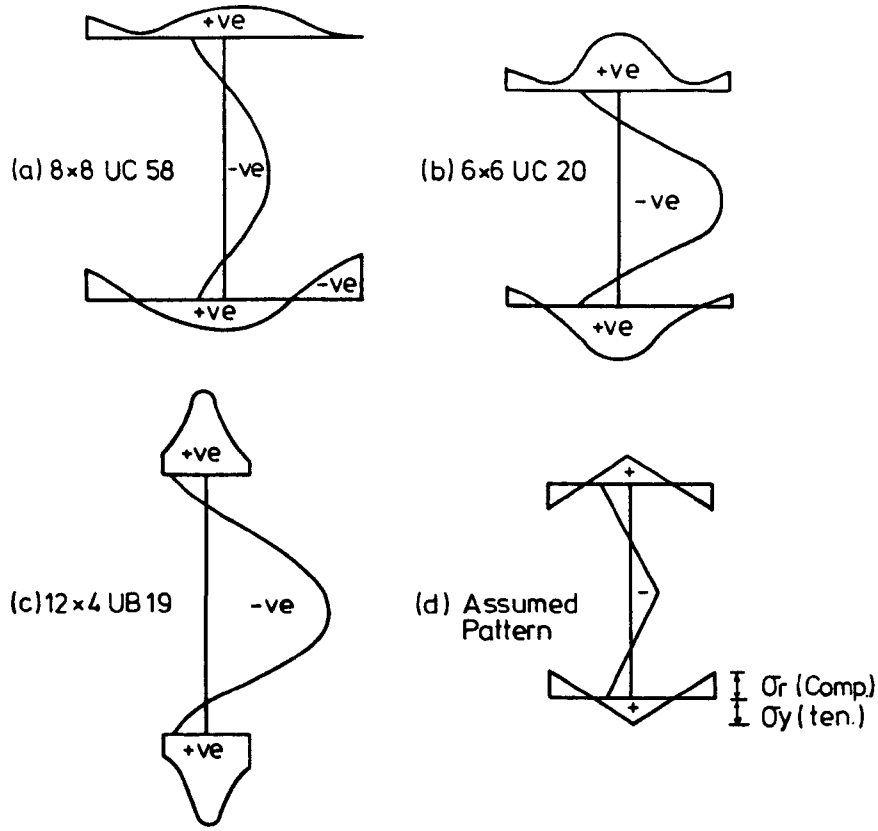

FIG. 4·18. OBSERVED (114) AND ASSUMED RESIDUAL STRESS PATTERNS.

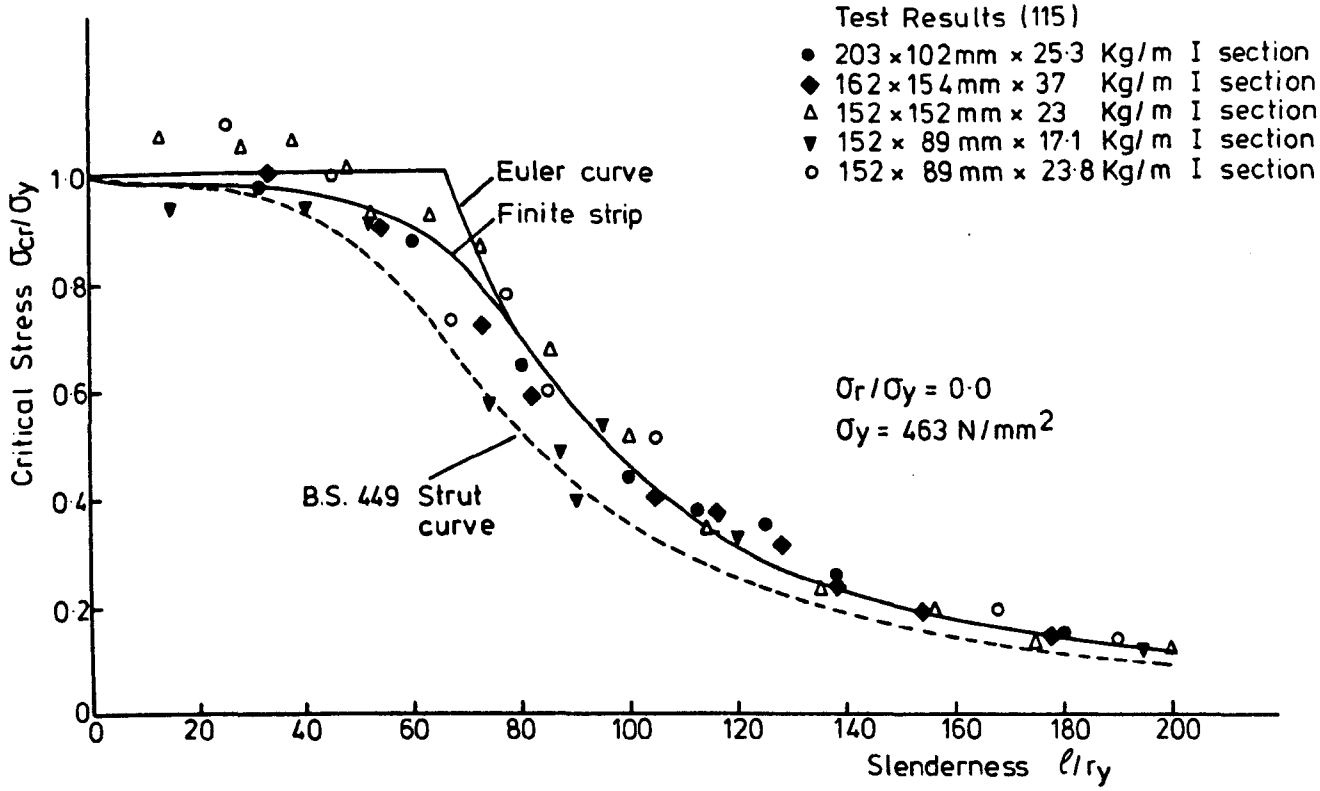

FIG. 4·19. COMPARISON BETWEEN FINITE STRIP AND HORSLEY RESULTS (115)

with a yield stress of 447 N/mm^2. Five sections of different geometry were studied over a wide range of slenderness ratios (ℓ/r). They investigated the influence of residual stresses by comparing the behaviour of as-rolled and stress-relieved stub columns and found that the residual stress made very little difference to the overall strength of the columns tested. They attributed this to the fact that the magnitudes of the residual stresses are influenced by the section geometry, rate of cooling and modulus of elasticity. Thus, as the modulus of elasticity is not greatly influenced by the yield stress, the residual stress will not depend on the type of steel, and influence of residual stresses on high strength steel is therefore less pronounced than on other steel. During the testing they observed that initial imperfections had very little effect on the final failure load.

To compare the test results, a 152 x 89 mm x 17.1 Kg/m I-section has been chosen for analysis using the finite strip method. Due to the lack of data regarding actual residual stress values it is assumed that the struts are initially stress-free. This would appear to be reasonable since the yield stress of the material is high. The results of the finite strip method together with corresponding curve B.S. 449 (116) - Addendum No. 1 (117) - are shown in Figure 4.19. It is clear that the finite strip method results are in good agreement with the test results whereas the B.S. 449 curve underestimates the test results over a wide range of ℓ/r_y. This is because the B.S. 449 strut curve was obtained for a strut with an initial imperfection.

The formula used to calculate the B.S. 449 curve is

$$K_2 P_c = \frac{(Y_s C_{L_m}) + (\eta + 1) C_o}{2} - \sqrt{\left(\frac{(Y_s C_{L_m}) + (\eta + 1) C_o}{2}\right)^2 - (Y_s C_{L_m}) C_o}$$

where P_c the permissible average stress, N/mm^2

K_2 load factor or coefficient

Y_s minimum yield stress, N/mm^2

C_o Euler critical stress $= \frac{\pi^2 E}{(\ell/r)^2}$

$\eta = 0.3\ (\ell/100r)^2$

ℓ/r slenderness ratio = effective length/radius of gyration

C_{L_m} is the weighted mean stress factor for the cross-section

$= \Sigma\ C_L bt / \Sigma\ bt$

C_L is the stress factor depending on b/t and Y_s. It is given in reference (117).

For short columns - $\ell/r < 50$ - the finite strip results and B.S. 449 are in good agreement but both underestimate the test results in this range. This may be due to the fact that the strain hardening parameter is neglected in both approaches. Moreover the effective length of the columns is assumed to be the distance between the supports although the two overhanging ends may have some effect on this. It seems also that the method of loading may have given some restraint to the rotation of the edge.

Nevertheless, the comparison appears to demonstrate that the current method is in good agreement with the available data.

4.6 Conclusion

In this chapter examples have been presented to assess the accuracy of the present approach by comparison with previously published theoretical and experimental work. Various plate structures - rectangular plates, stiffened panels, box columns, H-sections and channels - under axial compression or bending moments have been considered.

Convergence studies indicate that with each component of the structure divided into two strips, each of which is divided into 10 strips, sufficient accuracy is obtained.

In the light of the comparisons reported in this chapter it can be concluded that the current finite strip approach can be used to predict - with a reasonable degree of accuracy - the inelastic critical load for any plate assembly.

CHAPTER 5

INELASTIC STABILITY OF STIFFENED PANELS - A PARAMETRIC STUDY

5.1 Introduction

Two different stiffened panels have been considered in the current parametric study. The first is a square panel simply supported on the four edges and stiffened with four longitudinal flat, angle or tee stiffeners. The second is a very wide panel stiffened with flat ribs and simply supported at the loaded edges. William's approach (112) for the solution of a very wide panel has been used. In both cases the applied load is an axial longitudinal compressive stress.

The parameters to be varied in this study are:

1. The slenderness ratio of the plating.
2. The geometry and properties of the stiffeners.
3. The orientation of the angle stiffeners.
4. The yield stress of the stiffeners.
5. The residual stress level.
6. The longitudinal boundary conditions.
7. The distance between the transverse supports (for the very wide panel only).

The results for the very wide panel have enabled approximate design curves based on either the optimum panel length or the optimum stiffener dimensions to be established.

Finally, a stiffened box girder has been considered to show the capability of the present method for the analysis of a complete and complicated structure.

5.2 Square Panel Stiffened with Four Longitudinal Stiffeners

The square panels (Figure 5.1) considered in this section are reinforced with four flat, angle or tee stiffeners as shown in Figure 5.2. The distance between two adjacent stiffeners has been fixed (arbitrarily) at 200 mm and the plate thickness varies from 2 mm to 10 mm to achieve slenderness ratios β between 1.778 and 0.356. The yield stress σ_Y of both the plate and the stiffener is assumed to be 240 N/mm^2 and a number of different levels of residual stress σ_r are assumed, varying from zero to 0.5 σ_Y. The assumed residual stress patterns are shown in Figure 5.3. For the purpose of analysis using the finite strip method the plate between two adjacent stiffeners has been divided into two strips. The flat, angle and tee stiffeners have been modelled using one, two and three strips respectively. Every strip has been divided into ten substrips.

In the following sections, the influence of some of the important parameters on the inelastic buckling load are examined.

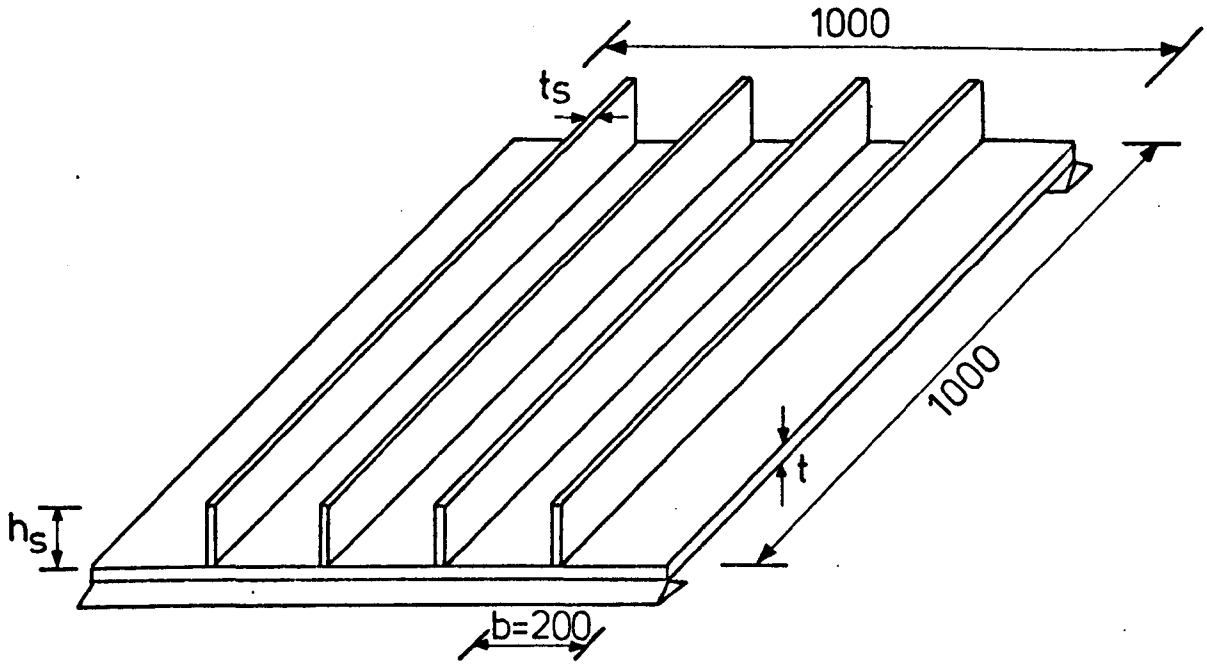

FIG.5·1. STIFFENED PANEL LIMITED BY THE END SUPPORTS.

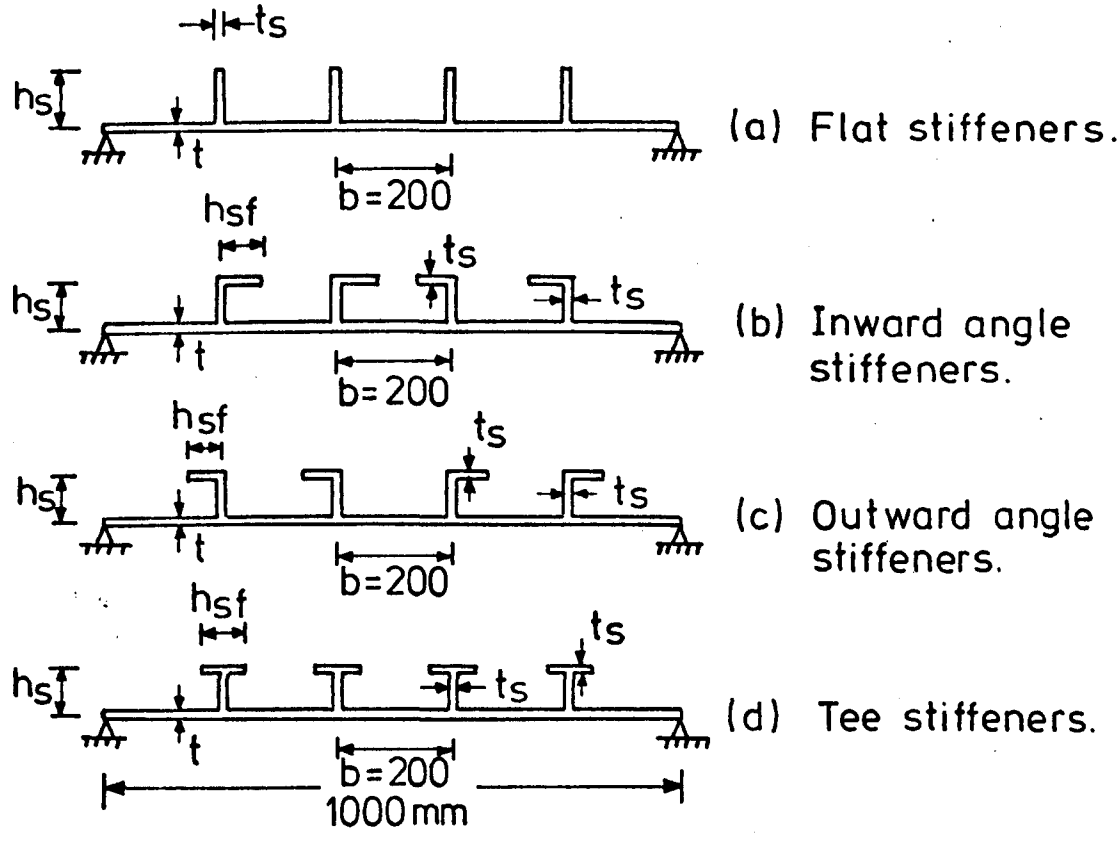

FIG. 5·2. STIFFENED PANELS TO BE ANALYSED.

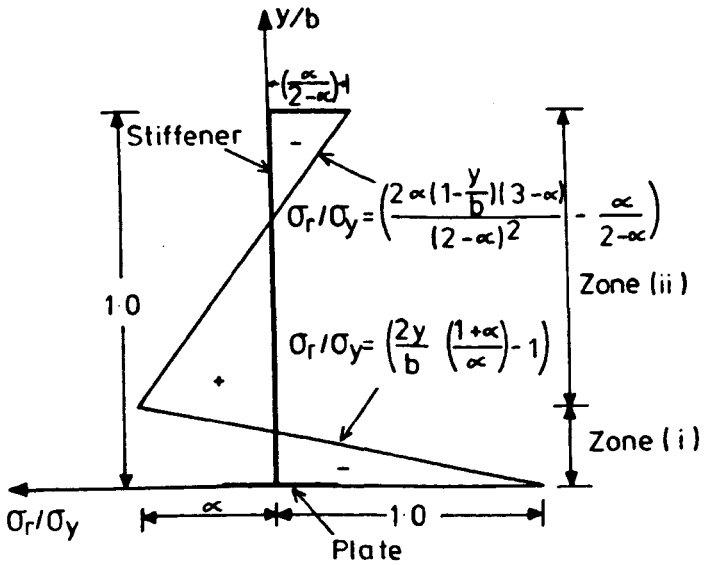

(a) Flat Stiffener.

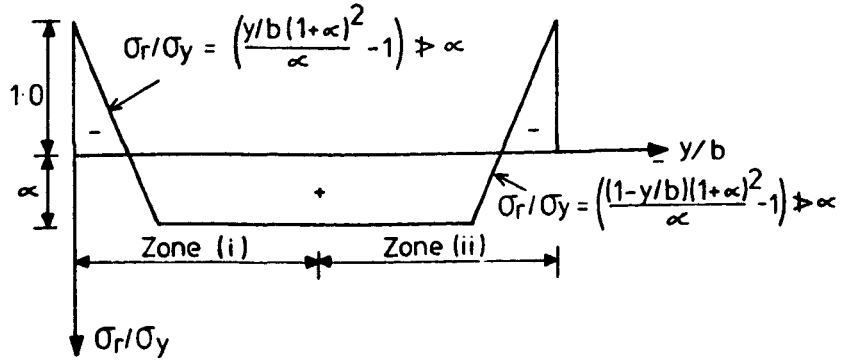

(b) Plate.

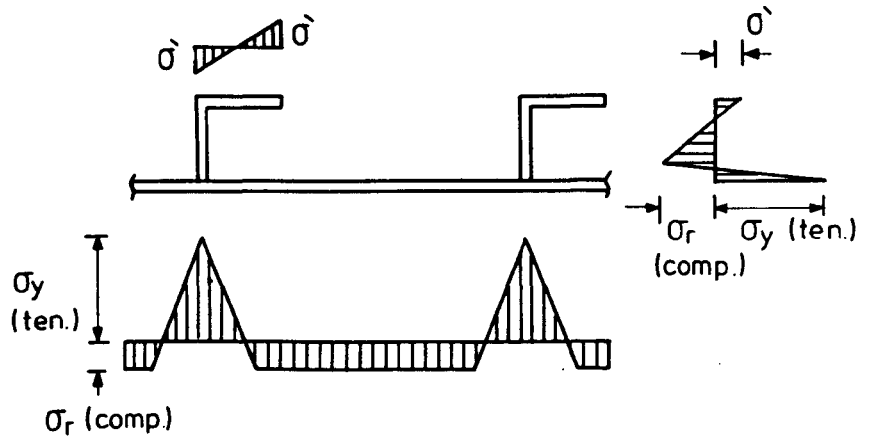

(c) Panel with angle stiffeners.

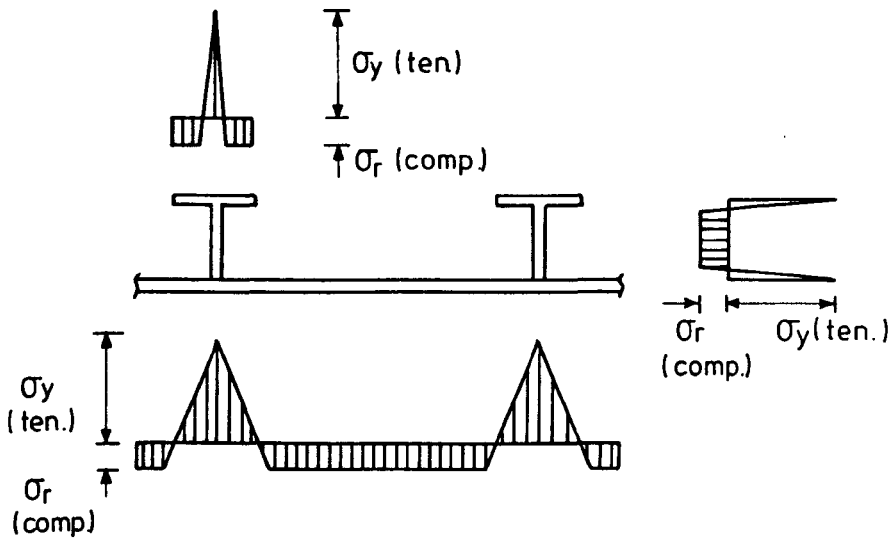

(b) Panel with T stiffeners.

FIG. 5·3. RESIDUAL STRESS PATTERNS.

5.2.1 Effect of Slenderness Ratio of the Plating Between Stiffeners

The effect of the slenderness ratio, β, of the plating between stiffeners on the critical buckling stress of the panel has been examined. This plate (i.e. the plate between two adjacent stiffeners) can be idealised simply as an isolated plate with specified longitudinal boundary conditions. The upper limit of the local buckling strength curve for a stiffened panel corresponds to a plate simply supported at one edge and built-in at the other edge. The lower limit is that for a plate simply supported on both edges. These two limits of the critical load will of course depend on the residual stress level. Three levels of residual stress - σ_r = 0.0, 0.3 σ_Y and 0.5 σ_Y - have been considered in this analysis, and for each of these the two bounds are shown in Figure 5.4 together with the Euler curve for a simply supported plate free of residual stress. For the lower bound curve (i.e. plate with simply supported edges) the half wavelength (λ) was assumed to be equal to the plate width (b). The upper limit was calculated for λ = 0.8b (1) as well as λ = b.

For an initially stress free simply supported plate the lower limit curve coincides with the Euler curve for slenderness ratios $\beta \geq 1.3$. For slenderness ratios less than this the buckling curve (lower limit) deviates from the Euler curve due to the effects of inelastic behaviour of the material. It is clear that in the absence of residual stress stocky plates with slenderness ratio

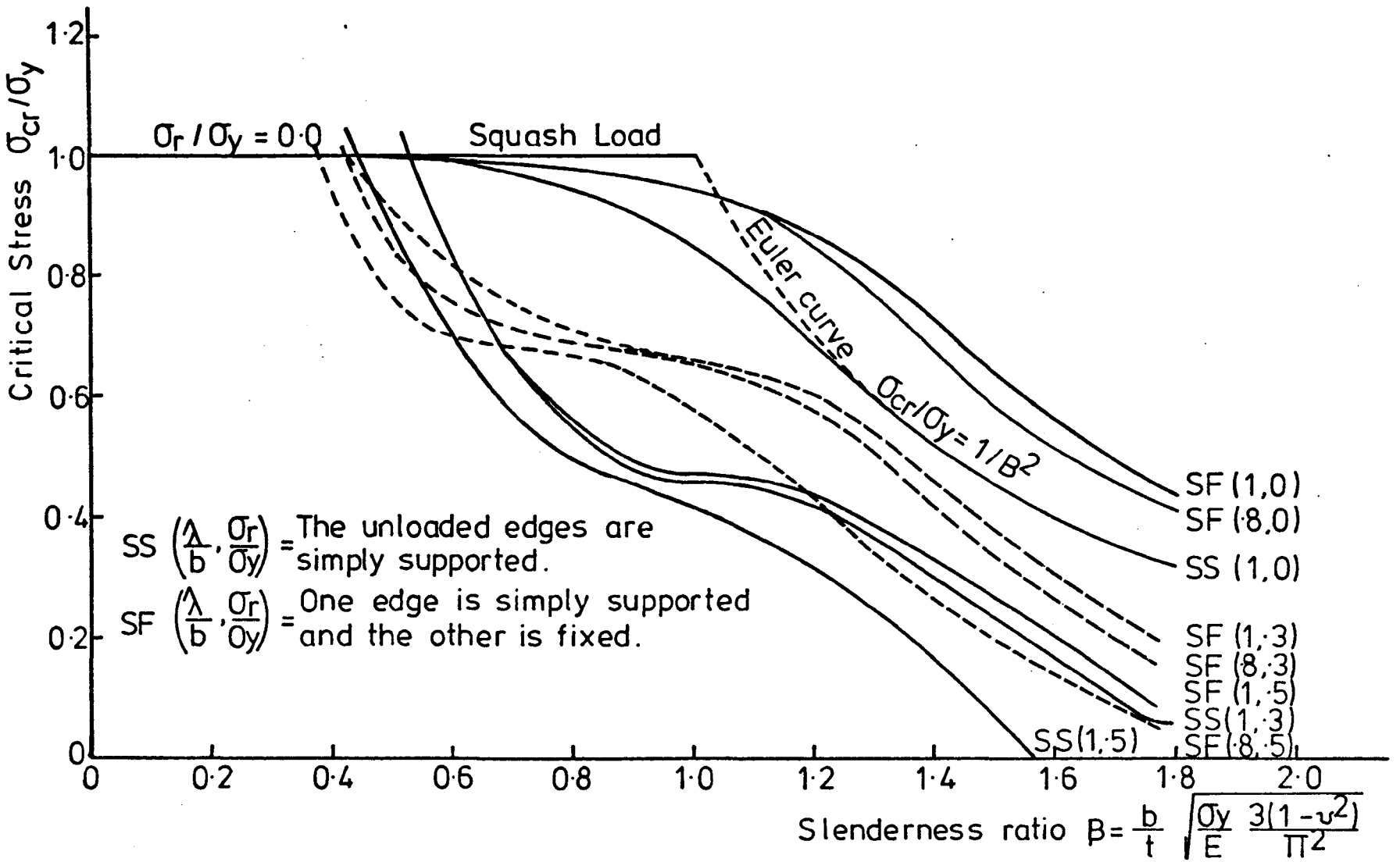

FIG.5·4. UPPER AND LOWER LIMITS FOR BUCKLING STRENGTH CURVES.

$\beta \leq 0.6$ are not affected by the out-of-plane boundary conditions of the longitudinal edge, but as β increases the effect of the edge conditions becomes more pronounced. This may be due to the fact that in the first range the plate yields before it buckles while in the second range the plate buckles elastically or inelastically. It is also clear that the effects of the boundary conditions and the half wavelength are more pronounced in the elastic buckling range - $\sigma_{cr} \leq (.8\ \sigma_Y - \sigma_r)$ - than in the inelastic buckling range.

The buckling strength curves for a plate with a residual stress level $\sigma_r = 0.3\ \sigma_Y$ and slenderness ratio $\beta \geq 0.8$ are similar to those for an initially stress free plate. For such a plate ($\sigma_r = 0.3$) with a slenderness ratio $0.9 > \beta > 0.7$ the critical load is approximately equal to the difference between the squash load and the residual stress. As the slenderness ratio increases ($\beta > 0.9$) the effect of the residual stress reduces and at $\beta = 1.8$ the reduction in the critical load is about $0.8\ \sigma_r$. For more stocky plates, the buckling strength increases as the slenderness ratio β decreases - $\beta \leq 0.8$ (built-in) and $\beta \leq 0.6$ (simply supported).

When the residual stress is increased to $0.5\ \sigma_y$ the buckling curves for plates with $\beta \geq 1.1$ have a pattern similar to $\sigma_r = 0$ curves. The buckling curves of a built-in plate become approximately horizontal in the range of $\beta = 0.9 \sim 1.2$ - corresponding to $\sigma_{cr}/\sigma_Y = 0.45 \sim 0.50$ -

while for a simply supported plate this plateau does not appear. It is clear that the plateaus (of the nearly constant strength) depend on the edge conditions and the residual stress level.

Again, for plates stockier than $\beta = 0.9$ ($\sigma_r = 0.50\ \sigma_Y$) the critical stress increases as the slenderness ratio β decreases. At slenderness ratio β less than about 0.6 the buckling strength curves become higher than those corresponding to $\sigma_r = 0.3\ \sigma_Y$. This may be due to the reduction of the plate area subjected to compressive residual stress as this stress, σ_r, increases.

A further point of interest is that a simply supported plate with slenderness ratio $\beta \geq 1.55$ and a residual stress $\sigma_r \geq 0.5\ \sigma_Y$ will buckle under the effect of the residual stress alone.

Let us now consider the case of buckling of a complete panel rather than the simplified case above where only local buckling was considered, and the plate was treated as an isolated plate. Buckling strength curves for panels stiffened with one of the three types of stiffener (flat, angle or tee) have been produced and are shown in Figures 5.5 and 5.6. By using two different values for the half wavelength - $\lambda = b$ and $\lambda = B$ - both local and overall buckling strengths have been obtained. The stiffeners were proportioned such that the depth to thickness ratio (h_s/t_s) was equal to 10 - the

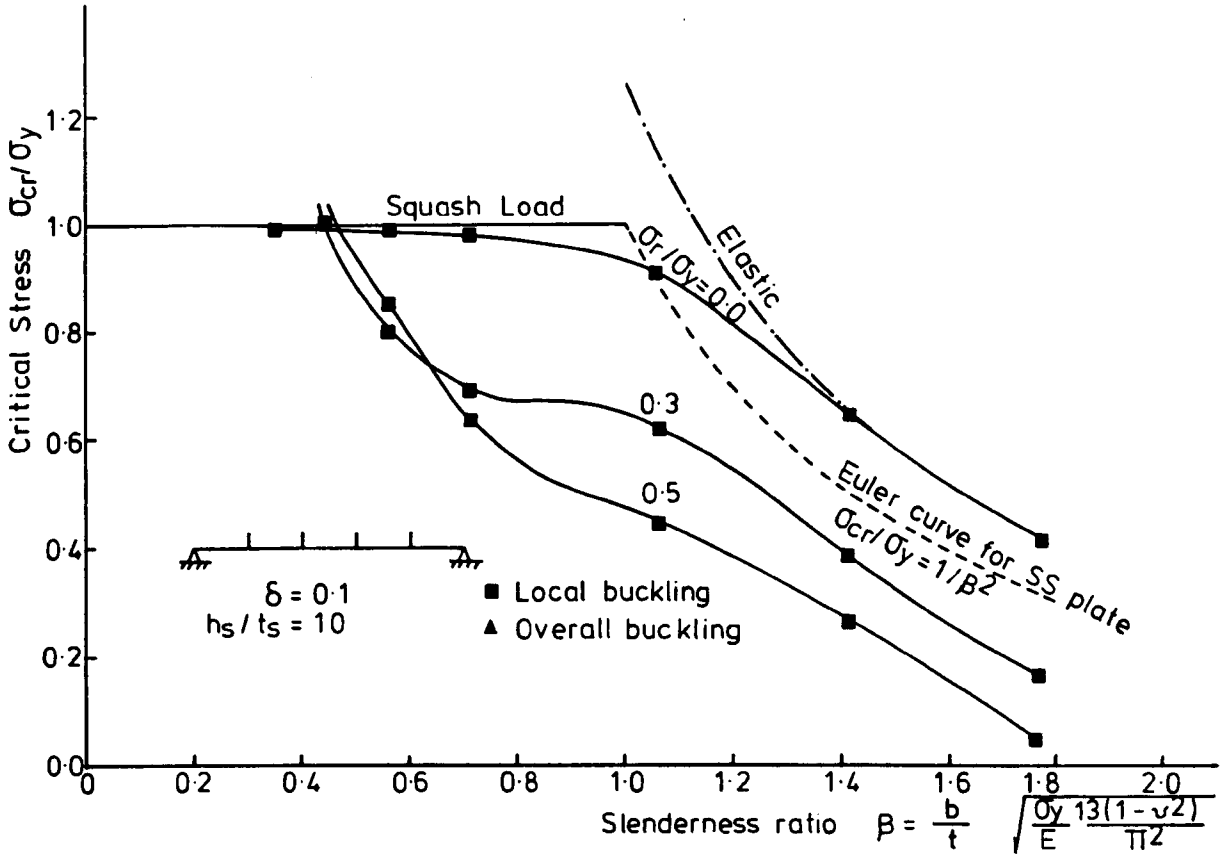

(a) Flat stiffeners.

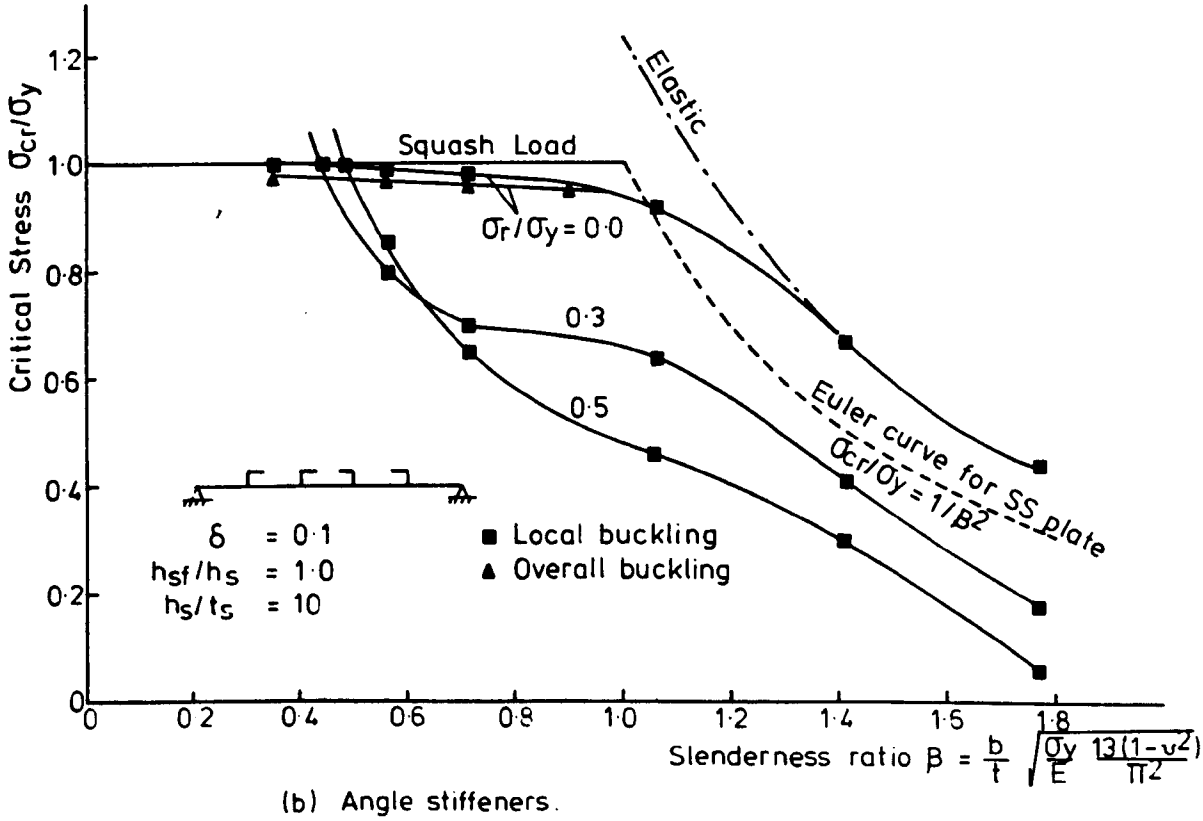

(b) Angle stiffeners.

FIG. 5·5. (Cont.....)

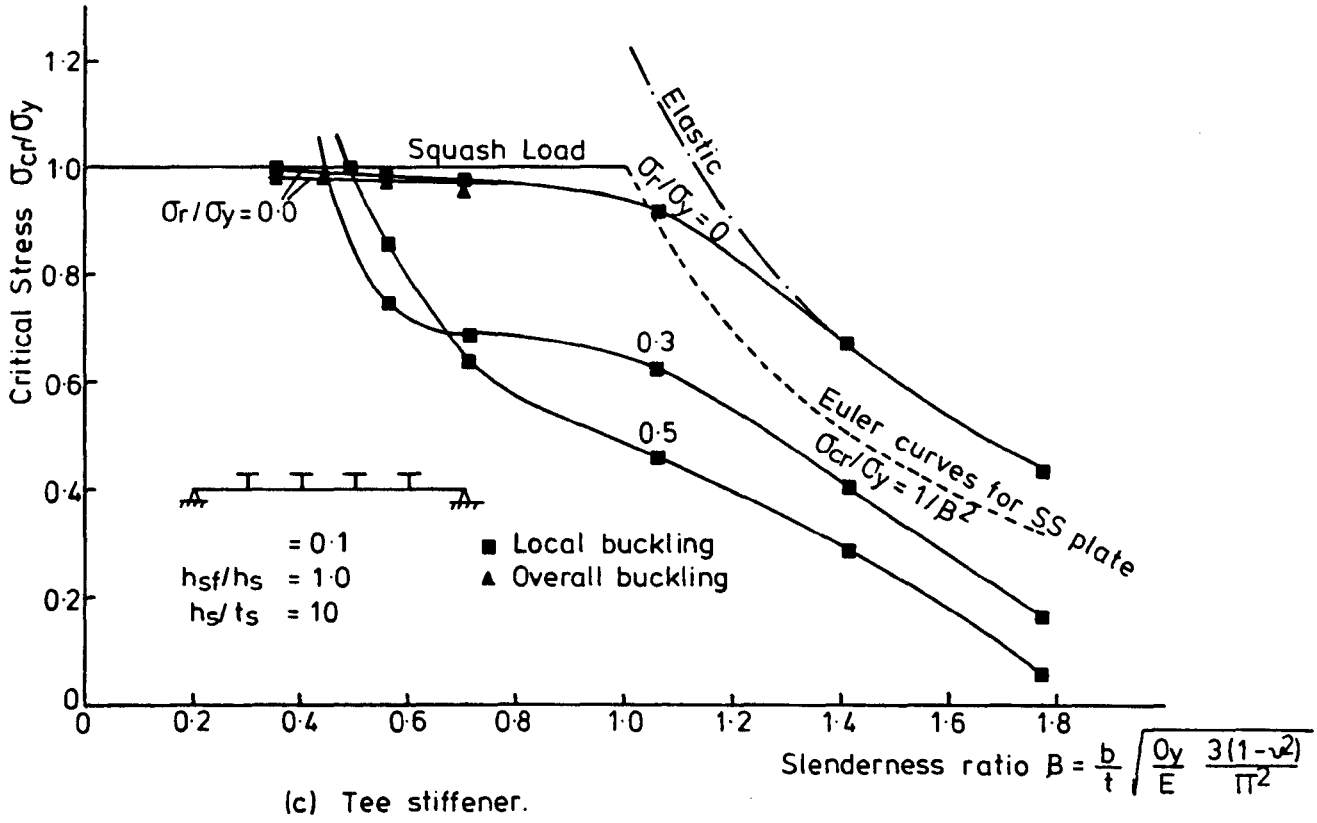

(c) Tee stiffener.

FIG. 5·5. BUCKLING STRENGTH CURVE FOR A STIFFENED PANEL.

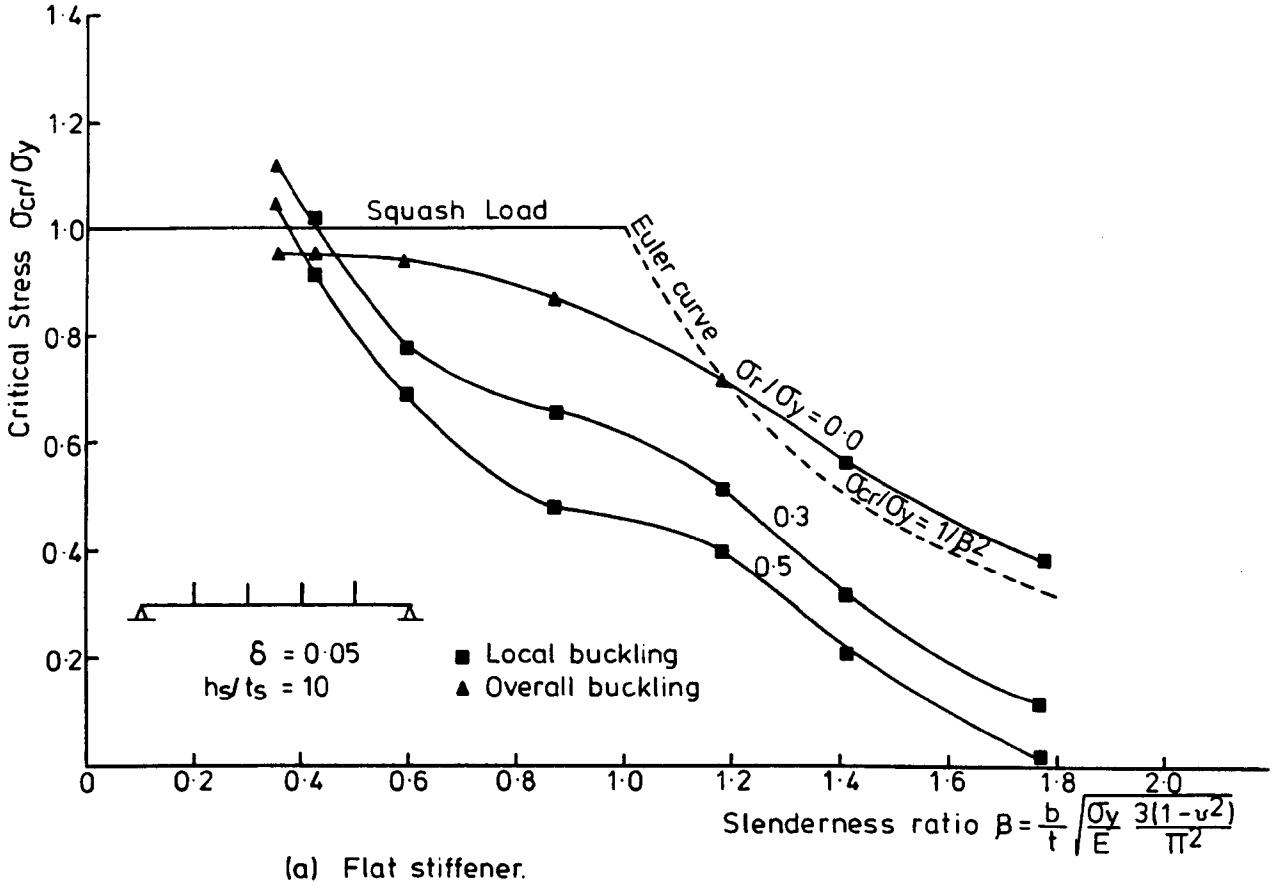

(a) Flat stiffener.

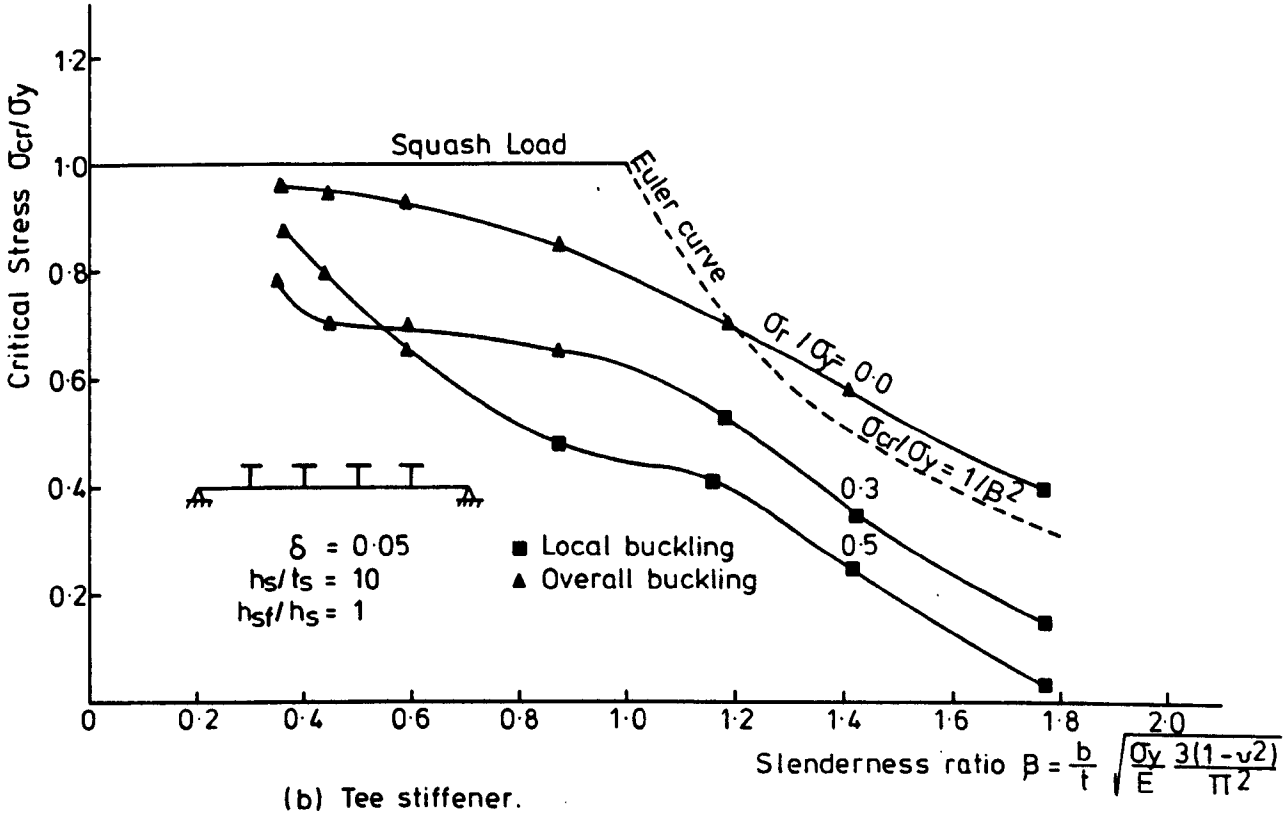

(b) Tee stiffener.

FIG. 5·6. BUCKLING STRENGTH CURVES FOR STIFFENED PANEL.

same value as used by Dowling (43) in his analysis. Two values of the ratio of the stiffener area to the plate area (δ) were considered - 0.05 and 0.1 - and the proportions of the stiffener were selected to ensure that local buckling of the stiffener outstand did not predominate.

The results for panels with relative stiffener area $\delta = 0.1$ are shown in Figure 5.5. It was found in most cases that short wavelength (local) buckling ($\lambda = b$) was critical and in these cases the curves for overall buckling ($\lambda = B$) are not shown. However, for an initially stress free panel stiffened with angle or tee stiffeners and with a slenderness ratio $\beta < 0.9$ overall buckling ($\lambda = B$) was the critical mode as shown in Figure 5.5 (b and c). The Euler curve for a simply supported plate - corresponding to the plating between stiffeners - and the elastic buckling curve of the panel ($\lambda = b$) are also shown for reference.

From the graphs it is clear that the elastic buckling curve of the panel is underestimated by the Euler buckling curve for a simply supported plate. This is due to the torsional resistance of the stiffeners and the transverse continuity with neighbouring sections of plate which provide some rotational restraint at the edges. These two factors are not included for a simply supported plate.

The initially stress free buckling curves coincide with the elastic buckling curve in the range of slenderness ratio

$\beta \geq 1.4$. When the slenderness ratio β of an initially stress free panel is reduced below unity, it is clear from Figure 5.5 that the gain in the critical stress is very small. Again, this is due to the fact that the failure of such panels is due to yielding. Comparing the buckling strength curve ($\sigma_r = 0$) with the two bounds given in Figure 5.4 it is clear that the curve coincides exactly with the upper bound ($\lambda = 0.8b$) for all slenderness ratios. This means that using stiffeners larger than $\delta = 0.1$ will not have any effect on the critical stress.

Panels with slenderness ratio $\beta > 1.3$ ($\sigma_r = 0.3\ \sigma_Y$) or $\beta > 1.4$ ($\sigma_r = 0.5\ \sigma_Y$) buckle elastically and in these elastic ranges - $\sigma_{cr} \leq (0.8\ \sigma_Y - \sigma_r)$ - the buckling curves have patterns similar to the elastic buckling curve. The reduction in the critical stress due to residual stress σ_r is approximately $0.85\ \sigma_r$ and $0.75\ \sigma_r$ respectively.

For slenderness ratio β between about 0.8 and 1.3 ($\sigma_r = 0.3\ \sigma_Y$) or 0.9 and 1.4 ($\sigma_r = 0.5\ \sigma_Y$) the effect of the residual stress becomes more pronounced. For lower values of β, the critical stress begins to increase more sharply and as the residual stress increases the critical stress increases. At a slenderness ratio $\beta \leq 0.65$ the buckling curve corresponding to a residual stress level of $0.5\ \sigma_Y$ indicates a higher critical stress than for a residual stress of $0.3\ \sigma_Y$ and this may be due to the fact that at such low slenderness ratios (because the residual stress pattern must be in self equilibrium) the central area of the plate which is subjected to residual compressive stress reduces as the residual stress increases.

Comparing the buckling strength curves - for panels with residual stress $\sigma_r = 0.3\ \sigma_Y$ and $\sigma_r = 0.5\ \sigma_Y$ - with the two bounds it is clear that these curves coincide with the upper bound ($\lambda = 0.8b$) for a wide range of slenderness ratio β. For slenderness ratios $\beta \leq 0.7$, the curve for the panel with $\sigma_r = 0.50\ \sigma_Y$ falls between the two limits and as the slenderness ratio decreases it becomes closer to the lower limit.

It is of interest to note that for panels with tee or angle stiffeners and $\beta > 0.7$, the buckling stress is about 5% higher than that corresponding to a similar panel with flat stiffeners for all values of residual stress. For a panel with flat or angle stiffeners and $\beta < 0.7$ the buckling curves are identical, being some 6% higher than the curve for a panel with tee stiffeners. This may be due to the residual stress pattern which is different for angle stiffeners and tee stiffeners as shown in Figure 5.2.

In general, for the panel with heavy stiffeners - $\delta = 0.1$ and $h_s/t_s = 10$ - the effect of the shape of the stiffeners on the buckling strength curves is relatively small. Moreover, it is also clear that the buckling strength curves are smooth curves and do not exhibit the sudden reduction which would occur at ($\sigma_{cr} = \sigma_Y - \sigma_r$) if an elastic perfectly plastic stress-strain relationship for the material had been assumed. In the present approach the more sophisticated stress-strain relationship (Chapter 3) leads to a gradual change from elastic buckling to inelastic buckling.

A similar study has been conducted using both flat and tee stiffeners of reduced size such that $\delta = 0.05$. This value has been chosen so that overall buckling ($\lambda = B$) will predominate over the local buckling ($\lambda = b$) of the panel which was critical for $\delta = 0.1$. The effect of the slenderness ratio of the plate on the critical stress of this panel is shown in Figure 5.6.

For an initially stress free panel with flat stiffeners and for slenderness ratios $\beta \leq 1.3$, the panel buckles in an overall mode but local buckling becomes critical as the slenderness ratio increases. A further point of interest is that the maximum critical load for the stockiest panel considered ($\beta = 0.35$) is only 95% of the squash load whereas for $\delta = 0.1$ it was equal to the squash load. This reduction is due to the fact that as this panel buckles in an overall mode, not only the slenderness ratio of the plating but also the stiffener properties have an effect on the buckling.

As the residual stress is increased ($\sigma_r = 0.3\ \sigma_Y$ and $0.5\ \sigma_Y$) the buckling mode changes to a more predominantly local mode ($\lambda = b$) and this is a reflection of the fact that local buckling is more sensitive to the level of residual stress than overall buckling.

It is of interest to note that the critical stress of the panels with very low slenderness ratios - $\beta < 0.4$ - exceeds the squash load. This may be due to the initial tensile stresses present in the panel required to maintain

equilibrium with the initial compressive residual stress. In general the buckling strength curves (Figure 5.6(a)) are similar to those for $\delta = 0.1$ (Figure 5.5(a)) but corresponding values of critical stress are lower for the panels with smaller stiffeners as would be expected. This difference depends on the slenderness ratio, the residual stress level and the half wavelength (i.e. mode of buckling).

It is clear from Figure 5.6(a) that a panel with slenderness ratio $\beta \geq 1.8$ will buckle locally ($\lambda = b$) under the effect of the residual stress alone if its value σ_r exceeds $0.5\ \sigma_Y$.

Comparing the curves for panels with flat stiffeners with the corresponding curves for panels with tee stiffeners, it appears that for the latter, the long wavelength (overall) buckling of the panel is critical (over a wider range of slenderness ratios β). This may be due to the more severe residual stress pattern assumed for the tee stiffener. This pattern leads to more substantial losses in the flexural rigidity of the stiffener accompanied by overall buckling of the panel.

For both types of stiffener - flat and tee - the slenderness ratio at which overall buckling ($\lambda = B$) becomes critical depends on the residual stress. Moreover, the range of slenderness ratio β for which the overall buckling

is critical is wider for panels with tee stiffeners than for panels with flat stiffeners, for all values of σ_r.

From the above discussion, it can be concluded that the buckling strength curves can be divided into three parts - elastic, inelastic and squash. The effect of the residual stress is more pronounced in the inelastic range than in the elastic range and the squash load may be overestimated if the panel is heavily welded.

5.2.2 Effect of Stiffener Geometry on the Buckling Strength

The effect of the stiffener area, the stiffener depth to thickness ratio h_s/t_s, the flange width to web depth ratio h_{sf}/h_s (for tee stiffener) and the stiffener shape (flat, angle and tee) on the buckling strength of a stiffened panel have been studied. The local buckling of the plating between stiffeners has been calculated from the short wavelength (λ = b) while the overall buckling has been determined from the long wavelength (λ = B). The buckling strength curves corresponding only to the critical mode are given, but in some cases the buckling strength curves corresponding to the two modes - local and overall - are given.

To investigate the effect of both the stiffener depth to thickness ratio and the stiffener shape on the buckling strength, only two panels - one buckling elastically and the other inelastically - have been considered.

5.2.2.1 The Effect of the Stiffener Area

To study the effect of stiffener area and the flange width to web depth ratio h_{sf}/h_s (of tee stiffener) on the buckling strength, the results for panels stiffened with flat or tee ribs with $h_s/t_s = 10$ and $\sigma_r = 0.3\ \sigma_y$ are reproduced in Figure 5.7 together with additional results for stiffeners with $h_s/t_s = 15$ and tee stiffeners with $h_{sf}/h_s = 0.5$.

It is clear that the more slender panels ($\beta \geq 1.4$) with flat stiffeners buckle in a local mode ($\lambda = b$) and the effect of h_s/t_s - 10, 15 - is small. As the slenderness ratio decreases, the effect of h_s/t_s increases. It is of interest to note that the buckling strength of panels with $h_s/t_s = 10$ is higher than the buckling strength of panels with $h_s/t_s = 15$ for all slenderness ratios β. This may be due to the fact that this panel buckles in a local mode.

It is also clear from Figure 5.7(a) that the stiffener area ($\delta = 0.1$ and 0.05) has no effect on the buckling strength of stocky panels ($\beta \leq 0.8$) as long as h_s/t_s ratio is constant ($h_s/t_s = 10$). Increasing the slenderness ratio of the panel, the stiffener area produces some increase in the local buckling strength. The effect of the stiffener area, on this strength, increases as the slenderness ratio increases.

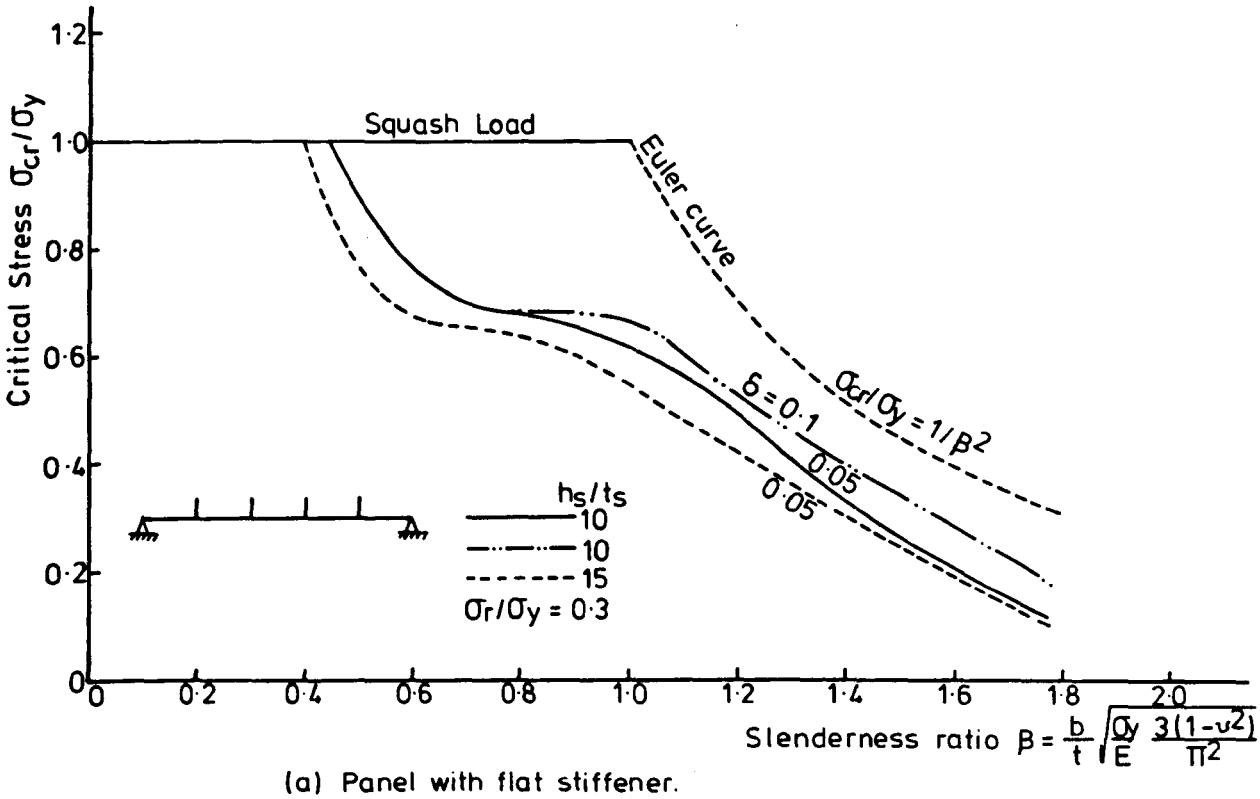

(a) Panel with flat stiffener.

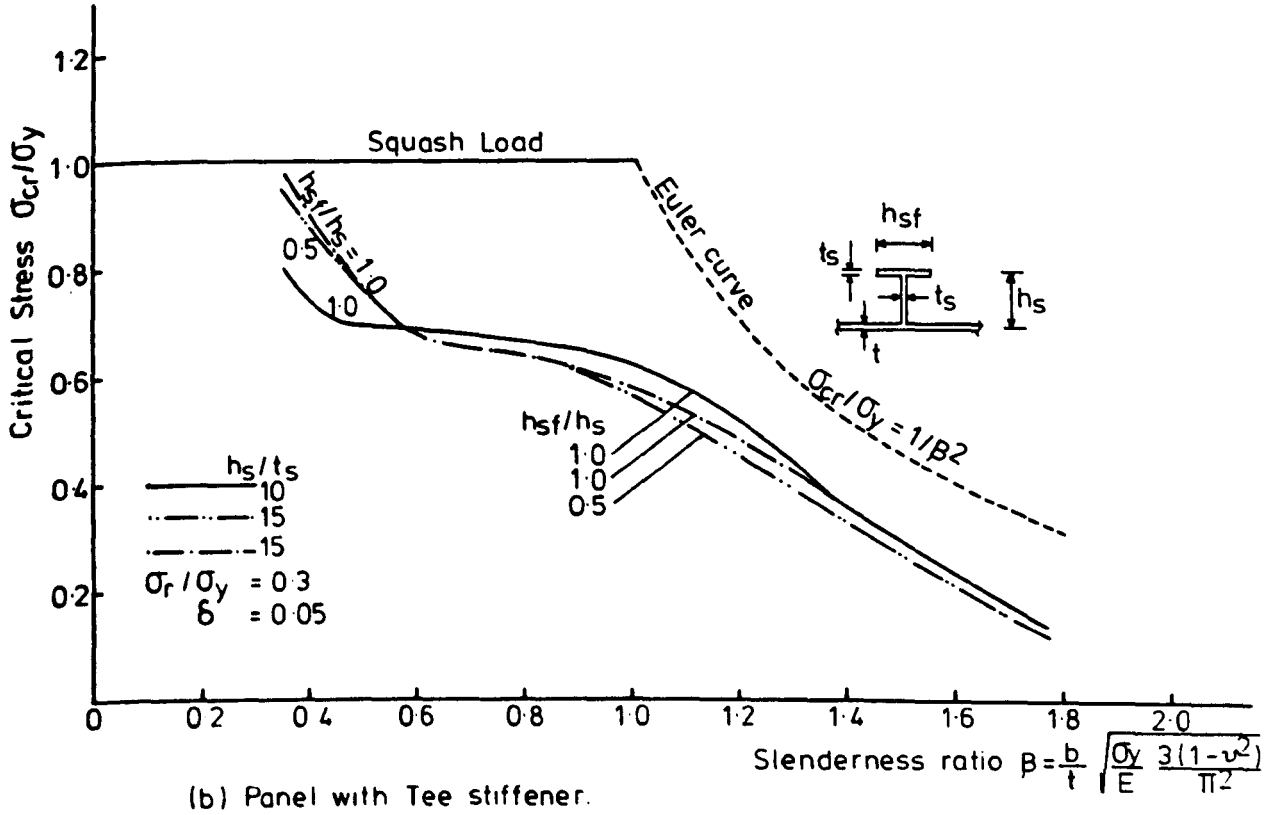

(b) Panel with Tee stiffener.

FIG. 5.7 VARIATION OF CRITICAL STRESS WITH SLENDERNESS RATIO FOR DIFFERENT STIFFENER DIMENSIONS

The panel with tee stiffeners (h_s/t_s = 15) behaves in a similar manner to the panel with tee stiffeners corresponding to h_s/t_s = 10 in the range of $\beta > 0.6$. Both panels buckle in a local mode. For slenderness ratios β less than this, there is an effect on the buckling strength due to the increase of the h_s/t_s ratio. The increase in the buckling strength for the panel with h_s/t_s = 15 is due to the fact that the panel buckles in an overall mode in the range of $\beta \leq 0.6$.

The effect of h_{sf}/h_s of the tee stiffener on the buckling strength for a wide range of slenderness ratio is very small. Fukumoto et al (60) also demonstrated this in their theoretical work. For panels with $\beta < 0.5$ the h_{sf}/h_s = 1.0 buckling curve is slightly higher than the h_{sf}/h_s = 0.5 buckling curve. This may be due to the increase in the flexural rigidity of the stiffener with higher h_{sf}/h_s.

The effect of h_{sf}/h_s and h_s/t_s on the buckling strength of a panel depends on the mode of buckling. The panels discussed above buckle in a local mode where this effect is small. But the strength of a panel buckling in an overall mode will increase as the h_{sf}/h_s ratio decreases. This is because the flexural rigidity rather than the torsional rigidity is the controlling factor.

5.2.2.2 Effect of Stiffener Depth to Thickness Ratio

Two panels with slenderness ratios β = 0.88 and 1.414 stiffened with flat, angle or tee stiffeners have been considered in a study of the relationship between the stiffener size and the critical stress. These two values of slenderness were chosen (from the previous section) to represent the inelastic and elastic ranges respectively. The stiffener thickness t_s was assumed to be equal to the plate thickness t and the stiffener depth h_s was varied from zero (unstiffened panel) to 16t. Three levels of residual stress - σ_r = 0, 0.3 σ_Y and 0.5 σ_Y - have been considered.

Figure 5.8 shows how, as the stiffener size is increased, the critical buckling mode of the panel changes from that of a predominantly overall mode (λ/b = 5.0) to a local mode for which the plate buckles between adjacent stiffeners (λ/b = 1.0). For the range of stiffener depths considered ($\leq$ 16t) local buckling of the stiffener outstand is not significant. It is clear from this graph that the local buckling of a panel with low h_s/t increases rapidly as h_s/t is increased, due to the increase in the torsional stiffness of the stiffener. Above a certain ratio however, the effect of h_s/t on the local buckling is very small (the torsional rigidity rather than the flexural rigidity is more effective), this ratio depending on the slenderness ratio of the plate β and the residual stress level σ_r.

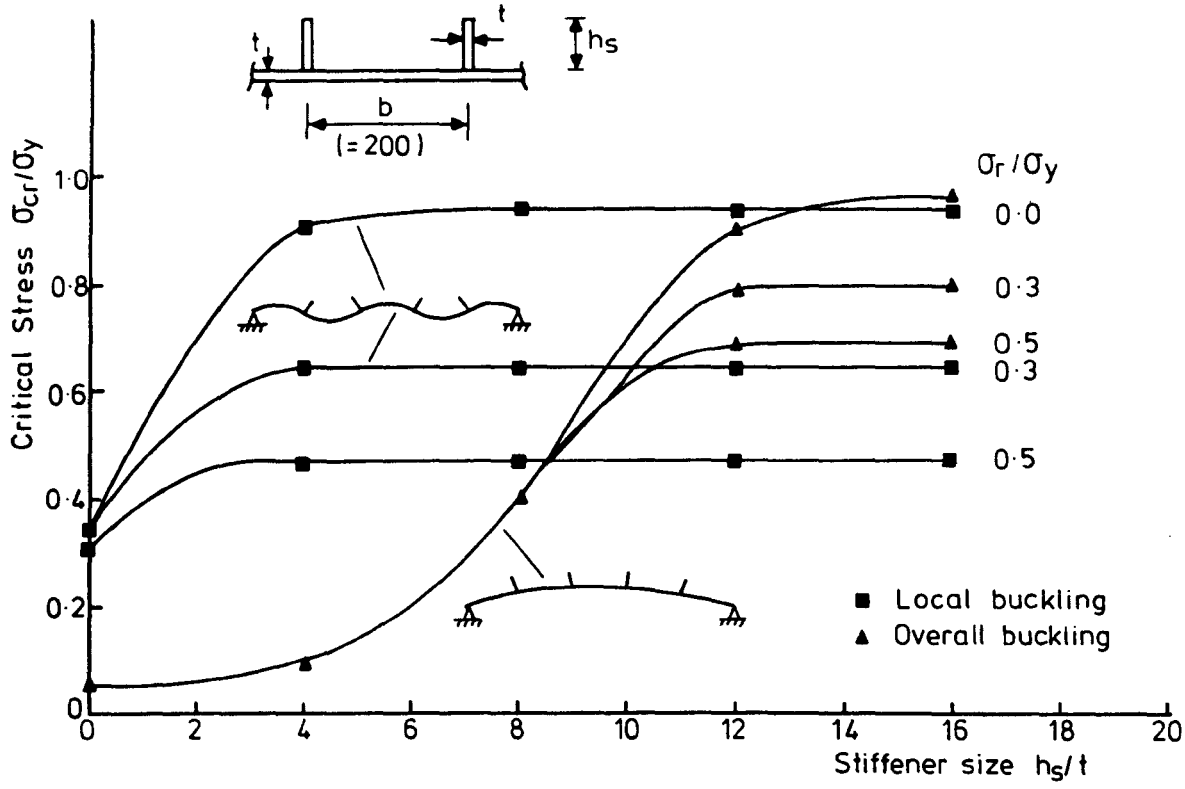

(a) β = 0·88 (t = 4)

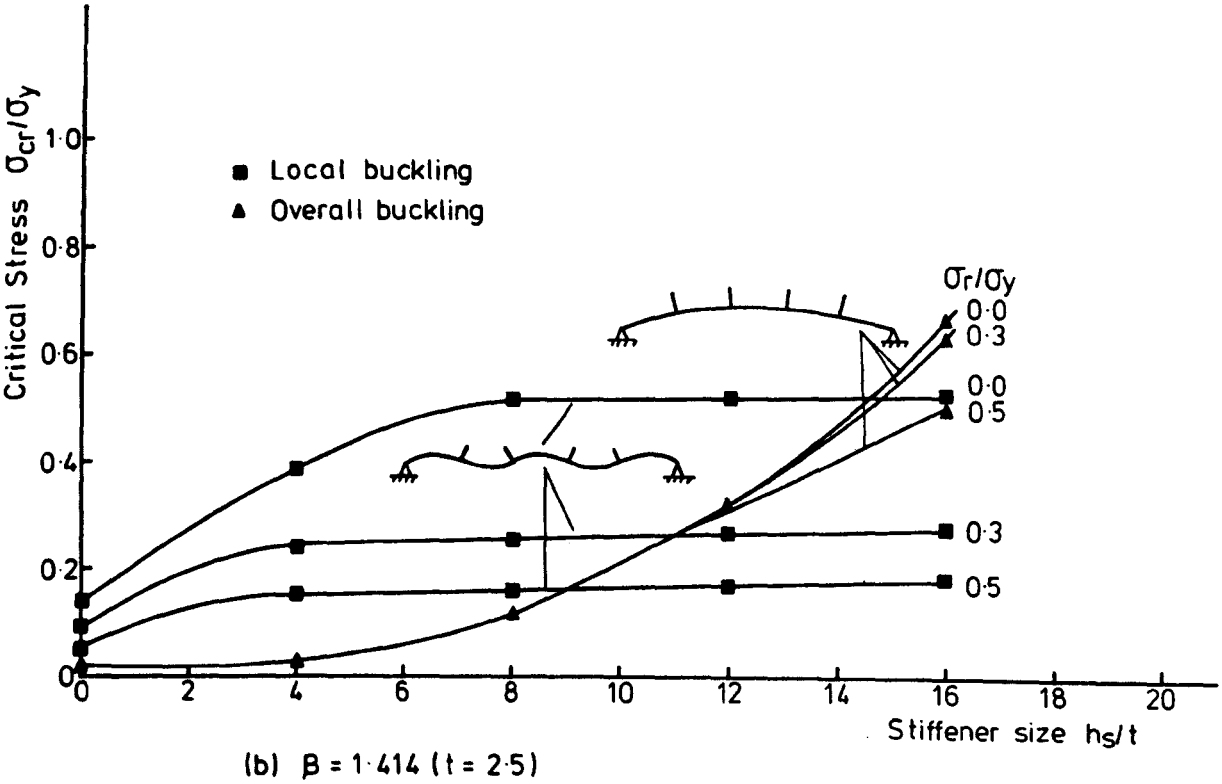

(b) β = 1·414 (t = 2·5)

FIG. 5·8. VARIATION OF CRITICAL STRESS WITH STIFFENER SIZE FOR A PANEL WITH FOUR FLAT STIFFENERS.

For panels with $h_s/t_s = 0$ (unstiffened) the effect of the residual stress level on local buckling is small. The effect of residual stress however increases as h_s/t increases until at a certain value of h_s/t the effect becomes constant and the local buckling curves for different σ_r-values become parallel.

It is clear that the more slender panel ($\beta = 1.414$) behaves elastically for the range of stiffener sizes considered, the critical stress being always less than ($0.8 \sigma_Y - \sigma_r$). While the overall buckling curves for the first panel, $\beta = 0.88$ become parallel to the local buckling curves at higher h_s/t, this does not occur for this panel as shown in Figure 5.8(b). This is due to the spread of yielding in the stiffeners of the first panel which reduces the effect of the stiffener (flexural rigidity) on the overall buckling strength. This spread of yielding also affects the local buckling of the panel. For the stockier panel the critical local buckling stress is approximately constant while for the other panel this critical local buckling increases slightly with the increase of the stiffener depth. For this panel, an increase in h_s/t of 50% leads to a 5% increase in the local buckling strength.

The intersection of the local buckling curves and the overall buckling curves leads to one of the possible definitions of the optimum size of the stiffeners. In designing stiffened plates, it may be that this optimum

stiffener size is required. From the comparison of the behaviour of the two panels - β = 0.88 and 1.414 - it is apparent that the optimum h_s/t increases as the slenderness ratio increases. For a 38% increase in the slenderness ratio of an initially stress free panel, the optimum h_s/t increases by 10%.

As an extension of this study similar panels with four angle or tee stiffeners have been examined. The results for the two panels with slenderness ratios, β = 0.88 and 1.414 and three levels of residual stress σ_r = 0.0, 0.3 σ_Y and 0.5 σ_Y - are shown in Figure 5.9. The general pattern of behaviour is similar to that shown in Figure 5.8 for a panel with flat stiffeners.

For the stockier panels there is no effect for h_s/t on the local buckling (λ = b) strength. The local buckling strength of the more slender panels increases by 12% as h_s/t is increased by 50%. This ratio, 12%, is more than twice the corresponding increase for flat stiffeners. However it is worth noting that although the increase in h_s/t is the same in both cases - 50% - the actual increase in the areas of the flat stiffeners and the tee stiffeners are 50% and 100% respectively.

The presence of residual stresses reduces the overall buckling of the stocky panel (β = 0.88) when $h_s/t > 5.0$ but for the more slender panel (β = 1.414) it has no effect. This may be due to the elastic behaviour of the slender panel. The optimum h_s/t reduces as the residual stresses

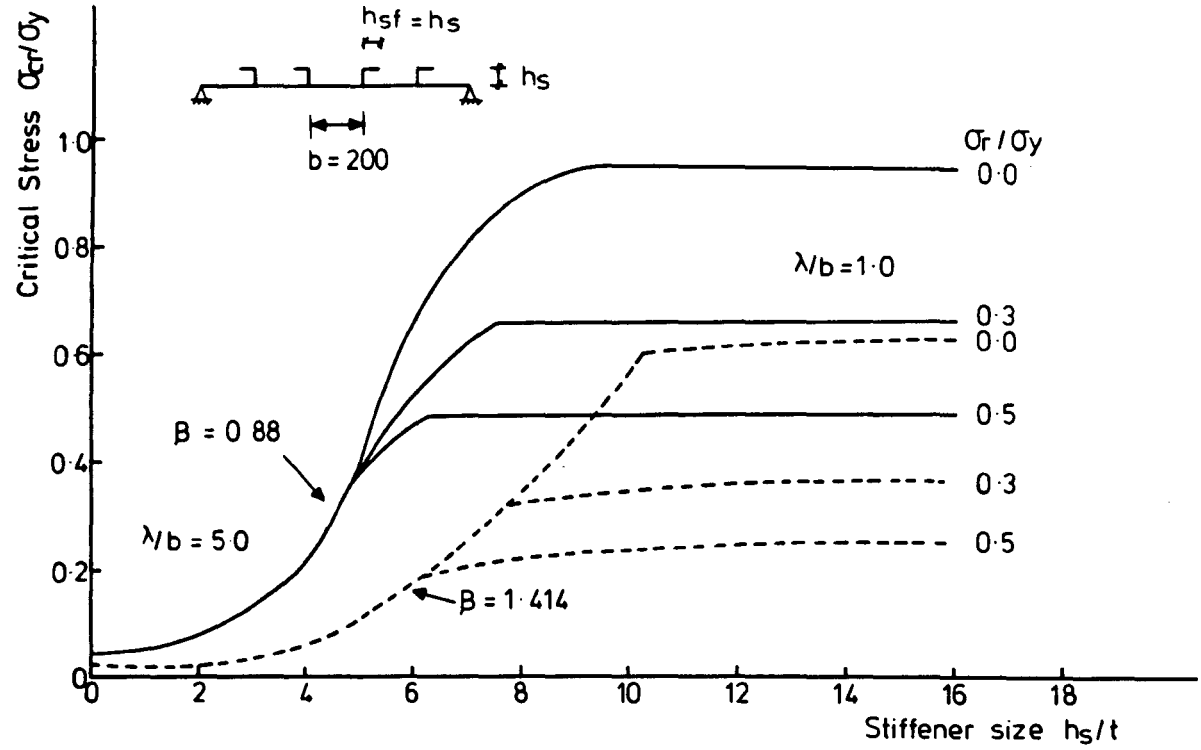

(a) Panel with angle stiffeners.

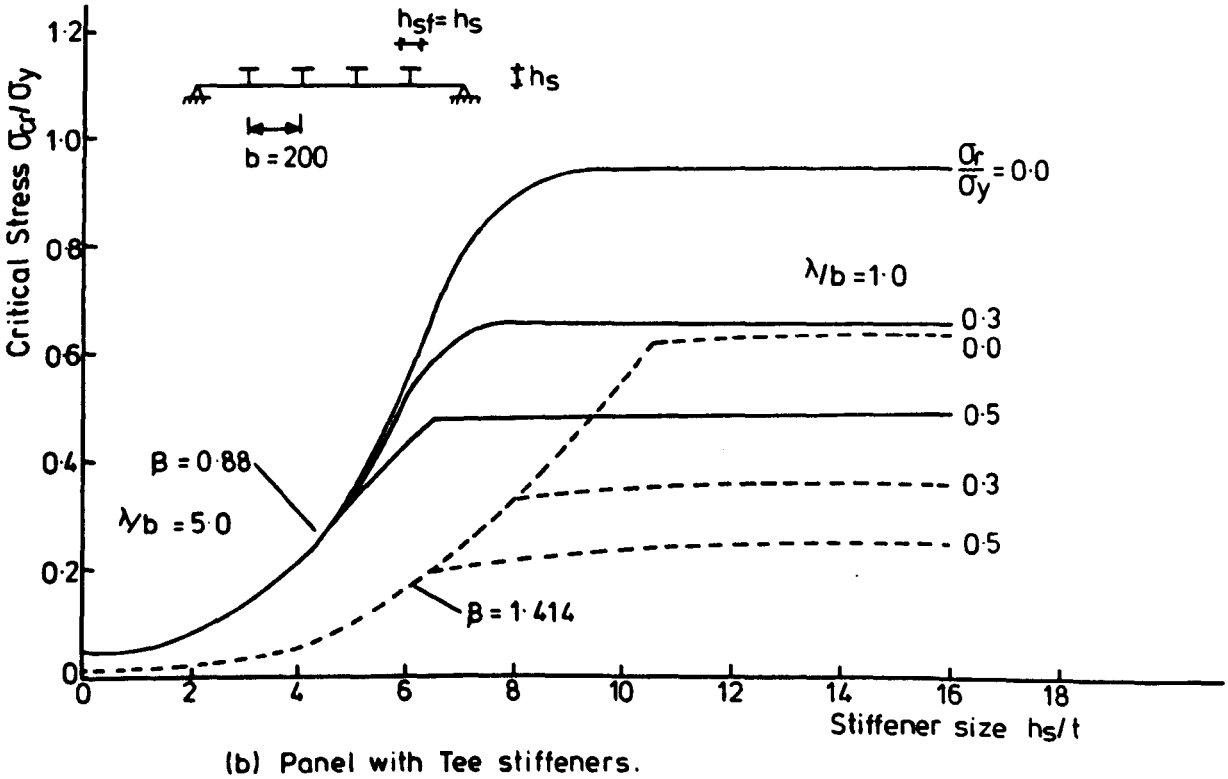

(b) Panel with Tee stiffeners.

FIG. 5·9. VARIATION OF CRITICAL STRESS WITH STIFFENER SIZE FOR DIFFERENT LEVELS OF RESIDUAL STRESS.

increase. This is because of an increase in the tendency towards local buckling, which is not greatly affected by the increase of the stiffener depth, h_s. When σ_r is changed from 0.0 to 0.5 σ_Y the optimum h_s/t reduces by about 28% and 40% for panels with β = 0.88 and 1.414 respectively.

5.2.2.3 Effect of the Stiffener Shape

Three identical panels stiffened with flat, angle and tee stiffeners have been considered in an attempt to establish the efficiency of the stiffener shape. The area of the three types are equal and their thicknesses are equal to the plate thickness. For three levels of residual stress - σ_r = 0, 0.3 σ_Y and 0.5 σ_Y - the variation of σ_{cr}/σ_Y against δ is shown in Figure 5.10 and Figure 5.11 for panels with slenderness ratios β = 1.414 and 0.88 respectively. The ratio of the stiffener area to the plate area (δ) is proportional to the amount of material spent on stiffening the flange; therefore the figures provide information on the effectiveness of the rib material in increasing the critical load.

For the more slender panel (β = 1.414) with flat stiffeners the results show clearly that for a wide range of δ the overall buckling (λ = B) stress is approximately 100% greater than the corresponding values for both the tee and angle stiffened panels. This range decreases as the residual stresses increase. While it is between δ = 0.012 ∿ 0.037 for an initially stress free panel, it reduces to

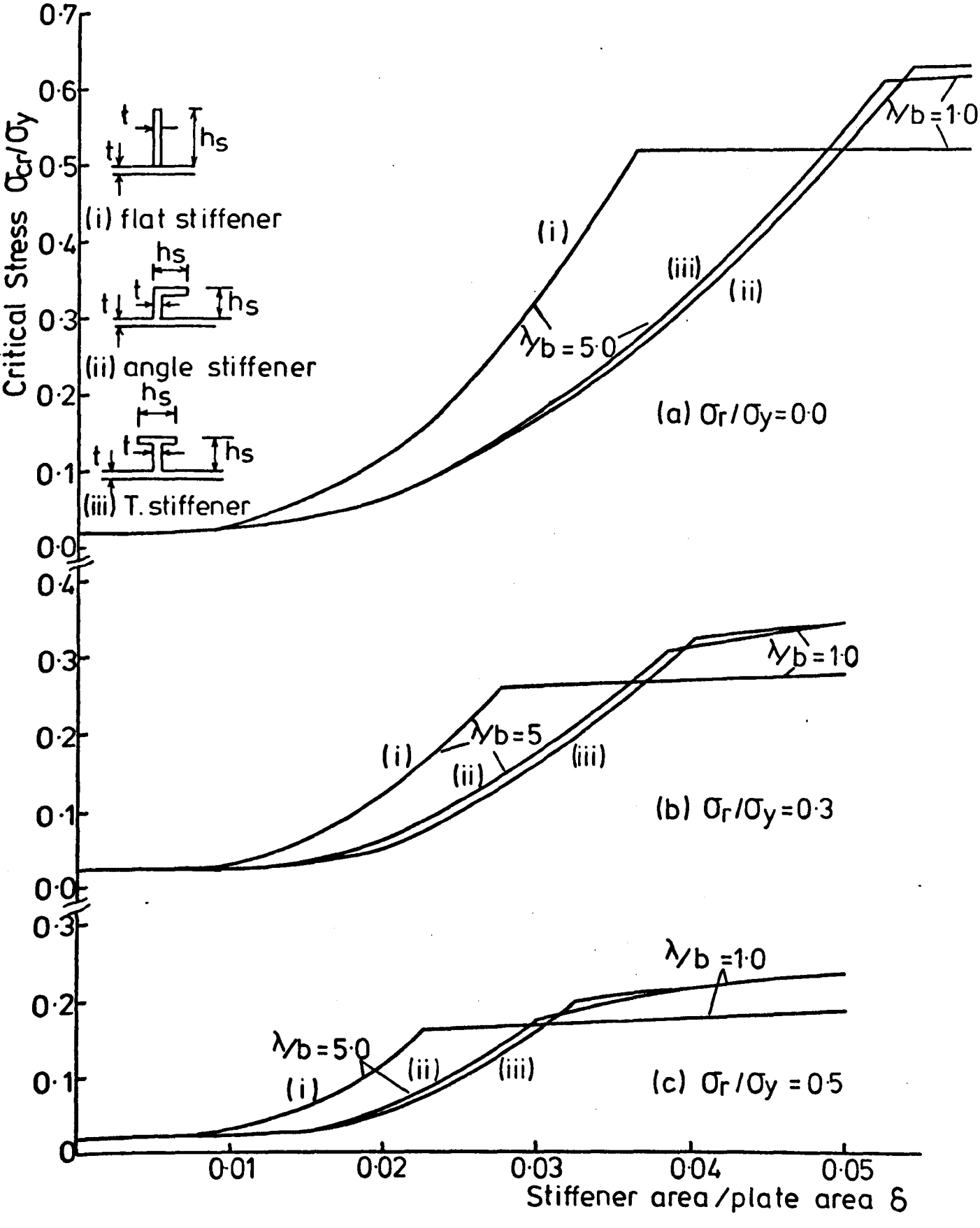

FIG. 5·10. VARIATION OF CRITICAL STRESS WITH STIFFENER SIZE FOR VARIOUS SHAPES OF STIFFENER CROSS-SECTION. ($\beta = 1·414$)

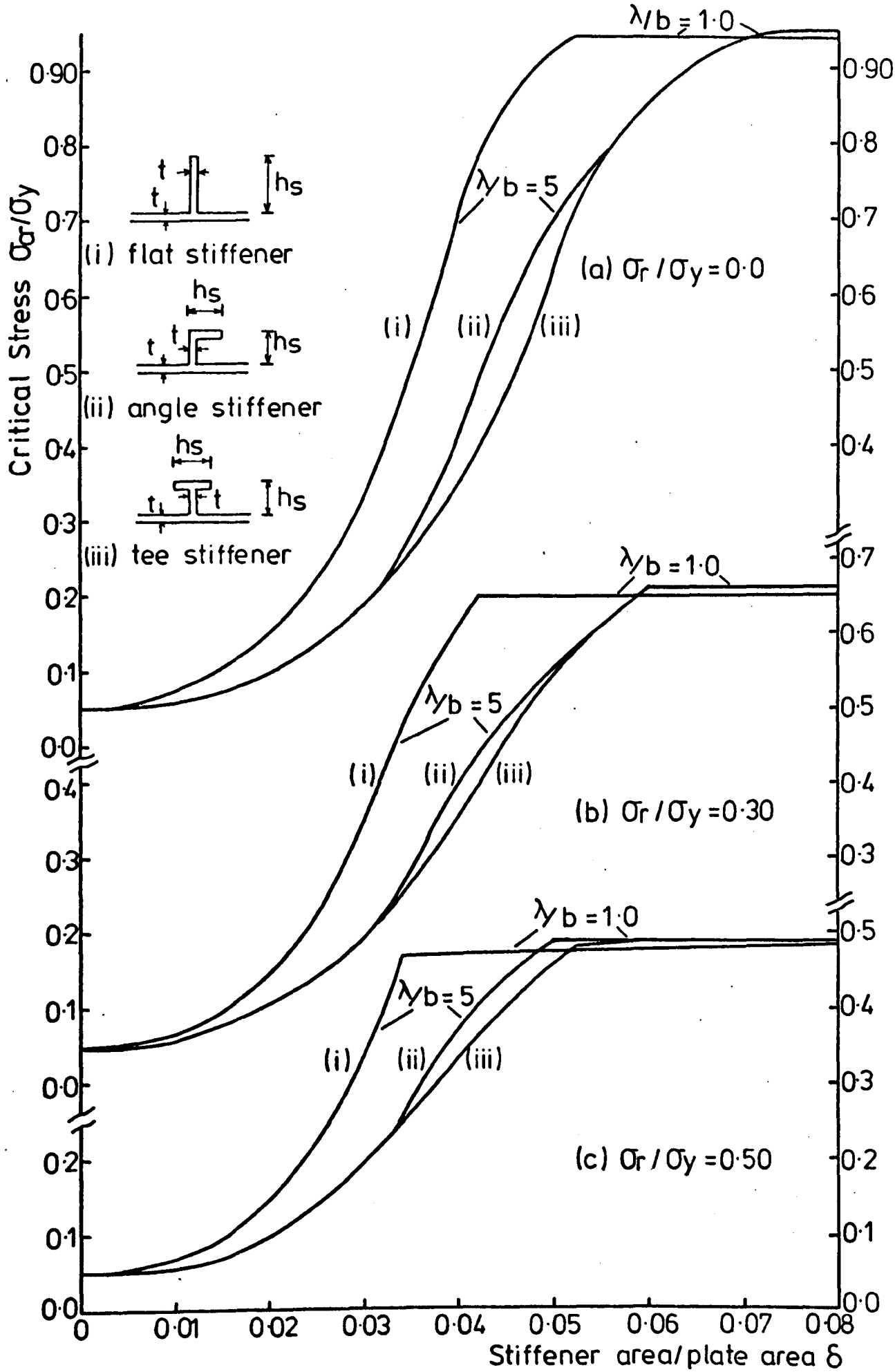

FIG. 5·11. VARIATION OF CRITICAL STRESS WITH STIFFENER SIZE FOR VARIOUS SHAPES OF STIFFENER CROSS-SECTION. ($\beta = 0{\cdot}88$)

δ = 0.012 $\sim$ 0.022 for a panel with $\sigma_r = 0.5\ \sigma_Y$. This is due to the early local buckling of the second panel.

For the initially stress free panel (β = 1.414) and at a value of δ of about 0.036 however, local buckling (λ = b) becomes critical for the flat stiffened panel and for values of δ greater than about 0.052 the angles and tee stiffened panels are more efficient. This value reduces to 0.038 and 0.030 for panels with $\sigma_r = 0.3\ \sigma_Y$ and $0.5\ \sigma_Y$ respectively. The increase in the local buckling stress due to using angle or tee stiffeners instead of the flat stiffeners is about 20% for an initially stress free panel. This value increases as the residual stress increases and for panels with $\sigma_r = 0.3\ \sigma_Y$ and $0.5\ \sigma_Y$ the value becomes 30% and 50% respectively.

The variation in the critical stress simply reflects the relative stiffnesses of the various sections for the different modes of buckling - local (λ = b) and overall (λ = B). It is of interest to note that the tee and angle stiffeners give results close to each other for any level of σ_r. The difference in the critical stress is about 6% on average. At a high ratio of δ the overall buckling of the panel with tee ribs, and the local buckling of the panel with angle ribs give the upper limits.

From Figure 5.10 and Figure 5.11 it is clear that as the slenderness ratio of the panel decreases, the effect of the stiffener shape (flat, tee and angle) on the critical -

local and overall - buckling stress decreases. For the stockier panel - $\beta = 0.88$ - this effect becomes approximately zero in the local buckling mode. The 100% increase in overall buckling stress observed in the slender panel ($\beta = 1.414$) with flat stiffeners reduces to 50% for the stockier one but its range becomes wider. It is worth noting that, for any stiffener shape, the change from the overall buckling mode ($\lambda = B$) to the local buckling mode ($\lambda = b$) is more gradual for the stockier panel with $\sigma_r = 0.0$.

Some designers and researchers suggest that the tee stiffener is more favourable than the rectangular stiffener. Fukumoto et al (60) referred this to the fact that the reduction of the effective flexural rigidity is much more gradual in tee cross-sections than in flat cross-sections. They found that the strength reduction due to yielding in the stiffeners are rather gradual in this type of stiffened plates. On the other hand Kristek et al (113) found that flat stiffeners are more efficient than any other type for a wide range of δ. Kristek's work was limited to initially stress free elastic panels.

From the present results, it is clear that it is not usual for tee or angle stiffeners to perform better than flat stiffeners. This is due to the fact that the flexural rigidity of a flat stiffener increases very quickly with the increase of δ (for constant thickness) but increases slowly

for other types of stiffeners until a limit where local buckling of the plate between stiffeners occurs. Any further increase in the flexural rigidity will have no effect on the panel with flat stiffeners but will continue to increase the critical stress for a panel with tee or angle stiffeners.

5.2.3 Effect of the Orientation of the Angle Stiffener

The orientation of the outstanding leg of the angle stiffener has been considered in connection with its effect on local (λ = b) and overall (λ = B) buckling. The results for a panel with slenderness ratio β = 1.414 under three levels of residual stress - σ_r = 0.0, 0.3 σ_Y and 0.5 σ_Y - are shown in Figure 5.12. The finite strip method and the folded plate theory (113) show that the orientation of the outstanding leg has some effect on the overall buckling stress. Kristek et al (113) referred this to the fact that the bending moments, through which the oustanding legs of the angle stiffeners act on the flange sheet, stabilize the buckled sheet in the case of the outward-orientated legs but enlarge the sheet flexure when the outstanding legs have an inward orientation. The two modes of buckling, local (λ = b) mode and overall (λ = B) mode used in the present analysis are similar to those used by Kristek.

From Figure 5.12 it is clear that there is no effect on the overall buckling stress for the orientation of a stiffener with $h_s/t \leq 5$. The increase in the critical

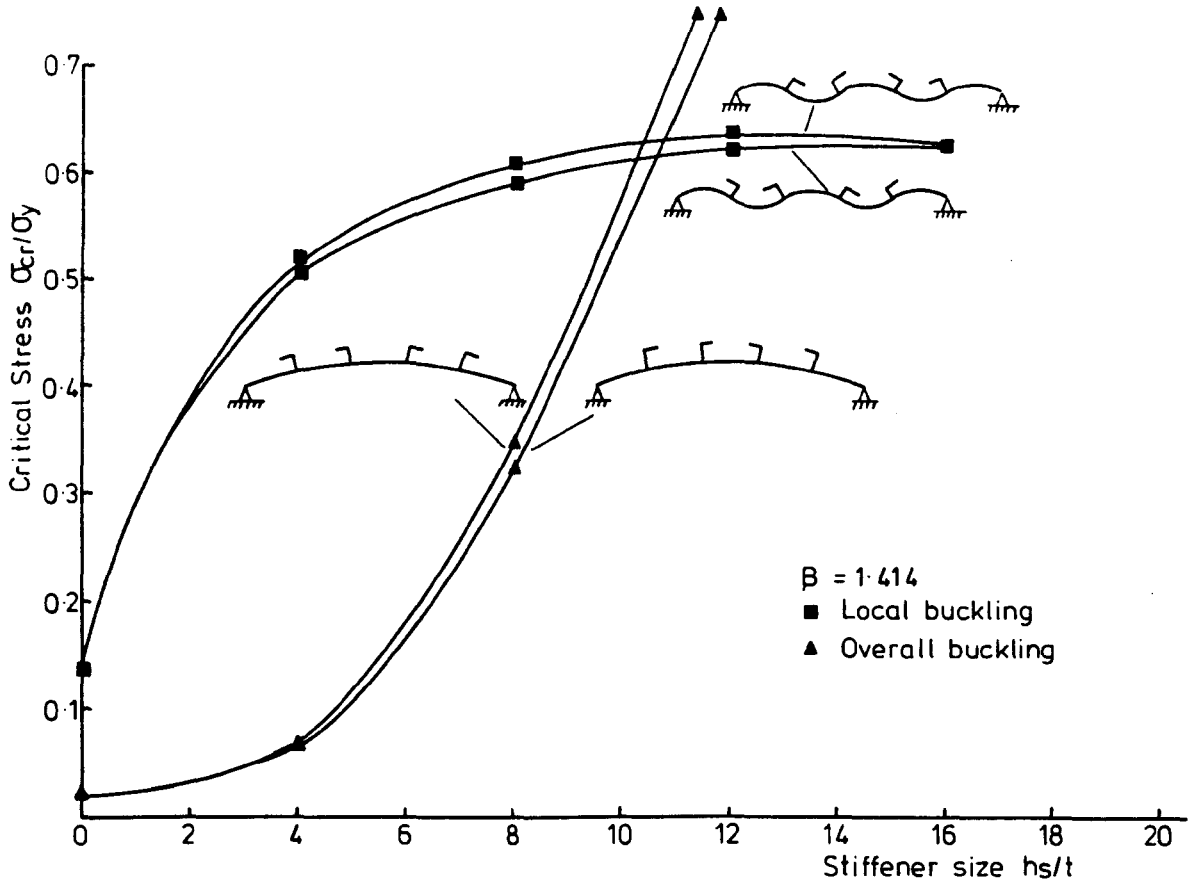

(a) Stress free panel. ($\sigma_r/\sigma_y = 0{\cdot}0$)

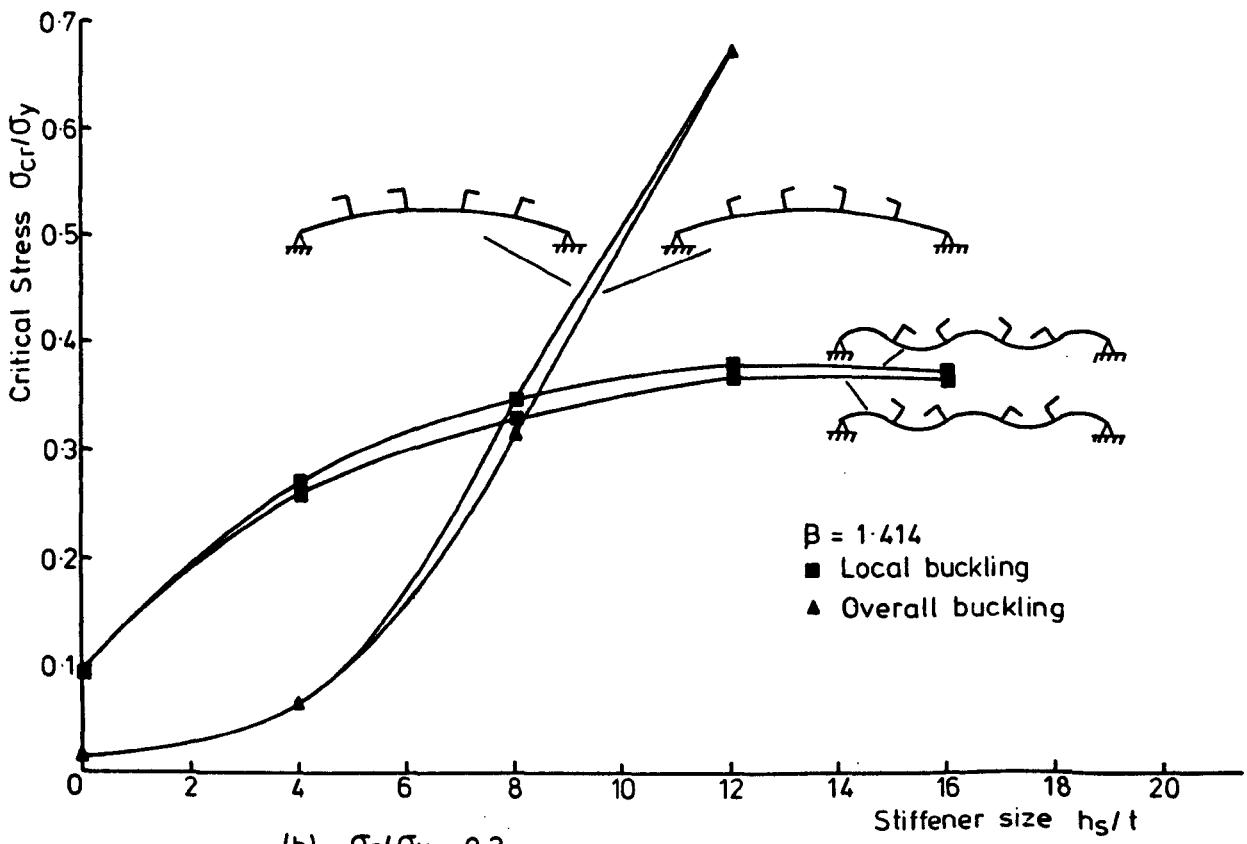

(b) $\sigma_r/\sigma_y = 0{\cdot}3$

FIG. 5·12 (Cont.....)

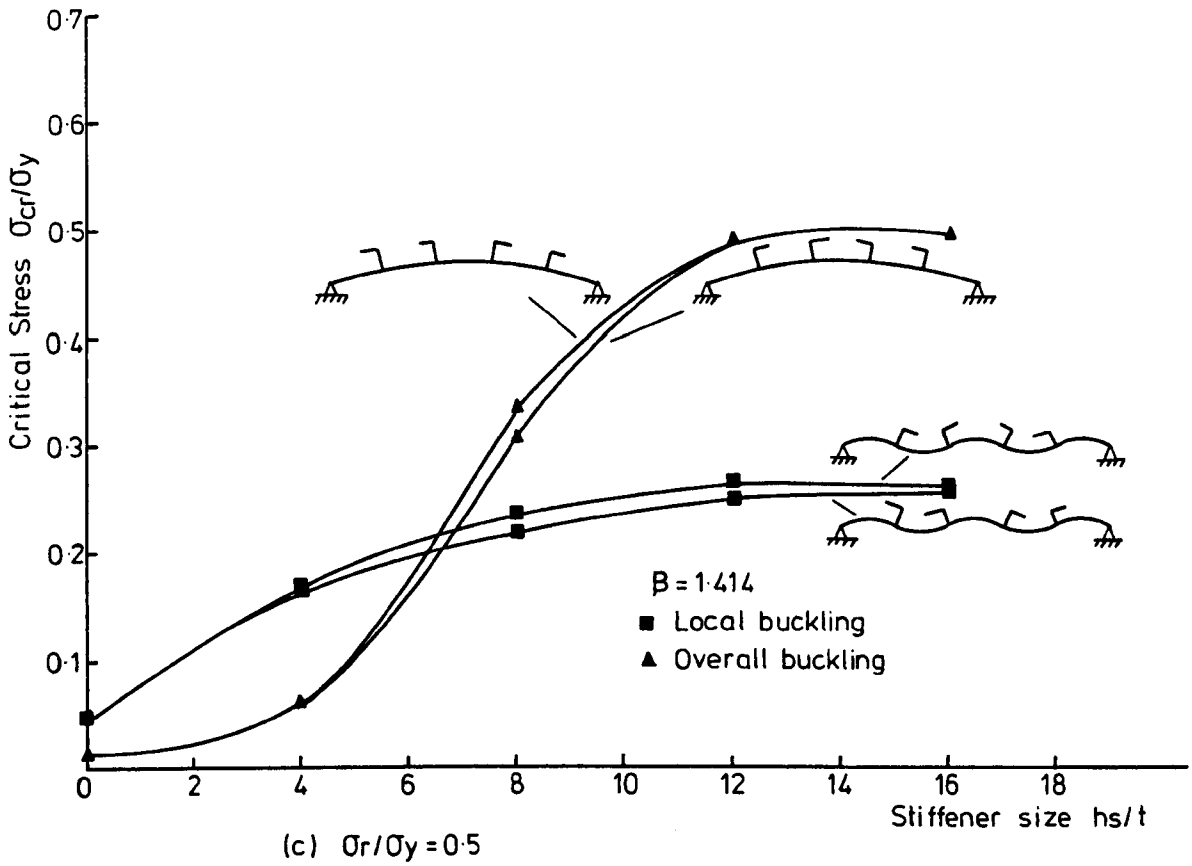

(c) $\sigma r/\sigma y = 0{\cdot}5$

FIG. 5·12. THE INFLUENCE OF THE ORIENTATION OF THE ANGLE STIFFENERS ON THE CRITICAL STRESS. ($\beta = 1{\cdot}414$)

stress, due to outward orientation, starts gradually as the stiffener depth h_s/t increases up to the optimum value h_s^*/t. Increasing the stiffener size over the optimum size will reduce the effect of the orientation on the overall buckling stress and it vanishes. As the residual stresses are increased the effect of the orientation of the outstanding leg increases. The overall buckling stress of an initially stress free panel with outward orientated stiffeners - at optimum h_s/t - is higher than the buckling stress of a panel with inward orientated stiffeners by 6%. This ratio icnreases to 12% for a panel with residual stress σ_r = 0.5 σ_Y.

For the local buckling mode (λ = b) the folded plate results (113) do not exhibit any influence of the orientation. The critical buckling stress of an inward orientated panel, based on the finite strip is higher than the critical stress of outward oriented panel. The effect of the orientation on local buckling stress reduces as h_s/t increases above its optimum value.

The optimum h_s^*/t for the inward orientation is higher than that for the outward orientation by 5% and 11% for panels with residual stress σ_r = 0.0 and 0.5 σ_Y respectively. The change in the critical stress with orientation may be due to the change in the out-of-plane displacements of the outstanding leg of the stiffener - which depends on the orientation - relative to the displacements of the plate.

Comparing both orientations, the smaller displacement of the outstanding leg of the angle stiffener leads to a higher overall buckling stress. It can be imagined that the angle stiffeners are replaced by an elastic support or springs. The stiffness of these springs is proportional to 1/w where w is the displacement of the centre of gravity of the stiffener. This displacement in overall buckling modes of a panel with outward orientated stiffeners is less than the displacement for a panel with inward orientated stiffener. So the stiffness of the springs is higher in the first case and the critical buckling load is higher. A similar analysis can be conducted for the local buckling mode.

From this it is clear that by choosing the better orientations of the outstanding leg of an angle stiffener a further increase in critical load could be obtained.

5.2.4 Influence of Residual Stress

The same two panels - β = 0.88 and 1.414 - with flat stiffeners and five levels of residual stress - σ_r = 0.0, 0.2 σ_Y, 0.3 σ_Y, 0.4 σ_Y and 0.5 σ_Y - have been used to study the effect of residual stresses on the stiffener size. The overall buckling mode (λ = B) and the local buckling mode (λ = b) have been considered and the results are shown in Figure 5.13.

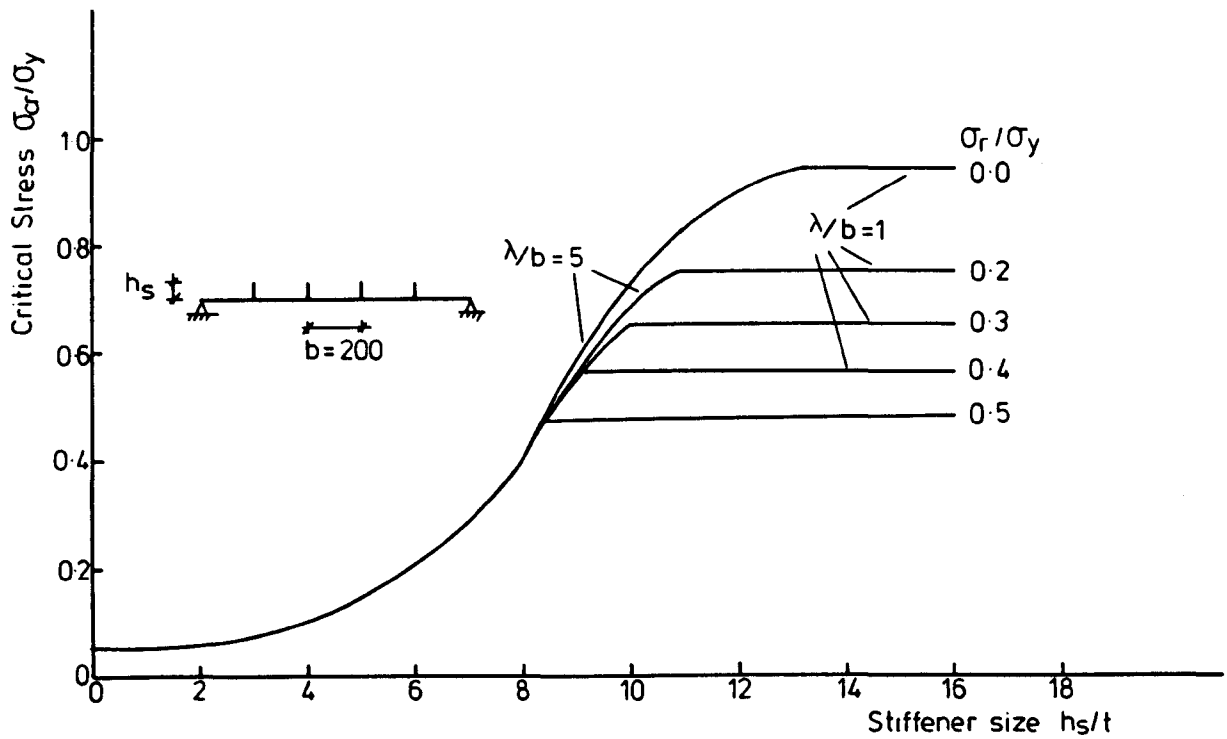

(a) β = 0·88 (t = 4·0)

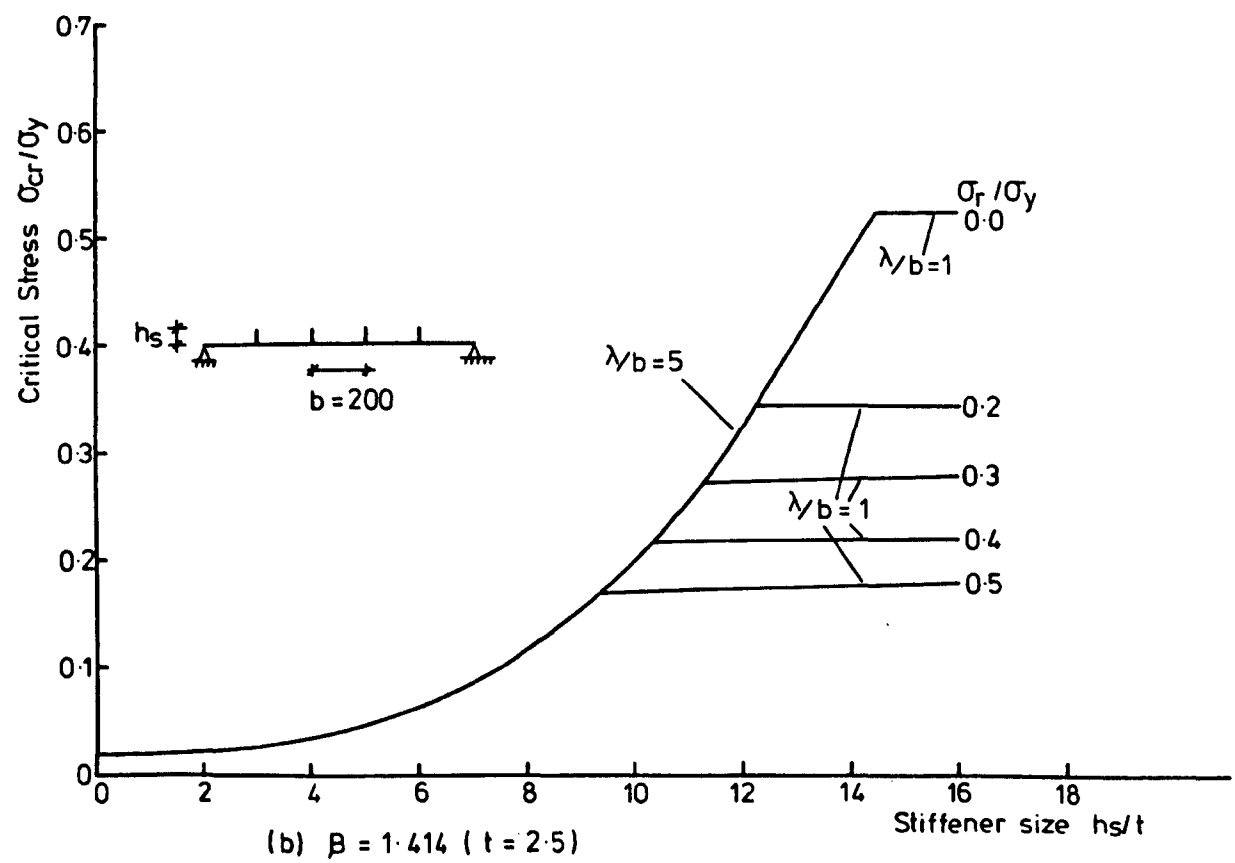

(b) β = 1·414 (t = 2·5)

FIG. 5·13. INFLUENCE OF RESIDUAL STRESS ON STIFFENER SIZE OF PANEL STIFFENED WITH FLAT RIBS.

For panels with light stiffeners (low values of h_s/t) for which overall buckling (λ = B) is the critical mode the residual stress has no effect on the critical stress. As the stiffener depth increases the tnedency towards local buckling - which is greatly affected by the residual stresses - increases. When the stiffener depth to thickness ratio $h_s/t_s \geq 8.5$, the residual stresses reduce the overall buckling of the stockier panel, $\beta = 0.88$. The reduction in the overall buckling stress increases as the residual stress σ_r decreases. This may be due to the increase of the plate area subjected to compressive residual stress. The more slender panel - $\beta = 1.414$ is not affected by the residual stress when it buckles in an overall mode.

One further point of interest is that for this panel - $\beta = 1.414$ - the reduction in local buckling stress due to residual stress $\sigma_r = 0.3\ \sigma_Y$ is of the order of 90% of σ_r, but the corresponding reduction for the stockier panel is almost equal to σ_r. For residual stress $\sigma_r = 0.5\ \sigma_Y$ the reductions become 75% and 90% of σ_r for the two panels respectively. This is because the former panel behaves elastically, whereas the latter is failing at a stress close to the yield stress and the influence of residual stress is therefore greater.

From these two graphs a relation between the residual stress level, the optimum stiffener size (h_s^*/t) and the critical buckling stress have been obtained - the results

are shown in Figure 5.14(a). The relationship is approximately linear; the slope of the σ_r/σ_Y vs h_s^*/t lines for the two panels - β = 0.88 and 1.414 - being almost equal. The slope of the σ_r/σ_Y vs σ_{cr}/σ_Y line for the more slender panel is slightly greater than the slope of the line for the stockier panel. This means that the later panel is more sensitive to the level of the residual stress. The 45^o line where

$$\sigma_r/\sigma_Y + \sigma_{cr}/\sigma_Y = 1.0$$

is also shown. The difference between the slope of this line and the slope of the other lines, may be due to the fact that in the first case the total area of the plate is assumed to be subjected to compressive σ_r, while in the later case this area reduces as σ_r increases. This difference reduces as the slenderness ratio of the panel reduces. For panels with β = 0.88 and 1.414 the difference between the slopes are 0.06 and 0.43 respectively which may be neglected for the stockier panel. It is clear from Figure 5.14(a) that the average reductions in the critical stress are 0.95 σ_r and 0.7 σ_r for the two panels respectively.

The same two panels but stiffened with angle or tee stiffeners have been considered and the results are shown in Figure 5.14(b) and Figure 5.14(c) respectively. The slopes of the σ_r/σ_Y vs h_s^*/t lines for these panels are

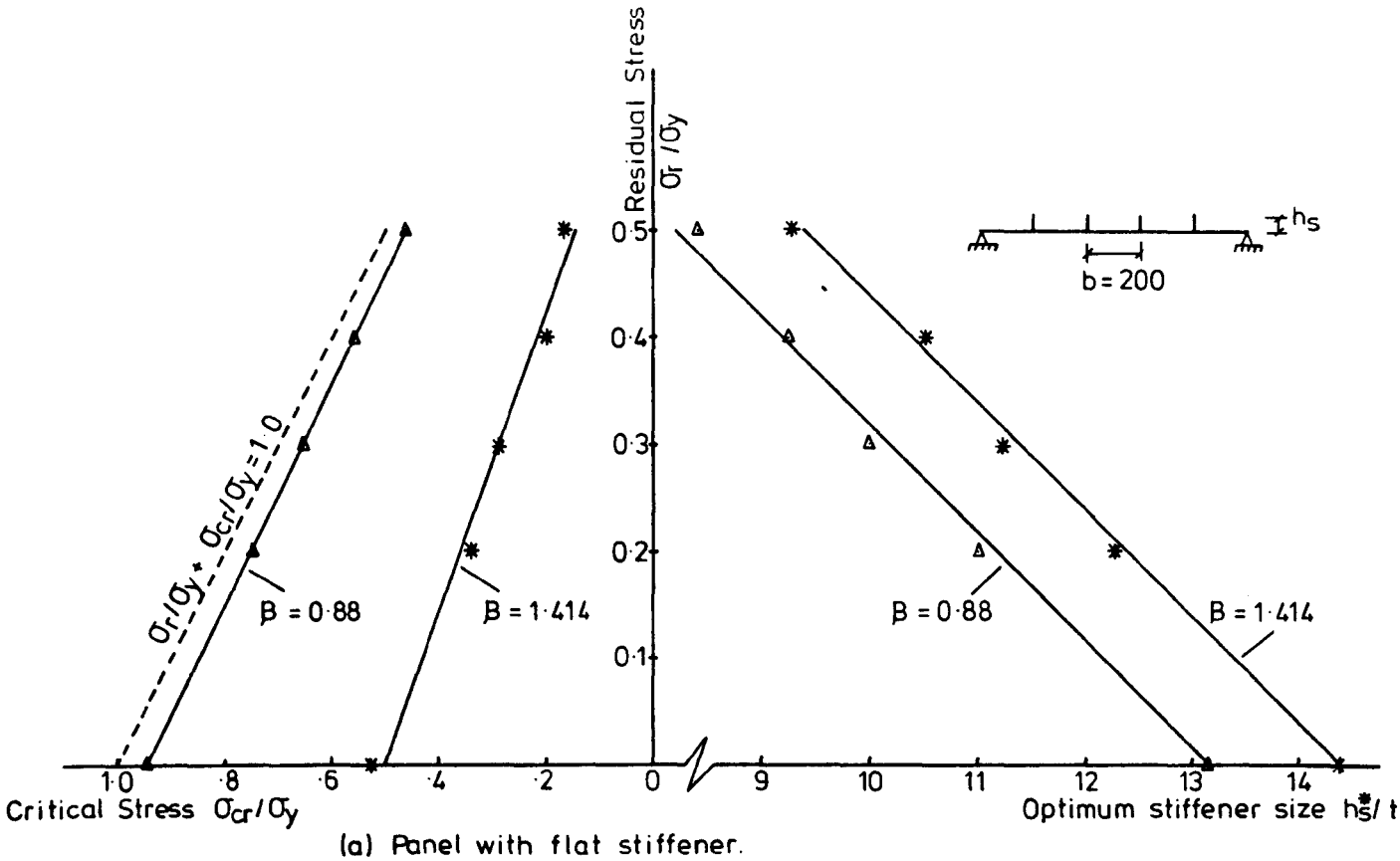

(a) Panel with flat stiffener.

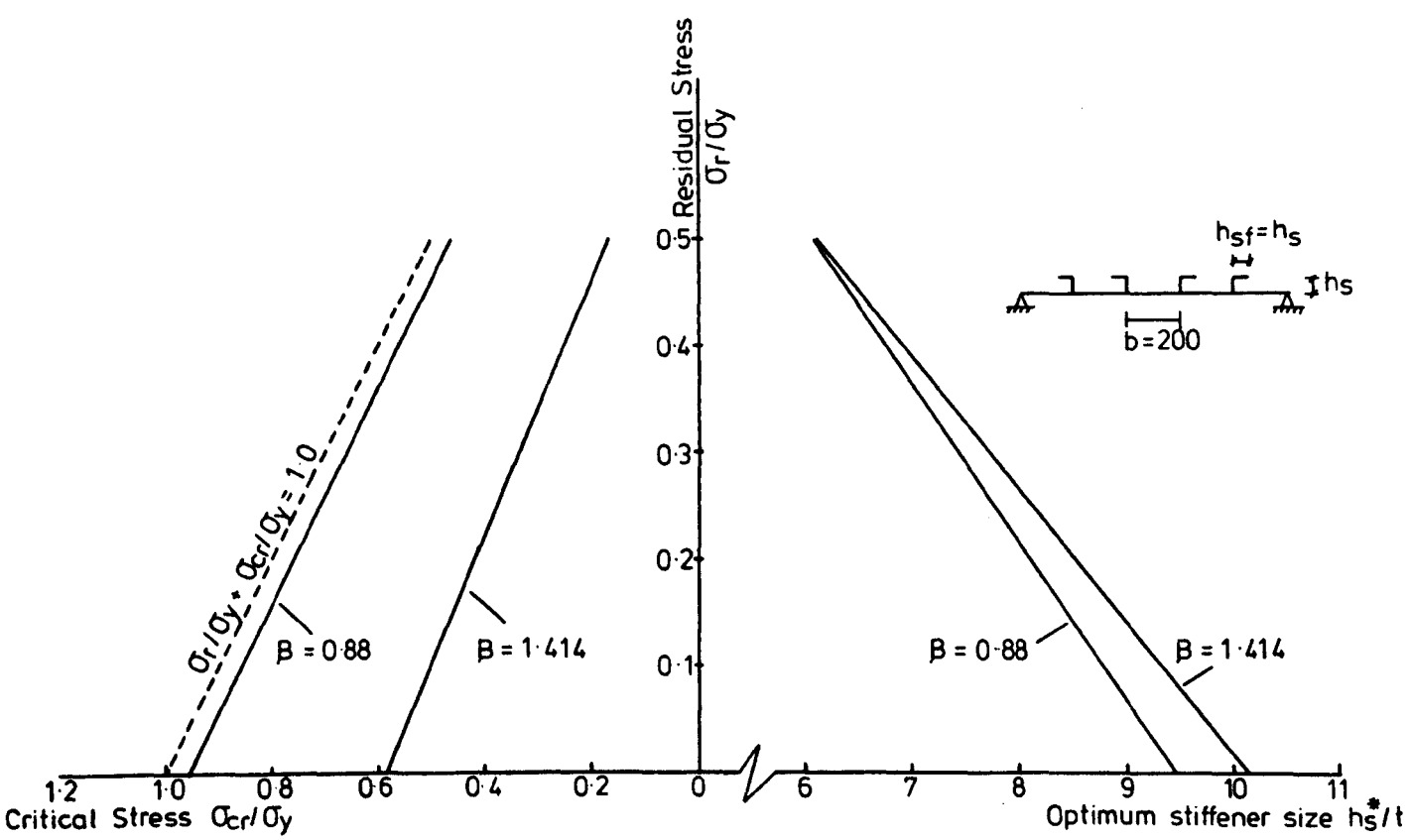

(b) Panel with angle stiffener.

FIG. 5·14 .(Cont.....)

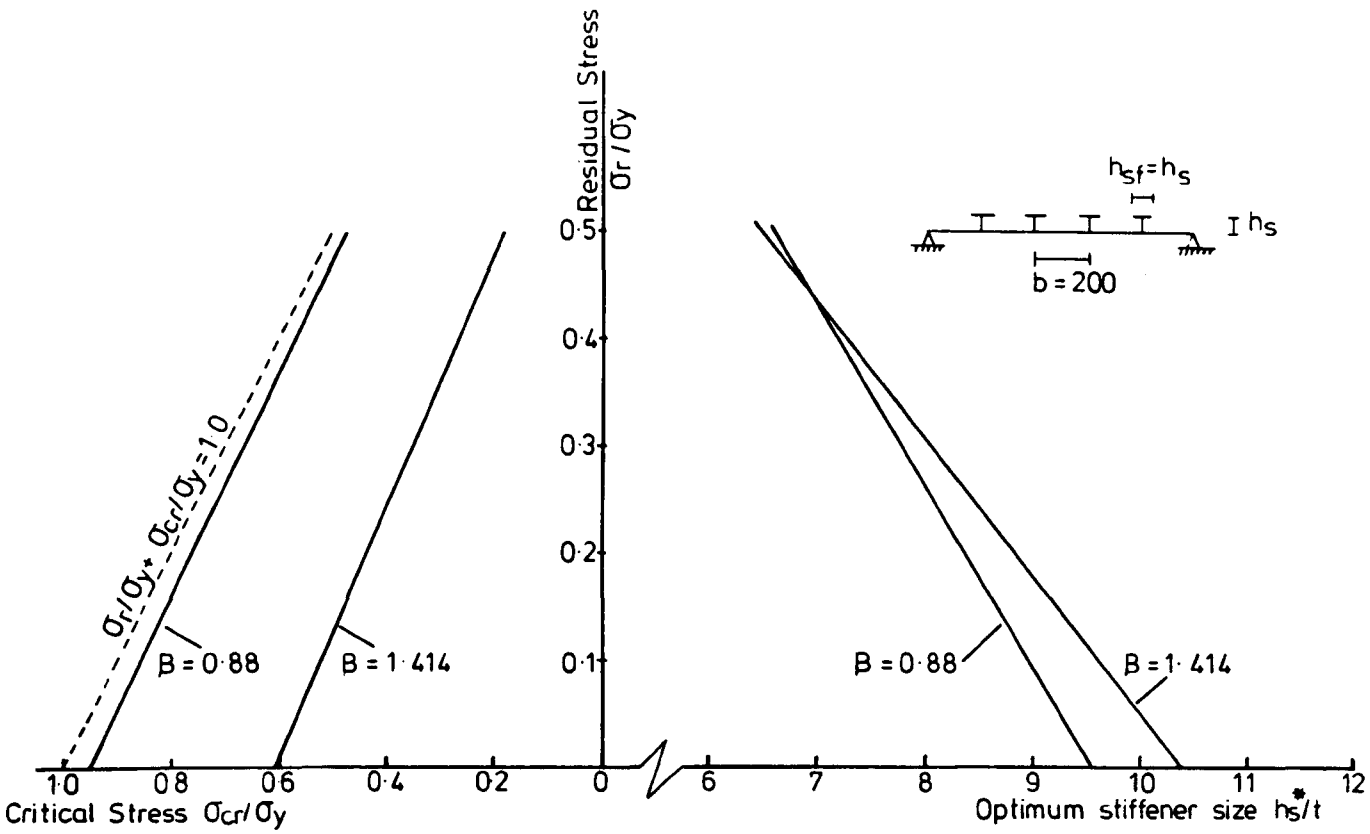

(c) Panel with Tee stiffener

FIG. 5·14. VARIATION OF RESIDUAL STRESS WITH OPTIMUM STIFFENER SIZE AND CRITICAL STRESS.

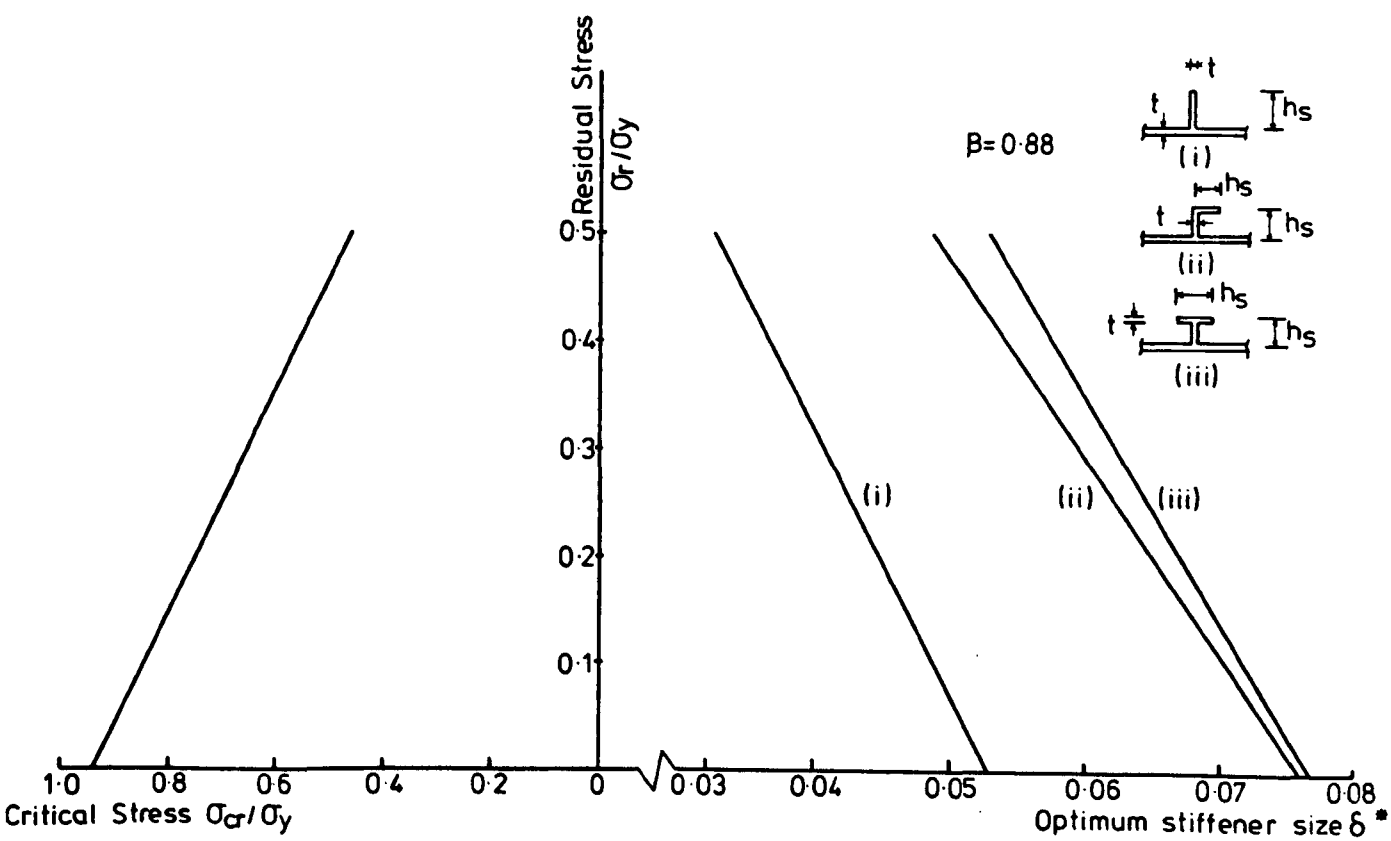

FIG. 5·15. VARIATION OF THE RESIDUAL STRESS WITH OPTIMUM STIFFENER SIZE FOR VARIOUS SHAPE OF STIFFENER CROSS-SECTION.

not equal. From the graphs it can be noted that the value of the optimum stiffener size of the stockier panel is less affected by the residual stress level than the more slender panel. The optimum h_s^*/t for the stockier panel with tee stiffener is higher than that required for the more slender panel in the range of residual stress $\sigma_r \geq 0.45\ \sigma_Y$. This may be due to the assumed pattern of the residual stress in this type of stiffener which makes the stiffener lose its rigidity rather more rapidly.

Considering the three panels with the same β (0.88) but stiffened with flat, angle and tee stiffeners the slopes of the σ_r/σ_Y vs δ^* lines are not constant as shown in Figure 5.15. In this figure the optimum relative stiffener area δ^* is used instead of the optimum stiffener depth h_s^*. Due to the fact that the assumed residual stress patterns for the flat, angle and tee stiffeners have no common base, a useful comparison cannot be obtained from Figure 5.15. It is of interest to note that for panels with tee or angle stiffeners having the same area and a panel with flat stiffeners having 70% of this area an equal strength can be obtained for any residual stress level. In general the difference between the optimum area of the tee and angle stiffeners for this panel is small compared with the flat stiffeners. The σ_{cr}/σ_Y against σ_r/σ_Y lines for the three shapes of stiffeners - flat, angle and tee - coincide with each other for the stockier

panel. For the more slender panel the shape of the stiffeners has some effect on the critical stress.

5.2.5 Hybrid Stiffened Panel

A panel stiffened with higher strength steel stiffeners has been considered to study the effect of the ratio of the stiffener yield stress to the plate yield stress σ_{YS}/σ_Y. The yield stress of the stiffeners σ_{YS} are taken as 1.0, 1.4 and 1.6 times the plate yield stress, σ_Y. Three levels of residual stress - σ_r = 0.0, 30% and 50% of the plate yield stress - have been considered for both plate and stiffeners. The results given in Figure 5.16 are nondimensionalized by using a modified yield stress $\bar{\sigma}_Y$, where $\bar{\sigma}_Y$ = maximum squash load/area of the panel.

The slenderness ratio of the plate is given by

$$\beta = \frac{b}{t}\sqrt{\frac{\bar{\sigma}_Y}{E}\,\frac{3(1-\nu^2)}{\pi^2}}$$

In Figure 5.17 the same results have been reproduced using the yield stress of the plate σ_Y to determine the ordinate and abscissa.

At high panel slendernesses, the panel buckles elastically and the higher yield stress of the stiffener has no effect on the critical load. In the inelastic range, the effect of the material yield stress depends on the

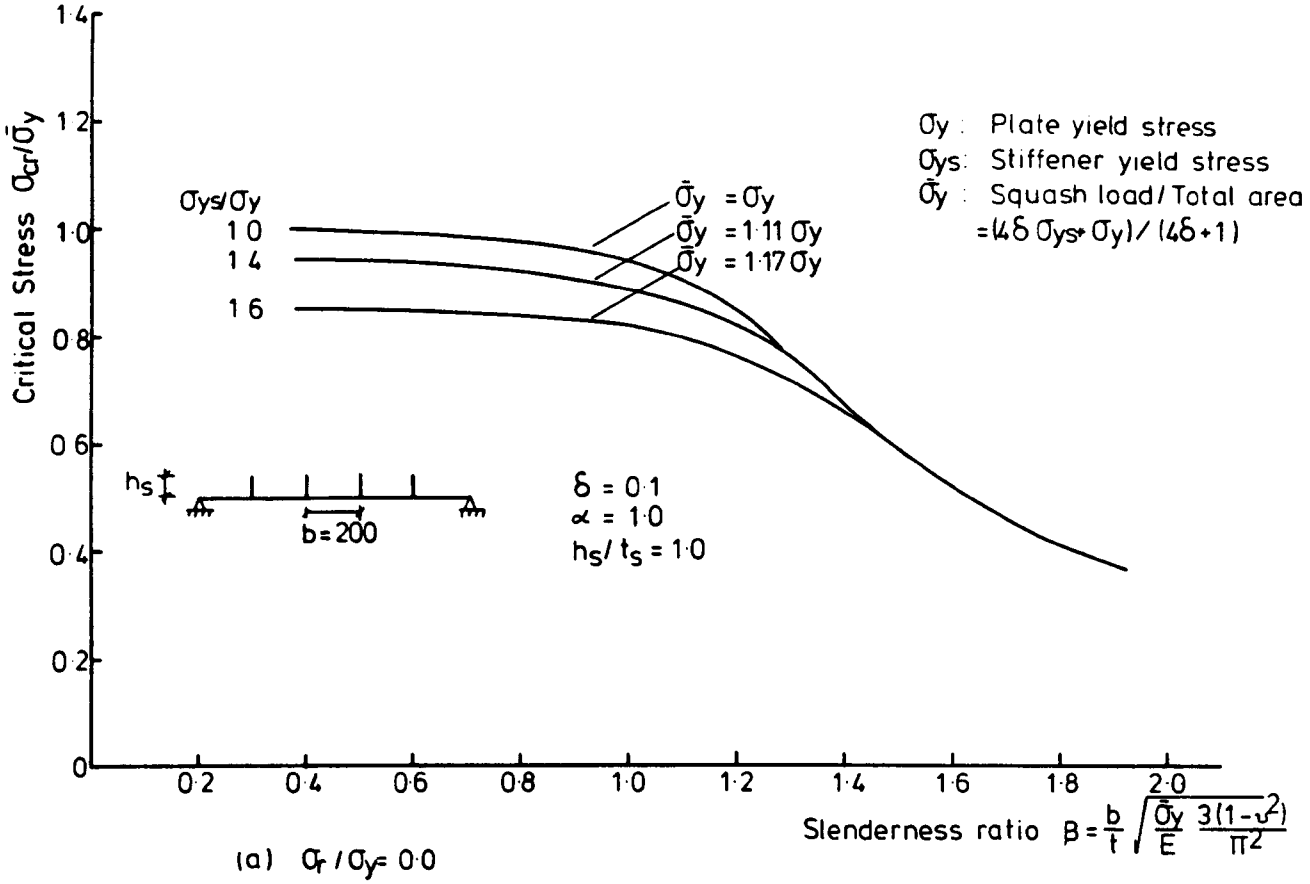

(a) σ_r/σ_y = 0·0

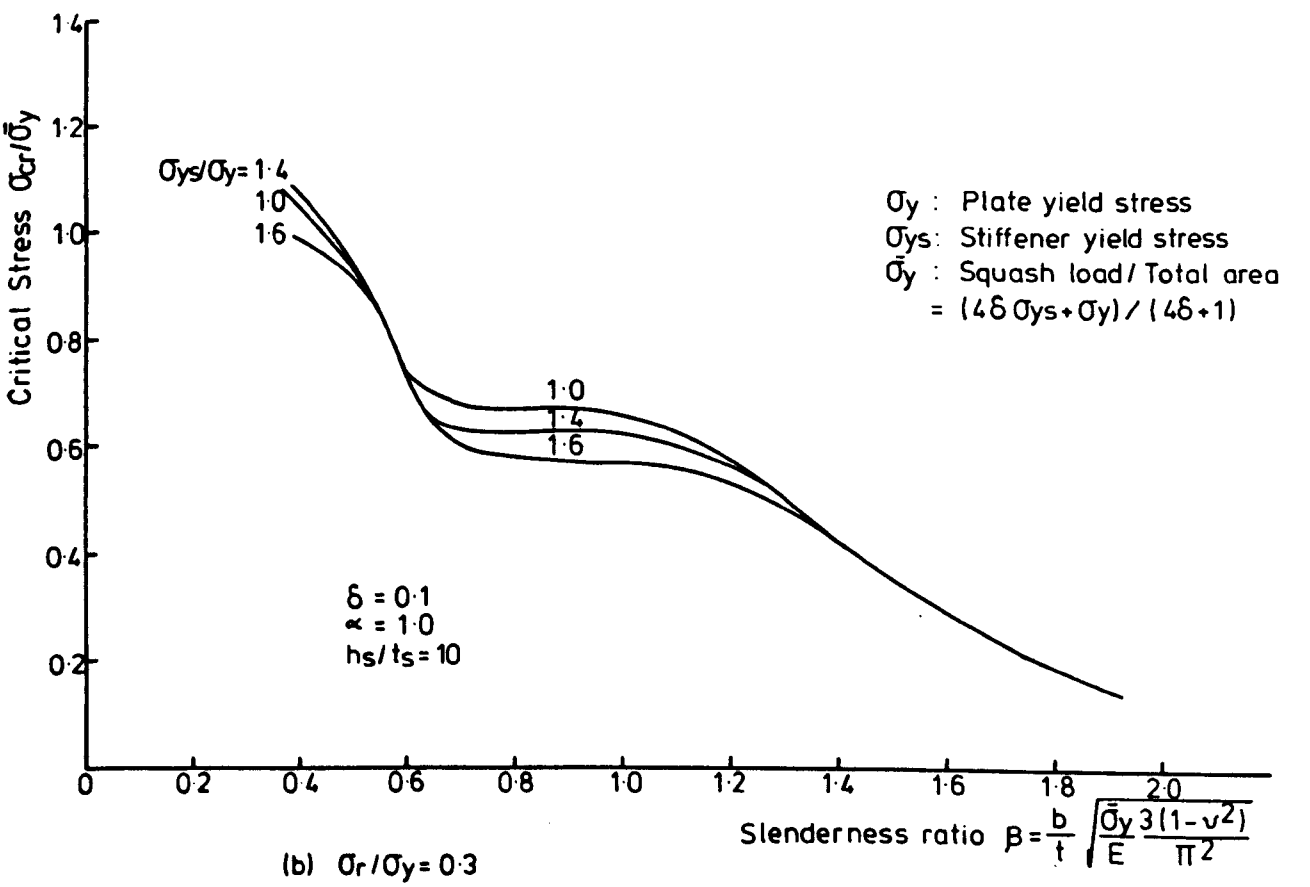

(b) σ_r/σ_y = 0·3

FIG. 5·16. (Cont.....)

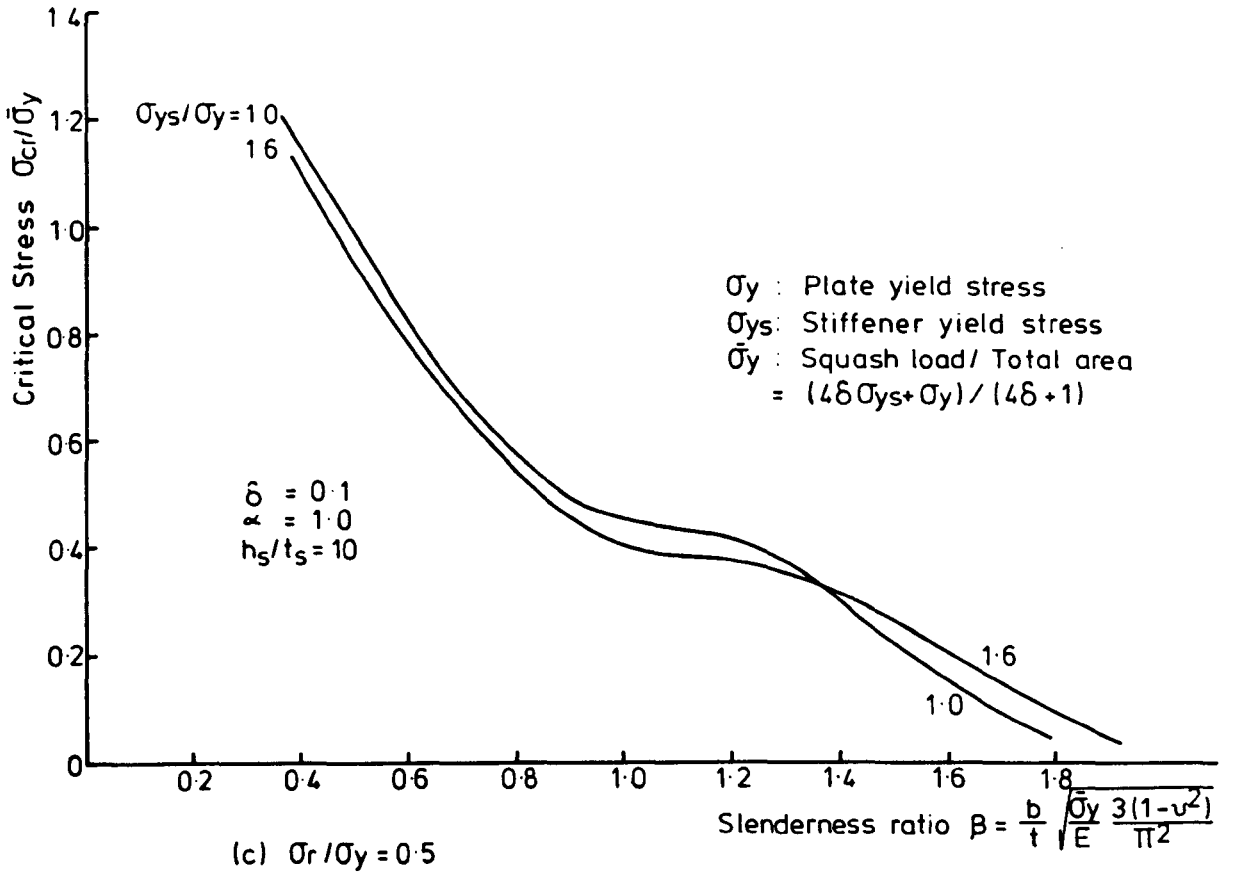

FIG. 5.16. BUCKLING STRENGTH CURVES OF HYBRID STIFFENED PLATE.

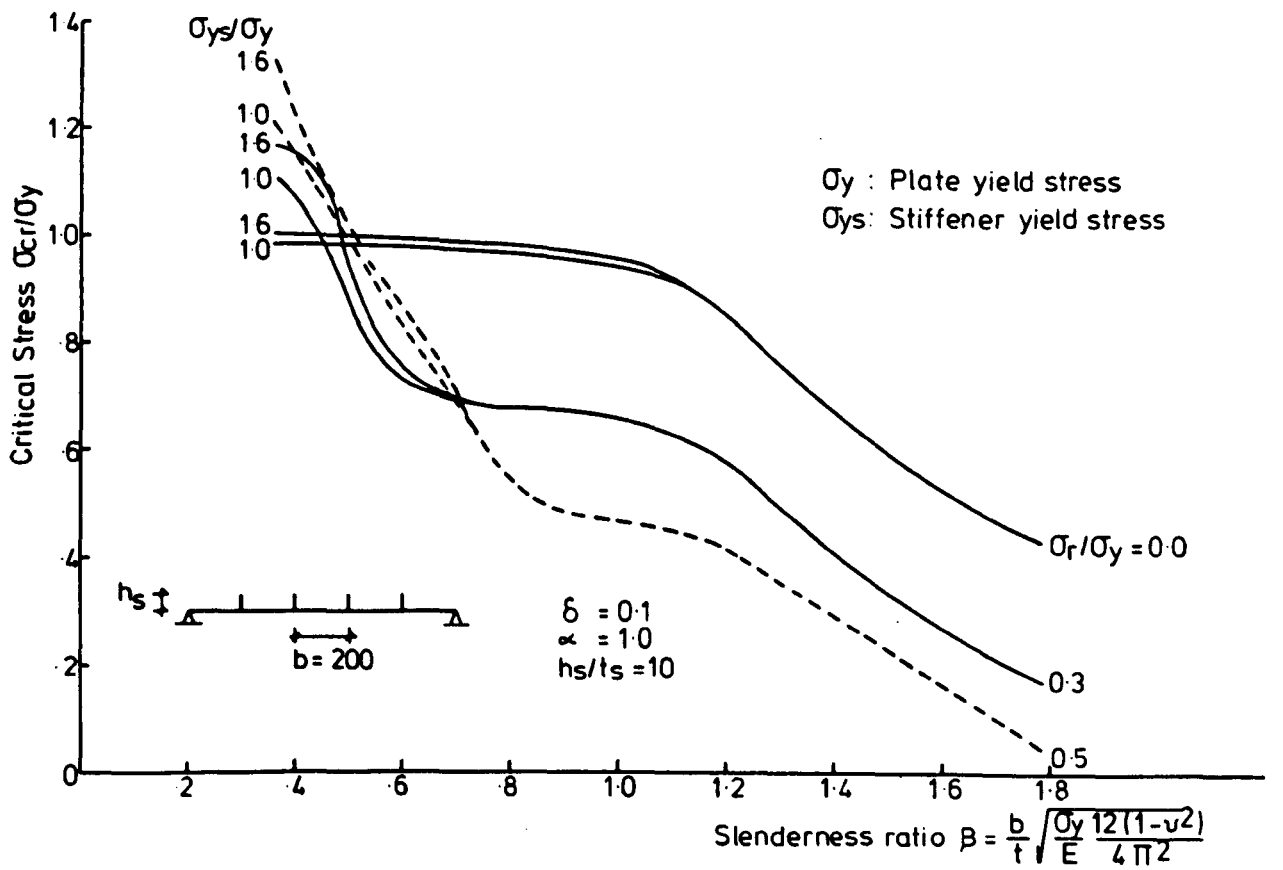

FIG. 5.17 BUCKLING STRENGTH CURVES OF HYBRID STIFFENED PLATE.

stiffener area, mode of buckling, residual stress, slenderness ratio of the panel and the ratio of stiffener yield stress to the plate yield stress σ_{YS}/σ_Y. For a panel with heavy stiffeners where the mode of buckling is usually a local mode, the effect of σ_{YS}/σ_Y is small. This effect increases as the slenderness ratio decreases. The maximum increase in the critical stress - for the panel considered - is 2% when σ_{YS}/σ_Y increases by 60% for an initially stress free panel. This value increases to 12% when the residual stress σ_r increases to 0.5 σ_Y.

From Figure 5.16 and Figure 5.17 it is clear that for a stocky panel with residual stress, the critical stress will exceed the squash load. This may be due to the fact that as the residual stress increases the area of the plate subjected to compressive residual stress decreases and the area subjected to tensile stress increase. The results obtained here are not sufficient to discuss the efficiency of this type of panel in detail, but generally, the little benefit from increasing the yield stress of the stiffener was expected for the assumed panels. Knowing that the panel with the smallest σ_{YS} has buckled in a local mode, the increase in σ_{YS} will not change this mode but will lead to a small increase in the buckling strength. This is due to the fact that the strength of the stiffener, after a certain limit, has a very small effect on the local buckling strength of the panel.

5.3 Very Wide Panel Stiffened With Flat Ribs

Usually the stiffened panels used in civil engineering projects have a width many times greater than their length. Such a panel behaves rather differently from the rectangular panel due to the lack of the longitudinal edge supports. Some studies on a panel like this have been carried out approximating the panel by a pin-ended column (19, 25, 44). Murray (19), Little (25), and Horne et al (44) neglected the continuity between the plate and the neighbouring panel and assumed that every stiffener together with its associated plate could be treated as a column.

Two buckling modes, a local mode (λ = b) and an overall mode (λ = a) have been considered. In the overall buckling there are differences between the present work and the previous work (19, 25, 44). In the previous work orthotropic plate action of the whole stiffened panel was not considered. In the present work it is assumed that the transverse cross-section can be distorted which means that the displacements at different points on this cross-section may be varied. The effect of any possible restraint arising at the edges of the panel due to transverse continuity with a neighbouring panel have also been included.

The approach given by Williams (112) is used to assemble the overall stiffness and stability matrices.

The parameters to be varied in this study are:

1. The residual stress level.
2. Stiffener depth to thickness ratio.
3. Stiffener area.
4. The length of the panel.
5. The slenderness ratio of the plate.

The geometry of the very wide panel is similar to the square panel except that the length of the panel changes from a = b (a = 200 mm) to a = 10b (a = 2000 mm).

A design chart has been developed to show the critical load of a very wide panel under longitudinal compressive stress.

5.3.1 Williams's Very Wide Panel Approach

Assume the panel shown in Figure 5.18 has nodal repetitive displacements δ_i. The equilibrium equations in matrix form are given by

$$[K]\{\delta\} = \{P\} \qquad (5.1)$$

where [K] is the stiffness matrix

{δ} is the displacement vector

{P} is the load vector

This stiffness matrix is of a very large order but can be divided into a number of submatrices as follows:

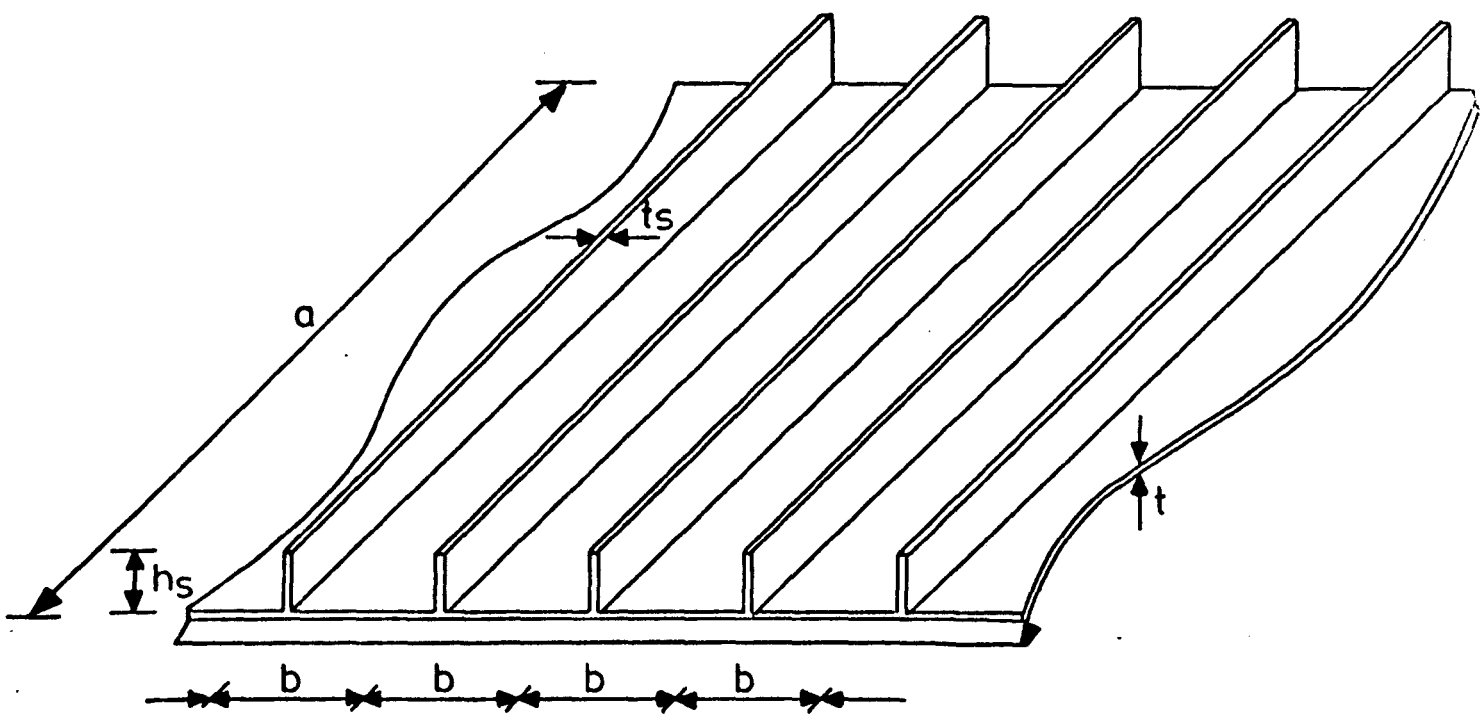

FIG .5·18.(a) VERY WIDE PANEL.

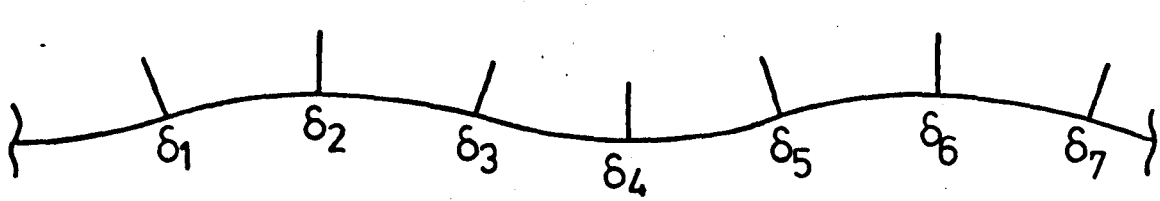

FIG.5·18. (b) DISPLACEMENT OF A VERY WIDE PANEL.

$$\begin{bmatrix} -- & -- & -- & 0 & 0 & 0 & 0 & 0 & 0 & 0 \\ 0 & K_{43} & K_{44} & K_{41} & 0 & 0 & 0 & 0 & 0 & 0 \\ 0 & 0 & K_{14} & K_{11} & K_{12} & 0 & 0 & 0 & 0 & 0 \\ 0 & 0 & 0 & K_{21} & K_{22} & K_{23} & 0 & 0 & 0 & 0 \\ 0 & 0 & 0 & 0 & K_{32} & K_{33} & K_{34} & 0 & 0 & 0 \\ 0 & 0 & 0 & 0 & 0 & K_{43} & K_{44} & K_{41} & 0 & 0 \\ 0 & 0 & 0 & 0 & 0 & 0 & K_{14} & K_{11} & K_{12} & 0 \\ 0 & 0 & 0 & 0 & 0 & 0 & 0 & -- & -- & -- \end{bmatrix} \begin{Bmatrix} -- \\ \delta_4 \\ \delta_1 \\ \delta_2 \\ \delta_3 \\ \delta_4 \\ \delta_1 \\ -- \end{Bmatrix} = \begin{Bmatrix} -- \\ P_4 \\ P_1 \\ P_2 \\ P_3 \\ P_4 \\ P_1 \\ -- \end{Bmatrix} \tag{5.2}$$

It is clear that the system consists of a set of equations which will be repeated many times. If there are n nodes in one complete wave-length there will be only (n - 1) new equations. These equations are (Figure 5.18(b))

$$K_{14}\,\delta_4 + K_{11}\,\delta_1 + K_{12}\,\delta_2 = P_1 \tag{5.3a}$$

$$K_{21}\,\delta_1 + K_{22}\,\delta_2 + K_{23}\,\delta_3 = P_2 \tag{5.3b}$$

$$K_{32}\,\delta_2 + K_{33}\,\delta_3 + K_{34}\,\delta_4 = P_3 \tag{5.3c}$$

$$K_{43}\,\delta_3 + K_{44}\,\delta_4 + K_{41}\,\delta_1 = P_4 \tag{5.3d}$$

Any other equation will be similar to one of these equations. Equations (5.3) can be put in matrix form as follows:

$$\begin{bmatrix} K_{11} & K_{12} & 0 & K_{14} \\ K_{21} & K_{22} & K_{23} & 0 \\ 0 & K_{32} & K_{33} & K_{34} \\ K_{41} & 0 & K_{43} & K_{44} \end{bmatrix} \begin{Bmatrix} \delta_1 \\ \delta_2 \\ \delta_3 \\ \delta_4 \end{Bmatrix} = \begin{Bmatrix} P_1 \\ P_2 \\ P_3 \\ P_4 \end{Bmatrix} \tag{5.4}$$

or simply

$$[\bar{K}]\ \{\bar{\delta}\} = [\bar{P}] \qquad (5.5)$$

Therefore the stiffness matrix of the very wide panel [K] is reduced to a square matrix $[\bar{K}]$ of order (n - 1) x (n - 1). This matrix can be used to determine the critical buckling stress using the Wittrick-Williams algorithm as usual (87).

5.3.2 Effect of the Panel Length on the Buckling Strength

Five values for the distance between the end supports (a) of a very wide panel have been considered

$$a = b,\ 2b,\ \ldots,\ 5b$$

where "b" is the distance between two adjacent stiffeners. Although full results for panels with residual stress σ_r = 0, 0.2 σ_Y and 0.4 σ_Y and h_s/t_s = 8, 12, 16 and 20 have been obtained, only the results for a panel with h_s/t_s = 12 and σ_r = 0.0 and 0.4 σ_Y are shown in Figure 5.19.

Three values for the relative stiffener area - δ = 0.1, 0.2 and 0.3 - have been used. It is clear that the buckling strength of the panel with the lightest stiffeners (δ = 0.1) reduces substantially as the panel length increases from a = b to a = 5b for both levels of residual stress - σ_r = 0.0 and 0.4 σ_Y. The maximum reductions are about 70% and 55% respectively. This may be due to the fact that the mode of

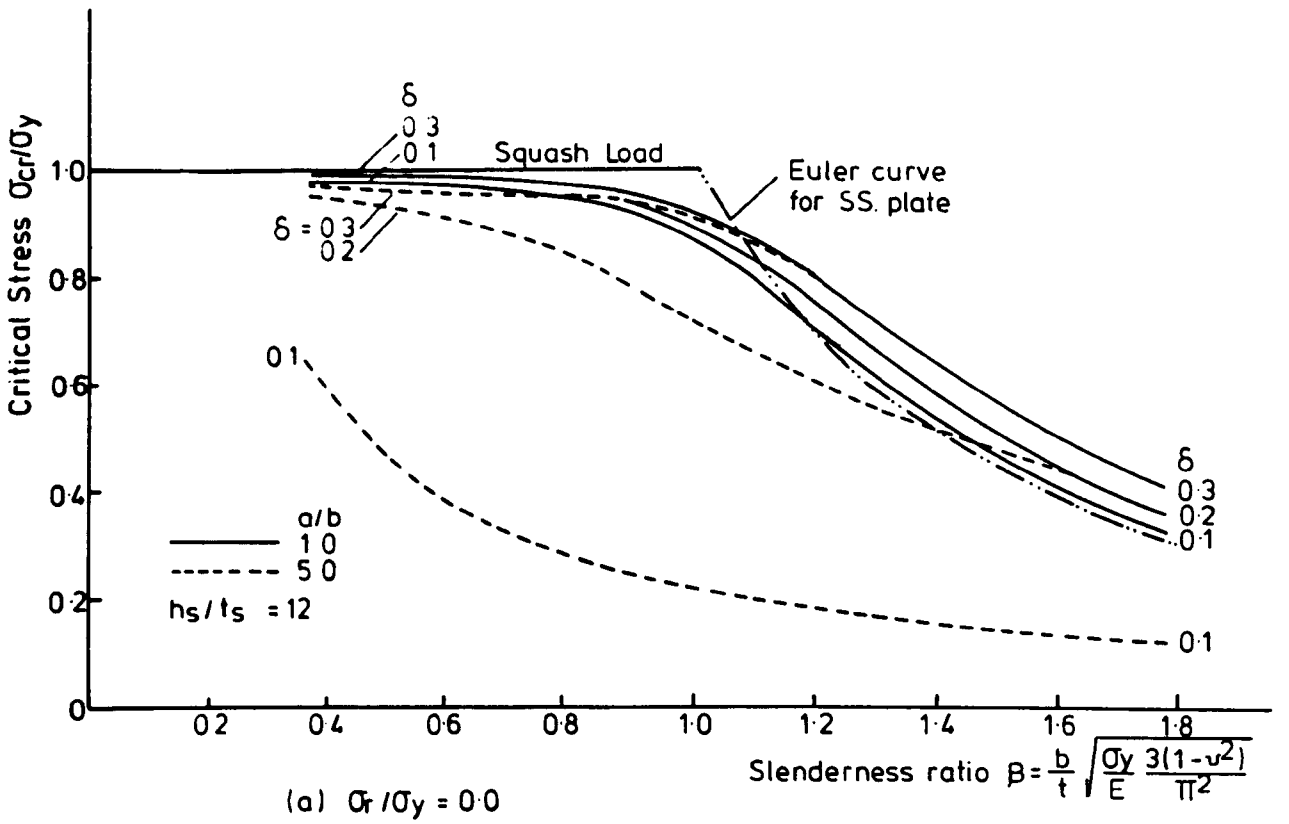

(a) $\sigma_r/\sigma_y = 0.0$

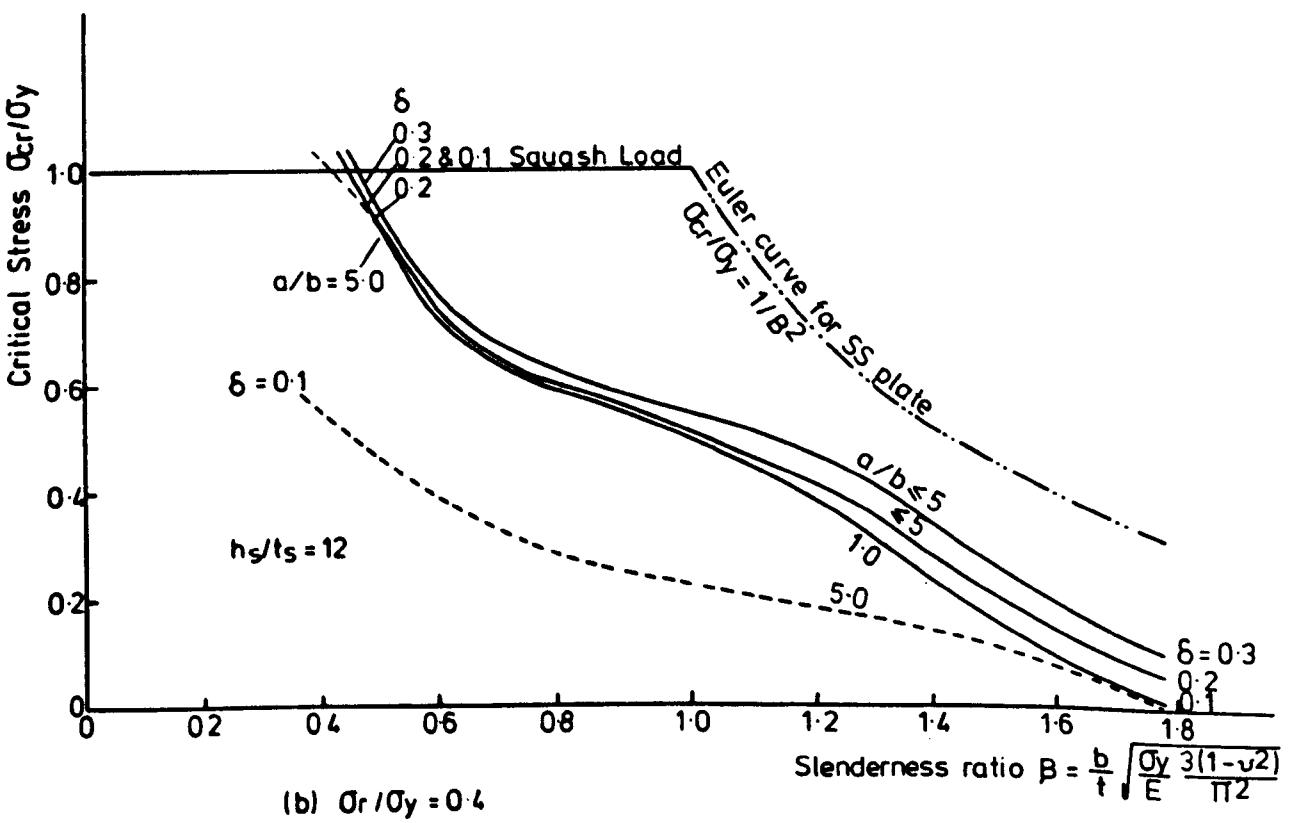

(b) $\sigma_r/\sigma_y = 0.4$

FIG. 5.19 EFFECT OF THE LENGTH OF THE PANEL ON THE BUCKLING STRENGTH.

buckling has changed from local (λ = b) to overall (λ = a). It is of interest to note that while the buckling strength for the panel with λ = b reduces when the residual stress increases, the buckling strength for the other panel (λ = 5b) is not affected.

As the stiffener area increases the reduction in the buckling strength decreases. For an initially stress free panel with stiffener area δ = 0.3, the maximum reduction - due to increasing the length of the panel from a = b to a = 5b - is 2%. The panel with higher residual stresses - $\sigma_r = 0.4\ \sigma_Y$ - is less affected by increasing its length to 5b. Again, this reflects the effect of the stiffener area and the residual stress on the local buckling strength. It is clear that panels with stiffener area $\delta > 0.1$, residual stress $\sigma_r = 0.4\ \sigma_Y$ and with length up to 5b buckle in a local mode.

From Figure 5.19, the effect of the stiffener area on the local buckling stress reduces as the slenderness ratio of the plate β reduces. Increasing the residual stress, the length of the panel can be increased to achieve a correlation between the local and the overall buckling because the residual stress affects the local buckling while the length of the panel affects the overall buckling.

5.3.3 Effect of Stiffener Depth to Thickness Ratio on Buckling Strength

Four values of the stiffener depth to thickness ratio - h_s/t_s = 8, 12, 16 and 20 - have been considered with the

relative stiffener area fixed at $\delta = 0.3$. The local buckling curves ($\lambda = b$) and the overall buckling curves for different lengths of the panel are shown in Figure 5.20. The residual stresses used in the analysis were $\sigma_r = 0$, $0.2\ \sigma_Y$ and $0.4\ \sigma_Y$.

It is clear from the graph that the local buckling stress increases as h_s/t_s reduces. This may be due to the reduction in torsional resistance of the slender stiffeners. As the slenderness ratio of the panel reduces the effect of h_s/t_s on the local buckling stress reduces. This is because the yield in the plate region between two adjacent stiffeners starts to spread and the limit in this case is an ultimate limit rather than a serviceability limit. The buckling mode changes from local ($\lambda = b$) to overall buckling ($\lambda = a$) as the length of the panel increases. In the overall mode the critical stress increases as h_s/t_s increases. In this mode the flexural resistance of the stiffener rather than the torsional resistance affects the critical stress.

5.3.4 Effect of the Residual Stress

The local buckling strength curves for three panels with relative stiffener area $\delta = 0.1$, 0.2 and 0.3 are shown in Figure 5.21. Three levels of residual stresses - $\sigma_r = 0.0$, $0.2\ \sigma_Y$ and $0.4\ \sigma_Y$ - have been considered. The stiffener depth to thickness ratios h_s/t_s are 12 and 20.

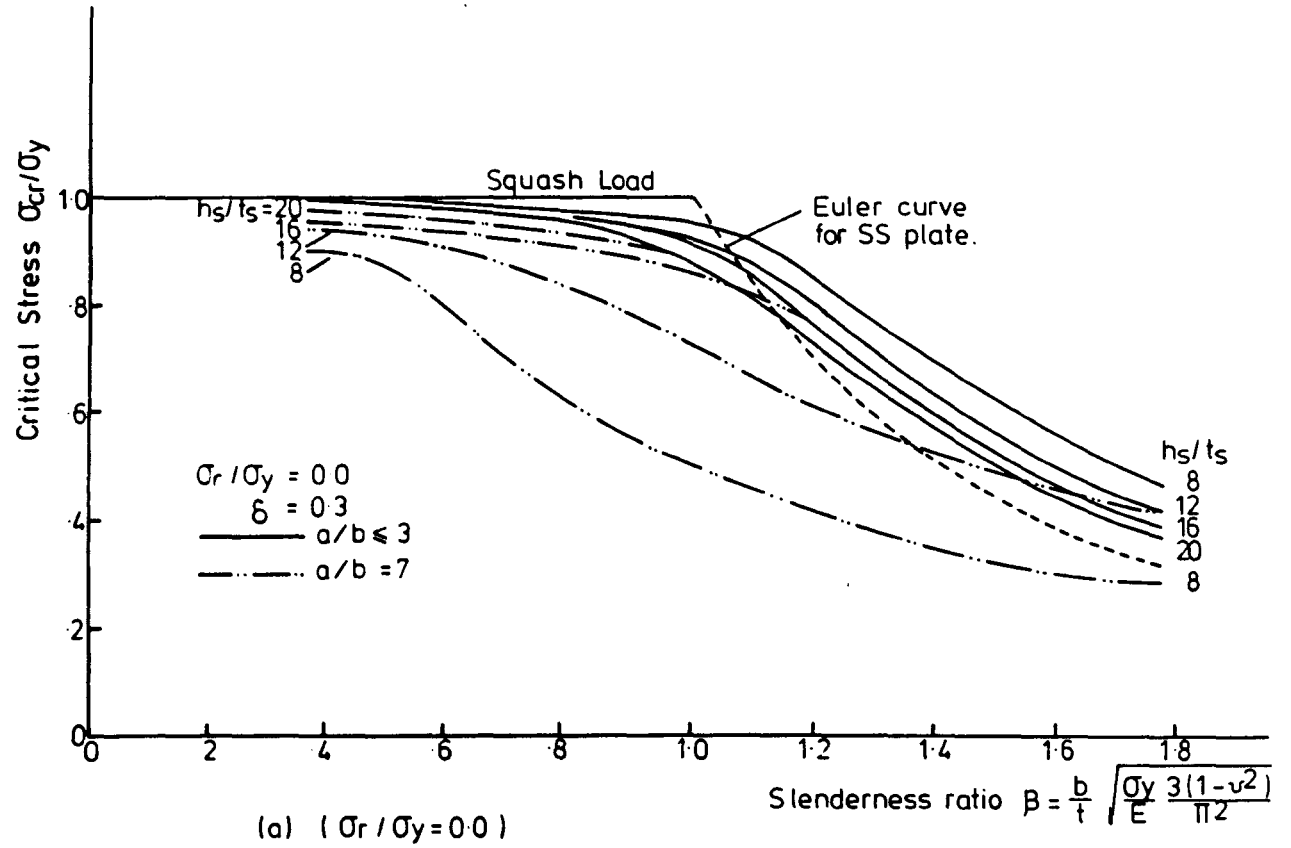

(a) ($\sigma_r/\sigma_y = 0{\cdot}0$)

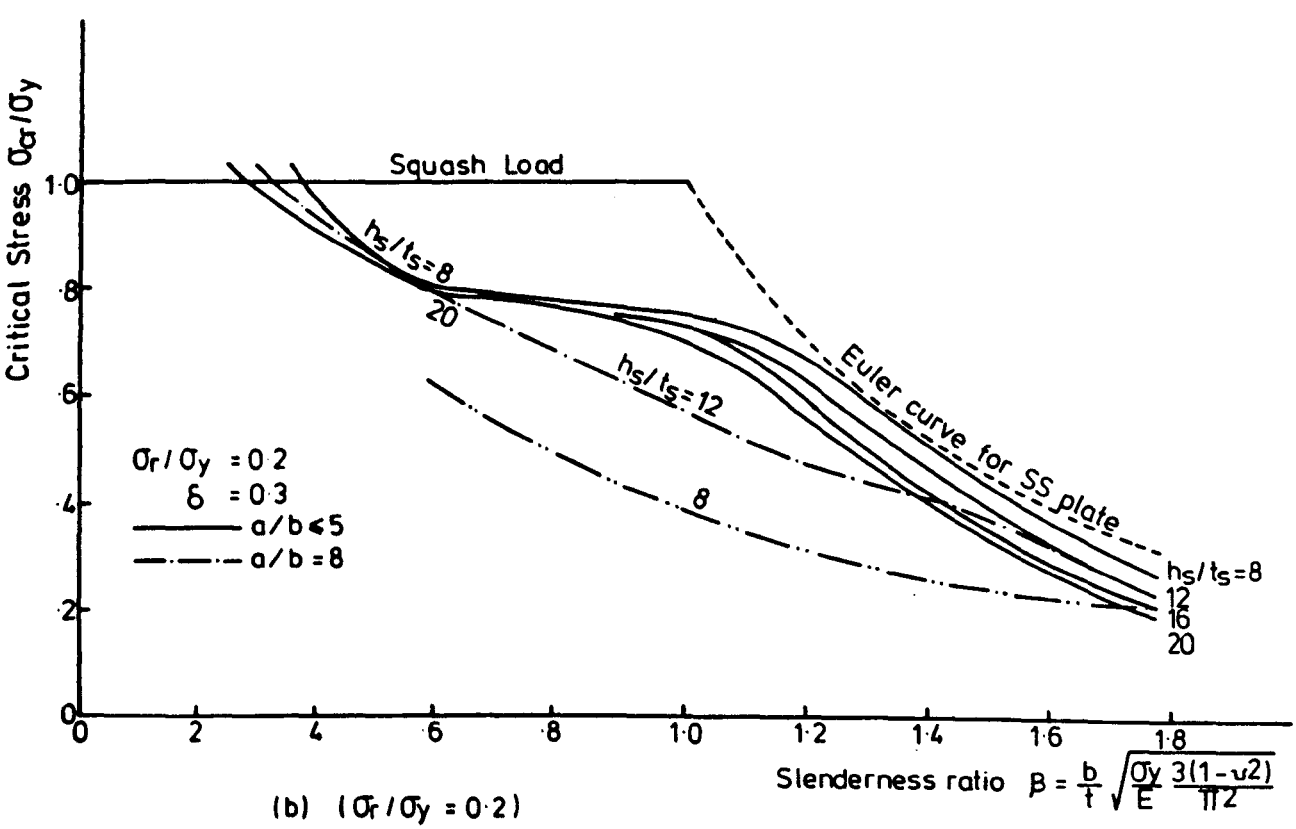

(b) ($\sigma_r/\sigma_y = 0{\cdot}2$)

FIG. 5·20. (Cont.....)

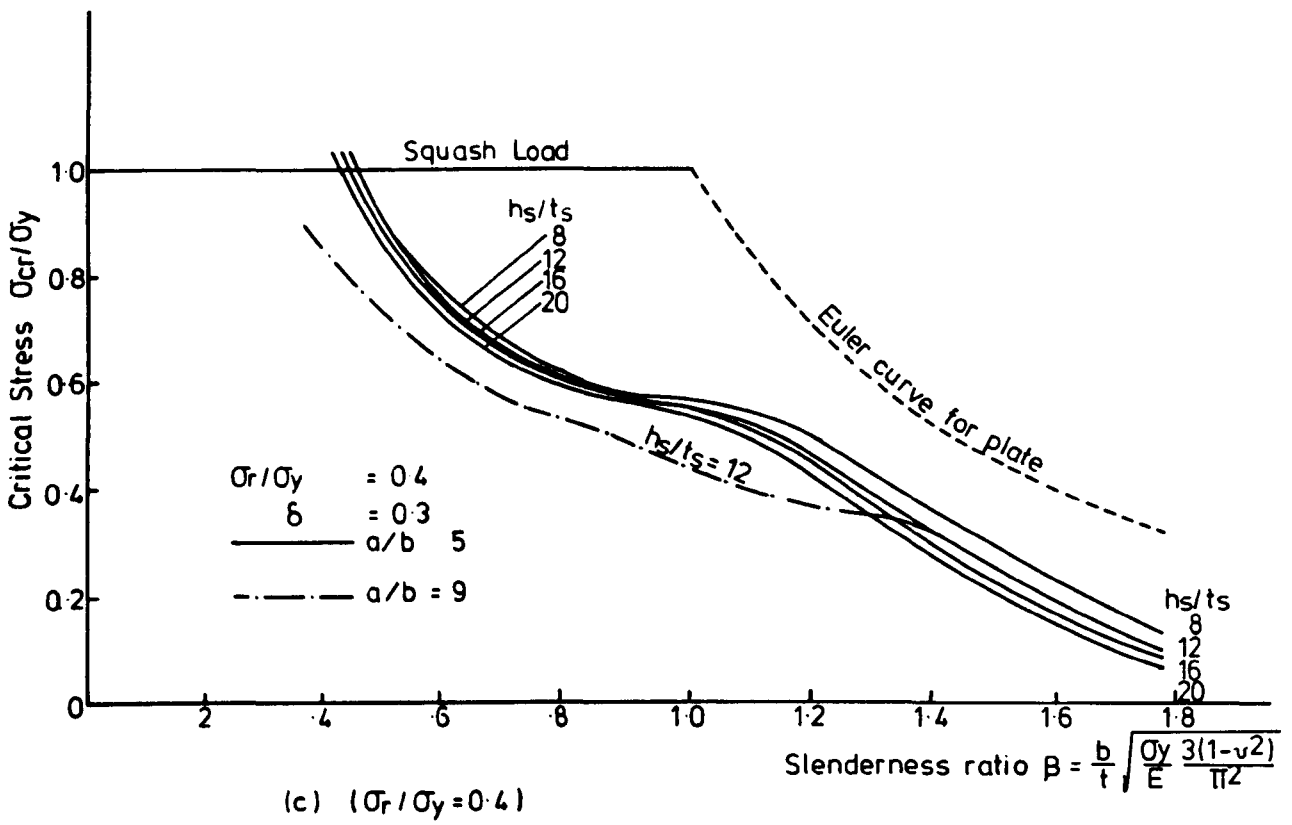

(c) ($\sigma_r / \sigma_y = 0.4$)

FIG. 5·20. EFFECT OF STIFFENER DEPTH TO THICKNESS RATIO ON BUCKLING STRENGTH.

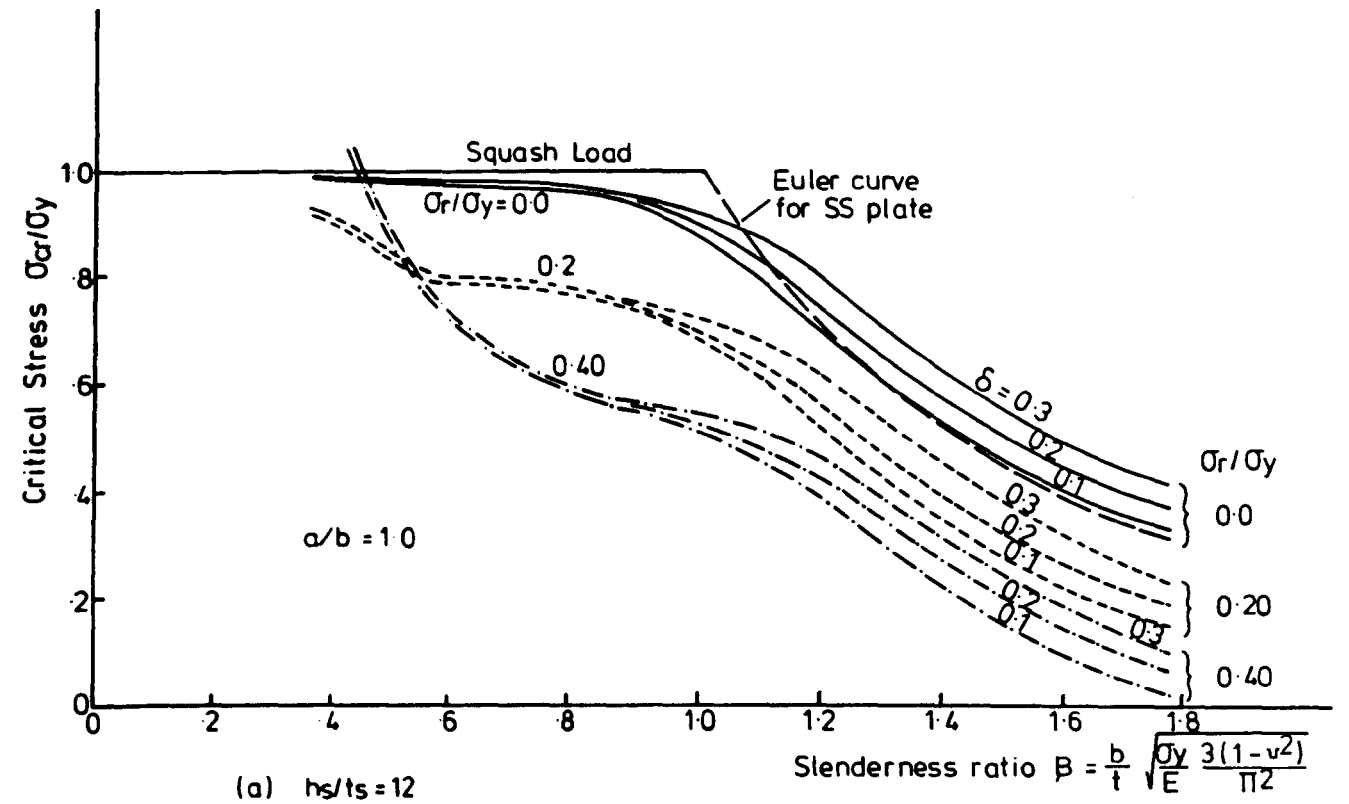

(a) hs/ts = 12

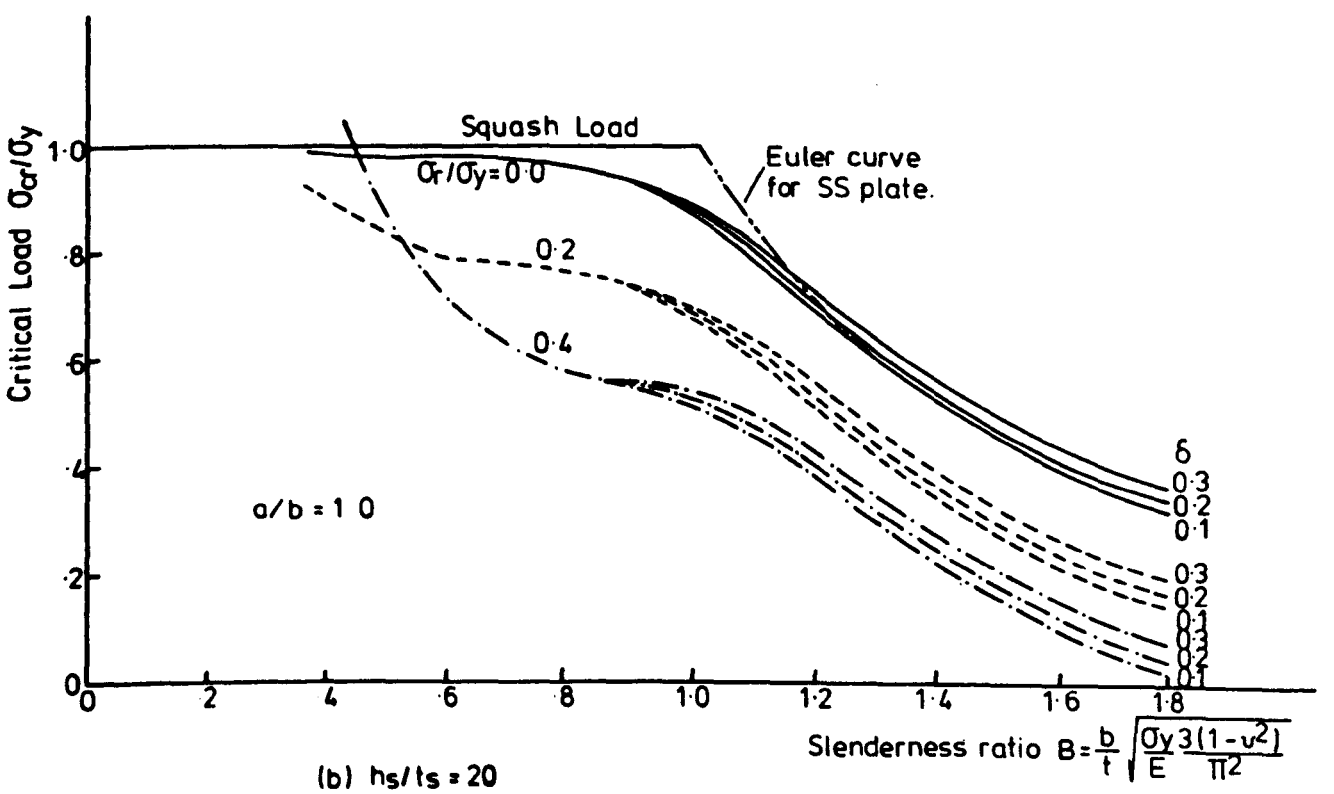

(b) hs/ts = 20

FIG. 5 21 EFFECT OF THE RESIDUAL STRESS ON BUCKLING STRENGTH.

From the graphs it is clear that for panels with a slenderness ratio $\beta \leq 0.9$ the effect of δ on the local buckling stress is very small for any level of σ_r. For a panel with slenderness ratio $\beta \leq 0.53$ the buckling strength curve for $\sigma_r = 0.4\ \sigma_Y$ exceeds the one for $\sigma_r = 0.2\ \sigma_Y$. When σ_r increases from 0.0 to 0.20 σ_Y the reduction in the strength of the panel with $h_s/t_s = 12$ and 20 is equal to 0.90 σ_r for any value of δ. As σ_r increases to 0.4 σ_Y this reduction reduces to 0.8 σ_r. This reduction is very high relative to the critical load of an initially stress free panel with slenderness ratio $\beta \geq 1.3$. A wide area of the plate in this panel is under compressive residual stresses.

As the slenderness ratio reduces, the reduction in the strength due to the residual stresses increases. In the range of $1.2 > \beta \geq 0.8$ the reduction in the strength equals σ_r and 0.95 σ_r for panels with residual stress $\sigma_r = 0.2\ \sigma_Y$ and $0.4\sigma_Y$ respectively. But it is worth mentioning that this reduction relative to the critical stress is less than that which occurs in the range $\beta > 1.2$.

The effect of the residual stress on the overall buckling strength is shown in Figure 5.22. The initially stress free panels with relative stiffener area, $\delta = 0.2$ and 0.3 buckle in an overall mode. This mode changes to a local mode when the residual stress increases to 0.4 σ_Y.

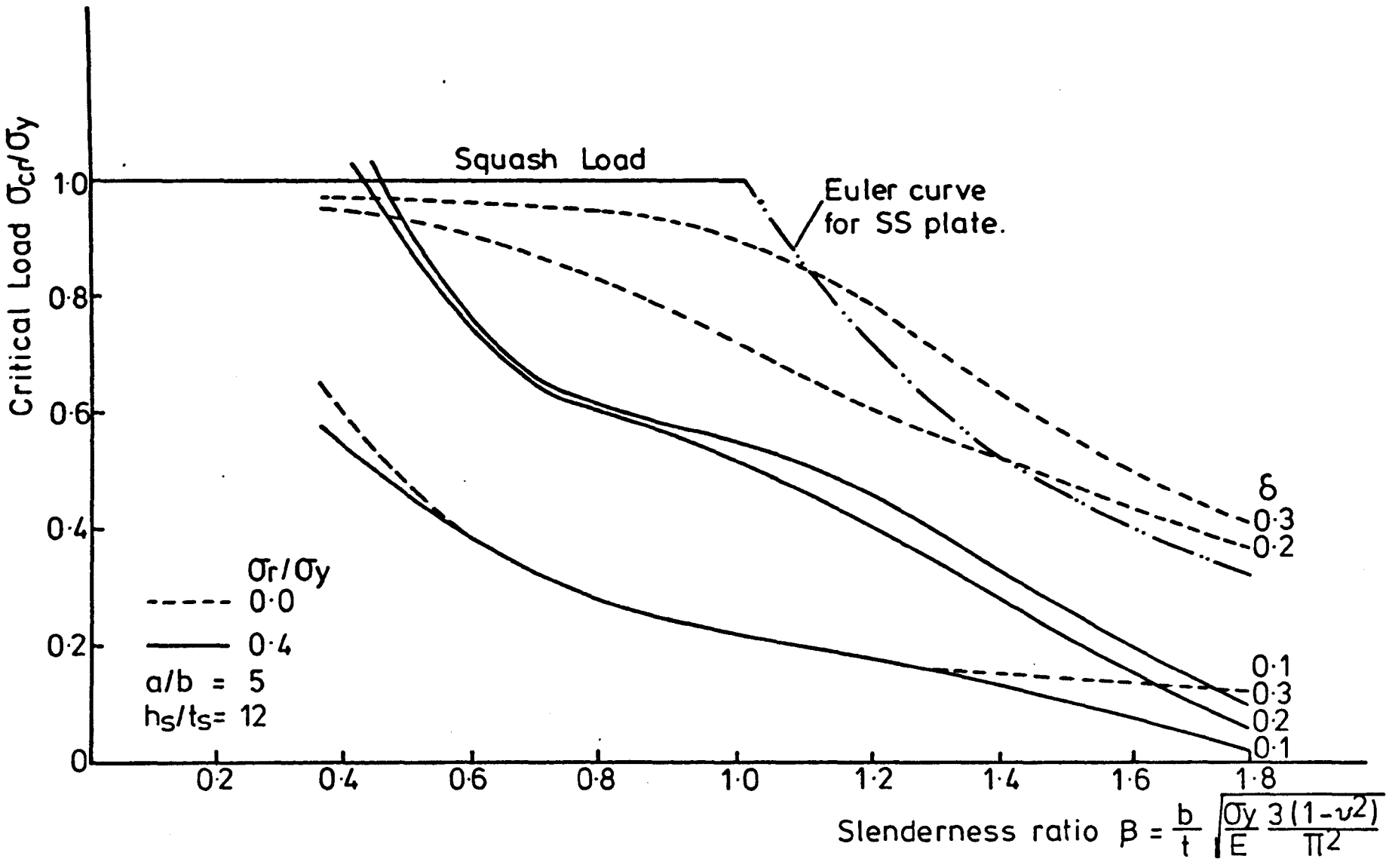

FIG. 5·22. EFFECT OF THE RESIDUAL STRESS ON THE BUCKLING STRENGTH.

The initially stress free panel with δ = 0.1 buckles in an overall mode and when the residual stress increases to 0.4 σ_Y the mode changes to a local mode for panels with slenderness ratio $\beta > 1.3$. For a very wide range of β there is no effect of the residual stress on the overall buckling strength for this panel. At $\beta \leq 0.4$ the residual stress reduces the strength of the panel by about 12%. This value of β will increase as the relative stiffener area δ increases.

5.4 Approximate Method for Design of Stiffened Panel

The intersection of the local buckling strength curves and the overall buckling strength curve leads to one possible definition of the optimum dimensions of the panel. The buckling strength of a panel depends on the distance between the transverse supports, the stiffener size and shape, the slenderness ratio of the plate and the residual stress level. Assume only one factor can be varied and that the value of this factor at which the overall buckling strength equals the local buckling strength is the optimum value.

Assume the length of the panel is the variable factor. The critical buckling stress for different values of plate slenderness ratio β, stiffener size h_s/t_s and δ and residual stress σ_r are given in Table 5.1.

To obtain the optimum length (a) for the panel a graph for λ/b against σ_{cr}/σ_Y is produced from this table. Figure 5.23 is an example for the case of a panel with residual stress $\sigma_r = 0.2\ \sigma_Y$ and the relative stiffener area $\delta = 0.1$. The intersection of the horizontal line for local σ_{cr}/σ_Y ($\lambda/b = 1.0$) with the corresponding buckling strength curve leads to the optimum length (a) of the panel. The slenderness ratio of the plate β varies between 0.36 and 1.78 ($b/t = 20 \sim 100$). Four values of stiffener depth to thickness ratio - $h_s/t_s = 8$, 12, 16 and 20 - have been considered.

For different values of δ and σ_r similar graphs have been obtained and the optimum panel length determined for every case.

In some cases where the graphs are almost flat, the optimum length of the panel has been obtained from Table 5.1 by interpolation.

The relation between the optimum length of the panel, the slenderness ratio β (b/t) and the critical stress is shown in Figure 5.24 for different stiffener sizes and residual stresses. To use this design chart:

1. Assume the values of both the residual stress - σ_r - and the relative stiffener area - δ.
2. Knowing the value of the applied compressive stress and choosing the stiffener depth to

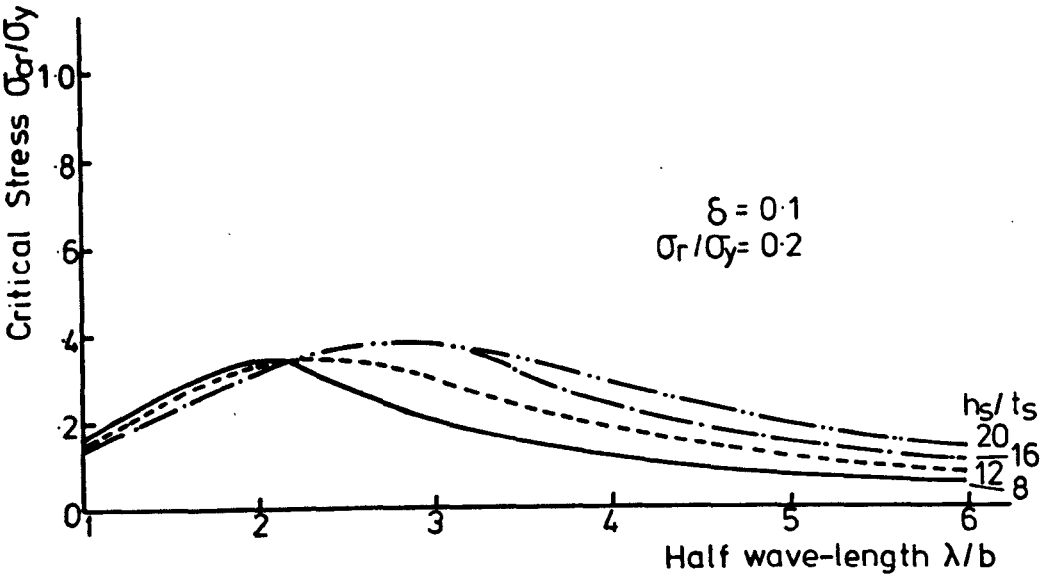

(a) β = 1·78 (b/t = 100)

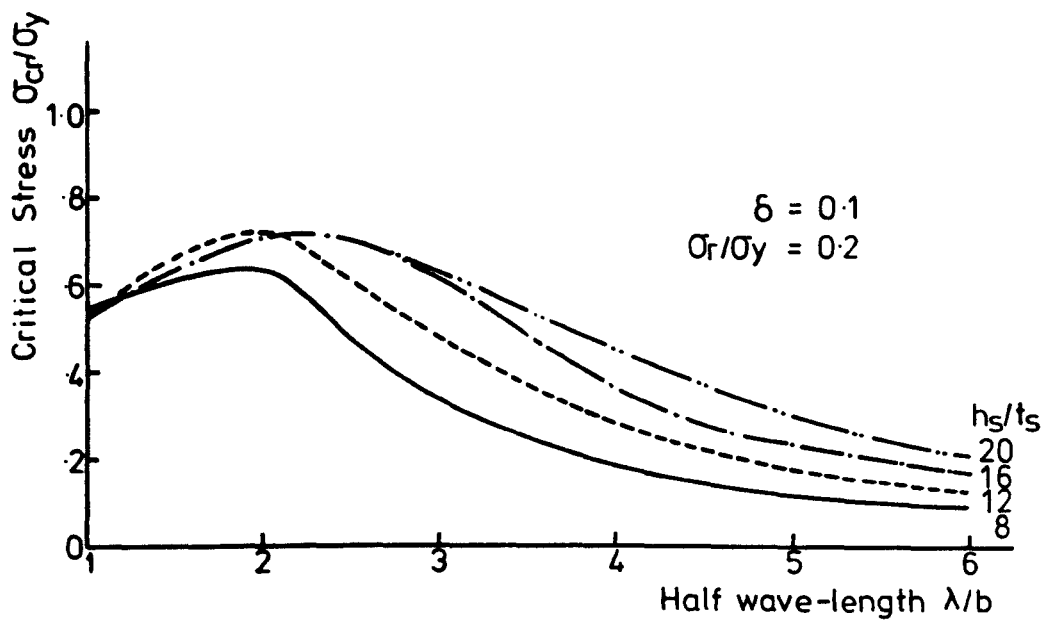

(b) β = 1·19 (b/t = 66·67)

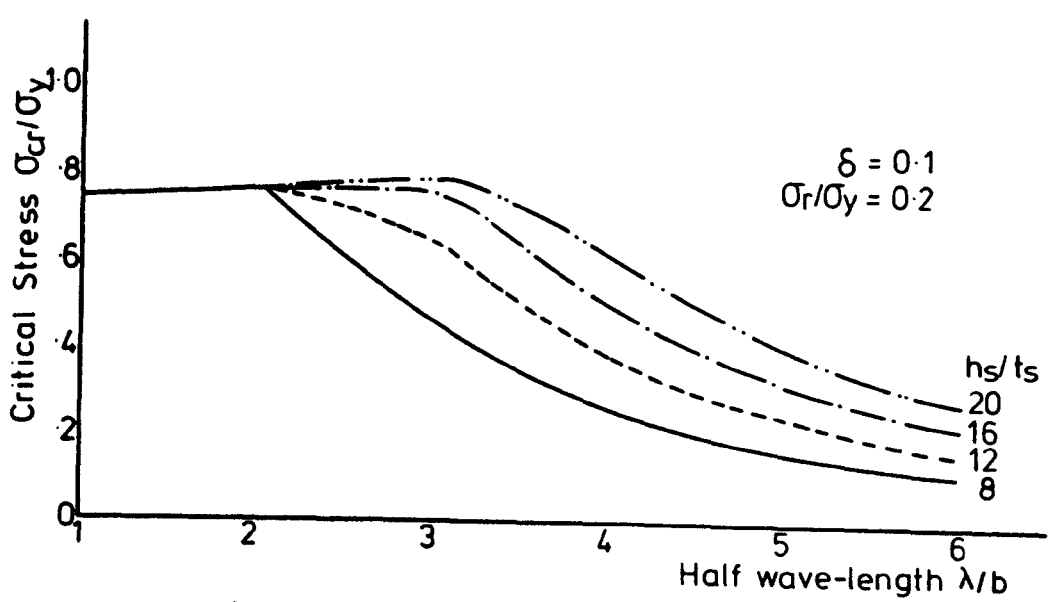

(c) β = 0·89 (b/t = 50)

FIG. 5·23 . (Cont.....)

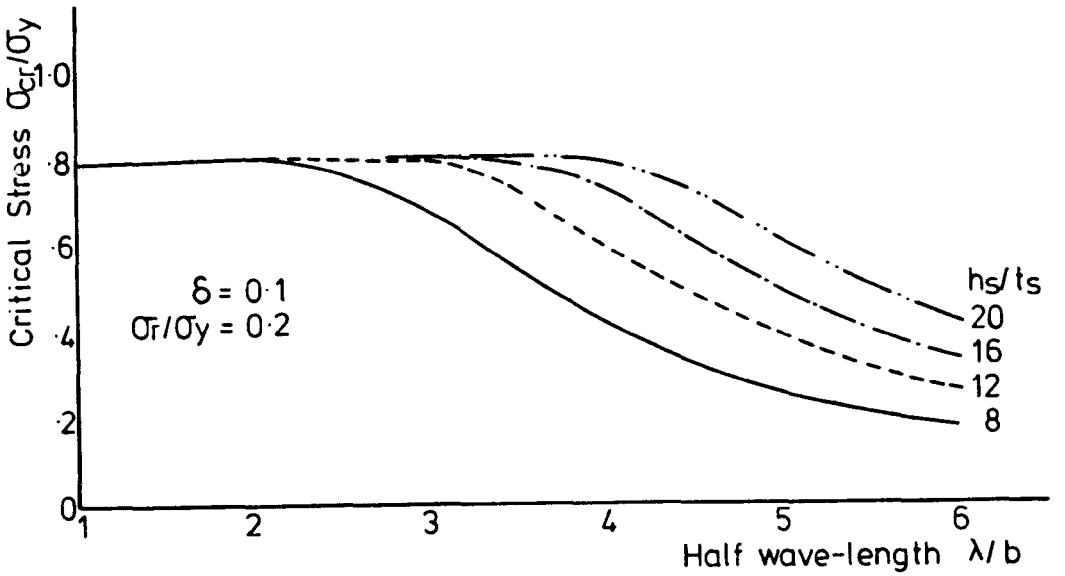

(d) β = 0·59 (b/t = 33·33)

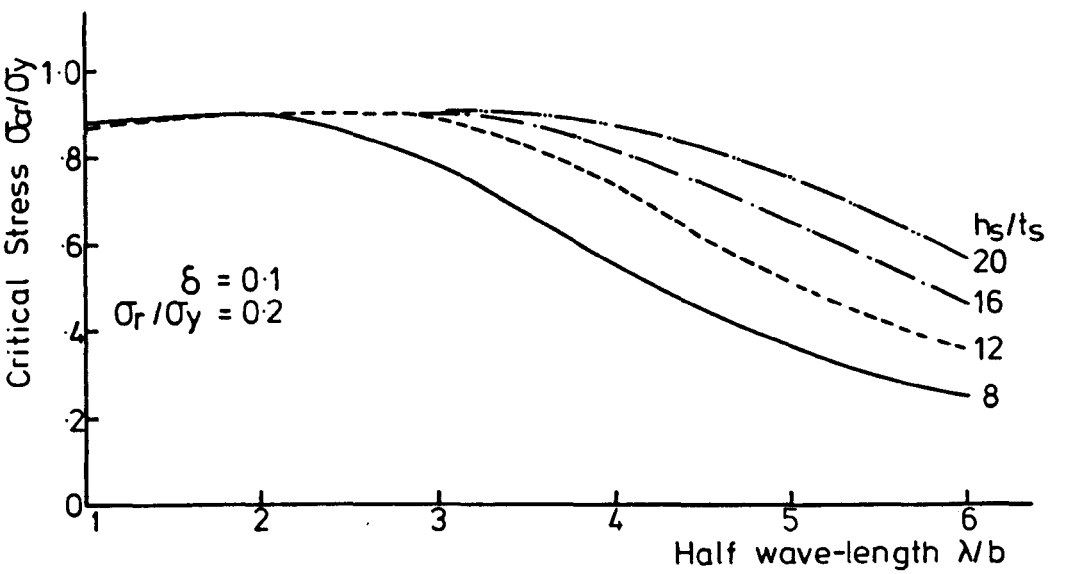

(e) β = 0·44 (b/t = 25)

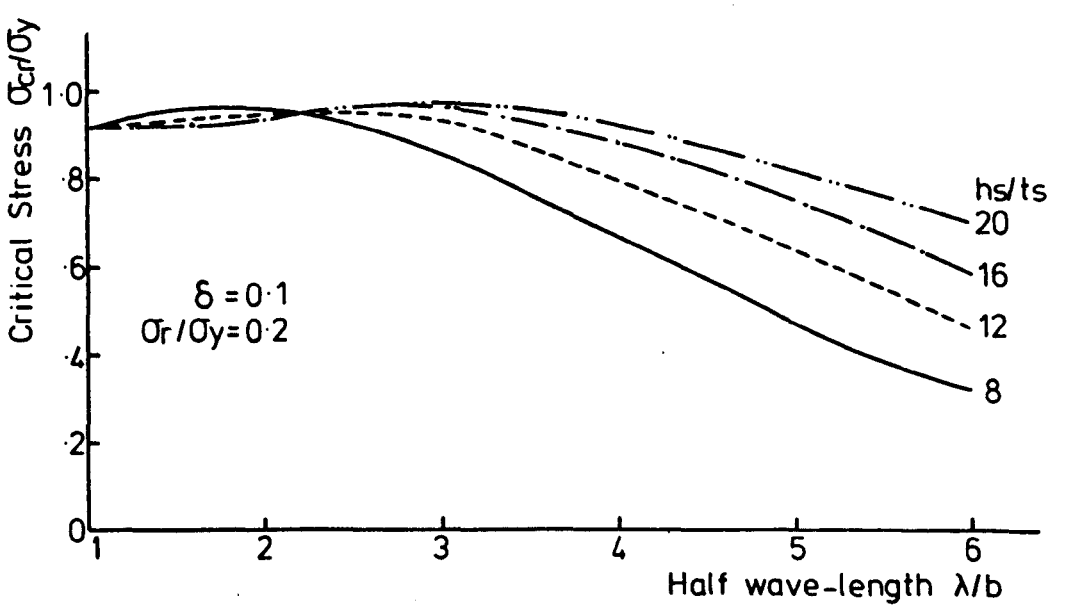

(f) β = 0·36 (b/t = 20)

FIG. 5·23. VARIATION OF THE CRITICAL STRESS WITH HALF WAVE-LENGTH.

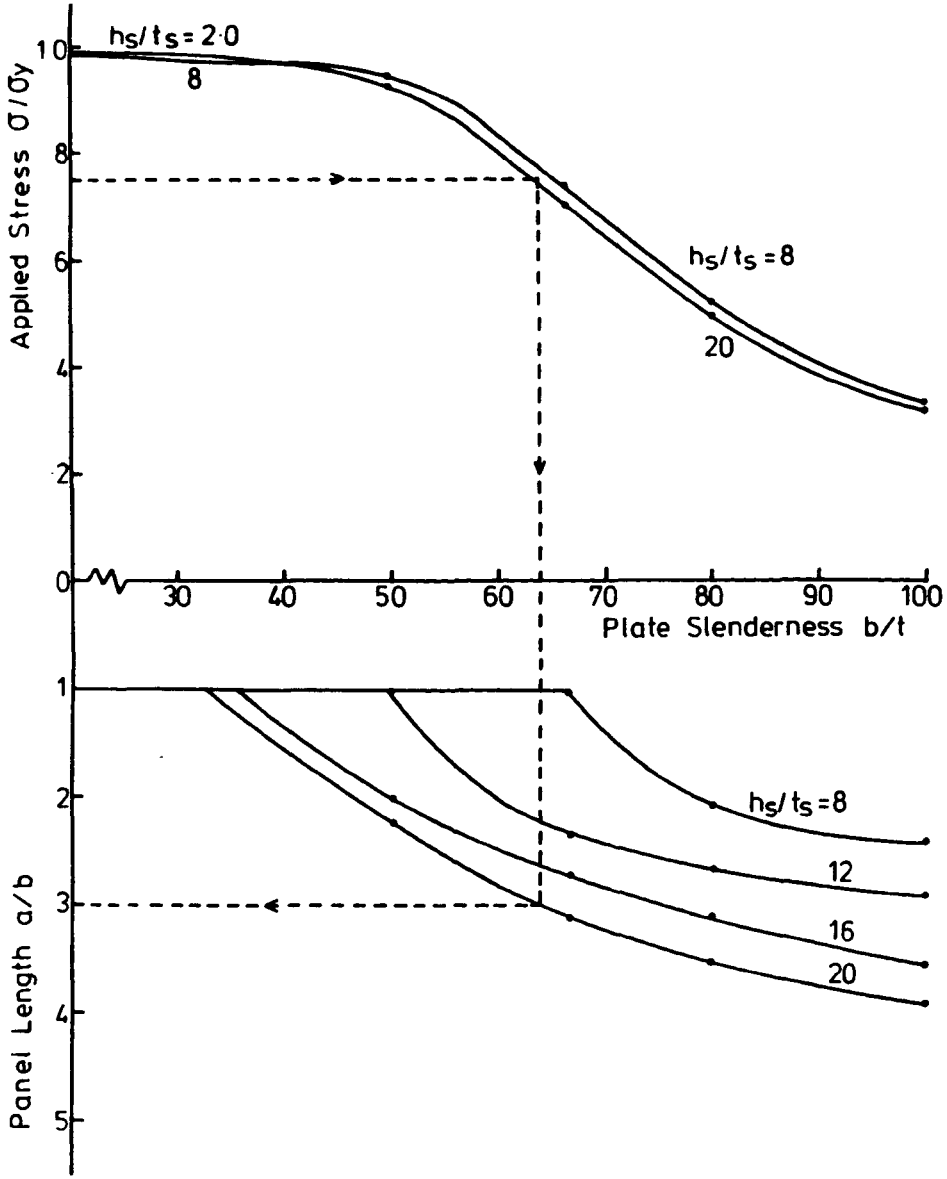

(a) $\sigma_r = 0{\cdot}0$ & $\delta = 0{\cdot}1$

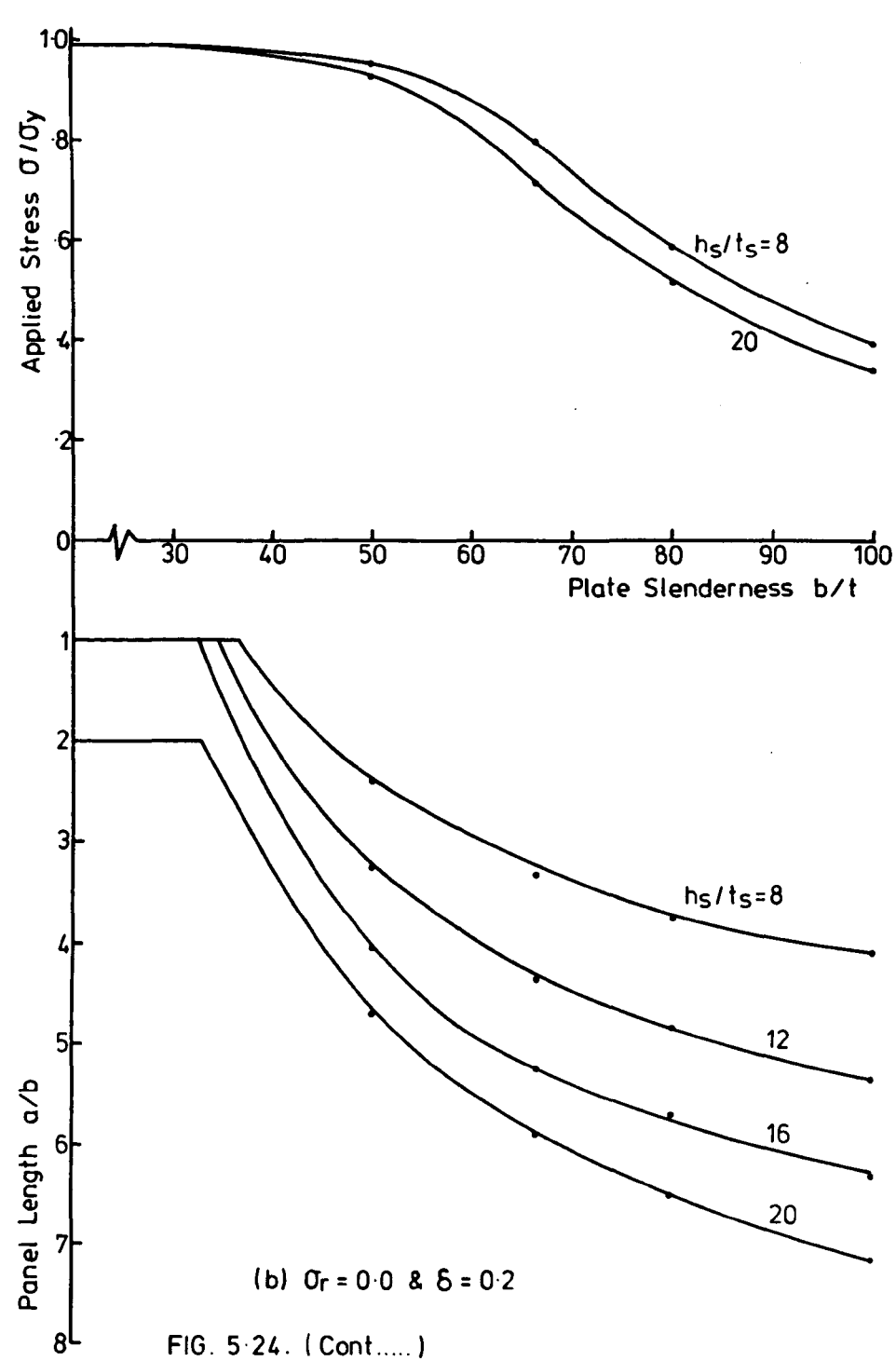

(b) $\sigma_r = 0{\cdot}0$ & $\delta = 0{\cdot}2$

FIG. 5·24. (Cont.....)

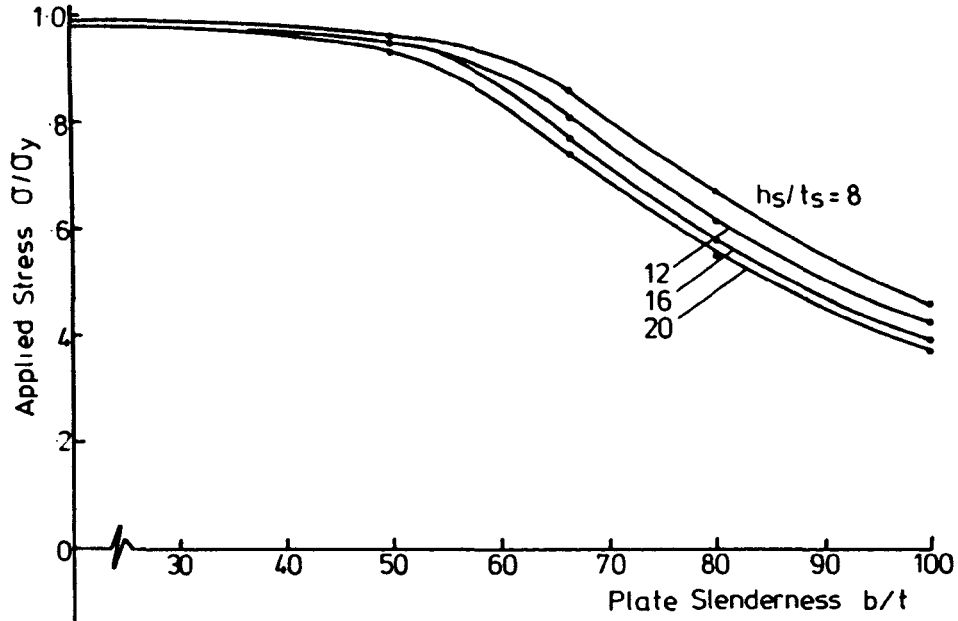
Applied Stress σ/σy
1·0
8
6
4
2
0
30
40
50
60
70
80
90
100
Plate Slenderness b/t
hs/ts = 8
12
16
20

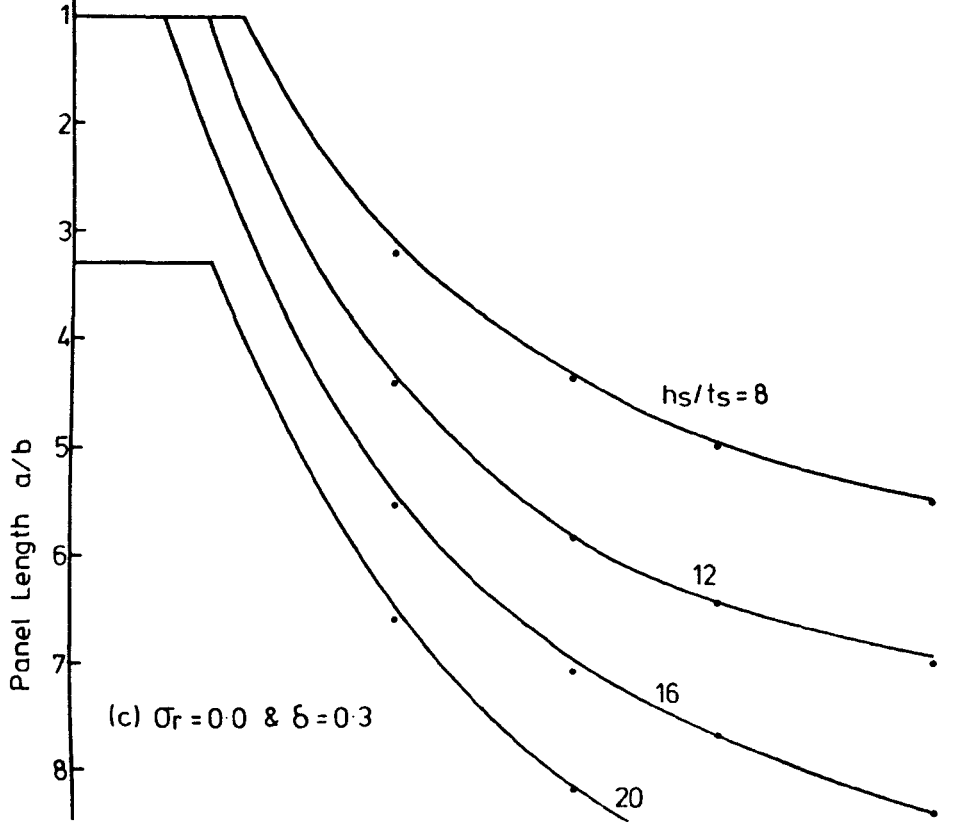
Panel Length a/b
1
2
3
4
5
6
7
8
hs/ts = 8
12
16
20
(c) σr = 0·0 & δ = 0·3

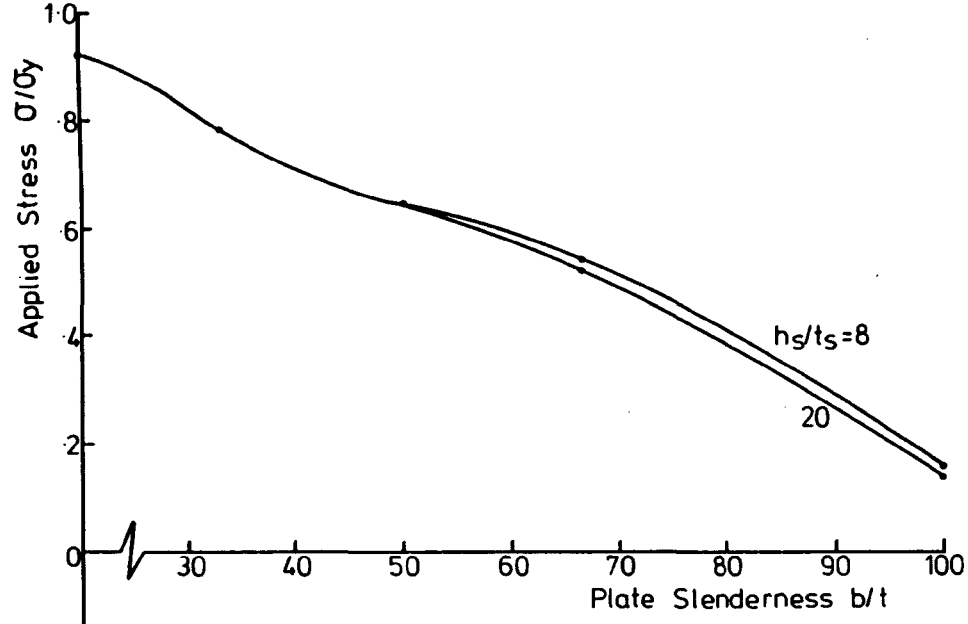
Applied Stress σ/σy
1·0
8
6
4
2
0
30
40
50
60
70
80
90
100
Plate Slenderness b/t
hs/ts=8
20

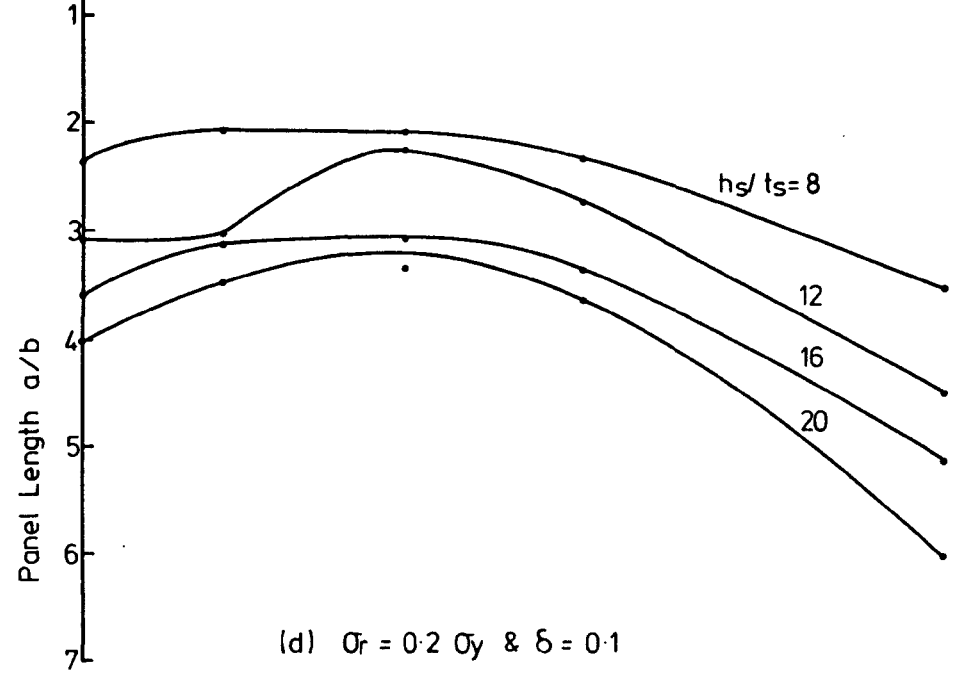
Panel Length a/b
1
2
3
4
5
6
7
hs/ts= 8
12
16
20
(d) σr = 0·2 σy & δ = 0·1

FIG. 5·24. (Cont.....)

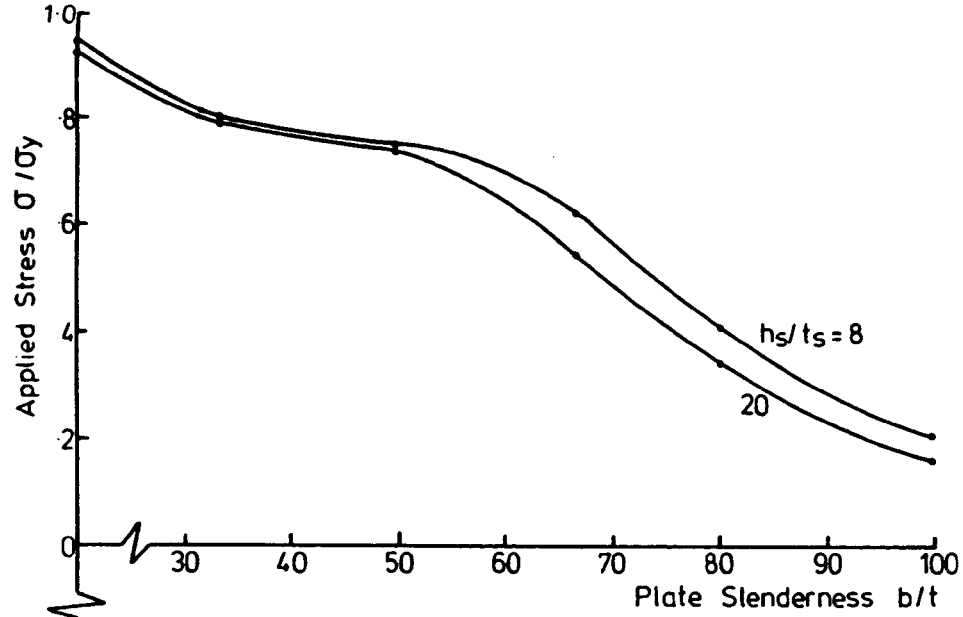

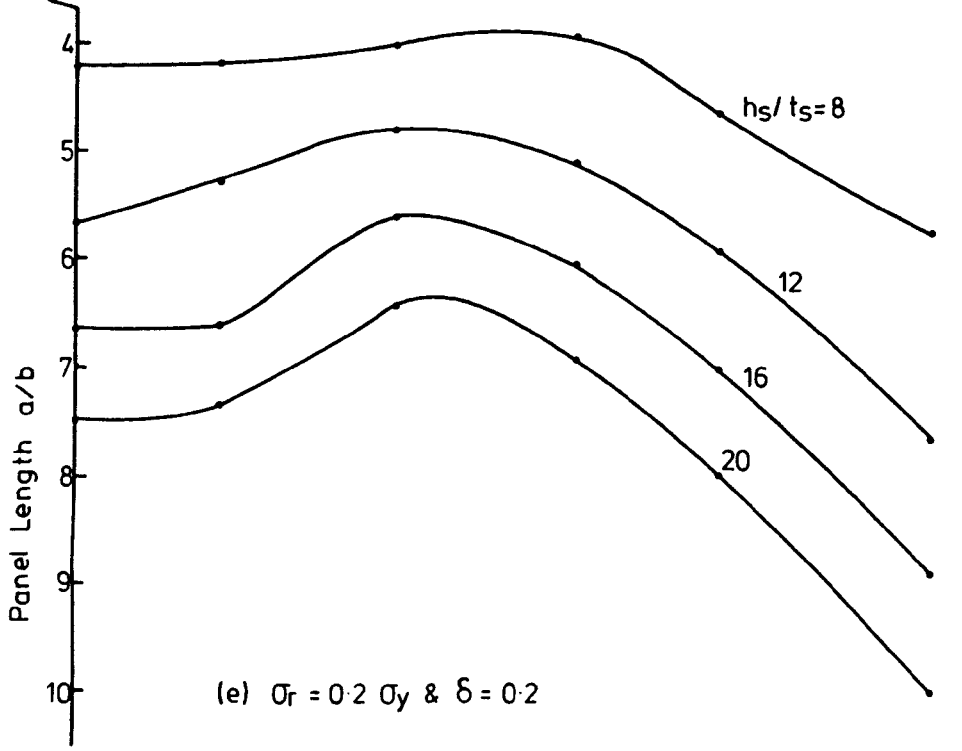

(e) $\sigma_r = 0{\cdot}2\ \sigma_y$ & $\delta = 0{\cdot}2$

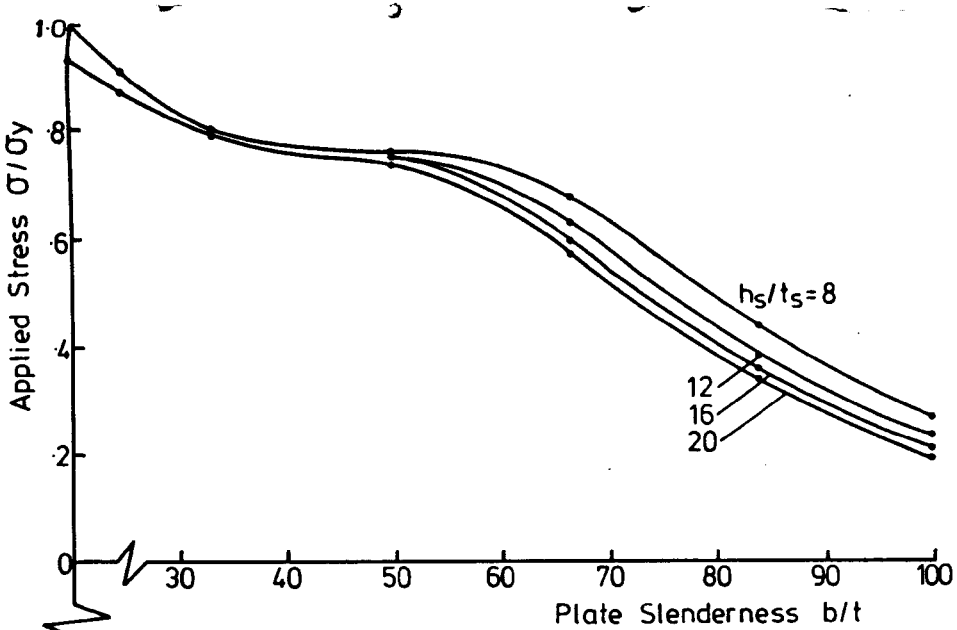

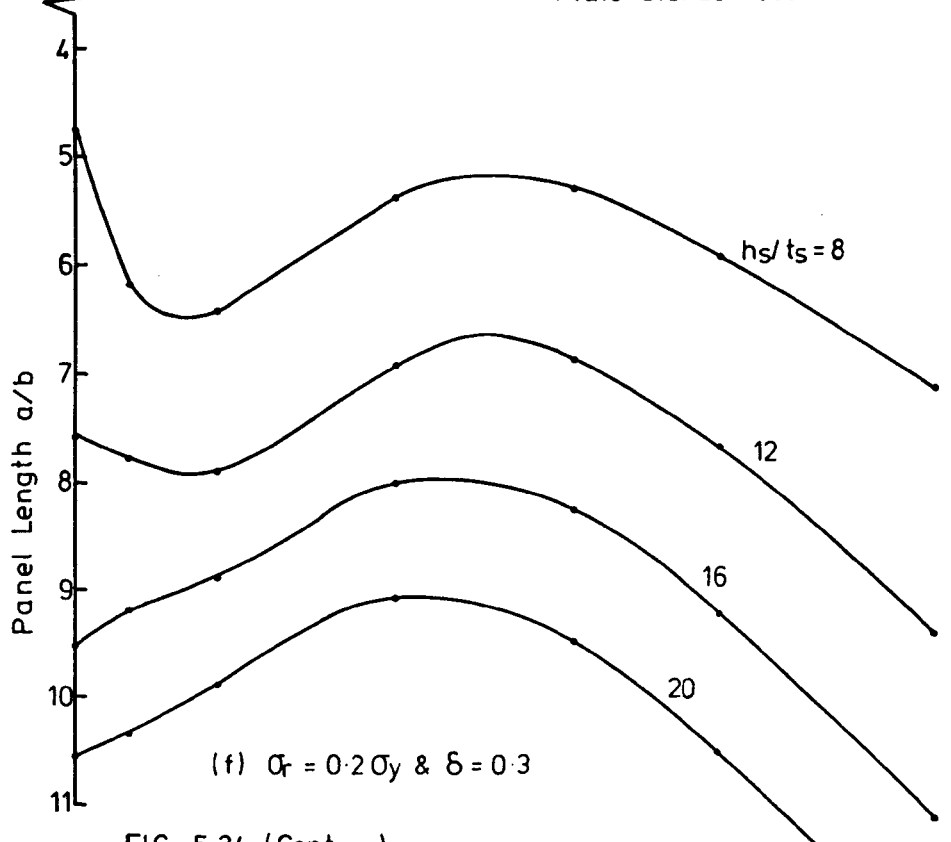

(f) $\sigma_r = 0{\cdot}2\sigma_y$ & $\delta = 0{\cdot}3$

FIG. 5·24. (Cont.....)

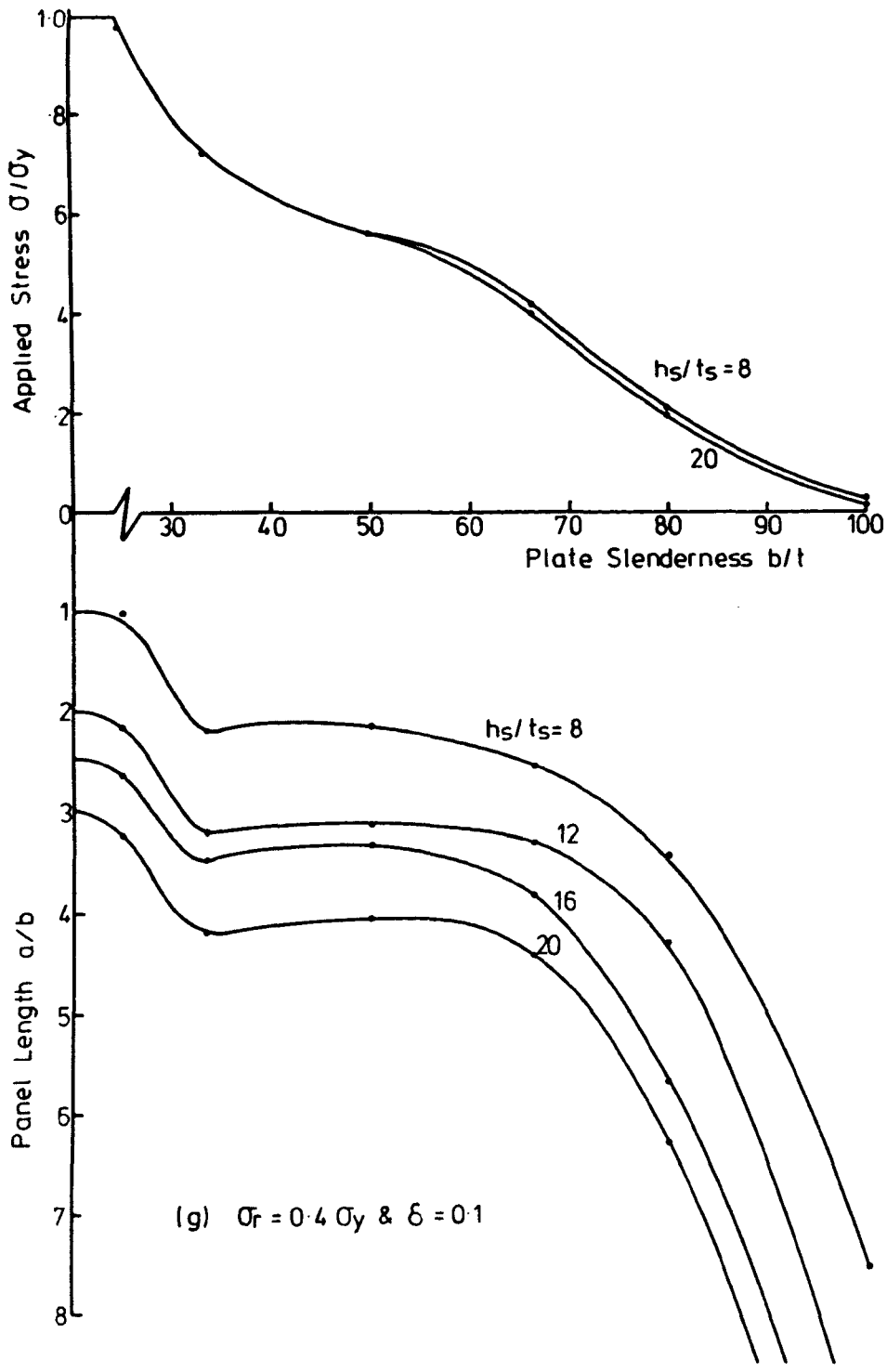
Applied Stress σ/σy
Plate Slenderness b/t
hs/ ts = 8
20
Panel Length a/b
hs/ ts= 8
12
16
20
(g) σr = 0·4 σy & δ = 0·1

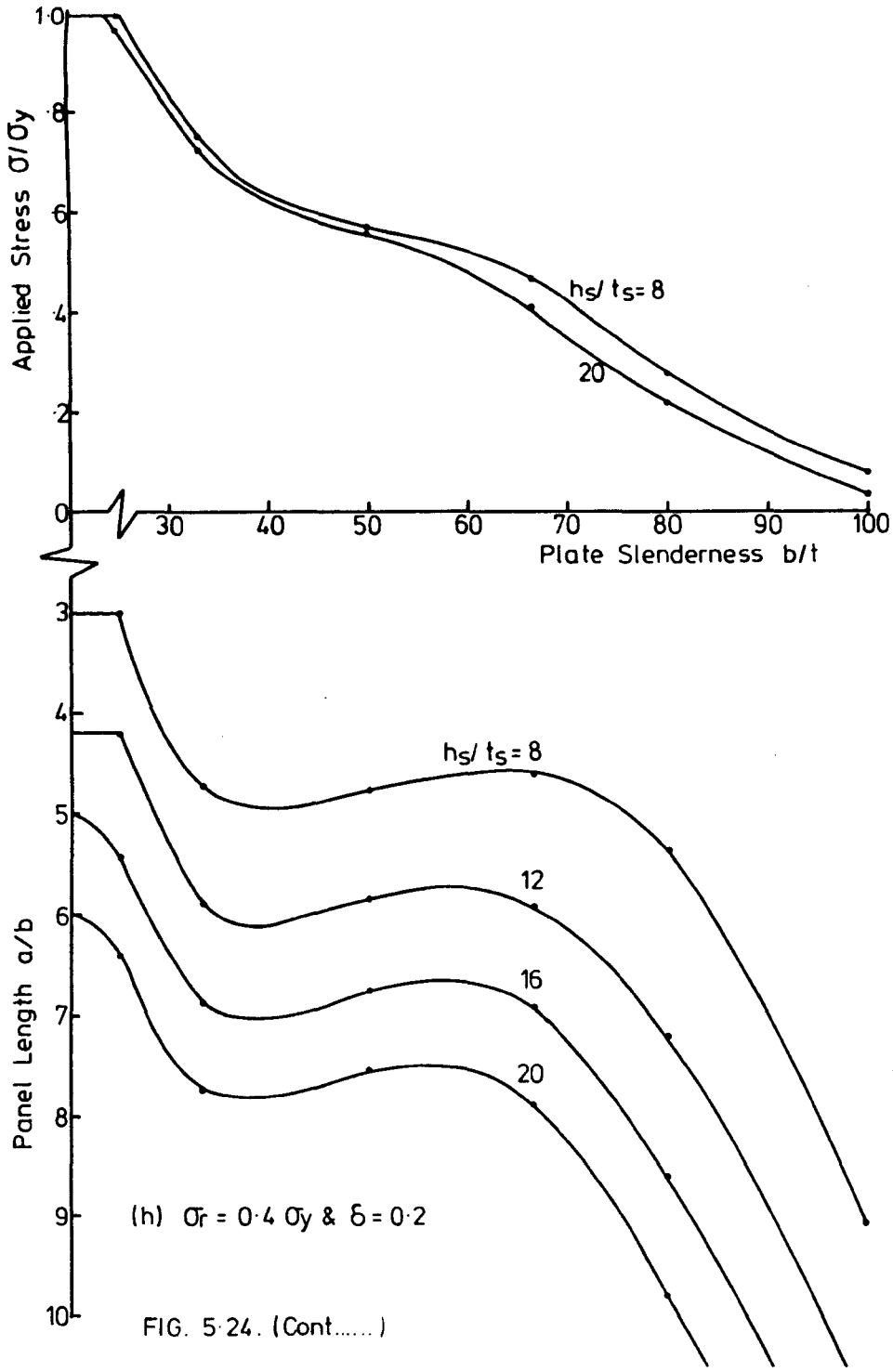
Applied Stress σ/σy
Plate Slenderness b/t
hs/ ts= 8
20
Panel Length a/b
hs/ ts = 8
12
16
20
(h) σr = 0·4 σy & δ = 0·2

FIG. 5·24. (Cont.....)

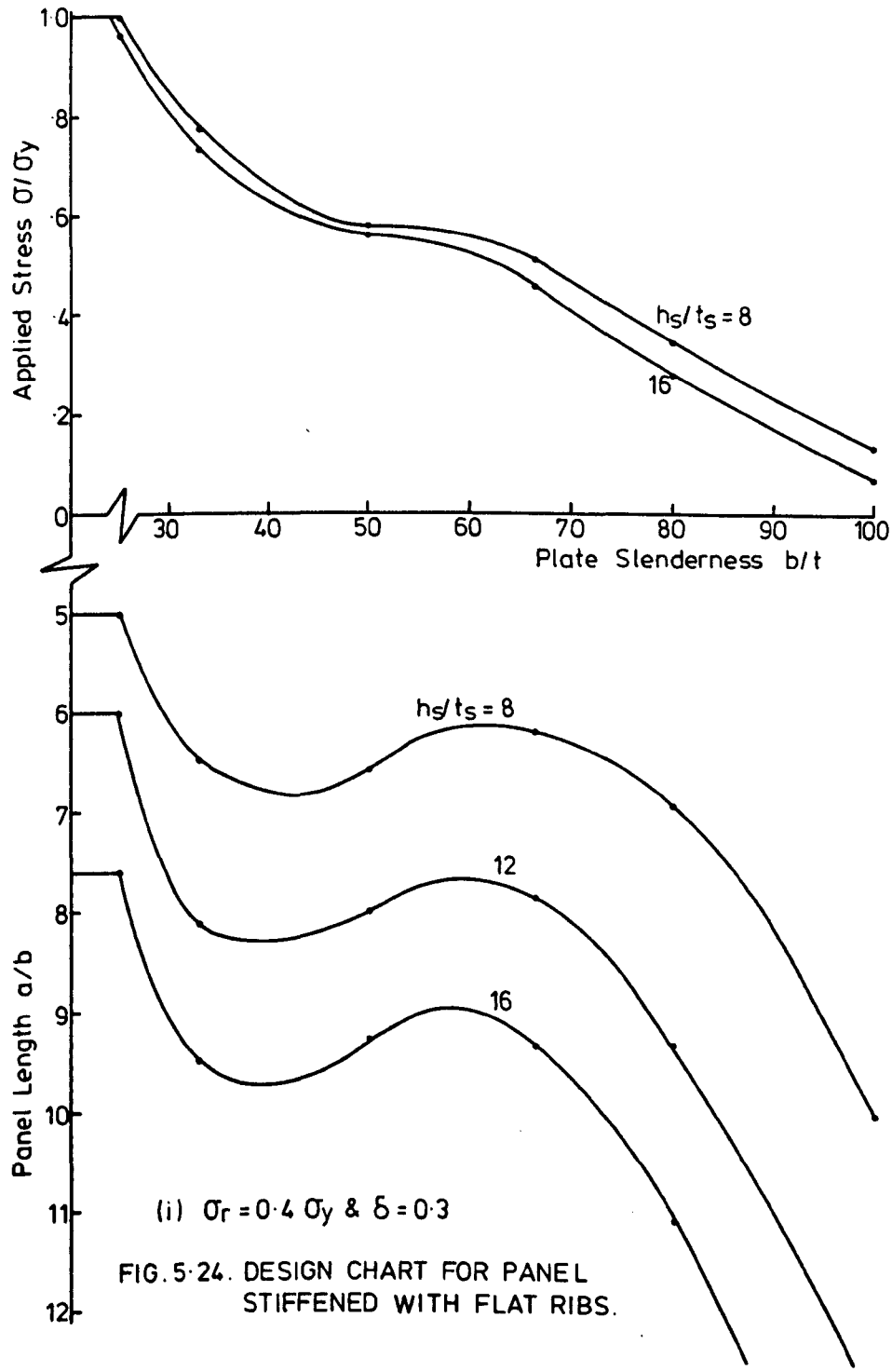

FIG. 5·24. DESIGN CHART FOR PANEL STIFFENED WITH FLAT RIBS.

thickness ratio - h_s/t_s between 8 and 20 - the slenderness ratio (b/t) of the panel - can be obtained.

3. From the relation between (b/t) and (a/b) the panel length (the distance between the transverse supports) can be obtained.

In the example shown assume an initially stress free panel stiffened with a number of ribs, the area of each rib relative to the area of the associated plate $\delta = 0.1$. Assume the applied stress $\sigma = 180$ N/mm^2 and choose $h_s/t_s = 20$. The optimum values for b/t and a/b will be 64 and 3.0 respectively.

From this, a very wide panel with the following dimensions

a : 600 mm

b : 200 mm

t : 3.125 mm

stiffener : 1.77 x 35.36 mm

σ_r : 0.0

σ_Y : 240.0 N/mm^2

will have local buckling strength equal to the overall buckling strength.

If the relative stiffener area δ is increased to 0.2 the optimum b/t and a/b will be 65 and 5.8 respectively.

The graphs can be used to determine any other two unknowns by using a similar approach.

In the previous section the optimum length of the panel was obtained from the graph of σ_{cr}/σ_Y against λ/b. The results given in Table 5.1 can be recast in the form of Figure 5.25 to obtain the optimum stiffener depth to thickness ratio h_s^*/t_s. The relation between the applied stress, the slenderness ratio of the plate and the optimum stiffener dimension h_s^*/t_s for a specified panel with length (a) are shown in Figure 5.26.

Use of this graph entails an exactly parallel process to that used with the length chart Figure 5.24.

5.5 Stability of Box Girder

The program has been developed to calculate the critical stress of a complete box section stiffened with any number of stiffeners on both the upper flange and the web. The applied stress can be axial compression with eccentricity varied from zero (pure compression) to infinity (pure bending). In order to take advantage of symmetry - both of the geometry and loading - only half of the box will be considered.

No parametric study has been done for this box section and the results shown in Figure 5.27 and Figure 5.28 are provided simply as an indication of the range of problems that can be analysed using the author's program.

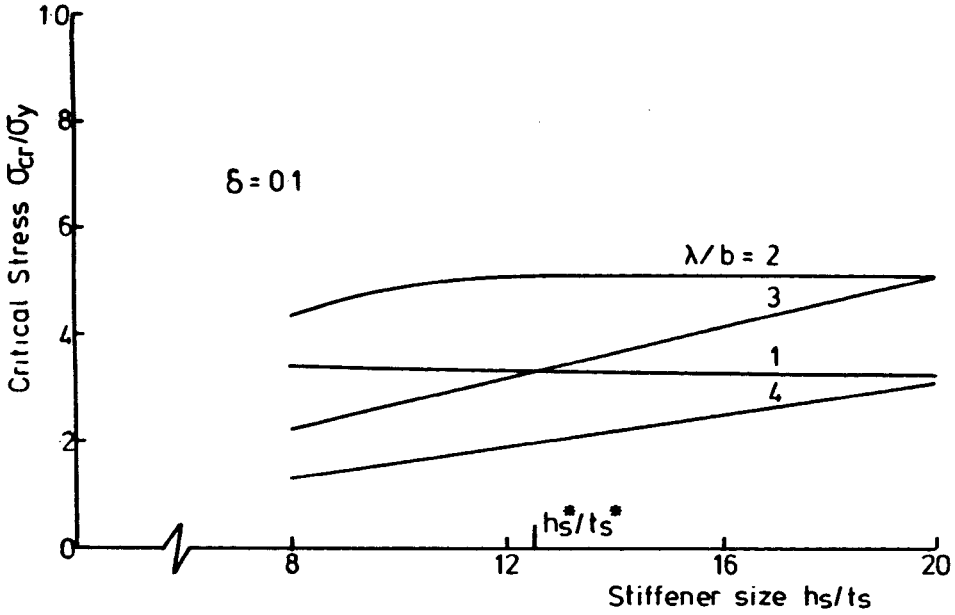

(a) β = 1·78 (b/t = 100)

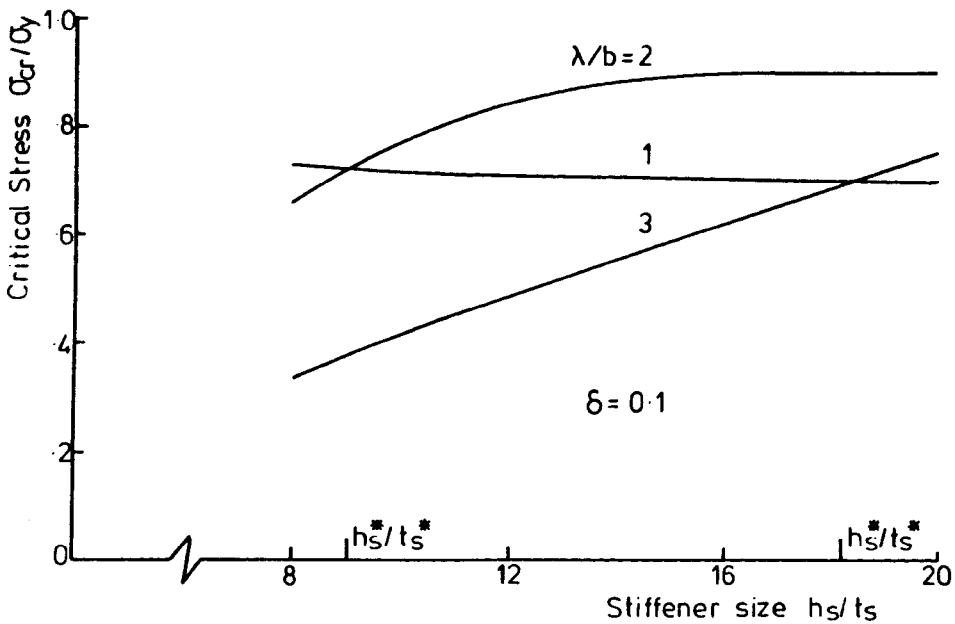

(b) β = 1·19 (b/t = 66·67)

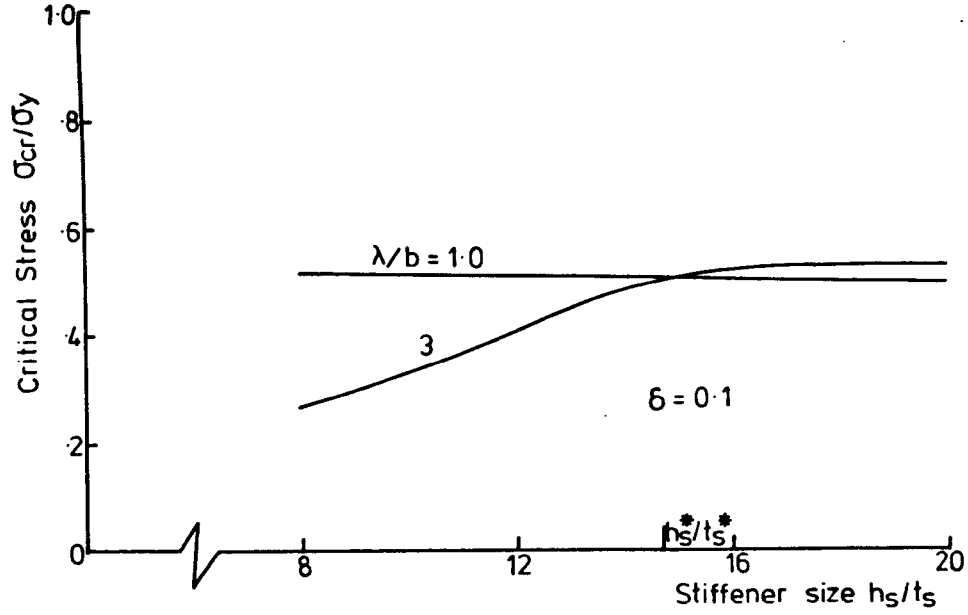

(c) β = 1·42 (b/t = 80)

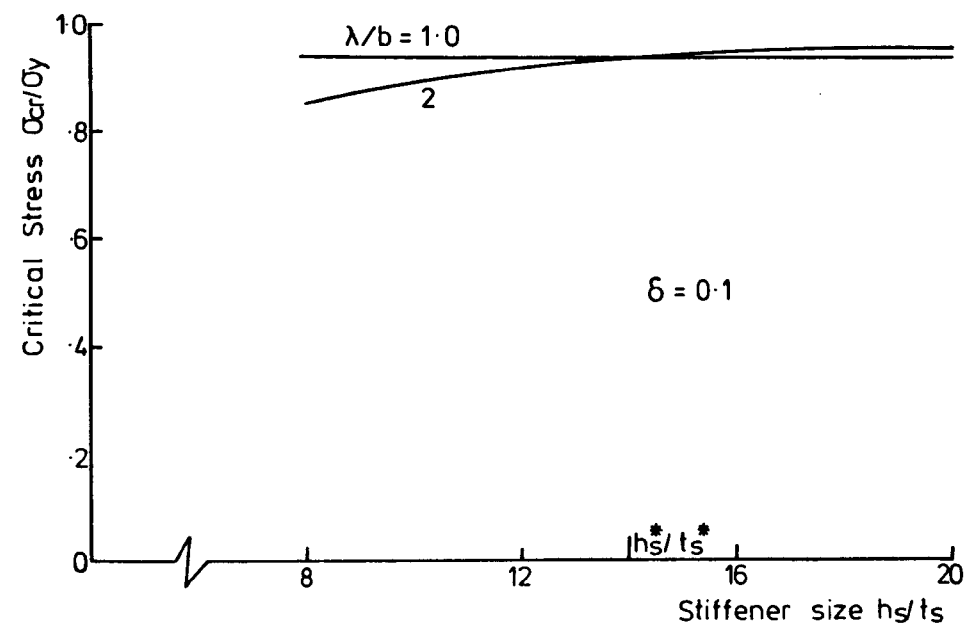

(d) β = 0·89 (b/t = 50)

FIG. 5·25. THE RELATION BETWEEN HALF WAVE-LENGTH AND STIFFENER DEPTH-TO-THICKNESS RATIO. (STRESS FREE PANEL)

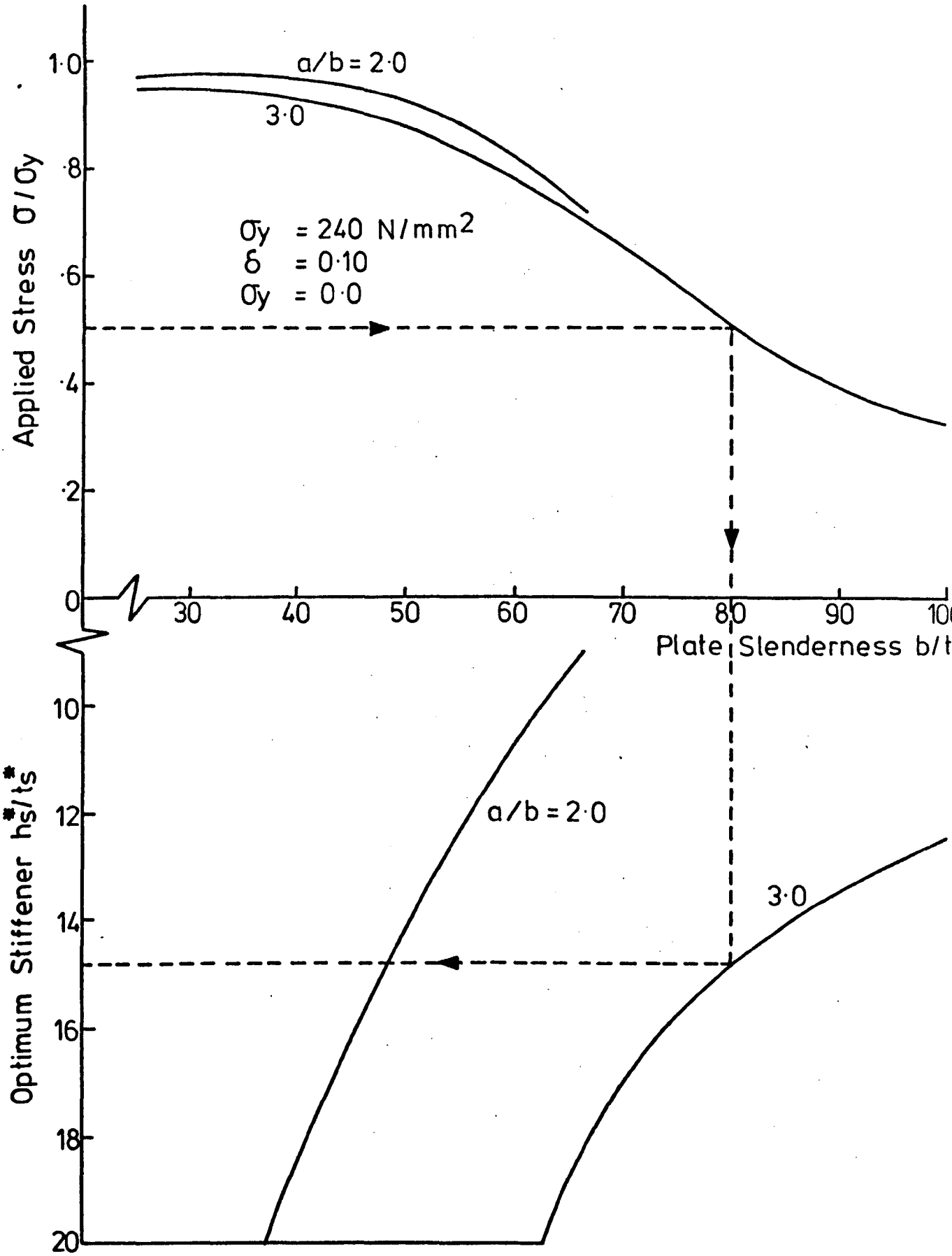

FIG. 5·26. A DESIGN CHART FOR OPTIMUM STIFFENER DEPTH-TO-THICKNESS RATIO, hs/ts.

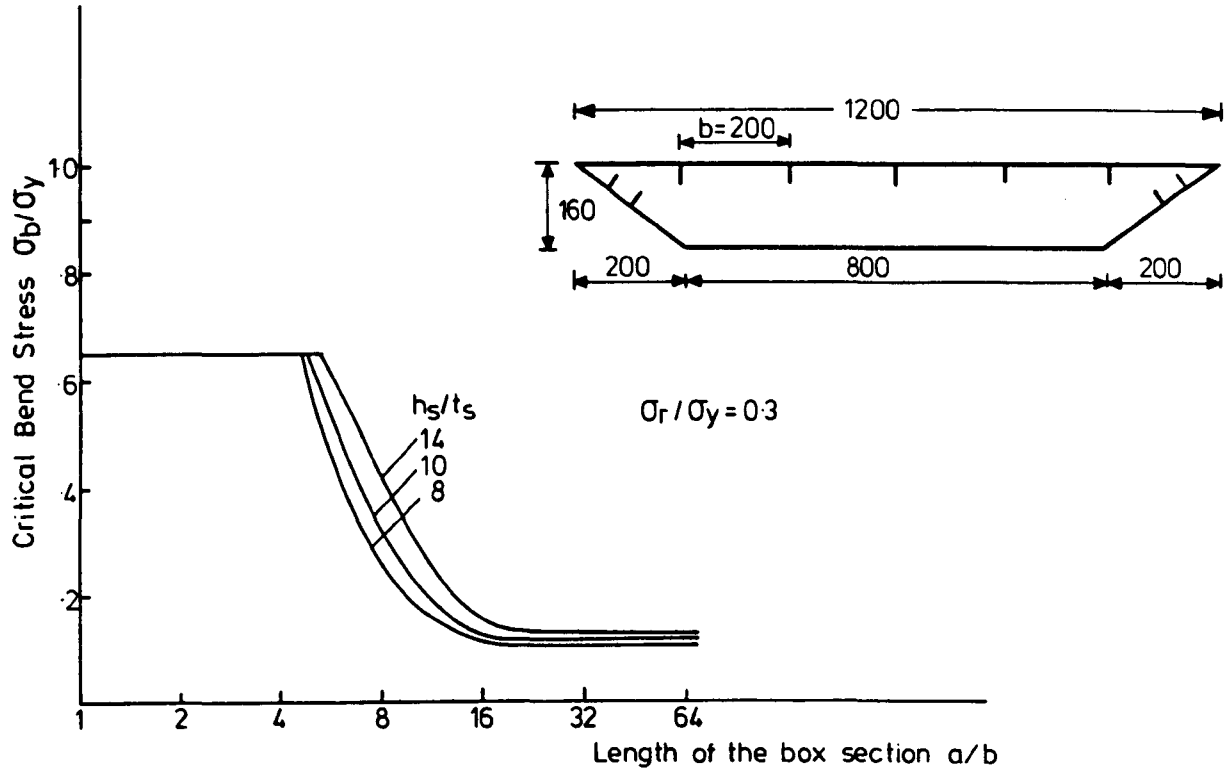

FIG. 5·27. EFFECT OF STIFFENER DIMENSION ON CRITICAL BENDING STRESS OF BOX SECTION.

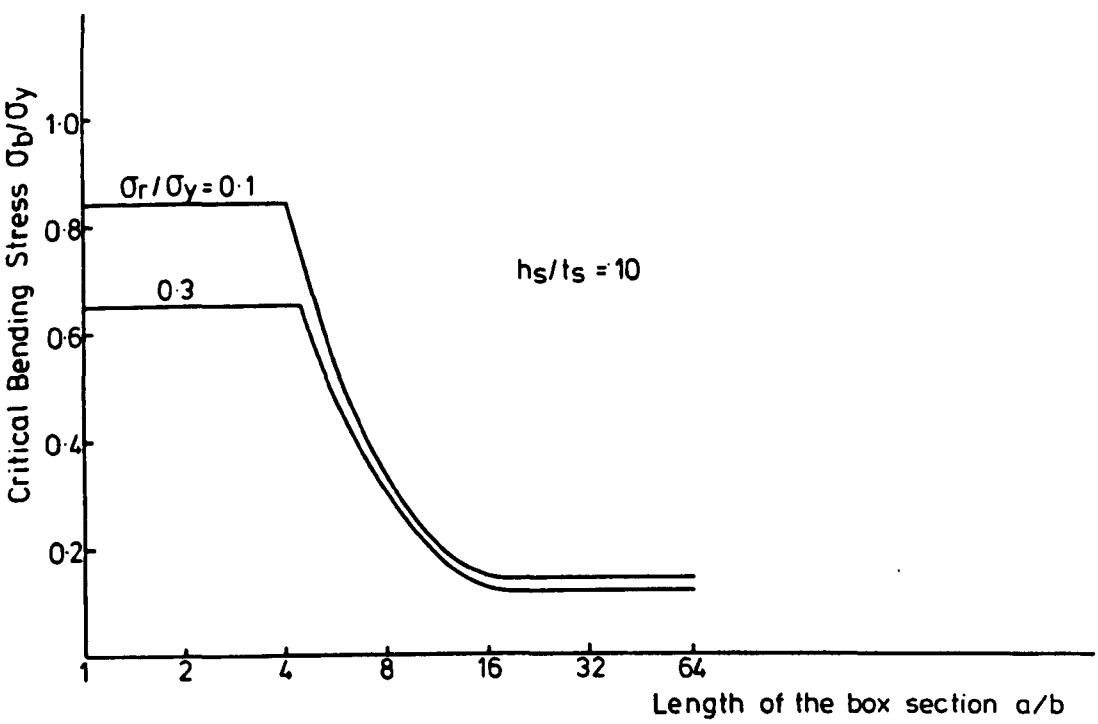

FIG. 5·28. EFFECT OF RESIDUAL STRESS ON CRITICAL BENDING STRESS OF BOX SECTION.

5.6 Concluding Remarks

The inelastic finite strip method has been used to study the buckling strength of stiffened panels. The effect of the slenderness ratio of the plating β, the residual stress, the shape and dimensions of the stiffener, the longitudinal boundary conditions and the yield stress of the material have all been considered. Results have been obtained for two main cases: a very wide panel and a square panel with four stiffeners.

The results from the analysis of the very wide panel have been used to develop an approximate design chart. This chart gives the optimum dimensions of a panel based on the condition that the overall buckling strength of the panel is equal to the local buckling strength of the plating; an example of its use is provided.

The main conclusions of the investigation of the square panels may be summarised as follows:

1. The present buckling strength curves show a smooth transition from elastic to inelastic buckling rather than the sudden reduction which would occur if an elastic perfectly plastic stress-strain relationship for the material had been assumed.

2. As the slenderness ratio of the plating β increases, the effect of the residual stresses reduces. For moderatly stocky panels strengths in excess of the value $(\sigma_Y - \sigma_r) \times$ area have been obtained at low β.

3. At low values of β the buckling strength curves for $\sigma_r = 0.5\ \sigma_Y$ become higher than those corresponding to $\sigma_r = 0.3\ \sigma_Y$. Moreover, for the very stocky panels, the critical stress may exceed the squash load.

4. At high values of the slenderness ratio of the plating β, increasing the stiffener area produces some increase in the local buckling strength.

5. Panels buckling in the inelastic range are affected more by the residual stresses than panels buckling in the elastic range.

6. The local buckling is more sensitive to the level of the residual stress than the overall buckling.

7. The torsional resistance of the stiffeners and the transverse continuity with neighbouring panels have some effect on the local buckling strength of the plating.

8. There is an optimum size for the stiffeners and using larger stiffeners will not have any effect on the buckling strength. This optimum size depends on the shape of the stiffener, slenderness ratio of the plating, level of residual stress and half wavelength of buckling.

9. The shape of the stiffener has some effect on the buckling strength. While flat stiffeners are most effective in preventing overall buckling, tee and

angle stiffener are more effective for local buckling. As β decreases, the effect of the stiffener shape on the critical buckling decreases.

10. There is a small effect for the flange width of a tee stiffener on the buckling strength of a stiffened panel.

11. The outward orientation of the outstanding leg of the angle stiffeners increases the overall buckling strength while the inward orientation increases the local buckling strength.

12. Some increases in the buckling strength of stiffened panels can be achieved by using stiffener material with a yield point higher than that of the plating.

b/t (β)	h_s/t_s \ λ/b	σ_{cr}/σ_Y					
		1	2	3	4	5	6
	8	0.341	0.429	0.220	0.128	0.083	0.058
	12	0.331	0.508	0.319	0.187	0.123	0.086
100.0	16	0.327	0.502	0.413	0.247	0.163	0.113
(1.76)	20	0.323	0.498	0.502	0.304	0.203	0.141
	8	0.729	0.672	0.338	0.195	0.127	0.088
	12	0.712	0.849	0.487	0.285	0.186	0.130
66.67	16	0.708	0.901	0.626	0.373	0.246	0.171
(1.17)	20	0.702	0.903	0.748	0.459	0.304	0.212
	8	0.937	0.848	0.457	0.264	0.172	0.119
	12	0.934	0.920	0.650	0.383	0.250	0.175
50.0	16	0.933	0.940	0.803	0.499	0.329	0.229
(0.88)	20	0.931	0.950	0.880	0.611	0.406	0.284
	8	0.972	0.932	0.693	0.407	0.265	0.185
	12	0.976	0.951	0.870	0.581	0.382	0.267
33.33	16	0.978	0.960	0.918	0.732	0.496	0.348
(0.59)	20	0.980	0.965	-	0.843	0.607	0.428
	8	0.978	0.951	0.858	0.555	0.363	0.253
	12	0.982	0.963	0.924	0.762	0.516	0.362
25.0	16	0.984	0.968	0.943	0.874	0.660	0.468
(0.44)	20	0.985	0.972	-	0.913	0.782	0.572
	8	0.982	0.960	0.913	0.701	0.465	0.326
	12	0.985	0.969	0.943	0.869	0.649	0.460
20.0	16	0.986	0.973	0.954	0.917	0.798	0.589
(0.35)	20	0.988	0.976	-	0.936	0.877	0.709

(a) $\sigma_r = 0.0$ and $\delta = 0.1$

(Table continued)

b/t (β)	λ/b / h_s/t_s	σ_{cr}/σ_Y						
		1	2	3	4	5	6	7
	8	0.397	0.584	0.665	0.415	0.279	0.195	0.143
	12	0.370	0.547	0.842	0.601	0.415	0.290	0.214
100.0	16	0.353	0.526	0.832	0.759	0.548	0.385	0.284
(1.76)	20	0.342	0.511	-	0.855	0.674	0.478	0.353
	8	0.799	0.927	0.880	0.622	0.415	0.292	0.215
	12	0.760	0.916	0.932	0.838	0.615	0.434	0.320
66.67	16	0.734	0.909	0.948	0.908	0.783	0.571	0.424
(1.17)	20	0.714	0.903	-	0.931	0.873	0.700	0.526
	8	0.947	0.960	0.928	0.796	0.556	0.390	0.288
	12	0.941	0.963	0.950	0.911	0.785	0.575	0.426
50.0	16	0.936	0.961	0.960	0.938	0.890	0.740	0.561
(0.88)	20	0.931	0.959	-	0.949	0.923	0.849	0.688
	8	0.983	0.971	0.953	0.915	0.794	0.583	0.433
	12	0.985	0.977	0.965	0.946	0.911	0.810	0.633
33.33	16	0.984	0.980	0.971	0.957	0.938	0.899	0.797
(0.59)	20	0.981	0.982	0.974	0.964	0.950	0.927	0.880
	8	0.987	0.977	0.963	0.941	0.895	0.757	0.577
	12	0.989	0.981	0.971	0.958	0.939	0.901	0.803
25.0	16	0.991	0.983	0.975	0.966	0.953	0.933	0.896
(0.44)	20	0.985	0.985	0.978	0.970	0.960	0.946	0.925
	8	0.990	0.980	0.969	0.952	0.927	0.863	
	12	0.991	0.984	0.975	0.965	0.950	0.929	
20.0	16	0.992	0.986	0.979	0.971	0.960	0.946	
(0.35)	20	0.985	0.987	0.981	0.974	0.966	0.956	

(b) σ_r = 0.0 and δ = 0.2

(Table continued)

b/t (β)	λ/b, h_s/t_s	σ_{cr}/σ_Y							
		1	2	3	4	5	6	7	8
	8	0.459	0.676	0.898	0.755	0.543	0.380	0.280	0.215
	12	0.417	0.603	0.869	0.897	0.776	0.564	0.418	0.321
100.0	16	0.389	-	0.844	0.929	0.887	0.731	0.552	0.426
(1.76)	20	0.369	0.531	-	0.929	0.921	0.845	0.679	0.529
	8	0.863	0.942	0.948	0.907	0.778	0.566	0.419	0.322
	12	0.813	0.928	0.960	0.942	0.908	0.798	0.618	0.479
66.67	16	0.771	-	0.956	0.954	0.937	0.895	0.787	0.636
(1.17)	20	0.735	0.902	-	0.961	0.949	0.925	0.876	0.762
	8	0.955	0.971	0.960	0.937	0.888	0.735	0.555	0.429
	12	0.948	0.967	0.969	0.956	0.937	0.896	0.788	0.631
50.0	16	0.940	-	0.973	0.964	0.952	0.931	0.891	0.798
(0.88)	20	0.932	0.958	-	0.969	0.960	0.946	0.923	0.881
	8	0.986	0.980	0.971	0.957	0.937	0.897	0.792	-
	12	0.986	0.983	0.976	0.968	0.956	0.940	0.911	0.851
33.33	16	0.984	0.985	0.980	0.974	0.965	0.953	0.938	0.914
(0.59)	20	0.978	0.983	0.982	0.976	0.970	0.961	0.950	0.935
	8	0.991	0.984	0.975	0.966	0.952	0.932	0.894	
	12	0.992	0.986	0.980	0.973	0.965	0.954	0.939	
25.0	16	0.993	0.988	0.983	0.977	0.971	0.963	0.953	
(0.44)	20	0.983	0.988	0.985	0.980	0.974	0.968	0.960	
	8	0.993	0.986	0.979	0.971	0.960	0.947		
	12	0.994	0.988	0.983	0.976	0.970	0.961		
20.0	16	0.993	0.990	0.985	0.980	0.974	0.968		
(0.35)	20	0.983	0.988	0.987	0.982	0.977	0.972		

(c) σ_Y = 0.0 and δ = 0.3

(Table continued)

b/t (δ)	λ/b / h_s/t_s	σ_{cr}/σ_Y					
		1	2	3	4	5	6
	8	0.160	0.340	0.200	0.120	0.080	0.060
	12	0.150	0.330	0.300	0.180	0.120	0.080
100.0	16	0.150	0.320	0.380	0.230	0.150	0.110
(1.76)	20	0.140	0.320	0.470	0.290	0.190	0.140
	8	0.550	0.630	0.330	0.190	0.120	0.090
	12	0.540	0.720	0.470	0.780	0.180	0.130
66.67	16	0.530	0.710	0.610	0.360	0.240	0.170
(1.17)	20	0.520	0.710	0.710	0.450	0.300	0.210
	8	0.740	0.760	0.450	0.260	0.170	0.120
	12	0.740	0.760	0.640	0.380	0.250	0.170
50.0	16	0.740	0.760	0.750	0.490	0.320	0.230
(0.88)	20	0.740	0.760	0.780	0.600	0.400	0.280
	8	0.790	0.800	0.680	0.400	0.260	0.180
	12	0.790	0.800	0.790	0.580	0.380	0.260
33.33	16	0.790	0.790	0.800	0.720	0.490	0.340
(0.59)	20	0.790	0.790	0.800	0.780	0.600	0.420
	8	0.880	0.900	0.780	0.550	0.360	0.250
	12	0.870	0.900	0.890	0.740	0.510	0.360
25.0	16	0.870	0.890	0.900	0.810	0.650	0.460
(0.44)	20	0.870	0.890	0.900	0.870	0.750	0.570
	8	0.920	0.960	0.850	0.690	0.460	0.320
	12	0.920	0.940	0.930	0.790	0.640	0.460
20.0	16	0.920	0.930	0.970	0.880	0.760	0.580
(0.35)	20	0.920	0.920	0.960	0.920	0.810	0.700

(d) $\sigma_r = 0.2\ \sigma_Y$ and $\delta = 0.1$

(Table continued)

b/t (β)	λ/b / h_s/t_s	σ_{cr}/σ_Y								
		1	2	3	4	5	6	7	8	9
	8	0.210	0.400	0.620	0.400	0.260	0.190	0.146	-	0.090
	12	0.190	0.370	0.660	0.580	0.390	0.280	0.217	0.167	0.133
100.0	16	0.180	0.360	0.650	0.710	0.510	0.368	0.287	0.221	0.175
(1.76)	20	0.170	0.340	0.640	0.740	0.630	0.457	0.357	0.275	0.218
	8	0.620	0.730	0.760	0.610	0.400	0.280	0.218	-	-
	12	0.580	0.720	0.760	0.770	0.590	0.420	0.323	-	-
66.67	16	0.560	0.720	0.760	0.770	0.740	0.555	0.427	-	-
(1.17)	20	0.540	0.710	0.760	0.770	0.780	0.676	0.529	-	-
	8	0.750	0.770	0.780	0.750	0.540	0.382	0.291	-	-
	12	0.750	0.770	0.780	0.790	0.740	0.562	0.429	-	-
50.0	16	0.740	0.770	0.780	0.780	0.790	0.710	0.564	-	-
(0.88)	20	0.740	0.760	0.780	0.780	0.790	0.779	0.684	-	-
	8	0.800	0.800	0.800	0.810	0.750	0.573	0.436	-	-
	12	0.800	0.800	0.800	0.800	0.820	0.760	0.633	-	-
33.33	16	0.790	0.800	0.800	0.800	0.800	0.841	0.759	-	-
(0.59)	20	0.790	0.790	0.800	0.800	0.800	0.837	0.816	0.745	-
	8	0.900	0.910	0.920	0.920	0.830	0.728	0.578	-	-
	12	0.880	0.900	0.910	0.910	0.920	0.844	0.760	-	-
25.0	16	0.870	0.890	0.900	0.910	0.910	0.912	0.846	-	-
(0.44)	20	0.870	0.880	0.890	0.900	0.910	0.913	0.911	0.827	-
	8	0.930	0.990	1.000	0.970	0.890	0.785	-	-	-
	12	0.920	0.950	0.980	1.000	0.960	0.901	-	-	-
20.0	16	0.920	0.920	0.940	0.970	0.990	0.954	0.912	-	-
(0.35)	20	0.920	0.920	0.920	0.940	0.980	0.980	0.951	0.902	-

(e) $\sigma_r = 0.2\ \sigma_Y$ and $\delta = 0.2$

(Table continued)

b/t (β)	λ/b / h_s/t_s	σ_{cr}/σ_Y									
		1	2	3	4	5	6	7	8	9	10
	8	0.273	0.497	0.707	0.710	0.508	0.382	0.282	0.216	-	-
	12	0.236	0.432	0.683	0.744	0.711	0.564	0.419	0.322	0.255	0.208
100.0	16	0.212	0.390	0.664	0.740	0.759	0.715	0.553	0.427	0.339	0.276
(1.76)	20	0.196	0.367	0.647	0.737	0.758	0.775	0.673	0.530	0.422	0.343
	8	0.677	0.748	0.769	0.779	0.728	0.566	0.421	0.323	-	-
	12	0.634	0.736	0.764	0.775	0.781	0.754	0.617	0.480	-	-
66.67	16	0.599	0.726	0.761	0.773	0.780	0.828	0.749	0.628	0.504	-
(1.17)	20	0.571	0.717	0.759	0.772	0.779	0.908	0.791	0.735	0.620	0.510
	8	0.764	0.779	0.786	0.790	0.793	0.717	0.556	0.430	-	-
	12	0.756	0.772	0.782	0.787	0.790	0.828	0.749	0.629	-	-
50.0	16	0.750	0.768	0.780	0.785	0.789	0.923	0.818	0.754	0.657	-
(0.88)	20	0.744	0.765	0.778	0.784	0.788	0.961	0.902	0.796	0.751	0.663
	8	0.799	0.800	0.841	0.866	0.880	0.830	0.751	-	-	-
	12	0.797	0.798	0.800	0.814	0.850	0.945	0.870	0.790	-	-
33.33	16	0.795	0.794	0.798	0.799	0.816	0.982	0.941	0.877	0.785	0.744
(0.59)	20	0.794	0.794	0.796	0.798	0.800	1.000	0.972	0.933	0.872	0.788
	8	0.907	0.917	0.919	0.920	0.932	0.924	0.821	-	-	-
	12	0.892	0.908	0.912	0.915	0.917	0.982	0.942	0.878	-	-
25.0	16	0.880	0.891	0.900	0.905	0.910	1.000	0.980	0.945	0.894	0.808
(0.44)	20	0.868	0.868	0.881	0.893	0.901	1.000	0.990	0.975	0.943	0.897
	8	0.995	1.000	1.000	1.000	0.993	0.962	-	-	-	-
	12	0.920	0.957	0.974	1.000	1.000	1.000	0.973	0.934	0.874	-
20.0	16	0.920	0.920	0.972	0.938	0.970	1.000	1.000	0.975	0.943	0.898
(0.35)	20	0.919	0.919	0.919	0.920	0.922	1.000	1.000	0.996	0.974	0.945

(f) $\sigma_Y = 0.2\ \sigma_Y$ and $\delta = 0.3$

(Table continued)

b/t (β)	h_s/t_s \ λ/b	σ_{cr}/σ_Y				
		1	2	3	4	5
	8	0.030	0.213	0.187	0.114	0.076
	12	0.023	0.204	0.276	0.171	0.116
100.0	16	0.019	0.199	0.360	0.226	0.155
(1.76)	20	0.017	0.197	0.429	0.281	0.195
	8	0.413	0.535	0.319	0.188	0.119
	12	0.403	0.535	0.457	0.276	0.179
66.67	16	0.398	0.539	0.554	0.361	0.238
(1.17)	20	0.394	0.533	0.568	0.443	0.300
	8	0.559	0.577	0.441	0.259	0.164
	12	0.557	0.576	0.574	0.376	0.243
50.0	16	0.556	0.575	0.590	0.486	0.321
(0.88)	20	0.556	0.575	0.590	0.566	0.398
	8	0.722	0.748	0.599	0.403	0.257
	12	0.718	0.744	0.763	0.551	0.373
33.33	16	0.715	0.742	0.768	0.656	0.483
(0.59)	20	0.712	0.740	0.767	0.752	0.567
	8	0.989	0.981	0.747	0.533	0.354
	12	0.983	1.000	0.892	0.674	0.499
25.0	16	0.979	1.000	0.965	0.789	0.592
(0.44)	20	0.974	1.000	1.000	0.870	0.698
	8	1.000	1.000	0.843	0.612	0.452
	12	1.000	1.000	0.962	0.775	0.580
20.0	16	1.000	1.000	1.000	0.880	0.678
(0.35)	20	1.000	1.000	1.000	0.945	0.803

(g) $\sigma_r = 0.4\ \sigma_Y$ and $\delta = 0.1$

(Table continued)

b/t (β)	λ/b, h_s/t_s	σ_{cr}/σ_Y							
		1	2	3	4	5	6	7	8
	8	0.079	0.279	0.507	0.386	0.272	0.188	0.136	0.103
	12	0.059	0.248	0.497	0.532	0.407	0.283	0.207	0.157
100.0	16	0.047	0.231	0.491	0.551	0.527	0.377	0.277	0.211
(1.76)	20	0.040	0.220	0.485	0.549	0.599	0.467	0.346	0.264
	8	0.467	0.548	0.573	0.563	0.410	0.285	0.208	-
	12	0.442	0.542	0.571	0.583	0.568	0.425	0.313	-
66.67	16	0.426	0.538	0.570	0.583	0.696	0.543	0.415	-
(1.17)	20	0.414	0.536	0.569	0.582	0.804	0.621	0.510	0.397
	8	0.567	0.582	0.596	0.683	0.532	0.382	0.281	-
	12	0.563	0.579	0.593	0.670	0.698	0.545	0.418	-
50.0	16	0.566	0.577	0.591	0.656	0.828	0.656	0.536	-
(0.88)	20	0.558	0.576	0.590	0.644	0.913	0.771	0.611	0.519
	8	0.746	0.766	0.787	0.876	0.703	0.549	0.424	-
	12	0.732	0.755	0.773	0.873	0.880	0.721	0.575	-
33.33	16	0.723	0.747	0.770	0.844	0.963	0.846	0.709	-
(0.59)	20	0.717	0.741	0.767	0.826	1.000	0.926	0.813	0.684
	8	1.000	1.000	1.000	0.969	0.835	0.664	0.545	-
	12	0.992	1.000	1.000	1.000	0.964	0.849	0.713	-
25.0	16	0.978	0.998	1.000	1.000	1.000	0.949	0.839	-
(0.44)	20	0.961	0.983	1.000	1.000	1.000	0.988	0.921	0.821
	8	1.000	1.000	1.000	1.000	0.921	0.782	-	-
	12	1.000	1.000	1.000	1.000	1.000	0.972	-	-
20.0	16	1.000	1.000	1.000	1.000	1.000	0.989	-	-
(0.35)	20	1.000	1.000	1.000	1.000	1.000	1.000	0.974	0.908

(h) $\sigma_r = 0.4\ \sigma_Y$ and $\delta = 0.2$

(Table continued)

b/t (β)	λ/b / h_s/t_s	σ_{cr}/σ_Y									
		1	2	3	4	5	6	7	8	9	10
	8	0.133	0.367	0.529	0.560	0.521	0.373	0.274	0.209	0.164	0.131
	12	0.101	0.309	0.514	0.556	0.677	0.535	0.409	0.314	0.248	0.200
100.0	16	0.082	0.276	0.503	0.553	0.820	0.635	0.528	0.417	-	0.268
(1.76)	20	0.069	0.254	0.493	0.551	0.857	0.757	0.591	0.511	0.412	0.335
	8	0.509	0.560	0.579	0.590	0.679	0.537	0.411	0.315	0.249	-
	12	0.482	0.552	0.545	0.586	0.873	0.701	0.565	0.467	0.373	-
66.67	16	0.460	0.545	0.572	0.584	0.961	0.838	0.688	0.570	0.489	0.401
(1.17)	20	0.441	0.540	0.570	0.583	1.000	0.924	0.803	0.664	0.567	0.494
	8	0.576	0.592	0.651	0.719	0.823	0.637	0.530	0.420	0.333	-
	12	0.570	0.584	0.606	0.690	0.962	0.839	0.689	0.571	0.490	-
50.0	16	0.565	0.581	0.594	0.673	1.000	0.944	0.829	0.701	0.583	0.521
(0.88)	20	0.562	0.578	0.592	0.653	1.000	0.988	0.917	0.814	0.693	0.586
	8	0.768	0.789	0.871	0.955	0.963	0.841	0.692	-	-	-
	12	0.750	0.768	0.793	0.903	1.000	0.970	0.882	0.765	0.637	-
33.33	16	0.736	0.754	0.772	0.844	1.000	1.000	0.966	0.889	0.790	0.679
(0.59)	20	0.725	0.742	0.765	0.811	1.000	1.000	1.000	0.957	0.885	0.795
	8	1.000	1.000	1.000	1.000	1.000	0.946	0.833	-	-	-
	12	1.000	1.000	1.000	1.000	1.000	1.000	0.967	-	-	-
25.0	16	0.981	0.990	1.000	1.000	1.000	1.000	1.000	0.970	-	0.823
(0.44)	20	0.954	0.953	0.996	1.000	1.000	1.000	1.000	1.000	0.968	0.911
	8	1.000	1.000	1.000	1.000	1.000	0.990	0.921	-	-	-
	12	1.000	1.000	1.000	1.000	1.000	1.000	1.000	0.958	0.887	-
20.0	16	1.000	1.000	1.000	1.000	1.000	1.000	1.000	1.000	0.968	0.912
(0.35)	20	1.000	1.000	1.000	1.000	1.000	1.000	1.000	1.000	1.000	0.970

(1) $\sigma_r = 0.4\ \sigma_Y$ and $\delta = 0.3$

Table 5.1. The Buckling Strength of a Very Wide Panel

CHAPTER 6

INELASTIC BUCKLING BEHAVIOUR OF COLUMNS, BEAMS AND BEAM-COLUMNS

6.1 Introduction

In this chapter the finite strip method described in the previous section is used to study the inelastic buckling of structural members under various types of loading. The columns, beams and beam-columns are all assumed to be pin-ended. Lateral deflection and twist at the ends are thus prevented but no resistance is provided against lateral bending nor is there any restraint (bracing) to the web or the flanges along the length. This type of structural member may buckle in one of the three basic modes,

1. Local buckling
2. Overall buckling
3. Combined overall and local buckling

Which of these modes will actually occur depends on many factors including,

1. The shape and dimensions of the cross-section
2. The length of the structural member
3. The magnitude and the pattern of the residual stresses
4. The initial imperfections and the eccentricity of the load

The local buckling of any component of the structural element depends largely on the width-to-thickness ratio of that component. For a low ratio the ultimate strength of the member may be reached before buckling occurs, while for a high ratio the component may exhibit some post-local-buckling strength. In this chapter any post-local-buckling strength is neglected.

In the conventional treatment of overall buckling, the components of a member are considered undistorted. This buckling may be flexural, torsional or flexural-torsional.

In the combined mode the overall buckling occurs at a load which is lower than that which the member would carry if local buckling of the components were prevented. This is due to the weakening effect of the local buckling. It is especially critical for intermediate length structural members containing plates with relatively large width-to-thickness ratios.

In this chapter the effects of the yield stress of the material, the slenderness ratio of the member, the cross-sectional shape and dimensions, the residual stress pattern and magntiude, the overall initial imperfection and the load eccentricity on the buckling strength of structural members have been considered.

6.2 Number of Strips, Number of Substrips and Accuracy

As described in Chapter 4, the current method requires the structural elements to be divided into a number of longitudinal strips and - where the stress is not uniform over the section - every strip is divided into a number of longitudinal substrips (segments). The number of strips required depends on some of the following factors,

1. The shape of the cross-section (H-section, channel, box section, etc.)
2. The type of the applied load (axial compression, bending moment, eccentric compression)
3. The mode of buckling (i.e. the half wavelength)
4. The residual stresses (pattern and magnitude)
5. The accuracy required

and these will now be discussed.

6.2.1 Section Under Concentric Longitudinal Compression

In Table 6.1 the effect of the number of strips on the elastic critical load is considered. Two cross-sections - an H-section and a channel - are divided into a number of strips as shown in Figure 6.1. Because the sections are under concentric axial load symmetrical divisions are considered (Figure 6.1). To study the effect of the buckling mode on the number of strips, five values for the half wavelength λ are used. It is clear that more strips are

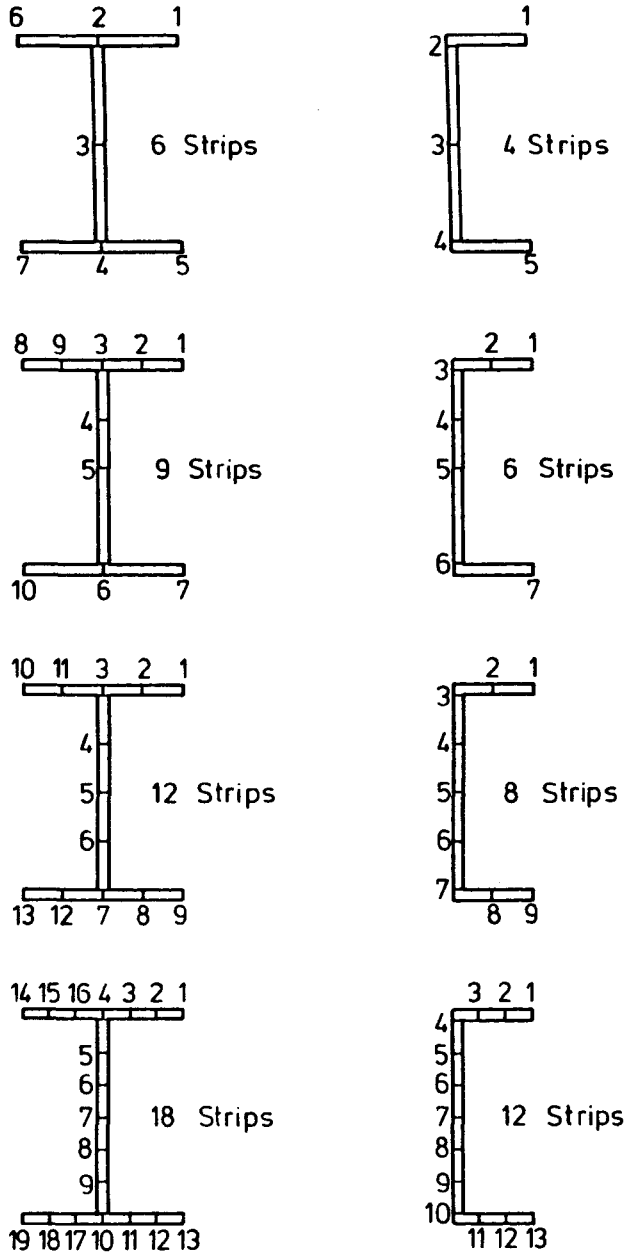

FIG. 6·1. STRIP IDEALIZATION OF H - SECTIONS AND CHANNELS.

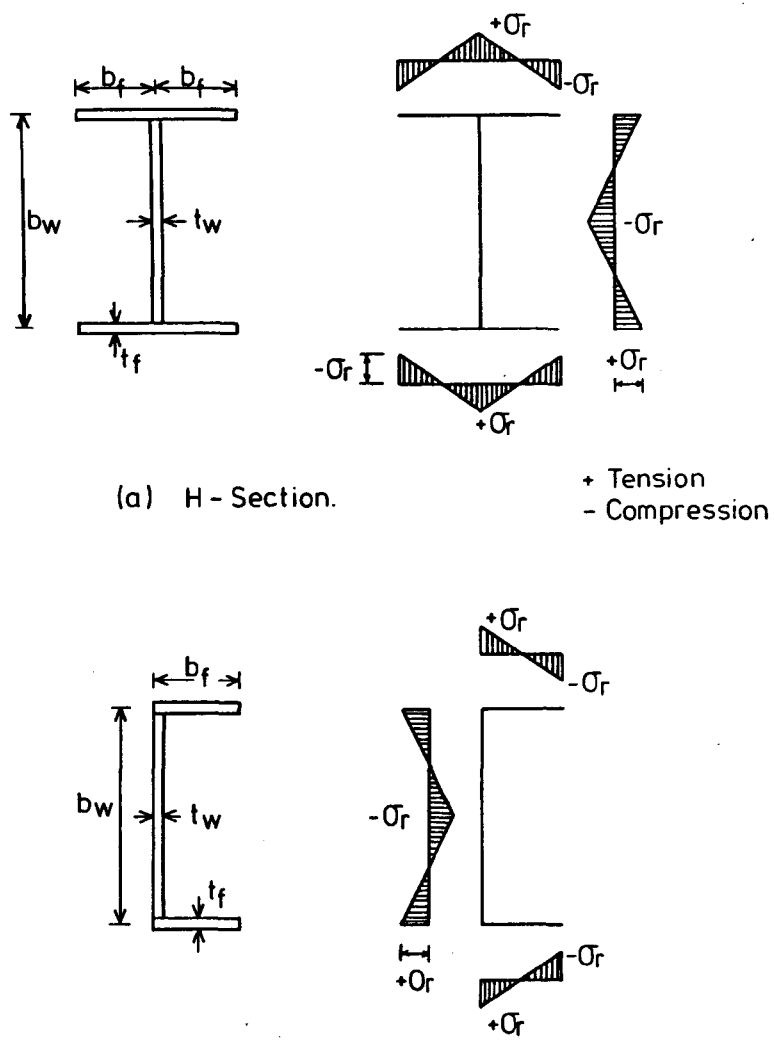

FIG. 6·2. THE RESIDUAL STRESS PATTERNS FOR ROLLED SECTIONS.

required for the local buckling analysis than are required for the other modes - i.e. the number of strips may be reduced as λ increases. For a wide range of λ, four strips for a channel section and six strips for an H-section are sufficient for the analysis of sections under pure compressive stress.

For a residual stress magnitude other than zero, every strip is divided into a number of substrips. The effect of this number on the accuracy is shown in Table 6.2. Two levels of the residual stress (Figure 6.2) are considered - σ_r = 0.3 σ_Y and 0.5 σ_Y. In Chapter 4 it was found that 10 substrips per strip were sufficient and from the current results it is clear that this will again give acceptable accuracy.

6.2.2 Sections Under Pure Bending

In this case three divisions - two symmetrical (Figures 6.1(a) and (c)) and one unsymmetrical (Figure 6.1(b)) - have been considered. The effect of the number of strips - for the H-section and channel - on the accuracy of the critical bending stress of beams under end moments is shown in Table 6.3. It is clear that there is no significant gain in accuracy from increasing the number of the strips on the tension side. Therefore 6 strips for a channel and 9 strips for an H-section will be used.

Table 6.4 confirms that 10 substrips per strip are again sufficient.

b_f/b_w	b_w/t_w	λ/b_w	$\sigma_{cr} \times 10^3/E$ (H-section)		$\sigma_{cr} \times 10^3/E$ (channel)		
			6 strips	12 strips	4 strips	8 strips	12 strips
0.5	50	0.25	6.406	6.345	6.429	6.369	6.351
		0.50	2.095	2.072	2.123	2.100	2.096
		1.00	1.067	1.063	1.128	1.118	1.118
		2.00	1.004	1.001	1.193	1.188	1.188
		4.00	1.753	1.750	2.425	2.416	2.417
0.25	50	0.25	6.676	6.648	6.620	6.606	6.599
		0.50	2.500	2.481	2.411	2.397	2.398
		1.00	1.760	1.751	1.625	1.616	1.616
		2.00	2.291	2.280	2.137	2.118	2.115
		4.00	3.816	3.773	2.467	2.411	2.403

Table 6.1. Effect of the number of strips on the accuracy for sections under axial compression (elastic)

Section	b_f/bw	λ/b_w	No. of strips	No. of sub-strips	$\sigma_{cr} \times 10^3/E$ (elastic)	σ_{cr}/σ_Y	
						$\sigma_r/\sigma_Y = 0.3$	$\sigma_r/\sigma_Y = 0.5$
Channel	0.50	4	4	10	2.425	0.834	0.756
				20		0.830	0.744
				30		0.830	0.744
H-section	0.50	4	6	10	1.753	0.794	0.694
				20		0.791	0.693
				30		0.793	0.692

Table 6.2. The effect of the number of substrips (segments) on the accuracy for sections under axial compression (inelastic)

b_f/b_w	b_w/t_w	λ/b_w	$\sigma_b \times 10^3/E$ (H-section)			$\sigma_b \times 10^3/E$ (channel)		
			6 strips	9 strips	12 strips	4 strips	6 strips	8 strips
0.50	50.0	0.25	6.494	6.378	6.378	6.550	6.401	6.401
		0.50	2.183	2.137	2.137	2.262	2.197	2.197
		1.00	1.211	1.193	1.193	1.356	1.332	1.332
		2.00	1.332	1.323	1.323	1.723	1.709	1.709
		4.00	2.732	2.727	2.723	3.876	3.853	3.848
0.25	50.0	0.25	8.819	8.545	8.545	9.103	8.740	8.740
		0.50	4.657	4.588	4.588	5.099	5.010	5.011
		1.00	4.295	4.276	4.276	5.178	5.510	5.146
		2.00	6.875	6.852	6.843	9.280	9.187	9.163
		4.00	9.503	9.298	9.294	5.169	4.992	4.987

Table 6.3. Effect of the number of strips on the accuracy for sections under pure bending (elastic)

Section	b_f/b_w	λ/b_w	No. of strips	No. of substrips	$\sigma_b \times 10^3/E$ (elastic)	σ_b/σ_Y	
						$\sigma_r/\sigma_Y = 0.3$	$\sigma_r/\sigma_Y = 0.5$
H-section	0.25	4.0	9	10	9.298	0.959	0.943
				20		0.955	0.939
				30		0.955	0.938
Channel	0.25	4.0	6	10	4.992	0.920	0.908
				20		0.920	0.908
				30		0.920	0.908

Table 6.4. The effect of the number of substrips on the accuracy for sections under pure bending (inelastic)

6.3 Buckling of Column Under Compressive Stress

One of the most important advantages of the finite strip method is its simplicity in obtaining the critical stress whatever the buckling mode. In the following analysis two cross-sectional shapes - an H-section and a channel section - have been considered. For both, the depth-to-thickness ratio of the web is constant at 50 and the thickness of the flange is taken as equal to the thickness of the web. Four values for the ratio of flange width divided by web depth - 1/8, 1/4, 3/8 and 1/2 for the channel and 1/4, 1/2, 3/4 and 1.0 for the H-section - have been considered.

Both the elastic buckling of sections free of residual stresses and the inelastic buckling of sections with different residual magnitudes have been investigated.

6.3.1 Elastic Buckling of Columns

The variation of elastic critical stress σ_{cr} with the half wavelength λ for both channels and H-columns is shown in Figure 6.3. For curves corresponding to b_f/b_w = 1/8, and 1/2 an indication of the different modes of buckling at different values of λ are also given. The curves have been obtained for subsequent comparison with the inelastic behaviour of these columns. Each curve can in fact be divided into three ranges depending on the buckling mode - overall buckling, interaction buckling and local buckling.

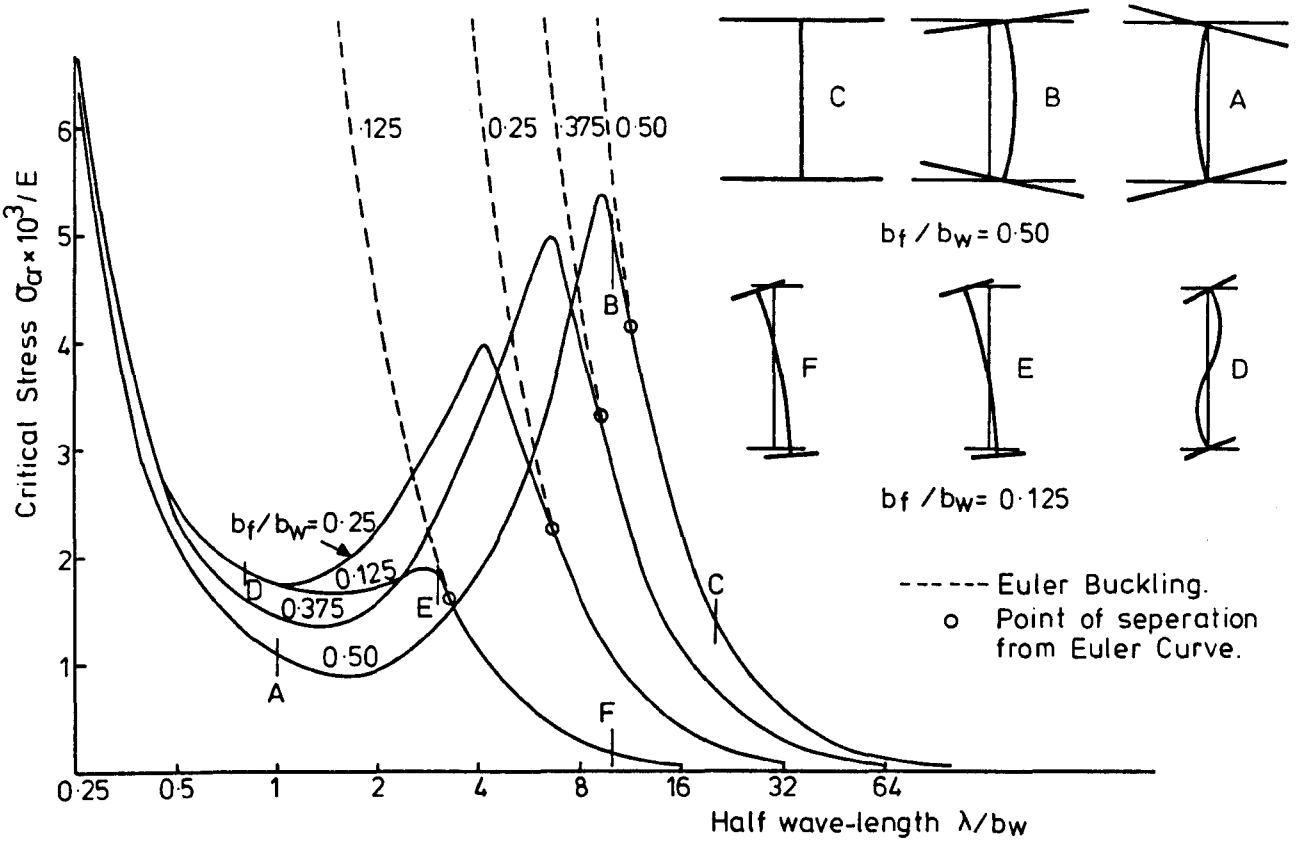

(a) H-Sections.

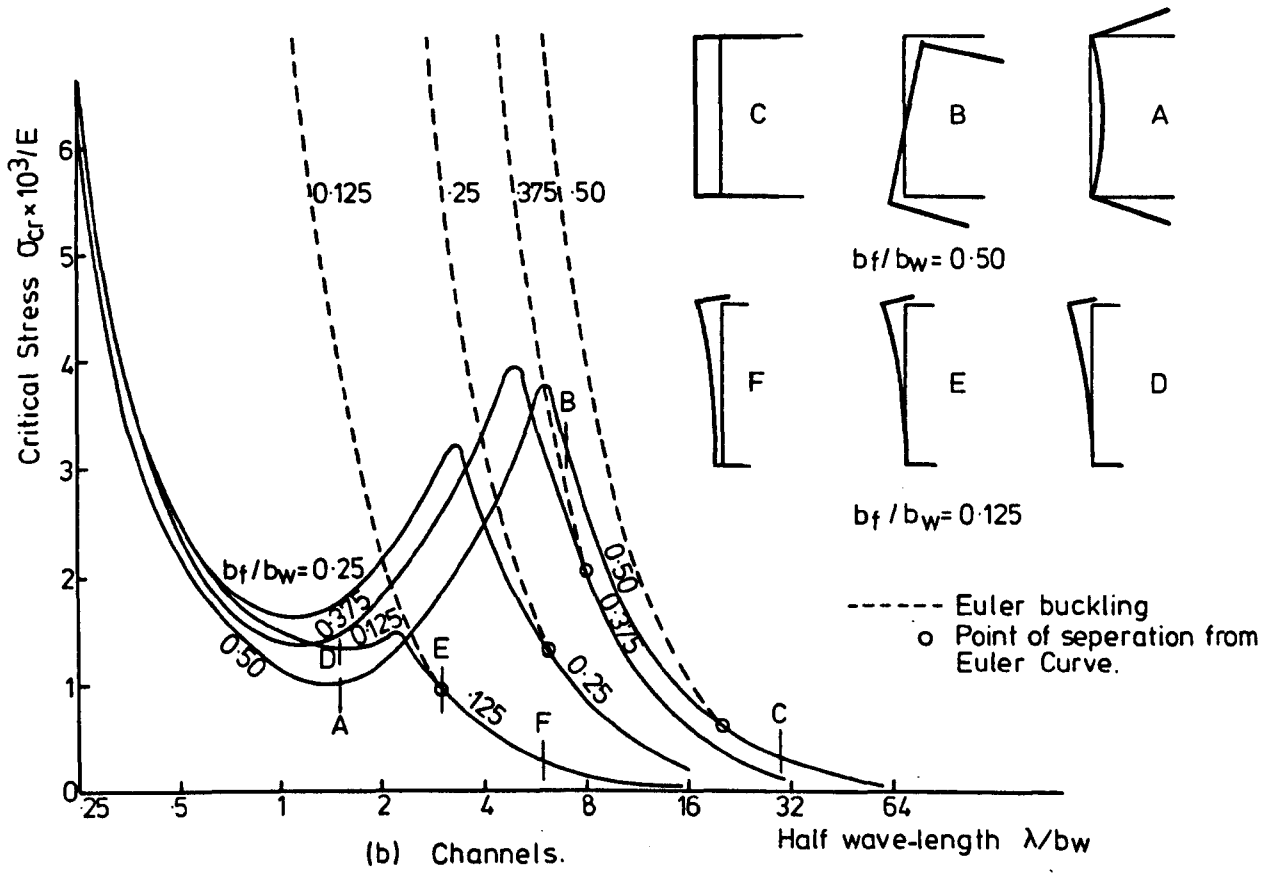

(b) Channels.

FIG. 6·3. ELASTIC BUCKLING STRESS CURVES FOR COLUMN.

At high values of half wavelength, the columns buckle in an overall buckling mode and the buckling curves coincide with the Euler curve. The critical stress σ_{cr} can thus be written,

$$\sigma_{cr} = \frac{\pi^2 E}{(\frac{\ell}{r})^2} \qquad (6.1)$$

where ℓ is the length of the column and in this case is equal to λ,

r is the minimum radius of gyration.

It is clear that there is no direct effect due to the shape i.e. individual plate slenderness, of the cross-section on this buckling strength since it depends only on the flexural rigidity of the cross-section. The columns with $b_f/b_w = 0.5$ buckle in an overall flexural, mode "C", while the columns with $b_f/b_w = 0.125$ buckle in an overall flexural-torsional, mode "F". This may be due to the large torsional rigidities of the long columns with $b_f/b_w = 0.5$. The overall flexural buckling of the channel with $b_f/b_w = 0.5$ (mode "C") changes to an overall torsional mode at $\lambda \leq 20\ b_w$. This may be the reason for the early separation of its buckling curve from Euler buckling curve.

The slenderness ratio of the cross-section of a column (ℓ/r) rather than the slenderness ratio of the components of the cross-section (β) has an effect on the overall buckling strength. Thus, for a column buckling in this mode, it is

more effective to add material in increasing the outer dimensions of the cross-section - depth and breadth - than to increase the thickness of the components. As the outer dimensions increase, the flexural rigidity of the cross-section increases, the slenderness ratio (ℓ/r) reduces leading to an improved overall buckling strength. On the other hand, increasing the thickness of the components, the slenderness ratio (β) - which has no effect on the overall buckling - reduces and no gain (relative to the first case) will result.

By reducing the half wavelength λ, the buckling curves start to deviate from the overall elastic buckling curves (Euler curve). This is due to the fact that the local buckling which occurs in some components of the sections leads to a reduction in the overall buckling strength. The shape and the dimensions of the cross-section have some effect, in this range, on:

1. The value of the half wavelength at which the interaction buckling starts
2. The range of the half wavelength where the interaction buckling mode occurs
3. The magnitude of the reduction in the overall buckling strength due to the interaction effect

If the channel with the largest ratio of flange width-to-web depth is excluded, the relation between λ/b_w and b_f/b_w for the other channels and H-sections can be

represented by a straight line as shown in Figure 6.4. For the channel with $b_f/b_w = 0.5$ the interaction between the local buckling and the overall buckling starts at a relatively high value of the half wavelength. While the range of λ where the interaction buckling occurs is about $2.5\ b_w \sim 3.0\ b_w$ for the H-sections with $b_f/b_w \sim 0.25$ it becomes $0.5\ b_w \sim 0.7\ b_w$ for the sections with $b_f/b_w = 0.125$. This range increases to about $20\ b_w$ for the channel with $b_d/b_w = 0.5$.

The reduction in the overall buckling strength due to this interaction depends on the half wavelength. As the half wavelength reduces, within the range, the reduction increases. Comparing the maximum reductions - at the end of the range - for all sections, it is clear that the minimum value is about 10% and occurs for the H-section with $b_f/b_w = 0.25$. The maximum value is about 35% and occurs for the channel with $b_f/b_w = 0.50$. It is of interest to note that the interaction buckling of the H-section with $b_f/b_w = 0.25$ occurs from the overall buckling and the local buckling of the web while the interaction buckling of the channel with $b_f/b_w = 0.5$ occurs from the overall buckling and the local buckling of the flanges (mode "B").

It is unsafe to design a column which buckles in this range by considering the full flexural rigidity of the cross-section and neglecting the weakening effects of the local buckling.

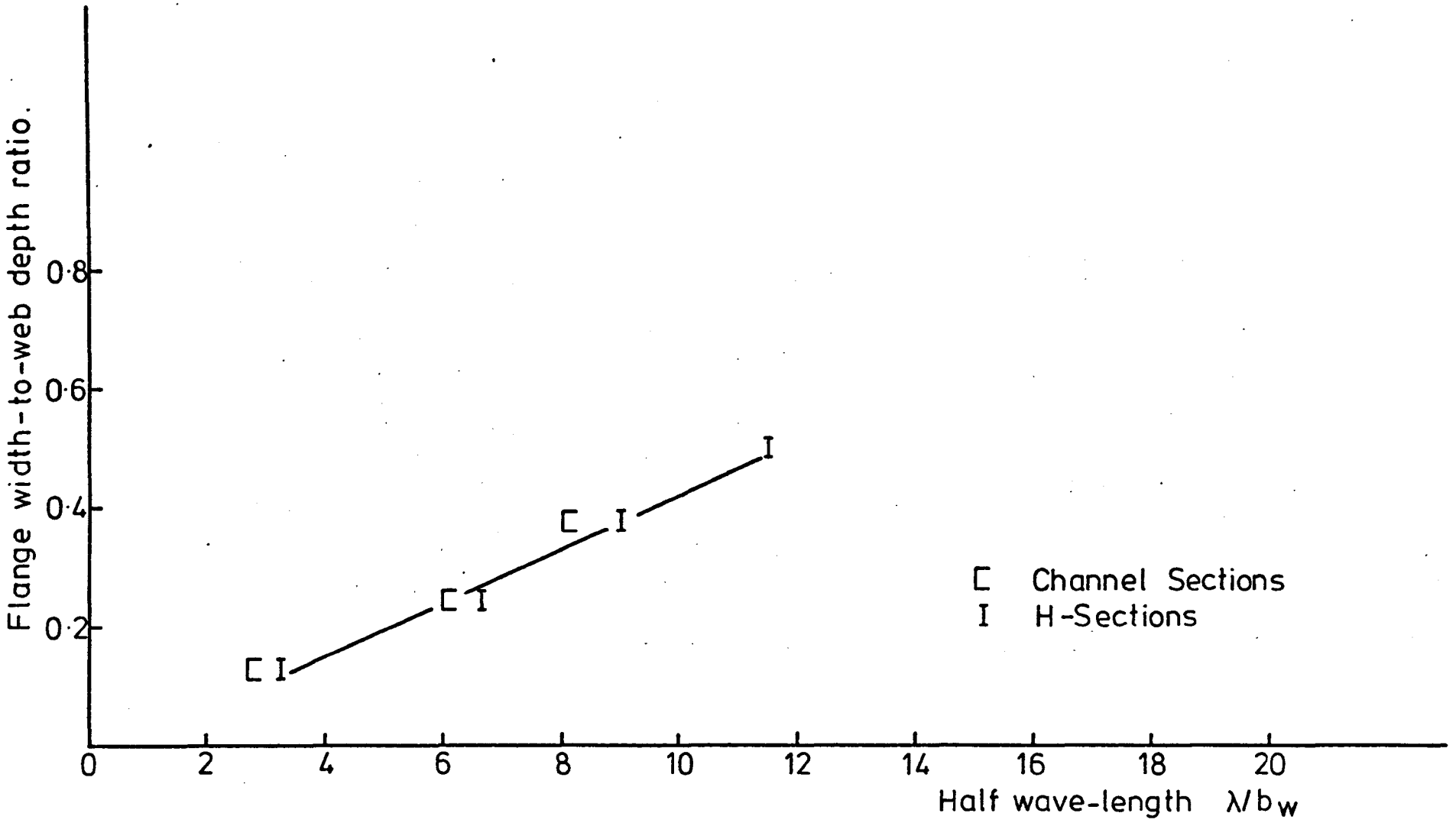

FIG. 6·4. λ/bw OF INTERSECTION OF THE OVERALL BUCKLING WITH THE COMBINED BUCKLING.

In the third range the sections buckle, in a local buckling mode at low half wavelength. The shape of the cross-section and the width-to-thickness ratio of its components have a large effect on the buckling strength. It is clear from Figure 6.3 that the minimum local buckling stress corresponds to a ratio of half wavelength-to-web depth of between 1 and 2.

For sections with small flange width-to-web depth ratios the local buckling of the web (mode "D") is more critical than the local buckling of the flanges (mode "A"). In this range it is more effective to increase the thickness of the cross-sectional components than to increase the breadth and the width of the column, i.e. reducing the slenderness ratio of the components (β) is more effective than reducing the slenderness ratio of the cross-section (ℓ/r).

From this discussion it is clear that the elastic-buckling mode depends on the half wavelength, the shape and the dimensions of the cross-section. While the compact section can offer a high resistance to the local buckling, its resistance to overall buckling is of course, much lower than a more slender section of comparable area.

6.3.2 Effect of Longitudinal Edge Conditions on Inelastic Buckling Strength

The buckling strength curves for the flanges and the web assuming different conditions of restraint at the junctions between them are considered. These idealised conditions

represent approximately upper and lower bounds to the actual behaviour of the complete section.

1. Built-in condition

The rotation and the out-of-plane displacement are restrained. This may model a section with a stiff web where the flange buckles in a local mode. It can also represent the local buckling of the web of H-sections with stiff flanges and a thin web. This condition is the upper limit for the local buckling curves of the section.

2. Free edges condition

It is assumed that the edges can rotate and move freely in any direction. This condition is the lower limit for the buckling curves of the sections. This case may represent the overall buckling mode of a very slender section at very high values of λ/b_w.

3. Simply supported condition

This case falls between the other two limits, free and built-in conditions. The rotation of the edge corresponding to the junction between the web and the flange is permitted, whilst the edge is restrained against out-of-plane displacement. Based on the relative dimensions of the cross-section components the local buckling strength of the section may be accurately modelled by this case. Thus, the approximate local buckling strength for the web and the flange can be obtained from this case. Due to the presence of some restraint to the rotation of the junction between the flanges

and the web in the actual section, this case is normally considered as a lower bound for the local buckling of any component.

These three cases are shown in Figure 6.5 with the buckling stress curves for a channel with $b_f/b_w = 0.5$. The modes of buckling for the complete channel at various half wavelengths are also shown. Three levels of residual stress have been considered with the pattern given in Figure 6.2. It is clear from Figure 6.6 that between $\lambda = 0.5$ and $\lambda = 4$ the buckling stress curve of the channel falls between the buckling stress curves of the flange with one edge simply supported (case 3) and built in (case 4). The other edge of the flange is free. The model where both edges of the web are simply supported (case 5) or built-in (case 6) over-estimates the buckling stress curve of the channel. This means that for this section the local buckling of the web will not occur before the local buckling of the flange or the overall buckling of the structural member, and this is also clear from the modes of buckling.

The main conclusion of this analysis is that the local buckling of the cross-section components - $\lambda/b_w > 4$ - falls between the two bounds. This is because there is always some sort of restraint to the rotation at the junction between the flange and the web - i.e. torsional resistance. For $\lambda/b_w > 4$ the mode of buckling is no longer local and these two bounds are invalid.

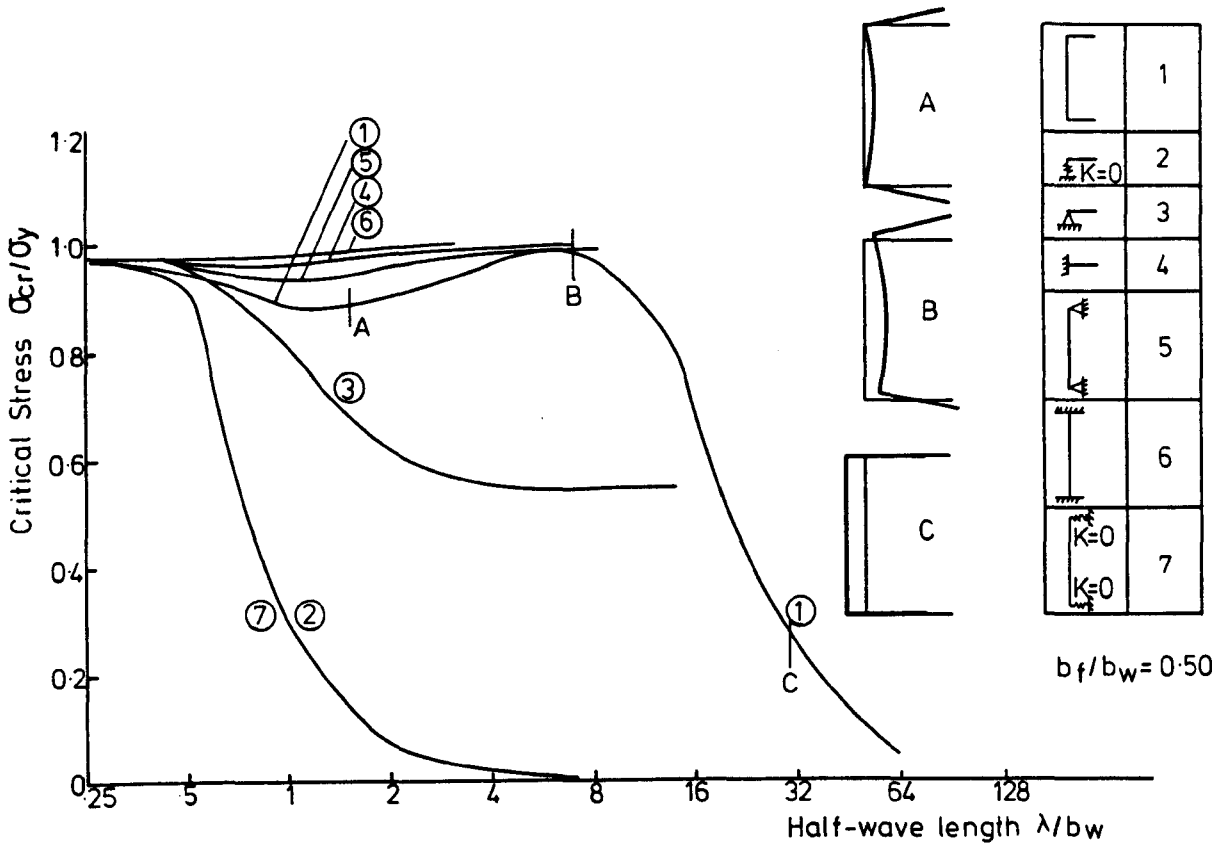

(a) $\sigma r / \sigma y = 0{\cdot}0$

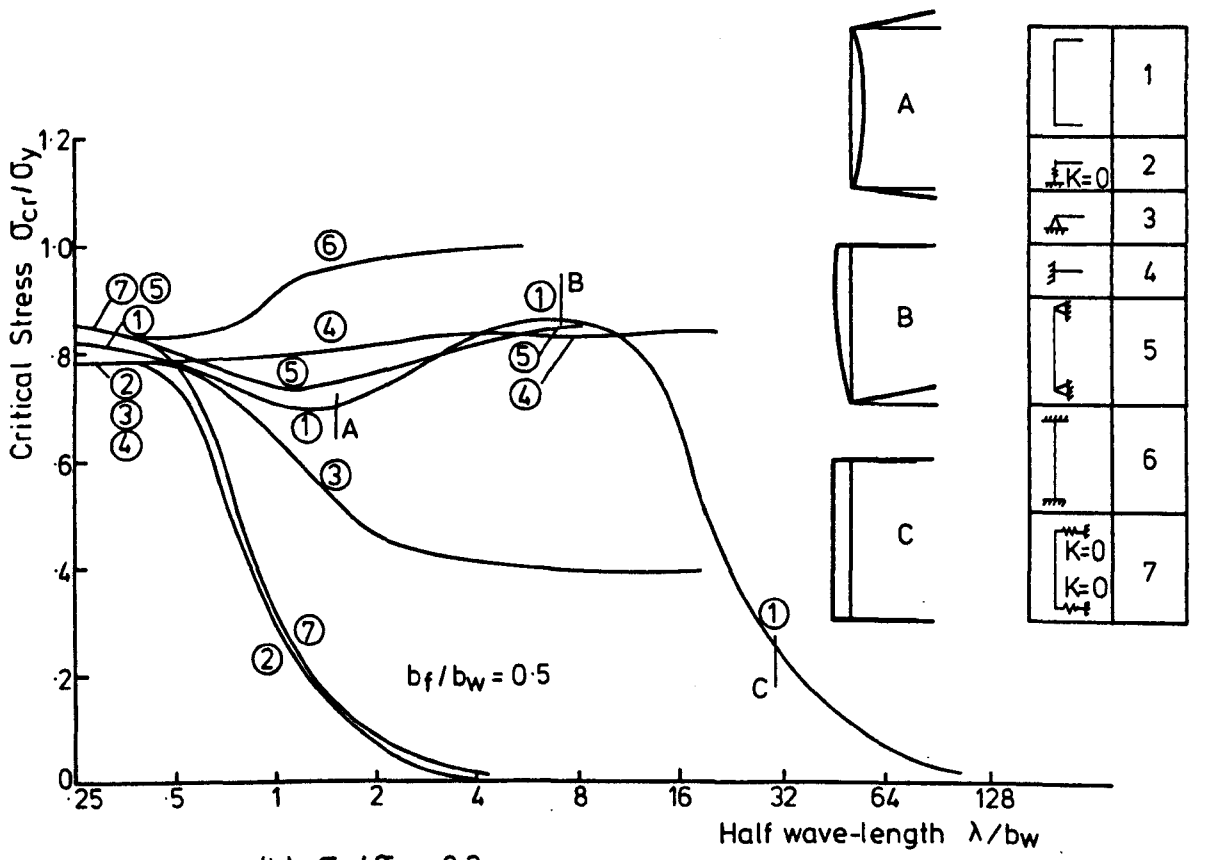

(b) $\sigma r / \sigma y = 0{\cdot}3$

FIG. 6·5. (Cont.....)

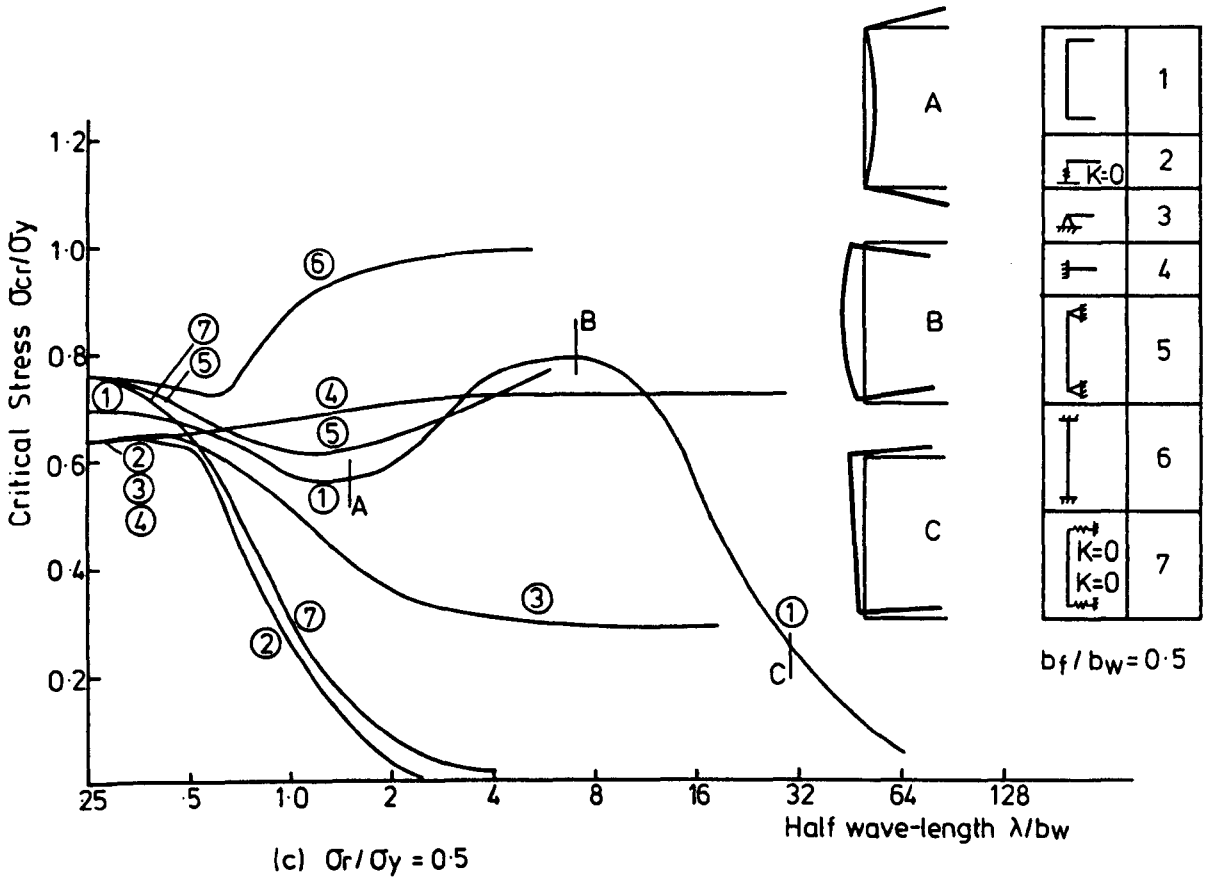

(c) $\sigma r / \sigma y = 0{\cdot}5$

FIG. 6·5. EFFECT OF DISPLACEMENT AND ROTATION RESTRAINED OF THE WEB-FLANGES JUNCTIONS.

6.3.3 Effect of the Cross-Section Dimensions

Two cross-sectional shapes, a channel and an H-section and four values for the flange width-to-web depth ratio have been considered. The yield stress of the material was assumed to be 240 N/mm^2. The buckling strength curves for three magnitudes of the residual stress - σ_r = 0.0, 0.3 σ_Y and 0.5 σ_Y - are shown in Figure 6.6 for channels and Figure 6.7 for H-sections. The elastic buckling curves are shown dotted.

The buckling curves of the columns can be divided into three ranges - large λ/b_w, intermediate λ/b_w and low λ/b_w. The value of λ/b_w which differentiates between these ranges depends on the shape and the dimensions of the cross-section and on the residual stress. At high value of half wavelength the columns buckle in an elastic overall mode. The shape of the cross-section and the residual stresses have no effect on the buckling strength in this range (as long as the column buckles flexurally).

By reducing the half wavelength, the buckling curve starts to deviate from the elastic overall buckling curve and this may be due to one of the following

- Inelastic overall buckling
- Elastic interaction buckling
- Inelastic interaction buckling

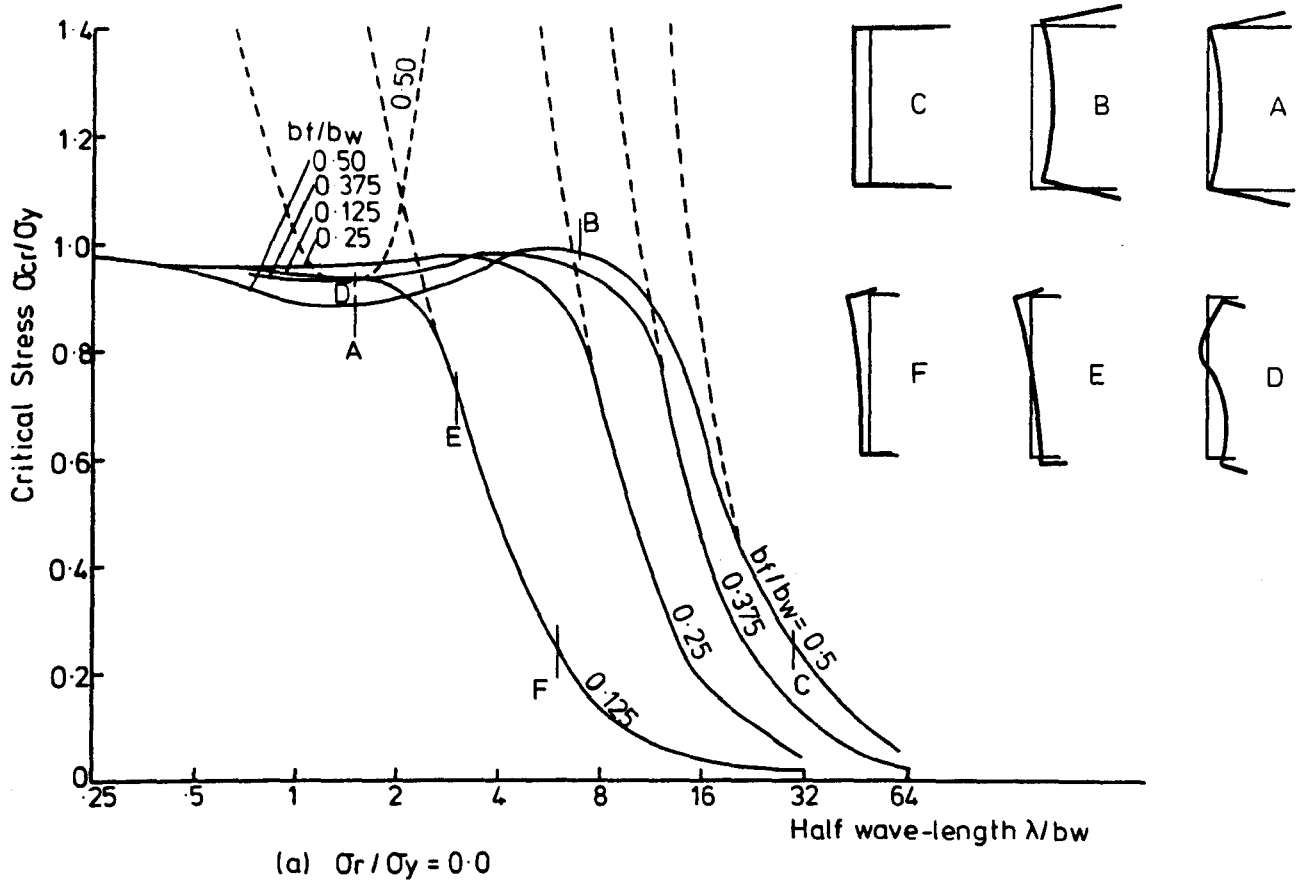

(a) $\sigma r / \sigma y = 0 \cdot 0$

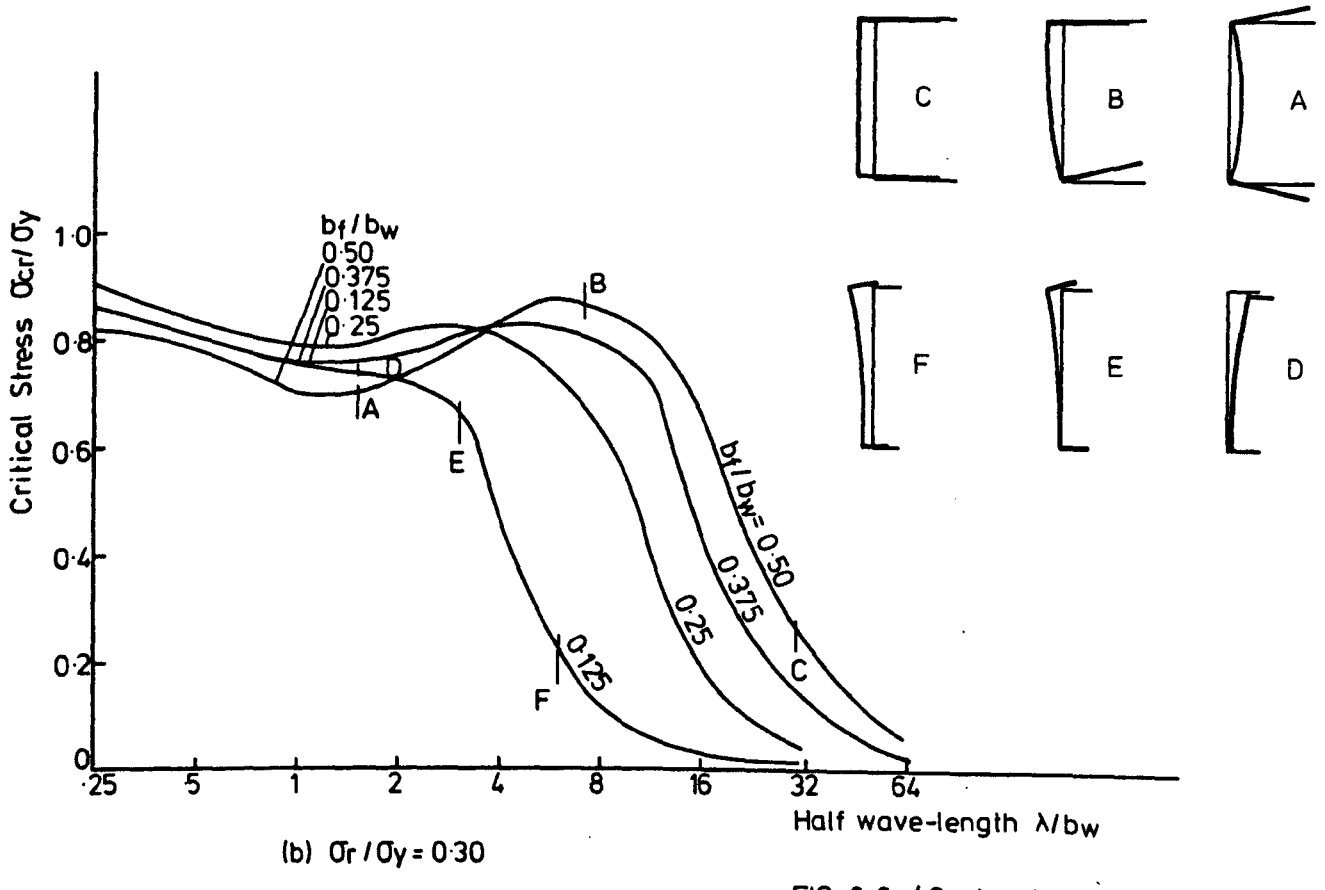

(b) $\sigma r / \sigma y = 0 \cdot 30$

FIG. 6·6. (Cont.....)

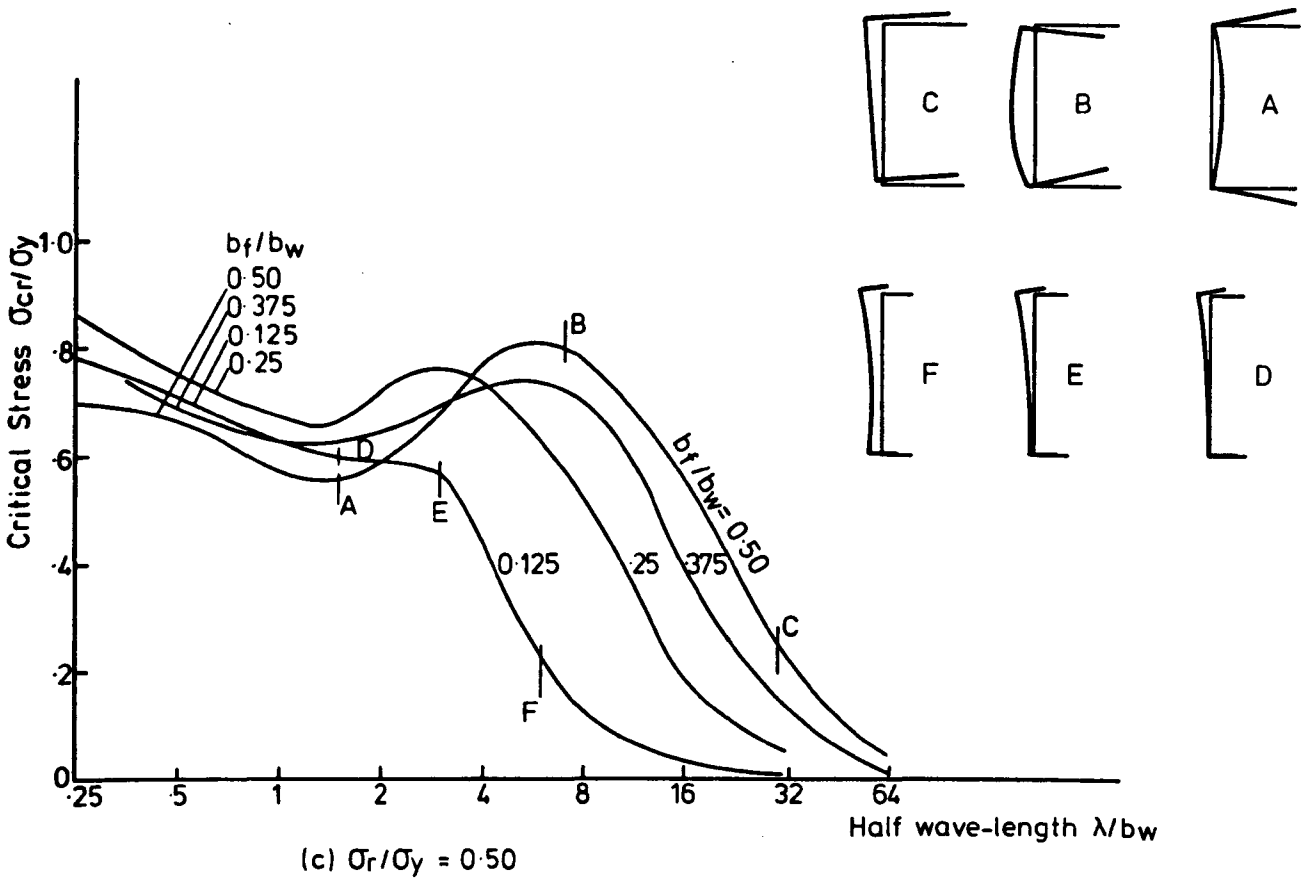

(c) $\sigma_r/\sigma_y = 0.50$

FIG. 6·6. INELASTIC BUCKLING STRESS CURVES FOR CHANNEL COLUMN.

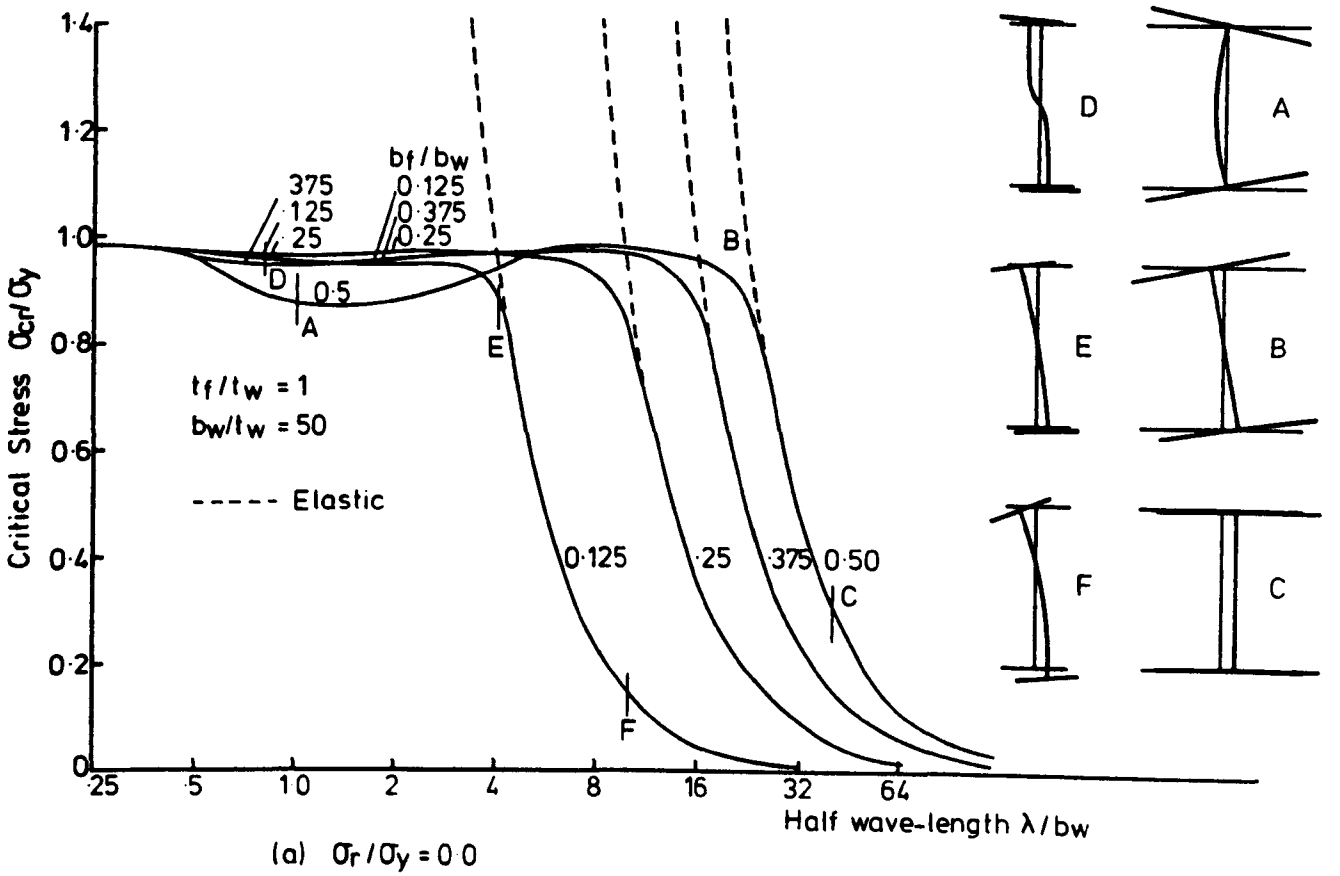

(a) $\sigma_r/\sigma_y = 0.0$

FIG. 6·7. (Cont....)

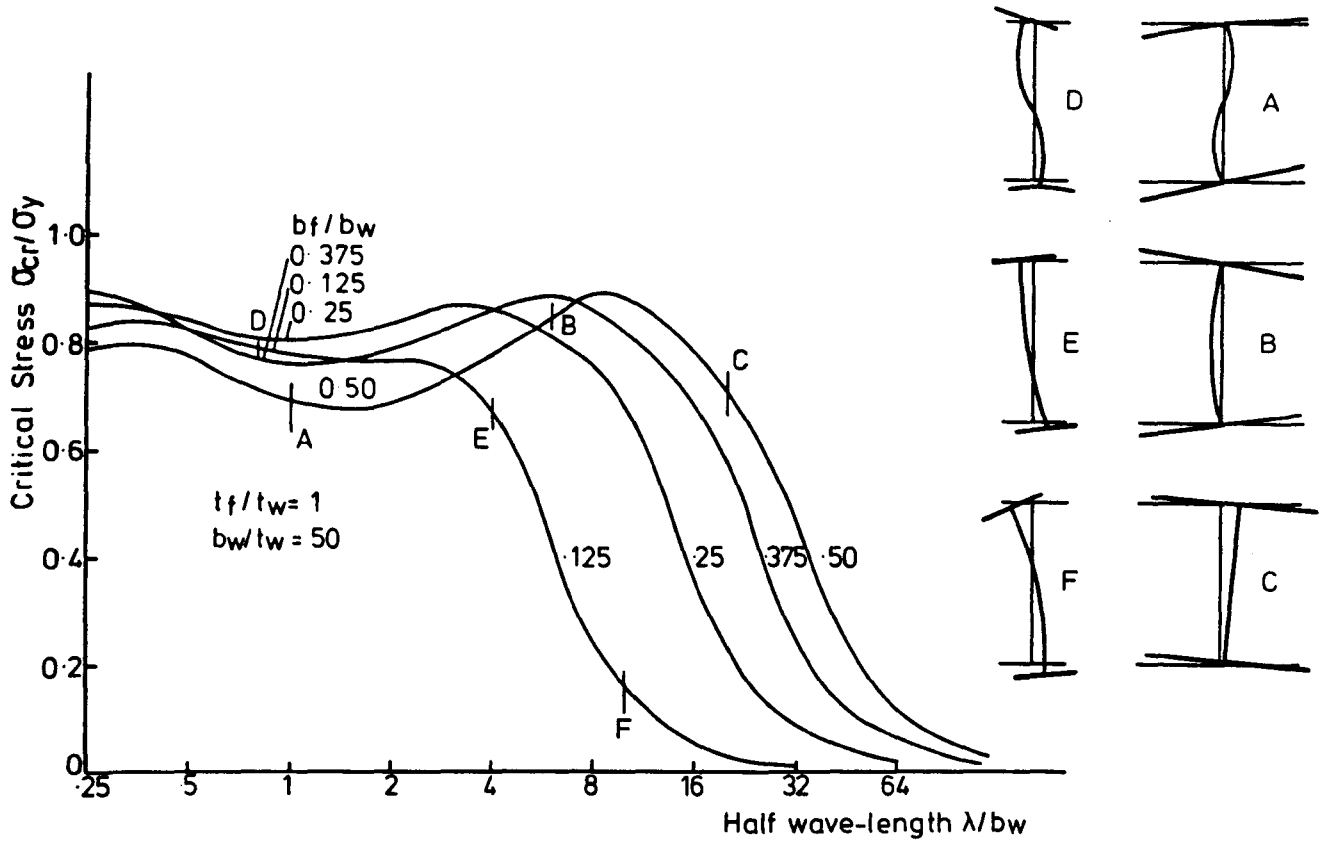

(b) $\sigma_r / \sigma_y = 0.3$

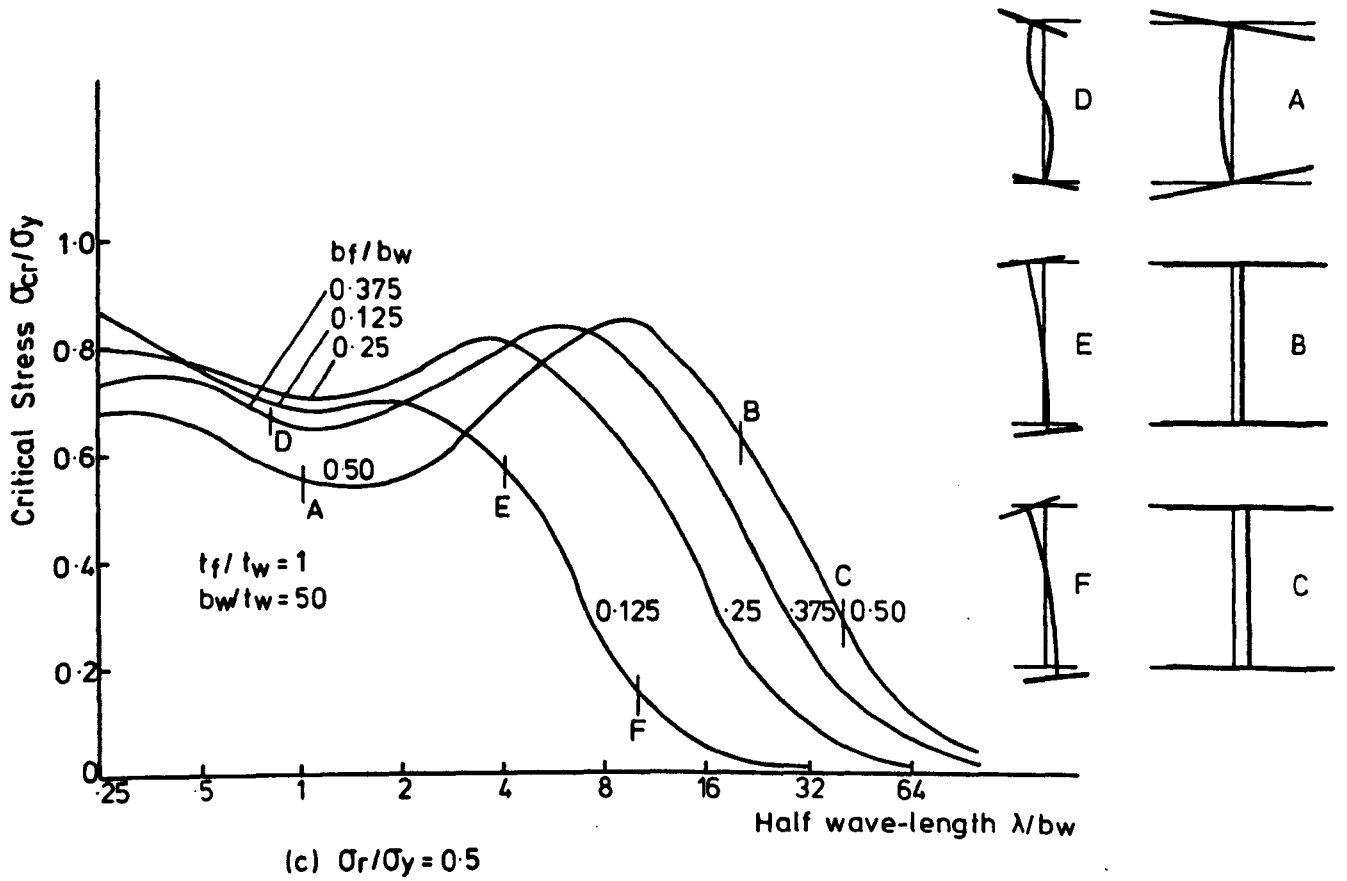

(c) $\sigma_r / \sigma_y = 0.5$

FIG. 6·7. INELASTIC BUCKLING STRESS CURVES FOR H-COLUMN IN COMPRESSION.

In this range at least one of these phenomena may be observed. The factors which affect behaviour are the half wavelength, the residual stress and the shape and the dimensions of the cross-section. At the beginning of the range - large λ/b_w - the possibility for inelastic overall buckling is high while at the end of the range the tendency for inelastic interaction buckling increases. In certain cases this range may disappear from the buckling curve and be replaced by a transition curve between the overall buckling and the ultimate strength (the squash load).

In the range of low λ/b_w ratios the section may reach its ultimate strength and/or buckle in a local mode either elastically or inelastically. This depends on the width-to-thickness ratio of the components of the member, the residual stress, the yield stress of the material and the half wavelength.

Considering the buckling curves shown in Figure 6.6(a) for the initially stress free channels with $b_f/b_w < 0.5$, it is clear that the sections buckle in an elastic overall mode at large ratios of λ/b_w (modes "C" and "F"). As λ/b_w reduces the buckling curves deviate from the elastic overall buckling curves. The deviation starts at $\sigma_{cr}/\sigma_y = 0.8$ thereby demonstrating that the deviation is due to an inelastic effect rather than an interaction effect. At an applied stress $> 0.8\ \sigma_y$ the stress strain relationship of the material is no longer linear. The ratios of b_f/b_w

have no effect on this deviation. For the channel with b_f/b_w = 0.5 the deviation starts in the elastic range at a half wavelength equal to the one obtained from the elastic buckling analysis. The deviation in this case is due to interaction buckling (mode "B"). The range where this interaction buckling occurs is clearer for this section than for the other sections.

The local buckling of the components of the cross-section occurs at a lower ratio of λ/b_w. This may be local buckling of the flanges (mode "A") or local buckling of the web (mode "D"). The width-to-thickness ratio of the component is the main factor controlling this buckling. For the present case the flanges of the channels with b_f = 0.375 b_w and b_f = 0.5 b_w have buckled before the web (mode "A") while for the other two channels the web has buckled (mode "D"). As b_f/b_w increases the minimum local buckling strength of the flange decreases while the local buckling strength of the web increases.

It is clear that the local buckling has a large effect on the strength of the structural members especially those with high residual stress levels. The ECCS (118) recommended prevention of the local buckling of the component elements and developed buckling curves based on this assumption.

Compare Figure 6.6(a) with σ_r = 0.0 and Figures 6.6(b) and (c) with σ_r = 0.3 σ_y and 0.5 σ_y respectively, it is clear that the three ranges become more clear as the

residual stress increases. In the overall buckling range the residual stress has no effect on the flexural buckling strength, but it reduces the local buckling strength and the interaction buckling strength. Due to this reduction the deviation of the buckling curve from the elastic overall buckling curve starts at a relatively high value of λ/b_w. As the residual stress increases the value of λ/b_w - where the deviation starts - increases. Moreover, the presence of the residual stress may change the local buckling of the section from web local buckling to flange local buckling. The local buckling of the flanges of the channel with b_f/b_w = 0.25 and $\sigma_r = 0.5\ \sigma_Y$ is more critical than the local buckling of the web while the web of the same channel with σ_r = 0.0 buckles before the flanges.

It is of interest to note that all the buckling curves diverge from the elastic buckling curves (Euler curve) at points where

$$\sigma_{cr}/\sigma_Y = 0.8 - \sigma_r/\sigma_Y \qquad (6.2)$$

From Figure 6.6 and Figure 6.7 it is clear that the ranges of the overall buckling are similar and there is no effect for the shape of the cross-section on the overall buckling strength. The local buckling of the flanges and the web of an H-section are different from the local buckling of the flanges and the web of a channel with the same b_f/b_w (modes "A" and "D", Figures 6.6(b) and 6.7(b)). This may be

due to the effect of the boundary conditions at the junctions between the flanges and the web. The flanges act as stiffeners to the web and it was shown in Chapter 5 that the local buckling of a plate (web) increases as the depth of stiffener increases up to a certain limit where it starts to decrease. So, by controlling the dimensions of the flanges, the maximum local buckling of the web can be obtained. The effect of the flanges (stiffeners) on the local buckling of the web depends on:

- The flanges are symmetrical (H-sections) or unsymmetrical (channels)
- The width-to-thickness ratio of the flanges
- The residual stress

Because the interaction buckling depends on the local buckling, it is clear that the range of the interaction buckling and the reduction in the strength due to it are affected by the shape of the cross-section (H-section or channel).

The main point arising from these 24 curves - Figures 6.6 and 6.7 - is that the inelastic buckling curve can also be divided into three ranges only one of which is similar to the corresponding elastic curve. The other two may or may not be similar to the corresponding elastic curve and this depends on many factors (discussed above).

6.3.4 Effect of the Residual Stress

H-sections and channels are fabricated by rolling or welding. Due to this rolling or welding some parts of the

cross-section are subjected to higher rates of cooling than the other parts. This leads to variation in the temperature and the parts which cool first contain residual compressive stress while the parts which cool later contain residual tension. The residual stresses also depend on the shape of the cross-section and the straightening procedures, the heavier the section the larger the magnitude of the residual stress.

To study the effect of the residual stress on the buckling strength, it is decided to reproduce some results from Figure 6.6 and Figure 6.7. Because the structural member may have one or more than one half wavelength λ along its length ℓ, the minimum critical stress is plotted against the length of the member. The ℓ/b_w ratio is used instead of λ/b_w ratio. Moreover, it is decided to plot the buckling curves of each section under three levels of residual stress σ_r = 0.0, 0.3 σ_Y and 0.5 σ_Y on one graph to investigate the effect of σ_r. Only four sections - two channels and two H-sections - have been considered. The results of the sections with flange width-to-web depth ratio b_f/b_w = 0.25 and 0.50 are shown in Figure 6.8 and Figure 6.9.

It is clear from Figure 6.8 and Figure 6.9 that while the residual stress has a large effect on the local buckling strength the effect becomes negligible on the overall buckling strength. The overall mode (flexural, torsional and flexural-torsional) however, may be affected by the residual stress magnitude. A column buckling laterally (mode "C" Figure 6.6(c)) may change to buckle

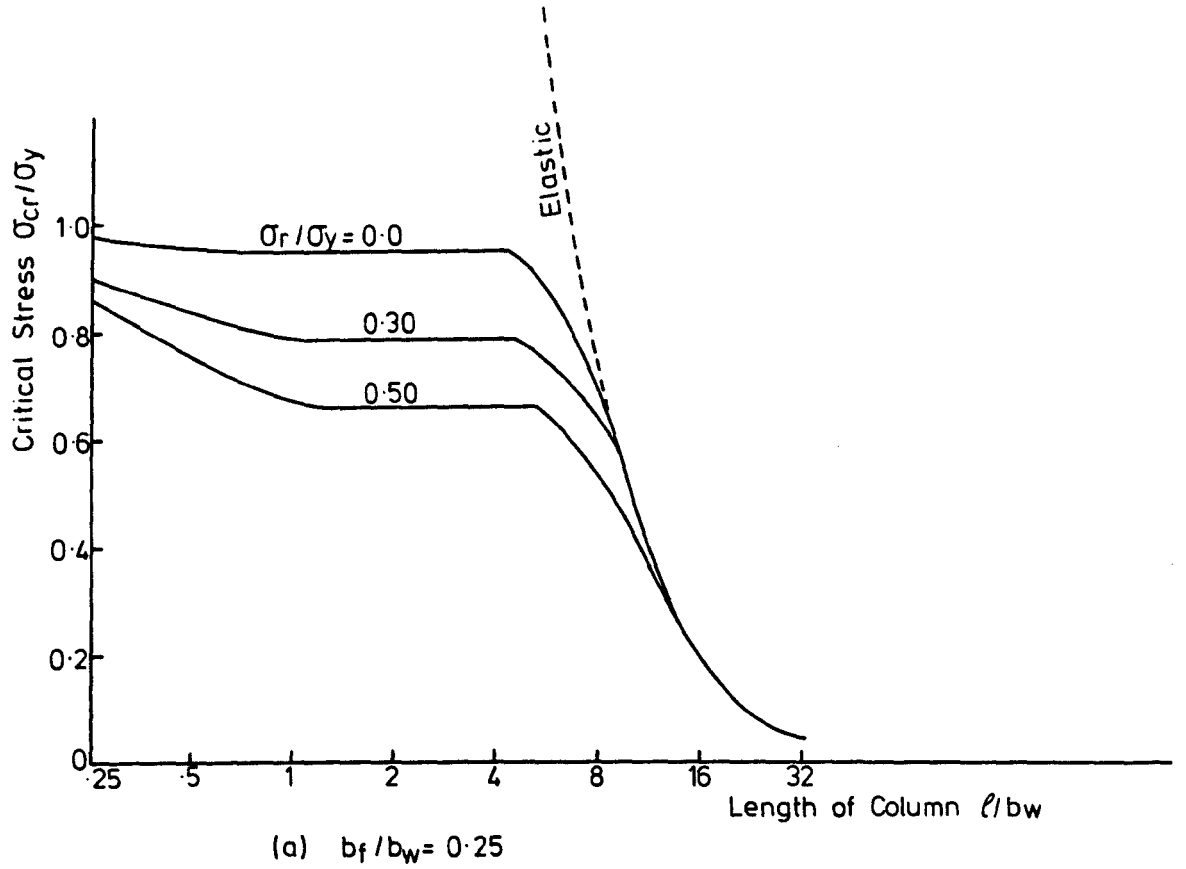

(a) $b_f/b_w = 0.25$

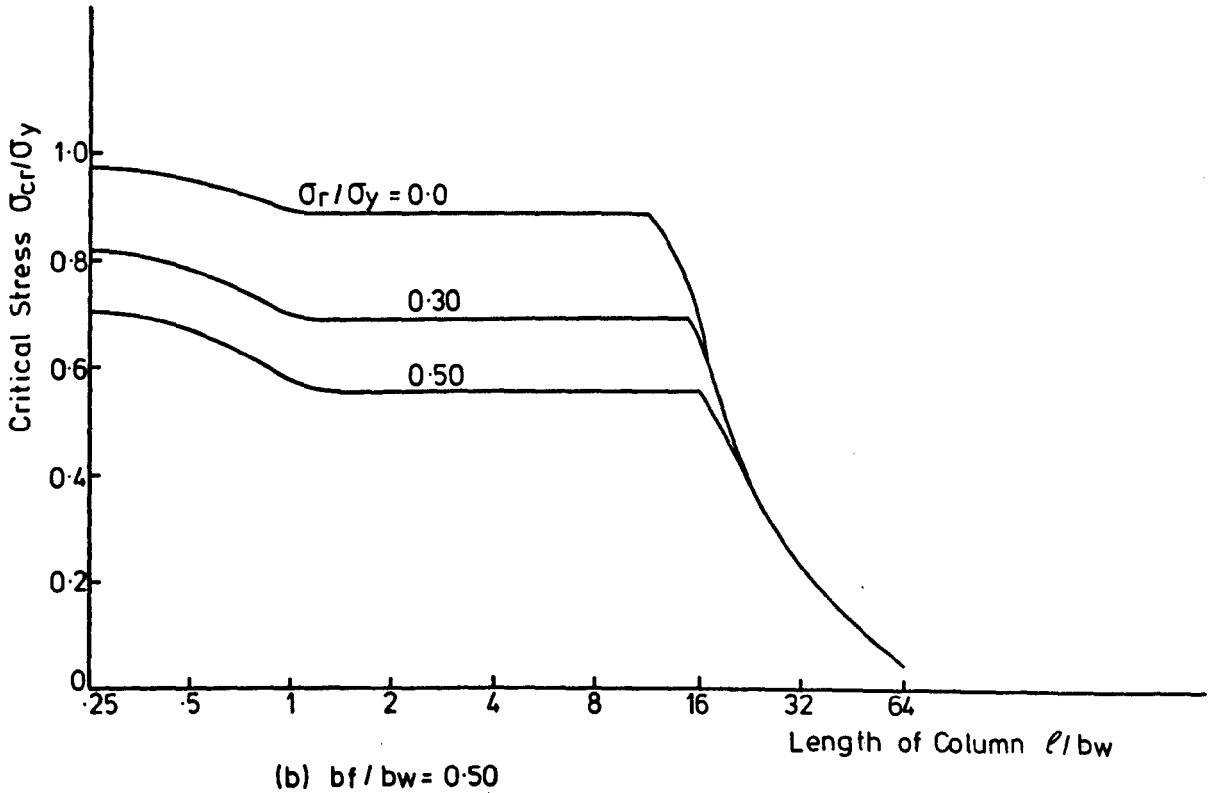

(b) $b_f/b_w = 0.50$

FIG. 6.8. THE INFLUENCE OF RESIDUAL STRESS ON THE CRITICAL STRESS OF CHANNEL COLUMN IN COMP.

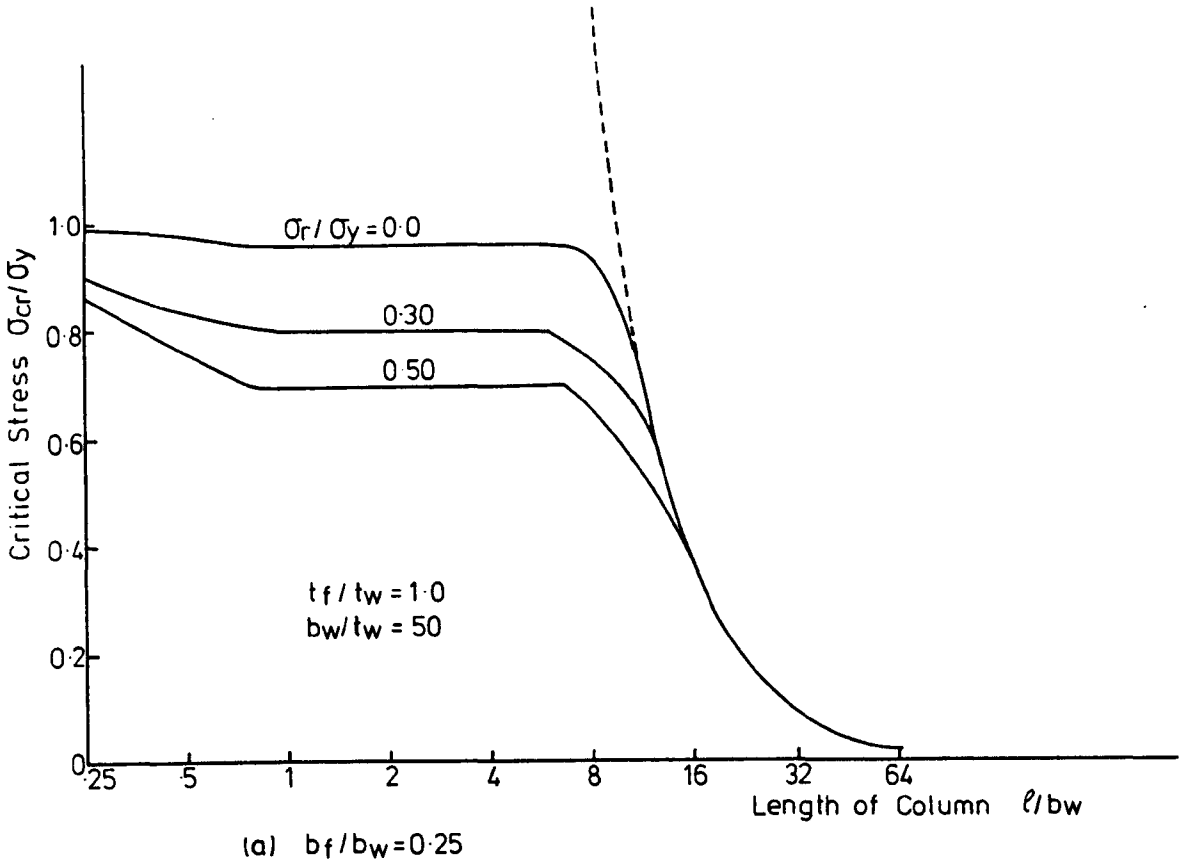

(a) $b_f/b_w = 0·25$

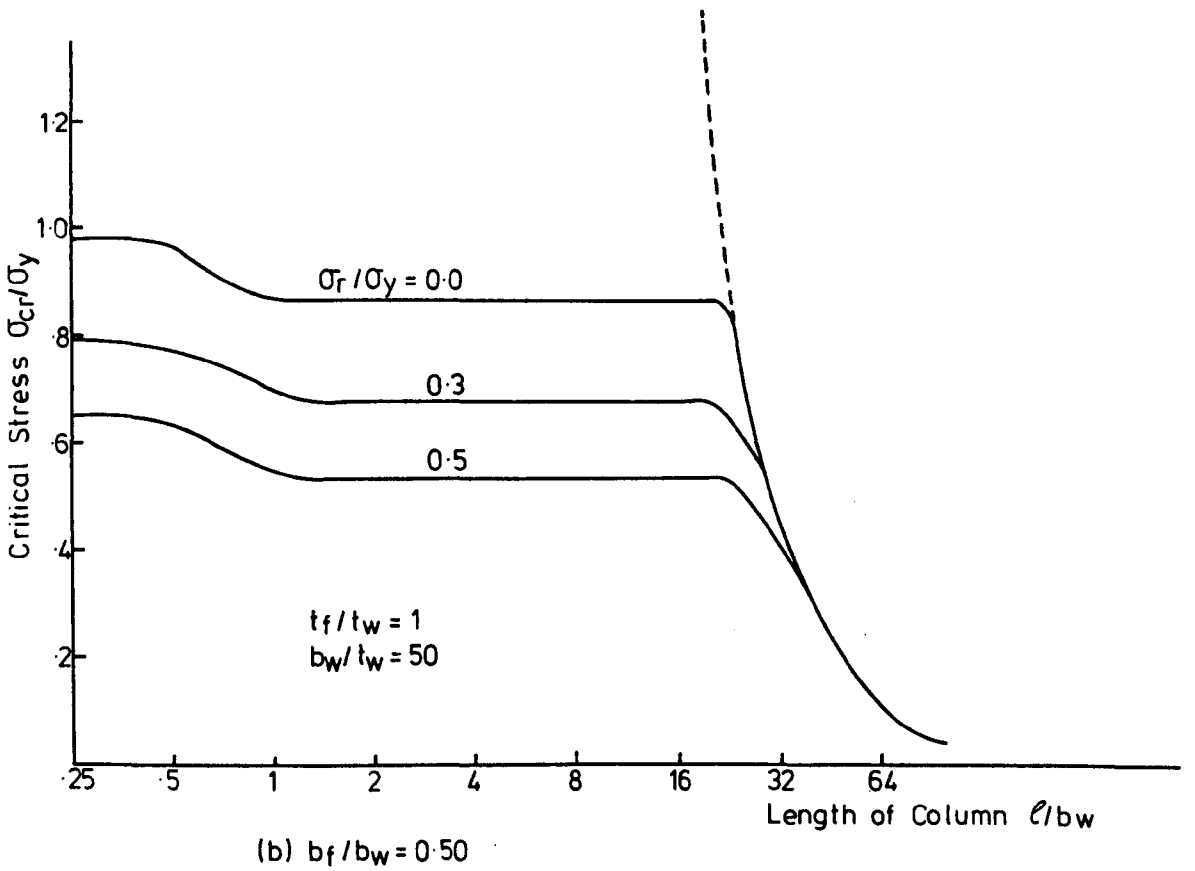

(b) $b_f/b_w = 0·50$

FIG. 6·9. THE INFLUENCE OF RESIDUAL STRESS ON THE CRITICAL STRESS OF H COLUMN IN COMP.

in lateral-torsional buckling (moxd "C" Figure 6.6(c)) as the residual stress increases. This may be due to the increase in the internal twisting moment as the residual stress increases. The internal twist moment is given by $\int \sigma_r (x^2 + y^2)\, dA$ (69) and it is clear that this value increases as the residual stress σ_r increases.

In the local buckling range, the effect of the residual stress depends on the shape and dimensions of the cross-section. For a channel with $b_f/b_w = 0.25$, increasing the residual stress from 0.0 to 0.3 and 0.5 leads to a reduction in the critical stress 17% and 30% respectively - in the range $\lambda = b_w \sim 4b_w$. When b_f/b_w is increased to 0.5 the reduction becomes 21% and 37% respectively - while the range becomes $\lambda = b_w \sim 12b_w$.

The effect of the residual stress on the local buckling of a component depends on the longitudinal boundary conditions of this component. A component with a free edge is more sensitive to the residual stress than that with elastically supported or simply supported edges. So, the flanges are more sensitive to the residual stress and by increasing σ_r the local buckling mode may change from web local buckling to flange local buckling.

For the H-sections the reductions in the buckling strength due to the residual stress are approximately the same as that of the channels but the range of λ increases slightly. It is clear that as the residual stresses increase the tendency for the local buckling increases.

6.3.5 Effect of the Cross-Sectional Shape

Three different cross-sections - an H-section, a channel and a box section - each with the same area have been considered. The thicknesses of all cross-section components are the same and equal to 0.25% of the cross-sectional area. The square box-column is divided into eight strips as was shown in Chapter 4. The patterns of the residual stresses in every section are shown in Figure 6.10 and their magnitudes are equal to 0.3 σ_y. The buckling strength curves are shown in Figure 6.10.

One of the important factors which is influenced by the cross-sectional shape is the magnitude and distribution of the residual stresses. For the box-section the pattern of the residual stresses is affected by the width-to-thickness ratio of the components. Because this pattern has an effect on the buckling strength, especially in the local buckling range, a useful comparison between the behaviour of different columns is difficult. But generally it is clear that three ranges for the buckling curves can be distinguished.

In the first range - where the section buckles in a local mode - the strength of the channel is less than the strength of the H-section. This is expected because the buckling occurs in the flanges of these sections. The strength of the box-column is higher than any other type although its residual stress pattern is more severe. This

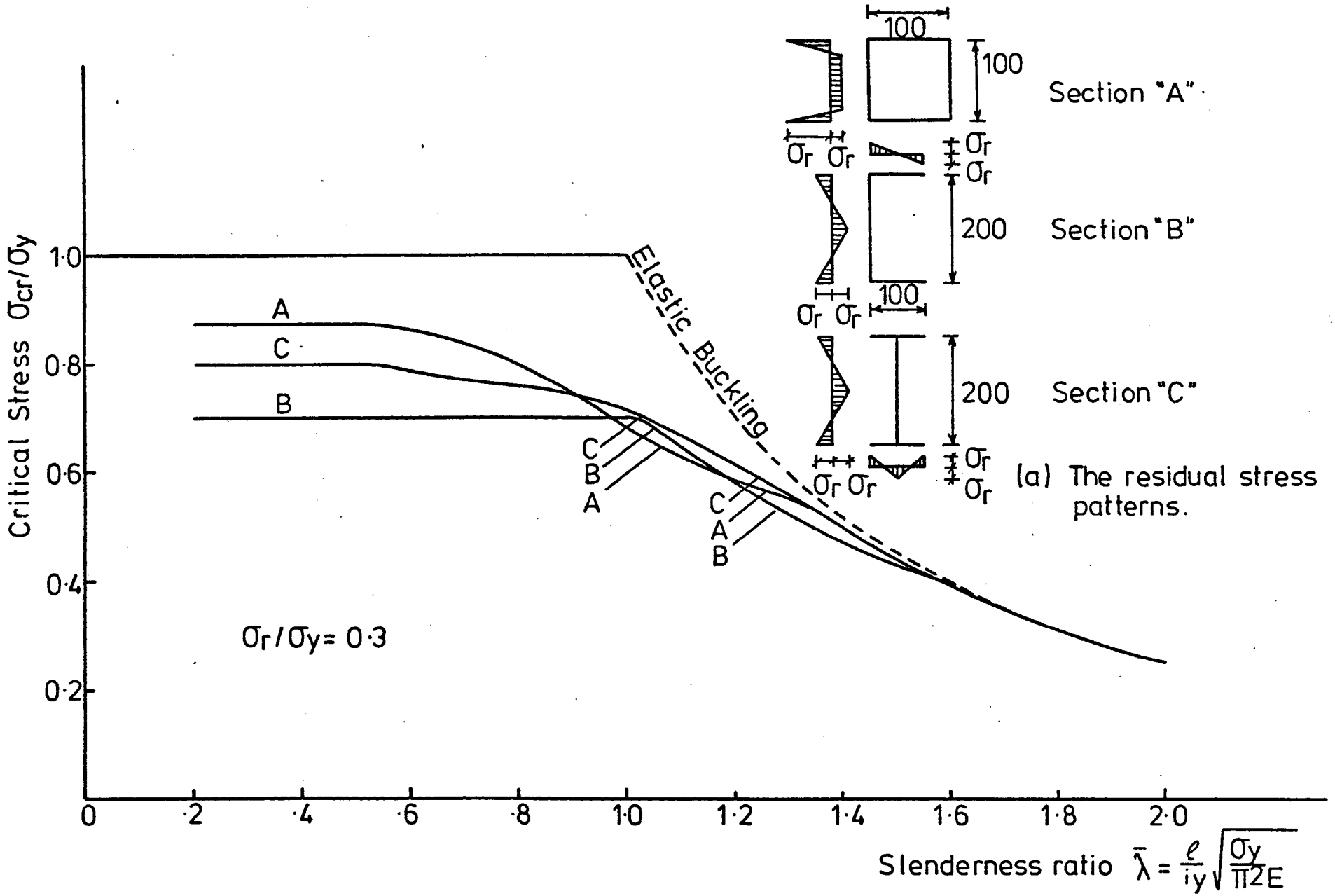

FIG. 6·10. EFFECT OF THE CROSS SECTIONAL SHAPE ON THE BUCKLING STRENGTH.

increase in the buckling strength may be due to the effect of the longitudinal boundary conditions. The boundary conditions of an open section's components differ from the boundary conditions of a closed section's components and there is a significant effect, particularly when the first section loses its stability due to the local buckling of the flange. Moreover, the shapes of the closed section (square-box or rectangular-box) have an effect on the local buckling of the components. It is clear from Figure 6.10 that while the local buckling of the box and H-sections occurs in a range of slenderness ratio $\bar{\lambda} \leq 0.5$, the local buckling of the channel section occurs at $\bar{\lambda} \leq 1.0$.

The second range corresponds to the interaction buckling mode. Because this mode depends on the local buckling it is clear that it starts at a lower $\bar{\lambda}$ for the box and H-sections than for the channel section. For slenderness ratio $1.6 > \bar{\lambda} > 0.9$ the three buckling curves become closer. At the beginning of this range ($1.2 > \bar{\lambda} > 1.0$) the buckling strengths of the channel and the H-section are higher than the buckling strength of the box-section. This may be due to the effect of the residual stress patterns. For higher slenderness ratios - $1.3 > \bar{\lambda} > 1.6$ - the effect of the residual stress becomes less and the buckling strength curve for the box-section coincides with the buckling strength curve for the H-section.

The cross-sectional shapes have no effect on the buckling strength of a column with a slenderness ratio higher than 1.6. The buckling curves for the three sections - channel, box and H-sections - coincide with the Euler buckling curve.

Based on the shape of the cross-section, the axis of buckling and the manufacturing procedures, the ECCS select four buckling curves to represent the column strength.

From this analysis it is clear that the shape of the cross-section has some effect on the buckling strength. This effect depends on the half wavelength (mode of buckling), the residual stresses and the boundary conditions along the longitudinal edges of the components. Generally, the sections can be divided into open sections and closed sections, which is better, depends on many other factors besides the shape of the cross-section. Thus, no general conclusion for the best choice of cross-sectional shape can be obtained from the present analysis.

6.3.6 Effect of the Material Yield Stress

Two cases have been considered, the first is an initially stress-free section and the second is a section containing residual stress. An H-section with $b_f/b_w = 0.25$ is assumed to be loaded by axial compressive stress. Three values for the yield stress of the material - $\sigma_Y = \sigma_Y^o$, $1.5\ \sigma_Y^o$, and $2\ \sigma_Y^o$ where $\sigma_Y^o = 240\ N/mm^2$ - are used. The results in terms of σ_{cr}/σ_Y against the slenderness ratio are shown in Figure 6.11.

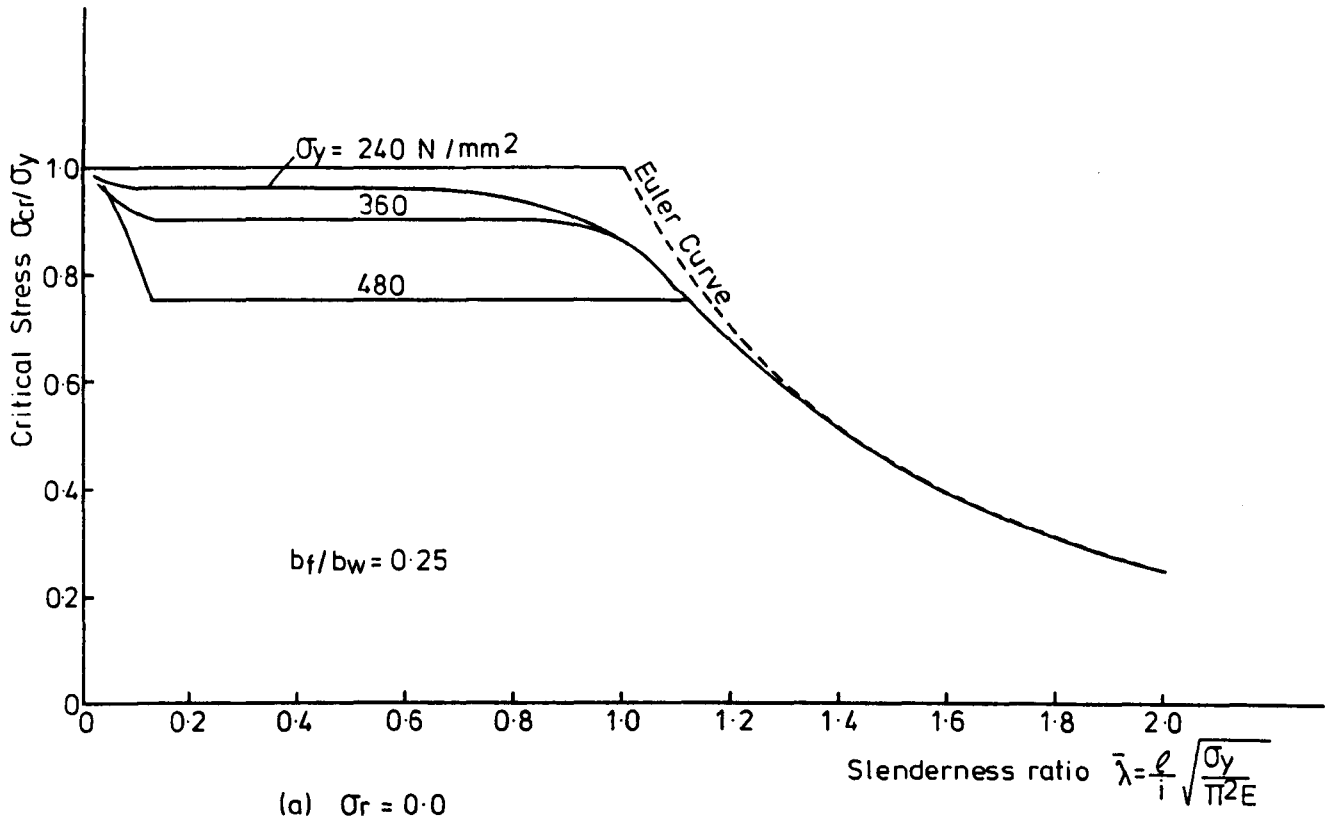

(a) $\sigma_r = 0{\cdot}0$

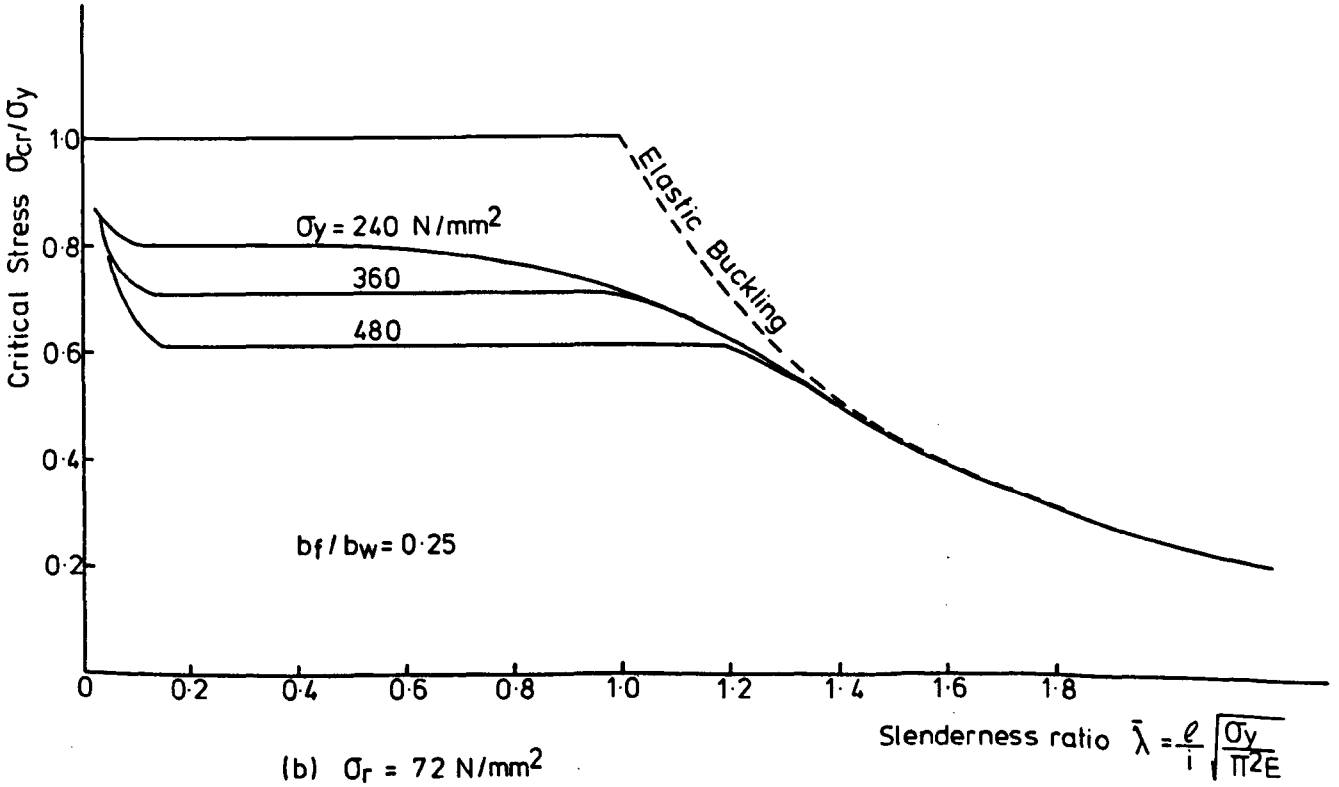

(b) $\sigma_r = 72\ N/mm^2$

FIG. 6·11. THE INFLUENCE OF THE YIELD STRESS σ_y ON THE CRITICAL STRESS OF H-SECTION.

It is known that the slenderness ratio is a nondimensional factor depending on the mode of buckling. For a member which buckles in an overall mode

$$\bar{\lambda} = \frac{\ell}{r}\sqrt{\frac{\sigma_Y}{\pi^2 E}} \tag{6.3}$$

while for the local buckling of the member's components:

$$\beta = \frac{b}{t}\sqrt{\frac{12\ \sigma_Y\ (1 - \nu^2)}{\pi^2\ E\ K}} \tag{6.4}$$

where b is the width of the buckled component

t is the thickness of the buckled component

K is a constant (buckling coefficient) depends on the boundary conditions.

In the elastic range there is a relation between the slenderness ratio $\bar{\lambda}$ and the critical stress σ_{cr}/σ_Y

$$\sigma_{cr}/\sigma_Y = \frac{1}{(\text{slenderness ratio})^2} \tag{6.5}$$

This parabolic equation is valid as long as

- The section does not yield
- The mode of buckling does not change.

In the present analysis different modes - overall, interaction and local buckling mode - have been developed along the buckling curve. For the initially stress-free section the buckling strength curve shown in Figure 6.11(a) can be divided into two ranges. The first is the overall buckling range where the member slenderness ratio $\bar{\lambda} \geq 1.4$,

equation (6.5) is valid. For $\bar{\lambda} < 1.4$ the mode of buckling changes to an interactive mode then a local mode and there is no relation between the member slenderness ratio $\bar{\lambda}$ and the critical stress. Changing the yield stresses leads to different buckling curves (in this range) as shown in Figure 6.11(a). It is worth noting that in the range of the local buckling mode using equation (6.4) with reasonable K instead of equation (6.3) will give a local buckling curve independent of the yield stress.

It is normally assumed that the residual stresses in the welded section depend on the yield stress while in the rolled sections the absolute values of the residual stress are not affected by the yield stress (118). For such sections the relative importance of this residual stress decreases with increasing yield stress. To study this effect the three values of the yield stress and a residual stress $\sigma_r = 0.3\ \sigma_Y^o$ are assumed, i.e. $\sigma_r = 0.3\ \sigma_Y$, $0.2\ \sigma_Y$ and $0.15\ \sigma_Y$ in the H-sections with $\sigma_Y = \sigma_Y^o$, $1.5\ \sigma_Y^o$ and $2\ \sigma_Y^o$ respectively. The buckling curves are shown in Figure 6.11(b). It is clear that at high slenderness ratios where the sections buckle in an overall mode there is no effect for the residual stress on the buckling strength. The maximum effect occurs in the range of slenderness ratios where the section buckles in a local mode. The local buckling of the cross-sectional components depends not only on the width-to-thickness ratio of this component but also on the yield stress of the material and the residual stress.

Some gain in the local buckling strength and the interactive buckling strength can be obtained by using a high

yield stress material for a section which is expected to have a certain amount of residual stress due to manufacture.

6.3.7 The Initial Imperfection

In practice there is no ideal straight structural member. Every member contains a certain initial imperfection and in practice the load is not concentric. From measurements on columns, the imperfection shapes were classified as shown in Figure 6.12.

The initial imperfection can exist in the member as an overall imperfection and/or local imperfection in the section's components. For the local out-of-flatness the nonlinear theory must be used and this will be considered in the next chapter. In the present section the overall imperfection is approximated by a sinusoidal curve. At first an approximate approach is discussed, then a study on the effect of the initial imperfection on the buckling strength is considered.

6.3.7.1 Approximate Approach

The imperfect member may be modelled by a perfect member under eccentric load, i.e. a member under axial load with equal and opposite end moments. The present approximation is based on the same model but assuming that the moment is varied sinusoidally along the length. This assumption is more sophisticated. Moreover, it is assumed that there is a variable shearing force along the length represented by a cosine shape. Because the imperfection is small the material properties are assumed to be constant

along the length. This assumption may lead to small underestimates of the buckling strength of the member. As the initial imperfection increases the variation of the distribution of the stress along the length increases and the underestimation increases.

Assume the centreline of the column has an initial bow in a sine form, the initial deflection at a distance x from the end is given by

$$w^o = \alpha_n \sin \frac{\pi x}{\ell} \tag{6.6a}$$

$$= \alpha_n \sin \frac{\pi x}{\lambda} \tag{6.6b}$$

$$= \alpha_n \sin \pi\eta \tag{6.6c}$$

where w^o is the initial imperfection at distance x

α_n is the amplitude of the initial imperfection

λ is the half wave-length

ℓ is the length of the member

At any cross-section of a perfect column there is only axial load while for an imperfect column there are axial compressive load N_x, bending moment M_y and shearing force Q_z,

$$N_x = \sigma_x A \tag{6.7}$$

$$M_y = N_x \alpha_n \sin \pi\eta \tag{6.8a}$$

$$= \sigma_x A\alpha_n \sin \pi\eta \tag{6.8b}$$

$$Q_z = N_x \overset{o}{\frac{dw}{dx}} \tag{6.9a}$$

$$= N_x \alpha_n \frac{\pi}{\lambda} \cos \pi\eta \tag{6.9b}$$

$$= \alpha_x A\alpha_n \frac{\pi}{\lambda} \cos \frac{\pi x}{\lambda} \tag{6.9c}$$

where A is the cross-sectional area.

Because the initial imperfection is usually very small it is assumed that its effect on the stiffness of the member can be neglected. So the stiffness matrices of the components can be obtained from the case of a perfect member. Only the stability matrix has been modified. This stability matrix can be divided into three matrices

1. <u>The stability matrix due to the axial stress</u>
   This matrix is given in Chapter 3 (equation (3.65)).
2. <u>The stability matrix due to the bending stress</u>
   Using the elastic theory, the bending stress is given by

$$\sigma_b = \frac{M}{Z} = \frac{\sigma_x A\alpha_n}{Z} \sin \frac{\sigma_x}{\lambda} \tag{6.10}$$

   where σ_b is the bending stress
   Z is the elastic modulus

Substitute equation (6.10) into equation (3.112) the stability matrix [S] due to bending is given by

$$[S] = \frac{4t\lambda b}{3\pi} \cdot \frac{\pi^2}{\lambda^2} \cdot \frac{A\alpha_n}{Z} \sigma_x \int_{-.5}^{.5} [\{X\}\{X\}^T + 2\{Y\}\{Y\}^T + 2\{Z\}\{Z\}^T] d\eta \qquad (6.11)$$

A more correct matrix can be obtained by numerical integration along the length of the member because the bending stress is not constant through this length. But in the present approximation a direct integration has been done. For a long column, the initial imperfection and hence the bending stresses are higher than the corresponding values for the short column. Fortunately, the long column usually buckles elastically and direct integration can be performed without any approximation. For a short column the initial imperfection and the bending stress are smaller, but direct integration leads to some underestimation in the column buckling strength.

3. The stability matrix due to shearing force

The shear stress can be obtained from equation (6.9c) and it will be in the form

$$\tau_{yx} = \sigma_x C \cos \pi\eta \qquad (6.12)$$

where C is a constant depending on the shape of the cross-section, the position of the strip and the value of the initial imperfection. Substitute equation (6.12) into equation (3.61) the stability matrix due to the shear stress is given by

$$[S] = \frac{\pi t b}{\lambda} \cdot \frac{4\lambda b}{3\pi} \sigma_x \int_{-.5}^{.5} C\,[-\{X\}\{X'\} - \{Y\}\{Y'\} + \{Z\}\{Z'\}]d\eta \qquad (6.13)$$

which is a symmetrical matrix.

Because the initial imperfection is usually assumed in the range of 0.001 of the length of the column this shear is small and may be neglected for simplicity.

6.3.7.2 Effect of the Initial Imperfection on the Buckling Strength

To check the accuracy of the present approach initially imperfect H-columns free from residual stress has been considered. The assumed amplitudes of the initial imperfection are $\ell/2000$, $\ell/1000$ and $\ell/500$. The buckling strength curves are shown in Figure 6.13. The buckling strength curves reproduced by ECCS (118) for an initially stress-free H-column similar to the assumed column - are also shown for comparison. It is clear that three ranges for the slenderness ratio can be distinguished. In the first range - where the slenderness ratio of the column $\bar{\lambda} < 0.7$ - the finite strip results underestimate the ECCS curves and this may be due to the following facts

1. The ECCS assumed that the local buckling of the cross-section is prevented while this buckling is allowed in the present work.

2. In the present work it is assumed that the material properties at any section are equal to the material properties of column midheight section. This section

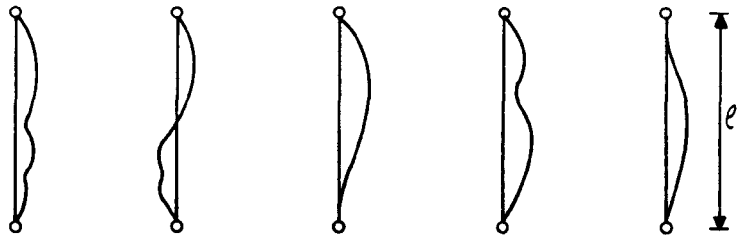

FIG. 6·12. THE MEASURED INITIAL IMPERFECTION. (Ref.118)

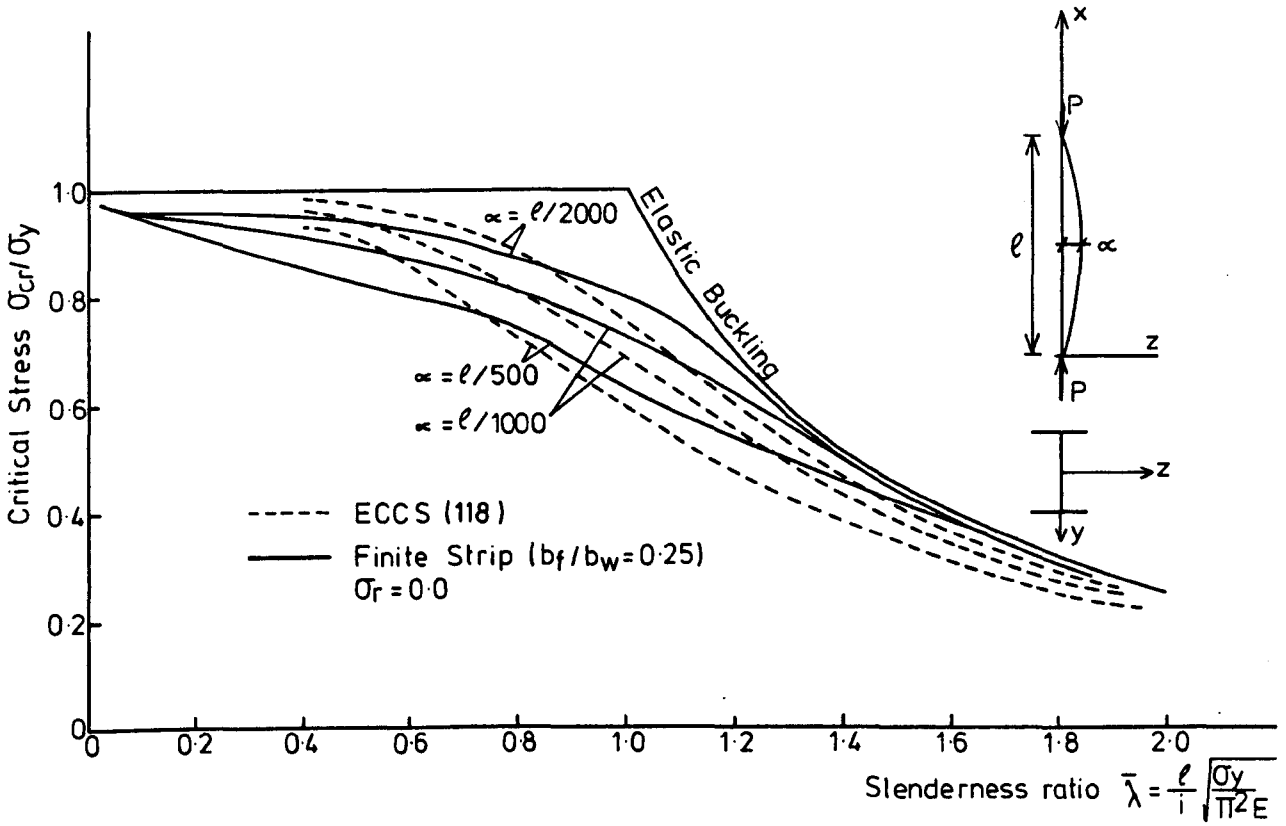

FIG. 6·13. COMPARISON BETWEEN THE FINITE STRIP AND ECCS BUCKLING CURVES FOR IMPERFECT COLUMN.

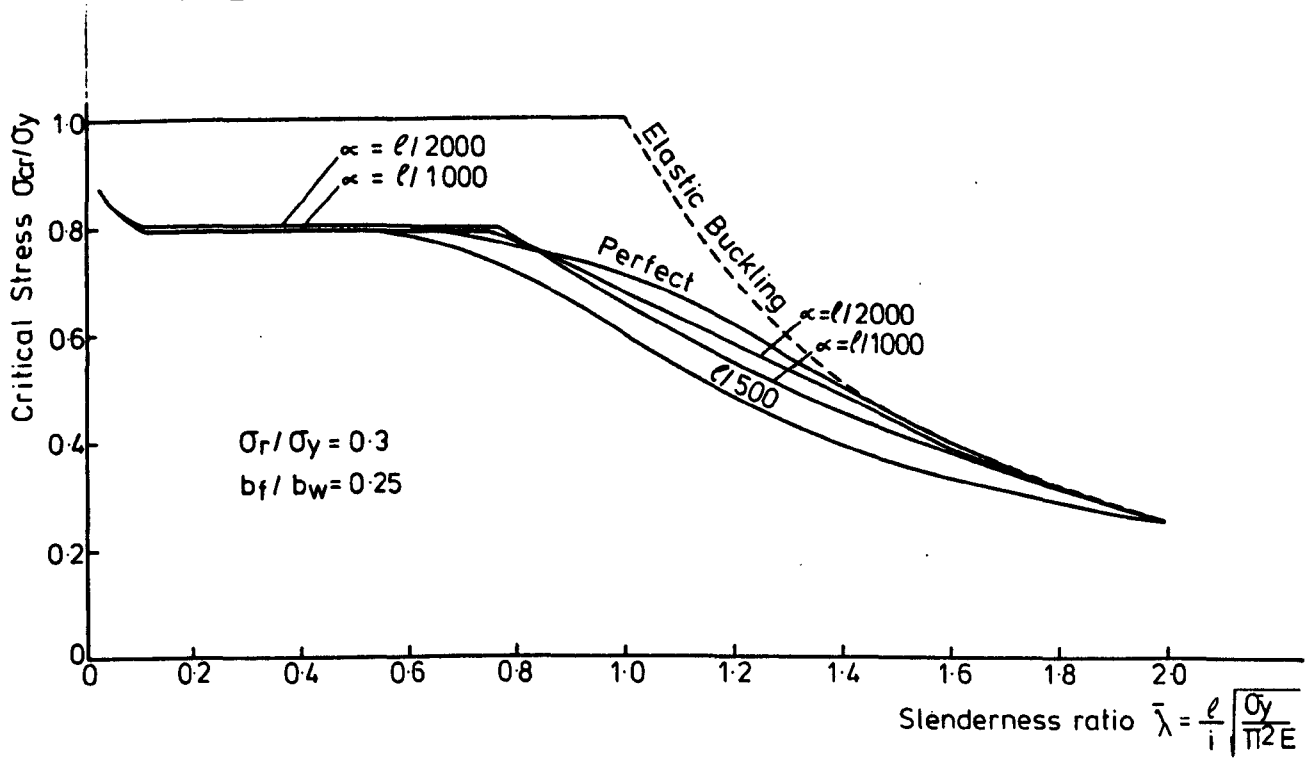

FIG. 6·14. EFFECT OF THE INITIAL IMPERFECTION ON THE BUCKLING STRENGTH.

starts to yield before any other section and behaves inelastically while the rest of the column may be still in the elastic state. The average of the maximum underestimation is 5.1% and this occurs at the lowest slenderness ratio, $\bar{\lambda} = 0.4$. As the slenderness ratio increases, this underestimation reduces and it becomes zero at $\bar{\lambda} = 0.75 \sim 0.85$, then it overestimates the ECCS results.

In the second range where the slenderness ratio of the column falls between 0.75 and 1.4 the finite strip result overestimates the ECCS curves by 6.4% average. For columns with slenderness ratios > 1.4 the finite strip result becomes very close to the Euler buckling curve and there is a small effect on the buckling strength due to the initial imperfection. The ECCS curves underestimate the Euler curve in this range. It is well known that as the slenderness ratio increases the effect of the initial imperfection decreases and this is clear in Figure 6.13.

In Figure 6.14 a perfect and imperfect column with initial bow equal to $\ell/2000$, $\ell/1000$ and $\ell/500$ are considered. The residual stress is assumed to be $0.3\ \sigma_y$. It is clear that for columns with slenderness ratios ≤ 0.65 there is a very small effect for the imperfection. This is because the section buckles in a local mode. In this range the local imperfection, the yield stress, the residual stress and the width-to-thickness ratio of the components are the factors controlling the buckling strength.

As the slenderness ratio $\bar{\lambda}$ of the column increases beyond 0.9, the effect of the imperfection on the buckling strength increases. At $\bar{\lambda} = 1.4$ this effect starts to decrease with increasing $\bar{\lambda}$. There is no effect for the imperfection on the buckling strength at a slenderness ratio $\bar{\lambda} \geq 1.9$.

6.3.8 Effect of the Load Eccentricity

Due to the erection of structures the joints may move in space and the axis of the structural members may deviate from ideal system geometry. This leads to an eccentricity of the applied load from the axis of the members. Moreover, the variations of the cross-section dimensions - along the length of the member due to manufacture procedure - produce an eccentric loading.

The eccentricity e of the load may be in any direction in the cross-sectional plane. When it tends to induce bending about the strong axis its effect is very small and can be neglected. The maximum effect occurs when it acts so as to induce bending of the section about the weak axis and this is the case which has been considered in the present section.

The buckling strength curves for an initially perfect H-section loaded by eccentric load with eccentricity e = 0.02, 0.04 and 0.06 of the flange width are shown in Figure 6.15. The section has a residual stress $\sigma_r = 0.3\ \sigma_Y$.

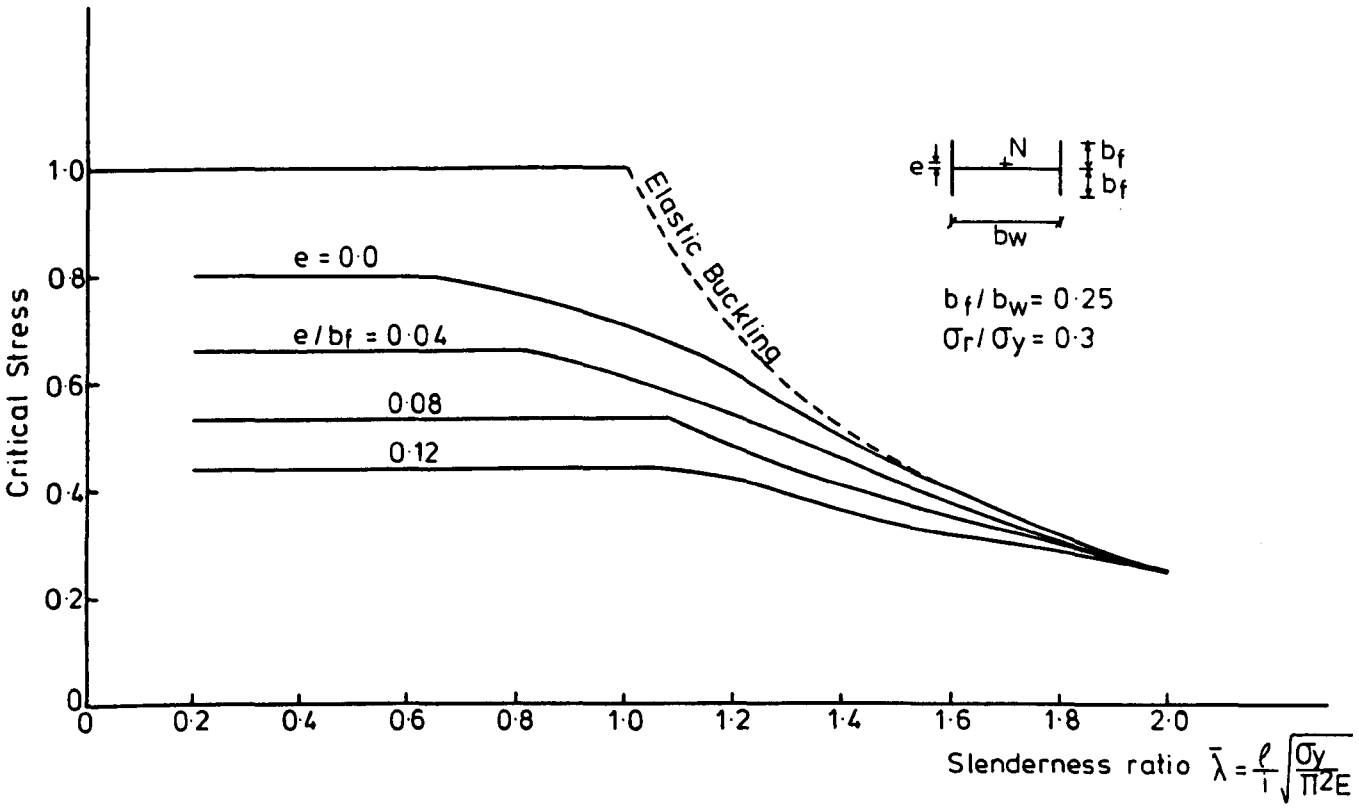

FIG. 6·15. EFFECT OF THE ECCENTRICITY ON THE BUCKLING STRENGTH.

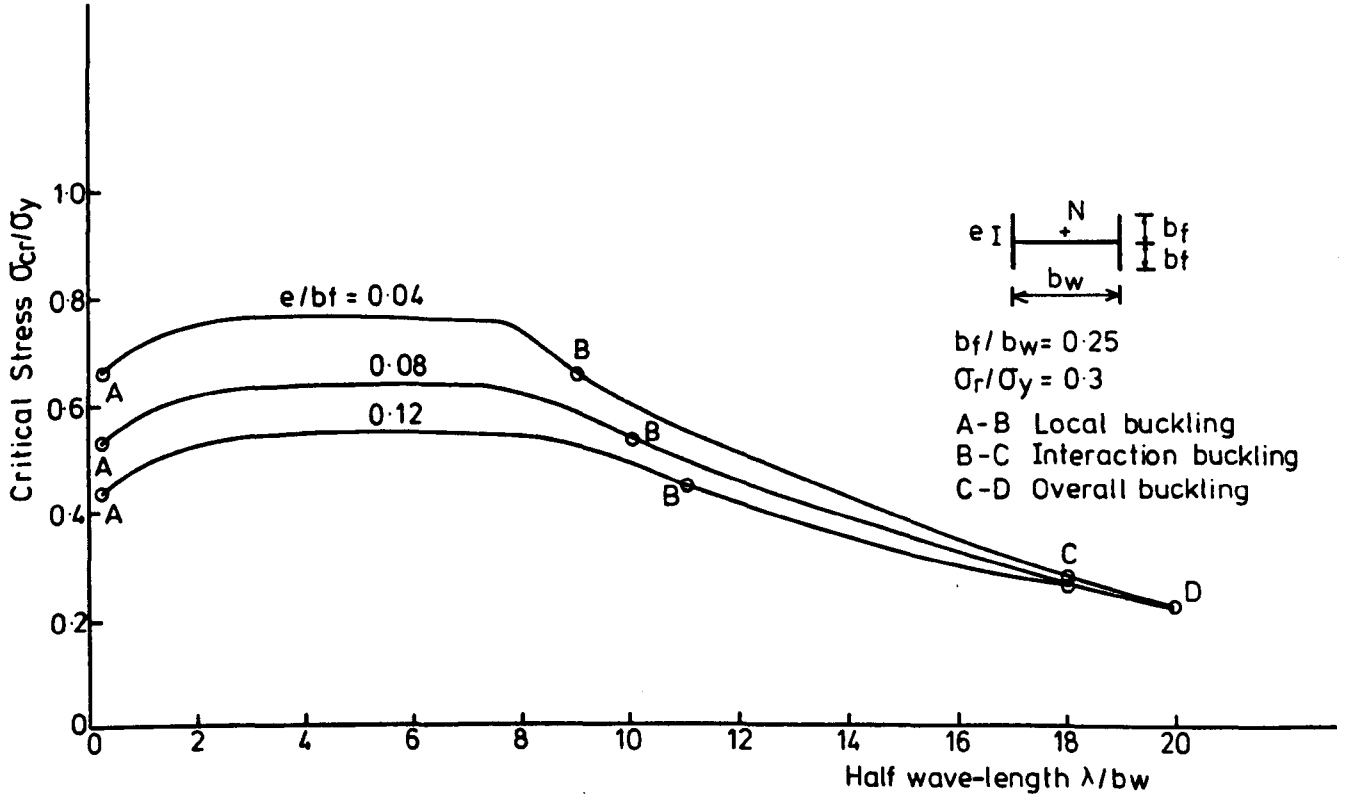

FIG. 6·16. THE CRITICAL STRESS VERSUS HALF WAVE-LENGTH OF ECCENTRIC COLUMN.

The reduction in the buckling strength due to the eccentricity depends on the slenderness ratio. For a very slender member - $\bar{\lambda} > 1.8$ - there is no effect for the eccentricity on the buckling strength. In this range the section buckles in an overall mode. The reduction increases as the slenderness ratio decreases up to a certain value then the strength becomes constant. The section buckles in an interaction mode. The interactive buckling strength depends on the overall buckling strength and the local buckling strength. It is clear that while the overall buckling strength is not affected by the eccentricity, the local buckling strength is greatly affected by it.

For the section considered, local buckling occurs in the flanges. Due to the eccentricity half of the flange is subjected to compressive stress (from the moment) while the other half is subjected to tensile stress. As the eccentricity increases, the moment increases and the bending stress increases. The maximum stress occurs at the free toes of the flanges and this reduces the local buckling strength significantly. When e/b_f increases from 0.0 to 0.04, 0.08 and 0.12, the local buckling strength reduces by about 17.5%, 33% and 45% respectively. These very large reductions are due to the fact that the ratios between the uniform compressive stress (e = 0.0) and the additional maximum bending stress are 24%, 48% and 72% for the three values of eccentricities respectively. It is clear from Figure 6.15 that the range of slenderness ratio - where the local buckling occurs - increases as the eccentricity

increases. When e/b_f increases from 0.04 to 0.08 this range increases from $\bar{\lambda} \leq 0.8$ to $\bar{\lambda} \leq 1.1$.

Figure 6.15 is reproduced in Figure 6.16 with the critical stress versus half wavelength instead of the critical stress versus the slenderness ratio. This is to show the effect of the eccentricity on the range where the interaction between the local and the overall buckling occurs.

6.4 Buckling of Beams Under Bending

A beam subjected to end moment about its strong axis will deflect in the plane of this moment. However, once the critical moment is reached, the beam may buckle in the lateral direction. This depends on the lateral stiffness of the beams and the lateral supporting arrangement. A short beam can carry the full plastic moment while a more slender beam may buckle at a moment which is significantly less than the plastic moment. If the width-to-thickness ratio of the flange is high, the flange may buckle locally before the plastic value of the applied moment is reached.

Two beams with different shape, a channel and an H-section under equal and opposite end moments have been considered. The beams are bent in their stiffer principal planes. This case is the model of the loaded beams shown in Figure 6.17(a). In general the beams are under moment gradient as shown in Figure 6.17(b). Only the first case - constant moment - is used to study the effect of the cross-sectional shapes and dimensions and the effect of the residual stress patterns and magnitudes on the buckling strength of the beams.

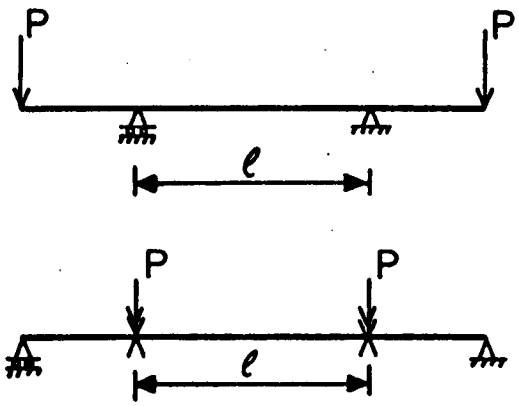

(a) Beams under constant moment.

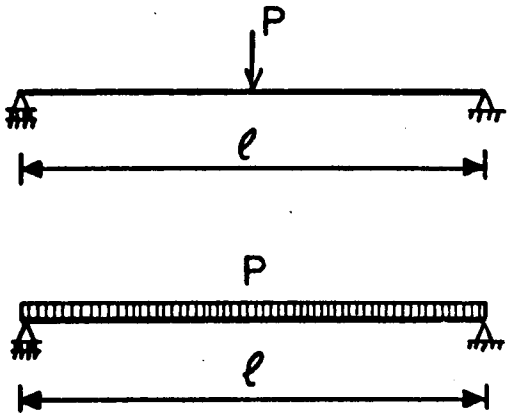

(b) Beams under moment gradinet.

FIG. 6·17. POSSIBLE LOADS ON BEAMS.

The problem of beams is more difficult than the problem of columns and the aim of the present section is to demonstrate the capability of the finite strip method for dealing with such problems rather than to investigate it in detail.

6.4.1 Elastic Buckling of Beams

Four values for the ratio b_f/b_w - 0.125, 0.25, 0.375 and 0.50 - have been considered. The channel is divided into 6 strips - 4 strips in the compression part and 2 strips in the tension part - while the H-section is divided into 9 strips - 6 strips in the compression part and 3 strips in the tension part (Figure 6.1). Every strip is divided into 10 substrips. The elastic buckling curves are shown in Figure 6.18 for the channels and in Figure 6.19 for the H-sections. Some modes of buckling at different half wavelengths are also shown. The elastic buckling strength curves have been obtained for subsequent comparison with the inelastic buckling behaviour of beams.

Because the beams are assumed to be initially perfectly straight, there are no out-of-plane displacements until the applied moments reach the critical values at which the beams buckle. The buckling curves of the beam can be divided into three ranges as in the case of columns. At a large ratio of λ/b_w the beams buckle in an overall mode. The buckling may be flexural, torsional (modes "F" Figure 6.18 and "C" Figure 6.19) or flexural-torsional (mode "C"

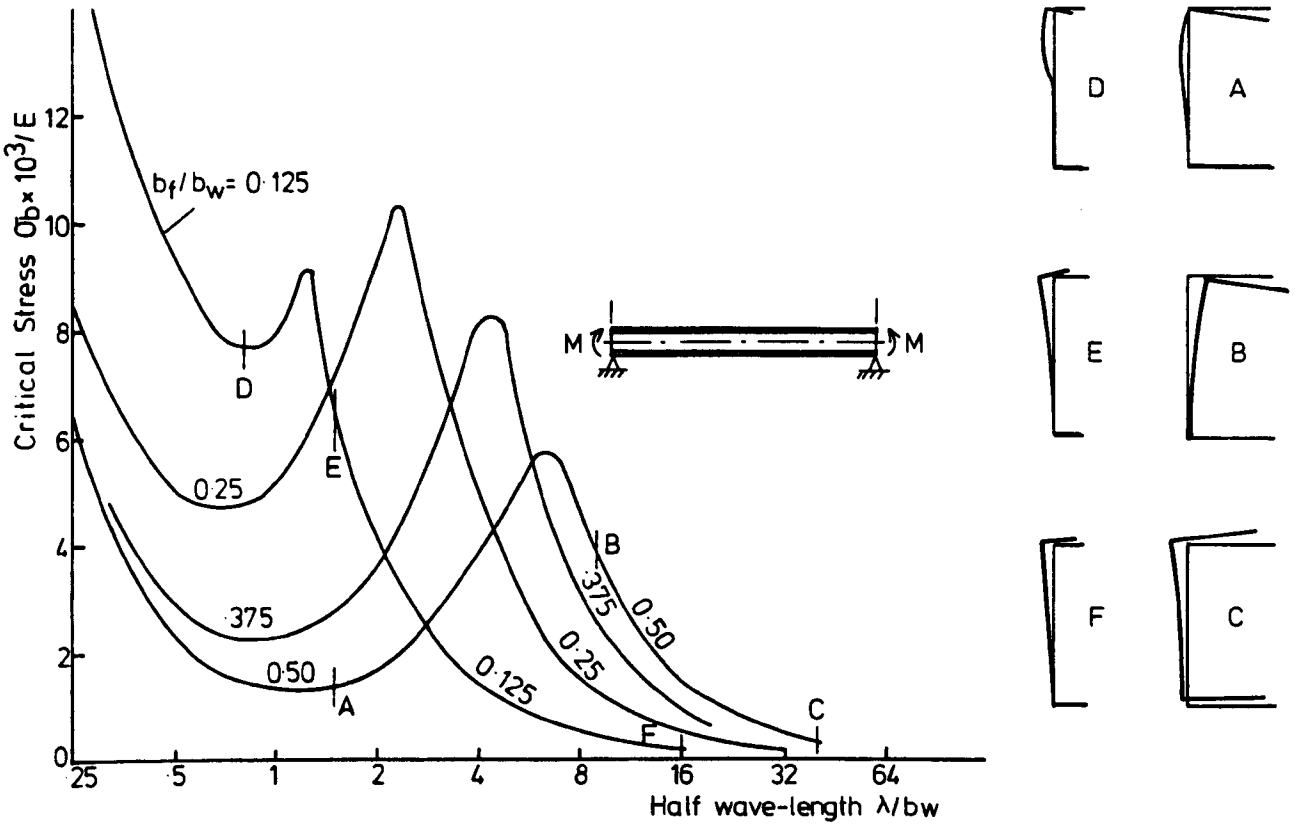

FIG. 6·18. ELASTIC σ_b/E VERSUS λ/bw FOR CHANNEL SECTIONS IN PURE BENDING.

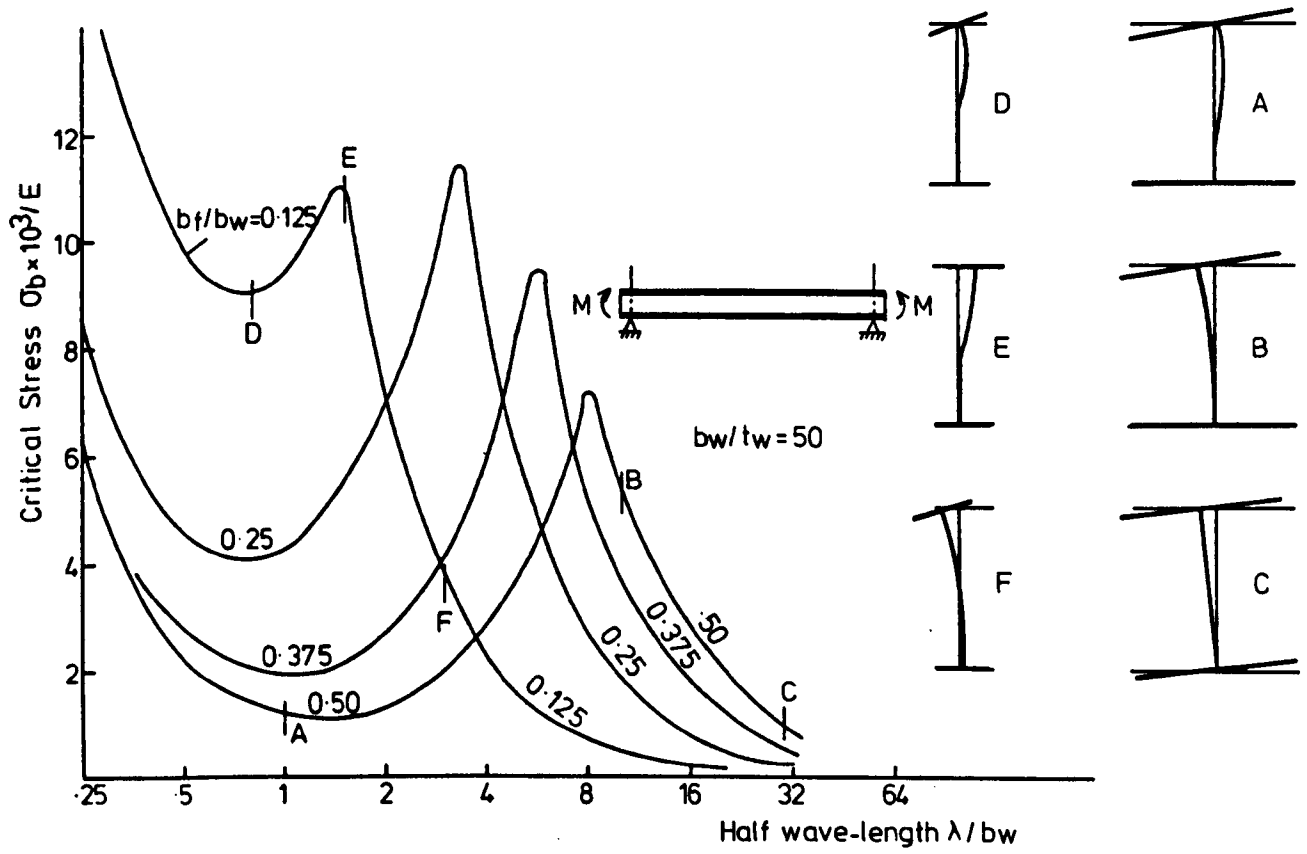

FIG. 6·19. ELASTIC σ_b/E VERSUS λ/bw FOR H-SECTION IN PURE BENDING.

Figure 6.18). This depends on the shape and dimensions of the cross-section.

For short beams, the local buckling occurs only in the compression flanges of the sections (modes "A" and "D"). In this range the buckling strength depends on the width-to-thickness ratio of the compression flange and the degree of restraint developed by the web.

In the intermediate range of λ/b_w, an interaction between the overall buckling and the local buckling occurs (modes "B" and "E"). Due to this interaction the beam buckles before it reaches its full overall buckling strength.

6.4.2 Effect of the Shape and Dimensions of the Cross-Section on the Inelastic Buckling Strength

Two cross-sectional shapes and four different dimensions for every cross-section are considered. The residual stress pattern Figure 6.2 with three levels of σ_r - 0.0, 0.3 σ_y and 0.5 σ_y - is assumed. The critical bending stresses against the half wavelength are shown with some modes of buckling in Figure 6.20 for the Channels and in Figure 6.21 for the H-sections.

It is clear from Figure 6.20(a) that the buckling strength curves can be divided into three parts. The first at large ratio of λ/b_w where the beams buckle in an overall mode (modes "C" and "F"). In this range the beams behave elastically and they may deflect laterally and/or

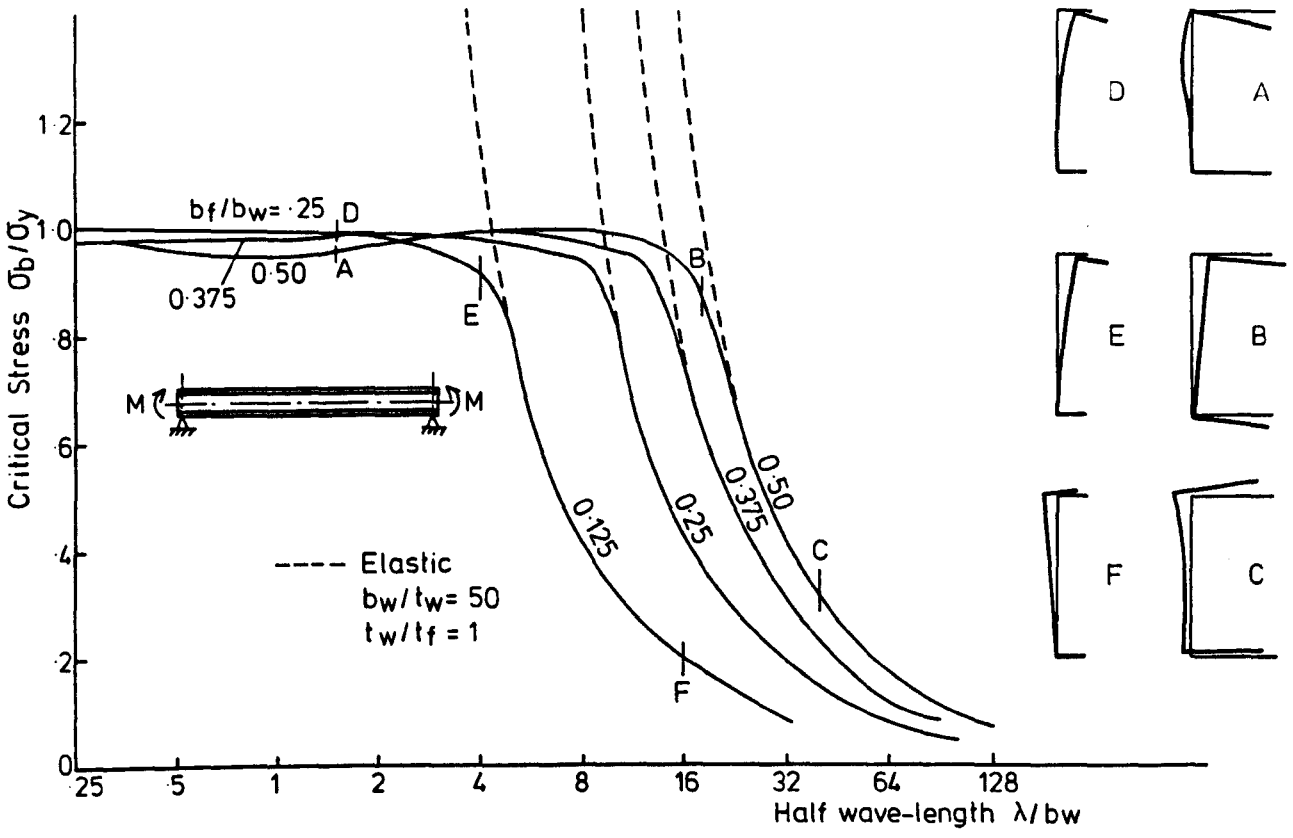

(a) σr / σy = 0·0

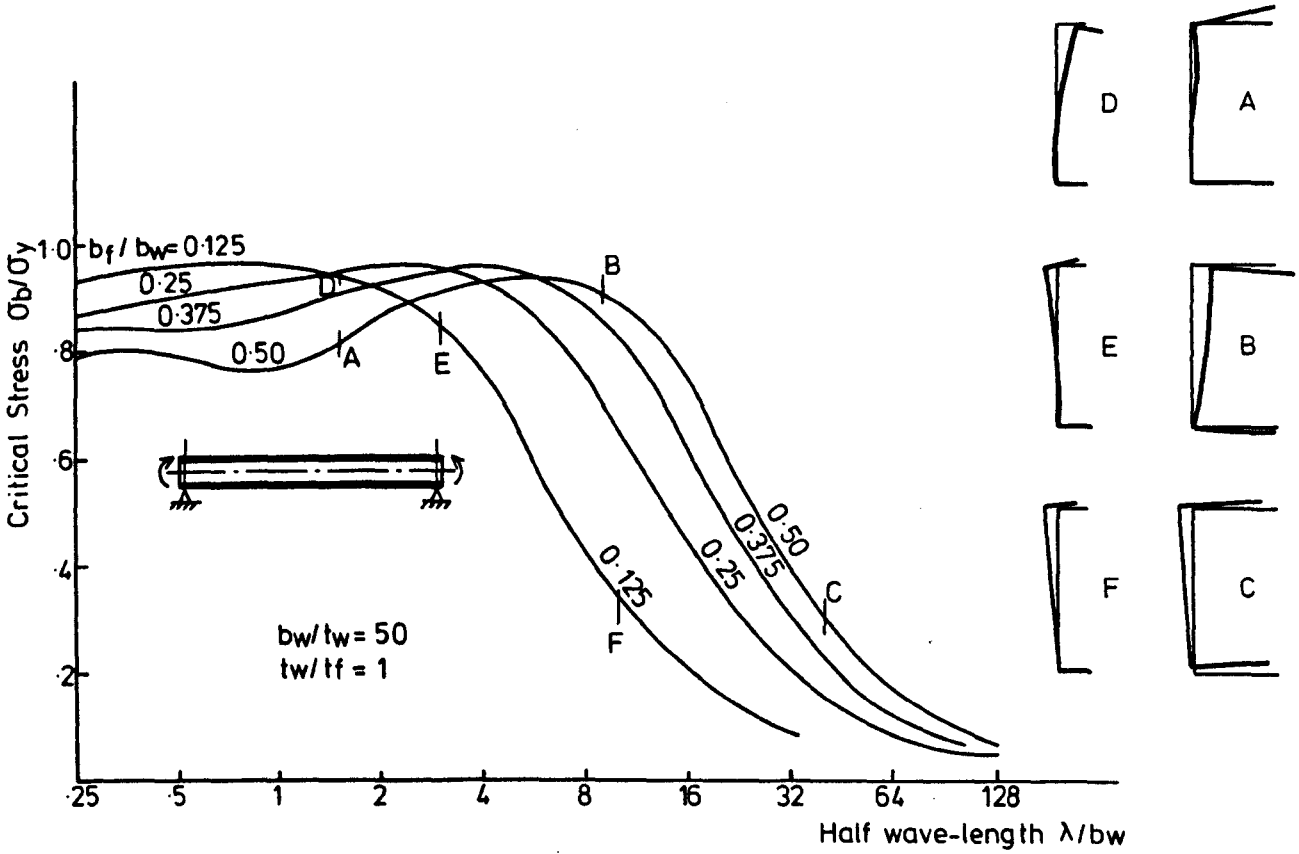

(b) σr / σy = 0·30

FIG. 6·20. (Cont.....)

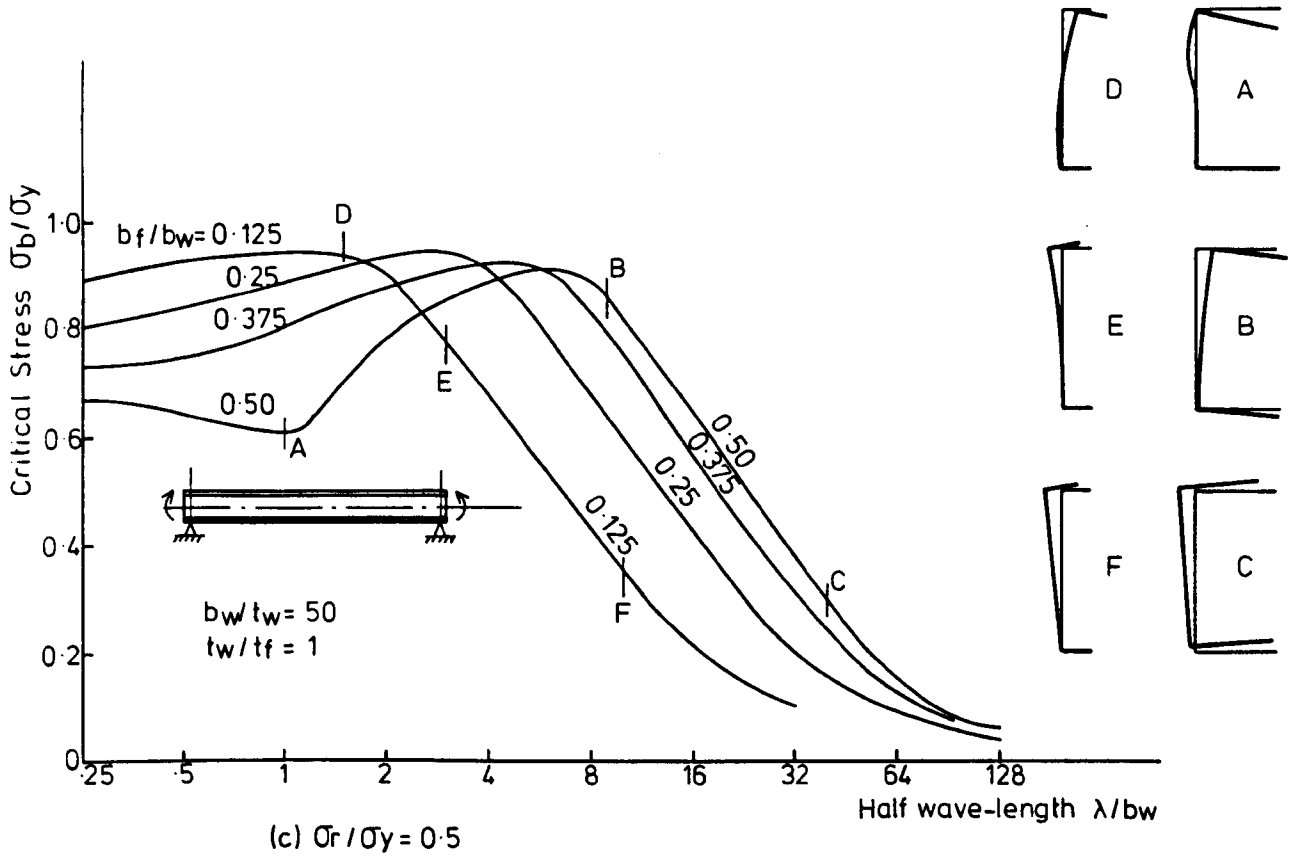

(c) σ_r/σ_y = 0·5

FIG. 6·20. INELASTIC σ_b/σ_y VERSUS λ/b_w FOR CHANNEL SECTIONS IN PURE BENDING.

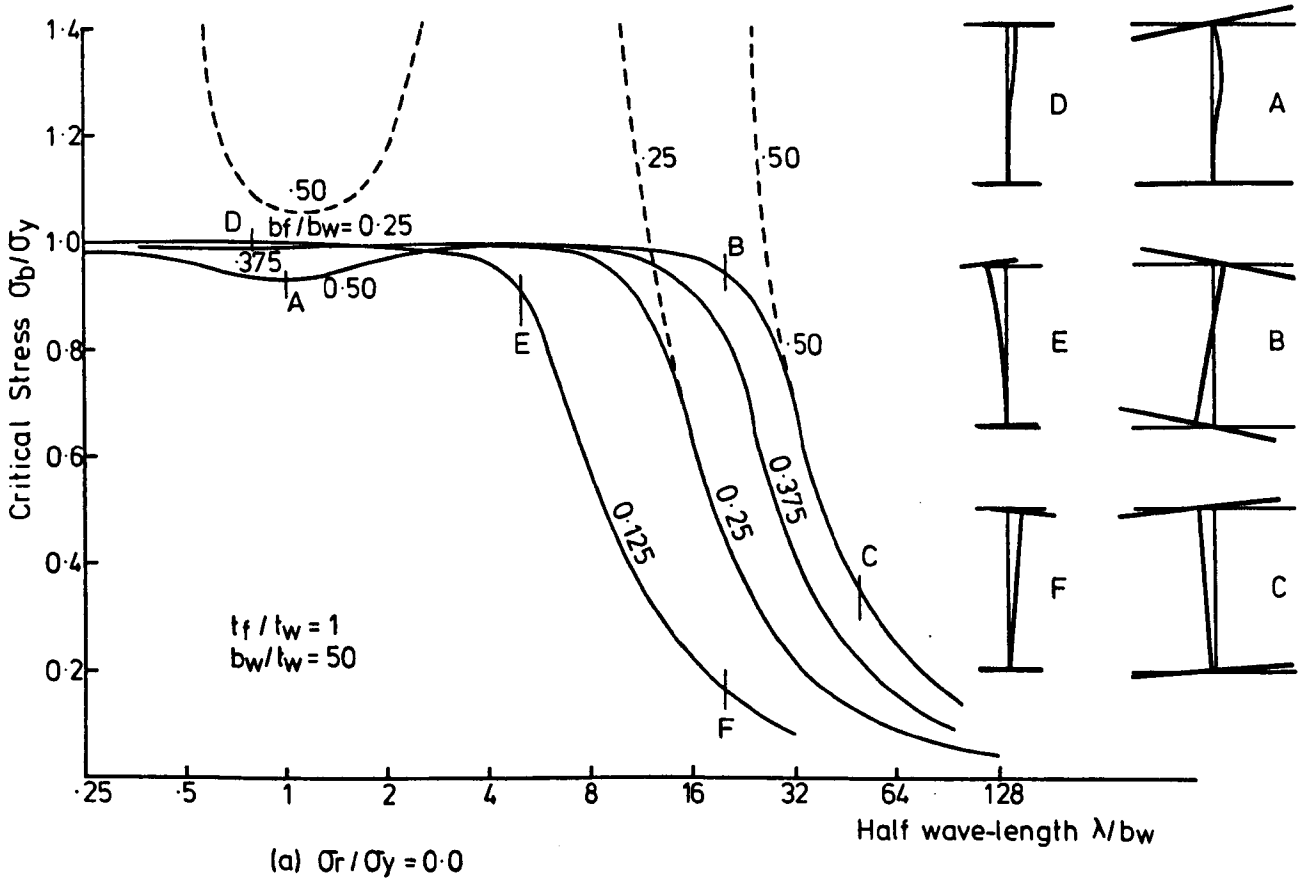

(a) σ_r/σ_y = 0·0

FIG. 6·21. (Cont.....)

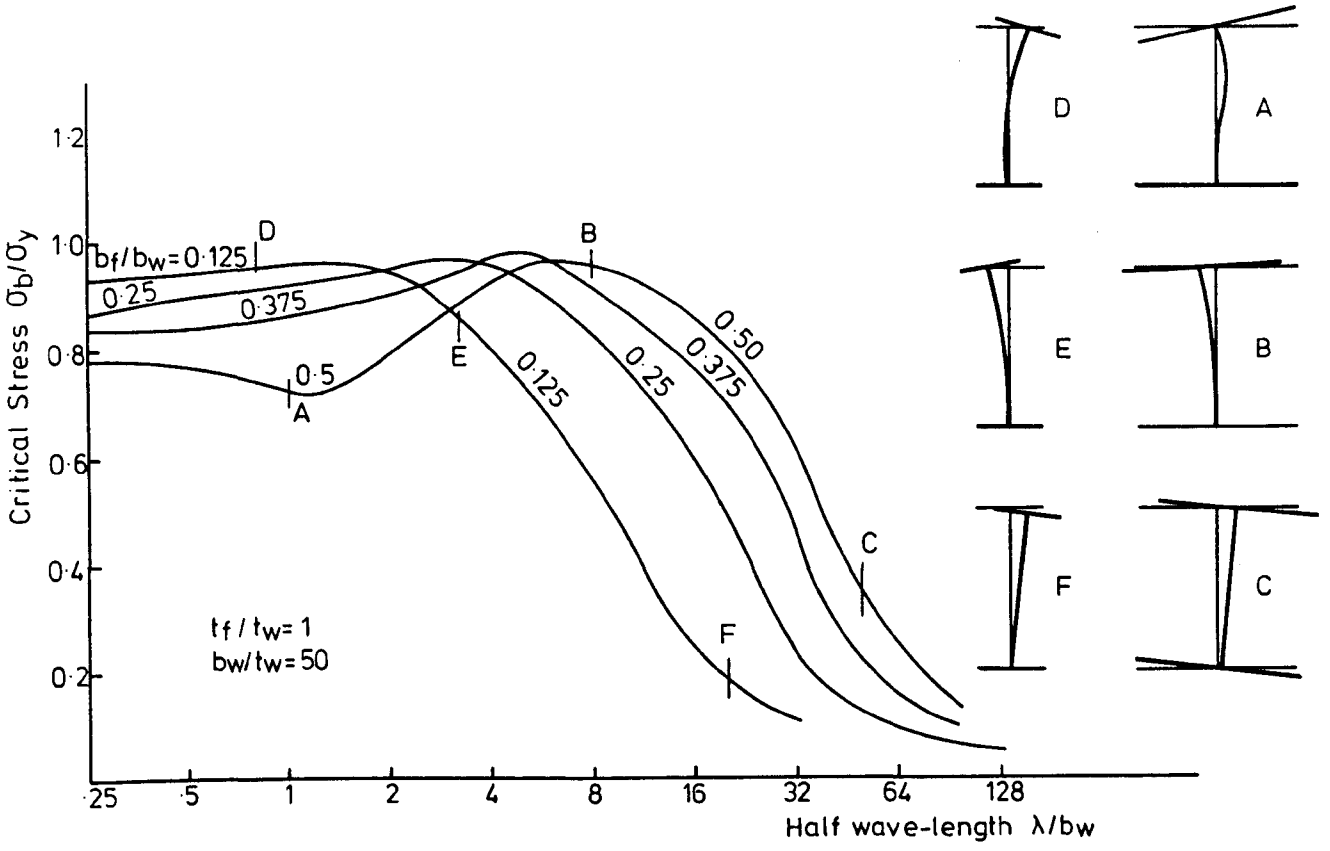

(b) $\sigma_r/\sigma_y = 0{\cdot}30$

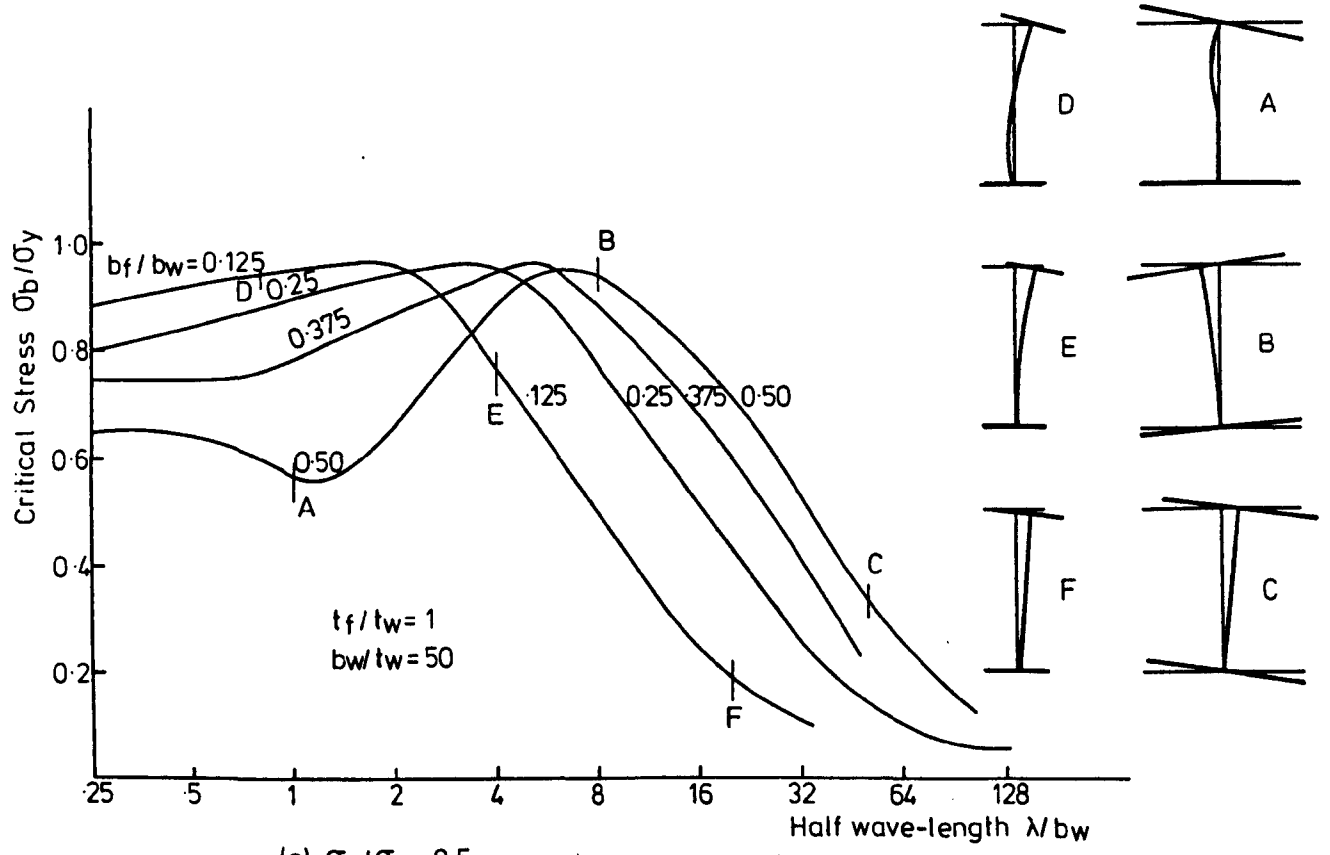

(c) $\sigma_r/\sigma_y = 0{\cdot}5$

FIG. 6·21. INELASTIC σ_b/σ_y VERSUS λ/bw FOR H-SECTION IN PURE BENDING.

twist. The torsional rigidity of the cross-section controls the deflected form.

As the half wavelengths reduce the buckling curves start to deviate from the elastic overall buckling strength curves. For the sections with wide flanges, an interactive buckling mode may occur in this range (mode "B"). The range of the half wavelength where this interaction mode occurs and the reduction in the overall buckling strength due to it depends on many factors as was shown for the case of columns. The buckling curves, for the other sections with small flange widths, seem to be transition curves between the elastic overall buckling curves and the full plastic strength of the flange. In this case the curves deviate at $\sigma_b/\sigma_Y = 0.8$ (Figure 6.20(a)) where the stress-strain relationship of the material becomes nonlinear.

The maximum strength for short beams depends on the width-to-thickness ratio of the compression flange. For sections with flanges of small width-to-thickness ratio, the flange may yield before it buckles while in the sections with high ratios the compression flange may buckle locally before reaching the ultimate strength (mode "A").

From Figures 6.20(a), (b) and (c), it is clear that the residual stress has no effect on the long beams buckling in an overall mode. For short beams, the local buckling strengths of the beams reduce significantly as the residual stress increases. The interactive buckling ranges become more clear due to the effect of the residual stress on the local buckling of the flanges.

Comparing the buckling strength curves Figure 6.20 and Figure 6.21, it can be noted that the H-beams behave in a similar manner to the channel beams. Because the two sets of graphs are not plotted with respect to the same slenderness ratio, no useful comparison can be obtained from them. The cross-sectional shape of the beam has an effect on the critical moment and this must be considered in any comparison.

6.4.3 Effect of the Residual Stress Pattern

The distribution of the compressive and tensile residual stresses depends on the cross-section geometry, the method of welding or rolling and many other factors. Open sections like H-sections or channels are affected by the variation of the residual stress pattern more than closed sections like box-sections and tubes (118).

In the previous sections some indications have been given of the effect of the magnitude of residual stresses on the buckling behaviour of various structural elements. In order to study the influence of the assumed pattern of residual stress on such behaviour, the H-section detailed in Figure 6.22(a) has been studied for the case of pure bending. Three different patterns have been assumed as shown in Figure 6.22 (b-d). These patterns are selected to represent H-section with as-rolled flanges (Figure 6.22(b) and (d)) and H-section with flame-cut flanges (Figure 6.22(c)). The critical stresses are computed over a range of wave-lengths. The results for σ_r/σ_Y of 0.3 and 0.5 are shown in Figure 6.23.

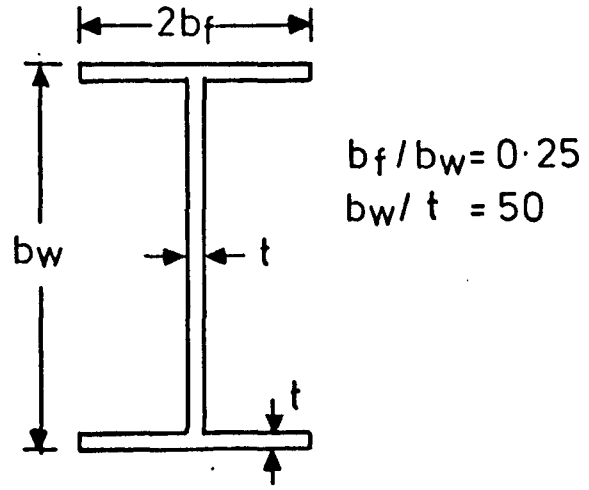

(a) Section Details.

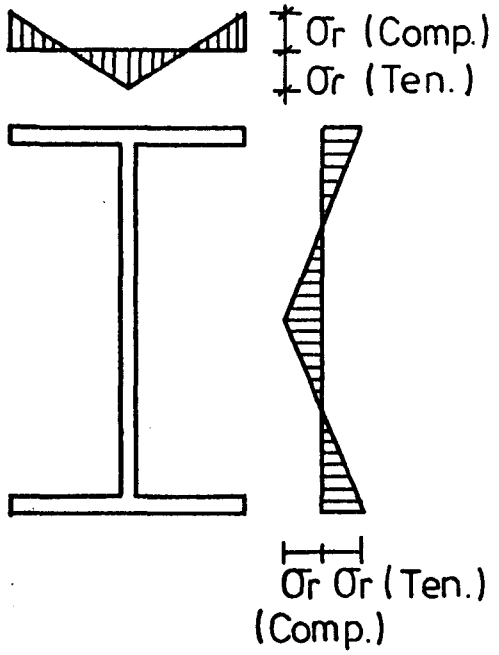

(b) Pattern A.

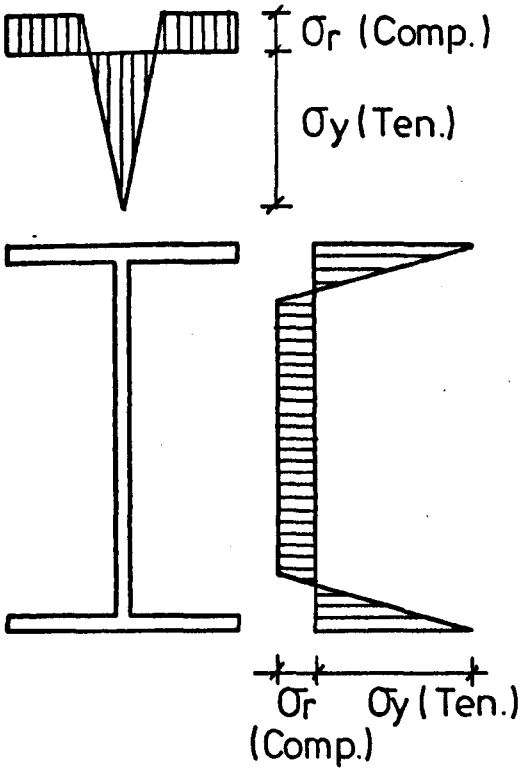

(c) Pattern B.

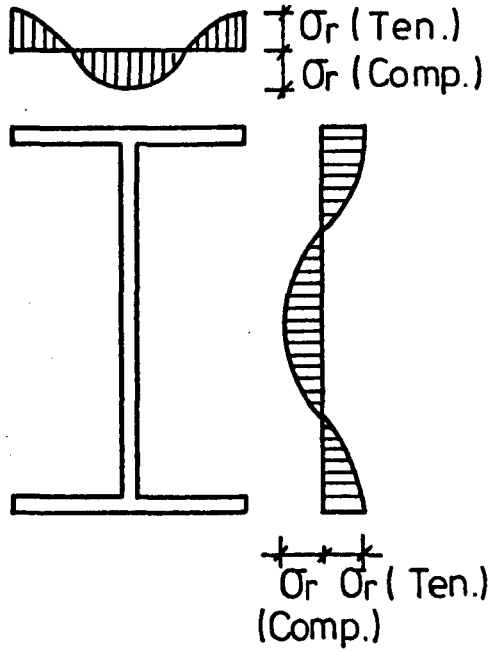

(d) Pattern C.

FIG. 6·22. DIFFERENT PATTERNS OF RESIDUAL STRESS FOR I-SECTIONS.

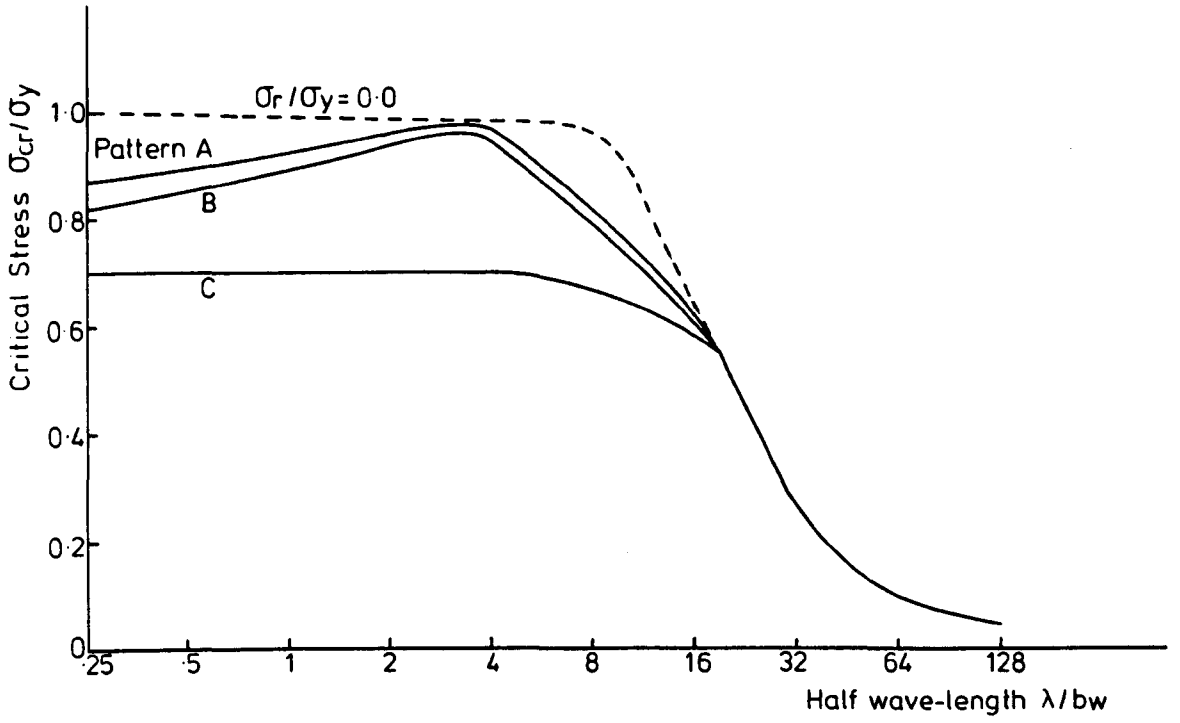

(a) $\sigma_r/\sigma_y = 0.3$

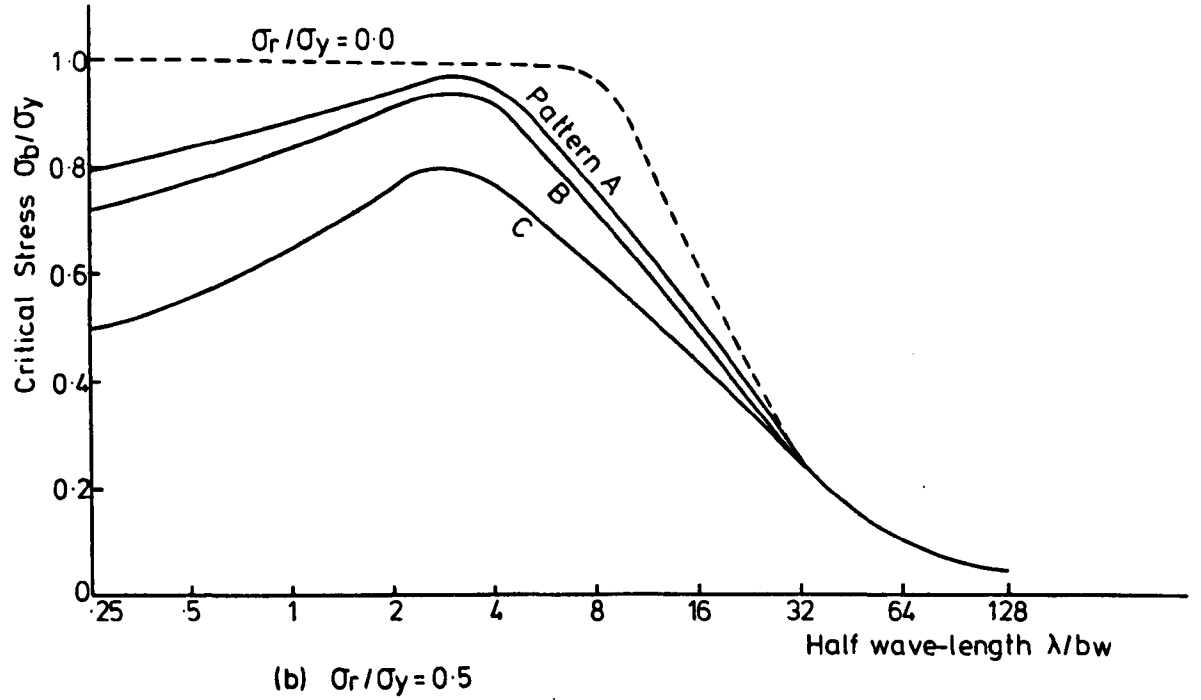

(b) $\sigma_r/\sigma_y = 0.5$

FIG. 6.23. EFFECT OF THE RESIDUAL STRESS PATTERN ON THE CRITICAL STRESS OF H-SECTION UNDER PURE BENDING.

In both cases the pattern of residual stress "A" is associated with critical stresses which are higher than for "B" and "C". For buckling at long wavelengths the differences between these are in fact very small. This is again a reflection of the fact that in the overall buckling mode, the influence of residual stress is very small.

At lower wavelengths, however, the difference is quite marked, being of the order of 30% and this clearly indicates the importance of idealising the residual stress distribution as accurately as possible when considering the local buckling behaviour of plated structures.

6.5 Buckling of Beam-Columns

A beam-column subjected to axial compressive force and moment about its stronger principal axis will deflect about this axis as long as the applied combined stress is less than the critical stress. When this critical stress is reached the long beam-column may buckle out-of-the plane of bending by deflecting laterally and twisting. For short beam-columns the cross-sectional components may buckle locally or the applied stress may reach the ultimate strength before it buckles. The most important factor controlling the mode of buckling is the moment-to-thrust ratio (the eccentricity).

In Figure 6.24 an H-section under eccentric load with different eccentricities has been studied. The residual stress is assumed to be 0.3 σ_Y and b_f/b_w is taken as = 0.25. It is clear that the effect of eccentricity on the local buckling strength is higher than its effect on the overall

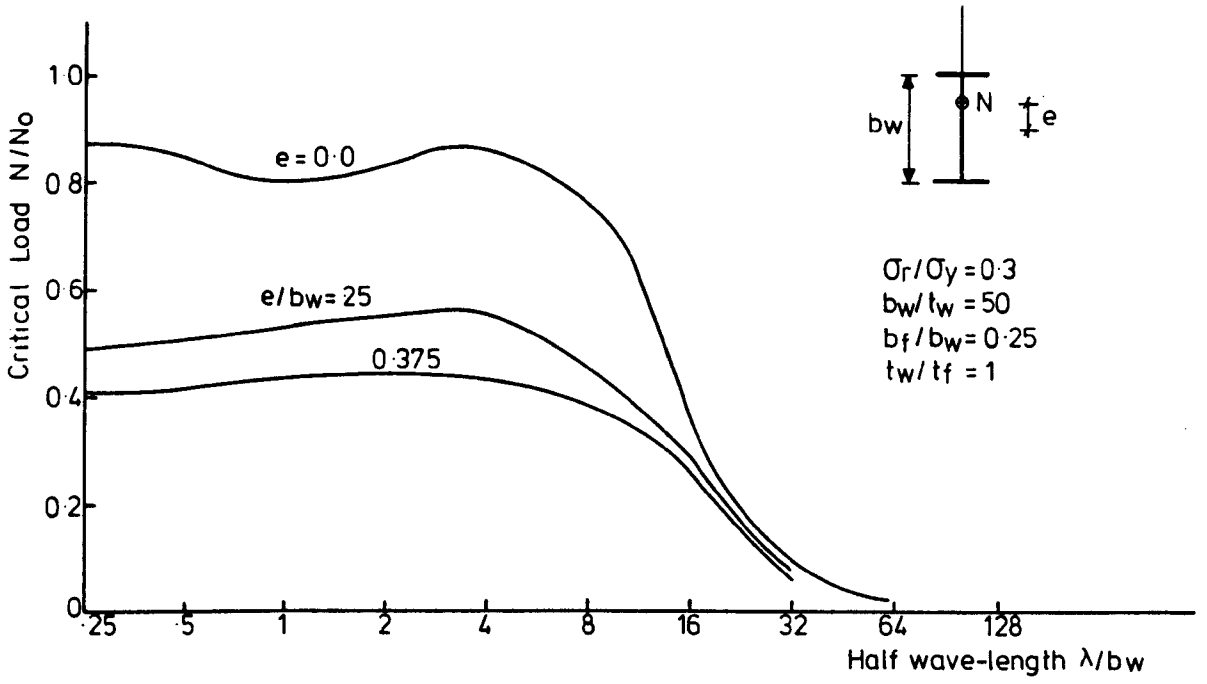

FIG. 6·24. EFFECT OF THE ECCENTRICITY ON THE CRITICAL STRESS OF H-SECTION.

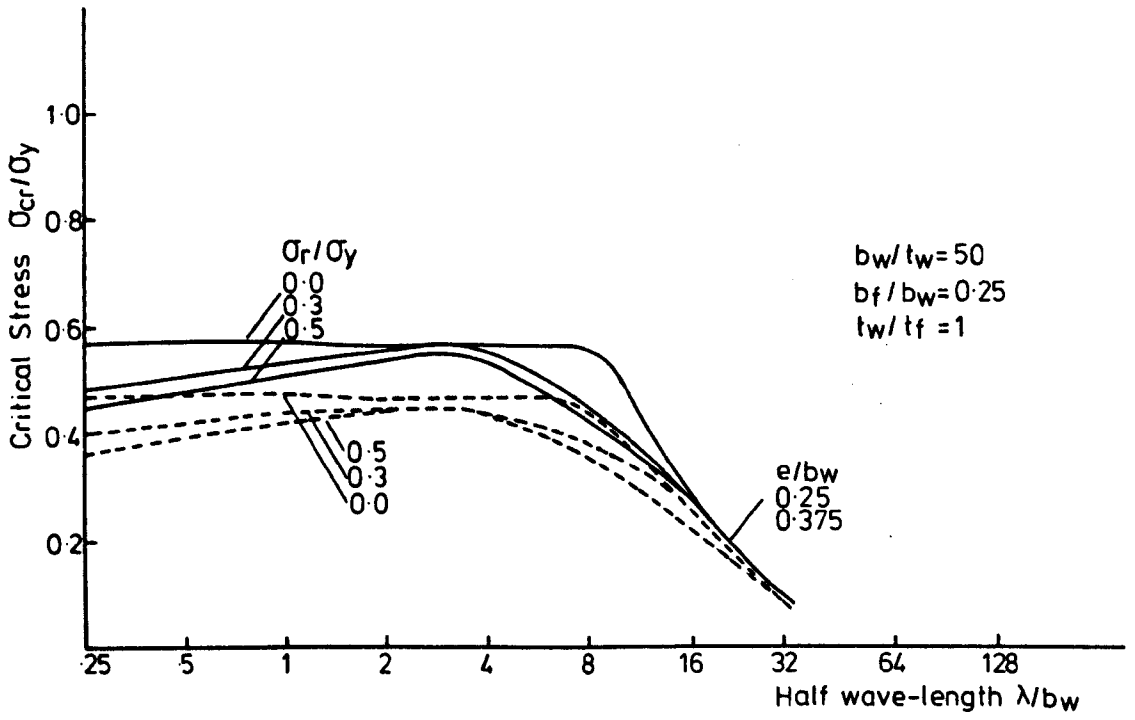

FIG. 6·25. INFLUENCE OF RESIDUAL STRESS ON THE CRITICAL STRESS OF H-SECTION ECCENTRICILY LOADED.

buckling strength. Increasing eccentricity e from 0.0 (pure compression) to 0.25 b_w and 0.375 b_w leads to a reduction in the local buckling strength of about 37% and 47% respectively. This reduction becomes 9% and 16% at half wavelength $\lambda = 20\ b_w$.

The influence of the residual stress on the buckling strength of an eccentrically loaded H-column is shown in Figure 6.25. Three levels of the residual stress - σ_r = 0.0, 0.3 σ_Y and 0.5 σ_Y - and two values for the eccentricity - e = 0.25 b_w and 0.375 b_w - have been considered. The reduction in the buckling strength - at $\lambda = b_w$ - due to an increases of σ_r from 0.0 to 0.3 σ_Y is 7% for both values of e. It is clear from Figure 6.25 that the effect of the residual stress on the buckling strength increase as the eccentricity e increases.

6.6 Concluding Remarks

The inelastic buckling of structural members under axial compression, pure bending and eccentric load has been considered. Convergence studies indicate that dividing any component of the cross-section into at least two strips is sufficient to obtain the desired accuracy. When residual stresses are present, every strip has been divided into 10 substrips.

The effect of certain parameters - the shape and dimensions of the cross-section, the length of the structural member, the magnitude and pattern of residual stress, the

initial imperfections and the eccentricity of the load - have been studied and the following conclusions may be drawn:

1. The buckling strength curve can be divided into three ranges - overall buckling, interactive buckling and local buckling. These three ranges become more clearly defined as the residual stresses increase.

2. The inelastic buckling curves diverge from the elastic buckling curves (Euler curve) at a point approximately corresponding to $\sigma_{cr}/\sigma_Y = 0.8 - \sigma_r/\sigma_Y$.

3. The overall buckling may be flexural, torsional or flexural-torsional.

4. The slenderness ratio of the structural member (ℓ/r) affects the overall buckling while the slenderness ratio of the components (β) affects the local buckling. There is very little effect for the shape of the cross-section on the overall buckling strength.

5. Due to the interaction between the overall and the local buckling, the buckling strength of the member has been reduced. In this range it is unsafe to design this member considering the full flexural rigidity of the cross-section.

6. The local buckling of any component of the cross-section falls between two bounds - upper bound (the displacement and the rotation of the longitudinal

edges are restrained) and lower bound (only the displacements of these edges are restrained).

7. The residual stress has no effect on the overall flexural buckling strength, but it reduces both the local and the interaction buckling strengths.

8. The presence of the residual stresses may change the local buckling of the section from web local buckling to flange local buckling. It may also change the overall flexural buckling to overall flexural-torsional buckling.

9. A component with a free edge is more sensitive to the presence of residual stress than a component with restrained - elastically, simply supported or fixed - edges, i.e. the flanges are more sensitive to the residual stress than the web.

10. The residual stress pattern has no effect on the overall buckling strength while the local and interactive buckling are greatly affected by this pattern.

11. The local buckling strength and the interactive buckling strength can be improved by using material with a higher yield point for a section which is expected to have a given level of residual stress.

12. The range of the interactive buckling and the reduction in the strength due to it are affected by the shape of the cross-section.

13. An approximate method has been proposed to take the overall initial imperfection into effect in a simple manner and the results have been compared with the results obtained by ECCS. The maximum difference between the two sets - FSM and ECCS - is about $\pm$ 6.0%.

14. The effect of this initial imperfection on the local buckling strength is very small while its effect on the interactive buckling and the overall buckling is relatively high. For a very slender column - $\bar{\lambda} \geq 1.9$ - the initial imperfection has no effect on the overall buckling strength.

15. The maximum effect of the load eccentricity occurs when it acts so as to induce bending of the section about the weak axis. For a very slender member - $\bar{\lambda} > 1.8$ - there is no effect for the eccentricity on the overall buckling strength while the local buckling strength is greatly affected by this eccentricity.

16. For beam-columns, the most important factor controlling the mode of buckling is the moment-to-thrust ratio. The effect of this ratio on the local buckling strength is greater than its effect on the overall buckling strength.

CHAPTER 7

A NON-LINEAR THEORY OF ELASTIC STABILITY

7.1 Introduction

For a slender plate the linear strain-displacement relationship (small deflection theory) leads to an underestimate of a plate's actual strength. This is due to the neglect of the post-buckling reserve which may, in certain cases, be much larger than the pre-buckling strength. Moreover, for this slender plate the presence of initial imperfections has a much more significant effect on strength than does material nonlinearity. It is the object of this chapter to extend the finite strip method to include the effects of geometric nonlinearity, leading to a study of the post-buckling behaviour of perfect and imperfect plates.

In the following analysis the large deflection theory (non-linear strain-displacement relationship) the Marguerre strain expression (119) for shallow shells will be used. The stress-strain relationship of the material is assumed to be linear elastic.

7.2 Non-Linear Elastic Behaviour

The classical linear elastic theory becomes invalid at loads in excess of the critical buckling load. A plot of the lateral displacement "$w_c/_t$" against the applied longitudinal compressive stress "σ/σ_{cr}" for a perfect plate

is shown in Figure 7.1. The load is assumed to act through a very rigid loading bar, thereby ensuring that the longitudinal displacement of the ends is uniform. The perfect plate does not deflect laterally at loads below the critical; the linear strain-displacement relationships can be applied in this range. However, the lateral displacements of the plate increase rapidly once applied stress exceeds this critical stress. The rate of growth of this displacement depends on the in-plane and out-of-plane boundary conditions at the longitudinal edges.

In practice plates are not perfect but contain initial imperfections. Up to a certain limit it is not unreasonable to neglect this imperfection and to consider the plate as perfectly flat (3). If the initial out-of-flatness exceeds this limit, then the post-buckling behaviour of the plate effectively represents a transition between that of a flat plate and that of a cylindrical shell. Plates containing large imperfections effectively buckle like a cylindrical shell, i.e. the in-plane boundary conditions have no effect on the ultimate load (107).

The plot of lateral displacement against the applied stress for an imperfect plate is shown in Figure 7.1. It does not exhibit a bifurcation point but a smooth increase in lateral deflections from the start of loading. Once the applied stress exceeds the critical, the effect of the initial bow reduces and the plate tends to behave rather like a perfect one.

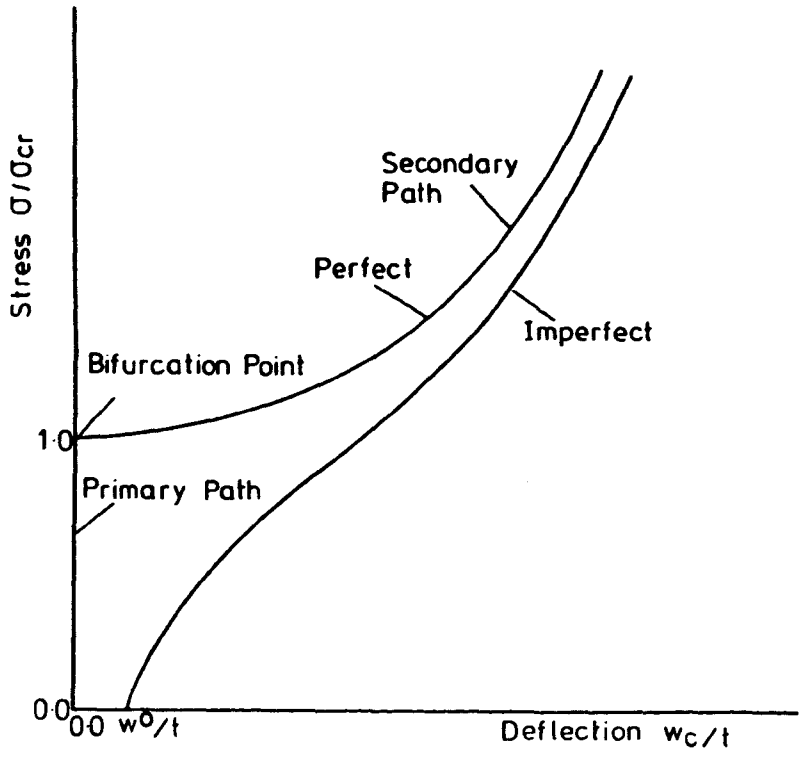

FIG.7·1. LARGE DEFLECTION OF PERFECT AND IMPERFECT PLATE UNDER IN-PLANE LOAD.

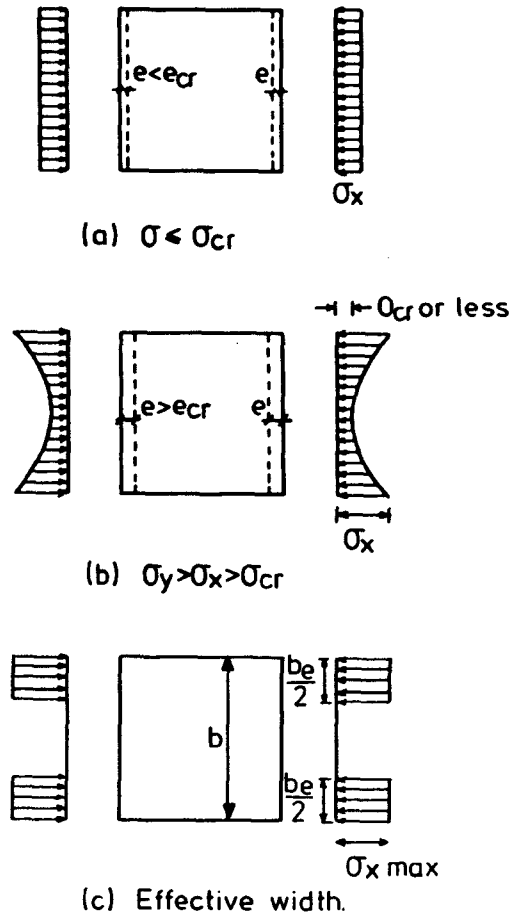

FIG.7·2. STRESS DISTRIBUTION ON A STRAIGHT COMPRESSED PLATE.

The presence of imperfections is considered in the general theory of elastic stability by introducing an imperfection parameter into the strain energy function.

7.3 Effective Width Method

Before buckling the axial compressive stress "σ_x" is uniformly distributed and proportionality exists between the strain and the compressive stress

$$\sigma_x = E\,\varepsilon_x \tag{7.1}$$

or $$\sigma_x = \frac{E\,\varepsilon_x}{(1-\nu^2)} \tag{7.2}$$

for the case of free and restrained longitudinal edges respectively. Above the critical load the plate deflects more in the middle than near the unloaded edges. Thus the stiffness of the central part reduces more quickly resulting in a nonuniform distribution of the compressive stress "σ_x" as illustrated by Figure 7.2. The stress in the centre of the loaded edge remains equal to or less than the critical. The actual distribution of these compressive stresses depends on the boundary conditions and the aspect ratio of the plate.

At failure the total compressive load is carried by two edge strips and the remainder of the plate contributes virtually nothing. This has led to the effective width concept suggested by von Karman et al (3). To obtain the

effective width of a plate they assumed that

1. The plate is initially perfect.
2. The stress is uniformly distributed over the two strips and equal to the maximum value.
3. The two strips have an equal width.

From this assumption, the effective width "b_e" is given by

$$b_e = \frac{1}{\sigma_{x\ max}} \int_{-B/2}^{B/2} \sigma_x \, dx \qquad (7.3)$$

where "B" is actual width of the plate, and
"$\sigma_{x\ max}$" is the value of the longitudinal stress at the unloaded edge.

The average longitudinal stress $\sigma_{x\ ave}$ is given by

$$\sigma_{x\ ave} = \frac{1}{B} \int_{-B/2}^{B/2} \sigma_x \, dx \qquad (7.4)$$

From equations (7.3) and (7.4)

$$b_e/B = \sigma_{x\ ave}/\sigma_{x\ max} \qquad (7.5)$$

Scheer et al (111) suggested a simple approximation to the minimum b_e/B ratio which may be adopted within the scope of the linear plate buckling theory. They assumed that the maximum edge stress is set equal to the yield

stress $\sigma_{x\ max} = \sigma_Y$ and the average stress is set equal to the critical stress $\sigma_{x\ ave} = \sigma_{cr}$. Thus equation (7.5) becomes

$$b_e/B = \sigma_{cr}/\sigma_Y \tag{7.6}$$

and the buckling stress curve can represent the effective width curve.

7.4 Solution of Non-Linear Equilibrium Equations

The strain-displacement relationship (in large deflection theory) has a non-linearity of second order (119), so the energy function has a non-linearity of fourth order. The equilibrium equations, which can be obtained from the first differentiation of the energy function, have a non-linearity of third order. Many numerical methods have been developed to solve this non-linear equation. The solution is usually attempted by one of the four basic techniques

1. Incremental or stepwise procedure.
2. Iterative or Newton method.
3. Step iterative or mixed procedure.
4. Perturbation procedure.

In the first three methods the load is applied first and the displacements obtained from the solution of the equations. These three methods are the most widely used for the solution of non-linear equations (22) and they are explained in detail in many text books (104,119).

In the incremental procedure the load is divided into many small increments which are usually equal. Every time an increment is applied the equations are assumed to be linear during that increment. An increment of the displacement can then be obtained from the solution of the equations. The total displacements can be obtained by accumulating the displacement increments. The procedure is shown in Figure 7.3(a).

In the iterative procedure the structure is fully loaded and the tangent stiffness at the origin is used to obtain the displacements (Figure 7.3(b)). From the equilibrium equations the corresponding load can be calculated, so the out-of-balance load can be obtained. After calculating the displacements due to this out-of-balance load, using the same tangent stiffness, the new out-of-balance load can be obtained. The tangent stiffness may be modified at every iteration (Figure 7.3(c)). This process is repeated until equilibrium is approximated to some acceptable degree, i.e. the out-of-balance loads become sufficiently small.

The mixed procedure is a combination between the incremental and iterative methods. The load is applied in increments and the displacement obtained in every increment by successive iteration. The method is shown in Figure 7.3(d).

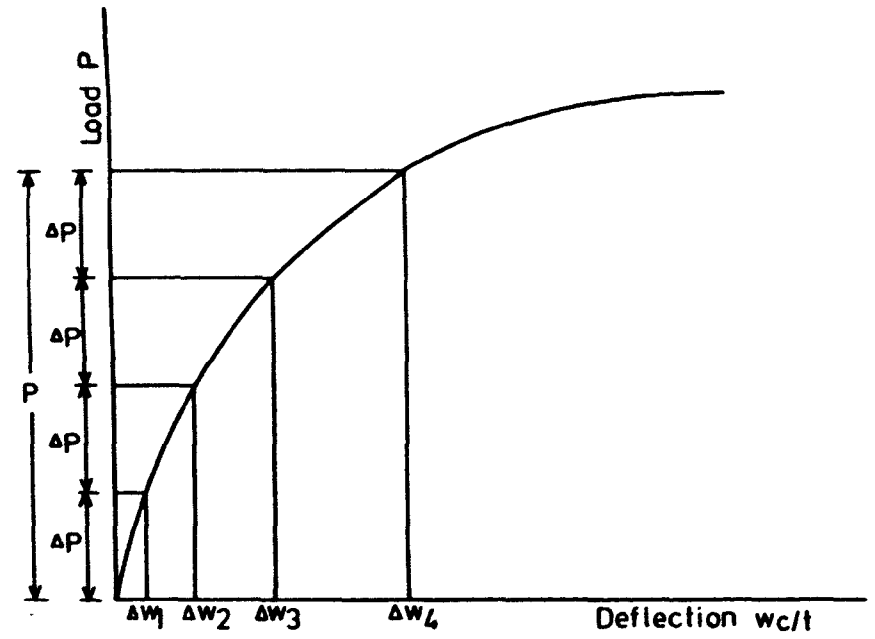

(a) Incremental method.

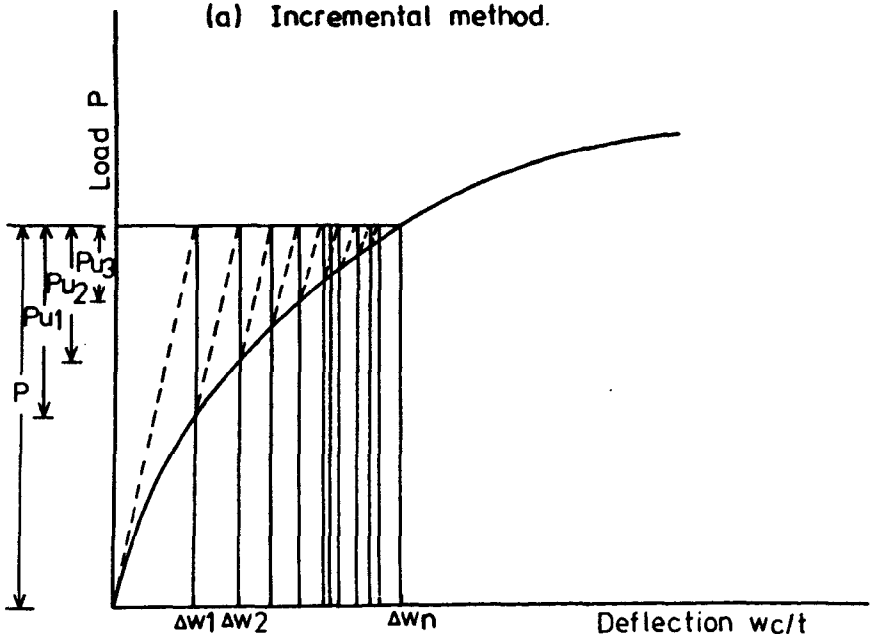

(b) Iteractive method.

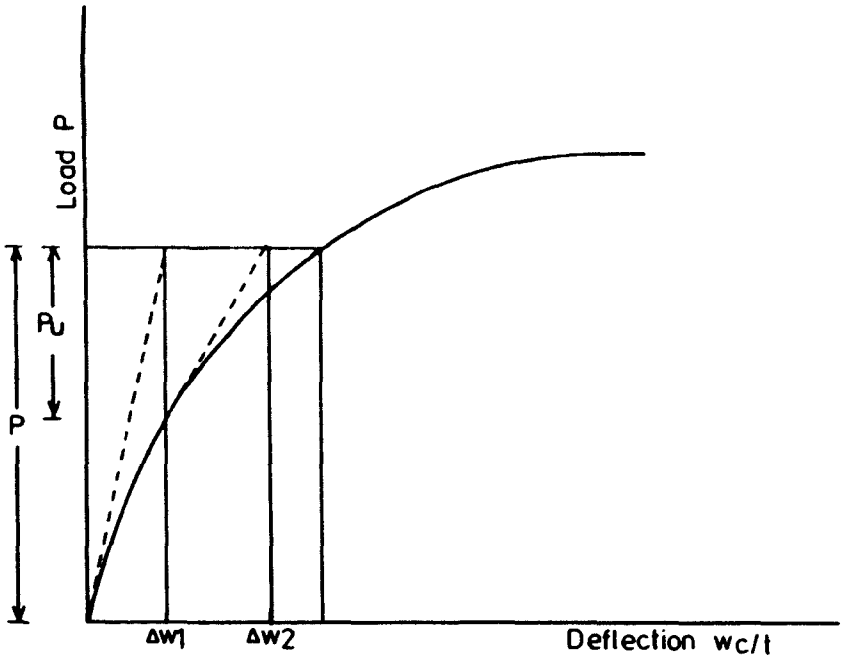

(c) Iterative method

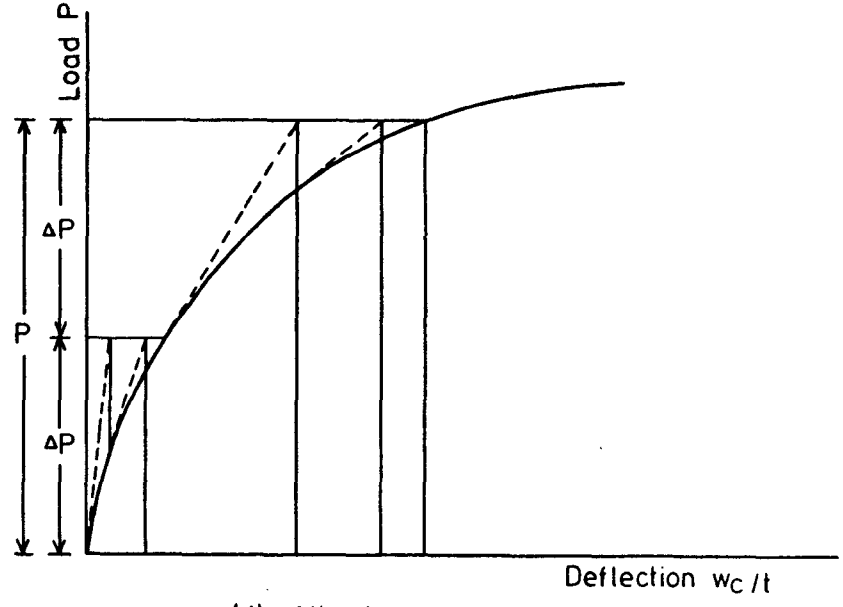

(d) Mixed procedure

FIG. 7·3. SOLUTION OF NON-LINEAR EQUATIONS.

The perturbation method is accurate for moderate non-linearity (22). Compared with the other methods, it is less time consuming (12). The method has been used in both finite element (22) and finite strip (99) post-buckling analysis. In this method the deformation δ_i and the stress σ are expressed in the form of a Maclaurin's series as follows

$$\delta_i = \frac{\partial \delta_i}{S} S + \frac{1}{2} \frac{\partial^2 \delta_i}{S^2} S^2 + \ldots \tag{7.7}$$

$$\sigma = \sigma_{cr} + \frac{\partial \sigma}{\partial S} S + \frac{1}{2} \frac{\partial^2 \sigma}{\partial S^2} S^2 + \ldots \tag{7.8}$$

where " S " is some, as yet undefined, perturbation parameter to be equated to one of the basic incremental variables "δ_i, σ". The derivatives of the equilibrium equations with respect to "S", as many times as is necessary for the required accuracy (12), are zero at "$\sigma = \sigma_{cr}$" and "$\delta_i = 0.0$". These derivatives with equations (7.7) and (7.8) are the basis of the perturbation method. Rojas-Gutierrez (22) discussed in detail the choice of the perturbation parameter " S " necessary for rapid convergence.

7.5 Large Deflection Energy Function of Rectangular Plate

Consider a rectangular plate with thickness "t" and orthogonal co-ordinates x, y and z. The "x" and "y" co-ordinates originate in the middle plane of the plate. The

z co-ordinate is normal to this plane. The change in displacements of any point on the plate due to external load are u, v and w in x, y and z directions respectively. The internal strains at this point are $\{\varepsilon\}$

$$\{\varepsilon\}^T = \{\varepsilon_x \ \varepsilon_y \ \gamma_{xy}\} \tag{7.9}$$

where "ε_x", "ε_y" and "γ_{xy}" are the longitudinal, transverse and the shear strains. These strains are composed of the in-plane strains (linear + nonlinear) and the bending strains. For an imperfect plate these strains include an extra linear term which is a function of the imperfection parameter.

The corresponding stresses are $\{N\}$

$$\{N\}^T = \{N_x \ N_y \ N_{xy}\} \tag{7.10}$$

For elastic material

$$\{N\} = [F] \{\varepsilon\} \tag{7.11}$$

The elastic matrix [F] is given by

$$[F] = \frac{E}{(1-\nu^2)} \begin{bmatrix} 1 & \nu & 0 \\ 0 & 1 & 0 \\ 0 & 0 & \frac{1-\nu}{2} \end{bmatrix} \tag{7.12}$$

where "E" is the elastic modulus,

"ν" is the Possion's ratio.

The strain energy of the plate is generally expressed as

$$W = \frac{1}{2} \int_{vol} \{N\}^T \{\varepsilon\} \, dvol \tag{7.13a}$$

$$= \frac{1}{2} \iiint \{\varepsilon\}^T [F] \{\varepsilon\} \, dx \, dy \, dz \tag{7.13b}$$

$$= \frac{1}{2} \frac{E}{(1-\nu^2)} \iiint (\varepsilon_x^2 + 2\nu \, \varepsilon_x \, \varepsilon_y + \varepsilon_y^2 + \frac{1-\nu}{2} \gamma_{xy}^2) dx \, dy \, dz \tag{7.13c}$$

7.5.1 Perfect Plate

For the large deflection analysis of a perfect plate, the strain-displacement relationship is given by

$$\{\varepsilon\} = \{\varepsilon_O\} + \{\varepsilon_N\} - z \{K\} \tag{7.14}$$

where $\{\varepsilon_O\}$ is the linear in-plane strain,

$\{\varepsilon_N\}$ is the non-linear strain due to the deflection of the middle plane,

$\{K\}$ is the curvature of the middle plane,

"z" is the depth of the point from the middle plane.

$$\{\varepsilon_O\}^T = \{\varepsilon_{xO} \; \varepsilon_{yO} \; \gamma_{xyO}\} \tag{7.15a}$$

$$= \{u_{,x} \; v_{,y} \; (u_{,y} + v_{,x})\} \tag{7.15b}$$

$$\{\varepsilon_N\}^T = \{\frac{1}{2} w_{,x}^2 \quad \frac{1}{2} w_{,y}^2 \quad w_{,x} \; w_{,y}\} \tag{7.16}$$

$$\{K\}^T = \{K_x \quad K_y \quad K_{xy}\} \tag{7.17a}$$

$$= \{w_{,xx} \quad w_{,yy} \quad 2w_{,xy}\} \tag{7.17b}$$

From equations (7.15b), (7.16) and (7.17b) equation (7.14) can be expressed by

$$\varepsilon_x = u_{,x} + \frac{1}{2} w_{,x}^2 - z\, w_{,xx} \tag{7.18a}$$

$$\varepsilon_y = v_{,y} + \frac{1}{2} w_{,y}^2 - z\, w_{,yy} \tag{7.18b}$$

$$\gamma_{xy} = u_{,y} + v_{,x} + w_{,x}\, w_{,y} - 2z\, w_{,xy} \tag{7.18c}$$

Substituting equation (7.18) into equation (7.13c) and integrating with respect to "z" to obtain the strain energy in terms of the displacements

$$W = \frac{1}{2} D \iint [w_{,xx}^2 + 2\nu\, w_{,xx}\, w_{,y} + w_{,yy}^2 + 2(1-\nu^2)\, w_{,xy}^2]\, dx\, dy$$

$$+ \frac{1}{2} F \iint [(u_{,x} + \frac{1}{2} w_{,x}^2)^2 + 2\,(u_{,x} + \frac{1}{2} w_{,x}^2)(v_{,y} + \frac{1}{2} w_{,y}^2)$$

$$+ (v_{,y} + \frac{1}{2} w_{,y}^2)^2 + \frac{1-\nu}{2} (u_{,y} + v_{,x} + w_{,x}\, w_{,y})^2]\, dx\, dy \tag{7.19}$$

where $D = \dfrac{E\, t^3}{12(1-\nu^2)}$ (7.20)

$$F = \frac{E\, t}{(1-\nu^2)} \tag{7.21}$$

The first term of equation (7.19) represents the strain energy of bending and the second term represents the strain energy of stretching of the plate.

7.5.2 Imperfect Plate

Consider now the same plate but with an initial imperfection. The total lateral displacement at a point is given by

$$w_t = w + w^o \tag{7.22}$$

where "w^o" is the initial imperfection at this point.

The strain displacement relationship for this plate can be obtained by modifying equation (7.18) (119).

$$\varepsilon_x = u_{,x} + \frac{1}{2} w_{,x}^2 - z\, w_{,xx} + w_{,x}\, w_{,x}^o \tag{7.23a}$$

$$\varepsilon_y = v_{,y} + \frac{1}{2} w_{,y}^2 - z\, w_{,yy} + w_{,y}\, w_{,y}^o \tag{7.23b}$$

$$\gamma_{xy} = u_{,y} + v_{,x} + w_{,x}\, w_{,y} - z\, 2w_{,xy} + w_{,y}\, w_{,x}^o + w_{,x}\, w_{,y}^o \tag{7.23c}$$

Substituting equation (7.23) into equation (7.13c) and integrating with respect to z, the strain energy of an imperfect plate can be obtained

$$W = \frac{1}{2} D \iint [w_{,xx}^2 + 2\nu\, w_{,xx}\, w_{,yy} + w_{,yy}^2 + 2(1-\nu^2)\, w_{,xy}^2]\, dx\, dy$$

$$+ \frac{1}{2} F \iint [(u_{,x} + \frac{1}{2} w_{,x}^2 + w_{,x}\, w_{,x}^{o})^2 + 2\nu\, (u_{,x} + \frac{1}{2} w_{,x}^2$$

$$+ w_{,x}\, w_{,x}^{o})(v_{,y} + \frac{1}{2} w_{,y}^2 + w_{,y}\, w_{,y}^{o}) + (v_{,y} + \frac{1}{2} w_{,y}^2$$

$$+ w_{,y}\, w_{,y}^{o})^2 + \frac{1-\nu}{2} (u_{,y} + v_{,x} + w_{,x}\, w_{,y} + w_{,x}\, w_{,y}^{o}$$

$$+ w_{,y}\, w_{,x}^{o})^2]\, dx\, dy \qquad (7.24)$$

7.6 The Finite Strip Analysis

The solution scheme already employed in the linear analysis of a plate will be used in the present section. The plate is divided into a number of longitudinal strips and displacement and shape functions which satisfy the boundary conditions assumed. The end displacement due to the longitudinal compressive stress is uniform due to the rigid loading bar. Once the potential energy of every strip for a given end displacement has been calculated the linear and the nonlinear equilibrium equations {E} may be obtained from the minimization of the energy function. The stiffness matrix for each strip can be then obtained from the corresponding equilibrium equations. By assuming a pattern of the initial imperfections the strain energy can be modified by the addition of a term which is linear in the displacement field. From the change in the strain energy, the stiffness matrix due to the imperfection can be

obtained. The overall linear and nonlinear stiffness matrices may be assembled and modified to include the effect of the longitudinal boundary conditions. A numerical method, e.g. Newton-Raphson iteration, can be used to solve the nonlinear equations. The deflected form of the plate and the magnitude and distribution of the membrane stresses can then be determined.

7.6.1 The Displacement and the Shape Function

It is difficult to assume a suitable deflection shape for a plate in general. The shape of the buckled plate, after reaching the first stage of buckling, may change as the load is increased beyond its critical value. These changes are always progressive. The aspect ratio of the plate, the in-plane and out-of-plane boundary conditions and the ratio between the applied stress and the critical stress are the factors which control the buckling mode and its changes. The first buckling mode keeps developing until the energy stored is sufficient to carry the plate into a second buckling mode and so on.

The deformed shape of the middle plane of a plate undergoing large deflections can be represented by displacement functions u, v and w in the x, y and z directions respectively. These functions must satisfy the geometric and static boundary conditions. In the following the longitudinal, transverse and out-of-plane displacement functions will be discussed in some detail.

7.6.1.1 The Longitudinal Displacement

The longitudinal compressive stress is assumed to act through a rigid loading bar, so the longitudinal displacement of the loaded edge is uniform. If the longitudinal strain at this edge is "e" the displacement "u" due to this strain is given by

$$u = e\,(\lambda/2 - x) \tag{7.25}$$

For a symmetrical plate the displacement "u" must be antisymmetrical in the longitudinal direction with the value $\pm e\lambda/2$ at the loaded edges. This can be achieved only if the chosen harmonic is $\sin \frac{m\pi x}{\lambda}$, where m = 0, 2, 4, 6,... . So the longitudinal displacement can be represented by

$$u = e(\lambda/2 - x) + \sum_{m=2}^{M} \{X\}^T \{\delta\} \sin \frac{m\pi x}{\lambda} \tag{7.26}$$

where $\{\delta\}$ is the nodal displacement of the strip,

"e" is the shortening of the plate/λ,

M is the number of harmonics chosen for a particular solution. As this number increases, the degrees of freedom increase. It is clear that the longitudinal harmonic series in this function differs from the one used in linear finite strip analysis (Chapter 3).

7.6.1.2 The Transverse Displacement

There are two cases for the transverse displacement functions depending on the conditions of the longitudinal edges of the plate or the conditions of the junctions between plates if a plate assembly is being considered. The first case is applicable for local buckling analysis of a plate while the second is applicable for overall buckling of a structure, i.e. in the first case it is assumed that the junction between plates in the assembly is restrained against out-of-plane displacement while in-plane displacements are allowed. In the second case no restrictions at all are placed on the displacement at those junctions. The second case is more general, more time consuming in computation, and cannot be approximated in the same way as the first (99).

Case I

In this case the transverse deformed shape of the middle plane of the strip is represented by

$$v = fy + \sum_{m}^{M} \{Y\}^T \{\delta\} \cos \frac{m\pi x}{\lambda} \qquad (7.27)$$

where "f" is a variable which controls the amplitude of the displacement function and may take any value. A similar function was assumed by Little (31) in his analysis of a simply supported plate. Graves Smith et al (98) replaced

the variable "f" by "ev" in their large deflection finite strip formulation. It is true that "f" is equal to "ev" as long as the longitudinal stress is equal to or less than the critical. If the applied stress exceeds this critical value the variable "f" may take any value. This displacement function satisfies the in-plane equilibrium equations (Appendix C). It is different from the displacement function used in linear finite strip analysis (Chapter 3). It is accurate for the large deflection analysis of a single plate but only approximate for the case of local post-buckling of a plated structure.

From equation (7.27) it is clear that the loaded edges are allowed to distort in the in-plane transverse direction. The unloaded edges are free to move or are maintained straight and move bodily in this direction. The number of longitudinal harmonic series may be 0, 2, 4, 6,... to achieve a symmetrical in-plane deformed mode.

Case II

This case applies to the unloaded edges of a simply supported plate restrained against any in-plane transverse displacement or where compatibility between the in-plane and out-of-plane displacements along the junctions of a plated structure is required. This is necessary in the overall buckling mode analysis. The displacement function must satisfy the geometric boundary conditions, but not

necessarily the governing differential equations (107). This longitudinal displacement function can be represented by

$$v = \sum_{n=1}^{N} \{Y\}^T \{\delta\} \sin \frac{n\pi x}{\lambda} \qquad (7.28)$$

where N is the number of the harmonic chosen for a particular solution. A similar function was assumed by Timoshenko (3) with N = 1 in his analysis of the post-buckling behaviour of a simply supported plate. He assumed that the longitudinal edges of the plate are restrained against the in-plane transverse displacement. Sridharan (99) used this function in the overall post-buckling analysis of a plated structure. He found that a large number of harmonics are required in this case, leading to a large number of degrees of freedom.

In this case the loaded edge will not distort. It is clear that the longitudinal harmonic of this function is similar to the longitudinal harmonic of the out-of-plane displacement function given in the next section. Moreover, the function is similar to that used in the linear finite strip analysis.

7.6.1.3 The Out-of-Plane Displacement

The displacement function is similar to that used in linear finite strip (discussed in detail in Chapter 3). For the assumption of a simply supported loaded edge the out-

of-plane displacement of a point in the middle plane is given by

$$w = \sum_{n=1}^{N} \{Z\}^T \{\delta\} \sin \frac{n\pi x}{\lambda} \qquad (7.29)$$

This function satisfies the boundary conditions at x = 0 and x = λ where the displacement and the curvature vanish.

$$w = w_{,xx} + \nu\, w_{,yy} = 0.0$$

7.6.1.4 The Shape Functions

The shape functions, which represents the change in the displacement in the transverse direction, are similar to those used in linear finite strip.

$$\{X_{im}\}^T = \{0 \quad 0 \quad 0 \quad C_{(4+2i)m}\}^T \qquad (7.30a)$$

$$\{Y_{im}\}^T = \{0 \quad 0 \quad C_{(3+2i)m} \quad 0\}^T \qquad (7.30b)$$

$$\{Z_{in}\} = \{C_{(2i-1)n} \quad C_{(2i)n} \quad 0 \quad 0\}^T \qquad (7.30c)$$

where "i" is the number of the node,

"C_{kl}" is a polynomial function (k = 1 ∿ 8, l = m or n) given by

$$C_{1n} = b/8\ (1 - 2\eta - 4\eta^2 + 8\eta^3) \qquad (7.31a)$$

$$C_{2n} = 1/2\ (1 - 3\eta + 4\eta^3) \qquad (7.31b)$$

$$C_{3n} = b/8\ (-1 - 2\eta + 4\eta^2 + 8\eta^3) \tag{7.31c}$$

$$C_{4n} = 1/2\ (1 + 3\eta - 4\eta^3) \tag{7.31d}$$

$$C_{5m} = 1/2\ (1 - 2\eta) \tag{7.31e}$$

$$C_{6m} = C_{5m} \tag{7.31f}$$

$$C_{7m} = 1/2\ (1 + 2\eta) \tag{7.31g}$$

and $$C_{8m} = C_{7m} \tag{7.31h}$$

The nodal displacement of a strip $\{\delta\}$ is given by

$$\{\delta_{in}\}^T = \{\theta_{in}\ w_{in}\ \ v_{im}\ u_{im}\}$$

where "i" is the number of the node. If a single harmonic is used for u, v and w, the nodal displacement becomes

$$\{\delta\}^T = \{\theta_{1,1}\ w_{1,1}\ v_{1,0}\ v_{1,2}\ u_{1,2}\ \theta_{2,1}\ w_{2,1}\ v_{2,0}\ v_{2,2}\ u_{2,2}\} \tag{7.32}$$

which means that there will be five degrees of freedom at every node. If two harmonics for the out-of-plane displacement "w" are used, the number of degrees of freedom becomes 11 per node.

In the present analysis the large deflections of a single plate are studied with the displacement function given by

$$u = e(\lambda/2 - x) + \sum_{m=2}^{M} \{X\}^T \{\delta\} \sin \frac{m\pi x}{\lambda}$$

$$v = fy + \sum_{m=2}^{M} \{Y\}^T \{\delta\} \cos \frac{m\pi x}{\lambda}$$

$$w = \sum_{n=1}^{N} \{Z\}^T \{\delta\} \sin \frac{n\pi x}{\lambda}$$

For completeness the analysis based on the displacement function

$$u = e(\lambda/2 - x) + \sum_{m=2}^{M} \{X\}^T \{\delta\} \sin \frac{m\pi x}{\lambda}$$

$$v = \sum_{n=1}^{N} \{Y\}^T \{\delta\} \sin \frac{n\pi x}{\lambda}$$

$$w = \sum_{n=1}^{N} \{Z\}^T \{\delta\} \sin \frac{n\pi x}{\lambda}$$

is given in Appendix D.

7.6.2 Linear and Nonlinear Stiffness Matrix

7.6.2.1 Perfect Plate

To find a relation between the strain at any point on a strip and the nodal displacement of this strip, differentiate equations (7.26), (7.27) and (7.29) and substitute into equation (7.23)

$$\varepsilon_x = - e + \sum_{n=1}^{N} \left(\frac{m\pi}{\lambda} \{X\}^T \{\delta\} \cos \frac{m\pi x}{\lambda} + \frac{1}{2} \frac{n^2 \pi^2}{\lambda^2} \{R\}^T \{\delta\} \cos^2 \right.$$

$$\left. \frac{n\pi x}{\lambda} + \frac{n^2 \pi^2}{\lambda^2} z \{Z\}^T \{\delta\} \sin \frac{n\pi x}{\lambda}\right) \qquad (7.33)$$

$$\varepsilon_y = f + \sum_{n=1}^{N} \left(\{Y'\}^T \{\delta\} \cos \frac{m\pi x}{\lambda} + \frac{1}{2} \{\bar{R}\}^T \{\delta\} \sin^2 \right.$$

$$\left. \frac{n\pi x}{\lambda} - z \{Z''\}^T \{\delta\} \sin \frac{n\pi x}{\lambda}\right) \qquad (7.34)$$

$$\gamma_{xy} = \sum_{n=1}^{N} \left(\{X'\}^T \{\delta\} \sin \frac{m\pi x}{\lambda} - \frac{m\pi}{\lambda} \{Y\}^T \{\delta\} \sin \frac{m\pi x}{\lambda} \right.$$

$$+ \frac{1}{2} \frac{n\pi}{\lambda} \sin \frac{n\pi x}{\lambda} \cos \frac{n\pi x}{\lambda} \{B\}^T \{\delta\} - 2 z \frac{n\pi x}{\lambda} \{Z'\}^T \{\delta\}$$

$$\left. \cos \frac{n\pi x}{\lambda}\right) \qquad (7.35)$$

The vectors $\{R\}$, $\{\bar{R}\}$ and $\{B\}$ are the contribution of the stretching of the middle plane due to the large deflections

$$\{R\}^T = \{\delta\}^T \{Z\} \{Z\}^T \qquad (7.36)$$

$$\{\bar{R}\}^T = \{\delta\}^T \{Z'\} \{Z'\}^T \qquad (7.37)$$

$$\{B\}^T = \{\delta\}^T \{Z'\} \{Z\}^T + \{\delta\}^T \{Z\} \{Z'\}^T \qquad (7.38)$$

Dashes denote differentiation with respect to y.

From equations (7.19), (7.26), (7.27) and (7.29) or from equations (7.13c), (7.33), (7.34) and (7.35) an expression for the strain energy in terms of the nodal

displacements, end shortening and the variable "f" can be obtained. The strain energy of a strip after integration through its depth is given in Table 7.1. It is clear that the highest order term in this equation is of fourth order.

The integration along the length of the strip can be done simply. Performing this integration, the first order terms "W_1" vanish for any value of (m). The quadratic membrane term "W_{2mb}" reduces to

$$W_{2mb} = F \int \lambda \{\delta\}^T \{Y'\} \{Y'\}^T \{\delta\} \, dy \quad \text{at } m = 0 \tag{7.39}$$

The cubic term "W_3" vanishes by integration for all values of "m" and "n" except when "m = 2n", i.e.

$$(n,m) = (1,2),(3,6),(5,10),...$$

The strain energy of the strip after this integration is given in Table 7.2.

For a given end shortening "e" of the plate the variable "f" and the nodal displacement $\{\delta\}$ will have constant values which can be found from the conditions that the strain energy of the plate "W_t" is a minimum; hence

$$\frac{\partial W_t}{\partial f} = 0.0 \tag{7.40}$$

$$\frac{\partial W_t}{\partial \{\delta_\ell\}^T} = 0.0 \tag{7.41}$$

Order	Formulation
Zero	$W_o = \frac{F}{2} \iint (e^2 + f^2 - 2\nu e f)\, dx\, dy$
Linear	$W_1 = \frac{F}{2} \iint C(m) \{2 \psi_3 (\nu f - e) \{X\} + 2(f - \nu e) \{Y'\}\} \{\delta\}\, dx\, dy$
Quadratic (membrane)	$W_{2mb} = \frac{F}{2} \iint \{\delta\}^T [(\psi_3^2 \{X\} \{X\}^T + \{Y'\} \{Y'\}^T + 2\nu \psi_3 \{X\} \{Y'\}^T) C^2(m) + S^2(m) (\frac{1-\nu}{2}) (\{X'\} \{X'\}^T + \psi_3^2 \{Y\} \{Y\}^T - 2\psi_3 \{X'\} \{Y\}^T)] \{\delta\}\, dx\, dy$
Quadratic (bending)	$W_{2b} = \frac{D}{2} \iint \{\delta\}^T [S^2(n) (\psi_1^4 \{Z\} \{Z\}^T - \nu \psi_1^2 (\{Z''\} \{Z\}^T + \{Z\} \{Z''\}^T) + \{Z''\} \{Z''\}^T) + C^2(n) (\frac{1-\nu}{2}) 4 \psi_1^2 \{Z'\} \{Z'\}^T] \{\delta\}\, dx\, dy$
Quadratic (stability)	$W_{2s} = \frac{F}{2} \iint \{C^2(n) \psi_1^2 (\nu f - e) \{R\} + S^2(n) (f - \nu e) \{\bar{R}\}\} \{\delta\}\, dx\, dy$
Cubic	$W_3 = \frac{F}{2} \iint \{\delta\}^T [\psi_1^2 C^2(n) C(m) \{\psi_3 \{X\} + \nu \{Y'\}\}^T \{R\} + S^2(n) C(m) \{\nu\psi_3 \{X\} + \{Y'\}\}^T \{\bar{R}\} + (\frac{1-\nu}{2}) \psi_1 S(m) S(n) C(n) \{\{X'\} - \psi_3 \{Y\}\}^T \{B\}] \{\delta\}\, dx\, dy$
Quartic	$W_4 = \frac{F}{2} \iint \{\delta\}^T [\frac{\psi 1^4}{4} C^4(n) \{R\} \{R\}^T + \frac{1}{4} S^4(n) \{\bar{R}\} \{\bar{R}\}^T + \psi_1^2 C^2(n) S^2(n) [\frac{\nu}{2} \{R\} \{\bar{R}\}^T + (\frac{1-\nu}{8}) \{B\} \{B\}^T]] \{\delta\}\, dx\, dy$

The strain energy $W = \sum_{n=1}^{N} (W_o + W_1 + W_{2mb} + W_{2b} + W_{2s} + W_3 + W_4)$

$\psi_1 = \frac{n\pi}{\lambda}$ $\quad$ $C(m) = \cos \frac{m\pi x}{\lambda}$

$\psi_3 = \frac{m\pi}{\lambda}$ $\quad$ $S(m) = \sin \frac{m\pi x}{\lambda}$

Table 7.1. The Strain Energy of a Strip

Order	Formulation	No. of harmonic
Zero	$W_o = \frac{F}{2} \int 2\lambda \ (e^2 + f^2 - 2\nu \ ef) \ dy$	
First	$W_1 = 0.0$	
Quadratic (membrane)	$W_{2mb} = F\lambda \int \{\delta\}^T \{Y'\} \{Y'\}^T \{\delta\} \ dy$	m = 0
Quadratic (membrane)	$W_{2mb} = \frac{F\lambda}{2} \int \{\delta\}^T [\psi_3^2 \{X\} \{X\}^T + \{Y'\} \{Y'\}^T + 2\nu \ \psi_3 \{X\} \{Y'\}^T + (\frac{1-\nu}{2}) [\{X'\} \{X'\}^T + \psi_3^2 \{Y\} \{Y\}^T - 2 \psi_3 \{X'\} \{Y\}^T]] \{\delta\} \ dy$	m = 2, 4, 6
Quadratic (bending)	$W_{2b} = \frac{D\lambda}{2} \int \{\delta\}^T [\psi_1^4 \{Z\} \{Z\}^T - \nu \ \psi_1^2 [\{Z''\} \{Z\}^T + \{Z\} \{Z''\}^T] + \{Z''\} \{Z''\}^T + (\frac{1-\nu}{2}) \ 4 \ \psi_1^2 \{Z'\} \{Z'\}^T] \{\delta\} \ dx \ dy$	n = 1, 3, 5
Quadratic (stability)	$W_{2s} = \frac{F\lambda}{2} \int \{\delta\}^T [\psi_1^2 \ (\nu f - e) \ \{Z\} \{Z\}^T + (f - \nu e) \ \{Z'\} \{Z'\}^T] \{\delta\} \ dy$	n = 1, 3, 5
Cubic	$W_3 = \frac{F\lambda}{4} \int \{\delta\}^T [\psi_1^2 \{A_1\} \{R\}^T - \{A_2\}\{\bar{R}\}^T + (\frac{1-\nu}{2}) \ \psi_1 \{A_3\} \{B\}^T] \{\delta\} \ dy$	n = 1, 3, 5 m = 2n
Quartic	$W_4 = \frac{F\lambda}{32} \int \{\delta\}^T [3 \ \psi_1^4 \{R\} \{R\} + 3 \{\bar{R}\} \{\bar{R}\} + 2\nu \ \psi_1^2 \{R\} \{\bar{R}\} + (\frac{1-\nu}{2}) \ \psi_1^2 \{B\} \{B\}] \{\delta\} \ dy$	n = 1, 3, 5
$\{A_1\} = \psi_3 \{X\} + \nu \{Y'\}$ $\{A_2\} = \nu \ \psi_3 \{X\} + \{Y'\}$ $\{A_3\} = \{X'\} - \psi_3 \{Y\}$		m = 2n m = 2, 6, 10

Table 7.2. The Strain Energy of the Strip

where "W_t" is the total strain energy of the plate which can be obtained by the acumulation of the strain energy of all strips. $\{\delta_\ell\}$ is the overall displacement vector. From equation (7.40) and Table 7.2

$$\frac{\partial W_t}{\partial f} = \sum_{1}^{M_s} \frac{F}{2} \int_{-b/2}^{b/2} (4\lambda(f - e\nu) + \lambda \{\delta\}^T [\nu\psi_1^2 \{Z\} \{Z\}^T + \{Z'\}\{Z'\}^T] \{\delta\}) \, dy \qquad (7.42)$$

where "M_s" is the number of strips into which the plate has been divided. Assuming

$$f = f_1 + e\nu \qquad (7.43)$$

equation (7.42) becomes

$$f_1 = \frac{-1}{4b\, M_s} \sum_{1}^{M_s} \int_{-b/2}^{b/2} \{\nu\psi_1^2 \{R\}^T + \{\bar{R}\}^T\} \{\delta\} \, dy \qquad (7.44)$$

For every iteration, the value of "f_1" can be obtained from equation (7.44) and the value of "f" from equation (7.43). Graves Smith et al (98) in their analysis assumed "$f = \nu e$" and did not mention "f_1".

The equilibrium equations {E} can be obtained by minimising the strain energy with respect to the displacement $\{\delta_\ell\}$

$$\{E\} = \partial W_t / \partial \{\delta_\ell\}^T \qquad (7.45a)$$

$$= 0.0 \tag{7.45b}$$

$$= [K]\{\delta_\ell\} \tag{7.45c}$$

where [K] is the overall stiffness matrix. In the following the stiffness matrix for one strip will be obtained and then the overall stiffness matrix will be assembled. Minimising Table 7.2 with respect to {δ}, the strip stiffness matrix has been obtained as shown in Table 7.3. The equilibrium equation of a strip is given by

$$\{E\} = [K]\{\delta\} \tag{7.46}$$

where

$$[K] = [Kl]_{mb} + [Kl]_b + [Kl]_s + [K2] + [K3] \tag{7.47}$$

It is clear from Table 7.3 that the matrices $[Kl]_{mb}$ and $[Kl]_b$ are similar to the inplane stiffness matrix and out-of-plane stiffness matrix obtained in the linear finite strip analysis (Chapter 3), respectively. It is worth noting that neglect of the nonlinearity leads to "$f_1 = 0.0$" and the matrix $[Kl]_s$ will be similar to the stability matrix used in Chapter 3.

By accumulating the equilibrium equations {E} for all strips and solving this nonlinear equation by any numerical method, the post-buckling behaviour of a rectangular plate can be obtained. In the present work,

Order of the equilibrium equation {E}	Formulation of the stiffness matrix	
Linear	$[K1]_{mb} = 2F\lambda \int \{Y'\}\{Y'\}\, dy$	m = 0
	$[K1]_{mb} = F\lambda \int [\psi_3^2 \{X\}\{X\}^T + \{Y'\}\{Y'\}^T + 2\nu\,\psi_3 \{X\}\{Y'\}^T + (\frac{1-\nu}{2})(\{X'\}\{X'\}^T + \psi_3^2 \{Y\}\{Y\}^T - 2\psi_3 \{X'\}\{Y\}^T)]\, dy$	m = 2, 4,.. 6,..
	$[K1]_b = D\lambda \int [\psi_1^4 \{Z\}\{Z\}^T - \nu\,\psi_1^2 (\{Z\}\{Z\}^T)'' + \{Z''\}\{Z''\}^T + 2\psi_1^2 \{Z'\}\{Z'\}^T]\, dy$	n = 1, 3,..
	$[K1]_s = Et\lambda \int [-e\,\psi_1^2 \{Z\}\{Z\}^T + \frac{f_1}{(1-\nu^2)}(\nu\,\psi_1^2 \{Z\}\{Z\}^T + \{Z'\}\{Z'\}^T)]\, dy$	n = 1, 3,..
Nonlinear (quadratic)	$[K2] = \frac{F\lambda}{2} \int [\psi_1^2 (\{R\}\{A_1\}^T + \frac{1}{2}\{A_1\}\{R\}^T) - (\{\bar{R}\}\{A_2\}^T + \frac{1}{2}\{A_2\}\{\bar{R}\}^T + (\frac{1-\nu}{2})\psi_1 (\{B\}\{A_3\}^T + \frac{1}{2}\{A_3\}\{B\})^T]\, dy$	n = 1, 3,.. m = 2n
Nonlinear (cubic)	$[K3] = \frac{F\lambda}{2} \int [\frac{3}{4}\psi_1^4 \{R\}\{R\}^T + \frac{3}{4}\{\bar{R}\}\{\bar{R}\}^T + \frac{\nu}{2}\psi_1^2 \{R\}\{\bar{R}\}^T + (\frac{1-\nu}{8})\psi_1^2 \{B\}\{B\}^T]\, dy$	n = 1, 3

Table 7.3. The Strip Stiffness Matrix

the approach of Clough et al (120) has been used, and in this way an incremental equilibrium equation {ET} can be developed from Table 7.3. Consider two configurations of the strip that are close to each other during deformation as shown in Figure 7.4. Obtaining the equilibrium equations of each of these strip configurations incremental relationships can then be determined by taking the difference between the two. The end shortening parameter "e" is assumed to be increased during this increment to "e + Δe". The incremental equlibrium equations and the incremental stiffness matrix for a strip are given in Table 7.4. The incremental equlibrium equation of the strip {ET} is given by

$$\{ET\} = [KT]\{\Delta\delta\} + \{\Delta P\} \tag{7.48a}$$

$$= 0.0 \tag{7.48b}$$

where

$$[KT] = [KT1]_{mb} + [KT1]_{b} + [KT1]_{s} + [KT2] + [KT3] \tag{7.49}$$

$$\{\Delta P\} = Et\lambda \int [-\Delta e\psi_1^2 \{Z\}\{Z\}^T + \frac{\Delta f_1}{(1-\nu^2)}(\nu\psi_1^2 \{Z\}\{Z\}^T + \{Z'\}\{Z'\}^T)]\{\delta\}\, dy \tag{7.50a}$$

$$= Et\lambda \int (-\Delta e\psi_1^2 \{R\} + \frac{\Delta f_1}{(1-\nu^2)}(\nu\psi_1^2 \{R\} + \{\bar{R}\}))\, dy \tag{7.50b}$$

$\{\Delta P\}$ is an imaginary load vector.

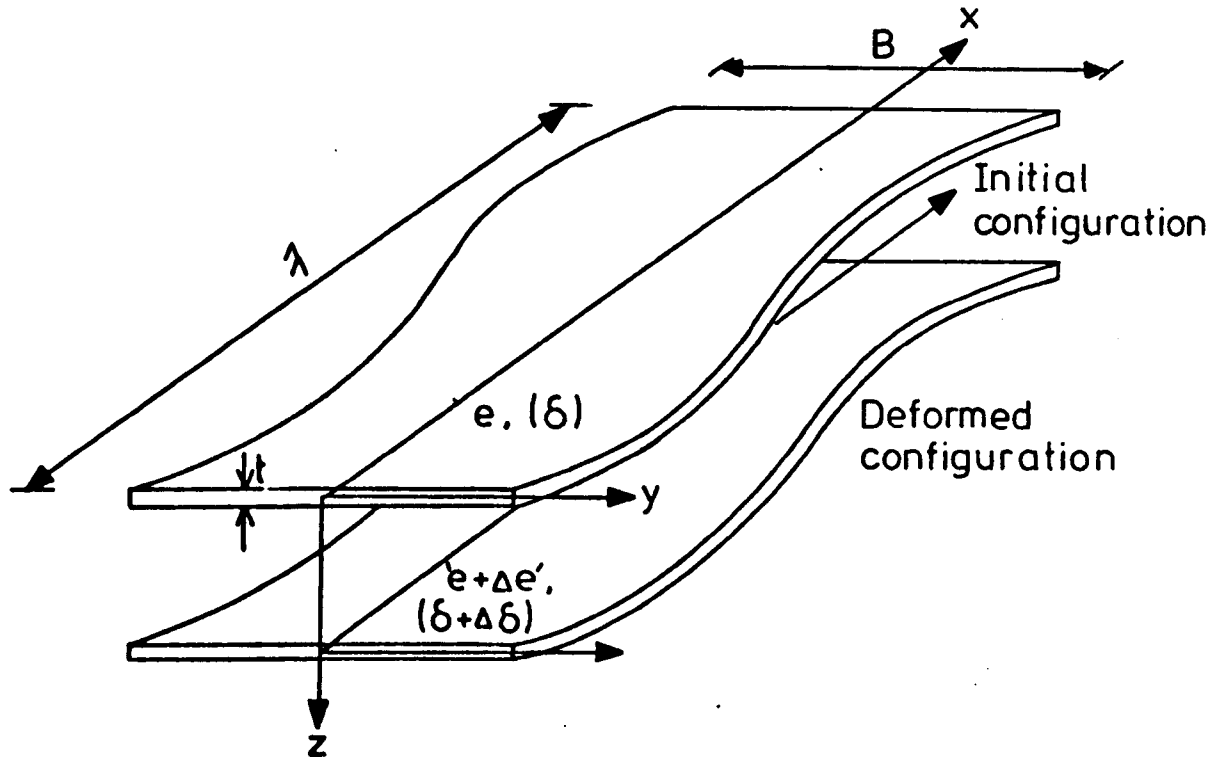

FIG. 7·4. INCREMENTAL DEFORMATION OF A STRIP.

Order of the incremental equilibrium equation	Formulation of the incremental stiffness matrix	
Linear	$[KT1]_{mb} = 2F\lambda \int \{Y'\}\{Y'\}^T dy$	$m = 0$
	$[KT1]_{mb} = F\lambda \int [\psi_3^2 \{X\}\{X\}^T + \{Y'\}\{Y'\}^T + 2\nu\,\psi_3 \{X\}\{Y'\}^T + (\frac{1-\nu}{2})(\{X'\}\{X'\}^T + \psi_3^2 \{Y\}\{Y\}^T - 2\psi_3 \{X'\}\{Y\}^T] dy$	$m = 2, 4, \ldots$
	$[KT1]_b = D\lambda \int [\psi_1^4 \{Z\}\{Z\}^T - \nu\,\psi_1^2 (\{Z\}\{Z\}^T)'' + \{Z''\}\{Z''\}^T + 2\psi_1^2 \{Z'\}\{Z'\}^T] dy$	$n = 1, 3, 5, \ldots$
	$[KT1]_s = Et\lambda \int [-e\,\psi_1^2 \{Z\}\{Z\}^T + \frac{f_1}{(1-\nu^2)}(\nu\,\psi_1^2 \{Z\}\{Z\}^T + \{Z'\}\{Z'\}^T)] dy$	$n = 1, 3, 5, \ldots$
Nonlinear (quadratic)	$[KT2] = \frac{F\lambda}{2} \int [\psi_1^2 (\{R\}\{A_1\}^T + \{A_1\}\{R\}^T) - (\{\bar{R}\}\{A_2\}^T + \{A_2\}\{\bar{R}\}^T) + (\frac{1-\nu}{2})\,\psi_1 (\{B\}\{A_3\}^T + \{A_3\}\{B\}^T)] dy$	$n = 1, 3, 5$ $m = 2n$
Nonlinear (cubic)	$[KT3] = \frac{3F\lambda}{2} \int [\frac{3}{4}\psi_1^4 \{R\}\{R\} + \frac{3}{4}\{\bar{R}\}\{\bar{R}\} + \frac{\nu}{2}\psi_1^2 \{R\}\{\bar{R}\} + (\frac{1-\nu}{8})\,\psi_1^2 \{B\}\{B\}] dy$	$n = 1, 3, 5$

Table 7.4. The Incremental Stiffness Matrix

Comparing the equilibrium equations (Table 7.3) and the incremental equlibrium equations (Table 7.4), it is clear that the linear terms do not change. The quadratic term in the incremental equation is symmetric although it is unsymmetric in Table 7.3. This fact has been noticed by Clough et al (120) and it is important since the incremental matrix will have to be inverted during end shortening incrementation.

7.6.2.2 Imperfect Plate

Assume the initial imperfection of the plate varies sinusoidally in "x" and "y" directions with an amplitude "$\alpha_{nn'}$". The initial displacement (w^o) of any point is given by

$$w^o = \sum_{n=1}^{N} \sum_{\bar{n}=1}^{\bar{N}} \alpha_{n\bar{n}} \sin \frac{n\pi x}{\lambda} \cos \frac{\bar{n}\pi y}{B} \qquad (7.51)$$

In the longitudinal direction this pattern is similar to the deformation of the plate after buckling. For simplicity assume $\bar{n}=1$, i.e. the initial deflection of the plate has one half wave in the transverse direction ($\alpha_{n\bar{n}} = \alpha_n$).

The initial imperfection of every strip relative to its local axes is given by

$$w^o = \sum_{n=1}^{N} \alpha_n \sin \frac{n\pi x}{\lambda} \cos \frac{\pi \bar{y}}{b} \qquad (7.52)$$

where $\bar{y} = (y + 0.5\ \beta b)/M_s$ (7.53)

b = the breadth of the strip

where M_s = total number of strips

β = a factor depending on the position of the strip relative to the plate given by

$$\beta = 2(L - \frac{M_{s+1}}{2}) \tag{7.54}$$

L = the strip number, for left edge strip L = 1 and for right edge strip L = M_s.

From equations (7.24), (7.26), (7.27) (7.29) and (7.52) the change in the strain energy $\bar{W}$ due to the initial imperfection can be obtained. The results are given in Table 7.5.

$$\bar{W} = \sum_{n=1}^{N} (\bar{W}_1 + \bar{W}_{20} + \bar{W}_{2i} + \bar{W}_3) \tag{7.55}$$

The results of integrating this strain energy function with respect to x are given in Table 7.6. The quadratic term due to the interaction between the membrane and bending strains will vanish for all values of m and n except when m = 2n, i.e.

$$(n,m) = (1,2), (3,6), (5,10), \ldots$$

Accumulating the total strain energy functions for all strips and minimising it with respect to f, equation (7.42) becomes

Order	Formulation
Linear	$\bar{w}_1 = F\,\alpha_n \iint \{\delta\}^T \{\psi_1^2\,(\nu f - e)\,C^2(n)\cos\frac{\pi\bar{y}}{b}\{z\} - \psi_2\,(f - \nu e)\,S^2(n)\sin\frac{\pi\bar{y}}{b}\{z'\}\}\,dx\,dy$
Quadratic (bending)	$\bar{w}_{2b} = \frac{1}{2}F\alpha_n^2 \iint \{\delta\}^T [\cos^2\frac{\pi\bar{y}}{b}\psi_1^2 C^2(n)\,(\psi_1^2 C^2(n)\{z\}\{z\}^T + (\frac{1-\nu}{2})\,S^2(n)\{z'\}\{z'\}^T)$ $+ \sin^2\frac{\pi\bar{y}}{b}\psi_2^2 S^2(n)\,(\psi_1^2 C^2(n)\,(\frac{1-\nu}{2})\{z\}\{z\}^T + S^2(n)\{z'\}\{z'\}^T)$ $- \sin\frac{2\pi\bar{y}}{b}\psi_1^2\psi_2 C^2(n)S^2(n)\,(\frac{1+\nu}{2})\{z\}\{z'\}^T]\{\delta\}\,dx\,dy$
Quadratic (interaction between membrane and bending)	$\bar{w}_{2i} = F\,\alpha_n \iint \{\delta\}^T [\psi_1^2 C(m)\,C^2(n)\cos\frac{\pi\bar{y}}{b}\{A_1\}\{z\}^T - \psi_2 C^2(m)\,S(n)\sin\frac{\pi\bar{y}}{b}\{A_2\}\{z'\}^T$ $- (\frac{1-\nu}{2})\psi_1 C(n)S(n)S(m)\{A_3\}\{\psi_2\sin\frac{\pi\bar{y}}{b}\{z\} - \cos\frac{\pi\bar{y}}{b}\{z'\}\}^T]\{\delta\}\,dx\,dy$
Cubic	$\bar{w}_3 = \frac{1}{2}F\,\alpha_n \iint \{\delta\}[\cos\frac{\pi\bar{y}}{b}\psi_1^2 C^2(n)\,(\psi_1^2 C^2(n)\{R\}\{z\}^T + S^2(n)(\nu\{\bar{R}\}\{z\}^T + (\frac{1-\nu}{2})\{B\}\{z'\}^T))$ $- \sin\frac{\pi\bar{y}}{b}\psi_2 S^2(n)\,(S^2(n)\{\bar{R}\}\{z'\}^T + \psi_1^2 C^2(n)\,(\nu\{R\}\{z'\}^T + (\frac{1-\nu}{2})\{B\}\{z\}^T)]\{\delta\}\,dx\,dy$
$\psi_1 = \frac{n\pi}{\lambda}$ $\psi_2 = \frac{\pi}{M_s.b}$ $C(n) = \cos\psi_1 x$ $S(n) = \sin\psi_1 x$	

Table 7.5. The Strain Energy Due to Initial Imperfection

Order	Formulation	
Linear	$\bar{W}_1 = \lambda F \alpha_n \int \{\delta\}^T \{\psi_1^2 (\nu f - e) \cos \frac{\pi\bar{y}}{b} \{z\} - \psi_2 (f - \nu e) \sin \frac{\pi\bar{y}}{b} \{z'\}\} dy$	$n = 1, 3, 5, \ldots$
Quadratic (bending)	$\bar{W}_{2b} = \frac{1}{8} F\lambda \alpha_n^2 \int \{\delta\}^T [\cos^2 \frac{\pi\bar{y}}{b} \psi_1^2 (3\psi_1^2 \{z\} \{z\}^T + (\frac{1-\nu}{2}) \{z'\} \{z'\}^T)$ $+ \sin^2 \frac{\pi\bar{y}}{b} \psi_2^2 (3 \{z'\} \{z'\}^T + \psi_1^2 (\frac{1-\nu}{2}) \{z\} \{z\}^T)$ $- \sin \frac{2\pi\bar{y}}{b} \psi_1^2 \psi_2 (\frac{1+\nu}{2}) \{z\} \{z'\}^T] \{\delta\} dy$	$n = 1, 3, 5, \ldots$
Quadratic (interaction between membrane and bending)	$\bar{W}_{2i} = \frac{1}{2} F\lambda \alpha_n \int \{\delta\}^T [\psi_1 \cos \frac{\pi\bar{y}}{b} (\psi_1 \{A_1\} \{z\}^T + (\frac{1-\nu}{2}) \{A_3\} \{z'\})$ $+ \psi_2 \sin \frac{\pi\bar{y}}{b} (\{A_2\} \{z'\} - (\frac{1-\nu}{2}) \psi_1 \{A_3\} \{z\})] \{\delta\} dy$	$n = 1, 3, 5$ $m = 2n$ $= 2, 6, 8$
Cubic	$\bar{W}_3 = \frac{1}{8} F\lambda \alpha_n \int \{\delta\}^T [\cos \frac{\pi\bar{y}}{b} \psi_1^2 (3 \psi_1^2 \{R\} \{z\}^T + \nu \{\bar{R}\} \{z\}^T + (\frac{1-\nu}{2}) \{B\} \{z'\}^T)$ $- \sin \frac{\pi\bar{y}}{b} \psi_2 (3 \{\bar{R}\} \{z'\} + \psi_1^2 (\nu\{R\} \{z'\}^T + (\frac{1-\nu}{2}) \{B\} \{z\}^T)] \{\delta\} dy$	$n = 1, 3, 5, \ldots$

Table 7.6. The Strain Energy Due to Initial Imperfection

$$\sum_{1}^{M_s}\sum_{n=1}^{N} F\lambda \int_{-b/2}^{b/2} [2(f - e\nu) + \frac{1}{2}\{\delta\}^T [\psi_1^2 \nu \{Z\}\{Z\}^T + \{Z'\}\{Z'\}^T]\{\delta\} + \nu\alpha_n \psi_1^2 \cos\frac{\pi\bar{y}}{b}\{\delta\}^T\{Z\} - \alpha_n \psi_2 \sin\frac{\pi\bar{y}}{b}\{\delta\}^T\{Z'\}] = 0.0 \quad (7.56)$$

Substituting equation (7.43) into (7.56), f_1 can then be expressed as follows

$$f_1 = \frac{-1}{4M_s b}\sum_{1}^{M_s}\sum_{n=1}^{N}\int_{-b/2}^{b/2} \{\psi_1^2 \nu\{R\} + \{\bar{R}\} + 2\nu\alpha_n \psi_1^2 \cos\frac{\pi\bar{y}}{b}\{Z\} - 2\alpha_n \psi_2 \sin\frac{\pi\bar{y}}{b}\{Z'\}\}^T\{\delta\}\, dy \quad (7.57)$$

To integrate the third term and the fourth term in this equation, where $\{Z\}$ and $\bar{y}$ are functions of y, the approach of integration by parts has been used (Appendix E).

Minimizing the strain energy function given in Table 7.6 with respect to the displacement $\{\delta\}$, the change in the equilibrium equations due to the initial imperfection can be obtained as shown in Table 7.7.

$$\{\bar{E}\} = \{P\} + [KO]\{\delta\} \quad (7.58)$$

The vector $\{P\}$ in Table 7.7 is an imaginery load vector dependent on the amplitude of the initial imperfection. The change in the stiffness matrix due to this

Order of the equilibrium equation	Change on the equilibrium equation	Formulation	
Zero	$\{P\}$	$\{P\} = \lambda F \alpha_n \int \{\psi_1^2 (\nu f - e) \cos \frac{\pi \bar{y}}{b} \{z\} - \psi_2 (f - \nu e) \sin \frac{\pi \bar{y}}{b} \{z\}\} dy$	$n = 1, 3, 5, \ldots$
First (bending)	$[K01]_b \{\delta\}$	$[K01]_b = \frac{1}{4} F\lambda \alpha_n^2 \int [\cos^2 \frac{\pi \bar{y}}{b} \psi_1^2 (3 \psi_1^2 \{z\} \{z\}^T + (\frac{1-\nu}{2}) \{z'\} \{z'\}^T) + \sin^2 \frac{\pi \bar{y}}{b} \psi_2^2 (3 \{z'\} \{z'\}^T + \psi_1^2 (\frac{1-\nu}{2}) \{z\} \{z\}^T) - \sin \frac{2\pi \bar{y}}{b} \psi_1^2 \psi_2 (\frac{1+\nu}{2}) \{z\} \{z'\}^T] dy$	$n = 1, 3, 5, \ldots$
First (interaction between membrane and bending)	$[K01]_i \{\delta\}$	$[K01]_i = \frac{1}{2} F\lambda \alpha_n \int [\psi_1^2 \cos \frac{\pi \bar{y}}{b} (\{A_1\} \{z\}^T + \{z\} \{A_1\}^T) + (\frac{1-\nu}{2}) \psi_1 \cos \frac{\pi \bar{y}}{b} (\{A_3\} \{z'\}^T + \{z'\} \{A_3\}^T) + \psi_2 \sin \frac{\pi \bar{y}}{b} (\{A_2\} \{z'\}^T + \{z'\} \{A_2\}^T) - (\frac{1-\nu}{2}) \psi_1 \psi_2 \sin \frac{\pi \bar{y}}{b} (\{A_3\} \{z\}^T + \{z\} \{A_3\}^T)] dy$	$n = 1, 3, 5, \ldots$ $m = 2n$ $= 2, 6, 10$
Quadratic	$[K02] \{\delta\}$	$[K02] = \frac{3}{8} F\lambda \alpha_n \int [\cos \frac{\pi \bar{y}}{b} \psi_1^2 (3 \psi_1^2 \{R\} \{z\}^T + \nu \{\bar{R}\} \{z\}^T + (\frac{1-\nu}{2}) \{B\} \{z'\}^T) - \sin \frac{\pi \bar{y}}{b} \psi_2 (3 \{\bar{R}\} \{z'\} + \psi_1^2 (\nu \{R\} \{z'\}^T + (\frac{1-\nu}{2}) \{B\} \{z\}^T)] dy$	$n = 1, 3, 5, \ldots$

Table 7.7. The Stiffness Matrix Due to Initial Imperfection

imperfection is given by

$$[KO] = [KO1]_b + [KO1]_i + [KO2] \tag{7.59}$$

All the integration with respect to y necessary to obtain the matrix [KO] (Table 7.7) can be carried out by parts. The change in the incremental stiffness matrix due to the initial imperfection can be obtained from Table 7.7. The vector {P} becomes {ΔP} by this increment but the two matrices $[KO1]_b$ and $[KO1]_i$ will not change. Multiplying the matrix [KO2] by a factor of order 2.0 enables the incremental one to be obtained. The incremental matrix of a strip [KOT] is given by

$$[KOT] = [KO1]_b + [KO1]_i + 2\,[KO2] \tag{7.60}$$

It is clear that the matrices [KO] and [KOT] are symmetrical matrices and this is an advantage of this approach since the matrix [KOT] + [KT] will have to be inverted during an increment of the end shortening.

The incremental load vector is given by

$$\{\Delta P\} = -\lambda\, Et\, \alpha_n\, \psi_1^{\,2}\, \Delta e \int \cos \frac{\pi \bar{y}}{b} \{Z\}\, dy$$

$$+ \frac{\lambda Et\, \alpha_n}{(1-\nu^2)} \Delta f_1 \int (\psi_1^{\,2}\, \nu \cos \frac{\pi \bar{y}}{b} \{Z\} - \psi_2 \sin \frac{\pi \bar{y}}{b} \{Z'\})\, dy \tag{7.61}$$

7.7 The Boundary Conditions

In the linear finite strip method only the out-of-plane boundary conditions of the longitudinal edge have any real effect on the pre-buckling behaviour of the structure. For the large deflection analysis not only the out-of-plane but also the in-plane boundary conditions affect the post-buckling results.

The loaded boundaries of the plate are taken to be simply supported (fundamental assumptions), with zero shear stress. The edges are maintained straight but move longitudinally under the applied longitudinal compressive stress (on the assumption that very rigid loading bars are present). These conditions may be written as

at $x = 0 \ \& \ \lambda$

$$w = w_{,xx} + \nu \, w_{,yy} = 0.0 \tag{7.62}$$

$$u = \pm \, e\lambda/2 \tag{7.63}$$

$$N_{xy} = 0.0 \tag{7.64}$$

The boundary conditions of the unloaded edges can be divided into

(a) out-of-plane boundary condition,

(b) in-plane boundary condition.

Considering the in-plane condition, there are two types of boundary as specified in reference (12)

b-i) The edges are free to move,

b-ii) The edges are maintained straight.

In the following these conditions will be discussed.

a) Out-of-plane boundary condition

The unloaded edges are simply supported and the shear stress is zero. This may be written as

at $y = \pm B/2$

$$w = w_{,yy} + \nu\, w_{,xx} = 0.0 \tag{7.65}$$

$$N_{xy} = 0.0 \tag{7.66}$$

b) In-plane boundary conditions

Case (b-i)

The edges are free to move in the plane of the plate. The stress resultant vanishes at this edge

at $y = \pm B/2$

$$v = \text{arbitrary} \tag{7.67}$$

$$N_y = 0.0 \tag{7.68}$$

Case (b-ii)

The unloaded edges are maintained straight by a distribution of normal stress, the resultant of which is zero. The edges may move bodily in the plane of the plate.

at $y = \pm B/2$

$$v_{,x} = 0.0 \tag{7.69}$$

$$\int_0^{\lambda} N_y \, dx = 0.0 \tag{7.70}$$

CHAPTER 8

THE COMPUTER PROGRAM

The computer program (written in Fortran IV) developed previously for the linear finite strip analysis has been extended to include the effects of large deflections and initial imperfections. There are four stages to this program:

1. Calculate the critical stress
2. Obtain the deformations at different points
3. Find the distribution of stresses and strains
4. Calculate the average longitudinal compressive stress

From the average stress and the maximum stress at the unloaded edges the effective width can be obtained. At first the program is used for the case where the transverse displacement "v" and the out-of-plane displacement "w" have different longitudinal harmonic series. Then, by modification of some constants, the same program can be used for the case where "v" and "w" have the same longitudinal harmonic series. This case is considered at the end of this chapter.

It is clear from Chapter 7 that the analysis makes use of two types of matrices. The first does not depend on the displacements and for this reason it is generated only once at the first cycle of the program and stored

for future use. This type corresponds to the linear equilibrium equations and throughout this work these will be termed "linear matrices". For a perfect plate divided into a number of similar strips, the linear matrices are the same for all strips, so only one strip will be considered in this case. The second type of matrix is a function of the deformation and needs to be generated at every increment of the end shortening. From these matrices the non-linear equilibrium equation can be obtained and so these will be termed "nonlinear matrices".

Figure 8.1 is a flow diagram of this computer program showing the main operations for the analysis of perfect or imperfect plates. As a first step only one term in the harmonic series has been considered. This single harmonic is chosen to reduce the number of degrees of freedom. It is assumed that n = 1 and m = 2. The main routines in the program are

1. Routine to generate linear matrices
   a - stiffness and stability matrices
   b - imperfect matrices
2. Routine to generate nonlinear matrices
   a - perfect matrix
   b - imperfect matrix
3. Routine to impose geometric boundary conditions
4. Routine to solve the equilibrium equations
5. Routine to calculate the stress and strain distribution.

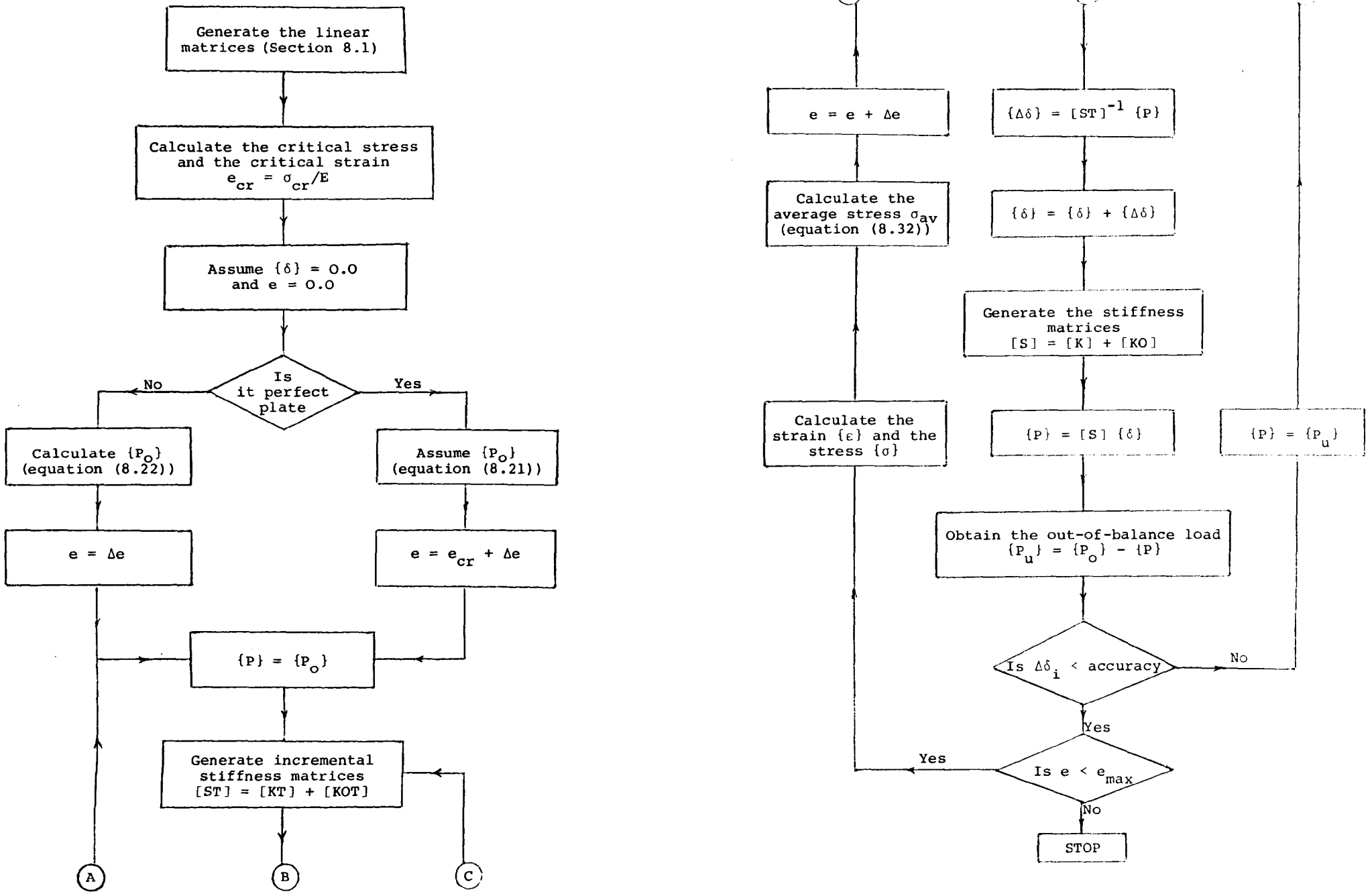

Figure 8.1. Flow Diagram for the Computer Program

In this chapter these routines will be described in some detail. The program will be checked for the case of a square, simply supported plate with different levels of imperfection under in-plane compressive stress.

8.1 Routine to Generate the Linear Matrices

8.1.1 Perfect Stiffness and Stability Matrices

For a perfect plate the same routines given in Chapter 3 will be used to generate the stiffness and the stability matrices of the strips. Once the overall matrix of the plate has been assembled use of the Wittrick-Williams algorithm enables the critical buckling load to be obtained. The critical end shortening parameter, e_{cr} is given by

$$e_{cr} = \sigma_{cr}/E \tag{8.1}$$

for the case of free transverse displacement of the unloaded edges. If this displacement is prevented equation (8.1) becomes

$$e_{cr} = (1-\nu^2)\ \sigma_{cr}/E \tag{8.2}$$

8.1.2 Imperfect Linear Matrices

Due to the initial imperfection the linear stiffness matrix will be modified. This modified matrix depends on the pattern of the initial out-of-flatness and on the

position of the strip. This matrix can be divided into two matrices. The first is an out-of-plane matrix given by

$$KOl_{i,j} = \int_{-b/2}^{b/2} (C_1 z_i z_j + C_2 z_i' z_j' + \cos \frac{2\pi\bar{y}}{b} (C_3 z_i' z_j' + C_4 z_i z_j) - \sin \frac{2\pi\bar{y}}{b} (C_5 z_i z_j')) dy \quad (8.3)$$

where C_1, C_2, ... are constants which can be obtained from Table 7.7 and the vector {Z} is given by equation (7.30c). Integrating this equation by parts the matrix can be obtained. Since $\bar{y}$ depends on the position of the strip, the matrix must be generated for each strip. The overall matrix may then be assembled and stored. This matrix has to be generated only once after which the program may use it at every increment of the end shortening.

The second matrix is generated from the interaction between the in-plane and out-of-plane shape functions, it is a symmetrical matrix given by

$$KOl_{i,j} = \int_{-b/2}^{b/2} (\cos \frac{\pi\bar{y}}{b} (C_6 al_i z_j + C_7 a3_i z_j') + \sin \frac{\pi\bar{y}}{b} (C_8 a2_i z_j' + C_9 a3_i z_j)) dy \quad (8.4)$$

where a's are the element of the vector {A}.

$$al_i = \frac{2\pi}{\lambda} x_i + \nu y_i \quad (8.5)$$

$$a2_i = \frac{2\nu\pi}{\lambda} x_i + y_i' \tag{8.6}$$

$$a3_i = x_i' - \frac{2\pi}{\lambda} y_i \tag{8.7}$$

The vectors {X} and {Y} are given by equations (7.30a) and (7.30b) respectively. The matrix may be integrated by parts, assembled into the overall matrix and stored. If α_n = 0.0 (perfect plate) the program will omit this routine.

8.2 Routine to Generate the Nonlinear Matrices

8.2.1 Perfect Strip

This matrix depends on the displacements of the strip, so it must be generated for every strip. At every increment of the end shortening the displacements change and the matrix has to be regenerated. In the present work at every iteration during the increment, the matrix is updated using the final displacements. The matrix can be divided into an out-of-plane matrix and a matrix covering the interaction between out-of-plane and membrane effects. The out-of-plane matrix is a symmetrical matrix given by

$$K3_{i,j} = \int_{-b/2}^{b/2} (C_{10}\, r_i\, r_j + C_{11}\, \bar{r}_i\, \bar{r}_j + C_{12}\, r_i\, \bar{r}_j + C_{13}\, b_i\, b_j)\, dy \tag{8.8}$$

where r, $\bar{r}$ and b are the elements of the vectors {R}, {$\bar{R}$} and {B} respectively. All these vectors are functions of the displacement given by

$$\{R\} = \{Z\}\ \{Z\}^T\ \{\delta\}$$

$$\{\bar{R}\} = \{Z'\}\ \{Z'\}^T\ \{\delta\}$$

$$\{B\} = \{Z\}\ \{Z'\}^T\ \{\delta\} + \{Z'\}\ \{Z\}^T\ \{\delta\}$$

It is clear that all these vectors are generated from the multiplication of constant matrices with the displacement vector. These matrices are generated only once and then stored for use at every iteration. They are identical for similar strips and thus only one strip will be considered to obtain the matrices $\{Z\}\ \{Z\}^T$, $\{Z'\}\ \{Z'\}^T$ and $\{Z\}\ \{Z'\}^T$. Having generated the matrix [K3] for every strip, the overall matrix can be obtained.

The matrix due to the interaction between the in-plane and the out-of-plane displacement is unsymmetrical. Not all the elements of the matrix have been calculated but only the elements which are given by

$$K2_{i,j} = \int_{-b/2}^{b/2} (C_{14}\ r_i\ al_j + C_{15}\ \bar{r}_i\ a2_j + C_{16}\ b_i\ a3_j)\ dy \qquad (8.9)$$

The other elements can be obtained from

$$K2_{j,i} = \frac{1}{2} K2_{i,j} \tag{8.10}$$

In the program the vectors {A1}, {A2} and {A3} are generated only once and stored for use at every iteration.

8.2.2 Imperfect Strip

This matrix is an out-of-plane symmetrical matrix. Knowing the vectors {R}, {$\bar{R}$} and {B} from the previous routine this matrix can be generated simply from the following equation

$$KO2_{i,j} = \cos \frac{\pi \bar{y}}{b} (C_{17}\, r_i\, z_j + C_{18}\, \bar{r}_i\, z_j + C_{19}\, b_i\, z'_j) + \sin \frac{\pi \bar{y}}{b} (C_{20}\, \bar{r}_i\, z'_j + C_{21}\, r_i\, z'_j + C_{22}\, b_i\, z_j) \tag{8.11}$$

The integrations have been carried out by parts, then repeated for all the other strips and the overall matrix assembled. If the plate is perfect ($\alpha_n = 0.0$) the program will omit this routine.

8.3 Routine to Impose Geometric Boundary Conditions

For the out-of-plane boundary conditions the same routine given in Chapter 3 will be used. In the present routine the in-plane boundary conditions will be considered. There are two cases for the in-plane boundary

conditions at the unloaded edges. Only the case where these edges are maintained straight have been included in the present routine. It can be expressed as (using equations (7.69) and (7.70))

$$v = \text{constant} \qquad \text{at } y = \pm B/2$$

$$v_{,x} = 0.0 \qquad \text{at } y = \pm B/2$$

$$\int N_y \, dx = 0.0 \qquad \text{at } y = \pm B/2$$

The transverse displacement is given by

$$v = \{Y\} \{\delta\} \cos \frac{m\pi x}{\lambda} + fy$$

by differentiation

$$v_{,x} = \frac{-m\pi}{\lambda} \{Y\} \{\delta\} \sin \frac{m\pi x}{\lambda} \tag{8.12}$$

substitute by $y = \pm B/2$ into equation (8.12), it gives

$$\sin \frac{m\pi x}{\lambda} \delta_3 = \sin \frac{m\pi x}{\lambda} \delta_{4(M_s+1)} = 0.0 \tag{8.13}$$

i.e.

$$\delta_3 = \delta_{4(M_s+1)} = 0.0 \tag{8.14a}$$

or $$m = 0 \tag{8.14b}$$

where δ_3 and $\delta_{4(M_s+1)}$ are the amplitudes of the transverse nodal displacements at the unloaded edges. The

corresponding diagonal elements of the stiffness matrix have been modified as shown in Chapter 3.

Equation (7.70) can be expressed as

$$\sum_{1}^{M_{s/2}} \int \frac{Et}{(1-\nu^2)} (\varepsilon_y + \nu \varepsilon_x) \, dx = 0.0 \qquad (8.15)$$

substitute for ε_x and ε_y by equations (A.1) and (A.2)

$$\sum_{1}^{M_{s/2}} \int (v_{,y} + \nu \, u_{,x}) + \frac{1}{2} (w_{,y}^{\,2} + \nu \, w_{,x}^{\,2}) = 0.0 \qquad (8.16)$$

The displacements u, v and w are given by equations (7.26), (7.27) and (7.29); thus the following equation can be obtained

$$\sum_{1}^{M_{s/2}} \int [f - \nu e) \cos \frac{2\pi x}{\lambda} \{A2\}^T \{\delta\} + \frac{1}{2} \sin^2 \frac{\pi x}{\lambda} \{P'\}^T \{\delta\} + \frac{\pi^2 \nu}{2\lambda^2} \cos^2 \frac{\pi x}{\lambda} \{P\}^T \{\delta\}] \, dx = 0.0 \qquad (8.17)$$

It is clear that this is the same equation as (7.42).

8.4 Routine to Solve the Nonlinear Equilibrium Equations

The general nonlinear equilibrium equation can be expressed as

$$[S] \{\delta\} = \{P\} \qquad (8.18)$$

To trace the post-buckling behaviour of a perfect plate a small constant uniformly distributed load "p" normal to

the original plane of the plate, is maintained on the plate throughout the analysis. The work done by this load is given by

$$W_s = \int\int pw \, dx \, dy \tag{8.19}$$

where w is the out-of-plane displacement,

p is the intensity of the load.

Substituting for w, equation (8.19) becomes

$$W_s = \int\int p \{Z\}^T \{\delta\} \sin \frac{\pi x}{\lambda} \, dx \, dy \tag{8.20a}$$

$$= \frac{4\lambda}{\pi} p \{\frac{b^2}{12} \frac{b}{2} 0 \; 0 \; \frac{-b^2}{12} \frac{b}{2} 0 \; 0\} \{\delta\} \tag{8.20b}$$

$$= \{P\} \{\delta\} \tag{8.20c}$$

where $\{P\}$ is the load vector for a strip

$$\{P\} = \frac{4\lambda}{\pi} p \{\frac{b^2}{12} \frac{b}{2} 0 \; 0 \; \frac{-b^2}{12} \frac{b}{2} 0 \; 0\} \tag{8.21}$$

Then the overall load vector can be obtained from the load vector of one strip. For the case of an imperfect plate this load is replaced by the imaginary load $\{P\}$ which is given by

$$\{P\} = \int [C_{23} \cos \frac{\pi \bar{y}}{b} \{Z\} + C_{24} \sin \frac{\pi \bar{y}}{b} \{Z'\}] \, dy \tag{8.22}$$

Knowing this the load vector for all the other strips may be generated leading to the assembly of the overall load vector.

To solve equation (8.18) Netwon Raphson iteration has been used. In this method the incremental matrices can be used directly (120). The incremental matrices can be obtained as follows:

1. The linear matrices will not change.
2. The nonlinear matrices.
   - i - [KT3] = 3[K3],
   - ii - [KT2] will be symmetrical and given by equation (8.9),
   - iii - [KOT2] = 2[KO2].

8.5 Routine to Calculate the Stress and Strain Distribution

Knowing the nodal displacement $\{\delta\}$, the strains at any point in a perfect plate can be obtained from the following equations

$$\varepsilon_x = - e + \psi_3 \{X\}^T \{\delta\} \cos \psi_3 x + \psi_1^2 z \{Z\}^T \{\delta\} \sin \psi_1 x + \frac{1}{2} \psi_1^2 \{R\}^T \{\delta\} \cos^2 \psi_1 x + \bar{\varepsilon}_x \quad (8.23)$$

$$\varepsilon_y = f + \{Y'\}^T \{\delta\} \cos \psi_3 x - z \{Z''\}^T \{\delta\} \sin \psi_1 x + \frac{1}{2} \{\bar{R}\}^T \{\delta\} \sin^2 \psi_1 x + \bar{\varepsilon}_y \quad (8.24)$$

$$\gamma_{xy} = \{\{X'\} - \psi_3 \{Y\}\}^T \{\delta\} \sin \psi_3 x - 2z \psi_1 \{Z'\}^T \{\delta\} \cos \psi_1 x$$

$$+ \frac{1}{4} \psi_1 \{B\}^T \{\delta\} \sin 2\psi_1 x + \bar{\gamma}_{xy} \qquad (8.25)$$

Only the vectors $\{R\}$, $\{\bar{R}\}$, $\{B\}$ and the factor "f" must be updated at every increment of the end shortening. All the other vectors and constants are calculated once and then used at any increment.

Where $\bar{\varepsilon}_x$, $\bar{\varepsilon}_y$ and $\bar{\gamma}_{xy}$ are the effect of the imperfections on the strains and given by

$$\bar{\varepsilon}_x = \alpha_n \psi_1^2 \{Z\} \{\delta\} \cos^2 \psi_1 x \cos \frac{\pi \bar{y}}{b}$$

$$\bar{\varepsilon}_y = - \alpha_n \psi_2 \{Z'\} \{\delta\} \sin^2 \psi_1 x \sin \frac{\pi \bar{y}}{b}$$

$$\bar{\gamma}_{xy} = \frac{1}{2} \alpha_n \psi_1 \{\{Z'\} - \psi_2 \{Z\}\}^T \{\delta\} \cos \frac{\pi \bar{y}}{b} \sin 2 \psi_1 x$$

The stress at the point can then be obtained from

$$\sigma_x = \frac{Et}{(1-\nu^2)} (\varepsilon_x + \nu \varepsilon_y) \qquad (8.29)$$

$$\sigma_y = \frac{Et}{(1-\nu^2)} (\varepsilon_y + \nu \varepsilon_x) \qquad (8.30)$$

$$\tau_{xy} = \frac{Et}{2(1+\nu)} \gamma_{xy} \qquad (8.31)$$

The mean applied compressive stress in the longitudinal direction σ_{av} is given by

$$\sigma_{av} = \frac{1}{\lambda B} \int_0^{\lambda} \int_{-B/2}^{B/2} \sigma_x \, dx \, dy \qquad (8.32)$$

8.6 Checking the Computer Program

A simply supported square plate under longitudinal in-plane compressive stress will be considered to check the computer program. The unloaded edges are assumed to be maintained straight but able to move bodily. The plate is initially perfect with a thickness to width ratio equal to 0.01. Because the program is not being used for a parametric study at this stage and in order to reduce the number of degrees of freedom and the computing time, the plate is divided into four strips only. A single longitudinal harmonic is used to reduce the number of degrees of freedom per node.

The post-buckling behaviour of this plate is compared in Figure 8.2 with the results presented by Yamaki (11). It is worth mentioning that in their work on the same problem Graves Smith et al (98) divided the plate into 24 strips to obtain a sufficiently accurate result. The present approximation leads to an overestimation in the post-buckling stress of about 11% and 14% at an applied stress level of twice and three times the critical stress respectively.

The same plate with a 0.1t initial imperfection has also been analysed and the results are also shown in Figure 8.2. At a stress equal to the critical, the finite strip underestimates the central deflection by about 11%.

These limited results do no more than indicate the potential of the current method and much additional work would be necessary to assess the accuracy, determine the required number of strips into which each plate should be divided for analysis and so on. Unfortunately due to lack of time this has not been possible.

8.7 Modification of the Program

There are two cases for the in-plane transverse displacement based on the assumed longitudinal harmonic function as described in Section 7.6.1. To consider the case where the transverse displacement "v" and the out-of-plane displacement "w" have the same longitudinal harmonic, the computer program has been modified in the following four areas:

1. The linear stiffness matrix used in Chapter 3 is modified by using the constant given in Table D. 3 instead of the constant given by equation (3.98).

2. The variable "f" vanishes and equations (7.38) and (7.50) become

$$f_1 = - e\nu$$

3. The vectors $\{A_1\}$, $\{A_2\}$ and $\{A_3\}$ are replaced by the vectors $\{\bar{A}_1\}$, $\{\bar{A}_2\}$ and $\{\bar{A}_3\}$ respectively, where

$$\{\bar{A}_1\} = \psi_3 \{X\} - \frac{8\nu}{3n\pi} \{Y'\}$$

$$\{\bar{A}_2\} = \psi_3 \{X\} + \frac{16}{3n\pi} \{Y'\}$$

$$\{\bar{A}_3\} = \{X'\} - \frac{8}{3\lambda} \{Y\}$$

4. An additional load given by

$$\{P\} = - \frac{2 F \lambda e\upsilon}{n\pi} \int \{Y'\} dy$$

considered to act on the plate.

Although this modification has been included in the computer program and some results have been obtained, these are incomplete due to lack of time and are therefore not included here.

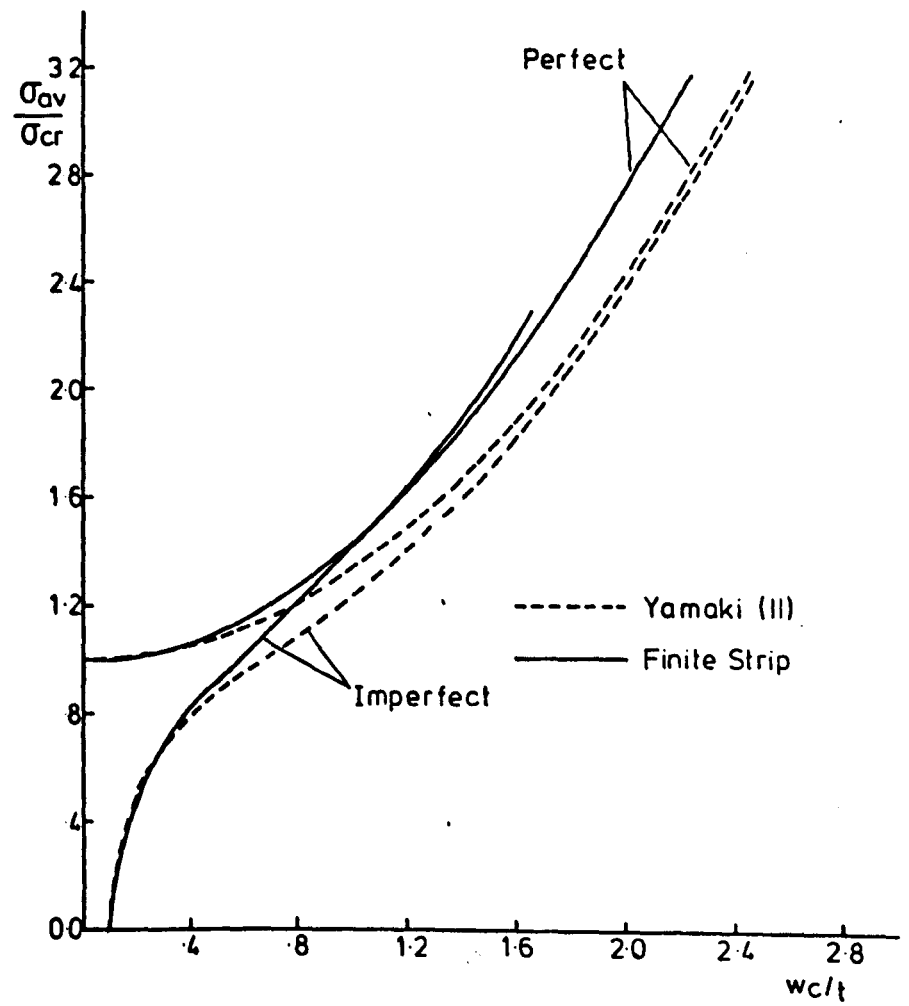

FIG. 8.2. CENTRAL DEFLECTION AGAINST AVERAGE STRESS. (THE UNLOADED EDGES MOVE BODILY)

CHAPTER 9

CONCLUSION AND SCOPE FOR FUTURE WORK

9.1 Scope of the Present Work

The present work can be divided into two parts, the first concentrated on the initial buckling while the second dealt with the post-buckling behaviour. The first part was intended to study the inelastic buckling of plate assemblies using the small deflection theory. The loaded ends of the component plates were limited to simply supported conditions. It was assumed that every strip was subjected to a range of in-plane longitudinal loads varying from pure compression to pure bending, no shear or transverse loading was considered. The analysis was restricted to perfect component plates, but plate assemblies with shallow overall imperfections were considered in some cases. There was no limitation on the mode of deformation of the whole plate assembly or the distortation of its components plates.

The parameters, which were varied to study the inelastic initial buckling of plate assemblies were:

1. Shape and dimensions of the cross-section (stiffened panels, rolled sections, box-section, etc.).
2. Number, orientation and geometrical properties of the stiffeners.

3. Pattern and magnitude of residual stress.
4. Material yield stress.
5. Boundary conditions of the unloaded edges.
6. Slenderness ratio of both plating and stiffened panel.
7. Mode of buckling (half wavelength).
8. Type of loading.

In the second part, the post-buckling behaviour was considered. The work was limited to the case of an initially stress free plate with simply supported loaded ends buckling in the elastic range. Only the case of plates under uniaxial longitudinal compressive stress was considered. It was assumed that the load was acting through two rigid loading bars, i.e. the longitudinal displacement at the loaded ends was uniform. A sinusoidal initial imperfection was assumed in the analysis. There was no limitation on the boundary conditions of the unloaded edges. No parametric study has been carried out in this part.

9.2 Conclusions from the Analysis

9.2.1 Theoretical Approaches

9.2.1.2 Initial Buckling

The theoretical approach for the determination of the initial buckling was based on the small deflection plate theory. This theory was applied through the finite strip

method which has been modified to include the effects of plasticity over parts of the cross-section. The critical buckling load has been obtained using Wittrick-Williams algorithm. The corresponding eigenvector was obtained from the solution of the reduced system of linear equations which has been developed by transforming the singular matrix (overall matrix) to a non-singular one. This was done by replacing a given column as the right-hand-side vector.

The general theory employed in this work provided a flexible and powerful method of analysis for the inelastic stability of any plate assembly. This theory was incorporated into a computer program to determine the critical load and the buckling mode of the plate assembly. The computer program could account for various patterns and magnitudes of residual stress.

9.2.1.2 Post-Buckling

In this theoretical approach, the large deflection plate theory was used with Marguerre's equation to account for the initial imperfection. The finite strip method was extended to determine the linear and non-linear stiffness matrices. The non-linear matrix, which was a function of the displacements, must be up-dated at every increment of load. Netwon-Raphson method was used to solve the non-linear equations. For the case of a perfect plate a very small disturbing surface load was applied. A computer program was developed to consider the following problem:

1. The determination of the bifurcation point, solution of the nonlinear equations and tracing the secondary path for a perfect plate. The change in the deformation of an imperfect plate can also be obtained by the same program.

2. The distribution of the stress and strain at any level of the applied load.

3. The determination of the average longitudinal compressive stress (the applied load).

9.2.2 Comparison with Previous Published Results

The accuracy of the method is demonstrated by comparison with previously published theoretical and experimental results from various sources, and some indications of the efficiency of the method were given. Various plate structures - isolated rectangular plates, box columns, stiffened panels and rolled sections - have been used. The comparisons cover the elastic and the inelastic behaviour of plate assemblies with different levels of residual stress.

9.2.3 Theoretical Parameters

A parametric study has been carried out on a number of plate assemblies under various loading conditions, and particular comments relating to the behaviour of each structures have been made in the relevant sections. Because only one or two parameters were usually varied

(while the other parameters were assumed to be constant) it was not possible to generalise the obtained results.

Three structural assemblies have been used in the present parametric studies, these are:

1. Square panels stiffened with four-flat, angle and tee - stiffeners.

2. Very wide panels stiffened with a large number of flat stiffeners.

3. Structural members - rolled H-sections and channels.

From the very wide panel results, a design chart is provided. Moreover, to demonstrate the capability of the current approach to analyse a complete plate structure, a box-section stiffened by any number of ribs on both the compression flange and the web has been used.

9.3 Recommendation for Future Work

The two parts of the investigation presented in this thesis can be extended in a number of ways. These will be mentioned briefly in the following.

Part I

This part was based on small deflection theory. The effect of a nonlinear stress-strain relationship and the effect of the residual stresses were included. The

computer program which has been developed can be used to investigate the initial buckling of various plate assemblies. This program may be applied to a well organized parametric study to cover any gap in the literature. The measured pattern of residual stress can be introduced and the approximation due to the use of an idealized pattern can be studied. Moreover, this computer program can be modified to investigate plate assemblies loaded by transverse stress, shear, combined load and/or lateral load.

Another extension, which is a simple matter in principle, will be the modification of the method to allow for end conditions different from those considered herein. A continuous structure over several supports, stiffened curved plate, etc. can also be studied after some modification in the present theory.

Finally, an extension which may be of importance, is to allow for the post-buckling in component plates. The large deflection of these plates, the initial imperfection and the residual stress can be accounted for by applying (to these component plates) one of the following approaches.

1. Theoretical load shortening curve.
2. Experimental results of stress-strain relationship.
3. The effective width approach.

This extension can produce a complete study on the interactive buckling. Similar work has been done by Wang et al (74, 75) where a combination of the finite element method based on small deflection theory with the effective width of the component plates was used. Little (82) has used the theoretical load shortening curve in conjunction with the moment-thrust-curvature relationship.

Part II

The work presented in this part can be extended to study the large deflection of plates under combined lateral and in-plane loads. The elastic post-buckling of a complete structure (e.g. box-girder) may be analysed by the computer program. To allow for the compatibility at the junction between two component plates, the longitudinal harmonic functions which have been developed recently by Hancock (78) can be used. Again the method can be modified to allow for end conditions different from those assumed herein. The theoretical approach can be extended to allow for inelastic behaviour and residual stress. The load shortening curves for perfect and imperfect plates with various boundary conditions can be obtained. Various plasticity theories and various yield criteria may be applied.

It is hoped that the present investigation has opened up new directions of research and providesasmall contribution towards better understanding of the instability problems.

APPENDIX A

EXPRESSION FOR THE STIFFNESS MATRIX [K]

From the equation of internal virtual work the stiffness matrix [K] is given in terms of the strain matrix [B] and the elsto-plastic matrix [F] by

$$[K] = \int_{vol} [B]^T [F] [B] \, dvol$$

$$= \lambda b \int_{-\frac{1}{2}}^{\frac{1}{2}} \int_{o}^{1} \int_{-t/2}^{t/2} [B]^T [F] [B] \, dz \, d\zeta \, d\eta \qquad (A.1)$$

The strain matrix [B] and its transpose $[B]^T$ are given by

$$[B] = \begin{bmatrix} \frac{-\pi}{\lambda}\{X\}^T + z\frac{\pi^2}{\lambda^2}\{Z\}^T \\ \frac{1}{b}\{Y,_\eta\}^T - z\frac{1}{b^2}\{Z,_{\eta\eta}\}^T \\ \frac{1}{b}\{X,_\eta\} + \frac{\pi}{\lambda}\{Y\}^T - z\frac{2\pi}{\lambda b}\{Z,_\eta\}^T \end{bmatrix} \begin{bmatrix} \sin\pi\zeta & \sin\pi\zeta & \cos\pi\zeta \end{bmatrix}$$

$$[B]^T = \begin{bmatrix} -\frac{\pi}{\lambda}\{X\} + z\frac{\pi^2}{\lambda^2}\{Z\} \\ \frac{1}{b}\{Y,_\eta\} - z\frac{1}{b^2}\{Z,_{\eta\eta}\} \\ \frac{1}{b}\{X,_\eta\} + \frac{\pi}{\lambda}\{Y\} - z\frac{2\pi}{\lambda b}\{Z,_\eta\} \end{bmatrix} \begin{bmatrix} \sin\pi\zeta & \sin\pi\zeta & \cos\pi\zeta \end{bmatrix} \qquad (A.2)$$

and the elasto-plastic matrix $[F] = \begin{bmatrix} F_{11} & F_{12} & 0 \\ F_{21} & F_{22} & 0 \\ 0 & 0 & F_{33} \end{bmatrix}$

Substituting $[B]^T$, $[F]$ and $[B]$ into equation (A.1), knowing that $\int_0^1 \lceil \sin\pi\zeta \quad \sin\pi\zeta \quad \cos\pi\zeta \rfloor \lceil \sin\pi\zeta \quad \sin\pi\zeta \quad \cos\pi\zeta \rfloor \, d\zeta = 1.0$ and carrying out the integration with respect to z, the stiffness matrix [K] will be given by

$$
\begin{aligned}
[K] = \int_{-.5}^{.5} & [a_1 F_{11} \{X\} \{X\}^T - a_2 F_{12} [\{Y,_\eta\} \{X\}^T \\
& + \{X\} \{Y,_\eta\}^T] + a_3 F_{22} \{Y,_\eta\} \{Y,_\eta\}^T \\
& + F_{33} [a_3 \{X,_\eta\} \{X,_\eta\}^T + a_2 [\{Y\} \{X,_\eta\}^T + \{X,_\eta\} \{Y\}^T] \\
& + a_1 \{Y\} \{Y\}^T] + a_4 F_{11} \{Z\} \{Z\}^T - a_5 F_{12} [\{Z,_{\eta\eta}\} \{Z\}^T \\
& + \{Z\} \{Z,_{\eta\eta}\}^T] + a_6 F_{22} \{Z,_{\eta\eta}\} \{Z,_{\eta\eta}\}^T \\
& + a_5 F_{33} \{Z,_\eta\} \{Z,_\eta\}^T] \, d\eta
\end{aligned}
\qquad \text{(A.3)}
$$

The elements of the matrix [F] are as follows

Element	Elastic	Inelastic
$F_{11} = F_{22}$	$\frac{E}{(1-\nu^2)}$	$\frac{E_t}{(1-\nu^2)}$
$F_{12} = F_{21}$	νF_{11}	νF_{11}
F_{33}	$\frac{E}{2(1+\nu)}$	$\frac{E_{sec}}{2(1+\nu)}$

The values of E_t and E_{sec} and effective ν are given in equations (3.22), (3.24) and (3.25). To obtain elastic or inelastic stiffness matrix substitute the appropriate [F] into equation (A.3). The constants in equation (A.3) are

$$a_1 = \pi^2 bt/\lambda,$$

$$a_2 = \pi t,$$

$$a_3 = \lambda t/b,$$

$$a_4 = \frac{1}{12}\pi^4 bt^3/\lambda^3,$$

$$a_5 = \frac{1}{12}\pi^2 t^3/\lambda b,$$

$$a_6 = \frac{1}{12}\lambda t^3/b^3 \qquad \text{(A.4)}$$

It is clear that if the stress is uniform the elements of the elasto-plastic matrix F_{11}, F_{12},... etc. will not change across the width of the strip and the integration through the width can be carried out as in the elastic analysis. In this case the results of the integration of the submatrices, in the right hand side of equation (A.3) will be as follows:

$$\int_{-.5}^{.5} \{X\}\{X\}^T d\eta = \begin{bmatrix} 0 & 0 & 0 & 0 & 0 & 0 & 0 & 0 \\ & 0 & 0 & 0 & 0 & 0 & 0 & 0 \\ & & 0 & 0 & 0 & 0 & 0 & 0 \\ & & & \frac{1}{3} & 0 & 0 & 0 & \frac{1}{6} \\ & & & & 0 & 0 & 0 & 0 \\ & & & & & 0 & 0 & 0 \\ & & & & & & 0 & 0 \\ \text{symmetrical} & & & & & & & \frac{1}{3} \end{bmatrix} \qquad \text{(A.5)}$$

$$\int_{-.5}^{.5} \{Y\}\{Y\}^T d\eta = \begin{bmatrix} 0 & 0 & 0 & 0 & 0 & 0 & 0 & 0 \\ & 0 & 0 & 0 & 0 & 0 & 0 & 0 \\ & & \frac{1}{3} & 0 & 0 & 0 & \frac{1}{6} & 0 \\ & & & 0 & 0 & 0 & 0 & 0 \\ & & & & 0 & 0 & 0 & 0 \\ & & & & & 0 & 0 & 0 \\ & & & & & & \frac{1}{3} & 0 \\ \text{symmetrical} & & & & & & & 0 \end{bmatrix} \qquad \text{(A.6)}$$

$$\int_{-.5}^{.5} \{X,_\eta\}\{X,_\eta\}^T d\eta = \begin{bmatrix} 0 & 0 & 0 & 0 & 0 & 0 & 0 & 0 \\ & 0 & 0 & 0 & 0 & 0 & 0 & 0 \\ & & 0 & 0 & 0 & 0 & 0 & 0 \\ & & & 1 & 0 & 0 & 0 & -1 \\ & & & & 0 & 0 & 0 & 0 \\ & & & & & 0 & 0 & 0 \\ & & & & & & 0 & 0 \\ \text{symmetrical} & & & & & & & 1 \end{bmatrix} \tag{A.7}$$

$$\int_{-.5}^{.5} \{Y,_\eta\}\{Y,_\eta\}^T d\eta = \begin{bmatrix} 0 & 0 & 0 & 0 & 0 & 0 & 0 & 0 \\ & 0 & 0 & 0 & 0 & 0 & 0 & 0 \\ & & 1 & 0 & 0 & 0 & -1 & 0 \\ & & & 0 & 0 & 0 & 0 & 0 \\ & & & & 0 & 0 & 0 & 0 \\ & & & & & 0 & 0 & 0 \\ & & & & & & 1 & 0 \\ \text{symmetrical} & & & & & & & 0 \end{bmatrix} \tag{A.8}$$

$$\int_{-.5}^{.5} \{Y,_\eta\}\{X\}^T + \{X,_\eta\}\{Y\}^T d\eta = \begin{bmatrix} 0 & 0 & 0 & 0 & 0 & 0 & 0 & 0 \\ & 0 & 0 & 0 & 0 & 0 & 0 & 0 \\ & & 0 & -\frac{1}{2} & 0 & 0 & 0 & -\frac{1}{2} \\ & & & 0 & 0 & 0 & \frac{1}{2} & 0 \\ & & & & 0 & 0 & 0 & 0 \\ & & & & & 0 & 0 & 0 \\ & & & & & & 0 & \frac{1}{2} \\ \text{symmetrical} & & & & & & & 0 \end{bmatrix} \tag{A.9}$$

$$\int_{-.5}^{.5} \{Y\}\{X,_\eta\}^T + \{X,_\eta\}\{Y\}^T d\eta = \begin{bmatrix} 0 & 0 & 0 & 0 & 0 & 0 & 0 & 0 \\ & 0 & 0 & 0 & 0 & 0 & 0 & 0 \\ & & 0 & -\frac{1}{2} & 0 & 0 & 0 & \frac{1}{2} \\ & & & 0 & 0 & 0 & -\frac{1}{2} & 0 \\ & & & & 0 & 0 & 0 & 0 \\ & & & & & 0 & 0 & 0 \\ & & & & & & 0 & \frac{1}{2} \\ \text{symmetrical} & & & & & & & 0 \end{bmatrix} \quad \text{(A.10)}$$

$$\int_{-.5}^{.5} \{z\}\{z\}^T d\eta = \frac{1}{420} \begin{bmatrix} 4b^2 & 22b & 0 & 0 & -3b^2 & 13b & 0 & 0 \\ & 156 & 0 & 0 & -13b & 54 & 0 & 0 \\ & & 0 & 0 & 0 & 0 & 0 & 0 \\ & & & 0 & 0 & 0 & 0 & 0 \\ & & & & 4b^2 & -22b & 0 & 0 \\ & & & & & 156 & 0 & 0 \\ & & & & & & 0 & 0 \\ \text{symmetrical} & & & & & & & 0 \end{bmatrix} \quad \text{(A.11)}$$

$$\int_{-.5}^{.5} \{z,_{\eta\eta}\}\{z\}^T + \{z\}\{z,_{\eta\eta}\}^T d\eta = \frac{1}{15} \begin{bmatrix} 4b^2 & -18b & 0 & 0 & b^2 & 3b & 0 & 0 \\ & -36 & 0 & 0 & -3b & 36 & 0 & 0 \\ & & 0 & 0 & 0 & 0 & 0 & 0 \\ & & & 0 & 0 & 0 & 0 & 0 \\ & & & & 4b^2 & 18b & 0 & 0 \\ & & & & & -36 & 0 & 0 \\ & & & & & & 0 & 0 \\ \text{symmetrical} & & & & & & & 0 \end{bmatrix} \quad \text{(A.12)}$$

$$\int_{-.5}^{.5} \{z,_{\eta\eta}\}\{z,_{\eta\eta}\}^T d\eta = \begin{bmatrix} 4b^2 & 6b & 0 & 0 & 2b^2 & -6b & 0 & 0 \\ & 12 & 0 & 0 & 6b & -12 & 0 & 0 \\ & & 0 & 0 & 0 & 0 & 0 & 0 \\ & & & 0 & 0 & 0 & 0 & 0 \\ & & & & 4b^2 & -6b & 0 & 0 \\ & & & & & 12 & 0 & 0 \\ & & & & & & 0 & 0 \\ \text{symmetrical} & & & & & & & 0 \end{bmatrix} \quad \text{(A.13)}$$

$$\int_{-.5}^{.5} \{\bar{z}\}\{\bar{z}\}^T d\eta = \frac{1}{30} \begin{bmatrix} 4b^2 & 3b & 0 & 0 & -b^2 & -3b & 0 & 0 \\ & 36 & 0 & 0 & 3b & -36 & 0 & 0 \\ & & 0 & 0 & 0 & 0 & 0 & 0 \\ & & & 0 & 0 & 0 & 0 & 0 \\ & & & & 4b^2 & -3b & 0 & 0 \\ & & & & & 36 & 0 & 0 \\ & & & & & & 0 & 0 \\ \text{symmetrical} & & & & & & & 0 \end{bmatrix} \quad \text{(A.14)}$$

Most of these matrices were obtained by Plank et al (76) and mentioned here for completeness.

APPENDIX B

EXPRESSION FOR THE STABILITY MATRIX [S]

From equation (3.55)

$$[S] = \int_{vol} \frac{\sigma_x}{\lambda^2} [N,_\zeta]^T [N,_\zeta] \, dvol$$

$$= \int_{-.5}^{.5} \int_{o}^{1} \int_{-t/2}^{t/2} \frac{b\sigma_x}{\lambda} [N,_\zeta]^T [N,_\zeta] \, dz \, d_\zeta \, d\eta \qquad (B.1)$$

where

$$[N] = [\{X\}^T \{Y\}^T \{Z\}^T]^T \lceil \cos\pi\zeta \quad \sin\pi\zeta \quad \sin\pi\zeta \rfloor \qquad (B.2)$$

Differentiating [N] with respect to ζ we obtain

$$[N,_\zeta] = \pi [-\{X\}^T \{Y\}^T \{Z\}^T]^T \lceil \sin\pi\zeta \quad \cos\pi\zeta \quad \cos\pi\zeta \rfloor \qquad (B.3)$$

and

$$[N,_\zeta]^T = \pi [-\{X\} \{Y\} \{Z\}] \lceil \sin\pi\zeta \quad \cos\pi\zeta \quad \cos\pi\zeta \rfloor \qquad (B.4)$$

Substituting equations (B.3) and (B.4) into equation (B.1), carrying out the integration with respect to z and ζ and knowing that

$$\int_{o}^{1} \lceil \sin\pi\zeta \quad \cos\pi\zeta \quad \cos\pi\zeta \rfloor \lceil \sin\pi\zeta \quad \cos\pi\zeta \quad \cos\pi\zeta \rfloor \, d\zeta = 1.0 \qquad (B.5)$$

we obtain

$$[S] = \frac{bt\pi^2}{\lambda} \int_{-.5}^{.5} \sigma x \, [\{X\} \{X\}^T + \{Y\} \{Y\}^T + \{Z\} \{Z\}^T] \, d\eta \quad \text{(B.6)}$$

For the case of uniform stress, the integration can be carried out through the width of the strip. But if the stress is not uniform due to the presence of residual stresses the integration must be carried out numerically by dividing the strip into a number of substrips and using any method of numerical integration such as the Trapezoidal Rule, Simpson's Rule or Weddle's Rule (110). The elements of the stability matrix [S] after integration over the width for the case of uniform stress are given by

$$[S] = \frac{\sigma_x \, tb\pi^2}{\lambda} \begin{bmatrix} 4b^2 & 22b & 0 & 0 & -3b^2 & 13b & 0 & 0 \\ & 156 & 0 & 0 & -13b & 54 & 0 & 0 \\ & & \frac{1}{3} & 0 & 0 & 0 & \frac{1}{6} & 0 \\ & & & \frac{1}{3} & 0 & 0 & 0 & \frac{1}{6} \\ & & & & 4b^2 & -22b & 0 & 0 \\ & & & & & 156 & 0 & 0 \\ & & & & & & \frac{1}{3} & 0 \\ \text{symmetrical} & & & & & & & \frac{1}{3} \end{bmatrix} \quad \text{(B.7)}$$

APPENDIX C

THE IN-PLANE EQUILIBRIUM EQUATIONS

To prove that the assumed displacement function satisfies the in-plane equilibrium equations assume the displacements of a point on the middle plane are u, v and w in x, y and z directions. The strains at this point are given by

$$\varepsilon_x = u_{,x} + \frac{1}{2} w_{,x}^2 \tag{C.1}$$

$$\varepsilon_y = v_{,y} + \frac{1}{2} w_{,y}^2 \tag{C.2}$$

$$\gamma_{xy} = u_{,y} + v_{,x} + w_{,x}\, w_{,y} \tag{C.3}$$

The corresponding stress resultants are given by

$$N_x = \frac{Et}{1-\nu^2} (\varepsilon_x + \nu\, \varepsilon_y) \tag{C.4}$$

$$N_y = \frac{Et}{1-\nu^2} (\varepsilon_y + \nu\, \varepsilon_x) \tag{C.5}$$

$$N_{xy} = \frac{Et}{2(1+\nu)} \gamma_{xy} \tag{C.6}$$

The in-plane equilibrium equations as derived by Timoshenko (3) are

$$\frac{\partial N_x}{\partial x} + \frac{\partial N_{yx}}{\partial y} = 0.0 \tag{C.7}$$

$$\frac{\partial N_y}{\partial y} + \frac{\partial N_{xy}}{\partial x} = 0.0 \qquad (C.8)$$

Substituting equations (C.1), (C.2) and (C.3) into equations (C.4), (C.5) and (C.6), the stress resultants can be expressed in terms of displacements

$$N_x = \frac{Et}{1-\nu^2} \left[(u_{,x} + \nu\, v_{,y}) + \frac{1}{2} (w_{,x}^2 + \nu\, w_{,y}^2) \right] \qquad (C.9)$$

$$N_y = \frac{Et}{1-\nu^2} \left[(v_{,y} + \nu\, u_{,x}) + \frac{1}{2} (w_{,y}^2 + \nu\, w_{,x}^2) \right] \qquad (C.10)$$

$$N_{xy} = \frac{Et}{2(1+\nu)} \left[(u_{,y} + v_{,x}) + w_{,x}\, w_{,y} \right] \qquad (C.11)$$

Differentiating equations (C.9), (C.10) and (C.11) and substituting equations (C.7) and (C.8), the in-plane equilibrium equations become

$$\left[u_{,xx} + \left(\frac{1+\nu}{2}\right) v_{,yx} + \left(\frac{1-\nu}{2}\right) u_{,yy}\right] + \left[w_{,x}\, w_{,xx} + \left(\frac{1+\nu}{2}\right) w_{,y}\, w_{,xy} + \left(\frac{1-\nu}{2}\right) w_{,x}\, w_{,yy}\right] = 0.0 \qquad (C.12)$$

$$\left[v_{,yy} + \left(\frac{1+\nu}{2}\right) u_{,xy} + \left(\frac{1-\nu}{2}\right) v_{,xx}\right] + \left[w_{,y}\, w_{,yy} + \left(\frac{1+\nu}{2}\right) w_{,x}\, w_{,xy} + \left(\frac{1-\nu}{2}\right) w_{,y}\, w_{,xx}\right] = 0.0 \qquad (C.13)$$

Differentiating the assumed displacement function

$$u = \sum_{m=1}^{M} \{X\}^T \{\delta\} \sin \frac{m\pi x}{\lambda} + e \left(\frac{\lambda}{2} - x\right)$$

$$v = \sum_{m=1}^{M} \{Y\}^T \{\delta\} \cos \frac{m\pi x}{\lambda} + fy$$

$$w = \sum_{n=1}^{N} \{Z\}^T \{\delta\} \sin \frac{n\pi x}{\lambda}$$

and substituting into equation (C.12)

$$\sum_{m=1}^{M} \sin \frac{m\pi x}{\lambda} \{C_1 \{X\} + C_2 \{Y'\} + C_3 \{X''\}\}^T \{\delta\}$$

$$+ \sum_{n=1}^{N} \sin \frac{n\pi x}{\lambda} \cos \frac{n\pi x}{\lambda} \{C_4 \{R\} + C_5 \{R'\} + C_6 \{R''\}\} \{\delta\} = 0.0 \qquad (C.14)$$

where C_1, C_2, C_3,... are a non-zero constants. Equation (C.14) may be expressed as

$$\sum_{m=1}^{M} a_m \sin \frac{m\pi x}{\lambda} + \sum_{n=1}^{N} b_n \left(\sin \frac{(n+n)\pi x}{\lambda} + \sin \frac{(n-n)\pi x}{\lambda}\right) = 0.0 \qquad (C.15)$$

From this it is clear that the condition of $m = n \pm n$, i.e. for $n = 1, 3, 5,\ldots$ $m = 0, 2, 4, 6,\ldots$ is a necessary and sufficient condition for the assumed displacement function to satisfy the in-plane equilibrium condition.

Similarly when the displacement function is differentiated and substituted into equation (C.13) the equilibrium equation becomes

$$\sum_{m=1}^{M} a_m \cos \frac{m\pi x}{\lambda} + \sum_{n=1}^{N} b_n \sin \frac{n\pi x}{\lambda} \sin \frac{n\pi x}{\lambda} = 0.0 \qquad (C.16)$$

$$\text{i.e. } \sum_{m=1}^{M} a_m \cos \frac{m\pi x}{\lambda} + \sum_{n=1}^{N} b_n \left(\cos \frac{(n-n)\pi x}{\lambda} - \cos \frac{(n+n)\pi x}{\lambda}\right) = 0.0 \tag{C.17}$$

and the sufficient condition is $m = n \pm n$.

APPENDIX D

THE STIFFNESS MATRICES FOR THE SECOND CASE

In this appendix the linear and nonlinear stiffness matrices have been obtained using the displacement functions given by

$$u = e(\frac{\lambda}{2} - x) + \sum_{m=2}^{M} \{X\}^T \{\delta\} \sin \frac{m\pi x}{\lambda} \tag{D.1}$$

$$v = \sum_{n=1}^{N} \{Y\}^T \{\delta\} \sin \frac{n\pi x}{\lambda} \tag{D.2}$$

$$w = \sum_{n=1}^{N} \{Z\}^T \{\delta\} \sin \frac{n\pi x}{\lambda} \tag{D.3}$$

The strains at any point on a perfect plate based on these functions can be expressed as

$$\varepsilon_x = - e + \sum_{m=2} (\psi_3 \{X\}^T \{\delta\} \cos \psi_3 x + \frac{1}{2} \psi_1^2 \{R\}^T \{\delta\} \cos^2 \psi_1 x$$

$$+ \psi_1^2 z \{Z\}^T \{\delta\} \sin \psi_1 x \tag{D.4}$$

$$\varepsilon_y = \sum_{m=2} \{Y'\}^T \{\delta\} \sin \psi_1 x + \frac{1}{2} \{\bar{R}\}^T \{\delta\} \sin^2 \psi_1 x$$

$$- z \{Z'\}^T \{\delta\} \sin \psi_1 x \tag{D.5}$$

$$\gamma_{xy} = \sum_{m=2} (\{X'\}^T \{\delta\} \sin \psi_3 x + \psi_1 \{Y\} \{\delta\} \cos \psi_1 x$$

$$+ \frac{1}{2} \psi_1 \sin \psi x \cos \psi_1 x \{B\}^T \{\delta\}$$

$$- 2z \psi_1 \{Z'\} \{\delta\} \cos \psi_1 x \tag{D.6}$$

where $\psi_1 = n\pi/\lambda$

$\psi_3 = m\pi/\lambda$

The vectors $\{R\}$, $\{\bar{R}\}$ and $\{B\}$ are given by equations (7.30), (7.31) and (7.32). Using equations (D.4), (D.5) and (D.6) the strain energy of the strip can be obtained. Table D1 is the modification of Table 7.1. It is clear that the quadratic (bending) term and the quartic term do not change. This is because these terms do not depend on the in plane displacement. In this appendix only the terms which have been affected by the modification are given in the tables. The other terms can be read from the earlier tables.

Integrating the strain energy function with respect to the length of the plate; Table 7.2 is modified as shown in Table D2.

The equilibrium equations $\{E\}$ can be obtained by minimizing this strain energy with respect to the nodal displacement $\{\delta\}$. The equilibrium equation is given by

$$\{E\} = [K]\{\delta\} + \{P\} \tag{D.7}$$

where $[K]$ is the stiffness matrix

$$[K] = [K1]_{mb} + [K1]_b + [K1]_s + [K2] + [K3] \tag{D.8}$$

Order	Formulation
Zero	$W_o = \frac{F}{2} \iint e^2 \, dx \, dy$
Linear	$W_1 = \frac{F}{2} \iint \{2C(m) \, \psi_3 \, (-e) \, \{X\}^T + 2 \, S(n) \, (-\nu e) \, \{Y'\}^T\} \{\delta\} \, dx \, dy$
Quadratic (membrane)	$W_{2mb} = \frac{F}{2} \iint \{\delta\}^T [(\psi_3^2 \, \{X\} \, \{X\}^T \, C^2(m) + \{Y'\} \, \{Y'\}^T S^2(n) + 2\nu \, \psi_3 \, \{X\} \, \{Y'\}^T \, C(m) \, S(n) + (\frac{1-\nu}{2}) \, (S^2(m) \, \{X'\} \, \{X'\}^T + \psi_1^2 \, \{Y\} \, \{Y\}^T \, C^2(n) + 2 \, \psi_1 \, \{X'\} \, \{Y\}^T \, S(m) \, C(n))] \, dx \, dy$
Quadratic (bending)	W_{2b}: Do not change
Quadratic (stability)	$W_{2s} = \frac{F}{2} \iint \{C^2(n) \, \psi_1^2 \, (-e) \, \{R\} + S^2(n) \, (-\nu e) \, \{\bar{R}\}\}^T \{\delta\} \, dx \, dy$
Cubic	$W_3 = \frac{F}{2} \iint \{\delta\}^T [\psi_1^2 \, C^2(n) \, \{C(m) \, \psi_3 \, \{X\} + \nu \, S(n) \, \{Y'\}\} \, \{R\}^T + S^2(n) \, \{C(m)\nu \, \psi_3 \, \{X\} + S(n) \, \{Y'\}\} \, \{\bar{R}\}^T + (\frac{1-\nu}{2}) \, \psi_1 \, S(n) \, C(n) \, \{S(m) \, \{X'\} + \psi_1 \, C(n) \, \{Y\}\} \, \{B\}^T] \{\delta\} \, dx \, dy$
Quartic	W_4: Do not change

Table D1. The Strain Energy

Order	Formulation	
Zero	$W_o = F \int \lambda e^2 \, dy$	
First	$W_1 = \frac{4F\lambda\nu e}{n\pi} \int \{Y'\}^T \{\delta\} \, dy$	$n = 1, 3, 5$
Quadratic (membrane)	$W_{2mb} = \frac{F\lambda}{2} \int \{\delta\} [\psi_3{}^2 \{X\} \{X\}^T + \{Y'\} \{Y'\}^T + \frac{8\psi_3{}^n}{(n^2-m^2)\pi} \{X\} \{Y'\}^T + (\frac{1-\nu}{2}) (\{X'\} \{X'\}^T$ $\psi_1{}^2 \{Y\} \{Y\}^T + \psi_1{}^2 \{Y\} \{Y\}^T + \frac{8\nu\psi_1{}^m}{(m^2-n^2)\pi} \{X'\} \{Y\}^T)] \{\delta\} \, dy$	$n = 1, 3, 5$ $m = 2, 4, 6$
Quadratic (bending)	W_{2b}: Do not change	
Quadratic (stability)	$W_{2s} = \frac{F\lambda}{2} \int \{\delta\} [-\psi_1{}^2 e \{Z\} \{Z\}^T - e\nu \{Z'\} \{Z'\}] \{\delta\} \, dy$	$n = 1, 3, 5$
Cubic	$W_3 = \frac{F\lambda}{4} \int \{\delta\} [\psi_1{}^2 \{\bar{A}_1\} \{R\}^T - \{\bar{A}_2\} \{\bar{R}\}^T + (\frac{1-\nu}{2}) \psi_1 \{\bar{A}_3\} \{\bar{B}\}^T] \{\delta\} \, dy$	$n = 1, 3, 5$ $m = 2n$
Quartic	W_4: Do not change	

$\{\bar{A}_1\} = \psi_3 \{X\} - \frac{8\nu}{3n\pi} \{Y'\}$ $\quad$ $\{\bar{A}_2\} = \nu \psi_3 \{X\} + \frac{16}{3n\pi} \{Y'\}$ $\quad$ $\{\bar{A}_3\} = \{X'\} - \frac{8\psi_1}{3n\pi} \{Y\}$

Table D2. The Strain Energy of a Strip

Those matrices can be obtained by modification of Table 7.3 as shown in Table D3. The minimization of the linear term "W_1" of the strain energy functions (Table D2) gives an imaginary load vector {P}.

$$\{P\} = \frac{2F\lambda e\nu}{n\pi} \int \{Y'\}\, dy \tag{D.9}$$

The incremental stiffness matrix can be obtained from Table D3 as follows:

1. The linear matrices do not change.
2. The quadratic incremental matrix is a symmetrical matrix given by

$$[KT2] = \frac{F\lambda}{2} \left[\psi_1^2 \{R\} \{\bar{A}1\}^T - \{\bar{R}\} \{\bar{A}2\}^T \right.$$

$$\left. - \left(\frac{1-\nu}{2}\right) \psi_1 \{B\} \{\bar{A}3\}^T\right] dy \tag{D.10}$$

3. The cubic incremental matrix is given by

$$[KT3] = 3\,[K3] \tag{D.11}$$

For an imperfect plate the strain energy, the equilibrium equations and the stiffness matrix can be obtained by substituting f = 0.0, {A1} = {$\bar{A}$1}, {A2} = {$\bar{A}$2} and {A3} = {$\bar{A}$3} in Tables 7.5, 7.6 and 7.7 respectively.

Order of the equilibrium equation	Formation of the stiffness matrix
Linear	$[Kl]_{mb} = F\,\lambda \int [\psi_3^{\,2}\,\{X\}\,\{X\}^T + \{Y'\}\,\{Y'\}^T - \frac{8\nu\,m\,n}{\lambda(m^2-n^2)}\{X\}\,\{Y'\}^T + (\frac{1-\nu}{2})\,(\{X'\}\,\{X'\}^T + \psi_1^{\,2}\,\{Y\}\,\{Y\}^T + \frac{8\,n\,m}{\lambda(m^2-n^2)}\{X'\}\,\{Y\}^T)]\,dy$ $[Kl]_b$: Do not change $[Kl]_s = F\,\lambda \int [-e\,\psi_1^{\,2}\,\{Z\}\,\{Z\}^T - e\nu\,\{Z'\}\,\{Z'\}^T]\,dy$
Nonlinear (quadratic)	$[K2] = \frac{F\lambda}{2} \int [\psi_1^{\,2}\,(\{R\}\,\{\bar{A}_1\}^T + \frac{1}{2}\{\bar{A}_1\}\,\{R\}^T) - (\{\bar{R}\}\,\{\bar{A}_2\}^T + \frac{1}{2}\{A_2\}\,\{\bar{R}\}^T) + (\frac{1-\nu}{2})\,\psi_1(\{B\}\,\{\bar{A}3\}^T + \frac{1}{2}\{A3\}\,\{B\}^T)]\,dy$
Nonlinear (cubic)	[K3]: Do not change

Table D3. The Strip Stiffness Matrix

APPENDIX E

INTEGRATION BY PARTS

Assume a general function

$$x = \int_a^b f(y) \sin^2 \alpha y \, dy \tag{E.1}$$

This function can be integrated by parts as follows:

$$\int_a^b f(y) \sin^2 \alpha y \, dy = \int_a^b \tfrac{1}{2} f(y) (1 - \cos 2\alpha y) \, dy \tag{E.2}$$

$$= \tfrac{1}{2} \int_a^b f(y) \, dy - \tfrac{1}{2} f(y) \cos 2\alpha y \, dy \tag{E.3}$$

$$= \tfrac{1}{2} \int_a^b f(y) \, dy - \left[\tfrac{1}{2} \left(\tfrac{1}{2\alpha}\right) f(y) \sin 2\alpha y\right]_a^b + \tfrac{1}{2} \left(\tfrac{1}{2\alpha}\right) \int_a^b f'(y) \sin 2\alpha y \, dy \tag{E.4}$$

$$\vdots$$

$$= \tfrac{1}{2} \int_a^b f(y) \, dy - \tfrac{1}{2} \left[\sin 2\alpha y \sum_{n=1} \left(\tfrac{1}{2\alpha}\right)^{2n-1} f^{2n-1} (-1)^{n+1}\right]_a^b - \tfrac{1}{2} \left[\cos 2\alpha y \sum_{n=1} \left(\tfrac{1}{2}\right)^{2n} \left(\tfrac{1}{\alpha}\right)^{2n} f^{2n} (-1)^{n+1}\right]_a^b \tag{E.5}$$

where f^{n+1} is the (n) differentiation of the function f(y)

$$f^{n+1} = \frac{\partial^n f}{\partial y^n} \tag{E.6}$$

Similarly,

$$\int_a^b f(y) \cos^2 \alpha y \, dy = \frac{1}{2} \int_a^b f(y) \, dy + \frac{1}{2} \left[\sin 2\alpha y \sum_{n=1} \left(\frac{1}{2\alpha}\right)^{2n-1} f^{2n-1} (-1)^{n+1}\right]_a^b + \frac{1}{2} \left[\cos 2\alpha y \sum_{n=1} \left(\frac{1}{2\alpha}\right)^{2n} f^{2n} (-1)^{n+1}\right]_a^b \tag{E.7}$$

$$\int_a^b f(y) \sin \alpha y \, dy = - \left[\cos \alpha y \sum_{n=1} \left(\frac{1}{\alpha}\right)^{2n-1} f^{2n-1} (-1)^{n+1}\right]_a^b + \left[\sin \alpha y \sum_{n=1} \left(\frac{1}{\alpha}\right)^{2n} f^{2n} (-1)^{n+1}\right]_a^b \tag{E.8}$$

$$\int_a^b f(y) \cos \alpha y \, dy = \left[\sin \alpha y \sum_{n=1} \left(\frac{1}{\alpha}\right)^{2n-1} f^{2n-1} (-1)^{n+1}\right]_a^b - \left[\cos \alpha y \sum_{n=1} \left(\frac{1}{\alpha}\right)^{2n} f^{2n} (-1)^{n+1}\right]_a^b \tag{E.9}$$

A routine has been developed to perform this integration. The function f(y) is differentiated many times until it vanishes. This function may be either in vector or matrix form. The results of the differentiation can be accumulated and multiplied by the corresponding harmonic function. The value of the integration can then be obtained by substituting the limits of the integration into the accumulated results.

REFERENCES

(1) Bleich, F. and Bleich, H. H. "Buckling Strength of Metal Structures". McGraw-Hill Book Co., New York, 1952.

(2) Timoshenko, S. P. "History of Strength of Materials". McGraw-Hill Book Co., New York, 1953.

(3) Timoshenko, S. P. and Gere, J. M. "Theory of Elastic Stability". Second Edition, McGraw-Hill Book Co., New York, 1961.

(4) Bulson, P. S. "The Stability of Flat Plates". Chatto and Windus, London, 1970.

(5) Mendelson, A. "Plasticity: Theory and Application". The Macmillan Co., New York, 1968.

(6) Bijlaard, P. P. "Some Contributions to the Theory of Elastic and Plastic Stability". IABSE, Vol. 8, pp. 17-80, 1947.

(7) Ilyushin, A. A. "Stability of Plates and Shells Beyond the Proportional Limit". Technical Memorandum 1116. Translation in NACA, 1948.

(8) Stowell, E. Z. "A Unified Theory of Plastic Buckling of Columns and Plates". Technical Notes 1556, NACA, 1948.

(9) Haaijer, G. "Plate Buckling in the Strain Hardening Range". Eng. Mech. Div., Proc. ASCE, Vol. 83, No. EM2, April 1957.

(10) Coan, J. M. "Large Deflection Theory for Plates with Small Initial Curvature Loaded in Edge

Compression". J. of App. Mech., pp. 143-151, June, 1951.

(11) Yamaki, N. "Postbuckling Behaviour of Rectangular Plates with Small Initial Curvature Loaded in Edge Compression". J. of App. Mech., pp. 407-414, September, 1959.

(12) Walker, A. C. "The Postbuckling Behaviour of a Simply Supported Square Plate". The Aeronautical Quarterly, pp. 203-222, August, 1969.

(13) Dawson, R. G. and Walker, A. C. "Postbuckling of Geometrically Imperfect Plates". J. of the Stru. Div., ASCE, Vol. 98, No. ST1, January, 1972.

(14) Williams, D. G. and Walker, A. C. "Explicit Solution for Plate Buckling Analysis". J. of the Eng. Mech. Div., ASCE, Vol. 103, No. EM4, pp. 549-569, August, 1977.

(15) Kalyanaraman, V. and Pekoz, T. "Analytical Study of Unstiffened Elements". J. of the Stru. Div., ASCE, Vol. 104, No. ST9, pp. 1507-1524, September, 1978.

(16) Alami, B. and Chapman, J. C. "Large Deflection Behaviour of Rectangular Orthotropic Plates Under Transverse and In-Plane Loads". Proc. of Inst. of Civil Engn., Vol. 42, p. 347, 1969.

(17) Rushton, K. R. "Postbuckling of Rectangular Plates With Various Boundary Conditions". The Aeronautical Quarterly, pp. 163-181, May, 1970.

(18) Frieze, P. A. and Dowling, P. J. "Interactive Buckling Analysis of Box Sections Using Dynamic Relaxation". Computer and Structures, Vol. 9, pp. 431-439, 1978.

(19) Murray, D. W. and Wilson, E. L. "Finite Element Postbuckling Analysis of Thin Elastic Plates". AIAA J., Vol. 17, No. 10, pp. 1915-1920, October, 1969.

(20) Vos, R. G. and Vann, W. P. "A Finite Element Tensor Approach to Plate Buckling and Postbuckling". Int. J. for Num. Meth. in Engn., Vol. 5, pp. 351-365, 1973.

(21) Crisfield, M. A. "Large Deflection Elasto-Plastic Buckling Analysis of Plate Using Finite Elements". TRRL Report LR 593, 1973.

(22) Rojas-Gutierrez, R. "Elastic Stability of Box Girder Sections". Ph.D. Thesis, University of Sheffield, 1978.

(23) Dwight, J. B. and Ratcliffe, A. T. "The Strength of Thin Plates in Compression". Symposium on Thin-Walled Steel Structures, Swansea, 1967.

(24) Dwight, J. B. and Moxham, K. E. "Compressive Strength of Welded Plates". Int. Colloguium on Stab. of Stru. Under Static and Dynamic Loads, pp. 462-481, New York, 1977.

(25) Little, G. H. "Plate Failure in Stiffened Steel Compression Panels". Cambridge University Report No. CUED/C-Struct/TR.33, 1973.

(26) Dwight, J. B. and Harrison, J. D. "Local Buckling Problems in Steel Columns". BWRA Research Report No. M9/63, March, 1963.

(27) Dwight, J. B., Chin, T. K. and Ratcliffe, A. T. "Local Buckling of Thin Walled Columns". CIRIA Research Report No. 12, Part 1, 1968.

(28) Moxham, K. E. "Compression in Welded Web Plates". Ph.D. Thesis, Cambridge University, July, 1970.

(29) Dwight, J. B. and Moxham, K. E. "Welded Steel Plates in Compression". Structural Engineer, Vol. 47, No. 2, pp. 49-66, February, 1969.

(30) Little, G. H. and Dwight, J. B. "Compressive Tests on Plates With Transverse Welds". Cambridge University Report No. CUED/C-Struct/TR.31, 1972.

(31) Little, G. H. "Rapid Analysis of Plate Collapse by Live-Energy Minimisation". Int. J. Mech. Sci., Vol. 19, pp. 725-744, 1977.

(32) Little, G. H. "The Collapse of Rectangular steel Plates Under Uniaxial Compression". The Structural Engineer, Vol. 58B, No. 3, pp. 45-61, September 1980.

(33) Crisfield, M. A. "On An Approximate Yield Criterion for Thin Steel Shells". TRRL, Crowthorne, Report LR 658, 1974.

(34) Neal, K. W. "Effect of Imperfection on the Plastic Buckling of Rectangular Plates". J. of Applied Mech., pp. 115-120, March, 1975.

(35) Frieze, P. A., Dowling, P. J. and Hobbs, R. E. "Ultimate Load Behaviour of Plates in Compression". An Int. Symposium on Steel Plated Stru., Imperial College, London, July, 1976.

(36) Harding, J. E., Hobbs, R. E. and Neal, B. G. "Ultimate Load Behaviour of Plates Under Combined Direct and Shear In-Plane Loading". An Int. Symposium on Steel Plated Stru., Imperial College, London, July, 1976.

(37) Wah, T. "Buckling of Longitudinally Stiffened Plates". The Aeronautical Quarterly, Vol. 8, p. 85, 1967.

(38) Huber, M. T. "Problem der Statik Technisch Wichtiger Orthotroper Platten". Warsaw (1929).

(39) Ratzersdorfer, J. "Rectangular Plates with Stiffeners". Aircraft Engineering, Vol. 14, p. 260, 1942.

(40) Seydel, E. "Wrinkling of Reinforced Plates Subjected to Shear Stress". NACA Technical Memorandum No. 602, 1931.

(41) Wittrick, W. H. "Correlation Between Some Stability Problems for Orthotropic and Isotropic Plates Under Biaxial and Uniaxial Direct Stress". The Aeronautical Quarterly, Vol. 4, p. 83, 1952.

(42) Elgaaly, M. "Correlation Between the Buckling of Uniformly Stiffened and Isotropic Plates". Int. Colloquium on Stab. of Stru. Under Static and Dynamic Loads, pp. 422-434, New York, 1977.

(43) Moolani, F. M. and Dowling, P. J. "Ultimate Load Behaviour of Stiffened Plates in Compression". An Int. Symposium on Steel Plated Structures, Imperial College, London, July, 1976.

(44) Horne, M. R. and Narayanan. "Strength of Axially Loaded Stiffened Panels". IABSE Memories, Vol. 36-I, April, 1976.

(45) Horne, M. R. and Narayanan, R. "Strength of Axially Loaded Stiffened Panels". Simon Engineering Laboratories, University of Manchester, July, 1974.

(46) Smith, C. S. and Kirkwood, W. "Influence of Initial Deformation and Residual Stress on Inelastic Flexural Buckling of Stiffened Plates and Shells". An Int. Symposium on Steel Plated Structures, Imperial College, London, July, 1976.

(47) Carlsen, C. A. "Simplified Collapse Analysis of Stiffened Plates". Norwegian Maritime Research No. 4, pp. 20-36, 1977.

(48) Massonnet, C. and Maquoi, R. "New Theory and Tests on the Ultimate Strength of Stiffened Box

Girders". Paper 9, Steel Box Girder Bridges, Institution of Civil Engineers, London, 1973.

(49) Djubek, K. and Skaloud, M. "Czechoslovak Approach to the Design of Longitudinally Stiffened Compression Flanges of Steel Box-Girder Bridges". Preliminary Report, Stability of Steel Structures, Liege, Belgium, 1977.

(50) Soreide, T. H., Bergan, P. G. and Moan, T. "Ultimate Collapse Behaviour of Stiffened Plates Using Alternative Finite Element Formulations". An Int. Symposium on Steel Plated Stru., Imperial College, London, July, 1976.

(51) Fujita, Y., Yoshida, K. and Takazawa, M. "On the Strength of Stiffened Plate Structures". Int. Colloquium on Stab. of Stru. Under Static and Dynamic Loads, pp. 487-502, New York, 1977.

(52) Tvergaard, V. and Needleman, A. "Buckling of Eccentrically Stiffened Elastic-Plastic Panels on Two Simple Supports or Multiply Supported". Int. J. Solids Stru., Vol. 11, pp. 647-663, 1975.

(53) Crisfield, M. A. "A Combined Rayleigh-Ritz/Finite Element Method for the Nonlinear Analysis of Stiffened Plated Structures". Computer and Stru., Vol. 8, pp. 679-689, 1978.

(54) Murray, N. W. "Buckling of Stiffened Panels Loaded Axially and in Bending". The Structural Engineer, Vol. 51, No. 8, August, 1973.

(55) Faulkner, D. "Compression Tests on Welded Eccentrically Stiffened Plate Panels". An Int. Symposium on Steel Plated Structures, Imperial College, London, July, 1976.

(56) Horne, M. R. and Marayanan, R. "Ultimate Load Capacity of Longitudinal Stiffened Panels". Simon Engineering Laboratories, University of Manchester, January, 1974.

(57) Horne, M. R. and Narayanan, R. "Further Tests on the Ultimate Load Capacity of Longitudinal Stiffened Panels". Simon Engineering Laboratories, University of Manchester, July, 1974.

(58) Horne, M. R. and Narayanan, R. "Ultimate Strength of Stiffened Panels Under Uniaxial Compression". An Int. Symposium on Steel Plated Stru., Imperial College, London, July, 1976.

(59) Merrison Committee. "Inquiry into the Basis of Design and Method of Erection of Steel Box Bridges". Appendix 1, Interim Design and Workmanship Rules, HMSO, London, 1973.

(60) Fukumoto, Y., Usami, T. and Yamaguchi, K. "Inelastic Buckling Strength of Stiffened Plates in Compression". IABSE Proceedings P-8, 1977.

(61) Dubas, P. "Plated Structures with Closed-Section Stiffeners". An Int. Symposium on Steel Plated Structures, Imperial College, London, July, 1976.

(62) Bijlaard, P. P. and Fisher, G. P. "Interaction of Column and Local Buckling in Compression Members". NACA T.N. 2540, March, 1952.

(63) Bijlaard, P. P. and Fisher, G. P. "Column Strength of H-Sections and Square Tubes in the Post-Buckling Range of Component Plates", NACA T.N. 2994, August, 1953.

(64) Cherry, S. "The Stability of Beams with Buckled Compression Flanges". The Structural Engineer, Vol. 38, pp. 277-285, 1960.

(65) Skaloud, M., and Zornerova, M. "Experimental Investigation into the Interaction of the Buckling of Compressed Thin-Walled Columns With the Buckling of Their Plate Elements". Acta Technica, CSAV, No. 4, Prague, Czechoslovakia, 1970.

(66) Goldberg, J. E., Bogdanoff, J. L. and Glonz, W. D. "Lateral and Torsional Buckling of Thin Walled Beams". IABSE, Vol. 24, pp. 91-100, 1964.

(67) De Wolfe, J. T., Pokoz, T. and Winter, G. "Local and Overall Buckling of Cold-Formed Members". J. of the Stru. Div., ASCE, Vol. 100, No. ST10, pp. 2017-2036, October, 1974.

(68) Kalyanaraman, V., Pokoz, T. and Winter, G. "Overall Column Stability After Local-Buckling". Int. Colloquium on Stability of Structures Under Static and Dynamic Loads, pp. 757-771, New York, 1977.

(69) Chen, W. F. and Astuta, T. "Theory of Beam-Columns". Volume 1 "In-Plane Behaviour and Design", 1976. Volume 2 "Space Behaviour and Design", 1977, McGraw-Hill, New York.

(70) Rajasekaran, S. and Murray, D. W. "Coupled Local Buckling in Wide-Flange Beam-Columns". J. of the Struct. Div., ASCE, Vol. 99, No. ST6, pp. 1003-1023, 1973.

(71) Johnson, C. P. and Will, K. M. "Beam Buckling by Finite Element Procedure". J. of the Struct. Div., ASCE, Vol. 100, No. ST9, pp. 669-685, 1974.

(72) Akay, H. U., Johnson, C. P. and Will, K. M. "Lateral and Local Buckling of Beams and Frames". J. of the Struct. Div., ASCE, Vol. 103, No. ST9, pp. 1821-1832, 1977.

(73) Bradford, A. and N. S. Trahair. "Distortional Buckling of I-Beams". The University of Sydney, School of Civil Engineering, Research Report No. R353, October, 1979.

(74) Wang, S. T. and Wright, R. S. "Torsional-Flexural Buckling of Locally Buckled Beams and

Columns". Int. Colloquium on Stability of Structures Under Static and Dynamic Loads, pp. 587-608, New York, 1977.

(75) Wang, S. T., Yost, M. L. and Tien, Y. L. "Lateral Buckling of Locally Buckled Beams Using Finite Element Techniques". Int. J. of Comp. and Struct., Vol. 11, p. 127, 1980.

(76) Plank, R. J. and Wittrick, W. H. "Buckling Under Combined Loading of Thin, Flat-Walled Structures by a Complex Finite Strip Method". Int. J. for Num. Meth. in Engn., Vol. 8, pp. 323-339, 1974.

(77) Hancock, J. G. "Local, Distrortional and Lateral Buckling of I-Beams". J. of the Struct. Div., ASCE, Vol. 104, No. ST11, pp. 1787-1798, November, 1978.

(78) Hancock, J. G. "Nonlinear Analysis of Thin Sections in Compression". The University of Sydney, School of Civil Engineering, Research Report R355, November 1979.

(79) Hancock, J. G. "Interaction Buckling in I-Section Columns". The University of Sydney, School of Civil Engineering, Research Report No. R360, March, 1980.

(80) Graves Smith, T. R. "The Ultimate Strength of Locally Buckled Columns of Arbitrary Length". Symposium on Thin-Walled Steel Structures, Swansea, 1967.

(81) Graves Smith, T. R. "The Effect of Initial Imperfections on the Strength of Thin-Walled Box Columns". Int. J. Mech. Sci., Vol. 13, pp. 911-925, 1971.

(82) Little, G. H. "Local and Overall Buckling of Square Box Columns". Cambridge Unviersity Report No. CUED/C-Struct/TR.56, 1976.

(83) Dwight, J. B. and Little, G. H. "Stiffened Steel Compression Flanges - A Simpler Approach". The Structural Engineer, Vol. 54, pp. 501-509, 1976.

(84) Wittrick, W. H. "A Unified Approach to the Initial Buckling of Stiffened Panels in Compression". Aeronautical Quarterly, Vol. 19, pp. 265-283, 1968.

(85) Wittrick, W. H. "General Sinusoidal Stiffness Matrices for Buckling and Vibration Analysis of Thin Flat-Walled Structures". Int. J. Mech. Sci., Vol. 10, pp. 949-966, 1968.

(86) Williams, F. W. and Wittrick, W. H. "Computational Procedures for a Matrix Analysis of the Stability and Vibration of Thin Flat-Walled Structures in Compression". Int. J. Mech. Sci., Vol. 11, pp. 979-998, 1969.

(87) Wittrick, W. H. and Williams, F. W. "An Algorithm for Computing Critical Buckling Loads of Elastic Structures", J. Struct. Mech., Vol. 1, pp. 497-518, 1973.

(88) Cheung, Y. K. "The Finite Strip Method in Structural Analysis". Pergamon Press Limited, 1976.

(89) Loo, Y. C. and Cusens, A. R. "The Finite Strip Method in Bridge Engineering". A Viewpoint, 1978.

(90) Hinton, E. "A Note on a Thick Finite Strip Method for the Free Vibration of Laminated Plates". Earthquake Eng. and Stru. Dynamic, Vol. 4, pp. 511-520, 1976.

(91) Chan, H. C. and Foo, O. "Buckling of Multi-Layer Sandwich Plates by the Finite Strip Method". Int. J. Mech. Sci., Vol. 19, pp. 447-456, 1977.

(92) Dawe, D. J. "Finite Strip Buckling Analysis of Curved Plate Assemblies Under Biaxial Loading". J. Solids Structures, Vol. 13, pp. 1141-1155, 1977.

(93) GravesSmith, T. R. and Sridharan, S. "A Finite Strip Method for the Buckling of Plate Structures Under Arbitrary Loading". Int. J. Mech. Sci., Vol. 20, pp. 685-693, 1978.

(94) Hinton, E. "Buckling of Initially Stressed Mindlin Plates Using a Finite Strip Method". Computer and Structures, Vol. 8, pp. 99-105, 1978.

(95) Thangham, P. V. and Reddy, D. V. "Stability Analysis of Skew Orthotropic Plates by the Finite Strip Method". Computer and Structures, Vol. 8, pp. 599-607, 1978.

(96) Yoshida, H. and Maegawa, K. "The Buckling Strength of Orthogonally Stiffened Plates Under Uniaxial Compression". J. Str. Mech., Vol. 7, pp. 161-191, 1979.

(97) Yoshida, H. and Maegawa, K. "Local and Member Buckling of H-Columns". J. Stru. Mech., Vol. 6, pp. 1-27, 1978.

(98) Grave Smith, T. R. and Sridharan, S. "A Finite Strip Method for the Post-Locally Buckled Analysis of Plate Structures". Int. J. Mech. Sci., Vol. 20, pp. 833-842, 1978.

(99) Sridharan, S. "Elastic Post-Buckling Behaviour and Crinkly Collapse of Plate Structures". Ph.D. Thesis, Southampton University, 1978.

(100) Plank, R. J. "The Initial Buckling of Thin Walled Structures Under Combined Loadings". Ph.D. Thesis, University of Birmingham, September, 1973.

(101) Zienkiewicz, O. C., Valliapan, S. and King, P. I. "Elasto-Plastic Solutions of Engineering Problems. Initial Stress, Finite Element Approach". Int. J. of Num. Meth. in Engn., Vol. 1, p. 75, 1969.

(102) Yamada, Y. N., Yoshimura, N. and Sakurai, T. "Plastic Stress-Strain Matrix and Its Application for the Solution of Elasto-Plastic Problems by the Finite Element Method". Int. J. of Mech. Sci., Vol. 10, p. 343, 1968.

(103) Ylinen, A. "Lateral Buckling of an I-Beam in Pure Bending Beyond the Limit of Proportionability". Proc. 2nd Conf. on Dimensioning and Strength Calculations, Budapest, p. 157, 1965.

(104) Desi, C. S. and Abel, J. F. "Introduction to the Finite Element Method". Van Nostrand Reinhold, 1972.

(105) Marshall, C. P. "Methods of Matrix Algebra". Academic Press, New York, 1965.

(106) Wilkinson, J. H. "Householder's Method for the Solution of the Algebraic Eigenproblem". Computer J., Vol. 3, pp. 23-27, 1960.

(107) Szilard, R. "Theory and Analysis of Plates, Classical and Numerical Methods". Prentice-Hall, New Jersey, 1974.

(108) Carlsen, C. A. and Czujko, J. "The Specification of Post-Welding Distortion Tolerances for Stiffened Plates in Compression". The Struc. Engn., Vol. 56A, No. 5, May, 1978.

(109) Dwight, J. B. and Moxham, K. E. "Welded Steel Plates in Compression". Struct. Eng., Vol. 47, No. 2, p. 49, February, 1969.

(110) Barnett, S. and Cronin, T. M. "Mathematical Formulae". Bradford University Press, 1975.

(111) Scheer, J. and Nölke, H. "The Background to the Future German Plate Buckling Design Rules". An Int. Symposium on Steel Plated Structures, Imperial College, London, July, 1976.

(112) Wittrick, W. H. and Williams, F. W. "A General Algorithm for Computing Natural Frequencies of Elastic Structures". Quarterly J. of Mechanics and Applied Mathematics, Vol. 14, Pt. 3, pp. 263-284, August, 1971.

(113) Skaloud, M. and Kristek, V. "Folded-Plate-Theory Analysis of the Effect of the Stiffener Configuration Upon the Buckling of Longitudinally Stiffened Compression Flanges". ACTA Technica Csav, No. 5, pp. 577-601, 1977.

(114) Dibley, J. E. "Lateral Torsional Buckling of I-Sections in Grade 55 Steel". Proc. of the Inst. of Civil Eng., Vol. 43, pp. 599-627, 1969.

(115) Strymowicz, G. and Horsley, P. D. M. "Strut Behaviour of a New High Yield Stress Structural Steel". The Structural Engineer, Vol. 47, No. 2, pp. 73-78, February, 1969.

(116) "Specification for the Use of Structural Steel in Building". BS449, Part 2, 1969.

(117) "Specification for the Use of Cold Formed Steel Sections in Building". Addendum No. 1 (to BS 449, Part 2, 1969), April, 1975.

(118) European Convention for Constructional Steelwork "Second International Colloquium on Stability". Introductory Report, 1976.

(119) Zienkiewicz, O. C. "The Finite Element Method". Third Edition, McGraw-Hill, 1977.

(120) Bergan, P. G. and Clough, R. W. "Large Deflection Analysis of Plates and Shallow Shells Using the Finite Element Method". Int. J. for Num. Meth. in Engn., Vol. 5, pp. 543-556, 1973.